
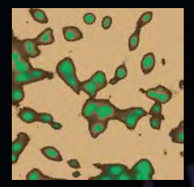
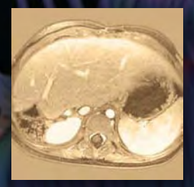
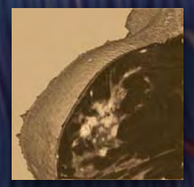
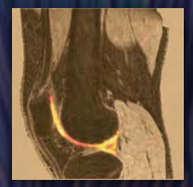
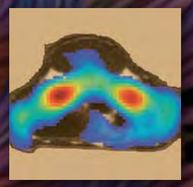
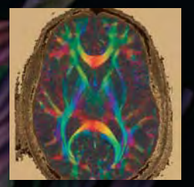


Lucas Center Annual Report 2008

Stanford University School of Medicine
Department of Radiology

Lucas Center Annual Report 2008

Stanford University School of Medicine
Department of Radiology

Richard M. Lucas Center for Imaging
Annual Report 2008

Stanford University School of Medicine
Department of Radiology


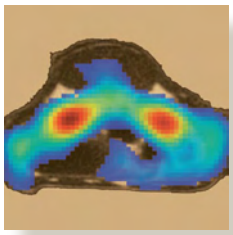
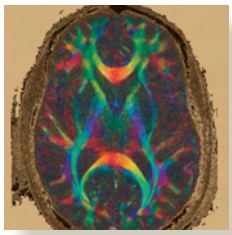
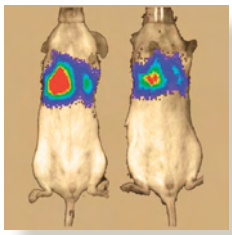

Richard M. Lucas Center for Imaging
Annual Report 2008

Stanford University School of Medicine
Department of Radiology


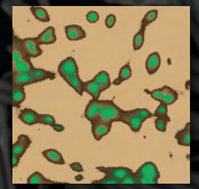
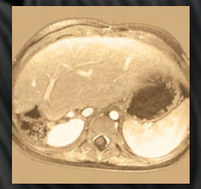
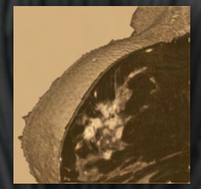

Contents


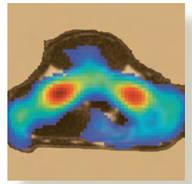
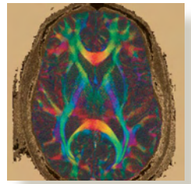
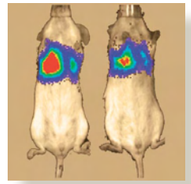

Cover Images:

Background: White matter fiber tracts are reconstructed using in vivo diffusion tensor imaging fiber tractography. Shown are medial lemniscus pathway and corticospinal tracts. The tracts were extracted from a set of diffusion-weighted images with a resolution of 0.86mm x 0.86mm x 2mm acquired on a GE 3T Signa MRI system using the SNAILS sequence (Chunlei Liu, PhD, Roland Bammer, PhD, Michael Moseley, PhD, Gary Glover, PhD).

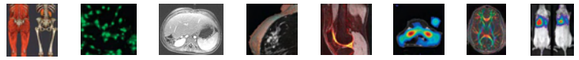

1. The CT image is a volume rendering of a whole body CT scan revealing muscular, skeletal, and vascular structures (Sandy Napel, PhD).

2. Immunofluorescence staining shows expression of vascular endothelial growth factor receptor type 2 (VEGF2) expression on mouse angiosarcoma SVR cells (Juergen Willmann, MD).

3. A 1.5 Tesla MR contrast-enhanced image from a child after a split liver transplant uses a novel three-dimensional k-space sampling sequence implemented in the Lucas Center. With this method, MRI has supplanted computed tomography (CT) for evaluating liver disease in children, thus reducing exposure to ionizing radiation to those most susceptible to its harmful effects (Shreyas Vasanawala, MD, PhD).

4. The MR image shows a contrast enhanced water-specific high resolution breast MRI, volume rendered, with cut-away to reveal a newly diagnosed multifocal invasive breast carcinoma (Brian Hargreaves, PhD, Bruce Daniel, MD).

5. The sodium sagittal image depicts a knee acquired at 3T in a subject with a prior ACL tear. The sodium signal in color correlates with the cartilage glycosaminoglycan content (Garry Gold, MD, Brian Hargreaves, PhD). See page 81.

6. This MR metabolic image is one of a series of images demonstrating lactate produced in rat kidneys following an injection of hyperpolarized $^{13}C_1$-pyruvate (Daniel Spielman, PhD, Dirk Mayer, PhD). See page 108.

7. This is a high-resolution diffusion tensor image (DTI) of the human brain. The image is acquired at 3T using a readout-segmented EPI sequence at a target in-plane resolution of 480 x 480 (Roland Bammer, PhD, Samantha Holdsworth, PhD). See page 136.

8. Bioluminescent imaging tracks genetically labeled mesenchymal stem cells (MSCs) homing, propagating, and differentiating in a breast cancer lung metastasis model (Xiaoyuan Chen, PhD). See page 112.

2008 Lucas Report Team:

Editor/Production: Susan Kopiwoda
Design: Amy Morris
Photography: Mark Riesenberger
Archiving: John Ralston
Printing: Lahlouh, Inc.

Building the Lucas Center

The View in 2008

As I approach the 20th anniversary of my arrival at Stanford University, I still vividly remember the excitement of conceptualizing and then building the Lucas Center. The initial dream of creating a world epicenter for medical imaging motivated several colleagues and me to move to California and get to work. What fun it has been to realize our dreams!

Today, the original Center and its expansion (known as Lucas I and Lucas II, respectively), as well as our other facilities on the Stanford campus, are overflowing with creative people. As you read this Annual Report, you will see an astonishing scope and great depth to our work. Our faculty champions continually reach out beyond the boundaries of their expertise to collaborate and to seek new ideas and information. They have published their research results in the leading scientific and medical journals; presented their work at major society meetings; and secured government funding or additional philanthropic financial support during this challenging funding climate.

Over the past year, we have been firing on all cylinders. We have created a Departmental section housed in the Lucas Center called Information Sciences in Imaging@Stanford (ISIS). One goal of ISIS is to bring together in new ways information from molecular medicine and imaging to speed the development of aspects of personalized medicine. We have also established the Center of Excellence for Cancer Early Detection. Supported by a generous gift from the Canary Foundation, this Center will become a major focus of the Department and Stanford University over the next five years as we work toward saving lives through the earlier detection of cancer. We are also very proud to have developed two major outpatient imaging centers for clinical care and translational research which house advanced technology in MRI and CT: Stanford Medicine Imaging Center, Palo Alto (SMIC) on Sherman Avenue, and Stanford Medicine Outpatient Center, Redwood City (SMOC). We expect that ideas generated and implemented at the Lucas Center will be transferred to these new outpatient centers to benefit our patients.

Collaborating with the Departments of Neurology, Psychiatry, and Psychology, we have also established the Center for the Aging Brain and Cognitive Disorders, which will focus on improving our understanding of Alzheimer's disease and the aging brain. The Lucas Foundation has seeded this effort, and I am pleased to report that we have identified and recruited a terrific imaging scientist who will lead our high-field MRI efforts in this area.

I have saved perhaps the biggest news for last. We have been given permission by the School and University to occupy approximately 30,000 square feet of space in the former Alza Building on California Avenue (less than three miles from the Lucas Center) starting in early 2009. All of these recent accomplishments and program developments, as well as those profiled throughout the Annual Report, would never have occurred without the Lucas family and Lucas Foundation's active support in so many ways. We now have more to look forward to than at any other time in our journey.

Gary M. Glazer, MD
Emma Pfeiffer Merner Professor in the Medical Sciences
Professor and Chairman
Department of Radiology
Stanford University School of Medicine

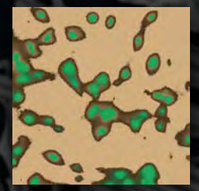

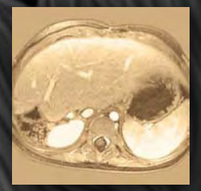

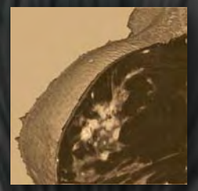

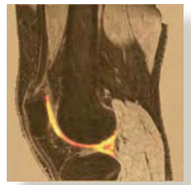

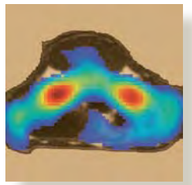

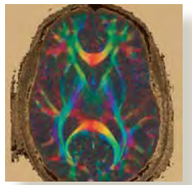

2008 Lucas Report Highlights

Highlights 2008

New Initiatives

During the last two years, Department leadership has made substantial commitment to early detection of disease, including noninvasive diagnosis, therapy, and monitoring of disease. There are currently a number of projects in varying stages of progress. For highlights of new initiatives, please see page 10.

Centers of Excellence

In addition to the many funded projects that our faculty lead, Stanford Radiology is also home for a number of NIH-funded Centers of Excellence. Highlights of these highly competitive and successful programs can be found on page 11.

Center of Excellence Cancer Early Detection

The Stanford Department of Radiology and the Canary Foundation have united to form The Center of Excellence in Early Cancer Detection. The Center will be led by Sam Gambhir, MD, PhD, and will focus on the development of blood and imaging tests, which will detect disease at its earliest and most treatable stage. A brief summary of the Center can be found on page 10.

Space

Stanford University and the School of Medicine has granted us permission to occupy 30,000 square feet of space in the former Alza Building on California Avenue (approximately three miles from the Lucas Center) starting in early 2009. See Dr. Glazer's "The View in 2008" on page 1, the Research Overview on page 8, and the Center of Excellence for Early Cancer Detection on page 10. We look forward to an expanded report on the new space in next year's Lucas Report.

ISIS

The Department of Radiology has recently created a new Section, Information Sciences in Imaging @ Stanford (ISIS), which will be co-directed by Professors Sandy Napel and Sylvia Plevritis. ISIS aims to gain new knowledge from imaging examinations by integrating and analyzing them with related clinical and molecular data. The section's goal is to explore the full spectrum of information-intensive activities in imaging and in non-imaging domains. For further details of ISIS and this new area of research, please see pages 12 and 13.

New Faculty

We have added several new faculty this year. Senior faculty joining us this year include Dr. Brian Rutt who will head up the High-Field Imaging Program and Dr. Michael Federle, who will focus on Education in Radiology. In addition, we have several other new faculty, science staff, and support staff who will help us advance in key areas of the Department. Please find details of the newest members of our research groups on pages 18-23.

Trainee Awards

Congratulations to the many postdoctoral fellows and scholars, graduate students, residents, clinical fellows, and medical students who have been recognized this year for their innovative projects and for their outstanding work. Please find trainee awards highlighted on page 30.

Outpatient Imaging

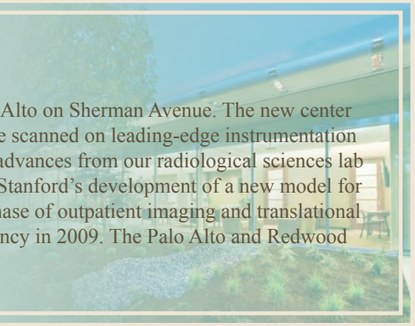

In June 2008, Stanford opened a state-of-the-art imaging center in Palo Alto on Sherman Avenue. The new center is a combined clinical and translational research facility. Patients will be scanned on leading-edge instrumentation from GE and Siemens, and will directly benefit from the translation of advances from our radiological sciences lab in the Lucas Center. The new outpatient center marks the first phase in Stanford's development of a new model for imaging service delivery featuring patient-centric facilities. The next phase of outpatient imaging and translational research at the Stanford Redwood City facility will be ready for occupancy in 2009. The Palo Alto and Redwood City facilities are highlighted on page 62.


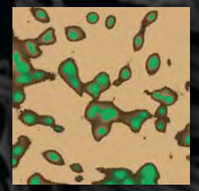
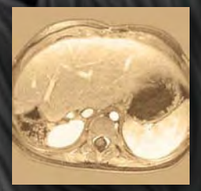
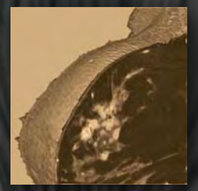
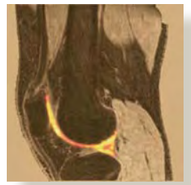
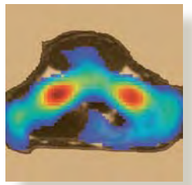
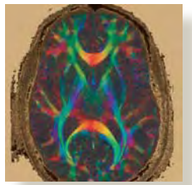


Lucas Center Overviews

Research Overview

Norbert Pelc, ScD, Associate Chair for Research
Susan Kopiwoda, MS, MPH, Director, Strategic Research Development

In 2008, our research program has experienced a phenomenal increase in the number of faculty, staff, and students. Since 2000, our ranks have expanded from 52 to over 200 (see Figure 1). The number of our scientific staff has increased the most (by 235%), followed by postdoctoral trainees (147%); administrative support (136%); faculty (108%); and graduate students (80%). Much of this growth derives from the addition of new faculty as each new scientist establishing his/her research lab attracts an average of seven to eight additional staff and trainees. This year, we welcomed nine new basic research faculty and senior scientists (see pages 18-23), which will lead to an increase in population to approximately 240 research personnel and trainees by 2009-10.

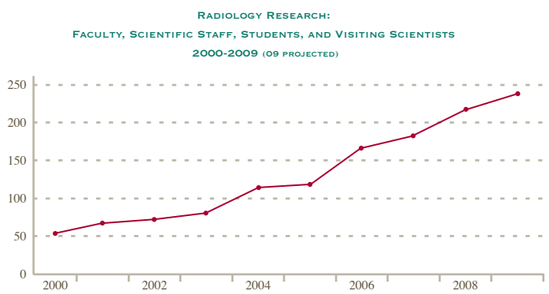

Figure 1 shows an increase of more than 300% in research personnel and trainees from 52 in 2000 to 211 in 2008

Our current space in the Lucas Center, Clark Center, Edwards Building, Grant Building, and the hospitals cannot accommodate our growth in people and programs. We are thrilled to report that radiology research personnel will occupy newly acquired research space on California Avenue in Palo Alto. The new Center of Excellence for Cancer Early Detection, supported by the Canary Foundation, will also initially occupy this space.

The Ultra High-Field MRI Program in the Stanford Radiology Department is another strategically important area undergoing major expansion. Led by Dr. Brian Rutt who was just recruited to our department, it will be centrally located in the Lucas Center and will include collaborations on instrumentation and application development and basic science. In his research, using MRI technology, Dr. Rutt targets vascular disease, cancer, neuroimaging, and cellular/molecular imaging. He has an outstanding record that includes numerous research grants from US and Canadian agencies. We welcome Brian and look forward to his contributions and programmatic expansion this coming year.

Our growth in research personnel has resulted in an increase in applications for funding and in newly funded projects. In Figure 2, the number of applications submitted since 2004 shows an increase of almost 100% from 2004 to 2008. The number of dollars requested during this period has increased from $55M in 2004 to approximately $92M in 2008. The peak in dollars proposed in 2005 was due to three large proposals submitted during that year: 1) the Center for Advanced Magnetic Resonance Technology at Stanford (CAMRT); 2) the In Vivo Cellular and Molecular Imaging Center (ICMIC); and the 3) Center for Cancer Nanotechnology Excellence Focused on Therapy Response (CCNE-TR). Each of these programs received new or continued funding

Our extramural funding is also greatly affected by the stagnation in the NIH budget, which began in 2003-2004. Adjusted for inflation, NIH's investment in science in constant dollars has dropped from $33B in 2004 to $28B in 2008, causing scientists across the country to explore avenues other than NIH for their research funding. While this funding picture has been worrisome, our faculty and research scientists have been persistent in submitting meritorious applications to NIH. Their hard work and astute response to NIH reviewer comments have led to 11 new or renewed NIH-funded projects this year. Of these, three are longstanding programs that were approved for an additional five years. For 2009, the United States Senate has proposed to increase the NIH budget by 2.9%, which would reverse the downward trend, staying ahead of a projected 2% inflation rate. Please see the American Association for the Advancement of Science (AAAS) website (http://www.aaas.org/spp/rd/nih09s.htm) for further details on this topic.

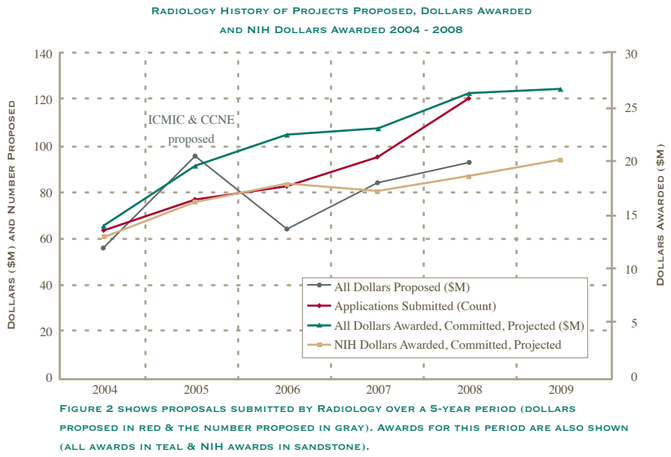

Figure 2 shows proposals submitted by Radiology over a 5-year period (dollars proposed in red & the number proposed in gray). Awards for this period are also shown (all awards in teal & NIH awards in sandstone).

The adjacent table shows the distribution of funded projects in the Radiology Department according to funding source. For a complete listing of all sponsored projects, see pages 206-11.

In the next few pages, you will read about emerging new initiatives, NIH-supported Centers of Excellence, and the three Stanford Radiology sections that make up our research effort: 1) our newest section, Information Sciences in Imaging @ Stanford (ISIS), co-led by Sandy Napel, PhD and Sylvia Plevritis, PhD; 2) the Radiological Sciences Lab (RSL), led by Gary Glover, PhD; and 3) the Molecular Imaging Program at Stanford (MIPS), led by Sam Sanjiv Gambhir, MD, PhD.

As the body of this report will highlight, supported by the Lucas and Canary Foundations, our research at the Lucas Center continues to have an important impact, bringing countless benefits to our trainees and, most importantly, addressing diagnostic and therapeutic needs of the patients we treat and care for every day.

2009 Sponsored Projects

Funding Source	Number
NIH supported projects	41
NIH sub-contracts	15
Industry-supported projects	30
Foundation-supported projects	22
DOD & California-supported porjects	12
Stanford-supported projects	4
Total	124

See pages 206-11 for a detailed list of all sponsored projects.

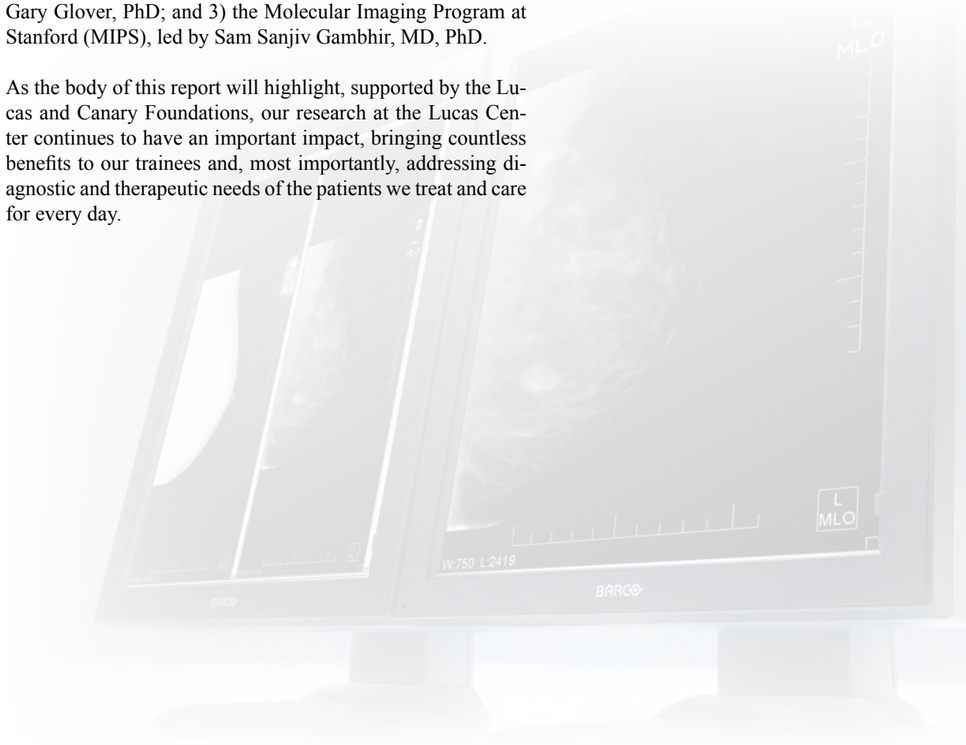

New Initiatives

The Aging Brain and Cognitive Disorders

The Center for the Aging Brain and Cognitive Disorders is a new collaboration among the Radiology, Neurology, Psychiatry, and Psychology Departments at Stanford. Dr. Brian Rutt, who has recently joined the Radiology Department and the Lucas Center faculty, will, in collaboration with Dr. Scott Atlas, lead the development of core MRI technologies and applications underlying this effort. This new collaboration is supported by generous funding from the Richard M. Lucas Foundation, which forms a multidisciplinary center-of-excellence that will focus on the aging brain, Alzheimer's disease, dementias, neurodegenerative disease, psychiatric disorders, and screening for preclinical cognitive decline. We will investigate and develop new diagnostic tools and therapies to care for patients with cognitive disorders. MR neuroimaging, especially at high field (7T), will play a large role in the development of this initiative.

Center for Biomedical Imaging at Stanford (CBIS)

The Center for Biomedical Imaging at Stanford emphasizes applied biomedical imaging and the identification of imaging resources to enable the development of innovative imaging methods. The Center provides the interdisciplinary networks for advancing biomedical imaging through its Web site (http://cbis.stanford.edu/), which offers access to imaging experts, research, programs, resources, training, and seminars. Bringing together a wide variety of imaging professionals, CBIS enhances human health by promoting the development of novel imaging technology, data acquisition, image reconstruction, analysis, modeling, visualization, simulation, and image interpretation.

Center of Excellence for Cancer Early Detection

Supported by an alliance between the Canary Foundation and the Stanford Department of Radiology, the Center of Excellence for Cancer Early Detection will be housed in a new off-campus facility of more than 10,000 square feet, and will focus on proteomics and molecular imaging in early cancer detection. Research will be performed in a proteomics facility focused on the development of blood screening tests. Tissue facilities as well as wet labs will facilitate the creation of molecular imaging strategies to identify and localize early cancer. Led by Sam Gambhir, MD, PhD, the Center will develop simple blood and imaging tests to predict the likelihood of disease; detect the presence of disease; plan and monitor therapy; and predict and monitor the progression and recurrence of disease. The Center's efforts will catalyze the work of early disease detection and intervention by creating synergies within the Department of Radiology, across campus, and outside of Stanford.

Information Sciences in Imaging at Stanford (ISIS)

The vision of ISIS is to gain new knowledge from imaging examinations by integrating and analyzing them with related clinical and molecular data. ISIS, co-directed by Sandy Napel, PhD, and Sylvia Plevritis, PhD, aims to achieve this goal by exploring the full spectrum of information-intensive activities in imaging (e.g., image management, storage, retrieval, processing, analysis, understanding, visualization, navigation, interpretation, reporting, and communications) and in non-imaging domains (e.g., pathology, molecular and genetic markers, family history, prior medical reports, and clinical outcomes). See pages 12-13 for details.

Centers of Excellence

The National Center for Advanced Magnetic Resonance Technology at Stanford (CAMRT)

The CAMRT is now in its fourteenth year of operation as a National Research Resource, directed by Gary Glover, PhD, and funded by a grant from the NIH's National Center for Research Resources. This Resource has six core technology development areas that include reconstruction methods (Dwight Nishimura and John Pauly, EE Department, core directors), imaging of brain activation (Gary Glover, core director and PI), diffusion and perfusion weighted imaging methods (Mike Moseley, core director), imaging of cardiovascular structure and function (Brian Hargreaves, core director), spectroscopic imaging development (Dan Spielman, core director) and interventional MRI technique development (Kim Butts Pauly, core director). In addition to development of technology projects, the CAMRT provides support for collaborations and service use of the facilities, with users in the Radiology department as well as more than 75 faculty and more than 200 other users from at least 14 departments.

The In Vivo Cellular and Molecular Imaging Center at Stanford (ICMIC)

The ICMIC, directed by Sam Gambhir, MD, PhD, brings together more than 50 faculty across the Stanford campus from 21 different departments, including the Department of Radiology. As only one of eight in vivo cellular and molecular imaging centers (ICMIC) in the country, the ICMIC studies disease by connecting preclinical models with clinical management through advances in multimodality molecular imaging. This molecular imaging program benefits from the highly regarded infrastructure provided by the CAMRT and RSL in the Richard M. Lucas Center for Imaging.

The Center for Cancer Nanotechnology Excellence-Focused on Therapy Response (CCNE-TR)

Stanford Radiology also has been identified as one of eight institutions in the nation to receive NIH support to develop a major nanotechnology center: the Center for Cancer Nanotechnology Excellence Focused on Therapy Response (CCNE-TR). This new center, led by Sam Gambhir, MD, PhD, includes scientists from Stanford and from six other sites across the country. The goal of this center is to use nanotechnology for the benefit of cancer patient management. The CCNE greatly expands our collaborative efforts, and we now work with an additional 35 faculty in more than 20 departments here at Stanford and across the country.

Center for Computational Modeling of Cancer Biology, an Integrative Cancer Biology Program (ICBP)

The Center for Computational Modeling of Cancer Biology, led by Sylvia Plevritis, PhD, consists of 9 academic faculty across 8 departments bridging the Schools of Medicine and Engineering. It is one of nine academic centers nation-wide, funded by the NIH/NCI Integrative Cancer Biology Program initiative, which promotes the analysis of cancer as a complex biological system. Our goal for the Stanford Center is to develop and apply the computational tools that will aid in the discovery of molecular perturbations implicated in cancer initiation and progression (http://icbp.stanford.edu/).

ISIS Overview

Information Sciences in Imaging at Stanford
Sandy Napel, PhD, and Sylvia Plevritis, PhD, co-Directors

ISIS core faculty members (from left to right): Daniel L. Rubin, Sandy Napel, Sylvia K. Plevritis, David S. Paik.

Information Sciences in Imaging at Stanford

In recent years, radiological imaging has seen unprecedented advances in spatial resolution and acquisition speed for visualizing and molecularly characterizing a variety of anatomical structures and lesions in the human body non-invasively. At the same time, molecular biology has witnessed break-through innovation with technologies that characterize excised tissue and biospecimens by their molecular signatures. The Department of Radiology has identified an interconnectedness of these advancements and recently created a new section, named ISIS for "Information Sciences in Imaging @ Stanford," that aims to gain new knowledge from imaging examinations by integrating and analyzing them with related clinical and molecular data. ISIS aims to achieve this goal by exploring the full spectrum of information-intensive activities in imaging (e.g., image management, storage, retrieval, processing, analysis, understanding, visualization, navigation, interpretation, reporting, and communications) and in non-imaging domains (e.g., pathology, molecular and genetic markers, family history, prior medical reports, and clinical outcomes). Critical to the ISIS mission is the development of a core capability to collect annotated imaging, clinical and molecular data, and to integrate them by creating databases and novel computational models that identify relationships among these data. Through these efforts, we believe that ISIS will improve the diagnostic and treatment planning value of images and lead to personalized, less-invasive approaches to early detection and treatment while also improving our understanding of human biology and disease.

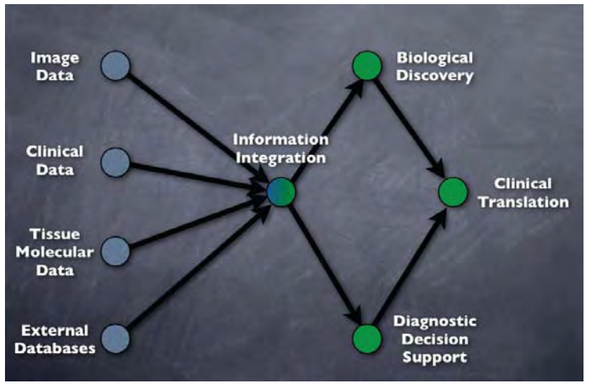

Figure 1: Key elements (grey nodes) and expected outcomes (green nodes) of ISIS

Figure 1 shows the key elements and expected outcomes of the ISIS effort. At the center of the Figure (Information Integration) is a database that is populated with correlated image, clinical, and molecular data (as obtained from non-invasive means, and/or through tissue samples), and novel computational models to analyze this richly annotated data. Image data can be annotated in several ways, including by human interpretation and by computer algorithms. These annotations are incorporated in the database as well. This database also is fed by external databases, such as are currently being developed by several national and international organizations (e.g., NIH, ACR, RSNA) and can, in turn, provide its correlated data to these efforts. The magic of ISIS happens through novel computational algorithms that mine the information in the database. The integration of genomic and proteomic tissue characterizations correlated to images, blood-based biomarkers, and clinical outcomes opens a new realm of basic scientific discovery of which ISIS will pursue three main efforts. First, ISIS will aim to identify imaging features that encode molecular properties of tissue. Second, ISIS will aim to derive new prognostic signatures based on the combination of imaging and molecular signatures. Finally, ISIS will aim to identify candidate molecular markers for molecularly-targeted imaging and therapy. All three efforts will be used to develop the primary outputs of ISIS: (1) an evidenced-based diagnostic decision support system, whereby patient-specific image, clinical and, if available, molecular data, can be compared to the database to suggest the most likely diagnoses, prognoses, and most relevant treatments, (2) biological discovery, i.e., synthesis and potential testing of hypotheses regarding the underlying biology in the development, progression, and hopeful eradication of specific diseases, and (3) the translation of these developments into clinical practice using computers and image storage systems that are ubiquitous in healthcare enterprises today.

Accordingly, we have established ISIS with an initial focus on three 5-year goals: (1) the establishment of a research program in data-driven Radiology Diagnosis and Decision Support, (2) the establishment of a research program in Integrative Biology that combines imaging data with high throughput molecular data to enable data-driven discovery in radiology, and (3) the translation and evaluation of the advances afforded by these two programs in clinical practice, ultimately improving health and influencing health policy. All of these efforts share the need for core resources for (1) database building and management, and (2) tissue processing, storage, and analysis. In order to accelerate the realization of our mission, we aim to leverage and broaden the industrial, international, and local collaborations that the Department has already established.

ISIS core faculty include Sandy Napel, Professor of Radiology and co-Director of the Radiology 3D Laboratory, Sylvia K. Plevritis, Associate Professor of Radiology, David S. Paik, Assistant Professor of Radiology. Daniel L. Rubin, who has expertise in medical and imaging informatics that is recognized at the national level, is expected to become the newest faculty member of the section as an assistant professor of radiology. ISIS also includes affiliate members; our first is Professor Robert J. Herfkens whose expertise will bridge ISIS to clinical imaging and information systems.

RSL Overview

Lucas Center, Radiological Sciences Laboratory and
The Center for Advanced MR Technology (CAMRT)
Gary H. Glover, PhD
Director, Radiological Sciences Laboratory

The Lucas Center is home to the Radiological Sciences Laboratory (RSL), a section of the Radiology Department, and in conjunction with the Electrical Engineering Department, is host to the Center for Advanced MR Technology, an NIH-funded National Research Resource. Its state of the art imaging facilities support research of the RSL and the entire Radiology department as well as hundreds of on-campus and extramural researchers as a core facility. The Center continues to be an exciting and lively nexus for fundamental imaging research.

The Radiological Sciences Laboratory

The RSL comprises 9 faculty, approximately 40 graduate and postdoctoral students, approximately 30 scientific staff and 8 administrative assistants, as well as the Lucas Center/RSL Administrative Services Director, Donna Cronister. This is a reduction of 3 from previous years due to the recent creation of the new Radiology department section, Information Science and Imaging at Stanford (ISIS). Sandy Napel and Sylvia Plevritis co-direct the new section, while David Paik is a third member and Daniel Rubin has recently joined the department and ISIS (see elsewhere in this report for more on ISIS).

However, we have been fortunate to attract Brian Rutt from Robarts Institute in Western Ontario to join our faculty this fall. Brian is internationally known for his expertise in many areas of MRI physics and engineering, and will head up our 7T research program. This is the culmination of a several year recruitment effort, and we are pleased to have such an exceptional outcome!

The faculty serves in a wide variety of advisory roles to government and foundation agencies such as the NIH and in policy-making positions for international scientific societies such as the ISMRM and RSNA. A number of our faculty, scientific staff, and students have garnered prestigious awards for their exceptional research achievements. Some of the Lab's honors of the past year are noted here with great pleasure.

The National Center for Advanced MR Technology at Stanford (CAMRT)

The CAMRT is now in its fourteenth year of operation as a Research Resource, sponsored by a grant from the NIH National Center for Research Resources. Outstanding progress has been made in all six of the core technology development areas that include reconstruction methods (Dwight Nishimura, Electrical Engineering Department, core director), imaging of brain activation (Gary Glover, core director and PI), diffusion and perfusion weighted imaging methods (Mike Moseley, core director), imaging of cardiovascular structure and function (Brian Hargreaves, core director, spectroscopic imaging development (Dan Spielman, core director) and interventional MRI technique development (Kim Butts, core director). Much of this exciting research is chronicled in the scientific reports that follow and is not duplicated here.

Lucas Center Facilities

With continued growth of our research enterprise, the Center continues to adapt to accommodate the new departmental initiatives. Renovation of the animal magnet lab for installation of a second 3T magnet was completed in 2007, and the system was installed and calibrated for use by June of 2008. The scanner is an investigational device cited in the Center by GE for evaluation by our various groups. It is a next-generation system with improvements in every subsystem of the machine, and evaluation is under way. It has impressive stability and other capabilities, and the scan suite has been completely outfitted for fMRI and other complex experimentation.

Plans are being finalized for renovation of the office space above the new 3T on the second floor, to accommodate more postdocs and senior staff. The current storage space and a closed office will be reduced somewhat, but much of the gain will come from more efficient layout.

The clinical arm of the 3D Lab, currently on the first floor, will be relocated to space in the Medical Center, which will be more efficient for their operation, and free up the Center to house the new ISIS section discussed above together with students.

MIPS Overview

Molecular Imaging Program at Stanford
Sanjiv S. Gambhir, MD, PhD
Director, Molecular Imaging Program at Stanford

The Molecular Imaging Program at Stanford (MIPS) (http://mips.stanford.edu) continues to experience significant growth. Many faculty within the Department of Radiology and from other Departments continue to help build the program. The faculty received several new grants from the NIH as well as other agencies over the last year. We are now in the fourth year of the NCI-funded In vivo Cellular Molecular Imaging Center (ICMIC) P50 grant. We are in the third year of the NCI Center for Cancer Nanotechnology Excellence (CCNE) U54 grant. We are also in the third year of the NIH R25T training grant, Stanford Molecular Imaging Scholars (SMIS), to train the next generation of cancer molecular imaging scholars. A new NIH post-doctoral training grant (T32) for cardiovascular molecular imaging is highly likely to be funded. In addition, all labs continue to grow with many new students, post-doctoral fellows, and outstanding research staff joining the program.

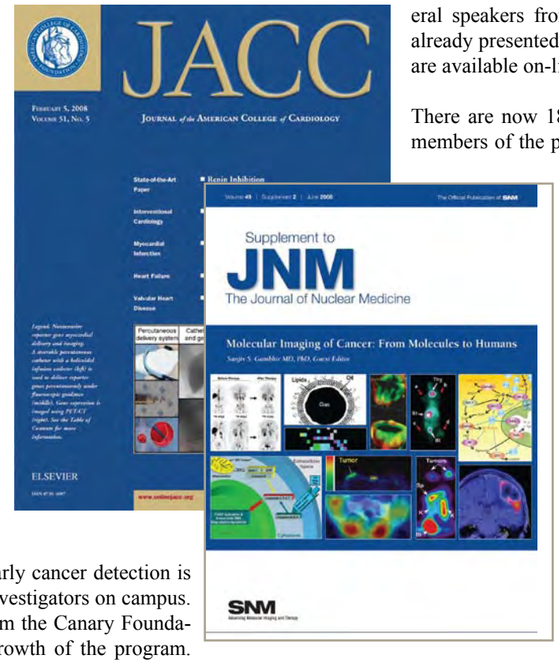

Funding from the Canary Foundation to develop a new center for early cancer detection is helping build bridges with many investigators on campus. Significantly increased funding from the Canary Foundation is expected with continued growth of the program. New off-campus space has recently been committed to for this effort in early cancer detection and includes facilities for blood/tissue based detection of disease. We are convinced that more investments are needed in the earlier detection of all disease, including cancer. The ability to detect disease earlier will substantially improve the potential for cure. This center will work on novel in vitro diagnostics (e.g., using patient blood samples) as well as new imaging strategies with high sensitivity to detect very low burden disease. It is hoped that in the next 3-5 years Stanford can become a world-leader in the important field of early cancer detection.

We continue to have several seminar series on campus to help educate scientists about molecular imaging. The molecular imaging seminar series (http://mips.stanford.edu/public/mi_seminar.adp) is now in its fourth year and has a large collection of videos available on-line of speakers from the last few years. This year we also initiated students presenting from different MIPS labs. The Nanobiotechnology seminar series (http://mips.stanford.edu/public/nanobiotech_seminar.adp), which focuses on new applications of nanotechnology to cancer continues to gain momentum. Several speakers from around the country have already presented in the series and all lectures are available on-line.

There are now 18 MIPS faculty that are full members of the program with many more associate members from all over campus. Many of the full members are from the Department of Radiology. The number of graduate students, MSTP students, post-doctoral fellows, research scientists, technicians, and administrative staff continues to grow and is currently approximately 150. We expect a significant growth over the next 2-3 years with the new center on early cancer detection and occupancy of new off-campus space.

We also continue to grow our industrial partnerships with key leaders in the molecular imaging community. Several projects to develop new imaging agents/strategies are underway with General Electric Global Research, General Electric Healthcare, Genentech, as well as Bayer-Schering. It is likely that additional industrial partners will enter into collaborative research relationships over the next several years. These will be key to helping to translate discoveries at Stanford to the patient bedside. Several faculty are also involved in new startup-company efforts with intellectual property from their laboratories at Stanford. These include new efforts in diagnostics, small animal imaging and clinical imaging.

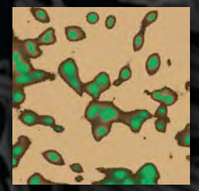

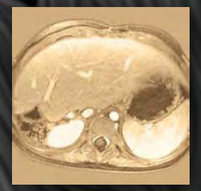

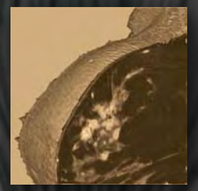

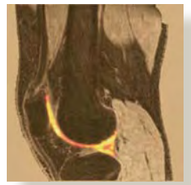

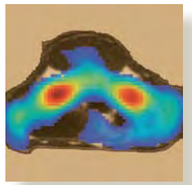

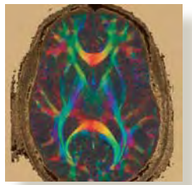

Faculty and Research Personnel

New Faculty Profiles

Michael Federle, MD

Professor of Radiology
Associate Chair for Education

Dr. Federle, who began his career in radiology at UCSF, joins our Department this fall as the Associate Chair for Education. Since 1989, Dr. Federle has practiced radiology at the University of Pittsburgh. During his tenure there, he served as the Chair of Radiology for three years and the Director of Abdominal Imaging for sixteen years. Prior to his affiliation with the University of Pittsburgh, he was Vice Chairman in the UCSF Department of Radiology and Chief of Medical Staff at the San Francisco General Hospital. Dr. Federle, who is internationally regarded as one of the best abdominal imaging radiologists in the world, has authored more than 10 definitive texts on abdominal imaging, more than 75 book chapters, and more than 200 publications during his career in radiology. In reading through Dr. Federle's long list of awards, it is apparent that teaching is his passion and as a testament to his gifts as a teacher, he has been awarded more than 10 teaching awards from students and colleagues during his career as an academic radiologist. In his new position as Associate Chair for Education, Dr. Federle's first objective is to make Stanford University the world's epicenter for medical student education in Radiology. With his experience and knowledge in this area, Dr. Federle will lead the development of a comprehensive plan to create the most attractive radiology medical student elective in the country.

Brian Rutt, Ph.D.

Professor of Radiology
Director of the High Field MRI Program

Dr. Rutt joined the Stanford faculty as Professor of Radiology effective Sept. 1, 2008. Dr. Rutt, who is the author of more than 120 peer reviewed journal articles, is an internationally recognized expert in Magnetic Resonance Imaging (MRI). Prior to coming to Stanford, Dr. Rutt was Professor of Diagnostic Radiology and Nuclear Medicine and Medical Biophysics at the University of Western Ontario and the recipient of the Barnett-Ivey Heart and Stroke Foundation of Ontario Endowed Research Chair. Dr. Rutt has made important contributions in both the basic technology of MRI (e.g., leading-edge work in insertable gradient coils and RF components), biophysical measurements using MR (e.g., combined T_1 and T_2 mapping using gradient imaging sequences), basic science applications of MR (e.g., the first demonstrations of in-vivo detection of a single mammalian cell using MRI and the use of MR to longitudinally monitor tumor growth deep within tissue starting from a single cell), and clinical applications, especially in cardiovascular disease. Dr. Rutt is especially interested in developing and using in-vivo ultra-high field (e.g. 7 Tesla) magnetic resonance techniques to study important human diseases. The increased sensitivity and enhanced contrast mechanisms at these high field strengths should provide insight to unsolved problems, especially in neuroscience and cancer.

Welcome New Faculty

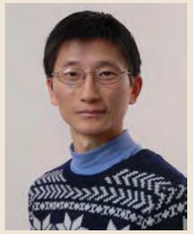

Zhen Cheng, PhD

Assistant Professor in the Department of Radiology
and the Molecular Imaging Program at Stanford (MIPS)

Zhen Cheng, PhD, Assistant Professor in the Department of Radiology and the Molecular Imaging Program at Stanford (MIPS) joined the Department in the fall of 2007 following a radio-biochemistry fellowship at Harvard Medical School and three years as a research scientist in the MIPS group. His superb training in chemistry and biology makes him uniquely qualified to conduct research in molecular imaging, which the NIH recognizes as one of the top seven research priority areas today. Dr. Cheng has been instrumental in the development of molecular imaging probes for cancer, especially for the early detection of breast cancer and melanoma. Dr. Cheng also studies protein scaffold-based agents as a generalizable strategy for tumor detection and imaging.

Daniel Rubin, MD, MS

assistant professor of radiology
Information Science in Imaging at Stanford (ISIS)

Daniel Rubin, MD, Assistant Professor of Radiology in the newly established Information Science in Imaging at Stanford (ISIS) section, is also director of scientific development for Stanford's National Center for Biomedical Ontology, a National Center for Biomedical Computing of the NIH Roadmap. He is chair of the RadLex Steering Committee of RSNA, chair of the Informatics Committee of the American College of Radiology Imaging Network (ACRIN), and co-chair of the Medical Imaging Systems Working Group of the American Medical Informatics Association. In addition to informatics, his background includes clinical and investigational radiology, as a radiologist and researcher. Dr. Rubin's academic focus is on 1) the intersection of biomedical informatics and imaging science; 2) developing computational methods and applications to access and integrate diverse clinical and imaging data; 3) extracting information and meaning from images; 4) enabling data mining and discovery of image biomarkers; and 5) translating these methods into practice by creating computer applications that will improve diagnostic accuracy and clinical effectiveness. He is currently undertaking the Annotation and Image Markup (AIM) project of the cancer Biomedical Informatics Grid (caBIG), an effort to create standards for making the semantic meaning in images explicit so that computers can help researchers to relate image data to other types of high-throughput data.

Juergen Willmann, MD

assistant professor of Radiology
Abdominal Imaging section and MIPS

Juergen Willmann, MD, an Assistant Professor of Radiology in the abdominal imaging section and a member of the Molecular Imaging Program at Stanford (MIPS) joined the Department in 2008. Dr. Willmann received his MD from the Albert-Ludwigs-University Freiburg, Germany in 1998 and did his radiology residency training at the University Hospital in Zurich, Switzerland, where he was also chief resident. In 2003, he was appointed clinical attending and was elected assistant professor of Radiology after he received the "venia legendi" from the University of Zurich, Switzerland. Between 2006 and 2008, he trained in the field of molecular imaging at Stanford. Dr. Willmann's research interests include multi-modality molecular imaging of angiogenesis and stem cell therapy and the development of new imaging probes. As a clinical radiologist, Dr. Willmann will teach and supervise residents and fellows in the abdominal imaging section. In addition, he will bridge the gap between basic and clinical research and establish his translational molecular and functional imaging laboratory with special focus on early detection and treatment monitoring of abdominal and pelvic diseases including cancer and inflammatory illnesses.

Welcome Senior Scientists

Frezghi Habte, PhD

Research and Development Engineer
Small Animal Imaging Facility

Frezghi Habte, PhD, is a former post-doctoral fellow and engineer from Dr. Craig Levin's laboratory and more recently was a post-doctoral fellow at Oak Ridge National Laboratory working on gamma imaging instruments. He is new to the Molecular Imaging Program at Stanford (MIPS) and the Small Animal Imaging Facility. Dr. Habte will provide image quantitation support for users of the imaging facility. He will provide quantitation training sessions regularly, will provide direct support on various molecular imaging related projects, and will perform studies on ways to characterize and improve image quantitation. He also supports the Small Animal Imaging Facility in performing instrument calibration.

Demir Akin, DVM, PhD

Instructor of Radiology
Deputy Director, Center for Cancer Nanotechnology Excellence

Demir Akin, DVM, PhD, Instructor of Radiology recently joined the Molecular Imaging Program at Stanford (MIPS) as the Deputy Director of the Center for Cancer Nanotechnology Excellence. Dr. Akin completed his PhD in comparative pathobiology at Purdue University, has a doctorate in veterinary medicine from Ankara University, and a master's degree in molecular biology from Mississippi State. Before joining the MIPS Radiology group, Dr. Akin was assistant professor of nanomedicine at Purdue in the Department of Biomedical Engineering and the Birck Nanotechnology Center. He managed the BioMEMS and BioNano Laboratories at the Birck Nanotechnology Center and was a member of the Oncological Sciences Center and the Bindley Biosciences Center and managed a group of interdisciplinary researchers from the fields of Engineering and Life Sciences. With more than ten years of experience in molecular diagnostics, image acquisition and processing, electrical engineering, and nanotechnology, Dr. Akin will be a rich resource for emerging multidisciplinary initiatives.

Andrei Iagaru, MD

Instructor of radiology
Nuclear Medicine section and MIPS

Andrei Iagaru, MD, Instructor of Radiology in the Department of Radiology recently joined our Department after completing a fellowship in nuclear medicine. Dr. Iagaru completed medical school at Carol Davila University of Medicine, Bucharest, Romania, and an internship at Drexel University College of Medicine, Graduate Hospital, in the Department of Medicine. He began his residency at the University of Southern California (USC) Keck School of Medicine, Los Angeles, in the division of nuclear medicine, where he was the chief resident. He finished his residency and completed a PET/CT fellowship at Stanford University School of Medicine in the Division of Nuclear Medicine. His research interests include whole-body MRI and F-18 and F-18 FDG PET/CT in metastases detection; Zevalin/Bexxar radioimmunotherapy; optical imaging of breast cancer; and PET-CT imaging for thyroid and breast cancer, melanoma, lymphoma, and sarcoma. With a strong clinical and research background, Dr. Iagaru looks forward to translating new PET/SPECT radiopharmaceuticals into clinical use.

Welcome Senior Scientists

Bonnie King, PhD

Instructor of Radiology
Deputy Director of the Center of Excellence for
Cancer Early Detection

Bonnie King, PhD, Instructor of Radiology and Deputy Director of the new Center of Excellence for Cancer Early Detection joined the Molecular Imaging Program at Stanford (MIPS) in September 2008. Dr. King earned her doctorate in Endocrinology at U.C. Berkeley, and did her postdoctoral fellowship at the Yale Medical School, where she joined the research faculty in the Department of Therapeutic Radiology. While at Yale, she developed a translational breast cancer research program focusing on mammary gland biology, molecular cancer genetics, and early detection.

Laura Pisani, PhD

MRI Physicist and Instrumentation Specialist in the
Small Animal Imaging Facility

Laura Pisani, PhD, a former post-doctoral fellow from Gary Glover's laboratory, has been hired as a full-time staff scientist, and is responsible for overseeing the MicroPET and fluorescent imaging modalities in the imaging core. During her first few months in the lab, Dr. Pisani focused her efforts on bringing the new 7T MRI small animal imaging system up to speed. She has provided an important link between the lab and industry by working closely with Varian, GEHC and Resonance Research Inc. It was through her thoughtful leadership on this project and these collaborations, that Dr. Pisani systematically identified hardware problems following installation and corrected them. Dr. Pisani has become a critical member of the team in the Small Animal Imaging Facility in many ways, including consulting and advising many groups here at Stanford as they expand their pre-clinical research to utilize the newly available MRI scanner.

New Administrative Support Staff

Bonita Crabbe works in the Clark Center with Dr. Gambhir and Elizabeth Gill.

Lin Davis, BS, works in the Lucas Center providing administrative support for Drs. Herfkens, Cheng, and Chin.

Mandeep Kaur, BA, graduated from UC Davis in 2003, and provides administrative support in the Lucas Center for Dr. Gary Glazer, Mary Bobel, Michelle Christierson, and Susie Spielman.

Armando Mendoza, RT (R) (MR), is a new MR technologist working in the Lucas Center providing research support for the many research studies that are carried out on the various MR systems at this site.

Teresa Newton, a graduate of UC Santa Cruz, works in the Lucas Center providing administrative support for Drs. Pelc, Butts Pauly, Zaharchuk, and the MR Lab Manager, Anne Sawyer.

Shannon Walters, BS, RT(MRI), a new 3D technologist, works in the Lucas and Clark centers, providing post-processing of CT and MRI images for clinical, research, and educational purposes.

Nancy Ware, RT (CT), is a new 3D technologist working in the Lucas and Clark centers, providing post-processing of CT and MRI images for clinical, research, and educational purposes.

Welcome

Faculty and Staff Awards

Recipient	Award
Patrick Barnes, MD	Herman Grossman Lecturer Award, Department of Radiology, Duke University Medical Center, In Appreciation for Your Contributions to Pediatric Radiology and the Eleventh Annual Herman Grossman Lecture, April 10, 2008.
Sandip Biswal, MD, SW Lee, PhD, A Kamaya, MD, D Behera, E Graves, PhD, Gold GE, MD	Moncada Award – 31st Annual Meeting of the Society of Computer Body Tomography and Magnetic Resonance for research entitled, "Nerves on Fire: Imaging Pain and Nociception with Manganese-Enhanced MRI (MEMR)." Society of Computed Body Tomography and Magnetic Resonance, 2008.
Carmel Chan, PhD	World Molecular Imaging Congress Travel Award, 2008
Terry Desser, MD	Journal of the American College of Radiology Best of 2007 award for best paper published in the Education category for Simulation based training: the next revolution in Radiology education?
Rebecca Fahrig, PhD	Selected as a 2008-09 faculty research fellow at the Michelle R. Clayman Institute
Nancy Fischbein, MD	Selected as a 2008 School of Medicine Faculty Fellow
Adam de la Zerda, Zavaleta, Keren, Vaithilingam, Bodapati, Liu, Levi, Smith, Ma, Oralkan, Cheng, Chen, Dai, Khuri-Yakub, Gambhir	Co-recipient of Senior Faculty of the Year award, 2007-2008.
Gambhir, MD, PhD, Lutz, MD, Willmann, MD, Cochran, PhD, Ray, PhD	The paper, "Carbon nanotubes as photoacoustic molecular imaging agents in living mice" published in Nature Nanotechnology has received significant media coverage in radio broadcasts (KCBS Radio, KGO Radio, KQED Radio) and in the press (Washington Post, U.S. News, Forbes, MSN Health, Springfield News-Sun, Medical Health Articles, Stay Healthy News, Your Total Health, Yahoo! News, Yahoo! Health, Dr. Koop).
Sam Gambhir, MD, PhD	The article, "Cancer Screening: A Mathematical Model Relating Secreted Blood Biomarker Levels to Tumor Sizes", published in PLOS Medicine covered in the news media (MSN, ScienceNews.org, WashingtonPost.com, Yahoo! News).
	Guest editor for a new special issue of the Journal of Nuclear Medicine reviewing multimodality molecular imaging of cancer. Over 10 articles covering all aspects of the latest developments in cancer imaging are included.
	Tesla Medal – United Kingdom Royal College of Radiologists for work in "Multimodality Molecular Imaging of Living Subjects," 2008.
	American Society of Clinical Investigation. Inducted as member in honor society for physicians/scientists at the Society's 100th year anniversary, 2008.
	Work in Dr. Gambhir's lab, Multimodality Molecular Imaging Lab, featured on the cover of the Journal of the American College of Cardiology (JACC), Feb 5, 2007.
Arun Ganguly, PhD	Received a SPIE Honorable Mention for her poster: "On the Angular Distribution of Bremsstrahlung", February 2008.
Garry Gold, MD	2007 International Skeletal Society President's Medal
Hargreaves, PhD; Neal Bangerter, PhD; Staroswiecki, PhD; Gurney, PhD; Nnewihe, MS; Daniel, MD; Gold, MD	Lauterbur Award by the Society of Computed Body Tomography and Magnetic Resonance (SCBT/MR) for their research project "Co-Registered Sodium and Proton MRI of Osteoarthritis and Breast Cancer."
Andrei Iagaru, MD	Best Essay Award, ACNP Annual Meeting: "I131 I-Tositumomab (Bexxar®) vs. 90Y-Ibritumomab (Zevalin®) in Refractory/Relapsed Non-Hodgkin's Lymphoma."
	Best Essay Award, ACNP Annual Meeting: "18F FDG PET/CT In Head and Neck Cancers: What is the Definition of "Whole Body" Scanning?"

NOTE: Please see pages 206-11 for Funded Research Awards (Sponsored Projects) and pages 30 and 31 for Trainee Awards.

Faculty and Staff Awards

Recipient	Award
Andrei Iagaru, MD	Alavi-Mandell Award, Society of Nuclear Medicine. Treatment of Thyrotoxicosis. Journal of Nuclear Medicine 2007;48(3):379-89.
	Clinician Educator of the Year Award, Stanford Radiology Residency Program.
Aya Kamaya, MD	2006-2007 Junior Faculty Teacher of the Year Award
Wulliam Kuo, MD	Awarded a Top 5 2007 Best Poster Award from the American College of Chest Physicians Annual Meeting
	Elected a Fellow of the American College of Chest Physicians (FCCP).
Ann Leung, MD	Stanford Radiology Senior Faculty of the Year 2007 – 2008
	Stanford School of Medicine Excellence in Teaching Award, 2007 - 2008.
Chunlei Liu, PhD	Selected as a finalist for the Young Investigator Award from the International Society of Magnetic Resonance in Medicine (ISMRM), 2007.
Amelie Lutz, MD	Swiss National Science Foundation Scholarship, 2007.
John D. MacKenzie, MD	2007 Radiological Society of North America Fellow Research Trainee Prize.
Michael Moseley, PhD	Elected as an honorary lifetime member of the Society of Magnetic Resonance Technologists
Norbert Pelc, ScD	Elected a Fellow of the American Association of Physicists in Medicine (AAPM), 2008
Sylvia Plevritis, PhD	The U56, Computational Modeling of Cancer Biology, lead by Dr. Plevritis, was identified as an exemplar of NCI-funded research, May 2008.
Daniel Sze, MD, PhD	His abstract was featured (top 5%) at the Society for Interventional Radiology Annual Meeting.
Willmann, MD, van Bruggen, PhD, Dinkelborg, PhD, Gambhir, MD, PhD	A review from the Multimodality Molecular Imaging Lab is featured on the cover of Nature Reviews Drug Discovery: "Molecular imaging in drug development" discusses applications of molecular imaging in drug development, and the challenges that need to be addressed to optimize its utility. It was written in collaboration with Genentech and Bayer-Schering.
Juergen Willmann, MD	2008 European Society of Gastrointestinal and Abdominal Radiology Bronze Award
	Travel Award - Society of Molecular Imaging and Academy of Molecular Imaging, Providence, September 2007
	2008 Editor's Recognition Award - awarded in recognition of outstanding service as a reviewer European Journal of Radiology & European Journal of Radiology Extra
	Selected as a Baxter Faculty Scholar, 2008-09.
Joseph Wu, MD, PhD	2008 Baxter Faculty Scholar.
	2007 Burroughs Wellcome Fund Career Award for Medical Scientist
	Research from Dr. Wu's lab, Cardiovascular Molecular Imaging Lab, was the cover feature of the Journal of Nuclear Medicine for cardiovascular molecular imaging of stem cell transplantation and gene therapy, December 2007.

NOTE: Please see pages 206-11 for Funded Research Awards (Sponsored Projects) and pages 30 and 31 for Trainee Awards.

Radiology Research Faculty, Staff, and Students

Our group photo represents approximately half of the 211 Radiology research personnel found in various locations on the medical school campus.

Trainees & Visitors

Post Doctoral Fellows

Stephanie Bailey, PhD
Deepak Behera, PhD
Ian Chen, PhD
Kai Chen, PhD
Ted Chu, PhD
Moses Darpolar, Ph.D.
Anca Dragulescu-Andrasi
Meng Gu, MS
Keith Hartman, PhD
Mei Huang, PhD
Michelle James, PhD
Brian Kim, MD
Richard Kimura, PhD
Allison Kurian, MD, MS
Zongjn Li, PhD
Hin-Tsu Jill Lin, PhD
Zhe Liu, PhD
Amelie Lutz, MD
Zheng Miao, PhD
Hua-Fan Minogue, PhD
Gang Niu, PhD
Natesh Parashurama, MD, PhD
Hao Peng, PhD
Jennifer Prescher, PhD
Gang Ren, PhD, MD
Hongjun Ren, PhD
Babak Shahbaba, PhD
Bryan Smith, PhD
Virginia Spanoudaki, PhD
Ning Sun, PhD
Kyung Sung, PhD
Moriah Thomason, PhD
Alessia Tognolini, MD
Ricky Tong, PhD
Stephanie van de Ven, MD
Arne Vandenbroucke, PhD
Wouter Veldhuis, M.D.
Hui Wang, PhD
Sen Wang, PhD
Yun Wu, PhD
Zuyong Xia, PhD
Fei Xiao, PhD
Yung Xing, PhD
Hequan Yao, PhD
Jin Yu, PhD
Cristina Zavaleta, Ph.D.
Yan Zhang, PhD

Radiology Scientific Research Personnel

Faculty & Staff

Faculty

Roland Bammer, PhD
*Sandip Biswal, MD
Kim Butts Pauly, PhD
Xiaoyuan Chen, PhD
Zhen Cheng, PhD
Rebecca Fahrig, PhD
Sam Gambhir, MD, PhD
Gary M. Glazer, MD
Gary H. Glover, PhD
Samira Guccione, PhD
Brian Hargreaves, PhD
Robert J. Herfkens, MD
*Rusty Hofmann, MD
Craig Levin, PhD
Michael E. Moseley, PhD
Sandy Napel, PhD
David Paik, PhD
Norbert J. Pelc, ScD
Sylvia K. Plevritis, PhD
Jianghong Rao, PhD
Daniel Rubin, MD, MS
Brian Rutt, PhD
Daniel M. Spielman, PhD
*Juergen Willmann, MD
Joseph Wu, MD, PhD
*Greg Zaharchuk, MD, PhD

*clinical scientists with Labs in the Lucas Center

Administrative & Support Staff

Mary Bobel, MBA
Maggie Bos
Michelle Christierson
Bonita Crabbe
Donna Cronister
Lin Davis, BS
Debra Frank
Elizabeth Gill
Sofia Gonzales, MS
Sondra Horn
Mandeep Kaur, BA
Susan Kopiwoda, MS, MPH
Marlys Lesene
John Mendoza
Donna Niernberger
Teresa Newton, BA
Kala Raman, MS
John Reuling
Lanzie Rivera
Julie Ruiz, PhD
David Russel
Monique Schareck, MHA
Judy Schwimmer, MBA, MA
Susan Singh
Jim Strommer, BA
Wei Xiong

Scientific Staff

Demir Akin, DVM, PhD
Marcus Alley, PhD
Priti Balchandani, PhD
Neal Bangerter, PhD
Wendy Baumgardner, RVT, LATg
Rhona Berganos, BS
Thomas Brosnan, PhD
Carmel Chan, PhD
Danye Cheng
Frederick Chin, PhD
Garry Chinn, PhD
David Clayton, PhD
Abhijit De, PhD
David Dick, PhD
Aloma D'Souza, PhD
Aihua Fu, PhD
Arundhuti Ganguly, PhD
Andrew Gentles, PhD
Gayatri Gowrishankar, PhD
Frezghi Habte, PhD
Lina He, PhD
Pam Hertz, RVT
Jung-Jin (Jason) Hsu, PhD
William Johnsen
Anitha Jununtula
Bonnie King, PhD
Seungbum Koo, Ph.D.
Keshni Kumar, CRT
Andrew Lamb
Malika Larabi, PhD
Jelena Levi, PhD
Chunlei Liu, PhD
Dirk Mayer, PhD
Sam Mazin, PhD
Mohammed Namavari, PhD
Linda Novello, RT
Manish Patel, PhD
Laura Pierce, MPA, RT
Laura Pisani, PhD
Paulmurgan Ramasamy, PhD
Pritha Ray, PhD
Robert Reeves, MA
Viola Rieke, PhD
Sandra Rodriguez, RT (R)(MR)
Jarrett Rosenberg, PhD
Ruminder Samra, RT
Ataya Sathirachinda
Anne Marie Sawyer, BS, RT (R)(MR)
Greig Scott, PhD
Bronislava Sigal, PhD
Stefan Skare, PhD
Marc Sofilos, RT
Matus Straka, PhD
Murugesan Subbarayan, PhD
Ron Watkins
Shahriar Yaghoubi, PhD
Yishan Yang, PhD
Sung-Won Yoon, PhD

Trainees & Visitors (continued)

Graduate Students

Murat Aksoy, MS
Jongduk Baek, MS
Christopher Caires, MS
Jing Chen, MS
Adam de la Zerda, BSc
Jessica Faruque, MS
Angela Foudray, MS
Erin Girard-Hughes, MS
Kristi Granlund, MS
Yi Gu, MS
Misung Han, MS
Andrew Holbrook, MS
Caroline Jordan, MS
Sonal Josan, MS
Elena Kaye, MS
Kranthi Kode, BS
Frances Lau, M.S.
Christine Law, MS
Andrew Lee, BS
Yakir Levin, PhD
Prasheel Lillaney, MS
Ray Lin, MS
Peter Olcott, M.S.
Jeremy Pearl, BS
Guillem Pratx, M.S.
Rebecca Rakow-Penner, BS, MS
Julia Rasooly, BS
Paul Reynolds, M.S.
Debashis Sahoo, MS
Meike Schipper, MD
Heiko Schmiedeskamp, MS
Florian Schmitzberger
Anthony Sherbondy, MS
Harpeet Singh
Jared Starman, MS
Ernesto Staroswiecki. MS
Emily Tsai, BS
Chardonnay Vance, MS
Adam Wang, MS
Kitch Wilson, MD
Jung Ho Won, MS
Serena Wong, M.S.
Tao Xu, PhD
David Yerushalmi, MS
Jian Zheng, MS

Visiting Researchers & Scholars

Ben Ahn, MD, PhD
Ya-Fang Chang, PhD
Hadassa Degani, Ph.D.
Mark Griffiths, M.D.
Maximilian Haeberlin, PhD
Joachim Hornegger, PhD
Sun Kim, PhD
Daniel Kopenigg, PhD
Carsten Nielsen, MSc
Zhengming Xiong, MD, PhD
Zianzhong Zhang, PhD


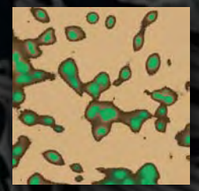
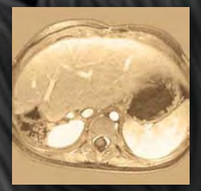
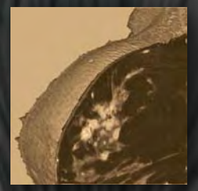
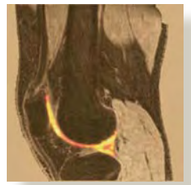
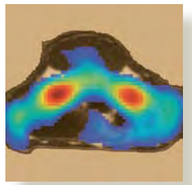
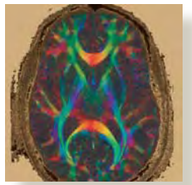


Education and Training

Trainee Awards

Recipient	Award
Priti Balchandani, PhD	2008 Young Investigator Award Finalist: Slice-Selective Tunable-Flip Adiabatic Low Peak-Power Excitation (STABLE) Pulse.
Michael Benoit, PhD	Career Development Award supported by the Center of Cancer Nanotechnology Excellence Focused-TR (CCNE-TR).
Chang, J, MD, Rao, J, PhD	2007 RSNA Trainee Research Prize for: "Functional Detection of Glucose Oxidase Activity by Electron Transfer to Quantum Dots."
Kai Chen, PhD	A research associate from the Molecular Imaging Probe Laboratory, is awarded 3rd place Young Professionals Committee (YPC) Best Basic Science Award, 2008 Society of Nuclear Medicine meeting.
Adam de la Zerda, BSc	2008 WMIC Student Travel Award. Bio-X Graduate Student Fellowship for research in the field of "Photoacoustic Molecular Imaging," 2008.
Riaz Dhanani, MD	Society of Interventional Radiology Resident Travel Award.
Bao Do, MD, JE Maley, S Biswal, MD	2007 RSNA Trainee Research Prize for: "Feedback natural language processing of fractures in unstructured reports of emergency department plain films."
Angela Foudray, MS	Awarded a full student scholarship to attend the 2007 International Workshop on Bayesian Inference and Maximum Entropy Methods, Saratoga Springs, N.Y.
Meng Gu, MS	2008 ISMRM Student Stipend Award. Career Development Award supported by the Center of Cancer Nanotechnology Excellence Focused-TR (CCNE-TR).
Mei Huang, PhD	2008 Dean's Fellowship.
Behara, MD, Kamaya, BS, Lee, MD, Graves, PhD, Yeomans, PhD, Biswal, MD	2007 RSNA Trainee Research Prize for: "Manganese-Enhanced MRI (MEMRI) Functionally Highlights Injured Peripheral Nerves in Neuropathic Pain."
B Kim, MD, E Mitra, PhD, H Dhatt, PhD, BH Do, MD, E Graves, PhD, S Biswal, MD	2007 RSNA Trainee Research Prize for: "A Difference in the Pattern of 18F-FDG Uptake is Observed Within the Spinal Canal in Low Back Pain Patients."
Frances Lau, MS	2007 IEEE Medical Imaging Conference Travel Grant to attend the 2007 Nuclear Science Symposium and Medical Imaging Conference. Bio-X Program Graduate Fellowship (2007-2010).
Levy, M, MD, Rubin, D, MD	2007 RSNA Trainee Research Prize for: "Is Current Radiology Reporting Sufficient for Evaluating the Clinical Response to Treatment? An analysis of Information Content in Radiology Images and Reports."
Zibo Li, PhD	Travel Award for the 2008 Society of Nuclear Medicine meeting. Awarded the Benedict Cassen Postdoctoral Fellowship from the Society of Nuclear Medicine, 2008.
Zongjin Li, PhD, MD	ACCF/Bristol-Myers Squibb Travel Award from the American College of Cardiology. Young Investigator Award from the Stanford University School of Medicine Cardiovascular Institute, 2008. Travel Award, 2008 International Society for Stem Cell Research (ISSCR) Annual Meeting. Finalist, Young Investigators Awards Competition, American College of Cardiology. Mitzi and William Blahd, MD Pilot Research Grant.
Chunlei Liu, PhD	Selected as a finalist for the Young Investigator Award from the ISMRM, 2007.
Jeff Liu	2008 Berson-Yalow Award, for the abstract "Analyzing the Recognition Sites of RGD Peptide on U87MG Tumor Cell Using a Competitive Binding Assay."

NOTE: Please see pages 206-11for Funded Research Awards (Sponsored Projects) and pages 24-25 for Faculty & Research Staff Awards

Trainee Awards

Recipient	Award
Yueyi, BS, Kamaya, MD, Desser, MD, Rubin, MD	2007 RSNA Trainee Research Prize for: "A Bayesian Approach to Decision Support for Evaluating Thyroid Nodules Based on Multi-variate Features."
Sam Mazin, PhD	Named a J.P. and Danyele Garnier Fellow for his contributions to the Stanford Graduate School of Business Summer Institute for Entrepreneurship Program.
Peter Olcott, MS	2007 IEEE Medical Imaging Conference Travel Grant, to attend the 2007 Nuclear Science Symposium and Medical Imaging Conference. One of two IEEE Nuclear and Plasma Sciences Society (NPSS) Student Paper Awards at the 2007 IEEE Medical Imaging conference.
Natesh Parashurama, PhD	Speaker and Travel Award for Stem Cell Bioengineering Conference, 2008. Dean's Fellowship Award for his proposal: "Molecular Imaging of the Cardiac Stem Cell Niche," 2008-09.
Hao Peng, PhD.	Stanford University Dean's Post-doctoral Fellowship Award for his proposal: "Investigation of a Miniature PET Camera Insert Dedicated to Simultaneous PET/MRI Mammography and MRI-guided Biopsy," 08-09. Travel Award - Society of Molecular Imaging and Academy of Molecular Imaging, Providence, September 2007.
Guillem Pratx, MS	IEEE Medical Imaging Conference Travel Award to attend the 2007 Nuclear Science Symposium and Medical Imaging Conference. Bio-X Graduate Student Fellowship Award, 2006-2009. 2008 Travel Award to attend the 2008 Society of Nuclear Medicine Meeting to present two papers: "Fast Maximum-Likelihood Image Reconstruction without a Line Search" and "Maximum a Posteriori event positioning in high-resolution PET CZT detectors".
Raman B., BS, Raman R, MD, Raman V., Phd, Desser T, MD	2007 RSNA Trainee Research Prize for: "Paperless Radiology Residency Conference Attendance Tracking Using Radiofrequency Identification (RFID) Technology."
Ricky Tong, PhD	2007 SNM Young Professional Committee – Best Scientific Award (first place).
Grace Tye, MD	Awarded a Society of Interventional Radiology (SIR) Resident Travel Award.
Maurice Van den Bosch, MD	Awarded a Society of Interventional Radiology Fellow Research Award and Fellow Travel Award.
Arne Vandenbrouke, PhD.	2007 IEEE Medical Imaging Conference Short Course Grant to attend the 2007 Nuclear Science Symposium and Medical Imaging Conference short course. Awarded 2008-2009 Belgian-American Educational Foundation (BAEF) Post-doctoral Fellowship.
David Wang, MD	Awarded a Society of Interventional Radiology Resident Travel Award.
Hui Wang, PhD	First Place, Society of Nuclear Medicine molecular imaging abstract: "Trafficking the Fate of Mesenchymal Stem Cells In Vivo."
Yingbing Wang, MD	Winner, 2008 Department of Radiology Norman Blank Award for the outstanding medical student in radiology.
Juergen Willmann, MD	Research Fellowship Award – Swiss Foundation for Medical-Biological Grants, 2007-2008. 2007 RSNA Trainee Research Prize for: "Molecular Imaging of Therapeutic Angiogenesis in Murine Hindlimb Ischemia Using PET and 64Cu-labeled Vascular Endothelial Growth Factor121."
Phyllis Yang, MD	Helena Anna Henzl-Gabor Young Women in Science Fund Travel Fellowship.

NOTE: Please see pages 206-11 for Funded Research Awards (Sponsored Projects) and pages 24-25 for Faculty & Research Staff Awards

Postgraduate Education

Continuing Medical Education Program

Susie Spielman

Director, Strategic Initiatives and Program Management

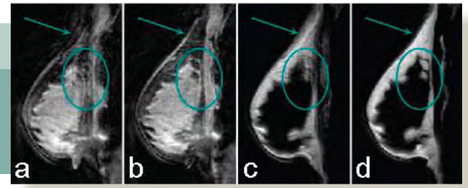

Over the past 18 years, Stanford University, Department of Radiology has constructed a world class CME program targeted to practicing physicians, academic scientists, radiology technologists, and industry-based engineers and scientists. Stanford Radiology is distinguished by an international reputation for excellence and innovation in postgraduate medical education. The Department was motivated to create such a program to fulfill their educational mission and disseminate radiological advances. Further the benefits of such an effort included an increase in reputation for the Department overall and for the individual faculty, as well as an opportunity to foster relationships globally with academic institutions and societies.

Radiology's CME program began in 1991 with small meetings and very few speakers. The Department made significant investments over the years, operating at a loss until 1999 and faced significant competition from a decade's old, dominant program at UCSF. A major emphasis on growth began in 1998 when high level administrative talented was recruited, many courses were changed to a three day format, and the marketing efforts were evolved. At that time, due to changes in the economic climate and professional needs of the target audience, Stanford moved away from primarily using "resort" settings and began to focus on large scientific meetings. Today Stanford Radiology has up to 16 efforts in a given year and reaches over 3,000 learners per year from more than 25 countries. These courses range from premiere scientific meetings on MDCT with up to 1,000 registrants to smaller on campus summer programs with leading Japanese technologists sponsored through the Japanese Society of Radiologic Technology.

Premier Scientific Meetings

The success of our program can be attributed to the strategic focus of our efforts and our focus on global partnerships. We construct large courses which are tailored to serve the changing educational needs of our target. By bringing together the world experts on key topics we are able to offer unique, high quality meetings. We continue to evolve our overall programs and in recent years offered new courses on PET/CT and advances in Interventional Techniques. In addition, our creative new meeting formats, innovative instruction techniques and careful selection of hotels and timing, allow us to differentiate our program from competing CME efforts.

We currently offer courses co-hosted by strategic partners in Japan, China and Europe in order to build international relationships for our faculty and to grow our international reach and reputation. Our goal is to continue to build these important efforts which have already led to vital scientific collaborations and show great promise for our future.

In August 2008 the School of Medicine issued a policy which restricts industry funding of specific programs in CME. Please visit http://cme.stanford.edu/documents/dean_letter.pdf to see the full policy. This new direction will provide us with quite a challenge but we remain committed to building our educational programs and are confident that we will thrive in the new environment.

Radiology National Institutes of Health (NIH) Training Programs

The Department of Radiology at Stanford University offers qualified individuals unique research opportunities through several programs that are home-based within the Radiological Sciences Lab (RSL) and the Molecular Imaging Program at Stanford (MIPS). Trainees in our programs will find unlimited opportunity to work with world-renowned faculty who are committed to sharing their knowledge and mentoring the future leaders in radiology. Our programs allow basic scientists (PhD) and clinical scientists (MD post-residency) to collaborate in an unparalleled environment that combines medical imaging sciences, clinical sciences, a strong cancer focus, and an institutional commitment to training academic radiologists and basic scientists in imaging science. The following training programs, listed in chronological order, give an idea of the success of the programs and the interests of current trainees.

NIH/NCI T32 CA09695

Advanced Techniques for Cancer Imaging and Detection - T32

PI – Gary M. Glazer, MD

Program Manager – Lanzie Rivera

The Advanced Techniques for Cancer Imaging and Detection Program, began its 16th year of training on February 1, 2008. The goal of our program is to provide MD and PhD research fellows with training in cancer-related imaging research. A specific aim of our training program is to position our trainees for a career in academic radiology. To date, we have graduated 26 trainees from our program. Our trainees continue to be extremely productive, and we often collaborate with them in their new positions both locally and throughout the country. This past year, we received the great news that NIH would continue to support our program for another five years, until January 31, 2013. We are grateful to the NIH for recognizing the strength and success of our training program. Listed below you will learn of our current trainees and their research interests and of past trainees and their latest appointments. NIH/NCI T32 CA09695 supports this T32 training program.

T32 Program Trainees and Research Interests

Stephanie Bailey, PhD. began her appointment in February 2007. She works with Dr. Sylvia Plevritis and her Computational Modeling group. Dr. Bailey's research interests in computational modeling and analysis of cancer outcomes, stochastic modeling of the natural history of cancer, health policy, and cost/benefit analysis are a natural fit for the Dr. Bailey and the Plevritis lab.

Rachel Bitton, PhD, began her appointment in March 2008. Her research interests are in photoacoustic imaging of micro-vasculature using high frequency ultrasonic transducers, MR temperature guidance for interventional high intensity focused ultrasound therapy, targeted contrast agents for photoacoustic imaging and therapy. Dr. Bitton is at home in the Interventional and Open MRI group led by Dr. Kim Butts Pauly.

Moses Darpolar, PhD, began his appointment in June 2008. His research interests are to apply multi-parametric MR and multimodality imaging in oncology. His previous and ongoing projects include DSC-MRI in conjunction with micro-CT imaging of vascular function and morphology of brain tumor with antiangiogenic treatment; 1H decoupled 31P CSI of tumor bioenergetics to detect early response of subsequent CPT11 and flavopiridol treatment; Hyperpolarized 13C imaging to detect early tumor response to radiation therapy. Dr. Darpolar is pleased to be among colleagues in the In Vivo Spectroscopy and Multinuclear Imaging lab led by Dr. Dan Spielman.

Cristina Zavaleta, PhD, joined Dr. Sanjiv Sam Gambhir's lab in 2006. Her research interests focus on the use of nanoparticles as imaging and drug delivery devices in cancer models. She is also interested in noninvasively imaging their accumulation in tumors using preclinical imaging techniques such as Raman Spectroscopy, MicroPET, and SPECT/CT.

T32 Program Graduates

NCI Fellow	Completed Training	Current Position	Current Institution	Primary Mentor
Byard Edwards, MD, PhD	2008	Research Scientist	Vanderbilt University, Nashville, TN	R. Brooke Jeffrey, MD
Jinha Park, MD, PhD	2008	Assistant Professor	University of Southern California, Los Angeles, CA	Sam Gambhir, MD,PhD
Anthony Faranesh, PhD	2007	Research Scientist	NIH, Washington, DC	Norbert Pelc, ScD & Brian Hargreaves, PhD
Lewis Shin, MD	2007	Assistant Professor	Radiology, Stanford University	Robert Herfkens, MD
Daniel Ennis, PhD	2006	Postdoctoral Fellow	University of Washington, Seattle, WA	Norbert Pelc, ScD
Daniel Margolis, MD	2005	Assistant Professor	Department of Radiology, UCLA, Los Angeles, CA	R. Brooke Jeffrey, MD
Jon Levin, MD	2004	Radiologist	St. Luke's Medical Center & Clinic, Minneapolis, MN	Robert Herfkens, MD, & Graham Sommer, MD
Laura Pisani, PhD	2004	Postdoctoral Fellow	Radiology, Stanford University	Gary Glover, PhD
Susan Hobbs, MD, PhD	2003	Resident	University of Minnesota	Mark Bednarski, PhD
Charles Liu, MD	2003	Radiologist	La Jolla Radiology, La Jolla, CA	Robert Herfkens, MD, & Graham Sommer, MD
Karl Vigen, PhD	2003	Research Scientist	University of Wisconsin-Madison, Madison, WS	Kim Butts Pauly, PhD
Lawrence Chow, MD	2002	Assistant Professor	University of Oregon, Eugene, OR	Graham Sommer, MD
Samira Guccione, PhD	2002	Assistant Professor	Radiology, Stanford University	Mark Bednarski, PhD
Yishan Yang, PhD	2002	Research Associate	Radiology, Stanford University	Mark Bednarski, PhD
Curtis Coulam, MD	2001	Radiologist	Gem State Radiology Group, Boise, ID	Graham Sommer, MD
Martin Blum, MD	2000	Researcher	Palo Alto, California	R. Brooke Jeffrey, MD
Steven Heiss, MD	1999	Radiologist	Radiology Imaging Associates, Denver, CO	King Li, MD
Roger Shifrin, MD	1998	Assistant Professor	University of Florida	Norbert Pelc, ScD & Robert Herfkens, MD
Esther Yuh, PhD	1998	Clinical Instructor	Radiology UCSF, San Francisco, CA	King Li, MD & Sandy Napel, PhD
Bruce Daniel, MD	1997	Associate Professor	Radiology, Stanford University	Robert Herfkens, MD
Garry Gold, MD	1997	Associate Professor	Radiology, Stanford University	Al Macovski, PhD
Yi-Fen Yen, PhD	1997	Research Scientist	GE Advanced Health Care	Gary Glover, PhD
Ian Chen, MD	1996	Radiologist	Southwest Washington Medical Center, Vancouver, WA	King Li, MD
Susan Lemieux, PhD	1996	Assistant Professor	Diagnostic Imaging Western Virginia University, Morgantown, WV	Gary Glover, PhD
John Strang, MD	1995	Assistant Professor	University of Rochester, Rochester, NY	Robert Herfkens, MD

NIH/NCI R25 CA118681

Stanford Molecular Imaging Scholars – SMIS R25

PI – Sam Gambhir, MD, PhD

Program Manager – Sofia Gonzales, MS

The Stanford Molecular Imaging Scholars (SMIS) program is a diverse training program bringing together more than 13 departments, predominantly from the Stanford Schools of Medicine and Engineering. Oncologic molecular imaging is a rapidly growing area within molecular imaging, which combines the disciplines of chemistry, cell/molecular biology, molecular pharmacology, bioengineering, imaging sciences, and clinical medicine to advance cancer research, diagnosis, and management. The goals of SMIS are to train postdoctoral fellows by providing mentorship through a diverse group of over 40 basic science and clinical faculty mentors representing eight program areas; by incorporating formal courses in molecular imaging, molecular pharmacology, cancer biology, cancer immunology, virology, and gene therapy; and by including a clinical component such as hematology/oncology rounds. To date, we have recruited 10 postdoctoral fellows. Three new fellows were recently selected to join the program, due to start later this year. Fellows in their first year have started their research projects and are preparing for clinical rounds. Fellows who are in their second year are continuing their research; they have participated in clinical rounds including Hematology/Oncology and Nuclear Medicine. In the upcoming year, they will each prepare a mock grant proposal.

Our first year of training began in September 2006. Six fellows have been recruited to the program. Four fellows are now in their second year of training. The following list summarizes where our new trainees are in the program. NIH/NCI R25 CA118681 supports the R25 program

R25 Program Trainees

SMIS Fellow	Training Period	Current Position	Institution	Primary Mentor
Richard Kimura, PhD	2006-2009	Postdoctoral Fellow	Stanford University	JenniferCochran, PhD
Jill Lin, PhD	2006-2009	Postdoctoral Fellow	Stanford University	David Paik, PhD
Jennifer Prescher, PhD	2006-2009	Postdoctoral Fellow	Stanford University (MIPS)	Christopher Contag, PhD
Bryan Smith, PhD	2006-2009	Postdoctoral Fellow	Stanford University (MIPS)	Sam Gambhir, MD, PhD
Ted Chu, PhD	2007-2010	Postdoctoral Fellow	Stanford University	William Kuo, MD
Hua Fan-Minogue, MD, PhD	2007-2010	Postdoctoral Fellow	Stanford University (MIPS)	Sam Gambhir, MD, PhD
Keith Hartman, PhD	2007-2010	Postdoctoral Fellow	Stanford University (MIPS)	Sam Gambhir, MD, PhD
Benjamin Cosgrove, PhD	2008-2011	Postdoctoral Fellow	Stanford University	Helen Blau, PhD
Henry Haeberle, PhD	2008-2011	Postdoctoral Fellow	Stanford University (MIPS)	Christopher Contag, PhD
Sharon Hori, PhD	2008-2011	Postdoctoral Fellow	Stanford University	TBD

NIH/NCI R25 CA118681

Stanford Molecular Imaging Scholars – SMIS R25

PI – Sam Gambhir, MD, PhD

Program Manager – Sofia Gonzales, MS

SMIS Trainee Research Interests

Richard Kimura, PhD, is a member of Dr. Jennifer Cochran's lab in the bioengineering department. He uses yeast surface display to evolve peptides to bind targets involves in cancer. He has developed several novel probes to detect and image angiogenesis and cancer cell surface markers.

Jill Lin, PhD, joined Dr. David Paik's lab in in 2006. She is working on building a computational simulation model to capture tumor growth in different types of cancer. Unlike all relevant and available technologies and systems, the proposed computational model will incorporate biochemical, biophysical and anatomical information on cells, tissues and organs to build a framework specifically for simulation of imaging processes in order to bridge the gap between modeling the micron level to milliliter level that can be observed and captured by current imaging technologies.

Jennifer Prescher, PhD, joined Dr. Christopher Contag's lab in 2006. Her research is focused on elucidating the molecular mechanisms of T cell homing and infiltration into tumor tissue. She is also interested in developing new tools to visualize the migration patterns of multiple immune cell types in vivo using in bioluminescence imaging.

Bryan Smith, PhD, joined Dr. Sanjiv Sam Gambhir's lab in 2006. His research interests involve monitoring and understanding the microscale behavior of various targeted and untargeted nanoparticles in real time in the tumors and vasculature of small living animals using intravital microscopy. This work is performed in order to accelerate the progression of nanoparticles into humans and to generate the data needed to optimize nanoparticle formulations to best target, image, and treat cancer.

Ted Chu, PhD, joined Dr. Calvin Kuo's lab in 2007. His research interests focus on developing cancer drug and siRNA delivery system in small animal tumor model and therapeutics for: 1. siRNA and drug delivery using carbon nanotube, antibody and RNA apatmers; 2. gene expression and regulation, biomarker identification for imaging.

Hua Fan-Minogue, MD, PhD, started her research in Dr. Sanjiv Sam Gambhir's lab in 2007. Her research currently focuses on developing optical imaging sensors for protein-protein interaction in vivo, which will not only provide a new way to monitor cell signaling in abnormal or tumor cells, but also for drug development for cancer therapy. She is also interested in stem cell imaging and early cancer detection using variety of imaging modalities.

Keith Hartman, PhD, joined Dr. Sanjiv Sam Gambhir's lab at the beginning of 2008. He in interested in applying his background as a materials chemist to the design of new molecularly-targeted nanomaterials for the imaging of cancer. He is also involved with the development of new medical imaging techniques, Raman imaging, and photoaccoustic tomography.

Benjamin Cosgrove, PhD, is interested in developing novel molecular imaging technologies to investigate stem cell signaling-phenotype relationships. These molecular imaging technologies will be employed to generate multivariate dynamic stem cell signaling-response data collected under a wide variety of microenvironmental stimuli, including tethered and soluble growth factors, in a multi-well three-dimensional hydrogel system, which will then be used to identify key intracellular signaling activities that govern specific stem cell differentation programs. This work will be conducted under the joint supervision of Drs. Sam Gambhir and Helen Blau.

Henry Haeberle, PhD, joined Dr. Christopher Contag's in September 2008. He is interested in developing molecular markers to better detect tumor margins in the central nervous system. I am particularly interested in developing fluorescent markers for the brain tumors medulloblastoma and glial blastoma.

Sharon Hori, PhD, Sharon Hori, PhD, began her appointment in September 2008. Her research interests include: 1) data-driven mechanistic biomodeling in relation to cancer and other diseases; 2) math modeling, parameter estimation and identifiability methods; 3) the development of imaging probes and optimization of their delivery to molecular targets via an integrative imaging/experimental and kinetic modeling approach. She is working with Dr. Sylvia Plevritis and Dr. Sanjiv Sam Gambhir.

NIH/NCI P50CA114747

In Vivo Cellular and Molecular Imaging - ICMIC P50

PI – Sam Gambhir, MD, PhD

Program Manager – Billie Robles, BS

Clinical Management of Cancer

The vision of the In Vivo Cellular and Molecular Imaging Center at Stanford (ICMIC@Stanford) is to bring together researchers from various disciplines to form synergistic teams that will make significant advances in the use of multimodality molecular imaging strategies for better linking pre-clinical models of cancer with the clinical management of cancer. The career development component of this P50 is designed to be as flexible as possible to attract highly qualified candidates with the passion and ability to make an impact on cancer research that will benefit patient care in terms of diagnosis, therapy, and monitoring. This overarching theme will guide the process of candidate selection and lead to successfully trained individuals who will be capable of leading their own independent research teams in the field of molecular imaging cancer research. As we enter the second year of the ICMIC@Stanford, we currently have four trainees in the program. Selected candidates attend various educational activities in the Molecular Imaging Program at Stanford (MIPS) and work to bridge activities between a minimum of two laboratories. The candidates invited to join the ICMIC@Stanford Program are expected to be well trained in basic science or in imaging science and to have the energy and drive to influence the growing field of molecular imaging cancer research. NIH/NCI P50CA114747 supports the P50 program.

P50 Program Trainees

ICMIC Fellow	Year Completed	Current Position	Current Institution	Primary Mentor
Frank Cochran, PhD	2008	Post Doctoral Fellow	Bioengineering, Stanford University	Jennifer Cochran, PhD
Mike Helms, PhD	2008	Post Doctoral Fellow	Pediatrics, Stanford University	Christopher Contag, PhD
Erhan Yenilmez, PhD	2007	Post Doctoral Scholar	Materials Science & Engineering, Stanford University	Nicholas Melosh, PhD
Sheen-Woo Lee, PhD	2005	Musculoskeletal Imaging Fellow	Asian Medical Center, Seoul, Korea	Sandip Biswal, MD

Lucas Center MR Systems Training and Support

1.5T, 3T (2), and 7T Whole Body Magnets

Anne Marie Sawyer, BS, RT (R)(MR)
Sandra Rodriguez, RT (R)(MR)
Armando Mendoza, RT (R)(MR)

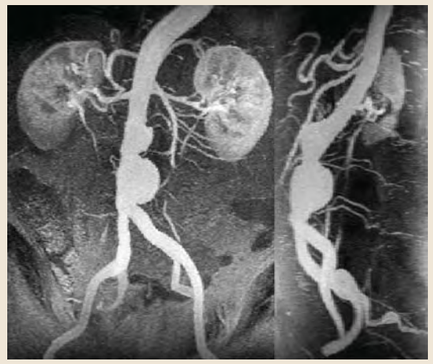

Figure 2. Two images from an MR 3D angiography examination demonstrate a bi-lobed aneurysm in the abdominal aorta. (Courtesy of A. Les, J. Yeung, P. Iyengar, C. Taylor and R. Dalman).

Safety training and system instruction have been provided to 137 new researchers conducting experimental MR studies at the Lucas Center over the last twelve months. Magnet safety training is provided twice a month and is an annual requirement for all researchers assisting or conducting studies on any of the magnet systems at the Lucas Center. A magnet safety refresher course was provided to 196 researchers this past spring. This ensures that all users and assistants are qualified to operate the systems and satisfies Lucas Center and University requirements for safety. System and safety support is provided to the researchers 7 days a week, 24 hours a day to ensure that research endeavors are successful, generate valuable data, and, above all, are safe for the researchers, the human subjects and the MR systems and components (Figures 1 and 2). Magnet safety is an on-going concern as the MR environment can be a potentially lethal setting without continuing education and support.

Safety Training

The research environment generates many new yet prototype designs in RF imaging coils, imaging accessories, monitoring and response devices such as button boxes, eye trackers, electroencephalogram (EEG) recorders, and sensory devices (Figure 3). Evaluation of these new devices is on-going to ensure that neither the image data, the safety of the human subject, nor the integrity of the MR system is compromised by the presence of these devices in the magnet room, in the bore of the magnet, or in the presence of an RF coil.

Figure 1. A subject is ready to be scanned at the 1.5T by Gilwoo Choi, MS (collaboration of Radiology, Mechanical Engineering and Vascular Surgery). The study includes imaging of the femoral arteries with a new MR-safe device that simulates weightbearing on a subjects lying in the supine position (B. Krasnow, Mag Design & Engineering, MagConcept.com).

Figure 3. Hooria Bittlingmayer, BA and Kelly Werner, PhD, from the Department of Psychology prepare a subject for a functional MRI of the brain at 3.0T using physiologic monitoring, button response boxes and video-projected images.


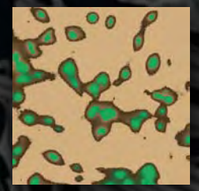
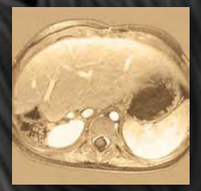
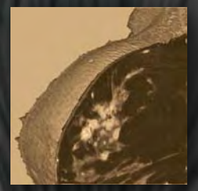
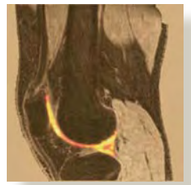
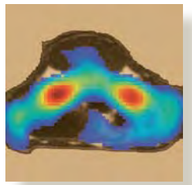
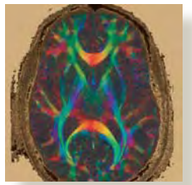


Research Group Updates

Research Group Updates

Advanced X-Ray Techniques

Inverse Geometry CT and Conventional CT

Norbert Pelc, ScD

left to right, back row: Jongduk Baek,, Adam Wang, Carolina Arboleda, Sam Mazin, and front row: Arun Ganguly and Norbert Pelc.

Work led by Dr. Pelc is in the technology and applications of computed tomography (CT). An important focus is aimed at understanding the basic limitations in current systems and, when physically possible, the development of solutions to effectively address these. One key motivating project in recent years is the development of an advanced CT platform that uses an inverted imaging geometry, and is therefore called inverse-geometry CT (IGCT). We are also working on a number of problems relevant to all CT configurations.

Our long-term aim is to push the limits in CT performance and to aid in the development of new applications. Our main current project is to develop a system that can image an arbitrarily thick section of anatomy (e.g. an entire organ) in a single fast rotation while producing uncompromised image quality and outstanding dose efficiency. The specific approach we are pursuing employs an inverse geometry (therefore the term IGCT), with one critical aspect being a distributed x-ray source whose length is comparable to the thickness of the section being imaged. The approach presents many opportunities, and we have already demonstrated excellent spatial resolution and complete freedom from cone beam artifacts (which can plague conventional systems when they try to image a thick region in a single scan). With funding from NIH and significant additional support from GE, we are collaborating with GE Global Research Center to build a gantry-based prototype. IGCT also presents a number of problems in the image reconstruction step. We report on two reconstruction algorithm advances that deliver improved image quality (Baek abstracts, page 75). In one, we take into account the possibly different statistics of rays measured along similar paths so as to minimize image noise. In the second, we optimally combine reconstructions from the multiple source rows in IGCT so as to obtain immunity from cone beam artifacts while efficiently using all the available ray path data.

Dose efficiency and image quality

In other projects, we studied the ability of energy selective CT to characterize tissues. We examined the ability of dual energy CT to separate iodine, bone and tissue (Arboleda abstract) and also the optimal way to process x-rays of different energies if photon counting energy discriminating detectors are available (Wang abstract, page 76). We always try to reduce the radiation dose to the patient necessary to obtain the needed diagnostic information. One technique being used in some clinical settings is the use “bismuth shields”, radiation absorbers placed on the surface of patients. We examined the degree to which these devices are an improvement over simple technique reductions.

Advanced X-Ray Techniques

X-Ray Guidance of Interventional Procedures

Rebecca Fahrig, PhD

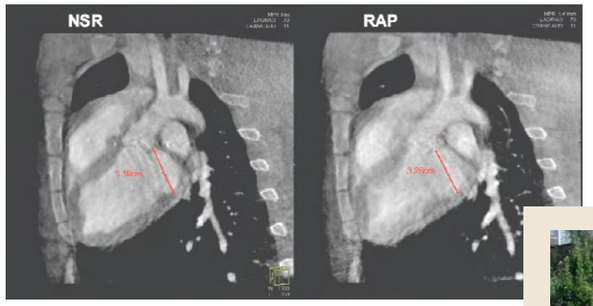

left to right: Jared Starman, Sungwon Yoon, Prasheel Lillaney, Marlys Lesene, Alessia Tognolini, Arun Ganguly and Rebecca Fahrig, and missing : Erin Girard-Hughes.

Our group continues to conduct research with the broad goal of improving the x-ray guidance of minimally invasive procedures. The Axiom Lab (C-arm CT system) is used for in vivo investigations and the Advanced X-Ray Imaging Lab for hardware and software development (table-top digital x-ray imaging, cone beam CT, and X-ray/MR system development).

Basic investigations into image quality improvement continue, including development of a new 1D approach to modulator-based scatter correction (Zhu abstract, page 70) and a forward bias technique to reduce the lag in amorphous silicon flat-panel detectors (Starman abstract, page 72).

The very high resolution of the C-arm CT system has been exploited in two studies. The first study used the C-arm system to acquire images of volunteers with stents in the superficial femoral artery. We have verified our analysis tools using custom-built jigs for conditions of pure extension and bending, demonstrating that stent deformation can be accurately quantified (Ganguly abstract, page 73) We have used the same capability to evaluate different bone healing techniques in a rabbit model (Ganguly abstract, page 73).

We have developed ECG-gated C-arm CT imaging to provide 3D images during cardiac procedures. We continue to evaluate image quality under different physiological conditions (Girard-Hughes abstract, page 73 and image above), and to develop new algorithms for image quality improvement. This technology has now moved from bench to bedside, with first clinical results reported at the American Heart Association meeting this year that demonstrate the advantages provided by gating. We have also shown that the location of the oesophagus can be tracked in the 3D images, which could have a significant impact on RF ablation for treatment of atrial fibrillation (Tognolini abstract, page 72).

Our NIH R01 grant for the development of a truly MR-compatible rotating anode x-ray tube was recently funded, and we have started to work on a modified motor design as well as electron optics for the x-ray tube (Lillaney abstract, page 71). This continues our development of a closed-bore X-ray/MR system with potential applications such as ‘one-stop’ stroke diagnosis and treatment.

Image Analysis, Bioinformatics, Computational Modeling

Paik Lab Research Group: Imaging Bioinformatics

David Paik, PhD

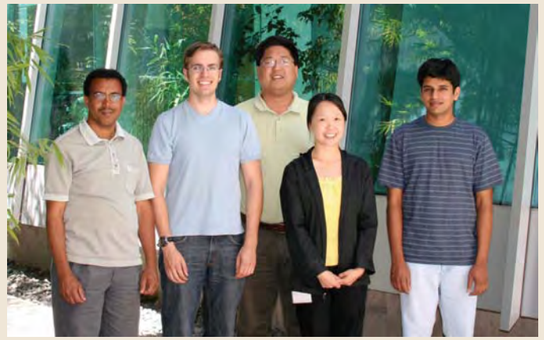

left to right: Frezghi Habte, Florian Schmitzberger, David Paik, Jill Lin, Kranthi Kode.

Our research group, led by Dr. Paik, is primarily interested in how biological information is extracted from both anatomic and molecular imaging, how it is represented, how it is modeled and how it is disseminated with an outlook toward how this imaging-derived information can be combined with other sources of biological and clinical information. The individual research projects span a gamut of application areas from extracting and encoding morphological features from chest CT to quantitation in molecular imaging to extracting and multiscale modeling of tumor growth kinetics in mouse models of cancer to computational methods to enable multiplexed analysis and imaging of tumors using nanoparticles to grid-based methods for distributed image interpretation trials to knowledgebases for cancer nanotechnology to novel statistical methods for evaluating imaging efficacy.

Our laboratory works closely with both the MIPS and RSL groups and is a member of the newly formed ISIS section. Currently, we run a quantitation and visualization core in the ICMIC@Stanford program as well as a bioinformatics core in the CCNE-TR program. We also work on dissemination efforts for Simbios, a National Center for Biomedical Computing as well as for the NCBC program as a whole. Dr. Paik also leads a national workgroup tasked with defining and driving forward the newly forming area of cancer nanotechnology informatics for the caBIG program at National Cancer Institute.

Quantitation and Visualization

Our long-term goal is to enable and simplify the problem of information extraction and information flow from medical/molecular imaging to be on par with that of genomic and proteomic profiling technologies so that these very different types of information may be treated as siblings computationally. Our philosophy is that for an integrative approach to imaging and non-imaging information to come to fruition, a major pre-requisite is to be able to maximally extract and represent information from imaging, with emphasis on the specificity of molecular imaging.

Image Analysis, Bioinformatics, Computational Modeling

Radiology 3D Laboratory

Sandy Napel, PhD; Christopher F. Beaulieu, MD, PhD; Dominik Fleischmann, MD; Justus Roos, MD; Geoffrey D. Rubin, PhD

left to right: Gennadiy Chuyeshov, Ushah Kiran Kommi Reddi, Bhargav Raman, Sandy Napel, Jessica Faruque, Johann Won, Markus Kukuk; Missing: Anthony Sherbondy, David Tran, Tejas Rakshe
Group Members who have left: Padmavathi Sundaram.

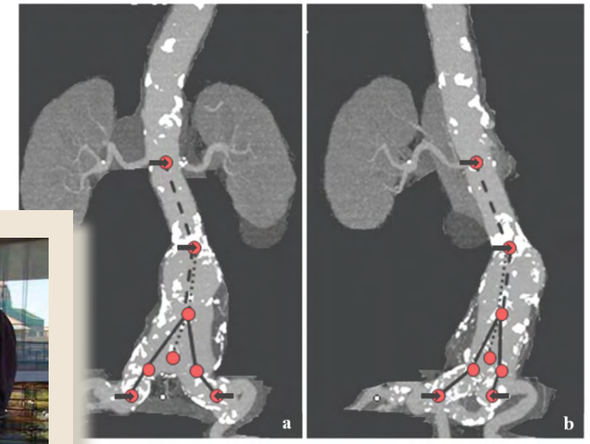

Our group addresses the field of image analysis, focusing on volumetric visualization, structure segmentation, quantitative analysis, and computer-aided detection of lesions. We see the future of radiology as benefiting from the continuously increasing "computations/dollar" in computing technology, as we continue to refine and evaluate these techniques and apply them and their derivatives to new areas. Advances here have impact in many technical and clinical areas. Examples are: automated visualization and quantitation of vascular image data (Raman and Won abstracts, pages 95, 97), virtual colonoscopy (Reddi abstract, page 99), intra-procedural registration of 2D fluoroscopic images of instruments with 3D volume data (Kukuk abstract, page 98), automated computation of peak flow velocity using a novel ultrasound transducer (Faruque abstract, page 96) for reproducible determinations of carotid stenosis, automatic generation of curved-planar images through blood vessels (Tran abstract, page 99), determination of likely neuronal connections of the visual tracts in the brain (Sherbondy abstract, page 98) for understanding human anatomy and patient-specific conditions. In addition, we have begun to develop new imaging informatics techniques (see ISIS Overview, page 12-13) to render human interpretation of radiological images amenable to biological discovery and future decision support (Rubin abstract, page 97). Our group is highly collaborative, working with many radiology department investigators (including Chris Beaulieu, Dominik Fleischmann, Rusty Hofmann, Brooke Jeffrey, Justus Roos, Geoff Rubin) as well as many other Stanford faculty (including Pierre Khuri-Yakub, electrical engineering; Brian Wandell, psychology). Based on our work, nine new manuscripts have been accepted for publication, and nine presentations were given at international meetings.

Image Analysis, Bioinformatics, Computational Modeling

Cancer Modeling Lab (CML)

Sylvia K. Plevritis, PhD

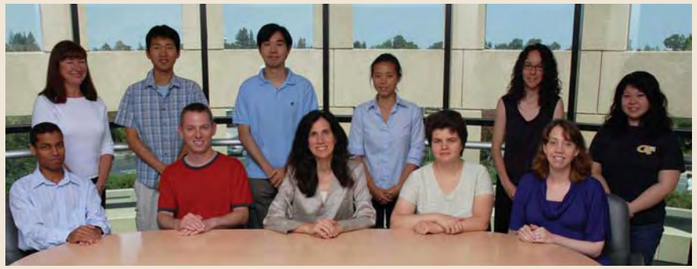

left to right, back row: Maggie Bos, Peng Qiu, Ray Lin, Emily Tsai, Stephanie Bailey, Linda Fong, and front row: Debashis Sahoo, Andrew Gentles, Sylvia Plevritis, Bronislava Sigal, Allison Kurian (missing Babak Shahbaba).

Our research program provides new insights into cancer early detection and treatment by integrating genomic, proteomic, pathological, imaging and patient outcomes data using novel mathematical and computational models. Our core research produces models of the natural history of cancer that describe the probabilistic behavior of tumor growth and metastatic spread. We apply these models to address important health policy questions, such as: what impact has screening mammography had on US breast cancer mortality; what impact has HRT had on the sensitivity of mammography and changes in US breast cancer incidence trends; what are expected outcomes for individuals at high risk for cancer who choose screening over prophylactic interventions; what impact could CT screening for lung cancer have on reducing lung cancer mortality and overall mortality. While these applied areas of our research are diverse they are fundamentally similar from a mathematical perspective, thus the breadth of our research demonstrates the power of modeling.

Novel mathematical and computational models

We also analyze cancer progression at the molecular level by developing and utilizing mathematical and computational models to understand how the "molecular circuitry"of cancer cells and their microenvironment are fundamentally different than that of normal cells. One of our major research goals is to analyze global gene and protein expression data to understand the transformation of lymphoma from low grade to high grade disease. Here we provide molecular biologists with molecular targets that may eradicate low grade disease before it progresses. We are also analyzing "–omics" data to identify markers predictive of the treatment response in prostate cancer. The goal of this work is to provide molecular biologists with novel markers for monitoring cancer patients. Both of these programs embrace a "systems biology approach" to the study of cancer biology by having computational researchers working side-by-side with biological experimentalists. We believe that computational models are a critical tool in developing a multi-scale understanding of cancer progression and ultimately will help to identify optimal approaches to eradicate the burden of cancer.

Magnetic Resonance Research

Body MR Imaging

Brian A. Hargreaves, PhD

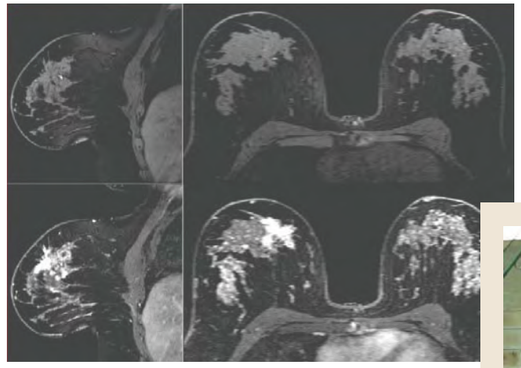

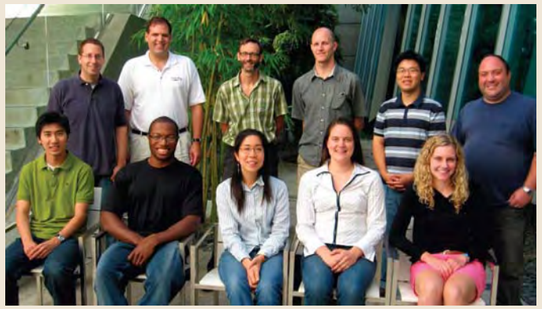

left to right back row: Neal Bangerter, Garry Gold, Marcus Alley, Brian Hargreaves, Seungbum Koo, Ernesto Staroswiecki, and front row: Ho Jin Kim, Anderson Nnewihe, Misung Han, Kristin Granlund, Caroline Jordan.

The body MR imaging group addresses applications of MRI to clinical body imaging. Our research includes abdominal imaging, musculoskeletal imaging, breast imaging, cardiovascular imaging, and collaborating with numerous clinical faculty, engineering faculty, and General Electric Healthcare.

Wenmiao Lu recently completed his PhD, and has continued to develop and characterize highly-efficient and robust methods to separate water and fat in MR images. This is of critical importance for breath-held scanning, where scan times currently limit the spatial resolution that can be achieved in 3D images. In addition, he has developed SEMAC, a robust method of MRI for patients with metallic implants. Misung Han has studied advanced parallel imaging techniques specifically tailored for bilateral breast MRI. These methods are now used in routine clinical care of over 1400 patients. Ernesto Staroswiecki continues to work on quantitative sodium MRI for applications including early detection of osteoarthritis and imaging of breast cancer in collaboration with Drs. Garry Gold and Bruce Daniel. Reduced sodium levels are an important indicator of cartilage degeneration, while elevated sodium levels correlate with malignancy. Kristin Granlund is working on robust fat/water separation for rapid breast MRI at 3T, as well as on non-contrast methods to assess perfusion. Anderson Nnewihe has built several new coils for sodium MRI, and is now concentrating on a high-density phased array coil for both rapid and high-resolution breast MRI on the new GE MRI scanners. Finally, Caroline Jordan has joined the group, modeling the susceptibility-induced off-resonance in particularly difficult extremities areas such as the ankle and breast. Research associate Seungbum Koo continues his work on automatic segmentation of cartilage for assessment of osteoarthritis. Marcus Alley continues to support a wide array of advanced clinical techniques for breast imaging, for dynamic contrast-enhanced MRI, for musculoskeletal MRI and many more. Kyung Sung will join the group in August as a post-doctoral fellow after completing his PhD at University of Southern California.

The body MR group continue to collaborate with numerous radiologists including Bruce Daniel, Bob Herfkens, Garry Gold, Shreyas Vasanawala, as well as researchers in radiation oncology, mechanical engineering, and electrical engineering.

Magnetic Resonance Research

Functional "Microvascular" Neuroimaging

Roland Bammer, PhD, and Michael Moseley, PhD

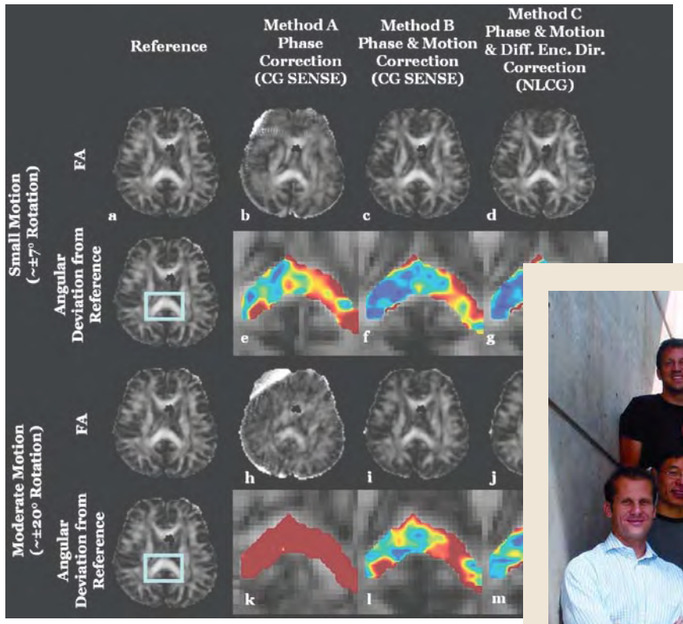

Left row (front to back), Roland Bammer, Chunlei Liu, Murat Aksoy, Daniel Kopeinigg, Matus Straka. Middle row (front to back), Samantha Holdsworth, Maximillian Haeberlin, Michael Moseley, Rexford Newbould. Right row (front to back), Lanzie Rivera, Heiko Schmiedeskamp, Jian Zhang, Stefan Skare.

State-of-the-art advances in magnetic resonance imaging (MRI) continue to improve adult and pediatric neuroimaging. Now, using functional MRI, dozens of times per day we routinely map and measure brain tissue water diffusion rates and direction, the perfusion of blood, and the brain's response to many functional activation tasks (such as vascular responses to mild reversible stresses) in a large number of diseases.

Over the past year, we have made significant progress in developing functional imaging technologies in several key areas. These included diffusion and perfusion techniques for the imaging of acute stroke and for the imaging of white matter structure and integrity. We are now funded to use the new 7 Tesla MRI whole-body scanner to improve higher-resolution tools of high-field and high-speed MRI. We focus on disease processes in "brain attacks" (cerebral stroke) in both adults and in children using diffusion MRI (DWI), tissue perfusion mapping (PWI), as well as the new field of mapping the brain connectivity, DTI. By responding to the needs of our collaborators and colleagues here at Stanford and worldwide, we have found that diffusion and perfusion techniques have significantly advanced far beyond the experimental arena into routine clinical applications in a wide variety of fields where they are being actively and effectively used in numerous individual and collaborative studies. The state-of-the-art in stroke MR imaging worldwide uses one of the sequences pioneered and developed here at Lucas.

Major strides have been made to improve research acquisition and reconstruction methods to our hospital systems with optimal performance to facilitate clinical studies. Moreover, considerable improvements in image quality have been achieved for DTI at 3T. In the next year, we are eager to move these methods from our scanners to those worldwide. With two clinical 3T MRIs now housed at Lucas and six being installed in our out-patient facilities, we will further advance our MR imaging tools and sharpen our focus on the critical clinical issues in the coming year with new experimental and clinical MR methods to predict eventual brain injury. We will detect diffuse abnormalities in the brain occult to conventional imaging, to further map how the brain and spine are "wired," understand the complex physiological stresses and changes that the brain experiences during ischemia and other pathologic processes, and extend these tools to better evaluate evolving therapies.

In addition to stroke, an intense focus has been made to reduce image blur and artifacts by developing real-time motion correction of MRI scans with a special focus on children. This prospective approach is a major paradigm shift and might help reduce the sedation needed while imaging children.

Over the last few years, a critical mass of highly qualified and remarkably creative researchers who are well sought-after in their respective fields has come together at the Lucas Center. Their unique expertise and industriousness have allowed them to design highly innovative methods that significantly strengthened the quality of both diffusion-weighted and perfusion-weighted MRI.

Pediatric and adult MR neuroimaging

Roland Bammer is an established faculty member at the Lucas Center, where he is being promoted to Associate Professor of Radiology and is the key imaging physicist for Pediatric Radiology. He has created collaborations with the Departments of Neurology and Pediatrics and has pioneered the active pediatric DTI program on the Lucile Packard Children's Hospital MRI scanner. Roland is an expert in parallel imaging with a special focus on applying this method to diffusion and perfusion imaging. He was a visiting professor at Bosporus University, Istanbul, Turkey, and he is also a university docent at the University of Graz, Austria. Roland has two funded peer- reviewed grants from the NIH. He directs multi-center trials, and has been named as "key personnel" on ten others. During the last year, Roland served as reviewer on several NIH study sections and is a full member on the editorial board of Magnetic Resonance in Medicine. Mike Moseley is a past president and Gold Medal winner of the International Society of Magnetic Resonance in Medicine (ISMRM) and last year he was elected a Lifetime Member of the Society of Magnetic Resonance Technologists (SMRT). Mike is a leading expert and pioneer of stroke imaging. He also sits on many NIH study sections and journal editorial boards.

The neuroimaging team remains involved in white matter tensor "fiber-tracking" neuroimaging projects as well as building collaborative programs. Jean-Marc Olivot continues to work with us as a Research Fellow. He is a stroke neurologist and is focusing on a comparative evaluation of Xenon-enhanced CT perfusion and MR perfusion. Jian Zhang is a fourth-year graduate student actively involved in 3D volume spiral imaging for diffusion applications. Chunlei Liu is a second- year Research Associate who has received a highly regarded K99/R00 award from the NIH on high-field-Tesla applications of DWI. Murat Aksoy is a fourth-year graduate student working with Roland on the exciting applications in fiber tractography and on motion correction projects. Rexford Newbould is a Research Associate with a background in IC design, and is currently involved in MR post-processing perfusion data and real-time motion correction with Roland. Lanzie Rivera is our administrative associate. Stefan Skare is a Research Associate and visiting scholar from Sweden focusing on multi-shot MR sequences for high-resolution diffusion in the presence of patient motion. Samantha Holdsworth, from New Zealand, is working on high-resolution diffusion sequences at 3T. Matus Straka, from the Vienna General Hospital (Austria) and the Computer Graphics Department of the University of Vienna, is focused on parallel computing issues for image reconstruction and quantitative parameter mapping. Heiko Schmiedeskamp, a graduate student from the ETH in Zurich, is a visiting researcher developing a promising new multi-echo sequence for functional MRI. Heiko was successfully admitted to the Stanford Bioengineering PhD Program and will stay for a couple more years in our lab. During the last year, Anders Nordell, from the Karolinska Institute in Stockholm, Sweden, has been working with us on selected topics of echo-planar imaging. Anders will continue working with us remotely as Stefan's graduate student in Stockholm. His clever work on EPI ghost correction led to significantly accelerated image reconstruction times. Daniel Kopeinigg is another visiting researcher who works with Roland, Marcus Alley, and Dominik Fleischmann on contrast-enhanced angiography with a special focus on improving contrast injection profiles to achieve desired enhancement profiles in the arterial system. Recently, visiting researcher Maximilian Haeberlin arrived from the ETH in Zurich. Max finished development of a reconstruction algorithm for highly undersampled MR data to improve temporal resolution.

Neuroimaging Functional Imaging – Technology Development

Gary Glover, PhD

The functional MRI group continues to develop and optimize methods for the acquisition of functional imaging data. Projects include the development of alternative fMRI contrast methods, real-time biofeedback for training brains, 3D fMRI acquisitions, and the calibration of fMRI using breath holding measurements. In addition, we continue to play an active role in the NCRR-funded FIRST BIRN schizophrenia test bed project, with Gary Glover as the chair of the calibration working group. The following are a few of the highlights; see abstracts for further details.

Graduate student Christine Law has concluded her development of spiral parallel imaging using a novel method of reconstruction in which the sensitivity maps are generated from every other, fully sampled acquisition. This provides a signal-to-noise ratio benefit by virtue of cross correlation between thermal noise in the sense maps and that in the reconstructed images. The work has been accepted for publication. She is writing her dissertation, which summarizes her extensive body of work in the use of spiral methods for fMRI.

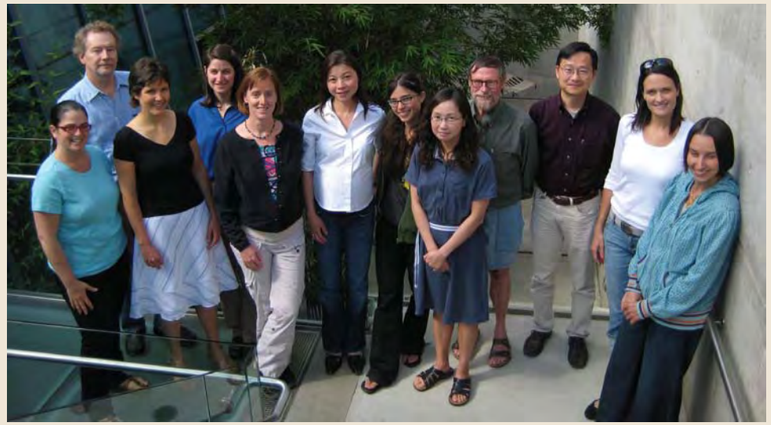

left to right: Rebecca Rakow-Penner, Paul Mazaika, Joelle Barral, Allyson Rosen, Laura Pisani, Fumiko Hoeft, Catie Chang, Christine Law, GHG, Jason Hsui, Moriah Thomason-Caires, Chardonnay Vance.

Jung Jiin (Jason) Hsu, a postdoctoral scholar, has developed a dynamic shimming method in which his local shim coils are adjusted separately for each slice. This allows much better optimization of field homogeneity in the frontal region. He has also been developing rapid methods of T1-based oximetry measurement in the CSF, working in conjunction with Greg Zaharchuk.

Chardonnay Vance has concluded her study of placental insufficiency using T1 relaxation times to characterize the stage of disease. Her results indicate that a simple scan procedure may be diagnostic and useful in treatment decisions. She is writing her dissertation and will be moving to U of Minnesota to continue her studies as a postdoc.

Graduate/MD student Rebecca Rakow-Penner, continues to develop functional methods to characterize breast cancer using Blood Oxygen Dependent contrast, induced by alternating periods of carbogen or hyperoxia and room air. She is also developing a liaison with a student at Hopkins who will bring near-infrared spectroscopy equipment to examine local oxygenation with this optical means concurrently with the fMRI scans.

Postdoc Moriah Thomason-Caires has published her work on functional connectivity in children undergoing executive processing (working memory) and has finished data collection for a study of depressed children with the COMT gene tic disposition. She has found that baseline cerebral blood flow is different in the two alleles, which may be an important marker.

Grad student Catherine (Catie) Chang has developed a new method to calibrate hemodynamic delays in the brain, which is very important in the study of resting state brain networks. She is also studying brain noise itself, and has developed a method to reduce the influence of physiological function (cardiac and respiration) in the fMRI signals.

Interventional and Open MRI

Kim Butts Pauly, PhD

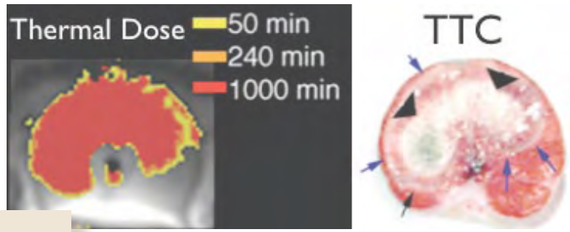

left to right, front row: Ron Watkins, Jing Chen, Elena Kay, Sonal Josan, Rachel Bitton, Kim Butts Pauly, and back row: Georgios Papadimitriou, Viola Rieke, Randy King, Andrew Holbrook, Will Grissom.

Our interventional and open MRI group is developing several MR-guided minimally invasive therapies in order to increase treatment options for prostate, breast, and liver cancers. This year, the iMRI group invcreased its effort in high intensity focused ultrasound, working with the InSightec ExAblate 2000 system installed on the 3T scanner.

BioE student Andrew Holbrook is working on the problem of MR thermometry in the liver, where respiratory motion can create artifacts that overwhelm the temperature measurement. Randy King, a BioE student who joined the group this year, started a small model liver tumor study for FUS ablation. In collaboration with Prof. Pierre Khuri-Yakub (EE Ultrasonics group), we continued the investigation of CMUTs (capacitive micromachined ultrasound transducers). Serena Wong, who received her Ph.D. in June, with Ron Watkins, found that CMUTs could, in fact, deliver the level of power needed for therapeutic applications. In addition, MRI temperature maps were acquired of a set of CMUTs heating a gel phantom. EE student Georgios Papadimitriou will now continue this work. Rachel Bitton, who joined our group as an NCI post-doc, started working on contrast agents for FUS. Research associate Viola Rieke worked with Annemarie Schmitz, a visiting physician from the Netherlands, and Prof. Bruce Daniel to investigate the use of HIFU in improving wire localization for breast tumors prior to surgery and found that this could be done in a reasonably short (~20 minute) timeframe. For non-thermal HIFU applications, EE student Jing Chen developed an improved method for MR monitoring of low duty cycle ultrasound through the MR imaging of the acoustic radiation force and optimized the gradient waveforms to minimize artifacts. In the area of MR-guided HIFU, Will Grissom, who joined the group as a post-doc from the University of Michigan, developed a new spatial spectral RF pulse that improves the quantitation of MR temperature in the presence of fat, without any loss of frame rate. Our group's other major project, MR monitoring of cryoablation of the prostate, continued with further developments in RF pulse design for ultrashort T2 quantitation by EE student Sonal Josan. Lena Kaye, also a student in EE, investigated the behavior of the proton resonance frequency shift as tissue freezes. We continued to collaborate with Prof. Chris Diederich from UCSF and Prof. Graham Sommer, in the area of MR-guided ultrasound ablation of the prostate and with Prof. Donna Bouley (Comparative Medicine) to investigate how MR images reflect the tissue changes over the initial few weeks after ablation. These contributions are only highlights from the work ongoing in the group, with more progress to be described next year.

Magnetic Resonance Research

Magnetic In Vivo Spectroscopy and Multinuclear Imaging

Daniel Spielman, PhD

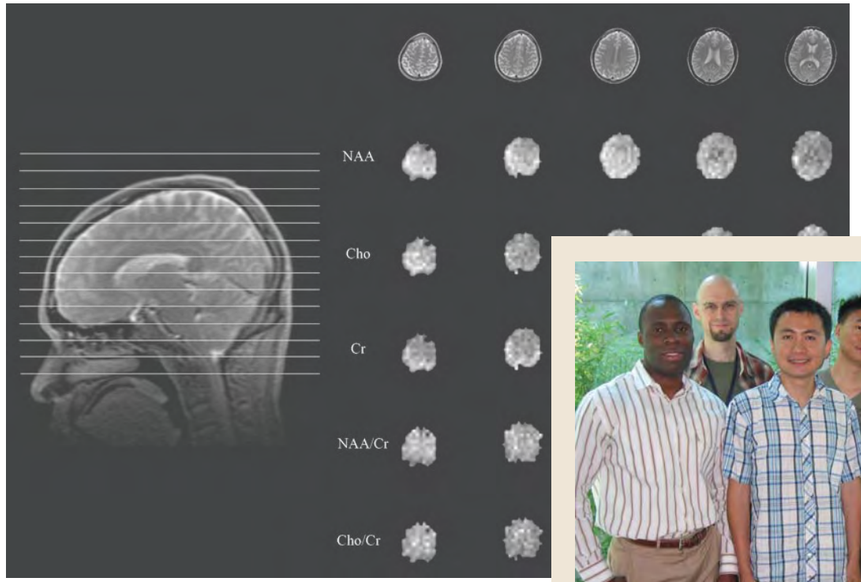

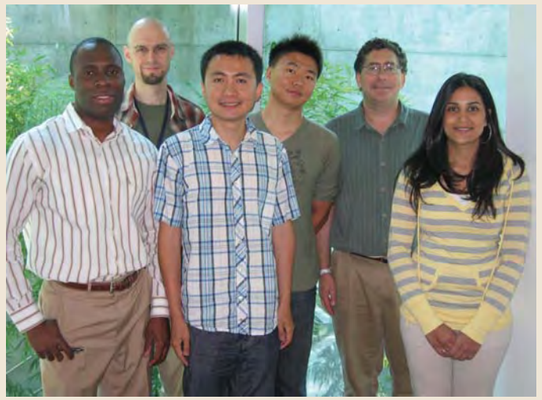

left to right: Moses Darpolor, Dirk Mayer, Calvin Lew, Meng Gu, Dan Spielman, Priti Balchandani.

The major thrust of our research in magnetic resonance spectroscopy (MRS) and spectroscopic imaging (MRSI) is focused along three distinct lines. Our work on the technical development of ultrahigh field (7T) proton spectroscopy of the brain continues from last year with an added emphasis on the design and evaluation of novel RF excitation pulses for addressing the magnetic field inhomogeneities encountered at 7T. We have an ongoing program in the development of volumetric 1H MRSI at 1.5 T and 3.0 T which is now funded through an NIBIB Bioengineering Partnership grant. Finally, our efforts in the area of hyperpolarized 13C MRS and MRSI continues to move forward at a rapid pace. Hyperpolarized 13C is an exciting new technology capable of directly probing key metabolic pathways by providing several orders of magnitude of increased signal than previously available. Over the past year we have successfully developed several fast MRSI protocols (temporal resolution = 375 ms/) and associated metabolic modeling tools, and are currently applying these techniques to the study of a number of pathologies including liver metabolic disorders, hepatocellular carcinoma, and pediatric arthritis.

Molecular Imaging

Cardiovascular Molecular Imaging Lab

Joseph Wu, MD, PhD

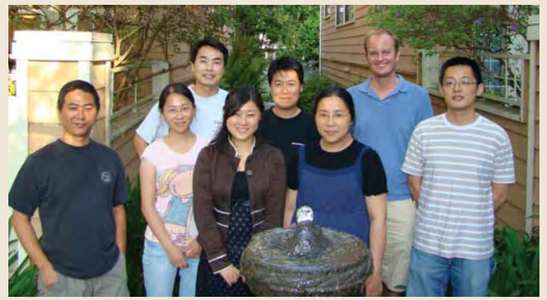

left to right: Fangjun Jia, Xiaoyan Xie, Joseph Wu, Jin Yu, Zongjin Li, Mei Huang, Kitch Wilson, Ning Sun.

Emerging molecular imaging techniques for clinical practice

Ischemic heart disease is the number one cause of morbidity and mortality in the United States. Repeated ischemic insults can lead to congestive heart failure, which is the leading cause of hospital admissions for people aged 65 years and over. With the advent of the human genome project, cardiovascular diseases will likely be targeted at the basic cellular and molecular levels. The cardiovascular molecular imaging lab is a multidisciplinary team that combines expertise in molecular and cell biology, cardiovascular physiology, and molecular imaging. To better understand stem cell biology in vivo, we use novel molecular markers that enable us to follow the fate of transplanted stem cells noninvasively. These include monitoring survival, proliferation, and differentiation as related to embryonic stem cells and bone marrow stem cells. The highly sensitive imaging devices we use include bioluminescence, fluorescence, positron emission tomography, and magnetic resonance scanners. We are actively engaged in studying the differentiation of human embryonic stem cells into endothelial and cardiac cells, which will have important applications for regenerative medicine applications in the future. Our lab also works on gene expression profiling of stem cell markers as well as optimizing cardiac gene therapy protocols. The eventual goal is to establish molecular imaging as a platform for translational research in cellular and gene therapies for ischemic heart disease in the 21st century.

Molecular Imaging

Cellular and Molecular Imaging Lab

Jianghong Rao, PhD

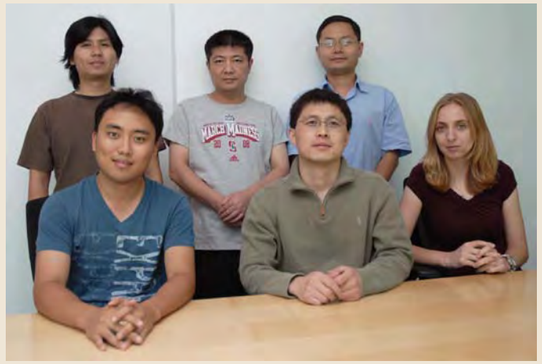

Sitting from left to right: Jungjoon Lee, JR, Anca Dragulescu-Andrasi
Standing from left to right: Zuyong Xia, Hongjun Ren, Gaolin Liang

The Rao lab works at the interface of biology and chemistry, combining synthetic and physical organic chemistry and molecular biology with imaging techniques, like fluorescence microscopy and whole-body fluorescence/bioluminescence imaging, to develop novel imaging probes and methods to image biology in living subjects. As part of the NCI-funded Center for Cancer Nanotechnology Excellence, we are developing nanosensors for the imaging and detection of tumor specific biomarkers with multiplexity and high sensitivity. The second area in which we are interested involves developing tools to visualize RNA localization through the use of RNA aptamers. Our understanding of RNA biology would greatly benefit from an imaging study of RNA in living subjects. We have successfully developed a ribozyme-mediated imaging system to enable the visualization of specific RNA in living cells and living animals. Last, we are interested in imaging infectious diseases in vivo. In collaborating with researchers at Texas A&M, we are currently working to develop probes to detect and image tuberculosis in vivo by targeting a bacterial enzyme beta-lactamase expressed by M. tuberculosis.

Molecular Imaging

Clinical Molecular Imaging Research

Andrew Quon, MD

left to right: Lindee Burton, Erik Mittra, Andrew Quon, Dana Peralta, (missing Maurice Zissen).

Our group is focused on applying emerging molecular imaging techniques into clinical practice. Recent projects have included the development of 3D volume rendered PET/CT acquisition and processing techniques for virtual colonography and bronchoscopy and the description of the importance of a truly integrated interpretation of PET and CT for bone metastases.

Currently, the group has been studying alternative PET radiotracers such as 18F-5FU (a radiolabelled form of the chemotherapy agent 5FU); 18F-NaF (a tracer specialized for bone imaging); and 18F-FLT (a cellular proliferation surrogate). Using these tracers, the goals of the group are to elucidate the effects of angiogenesis inhibitors on chemotherapy uptake in tumors; to evaluate PET/CT for imaging the skeleton in both oncological and non-oncological applications; and to evaluate the potential of 18F-FLT for evaluating GI malignancies.

Currently, the group is studying alternative PET radiotracers such as 18F-5FU (a radiolabelled form of the chemotherapy agent 5FU); 18F-NaF (a tracer specialized for bone imaging); and 18F-FLT (a cellular proliferation surrogate). Using these tracers, the goals of the group are to elucidate the effects of angiogenesis inhibitors on chemotherapy uptake in tumors; to evaluate PET/CT for imaging the skeleton in both oncological and non-oncological applications; and to evaluate the potential of 18F-FLT for evaluating GI malignancies. We have published our results of using18F-FLT in pancreatic cancer earlier this year.

Molecular Imaging

Molecular Imaging Instrumentation Laboratory (MIIL)

Craig Levin, PhD

left to right, back row: Guillem Pratx, Peter Olcott, Hao Peng, Yi Gu, Paul Reynolds, Arne Vandenbrouke, and front row: Jaeho Lee, Virginia Spanoudaki, Frances Lau, Craig Levin, Garry Chinn, Femi Olutade, Nahush Rao.

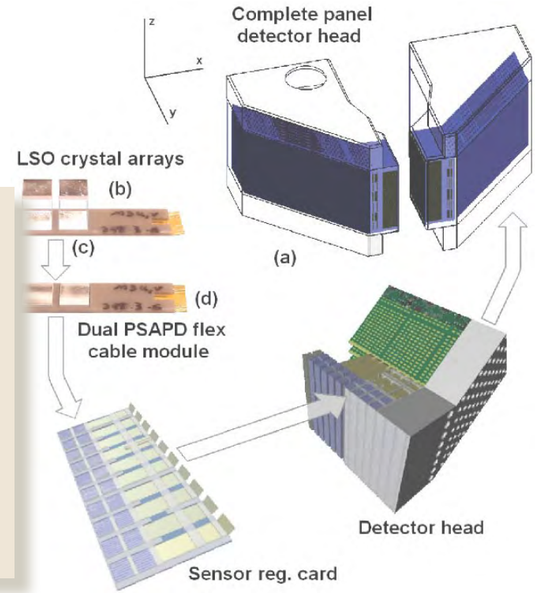

Our research interests are to advance instrumentation and algorithms for the non-invasive imaging of basic cellular and molecular signatures associated with disease. These new "cameras" image photon emissions from molecular probes designed to target specific molecular processes associated with disease in cells located deep within the tissues of living subjects. The technical goals of the instrumentation projects are to advance the photon detection efficiency and spatial, spectral, and temporal resolutions. The algorithmic goals are to understand the physical system comprising the subject tissues, photon transport, and camera, and to realize the best available reconstructed image quality and quantitative accuracy. The work involves the design, development, and testing of novel position sensitive photon sensors and systems; low-noise readout electronics; data acquisition electronics; computer modeling; computer graphics; tomographic image reconstruction algorithms; signal/image processing algorithms; and data/image analysis. Key goals of our research are to incorporate these innovations into practical imaging devices and introduce new in vivo imaging tools to advance studies of molecular mechanisms and aid discovery of novel treatments of disease in the clinic as well as in preclinical research. If successful, these novel system will substantially enhance the visualization and quantification of subtle molecular signatures associated with disease with the hope that molecular imaging can play a role in earlier disease management. The research is supported by grants from the National Cancer Institute, National Institute of Biomedical Imaging and Bioengineering, and GE Medical Systems. Fellowships are supported by Stanford's Bio-X Program and School of Medicine Deans Fellowship Program, the Society of Nuclear Medicine, and the Belgian-American Education Foundation.

Molecular Imaging of Musculoskeletal Illnesses

Sandip Biswal, MD

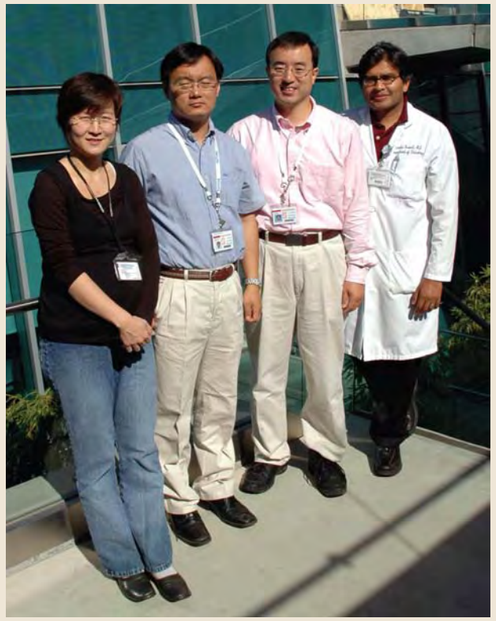

Sheen-Woo Lee, Tae Joo Joon, Sang Hoon Lee and Sandip Biswal. Not pictured are Deepak Behera, Harpreet Dhatt, Brian Kim, Vijay Rao and Bao Do

Dr. Sandip Biswal MD and members of the lab, Deepak Behera DNB, Harpreet Singh BS, Brian Kim MD, Bao Do MD and Shin Kamaya BS as well as recently departed Sheen-Woo Lee MD, Tae Joo Joon MD PhD, Sang Hoon Lee MD, and Andrew Tye, are interested in using mulitimodality molecular imaging techniques to study musculoskeletal inflammation and pain. Dr. Behera, Dr. Lee, Mr. Kamaya and Mr. Dhatt have employed manganese-enhanced magnetic resonance imaging (MEMRI) to study spinal cord activation in models of neuropathic and inflammatory pain using the now up-and-running 7.0T dedicated small animal MR in the Clark Center. They have also been studying the effects of analgesics on MEMRI patterns. Dr. Do, Dr. Kim, Mr. Dhatt and Mr. Tye continue to make significant inroads in understanding glucose metabolism in the human and animal spinal cord using 18F-FDG PET-CT. Furthermore, in addition to a number of MIPS research groups, our lab has formed productive collaborative relationships with Dr. David Yeoman's group focusing on pain research, Dr. Stuart Goodman's group studying prosthetic-induced osteolysis, and Dr. Blankenberg's group studying the role of Annexin V in pain. We are also fortunate to begin exciting new work to 'image pain' with Justin Dubois PhD, Associate Professor of Chemistry, by imaging voltage-gated sodium channels using a labeled saxitoxin. In the past year, we have been fortunate to present our work at a number of scientific meetings including RSNA, SNM, SBCT-MR and the Combined SMI/AMI Molecular Imaging meeting.

models of neuropathic and inflammatory pain

Molecular Imaging Probe Laboratory (MIPL)

Xiaoyuan (Shawn) Chen, PhD

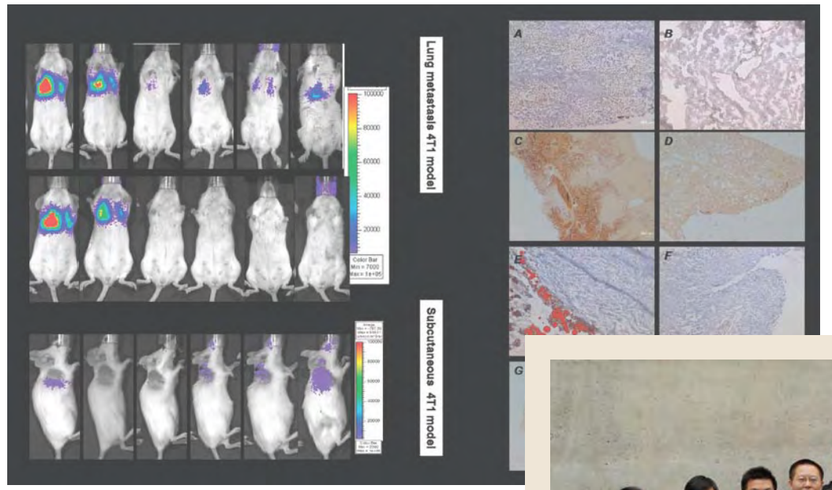

Front row (l-r): Xiaoyuan (Shawn) Chen, Qizhen Cao, Hui Wang, Dingtai Wei; mid row (l-r): Jinhua Wang, Yongjun Yan, Gang Niu, Zhaofei (Jeff) Liu, Kai Chen, Jin Xie; back row: Shuanglong (Scott) Liu

Shawn Chen's group is interested in developing and validating novel molecular imaging probes (nanoparticles, antibodies, proteins, peptides and small organic molecules) for the visualization and quantification of molecular targets that are aberrantly expressed during tumor growth, angiogenesis and metastasis. We are trying to combine both anatomical and molecular imaging techniques to pinpoint molecular and functional information related to tumor growth and dissemination, and monitor specific molecular therapeutic efficacy. We are currently working closely with two important angiogenesis targets: integrin alpha(v)beta(3) and vascular endothelial growth factor receptor subtype-2 (VEGFR-2). Integrins expressed on endothelial cells modulate cell migration and survival during angiogenesis. Integrins expressed on carcinoma cells potentiate metastasis by facilitating invasion and movement across blood vessels. In several malignancies, tumor expression of integrin alpha(v)beta(3) correlates well with tumor progression. VEGF is a key regulator of tumor angiogenesis and is the most potent endothelial cell mitogen. Binding of VEGF to its receptor on the endothelial cell membrane stimulates the VEGF signaling pathway. VEGFR-2 (KDR/Flk-1) is the primary VEGF receptor on endothelial cells. Specific projects include nanoplatform-based molecular imaging, multimodality imaging of angiogenesis and metastasis, as well as targeted delivery of gene, chemo, and radiotherapeutics.

Our research efforts are currently supported by NIH and DOD. Dr. Qizhen Cao received a 2-year postdoctoral fellowship from the Tobacco-Related Disease Research Program (TRDRP) to work on lung cancer imaging and therapy. Dr. Hui Wang won the First Place Award in the Molecular Imaging Abstract track for her abstract titled "Trafficking the fate of mesenchymal stem cells in vivo" from the SNM's Molecular Imaging Center of Excellence. Dr. Kai Chen was awarded 3rd place Young Professionals Committee (YPC) Best Basic Science Award for the 2008 Annual Convention of the Society of Nuclear Medicine. Visiting researcher Zhaofei (Jeff) Liu was awarded 2008 Society of Nuclear Medicine Berson-Yalow Award (1st place). Dr. Zibo Li was awarded Benedict Cassen Postdoctoral Fellowship from the Society of Nuclear Medicine. Numerous travel awards were also received by the Chen group to attend AMI/SMI and SNM annual conferences. Overall, we are proud to say that the year of 2008 has been very busy and productive.

Molecular Imaging

Multimodality Molecular Imaging Lab

Sanjiv Sam Gambhir, MD, PhD

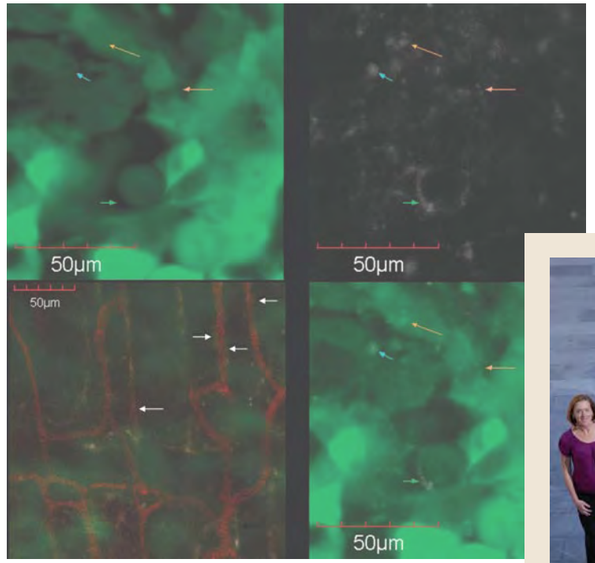

Front row: Laura Pisani, Anitha Junutula, Elizabeth Gill, Ataya Sathirachinda, Cristina Zavaleta, Gayatri Gowrishankar, Amelie Lutz, Sam Gambhir, Pritha Ray, Wei Xiong. Second row: Hua Fan-Minogue, Michelle James, Demir Akin, Shahriar Yaghoubi, Abhijit De, Paul Ramasamy, Sen Wang, Carsten Nielsen, Mohammad Namavari, David Yerushalmi. Last row: Bryan Smith, Keith Hartman, Robert Reeves, Adam de la Zerda, Bonnie King, Stephanie van de Ven, Carmel Chan, Natesh Parashurama, Ben Ahn, Bonita Crabbe, Andrew Forster.

molecular imaging for clinical applications

We are developing imaging assays to monitor fundamental cellular events in living subjects. We are actively investigating technologies such as micro-positron emission tomography (micro-PET); bioluminescence optical imaging with a charge coupled-device (CCD) camera; fluorescence optical imaging; micro-computerized axial tomography (microCAT); photoacoustics; and Raman spectroscopy in small animal models. Our goals are to marry fundamental advances in molecular/cell biology with those in biomedical imaging to advance the field of molecular imaging. We have a particular focus on cancer biology. We have developed several reporter genes/reporter probes compatible with all of the above imaging modalities. These reporter genes are being used in cell trafficking models, gene therapy models, as well as in transgenic models for studying cancer biology. Assays to interrogate cells for mRNA levels, cell surface antigens, protein-protein interactions, protein phosphorylation, and intramolecular folding are also under active development. We are also extending many of these approaches for human clinical applications. In particular we have done the first Raman Molecular Imaging studies in small living subjects this year while using surface enhanced Raman spectroscopy (SERS) nanoparticles as imaging agents.

Molecular Imaging

Proteomics, Biomarkers, and Nanoparticle Platforms for Imaging Therapeutics

Samira Guccione, PhD

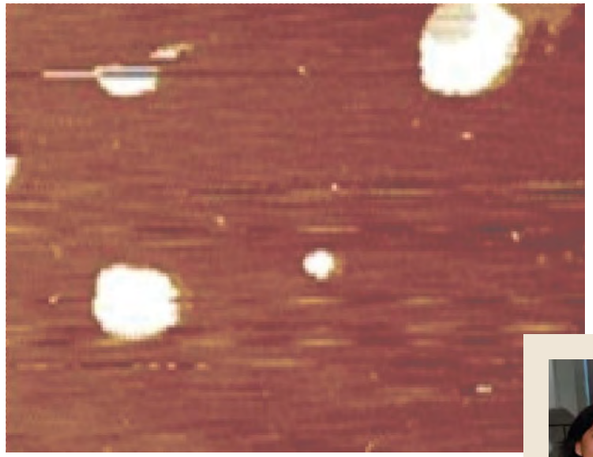

Yi-Shan Yang, Christopher Caires, Samira Guccione, Regina Bower, Steven Choi

The completion of the initial draft of the human genome and the rapid growth in high throughput assays, has opened a new era in translational research in medicine. The focus of our laboratory is translational research leading to agents for clinical use in detection, diagnosis, treatment, monitoring, and prognosis of clinical pathologies. We take a comprehensive approach in the design of agents that can span the "bench to bedside" timeline efficiently with our primary focus in development of novel agents for cancer. The research in our laboratory uses high throughput genomic and proteomic analysis on clinical pediatric and adult tissue samples to identify molecular targets. Ligands that bind these molecular targets are used to develop molecular imaging and therapeutic agents. We have developed a nanoparticle-based platform for attaching these ligands; thus creating targeted imaging and/or therapeutic agents. These targeted nanoparticles are first tested in vitro and used in in-vivo animal models, as molecular imaging probes. We have developed multimodality probes for MRI, gamma, fluorescent, and CT imaging. Visualization and quantitative evaluation of these targeted nanoparticles in vivo through molecular imaging, will provide information on the bio-distribution and accumulation of probes at the site of interest. Subsequently, we design therapeutic approaches including delivery of targeted chemo or radioactive agents, or non-viral-based genes for gene therapy. In specific, we have developed therapeutic and imaging agent targeting tumor vessels. In addition, we have successfully synthesized drug delivery agents controlled by external energy sources such as ultrasound. This is a powerful new approach that uses molecular imaging for identifying patients that will respond to treatment prior to choosing the best treatment regiment. We have successfully used this approach to image tumor vasculature in models of primary brain tumors, melanoma, and metastatic colon cancer to the liver and lung. A modified form of these nanoparticles was then successfully used for an antiangiogenic therapeutic approach to the tumor vasculature. We are currently performing toxicity studies as the preclinical requirement for clinical trials. Other research areas include tissue engineering applications in revascularization to enhance wound healing and vascularly compromised tissue; localized drug delivery systems; and biomarker development.


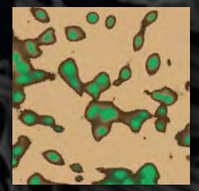
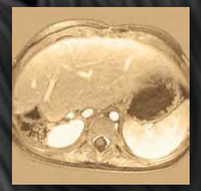
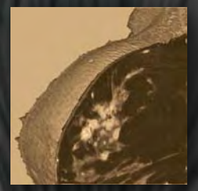
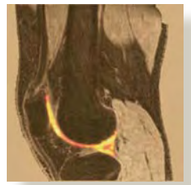
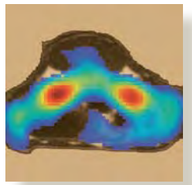
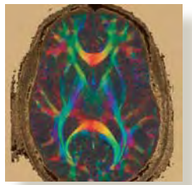


Facilities

Outpatient Imaging

Volney Van Dalsem, MD
Director
Susie Speilman
Director, Strategic Initiatives and Program Management

Growth in Outpatient Imaging

In June 2008, Stanford opened a state-of-the-art outpatient imaging center in Palo Alto on Sherman Avenue. Stanford Medicine Imaging Center (SMIC) was created to deliver an entirely new approach to medical imaging, offering patients access to the most advanced diagnostic imaging capabilities available, provided in a refined, private-practice like, "healing" environment. The 10,000-square foot space and serves as a combined clinical and research center and features the latest CT and MRI equipment, as well as the sub-specialty imaging expertise of Stanford radiologists.

Most imaging centers are designed to separate the patient from the professionals. We instead created a center where the physical layout promoted interaction between the patient, the radiologist and the technologist, under the premise that more communication results in better patient care. The design and exceptional service standards create a warm, private, and caring environment. We further included amenities such as individual rooms to enhance patient privacy, an on-site concierge, as well as a Stanford Health Library kiosk and patient education center.

The rapid advance of imaging technology (typically in 18 – 24 month cycles) requires frequent upgrading of equipment in order to stay at the forefront of clinical and research innovations. Such frequent upgrades are more easily facilitated in the outpatient setting. Stanford Medicine launched with the most advanced technology available with two state-of-the-art CT machines, and two next-generation 3T MRIs. We also have commitments from the Siemens and GE Healthcare in place to ensure the center will remain on the leading edge of the field through continual upgrades. In fact, one year from our opening, three of the four machines are scheduled to be replaced because newer technology will be available.

Equally important, community demand for imaging services continues to grow. Additional imaging capacity in close proximity to Stanford Hospital will relieve current scheduling backlogs, enable outreach to new patients in the community and offer another convenient location for individuals requiring outpatient imaging.

The center's commitment to staying ahead of the imaging technology curve makes the facility uniquely suited to a wide array of research activities, speeding the translation of research advances into clinical practice. The research performed in this center along with the efforts of the 200 researchers and scientists that are working every day at the Lucas Center will be translated directly to patient care. It's the software enhancements created by scientists in our laboratory that can have a markedly different and improved result on imaging studies. Many new MR methods developed by Stanford are not available on commercial scanners. However, we are able to takes these advances directly to SMIC and our other sites so patients can immediately benefit from our research. We implement this in many areas including breast cancer detection, stroke, and even new techniques in musculoskeletal imaging. Future advances and the availability of on-site blood testing capabilities will also draw healthy patients to the center for early diagnosis and treatment. The blood testing laboratory at SMIC will be an important tool for our new Center of Excellence in Early Cancer Detection as we work to link blood and imaging tests to predict the likelihood of disease.

A New Model of Patient Care

The new Palo Alto center marks the first phase in Stanford's development of new model for imaging service delivery, featuring patient-centric facilities, and a commitment to streamlined scheduling and faster report turnaround times. The Palo Alto center joins existing imaging facilities at Stanford Hospital, the Blake Wilbur Outpatient Center and Stanford Advanced Medicine Center. Together, these 4 locations, and a fifth center scheduled to open in February 2009 in Redwood City, will allow Stanford to greatly accelerate the delivery of imaging services, by doubling outpatient imaging capacity, and supporting Stanford's commitment to better serve our patients. The Stanford Medicine Outpatient Center (SMOC) in Redwood City includes two 3T MRI's and 1 CT with a focus on musculoskeletal and abdominal studies due to its adjacency to the new Orthopedics Clinic and Digestive Health Center which will be housed in these new buildings.

Stanford 3D medical imaging laboratory

Geoffrey Rubin, MD
Sandy Napel, PhD

Laura Pierce, MPA, RT (CT), Lab Manager

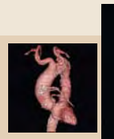

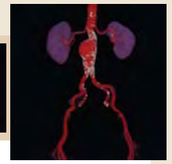

The Stanford 3D medical imaging laboratory is well into the second decade of service to the Stanford Medical community. The 3D laboratory continues to be guided by the mission of developing and applying innovative techniques for efficient analysis and display of medical imaging data through interdisciplinary collaboration. Our clinical goal is to deliver 3D imaging advances as rapidly as possible following validation to the Stanford and worldwide healthcare communities for the swift and accurate diagnosis and treatment of disease. Our educational goal is to disseminate knowledge and duplicate our 3D services at other institutions by providing training for local and international physicians and technologists in the latest developments in 3D imaging.

Progress

Clinical: Over the past year, the 3D laboratory has continued its operations simultaneously in two locations: the first floor of the Lucas Center as well as the third floor of the James H. Clark Center, a building dedicated to interdisciplinary science. Our average monthly 3D volume has increased to approximately 875 examinations, and we have processed over 57,000 examinations, for nearly every clinical department at the Stanford Medical Center, since our inception in 1996. The majority of our referrals come from vascular surgery, cardiothoracic surgery, gastroenterology, cardiology, urology, reconstructive surgery, orthopedics, and neurosurgery.

Education: The 3D lab is attended by a rotation of international visiting scholars, Stanford Radiology fellows, residents, and medical students who acquire skills in 3D interpretation as part of their medical training. Our 3D imaging technologists also train Stanford researchers from engineering and medical departments to acquire 3D images and data for research projects involving a variety of image types from an array of imaging devices, including video microscopy, electron microscopy, and multimodality small animal imagers. In response to the external demand for 3D post processing and management training, the 3D lab hosts visiting radiologists and technologists from other medical centers through our 3D clinical fellowship program. This past year, our visitors included teams from other major university medical centers, such as New York University, Cornell University, and University of Pennsylvania. These tertiary radiology departments are interested in duplicating our 3D workflow model at their institutions.

Infrastructure

3D imaging technologists include: Laura Pierce, 3D lab manager; senior 3D technologists Marc Sofilos and Linda Novello; Keshni Kumar; William Johnsen, and newly hired technologists Nancy Ware and Shannon Walters. Our technologists offer not only expertise in 3D imaging, but also experience in CT and MRI scanning techniques as well. We also employ administrative assistants Lakeesha Winston and Debra Frank, and a database administrator, Kala Raman. The research arm of the lab retains an annual average of 12 engineering graduate students and postdoctoral scholars as well as 2 clinical MD researchers. Both 3D lab locations include a central area table that invites professional collaboration and student desks and carrels for independent research. The lab encompasses a total of 13 advanced 3D workstations for processing clinical cases and for research and development. We also have three servers, which provide remote 3D rendering to the Stanford medical community, and two research and development servers for image and data storage. Two remote PACS workstations allow access to all Stanford medical imaging and reporting. The lab also houses a variety of PCs and printers for software development and support.

We continue our excellent relationships with corporate developers of 3D workstations (e.g., GE Healthcare, TeraRecon, and Vital Images) who place their hardware and software in the 3D lab in anticipation of our feedback. These relationships ensure that we maintain the most advanced multi-dimensional analytical technologies available. Future clinical applications under investigation include automatic pre-processing and pre-loading of patient examinations to improve efficiency; predefined workflow templates; automatic export of quantitative data to patient reports; and improvements to graphical user interfaces for simplicity and ease of use of clinical 3D software.

To facilitate the bridge between innovation and other clinical use of technology, we serve as an imaging core lab for medical device developers. These companies use our expertise to evaluate their current and future products in anticipation of FDA approval. Present industrial projects include the evaluation of data from pulmonary vein ablation procedures (to treat atrial fibrillation), as well as thoracic stent-graft deployment (for the treatment of thoracic aortic aneurysms).

Conclusion

The 3D Medical Imaging Lab continues to function as an international leader in clinical care, teaching, and research in medical imaging analysis. The confluence of talented, medical and engineering expertise as well as the most up-to-date equipment has been a consistent source of innovative developments in diagnostic and treatment planning approaches.

Developing & Managing Research Models for Medical Imaging

Wendy Baumgardner, RVT, LATg

Pam Hertz, RVT

Wendy Baumgardner and Pam Hertz demonstrate a uniquely designed transport cart supported with inhalant anesthesia and ventilation capabilities.

Research studies involving animal models at The Richard M. Lucas Center enhance both overall healthcare and diagnostic imaging. In our continuing efforts to provide support to the Radiology investigators, we are entrusted with the responsibility of overseeing all animal model protocols within our Department and all other Stanford departments conducting research at our center and satellite facilities. Two experienced California licensed veterinary nurses (RVTs) attend all animal model studies where diligent care is taken during all procedures. Animals are treated with great respect, compassion, and professional care. Deviation from the protocols is not permitted. All personnel working with animals under approved Institutional Animal Care and Use Committee (IACUC) protocols have attended "required" seminars from the University's Department of Comparative Medicine. Specifically tailored, one-on-one training is available for more advanced techniques. In addition, we ensure compliance to all government and university regulations and policies.

Committed to Quality Care

We realize that living subjects are needed to advance our knowledge, and commit to the proper respect for life in this quest. Work at the center develops and improves new invasive and non-invasive procedures that use magnetic resonance imaging, x-ray fluoroscopy, focused ultrasound, and computed x-ray tomography to guide them. Research studies currently involve the study of infarct modeling, stroke, liver and prostate cancers, neuroimaging of the brain, and stent/graft implantation. Research is enhanced by the ability to keep pace with the latest application of medical equipment and continuing education through conferences and seminars. The techniques currently being explored at the center all contribute to more efficient and effective medical treatment for illness and disease in both humans (adults and children) and animals. We look to the future with hope that through quality biomedical research the necessity for animal use will decrease with the increased use of computerized models or other non-living systems. With this in mind, we realize the privilege we are granted and strive for continued excellence in all research taking place within the Richard M. Lucas Center and the Department of Radiology.

Small Animal Imaging Center – SCi3

Tim Doyle, PhD

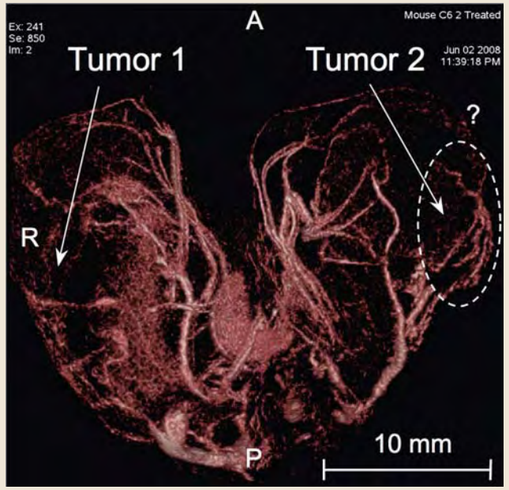

Mouse lower extremity vasculature with implanted C6 tumors treated with the anti-angiogenesis drug Avastin (Gambhir laboratory collaboration with Lars Wigstrom, GEHC).

2008 is the fifth year the small animal imaging facility has been in its present location in the basement of the Clark Center, and the third year of being a full university core facility, overseen by the Department of Pediatrics, with grant support from the Department of Radiology (ICMIC P50), the Stanford Cancer Center, and the Digestive Disease Core. We were able to bring the last major instrument online in the core with the new Varian/GEHC small animal 7 Tesla MRI system. The high field small bore MRI system became fully operational at the end of 2007 and, after a few teething problems, is now a major workhorse in the facility. November also saw the third year of the Small Animal Imaging Workshop, an opportunity for the MIPS program to educate the community on the power of small animal imaging, as well as providing hands-on demonstrations of each of the modalities in the core.

Mouse embryos at 15 days of gestation to study bacterial infections by Listeria monocytogenes that causes abortion and stillbirth (for Contag laboratory, Pediatrics.)

This year saw a "change of the guard" in the Small Animal Imaging Facility, with Dr. Shay Keren leaving. Dr Keren was a postdoc in Sam Gambhir's lab, in addition to overseeing the MicroPET and fluorescent imaging modalities in the imaging core. In addition to his tremendous efforts in the imaging facility, he was able to conduct some amazing research in Dr Gambhir's lab, and has now set up his own laboratory back in his native Israel. Dr Laura Pisani, a former post-doctoral fellow from Gary Glover's laboratory, has since been hired as a full-time staff member, and has taken over his responsibilities, as well as bringing the new MRI up to speed. Working closely with Varian, GEHC and Resonance Research Inc., Dr. Pisani has systematically identified hardware problems following installation and rectified them, and is now helping many groups here at Stanford to expand their pre-clinical research to utilize the newly available MRI scanner. Also joining the SCi3 team is Dr. Frezghi Habte, who with Dr David Paik will provide image quantification support for all of the users of the imaging facility. The Scientific Director of the facility, Dr. Tim Doyle, continues at the core's helm, working closely with faculty and students to provide access to one of the premier imaging facilities in the USA.

Cyclotron Suite Update

Frederick Chin, PhD

David Dick, PhD

Every year the Radiochemistry Facility develops and offers new radiotracers for both animal and human imaging in order to better understand, diagnose and stage disease. There are currently more than a dozen radiochemists including faculty, staff, and postdocs that use the facility on a routine basis and this number is expected to grow as we move into next year. In the past 12 months, a three-reactor automated radiosynthesis module, single-mode microwave apparatus, and multiple-plate radioactive thin layer chromatography scanner were installed to meet the increasing needs of our radiochemists to synthesize and analyze their new compounds. In addition, our efforts to foster new collaborative research with pharma and other groups have allowed us to acquire additional equipment including two more High Pressure Liquid Chromatography Pumps and another TRACERlab FX-FE module (Installation: September 2008) and use these equipment for our new projects.

Our staff continues to provide routine clinical tracers for use at the Stanford Hospital. Fluorine-18 labeled fluorodeoxyglucose (FDG) is still produced daily by the MX-FDG module and will soon be made with our new GE FASTlab module that was recently installed. Nitrogen-13 ammonia, used to assess myocardial perfusion, and Fluorine-18 sodium fluoride, used to image bones and joints, are also synthesized as needed by the clinic.

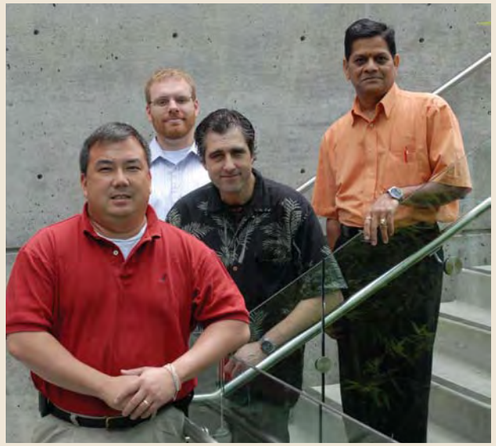

Frederick Chin, David Dick, Andrew Lamb, Murugesan Subbarayan

GE TRACERlab modules (FX-FN#1, FX-FN#2, FX-FE, FX-C Pro) are the workhorses in the lab and primarily carry out the syntheses of our ^{18}F and ^{11}C-labeled radiotracers and labeling agents for Stanford and other collaborative researchers including pharma. In addition, the final installation of the TRACERlab FX-C Pro and FX-FE modules have enabled us to perform new C-11 and electrophilic F-18 radiochemistries at Stanford and provide [^{11}C]PIB (imaging Alzheimer's Disease) and [^{18}F]Fluorouracil (monitoring chemotherapy treatment and efficacy) respectively for upcoming human studies. In the near future additional PET radiotracers that study the mechanisms and treatment of cancer as well as neurological disorders will become available to meet the increasing needs for performing preclinical (i.e. [^{11}C]Raclopride, [^{18}F]SPA-RQ) and clinical (i.e. [^{18}F]MISO, [^{18}F]EF-5, [^{18}F]Avid/Bayer compounds) research studies with PET.

Table summarizes an updated list of radiolabeled compounds that are made in the research radiochemistry lab excluding other research compounds protected under current confidentiality agreements.

Radiolabeled Compounds

Tracer	Use	Application
[^{11}C]NMSP	Imaging dopamine-2 receptors (D2R)	Monitoring D2R-related neurological disorders
[^{11}C]PIB	Imaging αβ amyloid in brain	Monitoring progression of Alzheimer disease in brain
[^{18}F]fluoroalkyne	Labeling agent used with "Click Chemistry"	Novel method for radiolabeling peptides
[^{18}F]Fluoro-BG-137	Imaging δ-opioid receptor	Imaging the process of chronic pain
[^{18}F] FAZA	Hypoxia imaging agent	Evaluating clinical-relevant hypoxia-directed cancer therapies
[^{18}F]MISO	Hypoxia imaging agent	Evaluating clinical-relevant hypoxia-directed cancer therapies
[^{18}F]EF-5	Hypoxia imaging agent	Evaluating clinical-relevant hypoxia-directed cancer therapies
[^{18}F]fluorobenzaldehyde	Prosthetic labeling group	1) Radiolabeling peptides for potential clinical use 2) Radiolabeled affibody for imaging of NER2neu
[^{18}F]fluorobenzoic acid	Prosthetic labeling group	Radiolabeling peptides for potential clinical use
[^{18}F]Fluoropropionic Acid	Prosthetic labeling group	Radiolabeling peptides for potential clinical use
[^{18}F]SFB	Prosthetic labeling group	Radiolabeling peptides for clinical use
[^{18}F]FDF	Imaging fructose metabolism and pentose pathway	Imaging fructose metabolism and the pentose pathway
[^{18}F]FEAU	Imaging substrates expressing mutant HSV1-sr39tk	1) Monitoring gene therapies targeting cancer 2) Monitoring cell therapies
[^{18}F]FHBG	Imaging agent for tumors expressing HSV1-tk	Monitoring various cancer therapies
[^{18}F]FLT	Imaging agent for tumor cell proliferation	Monitoring various cancer therapies
^{18}F-labeled RGD peptides	$\alpha_v\beta_3$ integrin imaging agent	Imaging tumor integrin expression

Lucas Center MR Systems

1.5T, 3.0T (2), and 7.0T Whole Body Magnets

Anne Marie Sawyer, BS, RT (R)(MR)
Sandra Rodriguez, RT (R)(MR)
Armando Mendoza, RT (R)(MR)

The 1.5 Tesla (Figure 1), 3.0 Tesla and 7.0 Tesla (Figure 2) G.E. Healthcare MR systems are currently operating at 12.0 M5 systems revision and a maximum slew rate of 150 milliTesla per meter per second and maximum gradient amplitudes of 50 milliTesla per meter (1.5T) and 40 milliTesla per meter (3.0T and 7.0T). The hardware currently allows the use of 8-channel phased array coils at 1.5T and 16-channel phased array coils at 3.0T and 7.0T.

Image 1. Sandra Rodriguez, MR Research Technologist and researchers Chunlei Liu, PhD and Wouter Veldhuis, MD, PhD, (left to right) at the 1.5T MR system, prepare a subject for an MR research examination of the breasts.

A second 3.0 Tesla MR system was recently installed at the Lucas Center (Figures 3 and 4). It is the first 20.x short bore 3.0T 750 (DVMR) system from G.E. Healthcare to be installed worldwide.

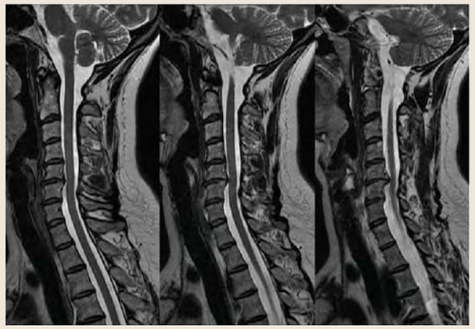

Image 4. Sagittal FRFSE-XL T2-weighted images acquired at the second 3.0T MR system at the Lucas Center.

Image 3. Sandra Rodriguez, MR Technologist, prepares a subject for a contrast-enhanced research MR examination of the hand at the second 3.0T system at the Lucas Center.

Daily support in MR system operation and screening and safety is provided to all researchers including faculty, post-doctoral fellows, graduate students, and visiting scholars in the Lucas Center and Department of Radiology; researchers from other University departments such as Psychology, Psychiatry, Neurology, Neurosurgery, and Nephrology; and service center users from outside of the University.

Image 2. Lucas Center faculty including (center to right) Roland Bammer, PhD, Mike Moseley, PhD, and Dan Spielman, PhD, collaborate with Atsushi Takahashi, PhD (left), from GE Healthcare in research studies being conducted at the 7.0T whole body MR system.


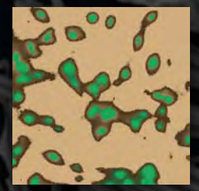
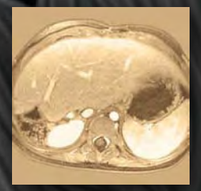
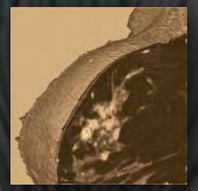
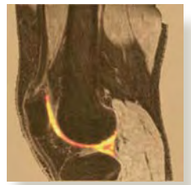
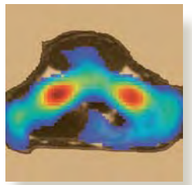
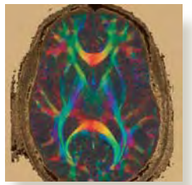


Abstracts

Advanced X-Ray Techniques

Scatter Correction for X-ray Conebeam CT Using One-dimensional Primary Modulation

L. Zhu[1,2], N. R. Bennett[1], R. Fahrig[1]
Departments of [1]Radiology, [2]Radiation Oncology

Recently, we developed an efficient scatter correction method for x-ray imaging using primary modulation. A two-dimensional (2D) primary modulator with spatially variant attenuating materials is inserted between the x-ray source and the object to separate primary and scatter signals in the Fourier domain. Due to the high modulation frequency in both directions, the 2D primary modulator has a strong scatter correction capability for objects with arbitrary geometries. However, signal processing on the modulated projection data requires knowledge of the modulator position and attenuation. In practical systems, mainly due to system gantry vibration and the ramp-filtering in the reconstruction, the insertion of the 2D primary modulator results in artifacts such as rings in the CT images if no post-processing is applied. In this work, we eliminate the source of artifacts in the primary modulation method by using a one-dimensional (1D) modulator. The modulator is aligned parallel to the ramp-filtering direction to avoid error magnification, while sufficient primary modulation is still achieved for scatter correction on a quasi-cylindrical object, such as a human body. The scatter correction algorithm is also greatly simplified for the convenience and stability in practical implementations. The method is evaluated on a clinical CBCT system using the Catphanc600 phantom. The result shows effective scatter suppression without introducing additional artifacts. In the selected region of interests, the reconstruction error is reduced from 187.2HU to 10.0HU if the proposed method is used.

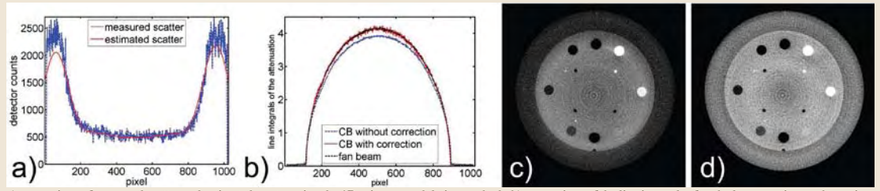

a) comparison of measured scatter and estimated scatter using the 1D primary modulation method; b) comparison of the line integrals after the log operation on the projection; c) reconstructed image of the Catphan phantom without scatter correction; d) reconstructed image of the Catphan phantom with scatter corrected using the proposed method.

References/Funding Source

NIH R21 EB008186
The Lucas Foundation

C-Arm CT Visualization of the Esophagus During Atrial Radio-Frequency (RF) Ablation

A. Tognolini[1], A. Al-Ahmad[2], E. Girard-Huges[1], T. Moore[3], R. Fahrig[1]
[1]Department of Radiology, [2]Cardiac Arrhytmia Service, [3]Siemens AG, Healthcare Sector, Forcheim, Germany

Purpose: During RF ablation of ectopic foci of atrial fibrillation, the esophagus may be at risk of thermal injuries. The purpose of this study was to test the feasibility, in comparison to a 64 MDCT system, of using C-arm CT without administration of oral contrast to visualize the esophagus and its relationship to left atrium (LA) and ostia of the pulmonary veins (PV).

Material and methods: Sixteen subjects underwent cardiac CT and C-arm CT imaging: 8 subjects were previously treated by RF ablation but volunteered to undergo imaging, the other 8 subjects were scheduled for RF-ablation. CT scans were obtained on a 64-slice MDCT (SOMATOM Sensation 64, Siemens AG, Healthcare Sector) using a CT left atrium ECG-gated protocol (120 KV, 250-350 mA, 1-1.5 reconstructed slices). C-arm CT scans were obtained on a C-arm system (AXIOM Artis dTA, Siemens AG, Healthcare Sector) modified to allow acquisition of four×4sec bi-directional sweeps with ECG gating in 13 patients, and non-gated in 3 (125 Kv/ 250-380 mA, 1-2 mm. reconstructed slices). All C-arm and CT scan were analyzed in a random order and findings were then compared (Fig.1) for the following criteria: a) esophagus visualization (yes/ no), b) esophagus relationship to the 4 PVs, c) direct contact/ absence of a fat pad between the esophagus and PVs antra/LA.

Axial planes obtained at the level of the ostium of the left inferior pulmonary vein of the same subject show esophagus (red arrow) on both C-arm CT (left side of the picture) and CT scan (right side).

Results:a) The esophagus was identified in all C-arm CT and CT scans. In 4 cases, orthogonal planes were needed on C-arm CT (inferior PVs level), b) in 7 patients (14/64 PV ostia examined), esophagus location on C-arm CT was different from CT, c) direct contact was reported in 19/64 (30%) segments examined on CT vs. 26/64 (41%) on C-arm CT. In 8% (5/64 segments), the C-arm CT images over-estimated a direct contact.

Conclusion: C-arm CT provides adequate images for esophagus visualization during RF atrial ablation.

References/Funding Source

Siemens Healthcare
AX
Forchheim Germany
The Lucas Foundation

Analysis of Lung Nodule Detectability and Anatomical Background Noise in Tomosynthesis Imaging of the Chest

S. Yoon[1], J. Siewerdsen[2], R. Fahrig[1]
[1]Department of Radiology, [2]Ontario Cancer Institute, Prince Margaret Hospital, Canada

Tomosynthesis is an imaging technique that is experiencing renewed interest with recent advancements of flat-panel digital detectors. Because of the wide range of potential applications, a systematic analysis of 3D tomosynthesis imaging systems would contribute to the understanding and development. We are carrying out a systematic evaluation of tomosynthetic imaging performance as a function of acquisition parameters, such as the number of projections, tomosynthesis orbital extent, and reconstruction filters in thoracic imaging. We evaluate lung nodule detectability as a function of tomosynthesis orbital extent (TOE) using anthropomorphic phantoms and a table-top acquisition system. Visual comparisons of different tomosynthesis reconstructions of 2 lung nodules show the progressive increase of anatomical clutter from off-focal planes into the reconstruction as the TOE decreases. Reconstructions for one of the nodules is shown in the figure (left). ROIs inside the nodule and the background region around the nodule were used to compute the signal difference to noise ratio (SDNR) values in order to quantify the anatomical clutter increase as the TOE decreases. As shown in the figure (right), SDNR for orbital extent greater than 50 degrees increased linearly with orbital extent. On the other hand, SDNR values for orbital extent smaller than 50 degrees varied less, suggesting strategies for identifying optimal orbital extent. Further evaluation in terms of anatomical background NPS, generalized NEQ, detectability index, and human observer performance will be used to validate and elucidate the dependence of image quality on TOE.

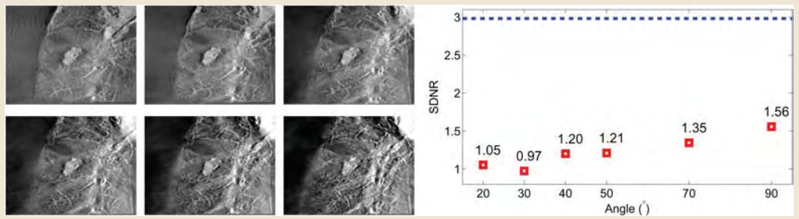

Effect of orbital extent on anatomical background noise and SDNR. Left: Tomosynthesis reconstructions of a nodule for progressively decreasing TOE (90, 70, 50, 40, 30, and 20 degrees, from left to right, top to bottom). Right: Nodule SDNR measured as a function of TOE (dotted line indicate the SDNR for the full-view reconstruction).

References/Funding Source

S. Yoon, J. Siewerdsen, D. Tward, S. Richard, R. Fahrig, Analysis of Lung Nodule Detectability and Anatomical Background Noise in Tomosynthesis Imaging of the Chest, submitted to SPIE Medical Imaging 2009.
NIH R01 CA112163
The Lucas Foundation

Optimized Focal Spot Control in MR-compatible X-Ray Tubes

P. Lillaney[1,2], R. Fahrig[1]
Departments of [1]Radiology, [2]Bioengineering

One of the major challenges in the development of hybrid X-Ray/MRI imaging systems is the close proximity of the x-ray source to the MR bore. As a result the MR fringe field can affect the electron optics of the x-ray source causing focal spot defocusing and deflection leading to degradation in image quality. One solution to this problem is to use small corrective Helmholtz coil pairs placed around the x-ray tube in order to locally cancel the MR fringe field in the region between the anode and cathode. When trying to correct for fringe fields on the order of 0.1 T problems arise with power consumption and corrective field homogeneity of the Helmholtz coil pairs. In order to optimize the position and sizes of the correction coils a linear programming (LP) framework for homogeneous magnet design [1] is used. The LP optimization procedure minimizes the power consumed by the correction coils and ensures field homogeneity over a region that can be arbitrarily specified by the user. The algorithm automatically chooses the minimum number of coils necessary to satisfy the above constraints. It is also possible to employ the algorithm iteratively over finer and finer search grids in order to determine the coil sizes and positions more precisely. By using this optimization procedure it is possible to exactly correct for a 0.1T unidirectional fringe field by using two correction coils. Both coils are required by the algorithm to have the same current density (800 A/cm2) but differ in their geometries and positioning relative to the homogeneity region.

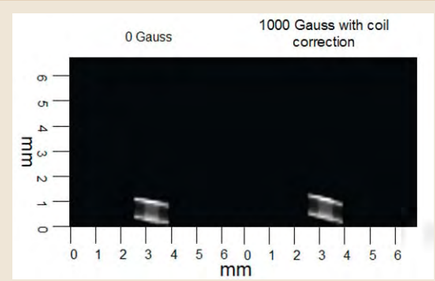

This image shows the result of a simulation carried out for the coils that were designed using the above-mentioned algorithm. On the left is the normal non-deflected focal spot with no external field or corrective field. On the right is the focal spot where a 0.1 T external field is present and a current of 800 A/cm2 is applied to the correction coils. The focal spots are virtually identical, demonstrating that the correction coils exactly cancel the 0.1 T external field.

References/Funding Source

Xu et al. Homogeneous Magnet Design Using Linear Programming IEEE Transactions on Magnetics, vol. 36, March 2000
NIH grant R01 EB007626
Stanford School of Medicine Bio-X Fellowship
The Lucas Foundation

Parameter Investigation and Results from a Flat Panel Detector with Forward Bias Capability

J. Starman[1,2], C. Tognina[3], G. Virshup[3], J. Star-Lack[3], I. Mollov[3], R. Fahrig[2]
Departments of [1]Electrical Engineering, [2]Radiology, [3]Varian Medical Systems, Palo Alto CA

Digital flat panel a-Si x-ray detectors can exhibit image lag of several percent. The image lag can limit the temporal resolution of the detector, and introduce artifacts into CT reconstructions. It is believed that the majority of image lag is due to defect states, or traps, in the a-Si layer. Software methods to characterize and correct for the image lag exist, but they may make assumptions such as the system behaves in a linear time-invariant manner. The proposed hardware method for lag reduction makes few additional hardware changes. For pulsed irradiation, the proposed method inserts a new stage in between the readout of the detector and the data collection stages. During this stage the pixel photodiode is operated in a forward bias mode, which fills the defect states with charge. Important parameters are current per diode and the current duration, which were investigated under light illumination by changing: 1.) forward bias voltage across the photodiode and TFT switch, 2.) number of rows simultaneously forward biased, and 3.)duration of the forward bias current. From the measurement data it was found that the forward biasing effectiveness was proportional to the total amount of charge injected into each photodiode (current per diode times duration). In Figure 1, the imager turn-on and turn-off responses are plotted vs frame number for several different forward bias charge amounts. For the modified Varian 4030CB imager used, a total injected charge of at least 6pC per photodiode gives maximal benefit in the reduction of image lag. Overall, the forward bias method has been found to reduce first frame lag by as much as 95% for direct light irradiation. For x-ray irradiation, lag improved (94% reduction) with forward biasing, but the temporal response of the scintillator became evident in the turn-on step response of the detector system.

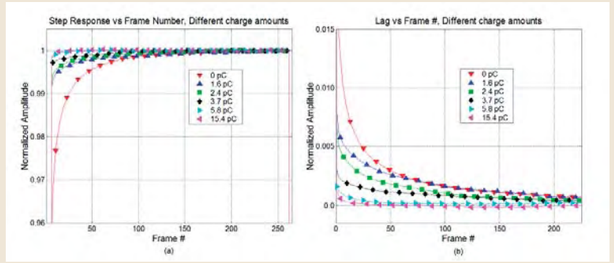

Light box step response and lag data plotted as a function of charge injected into each row. The different protocols used vary in the voltage, frequency, and number of active rows used. The quality of response correlates well with the amount of charge injected. Data taken at 10 fps.

References/Funding Source

J Starman, C Tognina, G Virshup, J Star-lack, I Mollov, R Fahrig, "Parameter investigation and first results from a digital flat panel detector with forward bias capability," Proc. of SPIE, 6913 (2008)
Varian Medical Systems
The Lucas Foundation
Stanford-NIH Biotechnology Traineeship

In vitro measurement of stent deformation using C-arm CT imaging

A. Ganguly[1], J. Simons[2], A. Schneider[3], B. Keck[4], R. Fahrig[1]
[1]Department of Radiology, RSL, [2]SRI International, Menlo Park, CA; [3] Formerly associated with The Richard M. Lucas Imaging Center, [4]Friedrich-Institut für Informatik, Alexander-Universität Erlangen-Nürnberg, Germany

Superficial femoral artery (SFA) stents have been reported to have a high breakage rate. We have investigated the cause for their breakage by studying their deformations. Here we describe a method for measurement of these deformations through in vitro imaging and analysis. This method was later used with in vivo studies in human subjects with SFA stents.

Mechanical testing devices were developed to measure force-deformation response of a stent under bending, axial and torsional loading. The response with increasing and decreasing load was measured. Volume images of the stents during deformation were obtained using an x-ray C-arm CT system (Axiom Artis dTA, Siemens Medical Solutions, Forchheim, Germany). Semi-automatic software was developed that calculated the stent centerline and allowed 'unwrapping' of the 3D image onto a 2D surface. From the centerline, the change in length due to axial loading and the change in curvature due to bending were calculated. The 'unwrapped' image allowed measurement of torsion. The results were compared with physical measurements of the changes in stent dimensions due to loading.

The results comparing the calculated and the physically measured values for the response of the stent are shown in Figure 1 (a)-(c). For bending, the results show good agreement at smaller bend angles. Since angles are calculated from successive centerline points, the larger values accumulate larger errors. The tension results agree well except for a few outliers. This may be due to sensitivity of the software to length change estimation. The torsion curves agree well during load increase. However, for decreasing loads, there are some disagreements. This could result from misidentification of gold marker pairs at opposite ends of the stent. We have developed a technique for calculating the deforming forces following the centerline identification and from the 'unwrapped' images.

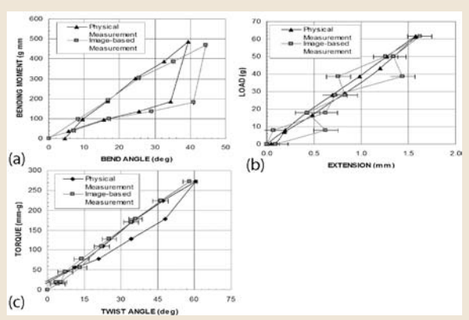

Fig. 9 Comparison of physical measurements and image-based measurements using the imaging technique for (a) bending (b) tension and (c) torsion of a stent

References/Funding Source

"In Vivo Imaging of Superficial Femoral Artery (SFA) Stents for Deformation Analysis", submitted to JVIR, July 2008.
The sponsors of the RESIStent program:
Abbott, Angiomed
Boston Scientific, Cordis
Medtronic, W. L. Gore
The Lucas Foundation

In vivo Imaging and Analysis of Bone Growth in a Rabbit Model

A. Ganguly[1], J. Starman[1], R. L. Smith[2], W. J. Maloney[2], R. Fahrig[1]
Departments of [1]Radiology, RSL, [2]Orthopedic Surgery

We have developed and in vivo imaging method combined with image processing to quantify the bone growth in critical sized defects in a rabbit model.

Critical size defects (1.5 cm) were created in the ulna in both forearms in twenty rabbits. The animals were divided into two groups: (1) the defect on one arm was left empty (2) the defects had de-mineralized bone matrix (DBM).

Three dimensional (3D) images of bone development were obtained at 2, 4, and 8 weeks post defect creation. For imaging, a C-arm CT system (Siemens Healthcare AX, Forchheim, Germany) was used. This system houses an x-ray tube and a solid-state flat panel detector (FPD) on either ends of a C-shaped arm. Twenty second scans at 96 kVp, each with 494 projections at a resolution of 394µm were used. The projections were then reconstructed using a kernel with Shepp-Logan-like behavior. An algorithm involving preprocessing, segmentation, volume registration and analysis of the new bone growth was developed. Following registration of the week4 and week8 datasets with the week2 volumes, the change in the number of voxels above 300HU in the cut region were calculated.

Fifty and sixty percent success rate was obtained in processing the data sets in groups one and two, respectively. From the processed data, it was observed that 48.8±13.2% and 53.7±32.2% total bone growth was observed in the empty defects in group1 and in the DBM filled defects in group2, respectively. In three cases in group2, the number of "bone" voxels at the center of the new bone decreased from week 4 to week 8 and was replaced by lower density material. We speculate that new bone marrow had formed in these regions. Using the high resolution volume imaging technique with post-processing, we were able to study in vivo bone growth.

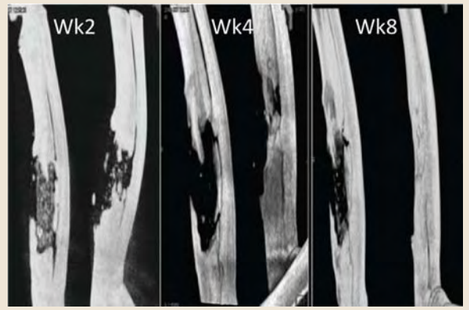

Bone development during weeks 2, 4, and eight in a rabbit with DBM material in the defect region on the right forearm

References/Funding Source

A research grant from Safamor-Danek Medtronic

Impact of Atrial Fibrillation on Accuracy of 3D Imaging of Left Atrium Using ECG Gated Multisweep C-arm CT

E Girard-Hughes[1], A Al-Ahmad[2], A Mehdizadeh[2], J Boese[3], G Lauritsch[3], P J Wang[2], H H Hsia[2], P C Zei[2], J Rosenberg[1], R Fahrig[1]
Departments of [1]Radiology, [2]Cardiovascular Medicine, [3]Siemens Healthcare AX, Forchheim, Germany

Radiofrequency ablation of the left atrium has become an important strategy in the treatment of atrial fibrillation (AF). Three-dimensional imaging with CT or MRI helps delineate left atrial (LA) and pulmonary vein (PV) anatomy and may be merged with an electroanatomical mapping system, but images are aquired days or weeks prior to ablation. We compare the accuracy of ECG gated C-arm CT system (DynaCT Cardiac, Siemens Medical Solutions, Forchheim, Germany) in swine with normal sinus rhythm (NSR) versus rapid atrial pacing (RAP) to simulate AF imaging during an interventional procedure.

Seven female swine were anesthetized and intubated and a transvenous pacing electrode was placed in the right atrium for rapid pacing during imaging. Gated C-arm CT was obtained in all animals with the electrode in place during NSR and then during RAP (500 bpm). 200 mL of iodinated contrast was injected peripherally in the inferior vena cava. After a 13-14 second delay, projection images were obtained over 6 sweeps with ECG for retrospective gating and during a breath hold (24-30 seconds). The LA was measured along its largest axis and the PVs were measured at the level of entry to the LA along two orthogonal dimensions at the largest cross sectional area. The measurements were compared between 3D images obtained during NSR and RAP.

RAP achieved a variable ventricular rate in all animals (110-220 bpm). Overall, RAP and NRS measurements were not significantly different (mean difference = .047cm; p<.40 by paired Wilcoxon test) and the overall concordance correlation was high (0.948, p<.001). RAP measurements were equivalent within 15% to NSR measurements and had a 2.4% bias. Overall, ECG Gated C-arm CT 3D imaging during simulated AF provides accurate measurements of the LA and PV, although during RAP, image quality was slightly more blurred and LA measurements tended to be larger.

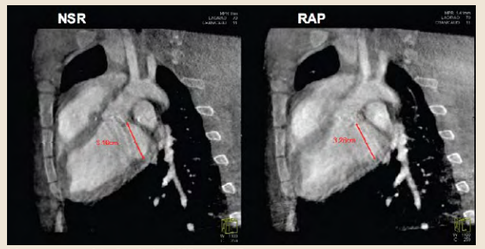

Measurements of the LA during NSR and RAP.

References/Funding Source

Girard-Hughes E, Al-Ahmad A, Mehdizadeh A, Boese J, Lauritsch G, Wang PJ, Zei PC, Hsia HH, Moore T, Rosenberg J, Fahrig R. The impact of atrial fibrillation on the accuracy of three-dimensional imaging of the left atrium: A study using ECG gated multisweep c-arm CT (DynaCT Cardiac). Annual Meeting of the Heart Rhythm Society; May 14-17, 2008; San Francisco, CA.
Siemens Sponsored Research Grant "Cardiac Imaging using C-arm CT: EP registration and perfusion"
The Lucas Foundation

Effectiveness of Breast Shields Combined with CT Dose Modulating Techniques

A. Ganguly[1], B. Newman[2], N. J. Pelc[1]
[1] Department of Radiology, RSL, [2]Pediatric Radiology, Lucille Packard Children's Hospital

Currently, there is an increased effort to reduce CT imaging dose, for example, to the developing breast tissue in pediatric patients(1). In-plane breast shields have been shown to reduce dose. Clinically, they are being used in addition to CT dose modulating techniques. However, they decrease image quality and it is unclear how the net effect compares to simply reducing the technique (e.g., mAs). We investigated this issue.

We imaged a 10cm diameter CT dose index (CTDI) measurement phantom using a 64 slice CT scanner (Siemens Medical Solutions, Forschheim, Germany). Protocols for imaging the following patients were used: [1] infant at 80 kVp [2] older child at 100 kVp, [3] adult at 120 [4] slim adult at 100 kVp, and [5] an obese adult at 100 kVp. The exposure values for the scans were obtained from topograms without the breast shield. The CT images were then obtained with and without the breast shield in combination with and without CareDose™ (Siemens method for mA modulation and dose control). When imaging without CareDose™ , the exposure was fixed at the value selected previously by CareDose™. The dose was measured using a pencil ion-chamber located 1cm below the top surface of the phantom. A 0.045mm lead equivalent bismuth-based breast shield was used (Figure 1).

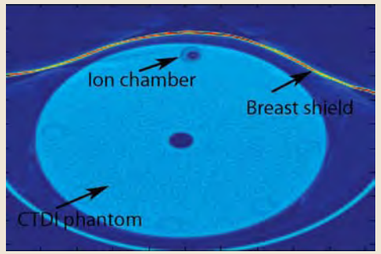

Cross-section CT image of CTDI phantom with breast shield

The dose reduction due to the shield in the five cases was: [1]28.1±0.2% [2]23.2±0.2% [3] 20.5±0.0% [4] 22.7±0.3% [5] 22.5±0.4%. In presence of the shield, the dose measured with CareDose was higher than without it in all but one case: [1] +3% , [2] +8% [3]+26% [4]+0.6% and [5]-7%. Per unit dose, the squared SNR in the region below the shield reduced by 9.2±3.5%. This suggests that a lower fixed exposure may actually be better than a breast shield at reducing dose while maintaining the same dose to squared-SNR ratio.

References/Funding Source

Bradley L. Fricke et al, 1) In-Plane Bismuth Breast Shields for Pediatric CT: Effects on Radiation Dose and Image Quality Using Experimental and Clinical Data, AJR:180, February 2003.
GE HealthCare
The Lucas Foundation.

A new Reconstruction Method to Improve SNR for an Inverse Geometry CT System

J. Baek[1,2], N. J. Pelc[2]
Departments of [1]Electrical Engineering, [2]Radiology, RSL

The inverse-geometry CT(IGCT) system uses a large-area scanned source and a 2D detector array with a smaller extent in the transverse direction. The acquired IGCT data can be significantly oversampled and the samples are not equally spaced in radial distance or angle. A previously proposed reconstruction algorithm used a modified gridding method to rebin the normalized and logged projection data into parallel projections. This approach can be suboptimal if the measured rays contributing to an output sample do not have the same signal-to-noise ratio (SNR) due to each ray having a different detected number of photons (due to different incident intensities). Reconstructed images may have better SNR if we consider the SNR of each ray in rebinning step. In this paper, we propose a new method to improve the SNR in the reconstructed image. In this method, input rays with different SNR were combined in the rebinning step by using weighted-least square fitting to produce SNR efficient output projection data. We simulated two cases: uniform, and triangular profiles of the detected number of photons across the detector array. For single slice 2D imaging, SNR improvements of 1% (uniform) and 21%(triangular) were observed. Experiments were also performed with air scan data acquired from a scanned source C-arm system (NovaRay, Inc., Palo Alto, CA). In this case, we observed SNR improvement as high as 20 %, depending on the intensity of non-uniformity across the detector.

References/Funding Source

GE Health care
The Lucas Foundation
NIH grant R01 EB006837

A Fourier Rebinning Algorithm for Cone-Beam CT

S. R. Mazin[1,2], N. J. Pelc[2,3]
Departments of [1]Electrical Engineering, [2]Radiology, [3]Bioengineering

It is known that x-ray projections collected from a circular orbit of an x-ray source are insufficient for accurate reconstruction of a 3D object. For each local region of the object (except in the plane containing the source trajectory) there is a conical volume in the object's spatial frequency space that is unmeasured due to the circular geometry. The Feldkamp, Davis and Kress (FDK) algorithm based on filtered backprojection (FBP) involves a 3D backprojection step so that these unmeasured spatial frequencies are set to zero, resulting in cone beam artifacts for certain objects. We present a new type of cone beam CT reconstruction algorithm based on the Fourier rebinning (FORE) framework of Defrise et al. The cone beam x-ray projection data are rebinned into a set of in-plane sinograms using the FORE rebinning approximation, followed by 2D FBP to reconstruct each axial slice. The algorithm is able to extrapolate data into the missing region of the object's frequency space in a computationally efficient way, allowing for a reduction of cone beam artifacts for certain objects. Unlike FDK, the algorithm is exact for an impulse object located anywhere along the axis of rotation. Reconstruction errors are dependent on the radial distance, cone angle, and the second- derivative of the projection data in the longitudinal direction. Finally, an extension to the algorithm was developed that permits reconstruction

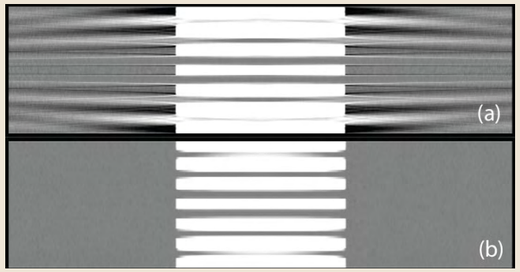

Coronal plane of a Defrise phantom showing a +/- 2 deg. cone-angle. (a) FDK reconstruction. (b) FORE-CB reconstruction.

in regions of the object that are not seen by the detector in every view. One potential application is imaging of the spine for reducing the cone-beam streak artifacts caused by the sharp edges of the vertebrae.

References/Funding Source

S. R. Mazin and N. J. Pelc, "A Fourier rebinning algorithm for cone beam CT", Proc. SPIE: Physics of Medical Imaging 6913, pp. 691323 (2008), DOI:10.1117/12.769575
GE Healthcare
NIH (R01 EB0006837)
The Lucas Foundation

SNR Efficient 3D Reconstruction Algorithm for Multi-Source Inverse Geometry CT system

J. Baek[1,2], N. J. Pelc[2]
Departments of [1]Electrical Engineering, [2]Radiology

The multi-source Inverse-Geometry CT(MS-IGCT) system uses a 2D array of sources opposite a smaller 2D detector array. One sample system design uses 3 rows of 21 sources each. Because the MS-IGCT system provides sufficient sampling in the axial direction, cone beam artifacts can be reduced. Projection data from the 21 sources at the same z-location can be rebinned into one cone beam projection, therefore, we can have 3 different cone beam projection data sets after rebinning, and reconstruction can be performed by using the FDK algorithm. However, if FDK is used, each of the three data sets by itself produces different cone beam artifacts. For example, the upper sources can provide artifact free images in the upper reconstruction volume, but cone beam artifacts can be observed in the central and lower reconstruction volume. The central and lower sources also provide artifact free image at different z-locations. We can achieve an artifact free volume by using artifact free images at different z-locations. However, if we could use all the data the SNR can be improved. In this study, we develop a method to combine reconstructed volumes in Fourier space, and the main goal is to keep the exactness and improve the SNR in the combined image. The method was tested with a simulation of a Defrise phantom and the proposed method, did not show cone beam artifacts. A noise simulation was also performed by using ideal bowtie filter so that all projection data had the same noise level. A noise simulation showed that the noise variance was ~1/3 of that in a single FDK reconstruction.

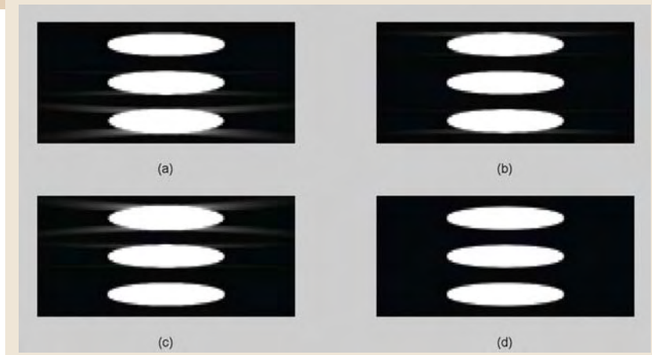

(a) Coronal plane of source 1 (b) Coronal plane of source 2 (c) Coronal plane of source 3 (d) Coronal plane of combined image

References/Funding Source

GE Health care
The Lucas Foundation
NIH grant R01 EB006837

Optimal Multi-Energy Binning in Photon Counting Detectors with Energy Discriminating Capabilities

A.S. Wang[1,2], N.J. Pelc[2,3]
Departments of [1]Electrical Engineering, [2]Radiology, [3]Bioengineering

It is well known that decomposing an object into attenuation or material basis functions provides additional imaging benefits such as contrast enhancement or material subtraction. This can be accomplished with photon counting x-ray detectors (PCXDs) with energy discriminating capabilities, which enable us to count x-ray photons and classify them based on their energies. The richness of the information contained in these measurements can depend heavily on how these photons are binned together.

Our goal is to identify a method that yields the optimal energy thresholds and/or weights for binning data from energy discriminating PCXDs. Additional energy information from these PCXDs allows us to use maximum-likelihood to estimate the amount of unknown calcium and water penetrated by the beam. However, due to inherent quantum noise or system limitations, these estimates are themselves noisy. We show that there are different optimal energy bin widths for different object sizes, and going from two energy bins to three has the benefit of noise reduction and robustness to changes in material thicknesses. However, for the cases examined, adding more energy bins results in diminishing returns.

Moreover, we show that for PCXDs that discriminate between low and high energy photons, it is beneficial to have a gap between the thresholds. Photons with energies that fall into this gap should either be discarded or counted separately to improve material separability. Also, if the PCXD can discern the energy of each photon, we show that when estimating the amount of each of two material basis functions, two appropriately weighted sums of the photon counts provide as much information as knowing the number of counts at each energy.

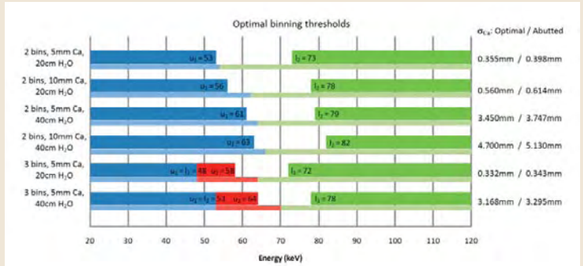

The thick bars illustrate optimal binning for a given number of bins and material thicknesses. The thin bars underneath show our results of optimal binning with abutted thresholds so that each photon goes into some bin. This yields up to an 11% higher uncertainty in our goal of estimating calcium thickness.

References/Funding Source

A.S. Wang and N.J. Pelc, "Optimal Multi-Energy Binning in Photon Counting Detectors with Energy Discriminating Capabilities," to be presented at RSNA 2008.
A.S. Wang and N.J. Pelc, "Optimal Energy Thresholds and Weights for Separating Materials Using Photon Counting X-Ray Detectors with Energy Discriminating Capabilities," submitted to SPIE Medical Imaging 2009: Physics of Medical Imaging.
GE Healthcare
NIH Grant EB006837
The Lucas Foundation

Relative Sensitivity of dual energy CT

C. A. Clavijo[1], N. J. Pelc[2]
[1]Escuela de Ingeniería de Antioquia, Universidad CES, Medellín, Colombia [2]Radiology

Dual-energy CT is known to enable possible improvement of material separation over regular CT, due to the strong energy dependence of the x-ray linear attenuation coefficient. Therefore, it could be useful in angiography to separate calcified tissue and iodinated contrast media and, eventually, enhance the visualization in the presence of implanted devices such as stents in order to facilitate the diagnosis of stent-restenosis. In clinical implementation, however, most of the current dual energy techniques show limited results due to their high sensitivity to noise. In this study, a dual energy separation method for iodinated contrast media, cortical bone and water was implemented; afterwards, its results in the noiseless and noisy cases, using both mono-energetic and poly-energetic spectrums, were analyzed in order to understand the main causes of the noise propagation. Furthermore, an optimization technique regarding the right distribution of radiation dose between the high and low energy images was proposed. Finally, a dose comparison between the traditional pre/post-contrast scans and the dual energy technique was performed, and the decomposition algorithm was tested for the stent-water-bone separation in the noiseless mono-energetic case.

Bioinformatics

Developing and Populating a Database of Cancer-related Nanotechnology

D. Paik[1], K. Kode[1,2], S. Guccione[1], N. Baker[3], D. Thomas[3], R. Pappu[4], P. Jones[3], M. Wang[5], L. Molnar[6], S. Pan[7], S. Gaheen[7]
Departments of [1]Radiology, [2]Civil and Environmental Engineering, Stanford University; Departments of [3]Biochemistry and Molecular Biophysics, [4]Biomedical Engineering, Washington University, St. Louis, MO; [5]Biomedical Engineering, Georgia Tech and Emory University, Atlanta, GA; [6]Office of Technology and Industrial Relations, NIH, [7]Center for Bioinformatics, NIH, Bethesda, MD.

Introduction: Nanotechnology is a promising approach to cancer diagnostics and therapeutics with applications in imaging, early detection, reporting efficacy, multifunctional therapeutics and combined theranostics. This is in part due to the combinatorics of designing nanoparticles from their constituent parts. Informatics has the potential to catalyze discoveries in this area, yet these tools have until now not been developed. Our multi-institutional collaboration has worked to design, implement and populate a caBIG-compliant database on nanoparticles called caNanoLab.

Materials and Methods: The caNanoLab portal is designed to facilitate sharing of nanoparticle related information, especially annotations of nanoparticles including physical, chemical and biological characterizations as well as the protocols used to create this data. caNanoLab has a web interface that uses a J2EE-based architecture. It also can be connected to the grid via caGrid so that the stored characterizations may be widely accessed by a federated approach. The backend is a MySQL database representing the nano object model. The concepts are using EVS standarized terminologies and the metadata are maintained in the caDSR metadata registry.

Results: Thus far, it has been populated with data on 173 different nanoparticles from various participating laboratories and it is one of the most federated data services on caGrid. Developing a domain model that captures the appropriate level of detail about the composition and functionalization of a nanoparticle so that future queries may be able to determine structurally similar nanoparticles of relevance has been one of the most significant challenges. Because nanotechnology encompasses such a broad swath of applications, designing an object model that works for all parties is particularly challenging.

Conclusion: Analogous to the DNA microarray community at its inception, the cancer nanotechnology community's informatics needs are just now being defined and the impact of caBIG and informatics on the discoveries in cancer nanotechnology is on the horizon.

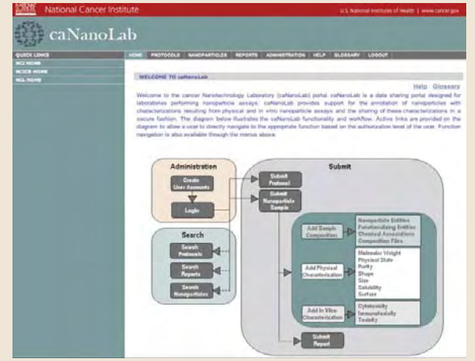

Figure 1: Screenshot of the caNanoLab workflow web interface.

References/Funding Source

Paik DS, Kode K, Guccione S, Baker NA, Thomas D, Pappu R, Jones P, Wang M, Molnar L, Pan S, Gaheen S, "Experience Developing and Populating a Database of Cancer-related Nanotechnology." caBIG 2008 Annual Meeting, Washington, DC, June 2008.
NIH U54 CA119367

Quantitative Unmixing of Multiplexed Raman Spectra from Nanoparticles in Cancer

K. Kode[1,2], C. Shachaf[3], S. Elchuri[4], C. Zavaleta[1], S. Gambhir[1,5], D. Paik[1]
Departments of [1]Radiology, [2]Civil and Environmental Engineering, [3]Microbiology and Immunology, [4]Neurology, [5]Bioengineering

Introduction: Raman spectroscopy is a technique used to identify molecular structures. Recently, Raman spectroscopy has gained interest as a tool for analyzing biological samples. Raman spectroscopy with its narrow and well-defined peaks can differentiate the spectral fingerprint of many molecules, resulting in high potential for multiplexed detection/imaging of multiple independently targeted nanoparticles. The goal of this work is to develop fundamentally new computational methods for unmixing these signals to allow for a more high throughput technique.

Materials and Methods: One of the problems in the analysis of Raman spectra is related to the presence of a relatively high fluorescence background. This necessitates the use of special mathematical procedures for (1) pre-processing the measured signal to remove background signals and (2) using more efficient unmixing techniques in order to accurately unmix the Raman spectra to determine the relative levels of each targeted protein. As the components of Raman Spectra increase, traditional linear least squares and its variants become increasingly inaccurate thus limiting the number of simultaneous proteins quantified.

Results: We are studying the effect of various background subtraction methods on the unmixing results. We have implemented some background subtraction methods from the literature and some novel methods and are in the midst of comparing their performance. Without knowledge of the true background vs. Raman signal in any given sample, it is very difficult to assess the effectiveness of these methods. Hence, we have developed a statistical model for generating simulated ground truth Raman spectra. Finally, we have developed an unmixing technique that allows for a degree of flexibility missing in standard least squares techniques.

Conclusion: While spectroscopic unmixing algorithms have been previously described in the literature, there are unique aspects to the Raman signals that we are leveraging to improve performance and eventually allow for 10 or more simultaneous signals to be unmixed, enabling much higher throughput studies than currently possible.

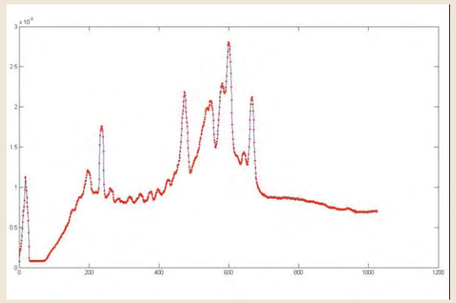

Fig1: Raman Spectra before preprocessing

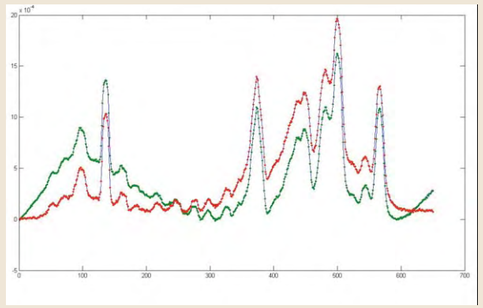

Fig 2: Results of two different background subtraction methods.

References/Funding Source

NIH U54 CA119367

Mathematical Modeling of Survival and Death Signals Predicts Oncogene Addiction

H. J. Lin[1], P. K. Bendapudi[2], P. T. Tran[2,3], S. Koh[2], J. Chen[2], G. Horng[2], D. W. Felsher[2], D. Paik[1]
Departments of [1]Radiology, [2]Oncology, [3]Radiation Oncology

Introduction: Oncogene-addiction is a biological phenomenon whereby tumors following oncogene-inactivation exhibit dramatic regression. This is widely appreciated clinically with the emergence of oncogene targeted therapies that expose a subset of human malignancies with this phenotype.

Materials and Methods: To explore mechanisms responsible for oncogene addiction, we developed multiscale mathematical models based on quantitative serial microCT imaging data acquired from oncogene-addicted and non-oncogene-addicted lung tumor ridden mice following a time course of oncogene targeted treatment. The model was built on the principle that the temporal changes in tumor volumes before and after oncogene inactivation were directed by the balance of two signals, a pro-proliferative/survival (S*(t)*) and a pro-death (D*(t)*) signals. In addition, each cell exhibits stochastic behavior and can be in either one of the three states (proliferation, homeostasis or apoptosis) in response to the signal input. This has led us to create an ordinary differential equation for the mechanism of oncogene-addiction.

Results: We derived our results from volume measurements of 20 weekly microCT scans on 11 lung tumors. Our model predicted lung tumor regression resulting from differences in decay of pro-survival and pro-death factors within tumor cells. This prediction was validated by experimental observations and supports *in vivo* the "oncogenic shock" hypothesis, a well-known hypothesis based on *in vitro* studies. In addition, for the non-oncogene-addicted tumors, we created a two-compartments model of the hypothesis that some tumor cells escape oncogene addiction and that subsequent inactivation of the oncogene causes regression only in subpopulation of addicted cells while the non-addicted cells are free to proliferate. Cells that are susceptible to oncogene addiction would undergo rapid apoptosis following oncogene inactivation. However, the growth of escaped cells will eventually overtake the decline of susceptible cells.

Conclusion: Our result suggests that a large number of cells escape oncogene addiction in the non-oncogene-addicted lung tumors while only a very small number of cells, if any at all, do in the oncogene-addicted lung tumors, with this difference being $p < 0.001$.

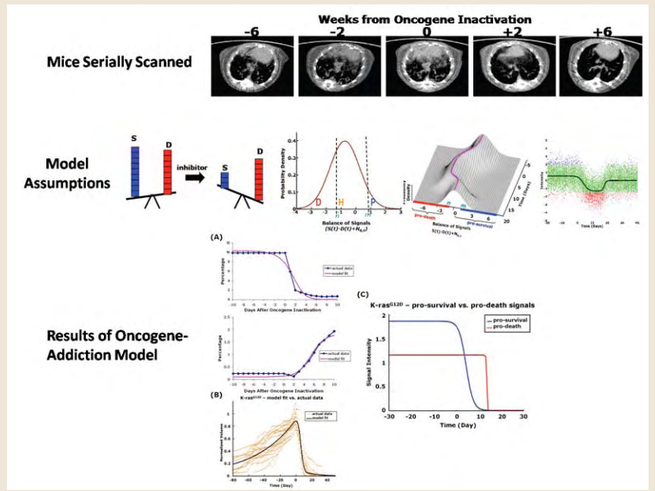

Figure 1: Quantitative model of oncogene addiction phenomenon in lung cancer.

References/Funding Source

RSNA Fellow Research grant (RF0801)
Parker B. Francis Fellowship
Henry S. Kaplan Research Fellow award (SUMC grant 1046297-100-KAVWO) (to P.T.T.)
HHMI Medical Student Research Fellowship (to P.K.B.)
SMIS Program - NIH R25 CA118681 (to H.J.L)
NIH/NCI R01-CA85610, R01-CA105102, 3R01CA089305-03S1
NIH/NCI ICMIC P50 CA114747
NIH/NCI Grant 1P20 CA112973
Leukemia and Lymphoma Society
Burroughs Wellcome Fund
Damon Runyon Lilly Clinical Investigator Award (to D.W.F.)

A Thin Client 2D+3D Architecture for Coordinating Multi-center CAD Trials

F. Schmitzberger[1,2], J. Roos[1], S. Napel[1], G. Rubin[1], D. Paik[1]
Departments of [1]Radiology, and [2]the Biomedical Informatics Training Program

Introduction: Geographically distributed CAD trials pose challenges in 1) setting a consensus gold standard, 2) displaying and recording CAD assisted reads and 3) reviewing and analyzing the collected data. The purpose of this study was to perform a needs assessment of informatics support for multi-center CAD trials and to design a solution using state of the art networking and visualization technologies.

Materials and Methods: Given the difficulties of geographic separation, we have defined several criteria for an ideal solution: (1) reduce needs for long distance software/hardware support, (2) minimize the need to distribute and synchronize large image datasets between sites, (3) eliminate the need for study coordinators at each site to collect and send in results, and (4) display 2D+3D rendered data using a fast and consistent interface that emulates a clinical readout environment.

Results: We considered the pros/cons of various system design possibilities including (1) no network (ship computers with software+images), (2) fat clients that each run a local copy of the software and (3) a thin client that connects to a centralized server. Each design was feasible but only the thin client design met our needs assessment criteria. Our system is designed around a network-capable 2D+3D (MIP and volume rendering) visualization SDK (provided by Fovia, Inc.) that renders images on a centralized server and sends the rendered images over the network at interactive frame rates (~10 fps). The client computing requirements are minimal (display calibration to be done by software). Datasets are stored only on the centralized server and data collection is done by the client display software and sent in real-time back to the server.

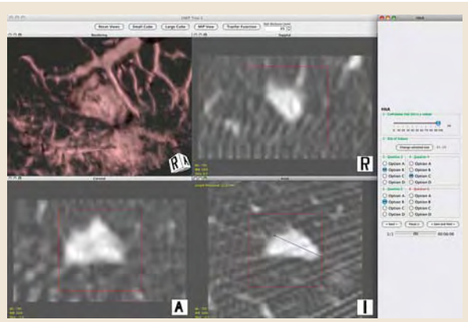

Figure 1: Screenshot of the system for running 2D+3D multi-center CAD trials over the grid.

Conclusion: This novel approach is able to greatly simplify the logistics of running a multi-center CAD trial. It is also a scalable solution that can enable much larger CAD trials that are needed to validate CAD for clinical use.

References/Funding Source

Schmitzberger FF, Roos JE, Napel S, Rubin GD, Paik DS, "A Thin Client 2D+3D Architecture for Coordinating Multicenter CAD Trials." accepted to Radiological Society of North America 94th Scientific Sessions, November 2008.
NIH R01 CA109089

External Validity of Cross-Validation on Computer-aided Detection (CAD) of Lung Nodules Enabled by the LIDC Dataset

D. S. Paik[1], D. A. Olsen[1], J. E. Roos[1], S. Napel[1], J. Pu[1], A. Aggarwal[1], G. D. Rubin[1]
[1] Department of Radiology

Introduction: Leave one out cross-validation (LOOVC) is widely used to evaluate algorithms in a "fair" way. However, it is fundamentally unable to demonstrate external validity (i.e., generalizability to new datasets). This study aimed to evaluate the external validity of our lung nodule CAD system by using the Lung Imaging Database Consortium (LIDC) datasets.

Method and Materials: Our own CAD system was tested and trained on two datasets. The first dataset (DS1) contained 20 MDCT scans (patient age range, 15–91 years; mean, 64 years) with 378 nodules (216 ≥ 3 mm), where the reference standard was established by two experienced thoracic radiologists in consensus. The second dataset (DS2) contained all 36 annotated chest MDCT scans with slice spacing ≤ 2mm from the LIDC dataset with 167 marked nodules (85 ≥ 3 mm). Each LIDC scan contained nodule markings from an un-blinded reading by four radiologists. None of our CAD developers reviewed the LIDC dataset prior to testing. The CAD system was tested (1) using a LOOCV on each dataset separately and (2) externally validating (EV) by training on one full dataset and testing on the other full dataset. FROC curves were created to measure performance on nodules marked by majority consensus in each dataset.

Results: CAD trained with LOOCV on DS1 had a FP/Pt rate of 1.7 and 2.3 at 60% and 70%, respectively. Similarly, LOOCV on DS2 had a FP/Pt rate of 2.2 and 3.6 at 60% and 70%, respectively. EV training on DS1 and testing on DS2 had a FP/Pt rate of 2.2 and 3.6 at 60% and 70%, respectively. EV training on DS2 and testing on DS1, the rates were 2.2 and 6.5.

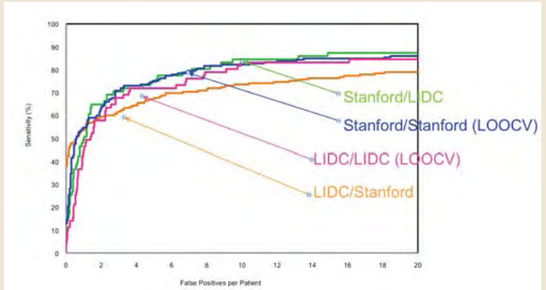

Figure 1: Internally cross validated results are within the range of externally validated results using both the Stanford lung dataset and the Lung Imaging Database Consortium (LIDC) dataset.

Conclusion: FROC curves for leave-one-out cross-validation on both datasets and the external validation test on DS2 were similar suggesting that the algorithm is robust to changes in patient population and training methodologies. The decreased FP rate when testing on DS1 with EV may reflect the difference in the quality of training data. In general, LOOCV led to slightly better results relative to external validation.

References/Funding Source

The Lucas Foundation

Body MR Imaging

In Vivo Whole-Knee Measurement of ^{23}Na at 3.0T in ACL Injured Patients

G. Gold[2], E. Staroswiecki[1,2], N. Bangerter[2], P. Gurney[1], S. Koo[1], R. Watkins[1], B. Hargreaves[1]
Departments of [1]Radiology, RSL, [2]Electrical Engineering

Early degenerative changes in articular cartilage leading to osteoarthritis are accompanied by proteoglycan depletion in the cartilage matrix. Subjects with prior tears to the anterior cruciate ligament (ACL) show early development of osteoarthritis. Sodium MRI has been shown to correlate with proteoglycan concentration, and may be useful in detecting and tracking early proteoglycan depletion. Sodium MRI is challenging due to relatively low ^{23}Na concentrations in biological tissues, and rapid signal decay. Despite these challenges, improved hardware coupled with higher field strengths enable diagnostic-quality sodium MRI in vivo in reasonable scan times. Short-TE gradient-spoiled sequences with efficient k-space trajectories are often employed to maximize sodium signal and minimize blurring from signal decay.

A fast gradient-spoiled sequence using the 3D cones k-space trajectory and a rapid (0.64 ms) RF excitation was developed for sodium image acquisition. The centric 3D cones trajectory permits short echo times and achieves very high SNR efficiency, while providing a relatively smooth k-space weighting and making efficient use of gradient resources. The sodium sequence was implemented on our 3T GE whole-body scanners. The whole knee cartilage was scanned in five normal subjects more than 3 years after ACL injury at 3T using custom sodium-tuned quadrature knee coil. Both the injured knee and uninjured knees were scanned. Conventional proton imaging was also done to look for cartilage loss.

We measured signal levels of sodium in the knee cartilage in both the healthy knees and knees of subjects at 3T. Results showed good sodium SNR in all cases, but lower sodium signal in the knee with ACL repair. Early detection of osteoarthritis before cartilage loss has occurred is important for development of drugs to treat this common disease before irreversible cartilage loss has occurred.

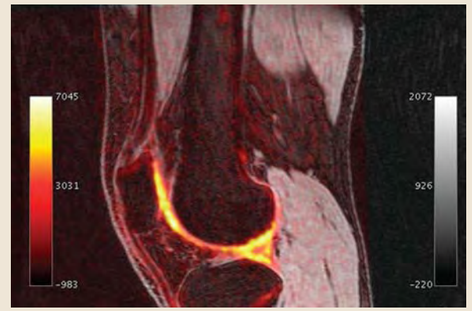

a) Sodium sagittal images of a knee acquired in a subject with a prior ACL tear. The sodium signal is overlaid in color and correlates with the cartilage glycosaminoglycan content. Sodium imaging has the potential to diagnose early osteoarthritis in these subjects before cartilage loss has occurred.

References/Funding Source

Staroswiecki, E, Bangerter, NK, Gurney, PT, Gold, GE, Holdsworth, SJ, Grafendorfer, T, Hargreaves, BA. In Vivo Measurement of ^{23}Na T2* in Human Articular Cartilage at 3T and 7T. Proc. Of 16th ISMRM, Toronto, 2008. p. 324.
NIH Grants EB002524, EB005790, and RR009789
GlaxoSmithKline
GE Healthcare
NCRR Grant P41-09784
The Lucas Foundation

In Vivo Measurement of ^{23}Na T2* in Human Articular Cartilage at 3T and 7T

E. Staroswiecki[1,2], N. Bangerter[2], P. Gurney[1], G. Gold[2], S. Holdsworth[2], T. Grafendorfer[3], B. Hargreaves[2]
Departments of [1]Electrical Engineering, [2]Radiology, RSL, [3]GE Healthcare, Waukesha, WI

Early degenerative changes in articular cartilage leading to osteoarthritis are accompanied by proteoglycan depletion in the cartilage matrix. Sodium MRI has been shown to correlate with proteoglycan concentration, and may be useful in detecting and tracking early proteoglycan depletion. Sodium MRI is challenging due to relatively low ^{23}Na concentrations in biological tissues, and a rapid bi-exponential signal decay. Despite these challenges, improved hardware coupled with higher field strengths enable diagnostic-quality sodium MRI in vivo in reasonable scan times. Short-TE gradient-spoiled sequences with efficient k-space trajectories are often employed to maximize sodium signal and minimize blurring from signal decay. In practice, accurate characterization of sodium T2* decay in a biological tissue of interest is required for sequence parameter optimization, and in some cases can be a marker of underlying physiologic structure. In this work, MR experiments were performed *in vivo* to measure and compare sodium T2* in human articular cartilage of the knee at both 3T and 7T.

A fast gradient-spoiled sequence using the 3D cones k-space trajectory and a rapid (0.64 ms) RF excitation was developed for sodium image acquisition. The centric 3D cones trajectory permits short echo times and achieves very high SNR efficiency, while providing a relatively smooth k-space weighting and making efficient use of gradient resources. The sodium sequence was implemented on our 3T and 7T GE whole-body scanners. The patellofemoral cartilage was scanned in five normal knees at *both* 3T and 7T using custom sodium-tuned transmit/receive 3" surface coils, with different echo times. A T2* exponential decay curve was fit to each pixel in the resulting data.

We measured T2* of sodium in patellofemoral cartilage in 5 knees at both 3T and 7T. Results consistently showed an exponential decay with average T2* of 15.5 ms and 13.2 ms at 3T and 7T respectively, consistent with those expected for a long-T2 component based on previously published results. Our long T2* measurements will be important in optimizing pulse sequence parameters for sodium imaging in vivo at high fields.

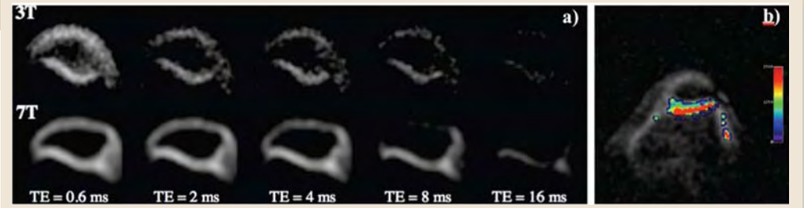

a) Sodium axial images of a knee acquired with different echo times (TE). The brighter signal corresponds to the patellofemoral cartilage. Signal from the subcutaneous sodium and the fluid is also visible. The signal decay as the TE increases is plainly visible. b) A color map showing the different values for T2* for each pixel of a sodium image.

References/Funding Source

Staroswiecki, E, Bangerter, NK, Gurney, PT, Gold, GE, Holdsworth, SJ, Grafendorfer, T, Hargreaves, BA. In Vivo Measurement of ^{23}Na T2* in Human Articular Cartilage at 3T and 7T. Proc. Of 16th ISMRM, Toronto, 2008. p. 324
NIH Grants EB002524, EB005790, and RR009789
GlaxoSmithKline
GE Healthcare
NCRR Grant P41-09784
The Lucas Foundation

Slab-Phase Modulation with Parallel Imaging in Bilateral Breast MRI

M. Han [1,2], B. L. Daniel[1], B. A. Hargreaves[1]
Departments of [1]Radiology and [2]Electrical Engineering

Slab-phase modulation reduces scan time in bilateral breast imaging by eliminating the need to image the space between the two breasts. In this work, we show effects of phase modulation combined with self-calibrated parallel imaging such as mSENSE and ARC on reconstructed image quality.

Eight volunteer scans were conducted using a GE 1.5T Excite scanner and an eight-channel breast coil. For each scan, two experiments were performed using a dual-slab spectral-spatial pulse. The first experiment used phase encoding over the entire volume with 192 sagittal sections. The second experiment used phase encoding over the two excited slabs, which were virtually shifted using slab-phase modulation, for a total of 128 sagittal sections. A 3D Cartesian readout was used, and both sets of volunteer scans were repeated twice to measure SNR by the "difference method."

To test parallel imaging, phase encode planes (k_z) were discarded to set the width of the undersampled slab FOV as the thickness of one slab. For the data without slab-phase modulation, k_z planes were undersampled by a factor of three and slice-direction acceleration used mSENSE with a factor of two and ARC with a factor of three. For the data with slab-phase modulation, k_z planes were undersampled by a factor of two and mSENSE and ARC accelerations of two were used. Additional 20 and 10 planes were used for calibration, respectively.

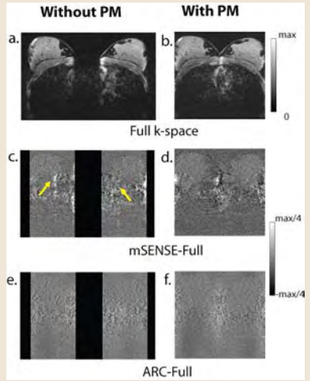

The reconstructed images from full k-space data without and with phase modulation (a-b), and difference images between unaccelerated images and accelerated images with mSENSE (c-d) and GRAPPA (e-f) were shown. SENSE residual artifacts due to misestimated sensitivity values are shown by arrows.

The figure show axially reformatted images from a single volunteer without and with phase modulation. We measured SNR from 74 ROIs in breast tissues over the eight volunteers and the average SNR efficiency increases were seen in mSENSE by 5% and ARC by 8% by incorporating phase modulation.

Slab-phase modulation improves image quality when combined with self-calibrated parallel imaging. SNR efficiency is increased with lower g-factors in average and reconstruction artifacts due to misestimated sensitivity values are reduced when mSENSE is applied.

References/Funding Source

M. Han, B. A. Hargreaves, Slab-Phase Modulation Combined with Parallel Imaging in Bilateral Breast Imaging. In: Proceedings of the 16th ISMRM Annual Meeting, Toronto, 2008, P. 2730.
[1] Hargreaves BA, et al., MRM, 57 (4):782-802, 2007.
[2] Wang J, et al., Proc., 1st Wurzburg Workshop on Parallel Imaging, P92, 2001.
[3] Beatty PJ, et al., Proc., 15th ISMRM, p1740, 2007.
[4] Pauly JM, et al., Proc., 11th ISMRM, p966, 2003.
[5] Reeder SB, et al., MRM, 54, 748-756, 2005.
[6] Firbank, et al., Phys Med Biol, 44, N261-N264, 1999.
NIH 2P41RR009784-11
NIH 5R01CA066785-0

Accelerated Bilateral DCE 3D Spiral Breast Imaging: Comparison between TSENSE and TGRAPPA

M. Han [1,2], B. L. Daniel[1], B. A. Hargreaves[1]
Departments of [1]Radiology and [2]Electrical Engineering

By combining slab phase modulation and 3D spiral imaging, both breast volumes can be efficiently imaged. We further increase temporal resolution through a time-interleaved acquisition of phase-encode planes, followed by parallel imaging reconstruction. We compared TSENSE and TGRAPPA techniques in bilateral DCE breast MRI.

Imaging was conducted with a GE 1.5T Excite scanner and an eight-channel phased-array breast coil. All scans used a "stack-of-spirals" imaging trajectory with a 40º flip angle, a 20 x 20 cm FOV, 1.05 x 1.05 mm resolution, 3.6 mm slice thickness and 32 sagittal sections over each breast. With an acceleration factor of 2, phase-encode planes were acquired in a time-interleaved manner alternating between even and odd planes. The scan time for a temporal frame was 10 s and a total of 20 temporal frames were acquired.

Both TSENSE and TGRAPPA reconstructions were applied to bilateral MRI exams from 15 patients. After 2D gridding, SENSE and GRAPPA reconstructions were applied in the slice direction. A full k-space reference data were acquired by averaging several temporal frames and sensitivity maps for SENSE and coil weight coefficients for GRAPPA were estimated from them.

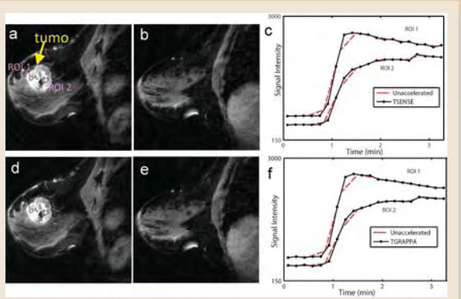

Post-contrast bilateral breast images. (a-b) Two unwrapped slices using TSENSE from the left breast (a) and the right breast. (c) Signal intensity curves measured in two ROIs located in the tumor. (d-e) Two unwrapped slices using TGRPAPA. Signal intensity curves were shown in (f). Curves from the unaccelerated images were also plotted in (c) and (f).

The figure shows two bilateral unfolded sagittal slices from the TSENSE (a-b) and TGRAPPA (c-d) from one patient. Signal intensity curves from accelerated and unaccelerated images were measured in two ROIs from a tumor. The increase in temporal resolution made possible by the acceleration is noticeable by the increased enhancement rate.

Both TSENSE and TGRAPPA reconstructions can provide diagnostic images with 10 s temporal resolution. In general, TGRAPPA provided less oscillation in DCE curves of the tumors from the 15 patients. For TSENSE, correct sensitivity-value estimation from dynamic images is sometimes challenging and localized residual aliasing artifacts can yield signal oscillation. Further investigation is needed to establish whether this affects the quantification of enhancement curves from tumors.

References/Funding Source

M. Han, B. L. Daniel, B. A. Hargreaves, Accelerated Bilateral DCE 3D Spiral Breast Imaging: Comparison between TSENSE and TGRAPPA. In: Proceedings of the 16th ISMRM Annual Meeting, Toronto, 2008, P. 2729.
[1] Pauly JM, et al., Proc., 11th ISMRM, p966, 2003.
[2] Hargreaves BA, et al., Magn Reson Med, 57 (4):782-802, 2007.
[3] Yen YF, et al., J Magn Reson Imaging, 11 (4): 351-359, 2000.
[4] Kellman P, et al., Magn Reson Med, 45: 846-852, 2001.
[5] Breuer FA, et al., Magn Reson Med, 53: 981-985, 2005.
NIH 2P41RR009784-11
NIH 5R01CA066785-0

Dual Tuned Helmholtz Coil for Breast Cancer Imaging

A. Nnewihe[1,2], E. Staroswiecki[1,3], N. Bangerter[1], B. Daniel[1], B. Hargreaves[1]
Departments of [1]Radiology, RSL, [2]Bioengineering, [3]Electrical Engineering

Clinical breast exams have limited specificity and sensitivity for detecting breast tumors [1,2]. Even X-ray mammography, which is used for early screening of breast tumors, has limited sensitivity and does not detect approximately 25% of breast cancers [3]. Dynamic contrast-enhanced MRI (DCE-MRI) has high sensitivity but low specificity; i.e., both cancerous and benign lesions enhance [2]. Additional imaging modalities such as sodium (23Na) MR have the potential to increase the sensitivity and specificity of breast cancer detection because ^{23}Na MR can reflect the disruption of the membrane Na-K pump associated with cancer. Moreover, recent advances in gradient hardware and pulse sequences have made ^{23}Na MR feasible for quantitative measurements of sodium concentration.

Preliminary results of multinuclear MRI using a receive-only H surface coil and a transmit/ receive ^{23}Na surface coil show elevated ^{23}Na signal in the tumor. Although the surface coil provides high SNR images, there is significant B1 inhomogeneity as modeled by Biot-Savart's law. For quantifying ^{23}Na concentration in the breast, we need an RF coil that improves B1 homogeneity without sacrificing SNR. The goals of this study were to build a dual-tuned Helmholtz coil, to investigate the difference between a dual-tuned Helmholtz coil and a dual-tuned surface coil in providing high SNR and high quality B1 homogeneity for multinuclear imaging, and to perform preliminary breast imaging using the dual-tuned Helmholtz coil.

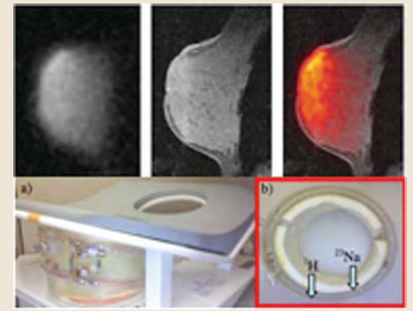

(Top) Breast images from a normal volunteer:
(Left) ^{23}Na; (Middle) 1H; (Right) ^{23}Na overlay.
(Bottom) Images of the dual-tuned Helmholtz coil.

Our novel coil design outperformed a dual tuned surface coil in both SNR and homogeneity. RF coils that provide high SNR enable high resolution imaging in reasonable scan times. Since we are using transmit/receive coils for ^{23}Na imaging, it is imperative that the RF coils exhibit a homogeneous B1 field. The homogeneous field and high SNR will facilitate more accurate measurements of ^{23}Na concentration in the breast. Our future coil designs will continue to improve upon these aspects of ^{23}Na imaging.

References/Funding Source

[1] Jacobs et al., Technol Cancer Res Treat 3.6, 2004
[2] Kopans, Breast Imaging, 2007
[3] Elmore et al., JAMA 293:1245-56,2005
[4] Jacobs, Eur Radiol 16, 2006
NIH Regenerative Medicine Training Grant
California Breast Cancer Research Program, IDEA Award
GlaxoSmithKline and the Richard M. Lucas Foundation

Multi-frequency Water/Fat Separation and Off-Resonance Correction for 3D Spiral Breast Imaging

K.L. Granlund[1,2], B.A. Hargreaves[2]
Departments of [1]Electrical Engineering and [2]Radiology, RSL

Field inhomogeneity can be problematic when scanning large volumes, such as in a bilateral breast exam. Inhomogeneity appears as blurring in spiral imaging sequences and also causes water/fat separation techniques to fail. This project aims to simultaneously correct both blurring and water/fat separation using a multi-frequency reconstruction algorithm for three-point water/fat separation using 3D spiral imaging. This multi-frequency approach allows for arbitrary field correction in three dimensions.

Images are acquired at three different echo times. Water and fat images are estimated using a least-squares three-point method. The least-squares residual image measures the quality of the reconstruction. Two residual functions are generated by repeating the least-squares method for different off-resonance frequencies: one by demodulating at the water frequency and one by demodulating at the fat frequency. A field map is generated by minimizing the sum of the water and fat residuals for each pixel. The image is reconstructed using the center frequency corresponding to the field map.

By considering both the water residual and the fat residual, we minimize the effects of blurring allowing for improved field correction. *In vivo* data shows improved water/fat separation and reduced blurring. This method is applicable to arbitrary k-space trajectories and should be very useful in studies with significant field variation over the imaging volume.

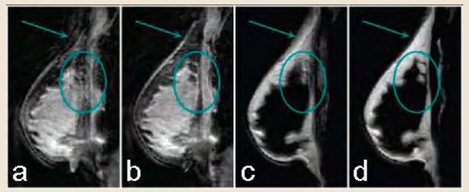

Volunteer data acquired at 3T: (a) single frequency water image, (b) multi-frequency water image, (c) single-frequency fat image, (d) multi-frequency fat image. The multi-frequency reconstruction images (b,d) show less blurring than the corresponding single frequency images (a,c), particularly at the skin (arrows) and glandular/fatty tissue boundaries (circled).

References/Funding Source

Granlund, KL, Hargreaves, BA. Multi-frequency Water/Fat Separation and Off-resonance Correction for 3D Spiral Breast Imaging. Proc. of 16th ISMRM, Toronto, 2008. p. 587.
NIH Grant RR009784
NSF GRFP
The Lucas Foundation

Towards Distortion-free MRI near Metallic Implants

W. Lu[1], K. Butts Pauly[1], G.E. Gold[1], J. Pauly[2], B. Hargreaves[1]
Departments of [1]Radiology, [2]Electrical Engineering
Stanford University Schools of Medicine and Engineering

Magnetic resonance imaging (MRI) is potentially the best modality for evaluating patients with metallic implants. However, MRI near metallic implants remains an unmet need due to severe artifacts, such as signal voids and pile-ups, which mainly stem from huge metal-induced field inhomogeneities. This work addresses MRI near metallic implants via an innovative imaging technique called ``Metal Artifact Reduction with View-angle-tilting and Encoded Locations" (MARVEL). The MARVEL technique provides robust spatial encoding against metal-induced field inhomogeneities by extending a view-angle-tilting (VAT) spin-echo (SE) sequence with additional z-phase encoding steps. While the VAT compensation gradient suppresses most in-plane distortions, the z-phase encoding steps resolve distorted excitation profiles that cause through-plane distortions. By positioning all the spins subject to metal-induced field inhomogeneities back to their actual spatial locations, the through-plane distortions can be corrected by summing up the resolved spins in each voxel.

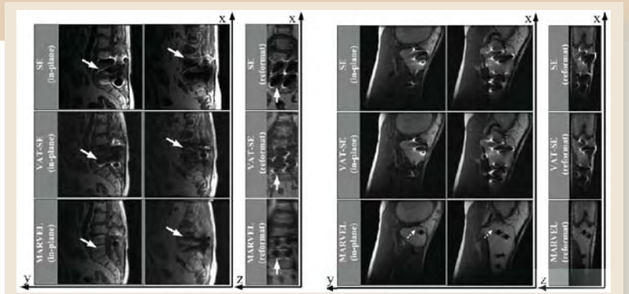

(a)Comparision of spine results obtained from spin-echo, VAT-SE sequences and the MARVEL technique

(b)Comparision of knee results obtained from spin-echo, VAT-SE sequences and the MARVEL technique

References/Funding Source

NIH-RR009784-11, NIH-EB002524-01
NIH-HL075803-01, NIH-CA077677-09
NIH 2P41RR009784-11
The Lucas Foundation

The MARVEL technique is validated in both spine and knee studies to greatly eliminate metal-induced distortions with feasible scan times. For imaging of the first subject with metallic fixture device in his spine, an eight-channel phased-array CTL coil and the following scan parameters were used: TE/TR=11/400 msec, acquisition matrix 256x128, FOV = 24 cm, readout bandwidth 125 kHz, nominal slab thickness 4 mm with no gap between slabs. Twenty-two slabs were prescribed to cover the spine and the device, and this scan took 14 minutes. The knee study used an eight-channel transmit/receive knee coil and the following scan parameters: TE/TR=12/555 msec, acquisition matrix = 256x128, FOV = 32 cm, readout bandwidth 166 kHz, nominal slab thickness 4 mm with no gap between slabs. Thirty-two slabs were prescribed to cover a volume containing the knee, and 18 minutes scan time was incurred. Figure 1 shows that the MARVEL technique successfully suppresses most metal-induced artifacts in the images obtained from spin-echo and VAT spin-echo sequences.

Noise considerations in Water-Fat Separation with Bipolar Multi-echo Sequences

W. Lu[1], H. Yu[2], A. Shimakawa[2], M. Alley[1], S. Reeder[3], B. Hargreaves[1]
Department of [1]Radiology, [2]GE Healthcare, [3]Biomedical Engineering, University of Wisconsin, Madison, WI

Bipolar multi-echo sequences (Fig. 1(a)) provide an efficient means to acquire multiple echoes in a single repetition for water-fat separation, which leads to shorter scan times, higher SNR-efficiency, and reduced motion-induced artifacts. One major technical problem is that the chemical-shift-induced misregistration between water and fat exists in opposite readout directions between even and odd echoes. It has been demonstrated that separating water/fat signals in k-space effectively eliminates the chemical-shift induced misregistration. The acquisition times at each k-space location are placed in an asymmetric pattern in the bipolar multi-echo sequence. That is, t3-t2 ≠ t2-t1 except at kx=0. Therefore, the k-space separation results in different noise amplification for different k-space locations.

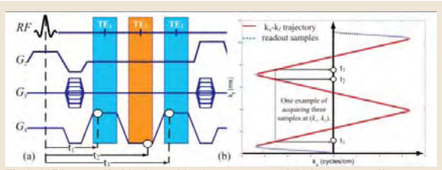

Fig.1: (a)Diagram of a bipolar multi-echo sequence, and (b) its corresponding k-space trajectory in k_y-k_x space. Note the asymmetric sampling pattern; i.e., t_3-$t_2 \neq t_2$-t_1 except at k_x=0

References/Funding Source

NIH RR009784
NIH EB002524
Lucas Foundation

The k-space signal model can be extended by including a noise vector, which models acquisition noise as zero-mean white Gaussian noise. The effect of the noise vector on the least-squares solution can be accounted for by the following noise amplification factor, which is the ratio of the variance of the noise present in the least-squares solution and the lowest achievable noise variance with a three-point acquisition. To verify the utility of the noise amplification factor in selecting regularization parameters, we used a bipolar multi-echo sequence to scan the knee of a healthy volunteer at 1.5 T with an extremity coil and the imaging parameters: matrix 256x256, FOV 20 cm, TR=11 ms, TE1,2,3=3.1, 5.3, 7.5 ms and BW 62.5 kHz. The imaging parameters result in greatly amplified high-frequency noise due to both insufficient water-fat phase differences developed at the boundary of the zigzag trajectory and the fact that the first and third echoes are nearly identical. This leads to an ill-conditioned inverse problem for separating k-space samples in high-frequency regions. To address the ill-conditioned separation, Tikhonov regularization is incorporated with the k-space separation in the high-frequency regions. The regularization significantly reduced the factor in the high-frequency regions. Fig. 2 shows that the imaging parameters causes the k-space separation to generate significant high-frequency noise in the separated image. Incorporating the regularization with the k-space separation eliminates not only the chemical–shift-induced artifacts but also the high-frequency noise.

Fig.2: Comparison of separated water images of a knee study (Case II) using (a) an image-domain method, and the k-space methods (b) without and (c) with Tikhonov regularization. The artifacts identified with arrows in (a) are eliminated in (b). The high-frequency noise in (b) is suppressed in (c).

High-Resolution 3D Bilateral Breast Imaging Using Slice Direction Autocalibrated Parallel Imaging

M.T. Alley[1], B.A. Hargreaves[1], B.L. Daniel[1], P.J. Beatty[2], AC Brau[2]
Department of [1]Radiology, Stanford University School of Medicine [2]GE Medical Systems ASL West, Menlo Park, CA

Dynamic Contrast Enhanced (DCE) breast imaging can provide high sensitivity in the detection of cancer[1]. Bilateral breast imaging is economically advantageous because it requires only one contrast injection and can also eliminate estrogen-level dependent contrast uptake differences between single breast exams performed on separate days. We have modified our high-resolution, fat-suppressed 3D sagittal sequence to use an auto-calibrated parallel imaging scheme to perform bilateral studies in a time comparable to traditional single breast acquisitions.

A typical imaging volume consisted of 160 1.5 – 2 mm slices to provide coverage over both breasts. A water excitation-only pulse was used for fat saturation. The in-plane matrix consisted of 192 phase encodes and 512 readout point with a fractional coverage in kx. Sparsely sampled k-space data were acquired in an elliptic-centric order to capture post-contrast enhancement at the beginning of the scan. The missing data were reconstructed using the Autocalibrating Reconstruction for Cartesian sampling (ARC) method2 using a 3-dimensional kernel.

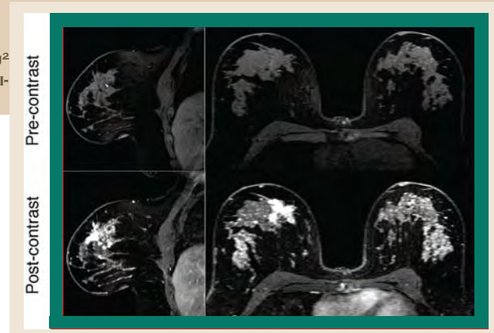

Pre-contrast (top row) and post-contrast (bottom row) images show the contrast uptake in a patient with invasive ductal carcinoma. The sagittal images in the left column were acquired with in-plane resolutions of 0.4 mm (A/P) x 1.0 mm (S/I). The axial reformatted images in the right column show that a slice thickness of 2.3 mm could provide full anatomic coverage.

References/Funding Source

1. C.D. Lehman, Role of MRI in screening women at high risk for breast cancer, JMRI, 24, ppgs. 964-970 (2006).
2. P. Beatty, et al., A Method for Autocalibrating 2D-Accelerated Volumetric Parallel Imaging with Clinically Practical Reconstruction Times. ISMRM-ESMRMB, 2007; Berlin, p. 1749.
NIH RR09784-11 and GE Healthcare

Because of the eight-channel breast coil profile, parallel imaging was performed only in the slice direction (R/L). An outer reduction factor of 2 was used. Autocalibration data for the reconstruction were provided by fully sampling a region of 20 x 96 central phase encodes in the kz-ky direction. Further time savings were performed by not acquiring the corners of ky-kz space. The total number of needed excitations could then be reduced by 47% (from 30720 to 16320) bringing the total scan time to approximately 6.2 minutes.

The ARC reconstruction produced consistently high quality images. The use of parallel imaging in the section direction reduced the scan time for bilateral imaging to that of an equivalent unilateral study. Future coil designs could allow parallel imaging to be used in the second phase encode direction for additional scan time reductions.

Automatic Segmentation of Articular Cartilage from MRI: A Multi-Contrast Approach

S. Koo[1], B. A. Hargreaves[1], T. P. Andriacchi[2,3], G. E. Gold[1]
Departments of [1]Radiology and [2]Mechanical Engineering, [3]Veterans' Administration, Palo Alto, CA

The regional variation in the morphology (thickness or volume) of articular cartilage is an important marker for evaluating the initiation and progression of osteoarthritis. Quantifying regional cartilage thickness or volume requires MR image segmentation and three-dimensional reconstruction. The tissue contrast in MRI can be adjusted using different contrast mechanisms (e.g. T1 or T2 weighting). The purpose of this study was to evaluate segmentation of knee articular cartilage automatically from multiple sets of MR images using the Support Vector Machine (SVM) method. Four 3D MR sequences, SPGR, DESS (1st and 2nd echo images), FIESTA and IDEAL-GRE (water and fat images), were run on an intact cadaveric knee to obtain six sets of MR images (matrix size 256x256x60) within 30 minutes. The bones in the MRI were automatically segmented to be used as landmarks to generate geometric information for each pixel. Each pixels were regarded as a vector with nine components, six MR intensity values and three pieces of geometric information, and mapped to a nine-dimensional space. Twenty percent of the pixels in the MRI volume were manually classified as cartilage and non-cartilage pixels to train the SVM and an optimal hyperplane that separate the two groups were calculated using the SVM algorithm. All pixels including the pixels used for training were tested using the hyper-plane and classified. Three-dimensional models of cartilage were created using the SVM testing result. True positive, false positive, true negative and false negative pixels were counted from the classification result (Figure 1(a)). The sensitivity and specificity were 98.95 % and 97.91 %, respectively. Three-dimensional cartilage models from manual segmentation (gold standard) and the classification result are shown in Figure 1(b) and 1(c) for qualitative comparison.

References/Funding Source

NIH EB002524
NIH EB005790

Figure 1. a) Classification result of a slice 1)false positive, 2) true positive, 3) false negative and 4)true negative, b) 3D model from the manual segmentation and c) 3D model from the classification results

Mapping and correction of vascular hemodynamic latency in the BOLD signal

C. Chang[1], M. E. Thomason[2], G. H. Glover[1,2,3]
Departments of [1]Electrical Engineering, [2]Psychology, and [3]Radiology

Correlation and causality metrics can be applied to blood-oxygen level dependent (BOLD) signal time series in order to infer neural synchrony and directions of information flow from fMRI data. However, the BOLD signal reflects both the underlying neural activity and the vascular response, the latter of which is governed by local vasomotor physiology. The presence of potential vascular latency differences thus poses a confound in the detection of neural synchrony as well as inferences about the causality of neural processes. In the present study, we investigate the use of a breath holding (BH) task for characterizing and correcting for voxel-wise neurovascular latency differences across the whole brain. We demonstrate that BH yields reliable measurements of relative timing differences between voxels, and further show that a BH-derived latency correction can impact both functional connectivity maps of the default-mode network and activation maps of an event-related working memory (WM) task.

References/Funding Source

Chang, C., Thomason, M.E., Glover, G.H., 2008. Mapping and correction of vascular hemodynamic latency in the BOLD signal. Neuroimage (in press).
NIH P41-RR09784 to GG
NIH T32-GM063495 to CC

Influence of Heart Rate on the BOLD signal: The Cardiac Response Function

C. Chang[1], J. P. Cunningham[1], G. H. Glover[1,2]
Departments of [1]Electrical Engineering and [2]Radiology

It has previously been shown that low-frequency fluctuations in both respiratory volume and cardiac rate can induce changes in the blood-oxygen level dependent (BOLD) signal. Such physiological noise can obscure the detection of neural activation using fMRI, and it is therefore important to model and remove its effects. While a hemodynamic response function relating respiratory variation (RV) and the BOLD signal has been described (Birn et al., 2008b), no such mapping for heart rate (HR) has been proposed. In the current study, we simultaneously deconvolve the effects of RV and HR from resting state fMRI. We demonstrate that a convolution model including RV and HR can explain significantly more variance in gray matter BOLD signal than a model that includes RV alone, and propose an average HR response function that well characterizes our subject population. We find that the voxel-wise morphology of the deconvolved RV responses is preserved when HR is included in the model, and is adequately modeled by Birn et al.'s previously-described respiration response function. We further demonstrate that modeling out RV and HR can significantly alter functional connectivity maps of the default-mode network.

References/Funding Source

NIH P41-RR09784 to GG
NIH T32-GM063495 to CC
NIH-NINDS-R01
Stanford Graduate Fellowship to JPC

BOLD Contrast in the Breast

R. Rakow-Penner[1], L. Pisani[1], S. Oberfoell[1], B. Daniel[1], G. Glover[1]
[1]Department of Radiology

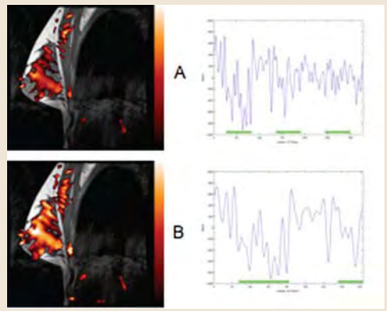

Figure 1. Left: Activation maps from one volunteer. Right: Time series (blue) corresponding to stimulus (green). In A, activation more closely correlated between the first half of the time series but attenuated over the second half. B shows the increased correlation activation map for the first half of the time series.

Introduction: Blood oxygen level dependent (BOLD) contrast imaging applied to breast tumors may provide useful clinical information on tumor oxygenation. We are developing a robust technique for measuring BOLD contrast in the breast.

Methods: A 2D gradient echo spiral pulse sequence, with fat saturation and heart saturation was designed for this study. Pure oxygen interleaved with room air delivered through a nasal cannula provided the BOLD stimulus with a block paradigm of 3 periods over 12 minutes. At 3T we developed our protocol and tested our most robust version on the left breasts of four healthy volunteers. A respiratory belt and pulse oximeter were placed on the volunteers to record respiratory motion and cardiac rate. The BOLD signal time series for each voxel was cross correlated with the periodic stimulus. Sigma and Fourier filters were applied to diminish noise artifact.. Coregistration parameters were evaluated to discount motion as causing periodic correlation with the stimulus.

Results: The figure displays the correlation between the stimulus and the breast tissue of one volunteer. The plots are filtered versions of the time series by frame number in relation to signal intensity of a designated ROI (selected based on activation). The activation maps are superimposed on T1 anatomical images. In two of the four studies, we found an inverse correlation between the stimulus and activation. In the other two volunteers we found a positive correlation to the stimulus.

Discussion: Results at 3T indicate that BOLD contrast in the breast can significantly vary from one person to another. We detected a strong correlation between the stimulus and either a positive or negative BOLD contrast measurement. We believe the results are real and a consequence of either variations in breast vasculature due to menstrual cycle and/or the difference in the fat and water content between volunteers.

References/Funding Source

Oral presentation at the 2008 ISMRM in Toronto, Canada.
NIH P41-RR09784
DOD W81XWH-06-1-0358.

Computational Modeling

A Survival Analysis of Alternative Cancer Risk Reduction Strategies for BRCA1/2 Mutation Carriers

A. W. Kurian[1,2], B. M. Sigal[3], S. K. Plevritis[3]
Departments of [1]Medicine, [2]Health Research and Policy, and [3]Radiology

Background: Women with mutations in the *BRCA1/2* cancer susceptibility genes inherit 5 to 20-fold increased lifetime risks of developing breast and ovarian cancer. Standard risk reduction options include prophylactic oophorectomy (PO), plus prophylactic mastectomy (PM) versus the alternative of high-risk screening with breast magnetic resonance imaging (MRI) and mammography (M). These strategies are variably acceptable to patients, and their efficacy has not been empirically compared; we performed a model-based analysis of their impact on survival.

Methods: We used a Monte Carlo model to simulate clinically relevant scenarios of no intervention, breast cancer screening with annual M and MRI (starting age 25), PM (starting age 25), and/or PO (starting age 40) in 25-year old female *BRCA1/2* mutation carriers. Characteristics of interventions were derived from published literature. We estimated resulting probabilities of death from breast cancer, ovarian cancer, and other causes by ages 70 or 80.

Results: PM at 25 plus PO at 40 yielded the highest survival probability by ages 70 (*BRCA1*, 0.79; *BRCA2*, 0.83; general population, 0.84) and 80 (*BRCA1*, 0.61; *BRCA2*, 0.65; general population, 0.66). Screening starting at 25 plus PO at 40 also yielded high survival probability by age 70 (*BRCA1*, 0.74; *BRCA2*, 0.80; general population, 0.84), and adding PM to this regimen provided little incremental benefit when performed at age 25 (*BRCA1*, 0.05; *BRCA2*, 0.03) or age 40 (*BRCA1*, 0.03; *BRCA2*, 0.02), with similar results by age 80. In the absence of PO, PM at age 25 yielded comparatively low survival probability by ages 70 (*BRCA1*, 0.66; *BRCA2*, 0.79; general population, 0.84) and 80 (*BRCA1*, 0.44; *BRCA2*, 0.61; general population, 0.66). These results are relatively insensitive to varying assumptions about tumor growth rate, and about impact of PO on breast cancer risk and other-cause mortality.

Conclusions: PM at 25 plus PO at 40 yields the highest survival probability for *BRCA1/2* mutation carriers; however, substituting M and MRI screening for PM, in women who have PO at 40, reduces estimated survival probability by only 2-5%. These results may assist patients and physicians to make the often difficult choice between high-risk breast screening and PM.

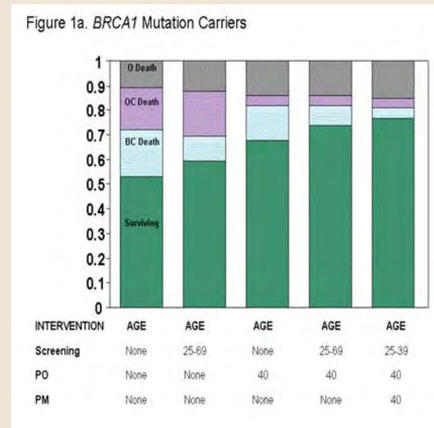

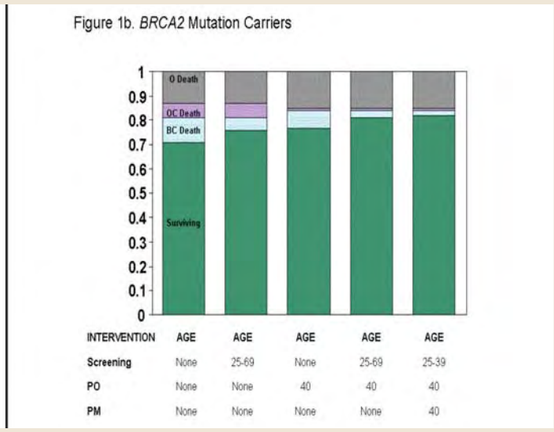

Figure 1a and b. Probability and causes of death, including breast cancer (BC), ovarian cancer (OC), and other causes (O), by age 70: intervention scenarios incorporate screening with mammography and MRI, PM, and PO in 25-year old women with mutations in a) *BRCA1* and b) *BRCA2*

References/Funding Source

NIH R01 CA829040, U01 CA088248, R01 CA66785 to Dr. Plevritis
Stanford Cancer Center 2007 Developmental Research Award in Population Sciences (to Drs. Plevritis and Kurian)
Robert Wood Johnson Foundation 2008 Physician Faculty Scholars Award (to Drs. Kurian and Plevritis)

Modeling the Onset of Fatal Metastases in Lung Cancer

R. S. Lin[1], B. M. Sigal[2], S. K. Plevritis[2]
Departments of [1]Biomedical Informatics and [2]Radiology

Introduction: Evaluating of the effectiveness of CT screening on lung cancer mortality has become a critical issue given divergent interpretations of the current evidence. The goal of this project is to predict the benefit of CT screening on reducing lung cancer mortality using a model of the natural history of lung cancer. This model is developed to predict the tumor size of lung cancer transition to lethal disease from metastases.

Methods: We developed a stochastic model of the onset of fatal metastasis of lung caner based on patient survival data. Growth of the primary tumor and the fatal metastatic burden are modeled as functions of time. The tumor size at the onset of fatal metastasis and the metastatic burden that will cause clinical detection and patient death are formulated in parametric forms. Model parameters were estimated from 30,691 Non Small Cell Lung Cancer cases in the Surveillance Epidemiology and End Results (SEER) database. The model was calibrated to tumor size and stage at clinical detection and patient survival. This model is more stable than existing models under the potential phenomenon of stage migration in lung cancer with advances in detection technology.

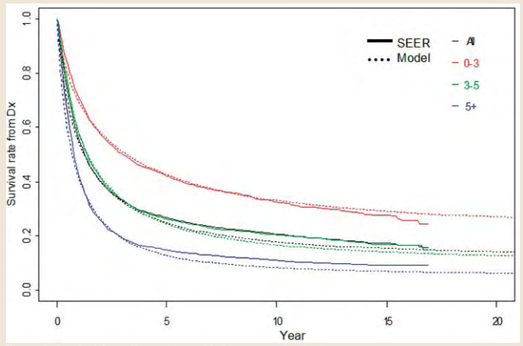

Figure 1. Survival from diagnosis, stratified by tumor size (cm).

Results: The model demonstrated good fit to the distribution of tumor size and stage at clinical detection and patient survival. Figure 1 shows the patient survival predicted by the model versus SEER, stratified by tumor size. The estimated median tumor diameter at onset of fatal metastasis is 10 mm and the estimated survival time from onset of fatal metastasis is 3.6 years. We estimated that 52% of lung cancer cases were detected due to the symptoms of primary tumors whereas the rest were due to metastases.

Future direction: We will use this natural history model to estimate the effect of CT screening on lung cancer mortality and estimate the effect of lung cancer biomarkers on screening outcomes.

References/Funding Source

NIH R01 CA105366
Canary Foundation

Integration of Copy Number and Gene Expression Information of Cancer

A.J. Gentles[1], S.K. Plevritis[1]
Department of [1]Radiology
Stanford University School of Medicine

Various high-throughput technologies exist for measuring changes in expression of genes, and changes in the number of copies of them in cancer genomes. Although there is usually some correlation between the copy number of a gene and its expression level, agreement is generally quite poor. We have developed a novel algorithm to integrate these data types in a unified model that substantially improves the concordant analysis, while providing more detailed hypotheses about changes driving cancer initiation and progression. We model gene expression as a function of both gene copy number, and the expression of upstream regulators, such as transcription factors. This utilizes known biological knowledge databases about regulatory interactions. In addition, we incorporate information on the strength of transcription factor binding motifs in gene regulatory regions, and the location of motifs relative to gene transcription initiation sites. We augment this with known annotated interactions by data from high-throughput protein-protein interaction experiments. Algorithmically, expression of each gene is modeled as a regression on these different data, and we impose sparsity constraints on the model using L1-regularization to reduce over-fitting. The statistical improvement in explaining the expression data is assessed by the proportion of variance explained, i.e. the fraction of actual observed variance in expression that is accounted for by the inferred model parameters. Furthermore, given the identified relationships between expression and copy number, we can refine analysis of copy number variations (CNVs). For example, a change in copy number of gene A can be considered equivalent to a change in copy number of a gene B that regulates it, if the latter change influences the expression of A in an appropriate way. This provides improved information regarding CNVs. Typically, only a subset of tumors from the same cancer share similar CNVs of specific gene loci. Our method permits a more unified view of the genomic changes that underlie cancer phenotypes.

References/Funding Source

NCI Integrative Cancer Biology Program U56 CA112973

Gene Module Regulatory Network Analysis Implicates Stem Cell Signatures in Follicular Lymphoma Transformation

A.J. Gentles[1], A.Alizadeh[2], S.I. Lee[3], B. Shahbaba[1], C.M. Shachaf[4], R. Levy[2], D. Koller[3], S.K. Plevritis[1]
Departments of [1]Radiology, [2]Medicine/Oncology, [3]Computer Science, [4]Microbiology and Immunology

The transformation of follicular lymphoma (FL) to diffuse large B cell lymphoma (DLBCL) is associated with drastically worse prognosis. Mechanisms underlying transformation are poorly understood, and implicate multiple pathways. To better understand the transformation process, we constructed a gene module regulatory network from microarray data on FL and DLBCL samples. Modules that significantly discriminate between FL and DLBCL were identified by supervised classification, in addition to modules that discriminate FL that are known to transform from FL that do not transform. A network of regulatory modules was constructed with a directed edge between pairs of modules if a gene in one module served as a regulator of the other module, as shown in Figure 1. The complete network includes modules that are highly enriched for genes involved in cell cycle progression (lowest False Discovery Rate, FDR=1.2x10-31), proliferation (FDR=2.4x10-25), cellular differentiation (FDR=3.1x10-17), and ribosomal protein activity (FDR=2.8x10-11). Other prominent modules are associated with: immune system function including; T-cell activation and receptor signaling (FDR=9.4x10-10), B-cell development and differentiation (FDR=3.3x10-12), and inflammatory response (FDR=9x10-12); components of the proteasome (FDR=9.3x10-5), hypoxia signaling (FDR=2.5x10-9), and mitochondrial function/oxidative phosphorylation (FDR=4.1x10-6). Known aspects of FL/DLBCL transformation, such as changes attributable to infiltrating T-cell populations were identified and served as internal validation. Core discriminant modules associated with transformation show expression signatures of cellular differentiation states, proliferative drive, deregulation of mitochondrial function, and increased proteasome activity impacting the cell cycle. Importantly, we illustrate how the network of gene modules can be used to generate hypotheses regarding processes driving transformation. This analysis suggests that Pax5 may be a critical factor during transformation of FL cells. In addition, we are able to suggest Bortezamib (a proteasome inhibitor) and Ecteinascidin-743 as potential treatments of FL and transformed DLBCL.

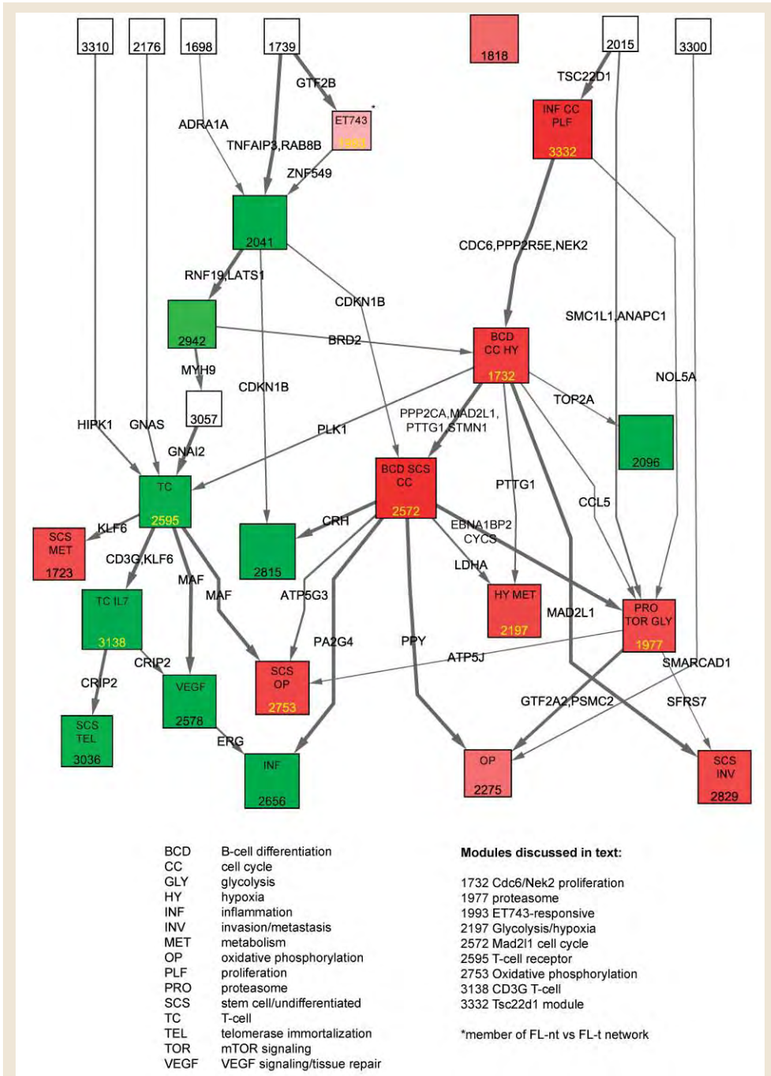

Figure1. Module network underlying follicular lymphoma transformation

References/Funding Source

NCI Integrative Cancer Biology Program U56 CA112973

Reducing the Computational Complexity of Reconstructing Gene Regulatory Networks Using Information Theoretic Approaches

P. Qiu[1], A. J. Gentles[1], S. K. Plevritis[1]
Department of [1]Radiology

Information theoretic approaches are increasingly being used for reconstructing gene regulatory networks from gene expression microarray data. Examples include the relevance network (RelNet), ARACNE, and the maximum relevance minimum redundance network (MRNet). These specific approaches and others start by computing the pairwise mutual information between all possible pairs of genes, resulting in a mutual information matrix. The mutual information matrix is then manipulated to identify regulatory relationships; for example, thresholding is applied in RelNet, the data processing inequality in ARACNE, and the maximum relevance minimum redundance criterion in MRNet. These approaches have been successfully applied to simulated data and real microarray data, identifying regulatory targets and pathways. The most time-consuming step in these approaches is computing the mutual information matrix. For example, in a recently analyzed B-cell data set consisting of 336 samples and 9563 genes per sample (Basso et al, *Nature Genetics* 2005), ARACNE takes about 142 hours to compute the mutual information matrix. In this work, we present two independent methods to reduce the computation time needed to compute the mutual information matrix.

We use spectral analysis to re-order the genes, such that genes that share regulatory relationship are more likely to be close to each other. We then apply a sliding window to examine subsets of the re-ordered genes. Since we compute the mutual information only among genes within the sliding window, only part of the mutual information matrix is computed. Depending on the window size, the computational complexity can be significantly reduced. Although only part of the mutual information matrix is computed, as long as connected genes are close to each other after the re-ordering, the reconstruction performance will not decrease much. With simulated data, we observed that our approach does not incur performance loss in operating regions of high precision and low recall. Using the above mentioned B-Cell data set, we show that with a small amount of reconstruction loss (<10%), our method reduces the computation time by 84%. We also developed a fast software implementation to calculate of the pairwise mutual information matrix based on kernel estimation. We noticed that the calculation of pairwise mutual information involves a few nested loops, which contain a lot of repeated operations. The essential idea of our fast implementation is to switch the order of the nested loops, so that the repeated operations can be pushed out of some of them. Our fast method reduces the computation time by 98%. Combining the two methods, the computation time for the above mentioned B-Cell data set can be reduced from 142 hours to less than 30 minutes.

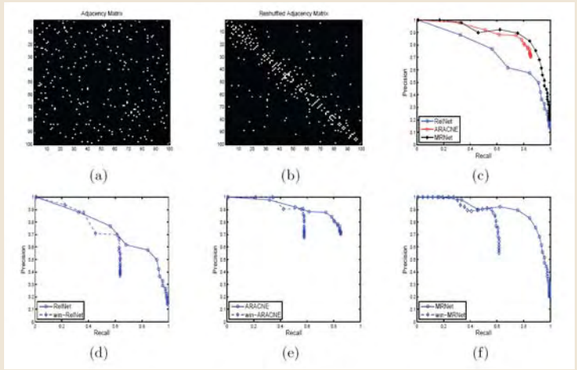

Fig (a) and (b) show effect of gene re-ordering. Fig (c-g) show the performance comparison of three information theoretic approaches and their corresponding versions when the proposed gene re-ordering and sliding window are applied.

References/Funding Source

P. Qiu, A. J. Gentles, S. K. Plevritis, "Reducing the Computational Complexity of Reconstructing Gene Regulatory Networks Using Information Theoretic Approaches", submitted to EURASIP Journal on Bioinformatics and Systems Biology, 2008.
P. Qiu, A. J. Gentles, S. K. Plevritis, "Fast Calculation of Pairwise Mutual Information for Gene Regulatory Network Reconstruction", submitted to Bioinformatics, 2008.
NCI Integrative Cancer Biology Program U56 CA112973

A Semi-supervised Method for Class Discovery and Classification of Microarray Data using Spectral Analysis

P. Qiu[1], S. K. Plevritis[1]
Department of [1]Radiology

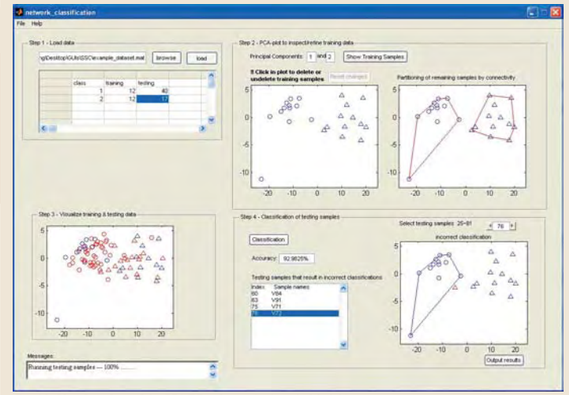

Graphic User Interface of the SPACC software (written in Matlab).

Classification methods are commonly used for mining microarray gene expression data to gain new biological insights. These methods are commonly divided into two categories: unsupervised versus supervised. Unsupervised methods have the ability to discover new classes, because the class label information is not utilized. However, they carry the risk of producing non-interpretable results. On the other hand, although supervised methods always find a decision rule that interprets the separation among different classes, the class label information plays such an important role that it confines the supervised methods by defining the possible classes. Consequently, supervised methods do not have the ability to discover new classes. Outliers and mislabeled samples in the training data may have a large undesirable effect on the classification. The limitations of unsupervised and supervised methods motivated us to propose a semi-supervised classification method, which utilizes the class label information to a less important role so as to perform class discovery and classification simultaneously.

We propose a semi-supervised method called SPACC (Spectral Analysis for Class discovery and Classification). In SPACC, we consider the training samples as inter-connected nodes that form an undirected weighted network. Using spectral analysis, the network is partitioned into two subnetworks in an unsupervised iterative manner, resulting in a top-down binary tree. The class labels are only used to define the criterion to stop partitioning. At the end of the process, the training samples are divided into several subsets, each of which is dominated by one class label. Because multiple subsets can correspond to the same class label, our approach can identify potentially new biologically meaningful subclasses or outliers. Classification of the testing samples can be performed using a variation of the nearest neighbor method. To the best of our knowledge, SPACC is the first approach that can simultaneously perform class discovery and classification. We have demonstrated SPACC's effectiveness on microarray gene expression data of clinical cancer samples. SPACC software is available for download at http://icbp.stanford.edu/software/SPACC/.

References/Funding Source

P. Qiu, "Semi-supervised classification based on network connectivity", invited talks in Integrative Cancer Biology Program (ICBP) Junior Investigator Meeting and Principal Investigator Meeting, 2007.
P. Qiu, S. K. Plevritis, "A Semi-supervised Method for Class Discovery and Classification of Microarray Data using Spectral Analysis", submitted to Bioinformatics, 2008.
NCI Integrative Cancer Biology Program U56 CA112973

Prediction of New Developmentally Regulated Genes Using Boolean Implications

D. Sahoo[1], J. Seita[3], D. Bhattacharya[3], I. L. Weissman[3], S. K. Plevritis[4], D. L. Dill[1,2]
Departments of [1]Electrical Engineering, [2]Computer Science, [3]Institute for Stem Cell Biology and Regenerative Medicine, [4]Radiology

We present a new method to discover developmentally regulated genes using large repositories of publicly available microarray data. The method uses Boolean implications (if-then rules) mined from existing data and conservation across species to predict genes whose expression is established as precursor cells differentiate to their progeny in the absence of data from cells at intermediate steps of development, which have not been previously identified. The algorithm was validated by applying it to B cell development, for which most developmental stages between hematopoietic stem cells and fully differentiated B cells are known and can be isolated. The algorithm predicted 19 genes that are expressed after the c-kit+ progenitor cell stage and remain expressed through CD19+ mature B cells. These predictions were validated by sorting 12 mouse hematopoietic populations at different stages of development ranging from hematopoietic stem cells to germinal center B-cells using fluorescence activated cell sorting. Empirical measurement of the expression of 14 of these predicted genes using qRT-PCR confirmed that the expression of 12 of these genes is indeed stably established during B-cell differentiation. Through combined inclusion of CD19 and AID, we expanded our list of predicted developmentally regulated genes to 62. Thirty-three of these genes have been ablated in mice, and 18 of these mutants have been reported to have defects in B cell function or development. Of the remaining 15 knockout strains, it is possible that B cell defects exist but have not been extensively evaluated. The expression patterns of five more selected genes were confirmed using qRT-PCR experiments. This study validated our prediction algorithm on B cell development. Based on this outcome, the method appears to have the potential to predict novel genes that are expressed early in other developmental pathways that are less well characterized than B cells.

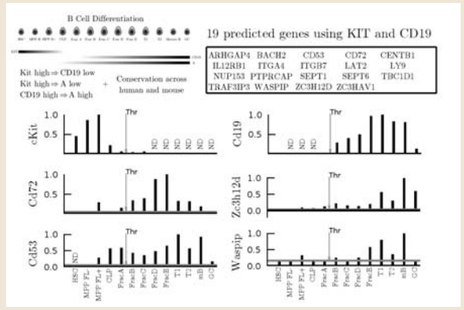

The prediction algorithm using Boolean implications is described in the top left. Top right space shows the 19 genes predicted using cKit and Cd19. Six qRT-PCR experiment is shown below that confirms the predicted gene expression pattern (turns on before Frac B and stay on till mature B cell). The threshold derived from HSC and MPP FL- stages of development is pointed by an arrow in each plot. The threshold for cKit is determined using its expression levels in mature B cell and Germinal Center B cell.

References/Funding Source

D. Sahoo, J. Seita, D. Bhattacharya, IL. Weissman, SK. Plevritis, DL. Dill. Prediction of New Developmentally Regulated Genes Using Boolean Implications. Nature Genetics (Submitted).
NIH award 5U56CA112973 (to S.K.P)
NIH award 5R01CA086065 (to I.L.W.)
NIH fellowship 5K01DK078318 (to D.B)
the California Institute of Regenerative Medicine fellowship (to J.S.).

Monte Carlo Simulation of the Mayo CT Study

B. M. Sigal[1], S. K. Plevritis[1]
The Department of [1]Radiology
Stanford University School of Medicine

Lung cancer is the leading cause of cancer death among US men and women. The effectiveness of the low-dose spiral computed tomography (CT) screening in reducing death from lung cancer is not known. Several randomized control studies are on the way, and the results are expected for several years. Given the differing interpretations over the current evidence underlying CT screening, we embarked on a decision analytic approach to predict the effectiveness of CT screening. In this study we developed a computer simulation model to simulate the Mayo CT study in order to estimate the lung cancer mortality reduction that would have been predicted by this study if it had been designed as a randomized control trial with a usual-care arm.

Mayo CT study is a prospective cohort (one arm) study that in 1999 enrolled 1,520 individuals aged 50 yr or older who had smoked 20 pack-years or more. Each participant underwent baseline CT screen and four subsequent annual screens. In total 66 persons were diagnosed with lung cancer during the study and 20 lung cancer deaths were reported. To simulate Mayo CT study we used the natural history of lung cancer model developed previously based on the Mayo Lung Project. CT detection threshold and delay between the time cancerous nodule first seen on the screen and the time of final diagnosis were estimated from Mayo CT data.

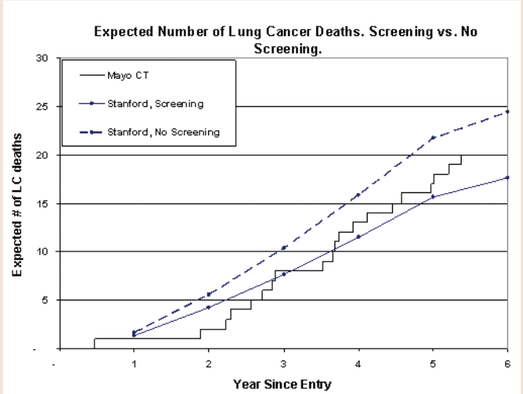

Expected number of lung cancer deaths in Mayo CT study in the presence and absence of screening.

We simulate both screened arm and hypothetical control or unscreened arm. Our simulation tends to underestimate the total number of cancers expected: 66 in Mayo CT versus 30 simulated. This could be indicative of over-diagnosis. To support this possibility, we show that our results are in a much better agreement when comparing advanced stage lung cancers: 18 Mayo CT versus 13.5 simulated. We also are in a good agreement with Mayo CT with respect to size and stage distribution for screen detected cancers. Compared to 20 lung cancer deaths in Mayo CT we predict 17.6 for screened arm, and for the hypothetical unscreened arm we estimate 24.4 deaths. Our analysis suggests that 6.8 deaths were prevented by CT screening in the Mayo CT study.

References/Funding Source

The Lucas Foundation

Bayesian Gene Set Analysis

B. Shahbaba[1], R. Tibshirani[2], S. K. Plevritis[1]
Departments of [1]Radiology and [2]Health Research and Policy
Stanford University School of Medicine

Gene expression microarray technologies provide simultaneous measurements of a large number of genes. Typical analyses of these data focus on individual genes, but recent work has demonstrated that evaluating changes in expression across predefined sets of genes produces more robust results. We introduce a new methodology for identifying gene sets that are differentially enriched under varying experimental conditions. Our approach uses a hierarchical Bayesian framework, shown in Figure 1, where the expected value of expression, y_{sgc}, for gene g in set s under condition c is modeled as the sum of its overall expression level, α_{sg}, and the change in the expression, β_{sgc}, due to condition c. Variation of gene expression under different conditions is captured by the variation of β_{sgc} as c changes. We treat the variance of β_{sgc} as a hyperparameter, τ^2_{sg}, which shrinks towards zero if the gene is not significant. Moreover, all hyperparameters τ^2_{sg} associated with genes in set s are controlled by a higher level hyperparameter, η^2_s, which itself shrinks towards zero if the set as a whole is not significant. We measure the enrichment of a gene set based on the magnitude of its corresponding hyperparameter, η^2. Using simulated data, we compare our proposed method to alternative approaches, such as Gene Set Enrichment Analysis (GSEA) and Gene Set Analysis (GSA). Our approach provides the best overall performance. We also show the application of our method to experimental data based on p53 mutation status in cancer cell lines.

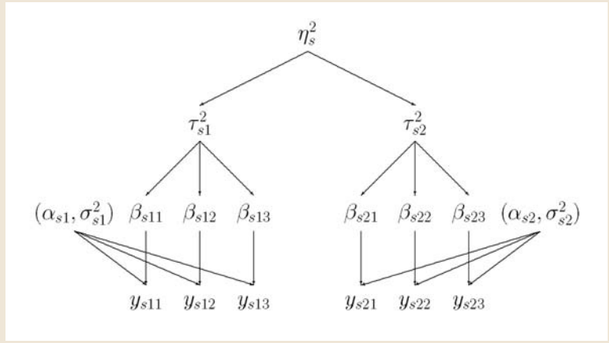

Figure 1: Schematic model representation. Expression level of two genes in set s under three different conditions are measured.

References/Funding Source

The Lucas Foundation

A Modified Dirichlet Process Mixture Model for Clustering Phosphopeptides Based on Their Response to Anti-Cancer Drug Perturbation

B. Shahbaba[1], E. Prenosil[2], A. Jain[2], S. K. Plevritis[1]
The Department of [1]Radiology, Stanford University School of Medicine, Stanford, CA
[2]Louis Warschaw Prostate Cancer Center, Los Angeles, CA

We present a new clustering method for identifying coordinated changes in tyrosine phosphorylation events in response to perturbation of the EGFR kinase signaling pathway. Several challenges posed by the experimental data make standard clustering methods inefficient. One major challenge is that the data include multiple replicates of the same phosphopeptide (generated from several experimental repeats) with some difference in patterns due to inherent variation in biological systems. Treating these replicates as independent observations is not appropriate and could lead to assigning a single phosphopeptide to multiple clusters. Another major challenge is that the number of clusters (i.e., distinct patterns) is not known a priori. To address these issues, we propose a modified version of Dirichlet process mixtures for clustering phosphopeptides. We apply our clustering algorithm to experimental data that measures the effect of EGF and erlotinib on tyrosine phosphorylation events in the A431 cell line. The identified clusters are shown in Figure 1. Five members of each cluster were independently tested and validated to belong to their assigned cluster.

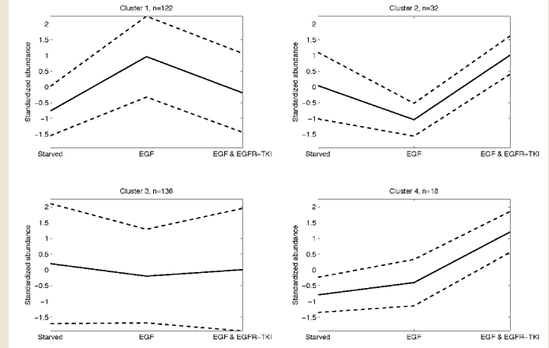

Figure 1. Identified clusters on phosphopeptide data

References/Funding Source

The Lucas Foundation

A Bayesian Nonparametric Method for Model Evaluation: Application to Gene-Disease Studies

B Shahbaba[1], A. J. Gentles[1], J. Beyene[2], S. K. Plevritis[1], C.M.T. Greenwood[2]
The Department of [1]Radiology, Stanford University School of Medicine, [2]Department of Public Health Sciences, University of Toronto, Ontario, Canada

Statistical models applied to gene-disease studies commonly assume linear relationships (between disease and risk factors) and simple distributional forms (by relying on asymptotic methods) for inference. However, when the sample size is small (which is the case in many health related studies), inference using traditional asymptotic models can be problematic. Moreover, the gene-disease relationship is not always linear. In most cases, we need to explicitly choose to investigate nonlinearity, for example, by including additional terms (e.g., nonlinear transformations of predictors) into our model. This is not a trivial task. Also, when the sample size is small, there is little power to correctly detect and model a nonlinear relationship using the traditional methods. In this work, we studied the problem of evaluating models (i.e., identifying significant predictors). We use a nonparametric Bayesian model based on Dirichlet process mixture of linear model, and we demonstrate the advantages of this approach particularly when the sample size is small and/or the true model is nonlinear as shown in Figure 1. We evaluate our approach on simulated data and find that it substantially performs better than alternative models. We also apply our method to two real studies: diagnosis of conventional high-grade nonmetastatic osteosarcoma, and survival in Burkitt's lymphoma.

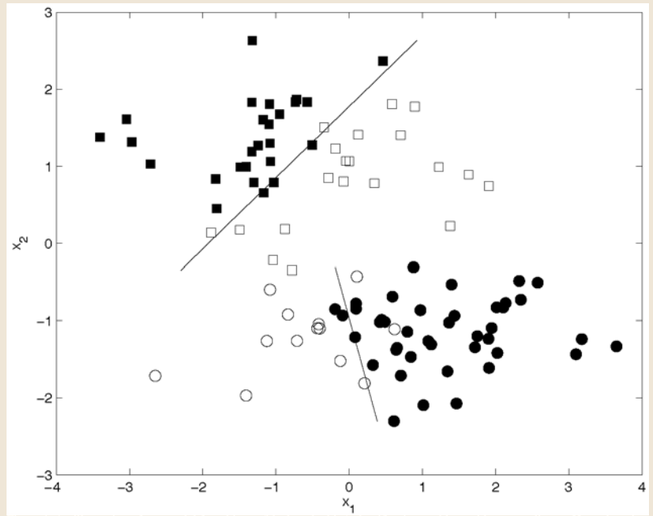

Figure 1. An illustration of our model for a binary (black and white) classification problem with two predictors. Here, the mixture has two components, which are shown with circles and squares. In each component, a logistic regression model separates the two classes into "black" or "white" with a linear decision boundary.

IMPACT OF TUMOR VOLUME DOUBLING TIME AND BREAST DENSITY ON MAMMOGRAPHY SENSITIVITY IN WOMEN AGES 40 TO 49 YEARS

S. BAILEY[1], B. SIGAL[1], S. PLEVRITIS[1]
THE DEPARTMENT OF [1]RADIOLOGY, STANFORD UNIVERSITY SCHOOL OF MEDICINE

Conventional screening mammography has been shown to reduce breast cancer mortality among women 50 to 69 years of age but its value among younger women is controversial. Compared to older women, breast cancer incidence is lower in younger women but the number of life years saved per breast cancer patient can be higher. One factor contributing to the lowered performance of screening mammography in younger women is its reduced sensitivity which is attributed to faster tumor growth and greater mammographically opaque breast tissue in younger women.

In this study, we evaluated the relative impact of faster tumor growth and greater breast density of younger women on mammography screening outcomes, specifically sensitivity and breast cancer mortality. This was done in a two step process. Fist, we estimated age-specific mammographic detection thresholds (DT) and tumor volume doubling times (TVDT). DT served as a measure of breast density. Age-specific DT and TVDT estimates were derived using a computer screening model that was calibrated across multiple U.S. birth cohorts to SEER breast cancer incidence and tumor sizes data from Breast Cancer Surveillance Consortium (BCSC). Second, we estimated the impact of a greater DT and a smaller TVDT in women 40 to 49 years compared to women 50 years of age and older on screening sensitivity and breast cancer mortality in a single birth cohort simulation model, as demonstrated in Figure 1.

The estimated relative contributions of greater breast density and faster tumor growth to lower program sensitivity in women 40 to 49 years compared to women 50 to 69 years are 79% and 21%, respectively, with comparable contributions of each to the breast cancer mortality reduction. Our results suggest that breast density is the primary factor for the lowered performance of screening among women 40 to 49 years of age, compared to women 50 to 69 years of age. The results underscore the importance of continued efforts to improve imaging in young women with dense breast tissue.

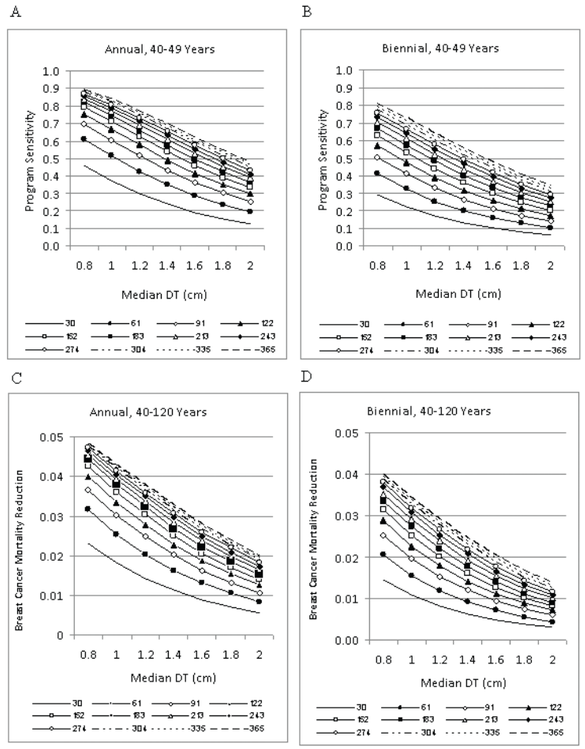

Figure 1: Impact of DT and TVDT on program sensitivity for annual screening (A) and biennial screening (B), and on breast cancer mortality reduction for annual screening (C), and biennial screening (D).

REFERENCES/FUNDING SOURCE

NCI U01 CA88248
Postdoctoral Research Fellowships in Advanced Techniques for Cancer Imaging and Detection

AUTOMATED QUANTIFICATION OF AORTOILIAC ANGULATION FOR CT ANGIOGRAPHY (CTA) OF ABDOMINAL AORTIC ANEURYSMS

B. RAMAN[1], R. RAMAN[2], S. NAPEL[2], G. D. RUBIN[2]
DEPARTMENTS OF [1]MEDICINE, [2]RADIOLOGY
STANFORD UNIVERSITY SCHOOL OF MEDICINE

Purpose: The degree of angulation of the infrarenal aorta and iliac arteries is an important factor in assessing eligibility for endovascular aneurysm repair (EVAR). We developed a 3D analysis algorithm to reduce the inter- and intra-observer variability of measurement of aortoiliac angulation.

Materials and Methods: The user must identify only four points at the superior boundary of the proximal neck, the superior boundary of the aneurysm, and 20 mm into each common iliac artery. The algorithm then calculates a centerline through the aorta. Best fit line segments approximating the centerline are derived, allowing measurement of angulation between line segments at the proximal neck, mid-aneurysm, and iliac artery origins. We evaluated the precision of our algorithm by comparing the variability of manual and automated measurement in CTA data from 11 patients. To assess accuracy, we created phantoms that simulated realistic aortic morphology as follows: a segmentation of the aorta was first obtained from one patient's CTA, and then computationally straightened to produce an aorta without angulation. Known amounts of angulation were then introduced computationally.

Results: For manual measurement, intraobserver variability was 8.23 ± 5.00° and interobserver variability was 5.59 ± 2.52°. For the automatic algorithm, intraobserver variability was 0.57 ± 0.77°($p<0.01$) and interobserver variability was 0.36 ± 0.38° ($p<0.01$). There was no statistically significant difference between manually and automatically measured angles ($p<0.05$). In phantoms, the mean error between the actual and measured angles was 0.86 ± 0.53 degrees. There was no statistically significant difference between angles measured by the automated algorithm and the known angle measurements ($p<0.05$).

Conclusions: Our automated algorithm reduces the variability in angle measurement to very low values, while maintaining good accuracy and reducing user interaction time. Our algorithm has the potential to enhance the clinical utility and reliability of CTA for preoperative assessment for EVAR.

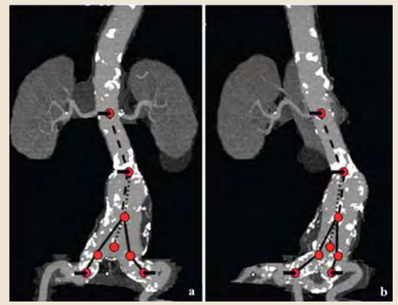

Antero-posterior (a) and oblique lateral maximum intensity projections (b) through the aorta and common iliac arteries. Black arrows indicate the user defined points that are used to delineate the boundaries of segments of the infrarenal aorta. The points that are subsequently calculated by the algorithm are shown as solid red circles. The four angles calculated by the algorithm are projected onto the MIP image: The proximal neck angle (dashed line), aneurysm angle (dotted line) and right and left common iliac angles (solid lines).

REFERENCES/FUNDING SOURCE

NIH 1RO1HL58915
NIH 1RO1HL67194

SEMI-AUTOMATED QUANTIFICATION OF THE MASS AND DISTRIBUTION OF VASCULAR CALCIFICATION USING MULTIDETECTOR CT

R. RAMAN[1], B. RAMAN[2], S. NAPEL[1], G. D. RUBIN[1]
THE DEPARTMENTS OF [1]MEDICINE AND [2]RADIOLOGY
STANFORD UNIVERSITY SCHOOL OF MEDICINE

Purpose: We developed a fast semi-automated method for quantifying the true mass and distribution of calcium in the systemic arteries without the need for separate calibration scans for each level of arterial contrast enhancement and without the need for calibration with complex phantoms.

Materials and Methods: Our quantification algorithm consists of two stages. First, the brightness-volume product (BVP) of each detected fragment is calculated using multiple thresholds. Second, these measurements are extrapolated to calculate BVP at a threshold of zero (water intensity). In-scan standards are then used to calculate the mass. This method corrects for arterial contrast enhancement to obtain the true mass of each fragment. We evaluated accuracy using phantoms and prospectively and retrospectively evaluated the algorithm in volunteers and patients, respectively.

Results: R2 for actual vs. measured mass in phantoms was 0.98; the absolute and relative errors were 1.2 mg and 9.1%, respectively, with no difference in error between unenhanced and contrast-enhanced scans ($p=0.95$). In a prospective study in 21 asymptomatic volunteers (10 women, mean age 60 years), calcium mass quantification in the extracoronary arteries had an interscan variability (v) of 24.9 ± 33.4 mg (6.3 ± 3.5%) compared to a significantly higher v of 991 ± 1820 units (45.2 ± 21.1%) for Agatston scoring (AS) ($p<0.01$). In coronary arteries, v was 55.5 ± 14.2 mg (10.9 ± 9.3%) while AS had a significantly higher v of 27.7 ± 56.5 units (23.7 ± 32.3%, $p<0.01$). In a retrospective study of CT scans of 10 patients with and 5 patients without known vascular disease, mean calcified mass was 321.3 mg (45-1443) and the mean number of fragments was 21 (6-254), with 67.8% of calcium in the infrarenal aorta.

Conclusion: Our method accurately quantifies the mass and distribution of calcification in simulated arteries, and can be applied in vivo with low interscan variability in both noncontrast and contrast-enhanced scans.

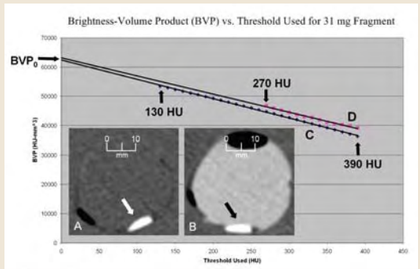

Axial CT image of a 31 mg calcium fragment (arrows) on the surface of an aortic phantom filled with water (A) and filled with contrast medium (B, 230HU). The graph shows the BVP as a function of threshold used to segment the calcium fragment. BVP values are calculated and plotted for thresholds every 10 HU starting at the calcium detection threshold. For the water-filled phantom, a best fit line (C) is calculated and projected back to determine the theoretical BVP of the fragment at a threshold of 0 HU (BVP). The process is repeated for the same fragment in the contrast filled phantom (Line D). The higher luminal contrast (230 HU) necessitates a higher minimum threshold of 270 HU. The extrapolated BVP0 shows little variation (1.3%) between unenhanced and contrast-enhanced scans.

REFERENCES/FUNDING SOURCE

Raman R, Raman B, Napel S, Rubin GD. Semiautomated quantification of the mass and distribution of vascular calcification with multidetector CT: method and evaluation. Radiology. 2008 Apr;247(1):241 50. Epub 2008 Feb 21.
NIH 1RO1HL58915 and NIH 1RO1HL67194

Automated Detection of Peak Blood Velocity (PBV) Using a Novel Transducer Array and Intelligent Software

J. Faruque[1], O. Oralkan[1], R. B. Jeffrey[2], B. T. Khuri-Yakub[1], S. Napel[2]
Departments of [1]Electrical Engineering, [2]Radiology
Stanford University Schools of Medicine and Engineering

Purpose: Ultrasound using pulsed Doppler for detection of PBV (correlated with carotid stenosis) is subject to inter- and intra-operator variability. We are developing an operator-independent method, using 5 parallel cross-sectional color Doppler images to be acquired from a capacitive micromachined ultrasonic transducer (cMUT) array. Our approach to PBV determination could reduce variability and make accurate and reproducible determination of stroke risk more widely available.

Materials and Methods: We developed software that automatically computes the vessel trajectory, Doppler angles and angle-corrected (AC) peak velocities for the 5-plane transducer. We simulated a straight tube with a concentric stenosis containing a time-varying velocity field and from it computed color Doppler ultrasound images on 5 parallel planes at a 35° angle to the vessel. We compared AC velocities to the simulated velocities. We also tested our method using an ultrasound vessel phantom, a conventional single-plane transducer, and a mechanical support system, to simulate the output of the 5-plane transducer, comparing the AC PBV to that obtained by the conventional longitudinal single-plane approach.

Results: Simulations: the linear regressions of the AC vs. known velocity magnitudes had slope=0.994 and R2=0.999, and slope=0.973 and R2=0.999, for the known (35°) and estimated (33.2°) Doppler angles, respectively. Using the estimated Doppler angle, AC PBV was estimated to within 1% of the known value, and, in the top 10% of velocities, the magnitude of the error was 2.682% ± 0.990% of the known velocities. Phantom: the PBVs were 11.0, 11.4, 10.6, 11.6, and 14.2 cm/s, at Doppler angles of 25, 30, 40, 45, 60 degrees respectively. PBV computed using the conventional approach was 11 cm/s.
Conclusions: PBVs can be determined automatically, accurately and precisely at a Doppler angle of 35°. Phantom experiments show that PBV using our method and the conventional method give similar results at Doppler angles below 45°.

Phantom experiment and results. (a). The experimental setup consists of (1) a vessel phantom simulating a single artery (courtesy of the Taylor lab) and (2) a transducer connected to (3) a Siemens Antares ultrasound machine. (b). Close-up image of the transducer (2) and phantom (1). The ends of the straight vessel phantom (3) are connected through tubes to a peristaltic pump to obtain pulsatile flow. A fixture (4) holds the transducer in place at a specified angle and allows for precise translation along the flow channel. (c). Plot showing the percent difference between the velocities determined using the conventional method and our method, as a function of known Doppler angle. As expected, the error increases with Doppler angle.

References/Funding Source

Bio-X Interdisciplinary Initiatives Program at Stanford
NIH Training Grant in Biomedical Computation
Siemens Medical Solutions, Ultrasound Division, Mountain View, CA

Tool to Incorporate Semantic Annotation and Markup of Images into the Research/Clinical Workflow

D. L. Rubin[1,2], C. F. Beaulieu[1], C. Rodriguez[1], P. Shah[3]
Departments of [1]Radiology, [2]Medical Informatics, Stanford, and [3]Computer Science

Purpose: Advances in radiology increasingly depend on analyzing quantitative and qualitative features of images; however, this information is currently not recorded in way that can be processed by computers. We developed an open-source tool, *iPad*, to enable researchers and clinicians to create semantic annotations on radiological images, making the image content computer-accessible.

Materials and Methods: *iPad* is a plug-in to OsiriX, an open-source image viewing application. It permits users to describe images and image regions using a graphical interface. In addition, *iPad* semi-automatically maps user textual descriptions to RadLex. *iPad* uses an ontology to check that the semantic content of the image annotations is appropriate to the image and that annotations are syntactically-complete. Two radiologists used *iPad* to annotate 10 radiological images acquired as part of a research study, and they evaluated *iPad* qualitatively in terms of usability and utility, compared to unassisted collection of image metadata.

Results: The radiologists reported that *iPad* enabled them to annotate the study images efficiently using a similar workflow to which they are accustomed, completing the 10 cases within 45 minutes. *iPad* collected detailed structured information about image findings and anatomy from the radiologists, but they reported that the manner in which it accomplishes this task did not hinder their work. *iPad* efficiently produced computer-accessible structured output of image measurements and observations. Based on these preliminary results with *iPad*, we believe such annotation tools can be introduced into the research workflow, as well as into clinical practice in the future.

Conclusions: *iPad* enables radiologists to create a structured description of image contents, thereby facilitating the use of image features in research projects that seek to discover relationships between clinical information, disease diagnosis, and prognosis. Providing such structured and computer-accessible format for image content will enable future data mining in large image-containing clinical databases.

iPad screenshot and workflow. An image is loaded in OsiriX (left screen) and geometric regions of interest are drawn (shown as rectangles in the image). The users types their observations about anatomy and abnormality in the iPad window (middle screen) while simultaneously receiving feedback from iPad about their annotation (e.g., controlled terms and spelling errors are highlighted). The annotations are saved as XML files in the AIM format (right).

References/Funding Source

Rubin DL, Rodriguez C, Shah P, Beaulieu C: iPad: Semantic Annotation and Markup of Radiological Images. Proc AMIA Symp 2008.
cancer Biomedical Informatics Grid (caBIG) Imaging Workspace, subcontract from Booz-Allen & Hamilton, Inc.
0970 370 X277 1390

Uncluttered Single-Image Visualization of Abdominal Aortic Vessel Tree using Global Optimization Methods

J. Won[1], J. Rosenberg[2], G. D. Rubin[2], S. Napel[2]
Departments of [1]Electrical Engineering and [2]Radiology

Purpose: We aim to develop a method to visualize the abdominal aorta and its branches, obtained by CT or MR angiography, in a single 2D image without any branches crossing each other.

Materials and Methods: The visualization problem is formulated as an optimization problem that finds a tree of bounding boxes of the flattened centerlines most similar to the anterior-posterior projection of the input, while not introducing intersection among the boxes. The optimization algorithm minimizes the distortion score regarding the deviation from the input and the overlap of the bounding boxes. The output of the algorithm is used to produce a stylistic visualization, made of the 2D centerlines modulated by the associated diameter information, on a plane. We performed a preliminary evaluation by asking 3 radiologists to label 10-13 arterial branches on 30 images produced by the algorithm. Each of 5 patients was presented in 6 different variant images, selected from 10 variants with the 3 lowest and 3 highest distortion scores. For each label, they assigned confidence and distortion ratings (low/med/high).

Results: The labeling accuracy of the three readers were 93.4%, 94.5%, and 95.4%, respectively. The corresponding 95% confidence intervals were respectively 90.4–95.7%, 92.7–97.3%, and 91.7–96.6%, for the 366 branches of the 30 visualizations. For the 1098 total samples (366 branches × 3 readers), the subjective distortion ratings were as follows: 77.4% were low. 10.5% were medium. 12.1% were high. The confidence ratings were as follows: 5.56% were low. 16.5% were medium. 77.9% were high. The algorithmic quantitative metrics for a visualization were significant predictors of a reader's subjective distortion rating (PA-GEE model, $p < .0001$).

Conclusions: Our algorithm for eliminating misleading false intersections in 2D projection of abdominal aortic tree conserves overall shape and does not lower the identifiability of the branches.

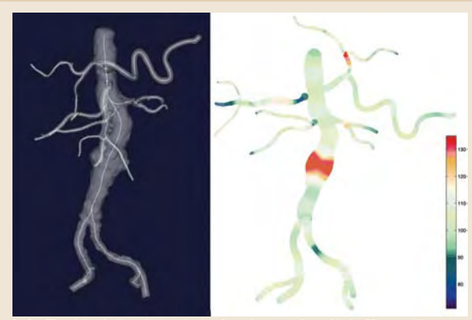

Left – The abdominal aortic vessel tree of a patient, together with the 3D centerlines, seen in the anterior-posterior viewing direction. Right – The Uncluttered Single-Image Visualization of the same vessel tree, produced using our stylistic renderer. The vessel segment widths were drawn proportionally to the associated vessel radii and color-coded by the relative percentage to the median radius of each segment.

References/Funding Source

Accepted for presentation at the 94th Annual RSNA, Chicago, 2008.
NIH grant 1R01HL67194

3D Endovascular Guidewire Reconstruction from a Single Fluoroscopic View Using the 3D Vessel Tree as a Prior

M. Kukuk[1], G. Chuyeshov[1], S. Napel[1]
Department of [1]Radiology

Purpose: To reconstruct in 3D the fluoroscopic projections of a guidewire in the context of a prior reconstruction of a vessel tree obtained from a CT acquisition.

Materials and Methods: We first compute the centerlines of the vessel tree and define all paths that connect its root to an endpoint. Pixels above a threshold in a mask-subtracted fluoro image are backprojected through the volume containing the centerlines, forming rays in the direction of the x-ray source. For each path, the 3D point on the ray closest to it is recorded along with a score that decreases exponentially with distance. Each path is then divided into short subsegments; for each, a density value is computed as the sum of all scores associated with that subsegment, normalized by its length. The wire is then reconstructed by considering all 3D points belonging to the longest continuous run of subsegments above a certain density. Testing was performed by simulating fluoro images of a wire by forward projecting subsections of smoothed centerlines and adding time-varying noise from real fluoro images. We simulated the wire insertion into 8 paths by iteratively increasing the length by 10 mm and estimated each wire's location at 324 uniformly distributed C-arm angles.

Results: A prediction containing more than one vessel was counted as an ambiguity. For a total of 4600 wires, the prediction was correct within 2 subsegments 50% of time w/o ambiguity, correct within 2 subsegments 79% of the time with ambiguity and incorrect 21% of the time.

Conclusion: The 3D location of an endovascular guidewire can correctly and uniquely be predicted in 50% of the cases. As expected, some projections (29%) through the complex vessel tree resulted in ambiguities. However, in these cases the number of predicted locations was small and ambiguities were resolved as the wire advanced.

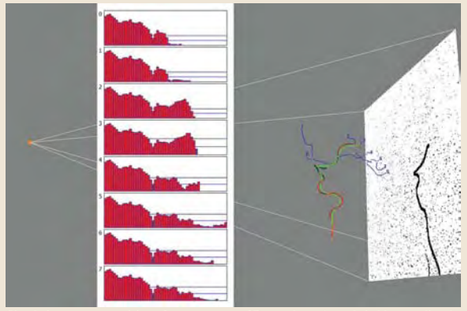

Simulation setup comprising of a x-ray source, 3D vessel tree (vessels in blue, predicted vessel in red and simulated wire in green) and fluoroscopic image. For each path (0 -7) from the root to an endpoint the scoring function is given, showing the score for each subsegment as a vertical red bar. A blue bar indicates a significant (more than 50%) drop in score with respect to the average of the previous six scores (indicated as the top horizontal blue line). Note how all scores drop significatnly at segment #22, where the wire passes the bifurcations leading to endpoints 4-7. While for paths 4-7 this represents a global minimum, it represents only a local minimum for all other paths, as the score picks up again to exceed the top blue line. For path 3, a second drop occurs at the very end, indicating that the wire reached this endpoint of the vessel tree.

References/Funding Source

Siemens Medical Solutions, Inc.

Digital Cleansing of Contrast-Opacified Colonic Residue Using Material Transition Models

U. K. Reddi[1], S. Napel[2], C. F. Beaulieu[2]
Departments of [1]Computer Science and [2]Radiology

Purpose: Current research in virtual colonoscopy aims for greater patient compliance and increased specificity of computer-aided detection (CAD) of polyps by allowing a less strict colon preparation wherein the patient intakes contrast agents to opacify (tag) fecal residue and water. The goal of our research is to develop a segmentation technique that digitally removes the 'tagged materials' thus ensuring a cleansed lumen for visualization and CAD.

Materials and Methods: Partial volume voxels at the different material transitions (air-tissue, air-tagged, tissue-tagged and air-tissue-tagged) are detected and addressed as follows. Each voxel in the colon is assumed to be comprised of three materials (air, tissue, tagged) in varying fractions. By considering CT vs. Gradient-CT values, models (arch model at two-material transitions and parachute model at three-material transitions) are constructed that best correspond to the behavior of CT values at material transitions. For each colonic edge voxel, its immediate neighborhood in the gradient direction is sampled and the pertinent model is fitted to estimate the model parameters (L, H for the arch model and L, M, H for the parachute model). Finally, the model is used to estimate the material fractions in each voxel in order to digitally replace the tagged fraction of the voxel with air.

Results: Applying the two-material transition model to colonic edge voxels resulted in the proper reconstruction of the mucosal layer. However, cleansing is adversely affected at thin haustral folds containing tagged material and artifacts that resemble a bath-tub ring are formed at three-material transition regions.

Conclusions: The thin haustral folds require special processing still under development, and the artifacts caused by not incorporating the three-material transition model, though small in size (< 5 mm), unfavorably affect the sensitivity of CAD.

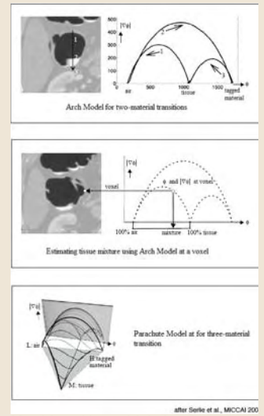

Material transition models in the colon.

References/Funding Source

Serlie, et al. "Computed Cleansing for Virtual Colonoscopy Using a Three-Material Transition Model", MICCAI 2003
NIH/NCI Grant RO1CA72023 "Three Dimensional Spiral CT Colonography"

Identifying the Human Optic Radiation Using Diffusion Imaging and Fiber Tractography

A. J. Sherbondy[1], R. F. Dougherty[2], S. Napel[3], B. A. Wandell[2]
Department of [1]Electrical Engineering, [2]Psychology, [3]Radiology

Purpose: Measuring the properties of the white matter pathways from retina to cortex in the living human brain will have many uses for understanding visual performance and disabilities. We use diffusion tensor magnetic resonance imaging (DTI) and a novel fiber tractography (DTI-FT) method, ConTrack, to identify Meyer's loop in the optic radiation (OR) in the living human brain.

Methods and Materials: We used our previously published method, ConTrack (Sherbondy, et al, 2008) to identify the most likely pathway between the lateral geniculate nucleus (LGN) and the calcarine sulcus in 8 human subjects studied with a diffusion-weighted single-shot spin-echo, echo-planar imaging sequence (63ms TE; 6s TR; 260mm FOV; 128x128 matrix) at two b values (0, 800 s/mm^2). In each of the 16 hemispheres, we compared key OR landmarks to locations derived using dissection methods (Ebeling & Reulen, 1988). In order to compare the OR estimated by ConTrack with the results from dissection studies, we identified the following anatomical landmarks: anterior tip of the temporal pole (TP), anterior tip of Meyer's loop (MLa), anterior tip of the temporal horn (TH), and the posterior tip of the occipital pole.

Results: The most anterior position of the Meyer's loop was found to be an average distance of 28mm from the temporal pole, in agreement with the dissection results of Ebeling et al. Furthermore, the measurements of the distance between the anterior location of the Meyer's loop and the occipital pole as well as the location of this point of the OR with respect to the tip of the temporal horn agree quite well with the dissection results.

Conclusions: Our approach improves upon previous methods, which, in most cases, cannot track Meyer's loop at all, and is the first method to be shown to be consistent with quantitative measurements made by high quality dissection techniques.

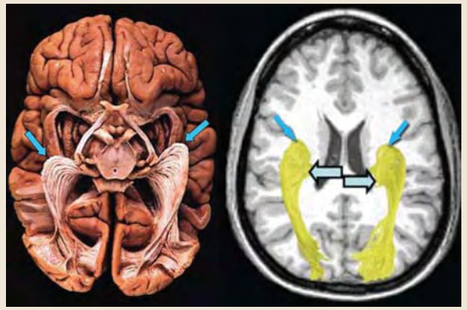

(left) Dissection of human brain (courtesy of University of Iowa Virtual Hospital) showing Meyer's loop (diagonal blue arrows). (right) Fiber tracts (yellow) corresponding to Meyer's loop, as estimated by our algorithm on one of 8 subjects studied with diffusion weighted MRI, superimposed on a T1-weighted image. Horizontal arrows indicate the LGN.

References/Funding Source

A. J. Sherbondy, R. F. Dougherty, S. Napel, and B. Wandell, "Identifying the human optic radiation using diffusion imaging and fiber tractography." Journal of Vision, Submitted.
NIH RO1 EY015000-01

Comparison of Automated Centerline Estimation Algorithms for Femoropopliteal Artery Occlusions

D. N. Tran[1], J. E. Roos[2], T. Rakshe[2], M. Straka[2], J. Rosenberg[2], S. Napel[2], D. Fleischmann[2]
Departments of [1]Medicine and [2]Radiology

Purpose: Existing centerline-extraction algorithms needed to generate curved planar reformations (CPR) in lower extremity CTA consistently fail in severely diseased and occluded arterial segments. We aimed to assess the precision of two new shape-based algorithms in patients with femoropopliteal artery occlusions.

Materials and Methods: Twenty-four patients (9m/15f, mean 75yo, range 30-89yo) with femoropopliteal artery occlusions (38 total, mean 120mm, range 15-398mm) were retrospectively identified. Centerlines of occluded segments were manually determined by four readers and the mean of them served as the reference centerline. The knowledge-based (KB) algorithm (using a database of shapes) and the contralateral-based (CB) algorithm (using a patient's contralateral vessel shape, when available [in 35 of 38 occlusions]) interpolated the same occlusions. Performance was computed by two measures, the maximum distance from the reference and how often the interpolation remained within an assumed vessel radius of 3mm. Subjective CPR image quality was determined independently by two readers.

Methods: For all occlusion lengths (<50, 50-100, 100-200, >200mm): there was little inter-reader variability (0.40, 0.76, 0.79, 1.62mm, respectively), the KB algorithm's error (1.58, 2.81, 9.17, 18.68mm, respectively) was overall greater compared to the CB algorithm's error (1.39, 5.06, 7.10, 6.75mm, respectively), and the KB interpolation was contained within a 3mm vessel radius overall less often (91.2, 54.2, 23.7, 18.4%, respectively) than the CB algorithm (97.3, 36.7, 71.9, 45.8%, respectively). CPR quality was rated diagnostic in 23 of 38 KB interpolated occlusions compared to 25 of 35 CB interpolated occlusions.

Conclusion: Shape-based centerline extraction of femoropopliteal occlusions in lower extremity CTA is feasible. When contralateral shape information is available, the CB algorithm is generally more accurate in interpolating occlusions. Shape-based centerline extraction does not depend on attenuation values, thus may overcome the fundamental limitation of current gradient-based algorithms in severely diseased and occluded arteries.

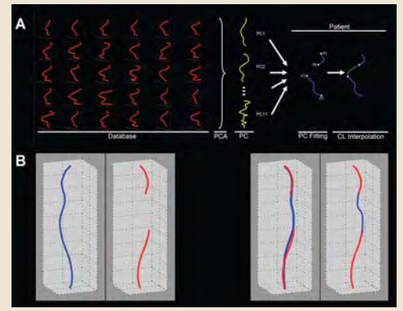

Automated interpolation of occluded centerlines. Panel A: Illustration of knowledge-based algorithm showing an occluded femoropopliteal centerline interpolated from a database of patient femoropopliteal centerlines using principle component analysis (PCA). The PCA computes the principle components (PC) that are fitted to the patent centerline segments to interpolate the occlusion. Panel B: Illustration of contralateral shape-based method, showing a patient's femoropopliteal centerlines (left pair) with an occluded (missing) segment. Since the contralateral artery is patent, the contralataeral shape information is used to interpolate the occlusion (right pair). The left image in this pair shows the patent centerline (blue) being fitted to the vessel with occlusion (red), and the right image in this pair shows the fitted patent centerline being used to interpolate the occluded segment.

Capacitive Micromachined Ultrasonic Transducers for MR-guided Therapeutic Ultrasound

S. H. Wong[1], R. D. Watkins[2], M. Kupnik[1], K. Butts Pauly[2], B. T. Khuri-Yakub[1]
Departments of [1]Electrical Engineering and [2]Radiology

High intensity focused ultrasound (HIFU) guided by magnetic resonance imaging (MRI) is a noninvasive treatment that potentially reduces patient morbidity, lowers costs, and increases treatment accessibility. Traditionally, piezoelectric transducers are used for HIFU, but capacitive micromachined ultrasonic transducers (CMUTs) have many advantages, including fabrication flexibility, low loss, and efficient transmission. We designed, fabricated, and tested HIFU CMUTs for use under MRI guidance and have demonstrated continuous wave (CW) focusing.

CMUT cells were designed with 70 micron radius, 6 micron thick conductive membranes, and 0.4 micron gap heights. We fabricated 2.5 mm by 2.5 mm unfocused transducers and 2.2 cm diameter, 4-element, equal-area concentric ring arrays. The transducers' output pressure and frequency response were measured in soybean oil and compared to finite element models (FEMs). We used the test transducer to heat phantoms, monitored under MRI. Finally, the ring array was focused to 3.5 cm using custom electronics; the beam profile in the focal plane was measured using a hydrophone.

The devices demonstrated a center frequency of 3 MHz and a fractional bandwidth of 100%, which matched FEM. When operated at 2.5 MHz with a 250 VPP sinusoidal AC voltage superimposed on a DC bias voltage (60% of pull-in voltage), the CMUT demonstrated 1.3 MPa peak to peak output pressure. When monitored under MR temperature maps with this input, a phantom heated by 18.6 degrees Celsius after 5 minutes. Finally, focusing the ring array, we obtained a beamwidth of 2 mm and sidelobe suppression to -10 dB, which matches simulation.

Our results demonstrate that CMUTs can be designed for therapeutic ultrasound. Unfocused heating was achieved and monitored under MR guidance. Finally we demonstrated a focused CMUT array whose beam profile matched well with simulation. In the future, we will expand the array and system for noninvasive cancer therapy.

References/Funding Source

NIH R01 CA77677
NIH R01 CA 121163
NIH F31EB007170-01

HIFU Liver Ablation Through the Ribcage and Cartilage in a Rodent Model

R. King[1], V. Rieke[2], K. Butts Pauly[2]
Departments of [1]Bioengineering and [2]Radiology

We are currently examining the feasibility of the rat model for the study of high-intensity focused ultrasound (HIFU) treatment of liver cancer. In patients, obstruction of the ultrasound by the ribs poses a significant problem, and current studies are under way which look at the efficacy of focusing around or sonicating between the ribs. Such techniques show promise for patient treatments, but such schemes are not feasible when using rodent models. Six recently euthanized (within the hour) Sprague-Dewey rats were used to test if it is possible to deliver ultrasound to the liver by sonicating through the ribs. Sonications were performed with the Insightec Exablate system at 0.95 MHz, 1.1 MHz, and 1.35MHz through the rib cage. Temperature rise was monitored with MRI-based thermometry. Lesions were created in the livers of 5/6 rats. In the five rats, energy levels between 572-1194 Joules produced lesions every time. With energies greater than 1393 Joules, skin damaged was observed which prevented the ultrasound from propagating through on subsequent sonications, accounting for the one study that failed to produce thermal lesions in the liver. No thermal damage was observed at the skin with sonications that resulted in liver lesions, and no significant heating was observed at or near the skin in the MRI temperature maps. It is possible to ignore the effect of ribs, cartilage and sternum in rodents and create lesions within the rat liver. This technique opens the door to using hepatocellular carcinoma rodent models in HIFU studies. Having shown that treatment through the ribcage is possible, the next step is to implant hepatocellular carcinoma tumors in the livers of rats and treat the tumor using the same HIFU technique.

References/Funding Source

NIH CA121163

Contribution of T1-change, Slice Thickness, and Positioning to an Artifact in Temperature Images of FUS Heating

V. Rieke[1], K. Butts Pauly[1]
Department of [1]Radiology

Proton resonance frequency (PRF) based temperature mapping is commonly used to monitor focused ultrasound (FUS) ablation. Accurate temperature measurements are necessary to calculate the thermal dose, which is an indicator for tissue viability. Because of the small dimensions of the heating region compared to the MR slice thickness, partial volume effects have to be considered. During FUS treatment, the tissue heating is usually monitored in a scan plane transverse through the FUS spot, because partial volume effects along this direction are small. However, it is often desirable to monitor the lesion along it longitudinal direction. In this orientation, an underestimation of the temperature due to partial voluming was expected. However, an additional artifact was seen, shown in Fig. 1. The artifact appears as a dip in the measured temperature in the middle of the heating region where temperatures were expected to be highest. The purpose of this work was to investigate the source of this artifact.

The influence of slice thickness, slice positioning, and temperature dependent T1-change on PRF-based temperature maps was simulated. MR temperature maps were acquired during FUS heating with different slice thickness and positioning. The following trends were observed: no dip artifacts occurred for slices centered on the FUS spot and for low FUS power levels. Moving the imaging slice away from the FUS spot creates a dip artifact, which is more pronounced at high FUS power levels. The artifact is larger for thicker slices. The simulations confirmed the experimental observations although quantitative evaluation was difficult because it was not possible to heat the same position in the gel phantom consecutively without melting the phantom and moving the focal spot to a different location introduced uncertainty. A discrepancy was found between simulation and experiment: Whereas in experiment, dips occurred for large heating spots and thin slice thickness, the simulations only resulted in dips for narrow heating spots and thick slices.

Experimental results and simulations have demonstrated that off-center slice position together with partial voluming and temperature dependent T1-change can cause a dip artifact in the temperature measurements.

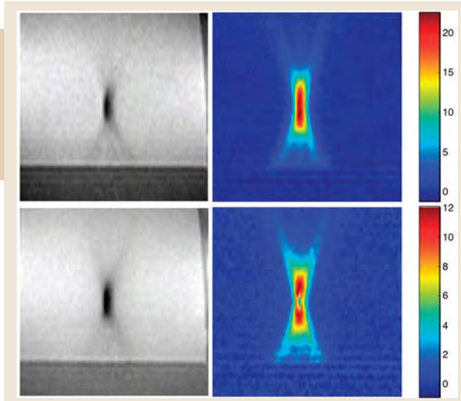

Magnitude and temperature images of two identical FUS heating spots. No artifact is present in the slice centered on the sonication (upper row). In a slice 3 mm offcenter, the dip artifact is visible (lower row).

References/Funding Source

NIH R01 CA111891
NIH P41 RR009784
NIH R01 CA077677
NIH R01 CA121163

Optimization of MR Acoustic Radiation Force Imaging

J. Chen [1, 2], K. Butts Pauly[2]
Departments of [1]Electrical Engineering and Radiology, RSL

For HIFU treatments without significant heating, MR monitoring could be done by imaging the acoustic radiation force (MR-ARFI). The ultrasound is triggered on during large gradients, which encode the displacement from the radiation force into the phase of the image. Unfortunately, large conventional singles lobes gradients render the image sensitive to motion, low, and susceptible to artifacts, which are seen as a non-linear background phase and can be larger than the displacement-induced phase. In this work, MR-ARFI encoding gradients are optimized to minimize these problems.

Imaging was performed with a line scan sequence on a 3T MR-scanner equipped with an MR-compatible HIFU system. Three encoding gradient sets were compared: 1) conventional two-unipolar gradient set; 2) a repeated bipolars set with two identical bipolar gradients around the 180° refocusing pulse; and 3) an inverted bipolars set with opposite bipolars around the 180°. The HIFU system was triggered by the MR sequence to emit ultrasound synchronized with the encoding gradients with a duty cycle less than 5%.

The baseline images for the three encoding gradient sets are shown in the first row of the figure. The repeated bipolar encoding gradients significantly reduce the nonlinear background phase, such that a further background correction step is no longer required. In addition, the b value is greatly decreased from over 1000 s/mm2 with the unipolars, to less than 300 s/mm2 with the bipolars. Therefore the signal noise ratio (SNR) is enhanced at no cost to displacement sensitivity, as demonstrated in the second row of the figure. With the enhanced image quality, a displacement of less than 0.1 µm was successfully detected.

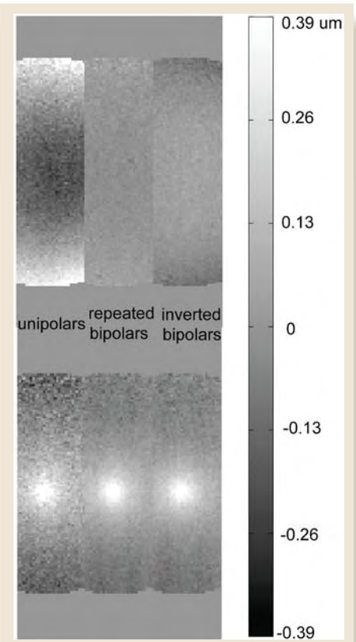

The first row of the figure demonstrates the reduction of background phase with the proposed repeated bipolar gradients. The bipolar gradients significantly improved the SNR of the displacement map, as shown in the second row of the figure.

References/Funding Source

J. Chen, R. Watkins, K. Butts Pauly, MR Acoustic Radiation Force Imaging: Comparison of Enconding Gradients.16th ISMRM, Toronto, 2008
NIH RO1 CA111981
NIH RO1 CA121163
NIH P41 RR009784

Proton Resonance Frequency Shift in Frozen ex vivo Renal Tissue at 7T

E. Kaye[1,2], S. Lynch[3], C. C. Caires[3], K. Butts Pauly[2]
Departments of [1]Electrical Engineering, [2]Radiology, and [3]Chemistry

Introduction: Image-guided cryoablation is a minimally invasive therapy for renal cancer. During cryoablation, temperature monitoring is desired. MR parameters of frozen tissue have been measured with ultrashort TE MR imaging on a low field interventional system [1,2]. Phase changes have been observed as tissue freezes [3], but understanding of the contribution of the proton resonant frequency (PRF) shift to the phase changes have been limited by the SNR of the frozen tissue at low field. The purpose of this study was to measure PRF shift in frozen tissue on a high field spectrometer.

Methods: Freshly excised kidney samples (n=3) were placed into a 10 mm diameter tube. A 100 ml acetone solution in a 3 mm tube was inserted into the tissue tube. During the experiments the Varian 300 MHz NMR system was locked to the deuterium resonance of the acetone to account for magnetic field drift. Tissue temperature was decreased to –30°C in steps. A fiber-optic temperature sensor measured the sample temperature during imaging. The ^{1}H frequency at room temperature was used as a baseline. To calculate ^{1}H frequency shift with temperature Δf(T) the baseline was subtracted from the ^{1}H frequency at every temperature.

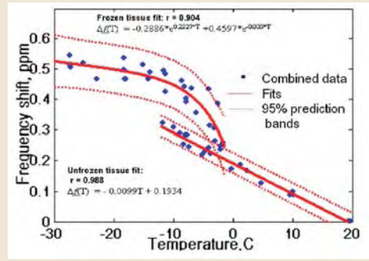

Figure 1. Frequency Shift vs Temperature.

Results: In our study we observed that the PRF shift as a function of temperature has a discontinuity at the freezing point. Frequency shift follows the known linear PRF shift of -0.01ppm/C until tissue freezes. Following the transition to the solid phase, the behavior of the PRF shift with temperature changes from linear to exponential (Fig. 1).

Discussion: In this study we report on the ^{1}H frequency shift of frozen ex vivo renal tissue. In frozen tissue, the observed ^{1}H frequency changes nonlinearly with temperature. This behavior resembles previously published ^{1}H frequency shift in HCl-doped ice [4].

References/Funding Source

ISMRM 2008 abstract.
[1] Wansapura JP, Daniel BL, Vigen KK, Butts K, Acad Radiol. 2005
[2] Kaye E, Josan S, Lu A, K.B.Pauly, ISMRM 2006
[3] Kaye E, Josan S, Lu A, K.B.Pauly, ISMRM 2007.
[4] EW Hansen, A Ninequillibrium. J.Chem.Eng.Data 1988, 33,99-104.
RO1 CA09061
P41 RR009784

HIU Ablation of the Canine Prostate: MR Monitoring and Post-Procedural Assessment

V. Rieke[1], J. Chen[1], A. B. Holbrook[1], D. M. Bouley[2], C. J. Diederich[3], G. Sommer[1], K. Butts Pauly[1]
Departments of [1]Radiology and [2]Comparative Medicine, Stanford University, [3]Radiation Oncology, University of California, San Francisco

High intensity ultrasound (HIU) ablation is a minimally invasive treatment that potentially provides focal control of prostate cancer. In this study, we investigate the performance of MRI for monitoring and assessing thermal therapy.

Experiments were performed in 18 canine prostates undergoing thermal ablations using transurethral or interstitial ultrasound applicators. Imaging was performed in at 0.5T using an endorectal receive coil. Temperature distribution within the prostate was monitored in real-time using the proton resonance frequency method and thermal dose maps were calculated. Following treatment, tissue changes due were imaged with diffusion weighted imaging (DWI), magnetization transfer (MT) and contrast enhanced (CE) imaging. The prostates were harvested, sliced, and stained with TTC and H&E.

Microscopically, discrete zones of injury can be distinguished. The heat fixed zone (HFZ) in the center of the ablation was surrounded by the transition zone (TZ) where damage to the glands and interstitial vasculature was less severe or sublethal. The TZ then merged irregularly with the normal, untreated glands. Temperature and thermal dose maps gave a good prediction of the area of thermal damage. On CE images the HFZ appears as hypointense non-enhancing area often surrounded by a hyper-enhancing ring. DWI showed a decrease in apparent diffusion coefficient (ADC) immediately after treatment. In chronic experiments, the ADC value increased as the tissue recovered and regenerated. None of the prostates showed a significant MT effect immediately after treatment, but became detectable within 60-90 minutes. When imaging was repeated after 4 days the MT effect was prominent.

MRI offers a variety of imaging methods that supply complementary information for monitoring and assessing thermal treatment and help predicting cell death in the target area. The different contrast mechanisms help to interpret the underlying histopathology and to understand the mechanisms of cell death and tissue regeneration.

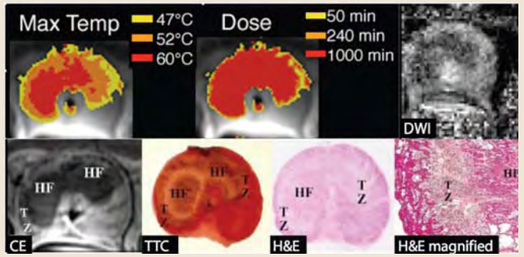

MR imaging (temperature, thermal dose, DWI and CE) for therapy monitoring and assessment, compared to histology (TTC and H&E staining).

References/Funding Source

NIH R01 CA111891
NIH P41 RR009784
NIH R01 CA077677
NIH R01 CA121163

Maximum-Phase Spectral-Spatial Excitation for Frame Rate Enhancement in PRF-Shift MR Thermometry

W. A. Grissom[1], A. Kerr1, A. Holbrook[2], J. M. Pauly[1], K. Butts Pauly[3]
Departments of [1]Electrical Engineering, [2]Bioengineering, and [3]Radiology

Proton resonance frequency (PRF)-shift MR thermometry is an imaging method that can be used to noninvasively monitor temperature during targeted thermal therapy. However, fat can corrupt PRF-shift temperature measurements, since it does not experience a temperature-induced resonance shift. One approach to avoiding this problem is to perform excitation with spectral-spatial (SPSP) RF pulses that excite water only [1]. Conventional pulses used for this purpose allow the TE period to start in the middle of the pulse. Here we demonstrate a maximum linear-phase SPSP pulse, for which the TE period starts near the beginning of the pulse. This permits signal readout to begin closer to the end of the new pulse and a shorter TR, resulting in equivalent temperature maps acquired at a higher frame rate, thereby improving the sequence's robustness to patient motion.

Our pulse is designed using an iterative method [2]. We compared it experimentally with a conventional linear-phase pulse on a 3.0T scanner. The pulses were designed along a 7-lobe, 6.97 ms flyback echo-planar trajectory. The difference in TE starting times was 2.53 ms.

An InSightec HIFU system (InSightec Ltd., Tirat Carmel, Israel) was used to heat a QA phantom. Images were acquired during two sonication runs, one for each pulse. A 2DFT sequence was used, with TE = 15.7 ms. The TR's were as short as possible, 25 ms (conventional linear-phase) and 22.5 ms (maximum linear-phase).

The figure shows an image acquired using the maximum-phase pulse prior to heating. The temperature recorded in the hot spot is also plotted for both pulses. In our experiment, the maximum-phase pulse improved the frame rate by 10%. Larger frame rate improvements will be achieved in sequences with shorter TR's, or at lower main field strengths for which pulse duration must increase to achieve the same quality of fat suppression.

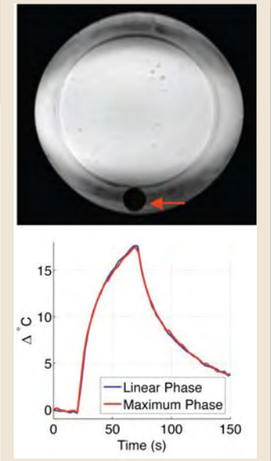

Left: Image of the phantom acquired before heating, using the proposed pulse design. The red arrow indicates an oil-filled vial, confirming fat suppression. The hot spot was in the phantom's center. Right: Temperature measured in the voxel corresponding to the hot spot center indicated in Fig. 1. Excellent agreement is observed between maps acquired with the two pulses.

References/Funding Source

[1] J.A. de Zwart et al. Magn Reson Med, 42(1):53-59, 1999.
[2] C.-Y. Yip et al. Magn Reson Med, 54(4): 908-917, 2005.

Real Time Sleep MRI and Physiologic Monitoring of Patients with Obstructive Sleep Apnea

A. B. Holbrook[1,2], J. M. Santos[3], J. Barrera[4], G. Popelka[4], K. Butts Pauly[2]
Departments of [1]Bioengineering, [2]Radiology, [3]Electrical Engineering, and [4]Otolaryngology

Sleep disordered breathing is a spectrum of syndromes comprised by snoring, upper airway resistance, and obstructive sleep apnea (OSA). Airway obstructions in OSA can cause lack of sleep that limits productivity at best and causes death at worst. Current standards of OSA diagnosis are compromised by their inability to document the actual anatomical abnormality under sleep conditions and the inability to provide physiological information in relation to specific obstructions. A potential solution to these limitations is to combine real-time MRI with simultaneous physiological measures provided by a medical device currently used in outpatient OSA care (Watchpat WP100, Itamar, Caesarea, Israel). Real-time MRI can display dynamic anatomic information about the upper airway in a sleeping patient and the Watchpat can provide simultaneous physiologic measures like pulse, pulse arterial tone, oxygen saturation, and whether the patient is asleep. The purpose of this study was to determine if the conditions underlying OSA can be more accurately specified.

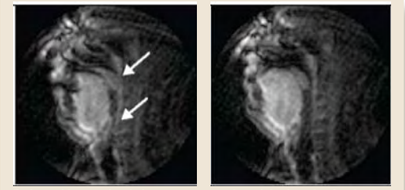

Patient with constricted airway space near the epiglottis and soft palate (left, denoted with arrows), and open posterior airway space (right).

Ten patients with mild to severe OSA were continuously imaged within a 0.5T Signa SP MRI scanner (GE Healthcare, Waukesha WI). The patients were asked to sleep without use of any pharmaceuticals while wearing the Watchpat WP100 device. Images were acquired using the RTHawk real-time system and 2D spiral sequence with 6 interleaves that was capable of acquiring at 5.5 fps. A sagittal view through the patient's midline of the upper airway was selected.

Ten patients were successfully imaged. Based on the physiological data, all fell asleep for a period of time during the ninety-minute session. Tongue and soft palate movements during an airway obstruction occurred at a much slower rate than the imaging frame rate, which allowed accurate continuous monitoring for respiratory obstructions. Furthermore, physiological data from the WatchPat was synchronized to the MR images, allowing for comparisons of this data with the observed MRI changes.

Simultaneous real-time MRI scans and Watchpat recording while sleeping appear to be an innovative and improved method for more precisely characterizing airway obstructions for patients with OSA. The changes in PAT amplitude and blood oxygen level could be useful in diagnosis, although longer video sequences are needed to ensure the capture of an entire respiratory event. This approach is also valuable for planning surgical treatments, potentially improving the success of these procedures.

References/Funding Source

Holbrook AB, Santos JM, Barrera J, Popelka, G, and K Butts Pauly. Real Time Sleep MRI and Physiologic Monitoring of Patients with Obstructive Sleep Apnea. 17th Scientific Meeting of the ISMRM. Toronto, May 2008.
R01 CA077677
P41 RR009784
R01 CA111981
R01 CA121163

Improved Half RmF Slice Selectivity in Presence of Eddy Currents with Quadratic Phase Saturation

S. Josan[1,2], J. Pauly[1], B.L. Daniel[2], K. Butts Pauly[2]
Departments of [1]Electrical Engineering and [2]Radiology

MRI-guided cryoablation is a promising minimally invasive therapy for prostate cancer. MRI provides the promise of temperature mapping throughout the frozen area to better guide the procedure than the placement of discrete thermocouples. Previous studies have shown the tissue transverse relaxation rate $R2^*(1/T2^*)$ to be relatively linear over the temperature range of interest. In order to quantitate $R2^*$ in frozen tissue, ultrashort echo times are obtained with specialized RF pulses, called half pulses. The half pulse slice profile is sensitive to gradient imperfections such as eddy currents that result in out-of-slice signal contamination, and make it difficult to quantitate $R2^*$. The purpose of this work was to develop a simple and robust method for accurate $R2^*$ quantitation in the presence of eddy currents.

A quadratic phase saturation RF pulse with high bandwidth and selectivity was designed to suppress the out-of-slice signal. Experiments were performed on a 0.5T GE Signa SP interventional MR scanner. The effectiveness of the quadratic phase saturation bands in improving the slice profile of the half RF pulse is demonstrated in the figure.

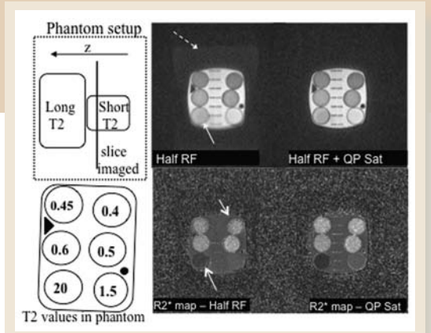

A short T2 phantom was imaged with a long T2 phantom placed out-of-slice. Without the saturation bands, out-of-slice signal from the long T2 phantom introduces errors in the magnitude image and $R2^*$ measurements. These artifacts are removed by out-of-slice saturation.

A short T2 phantom was imaged with a long T2 phantom placed adjacently in the slice direction. $R2^*$ maps were obtained by an exponential fit of images acquired at echo times of 0.1, 0.4, 0.7, 1.0 ms. The half RF pulse image has significant out-of-slice signal due to eddy current distortions, which corrupts the $R2^*$ measurements. The out-of-slice signal is greatly reduced with the quadratic phase saturation pulse, giving cleaner $R2^*$ measurements.

References/Funding Source

Josan S, Pauly JM, Daniel BL, Butts Pauly K. "Improved half RF slice selectivity in presence of eddy currents with out-of-slice saturation". Accepted, Magn. Reson. Med.
NIH CA092061
NIH P41 RR009784

Acute and Chronic Magnetization Transfer Ratio Observations in Canine Cryoablation

A. B. Holbrook[1,2], S. Josan[2,3], D. M. Bouley[4], B. Daniel[2], K. Butts Pauly[2]
Departments of [1]Bioengineering, [2]Radiology, [3]Electrical Engineering, and [4]Comparative Medicine

Prostate cancer is the most common invasive neoplasm in men in the United States. A potential minimally invasive treatment is cryoablation. With MR guidance, this treatment option could prove effective in locally ablating prostate tissue while preserving sensitive structures like the urethra or rectal wall. While iceball formation can be monitored with MR, assessment of tissue damage afterwards is less clear. Perfusion can be assessed with contrast enhanced (CE) imaging, but further tissue characterization of healing is desired. In previous studies, we noticed regions of low magnetization transfer (MT) contrast in cryolesions fourteen and fifty-three days after treatment. This current study follows the MT effect in cryolesions created in three canines, from immediately after treatment to weeks later when the dogs were sacrificed. The purpose of this work was to investigate if the lack of MT effect was evident immediately following treatment and to monitor how it progressed over time, comparing MT effect to CE and histology.

Three MRI-guided canine prostate cryoablations were performed *in vivo* on a 0.5T Signa SP scanner (GE Healthcare, Waukesha, WI). Each cryoablation procedure created multiple lesions within the prostate. After ablation, all dogs were imaged with MT pulse sequences, followed by Gadolinium CE imaging. Two dogs (Dogs 1 and 2) were imaged with the same follow-up imaging protocol at seven days and at study termination - twenty-one days after treatment, while the third dog (Dog 3) was imaged at seven days and fourteen days (study termination). After the final imaging session, each dog was euthanized and the prostate harvested for histological analysis.

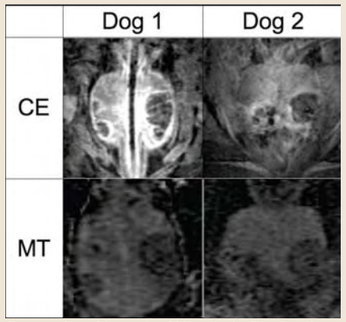

Contrast enhanced (top row) and Magnetization Transfer ratio (bottom row) images of slices of lesions in dogs 1 and 2 on the day of cryoablation. The MT lesion is hypointense.

Immediately following treatment, cryolesions could be visualized with MT, which was not the finding in previous canine thermal ablation experiments. Over the following weeks, MT visualization of lesions persisted. Histologically lesions after 2-3 weeks were minimally hemorrhagic and consisted of regenerating glands, granulation/scar tissue and fragmented smooth muscle fibers. In Dog 2, one lesion developed into a fluid filled cavity.

There is currently no planned work on MT prostate cryoablations, however future work will include analyzing MT contrast in other animal models for thermal ablations, particularly to answer the question of why cryolesion MT contrast begins earlier than in thermal lesions.

References/Funding Source

Holbrook AB, Josan S, Bouley DM, Daniel B, and K Butts Pauly. Acute and Chronic Magnetization Transfer Ratio Observations in Canine Cryoablation. 17th Scientific Meeting of the ISMRM. Toronto, May 2008.
R01 CA077677
P41 RR009784
R01 CA111981
R01 CA121163

MRI-guided cryoablation: In vivo assessment of canine prostate cryolesions

S. Josan[1], D. Bouley[2], B. L. Daniel[1], K. Butts Pauly[1]
Departments of [1]Radiology and [2]Comparative Medicine

MRI-guided cryoablation is a promising minimally invasive therapy for localized prostate cancer. The purpose of this work was to investigate the appearance of acute and chronic canine prostate cryolesions on conventional T1-weighted (T1w) and T2-weighted (T2w) MR images, and compare them to contrast-enhanced (CE) MRI and histology.

Cryoablation was performed on fourteen dogs in the 0.5T GE Signa SP interventional MRI scanner. Each dog prostate was subjected to two different freezing protocols: single slow freeze, passive thaw; and two fast freeze/thaw cycles.

The T2w signal increased pre-to-post ablation, presumably from edema & hemorrhage. Acutely post-ablation, this T2w contrast was greater for a shorter freeze duration, which corresponds to a faster freezing rate. Over time, the contrast for the fast double freeze first increased, and then decreased; while the contrast for the slow single freeze lesions decreased from the acute value. The T2 lesion area was greater than the non-enhancing area on CE images, but smaller than the non-enhancing CE lesion plus the hyperemic rim.

The appearance of the acute T1w lesions ranged from isointense to slightly hypointense and they were generally surrounded by a dark rim. Over time, the T1w lesions demonstrated T1 shortening and appeared hyperintense, and then developed a hypointense outer border (longer T1), till gradually the entire lesion was hypointense. Thus, the T1 changes progress from the rim of the lesion inwards, as the hemorrhage is resolved into blood cell breakdown products.

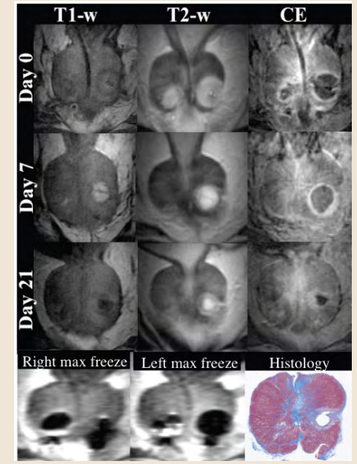

Example images from one study shows the evolution of the cryolesion over time on T1-weighted, T2-weighted, and contrast-enhanced MR images – left lesion is fast double freeze. Images acquired during freezing show the maximum extent of the iceball. The trichrome stained histology section depicts scar tissue and regenerating glands at the site of the left lesion.

Histologically, acute cryolesions appeared hemorrhagic with severe gland fragmentation and necrosis. As time progressed, the lesions became less hemorrhagic and contained more regenerating glands, and scar tissue. Overall, the slow single freeze lesions were smaller and regenerated more quickly.

Prostate cryolesions appear with different contrast on various imaging techniques as the lesions heal. Compared to CE imaging, T1 and T2w imaging can be conveniently repeated, and can potentially be used to monitor tissue response over time following cryoablation.

References/Funding Source

NIH CA092061
NIH P41 RR009784

MR-guided FUS Ablation for Pre-operative Localization of Non-palpable Breast Tumors

A. C. Schmitz[1], M. A. A. J. van den Bosch[1], V. Rieke[2], F. M. Dirbas[3], K. Butts Pauly[2], W. P. Mali[1], B. L. Daniel[2]
Department of [1]Radiology, University Medical Center, Utrecht, The Netherlands, Departments of [2]Radiology, RSL, [3]Surgery, Stanford University

Breast cancer screening has led to an increased detection of early stage and non-palpable breast cancer. MR-guided needle wire placement (MRgNW) is a standard method to localize these tumors. Although it is a relatively simple procedure, positive tumor margin are found in around 40% of patients. Here, we investigate if MR-guided focused ultrasound (MRgFUS) can be used to mark a non-palpable breast tumor by creating a palpable and visible template caused by necrosis. The results are compared to MRgNW placement.

In this study, 16 turkey breasts were used as phantom model. In each phantom an artificial non-palpable tumor was created by injecting an aqueous gel containing gadolinium. Both localization techniques were performed in a 3.0T MR scanner. MRgFUS (n=8) was performed with the InSightec ExAblate 2000 system. Multiple ablations around the non-palpable tumor were used to create a visible and palpable template. MRgNW (n=8) was performed by placement of an MR-compatible needle wire centrally through the tumor. After both localization techniques, the tumor was excised. MR images were used to evaluate tumor-free margins (neg/pos), minimum tumor-free margin (mm) and the excised tissue volume (cm^3).

With MRgFUS no positive margins were found (0%) and with MRgNW 2 phantoms (25%) had positive margins (P=0.48) The mean minimum tumor-free margin ±SD with MRgFUS was significantly larger (5.5 ±2.4mm), than with MRgNW (0.9 ±1.4mm) (P<0.001). The mean volume ±SD of excised tissue was 44.8 (±9.0cm^3) after MRgFUS and 39.5 (±10.7cm^3) after MRgNW (P=0.3).

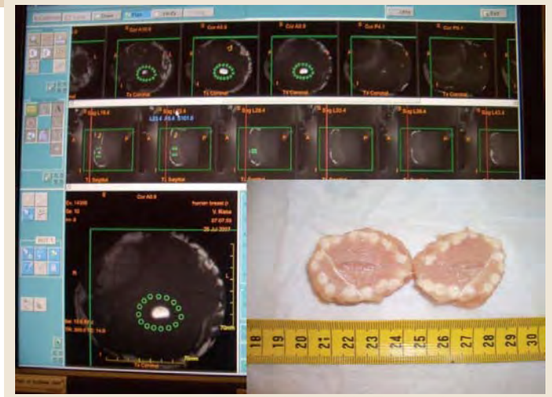

Photograph of excised tissue after MRgFUS localization (lower right). The arrow points to the injected tumor. The background picture shows a screenshot of the InSightec treatment planning software with selected sonications locations around the bright, gadolinium enhanced tumor.

The results of this experimental study indicate that MRgFUS is as accurate as MRgNW for pre-operative localization of non-palpable breast tumors and provides more adequate tumor-free margins.

References/Funding Source

NIH P41 RR009784

Real Time Temperature Imaging of HIFU Ablations

A. B. Holbrook[1,2], E. Kaye[2,3], V. Rieke[2], J. M. Santos[3], K. Butts Pauly[2]
Departments of [1]Bioengineering, [2]Radiology, and [3]Electrical Engineering

High Intensity Focused Ultrasound (HIFU) is a promising technique for treating cancer. HIFU can noninvasively focus nonionizing energy deep in tissue, creating temperature rises that lead to tissue necrosis. These thermal therapies can be monitored with MRI, utilizing Proton Resonant Frequency (PRF) PRF thermometry to determine temperature rises and thermal doses of HIFU sonications. However, respiratory motion during imaging can greatly distort the results. Conventional PRF requires a baseline phase image (pre-heat) that is subtracted from subsequent phase images (during and after heating); the presence of motion makes registration compulsory. An alternative approach utilizes referenceless thermometry, which estimates the background phase from the unheated portions of the image to determine the applied temperature. This technique can be utilized for real time imaging of the hot spot regardless of motion.

We are currently focused on developing a pulse sequence that can be run in real-time, mitigating the effects of motion. The pulse sequence is a combination of a polynomial phase spatial saturation pulse, a spatial-spectral excitation pulse, and a flyback EPI readout trajectory. The combination of these three components allows for acquiring high spatial resolution images at a fast frame rate, while minimizing effects from off-resonance. The phase images from this sequence can then be converted to temperature images with referenceless PRF thermometry.

We have tested the sequence by sonicating a phantom with an Insightec ExAblate2000 extracorporeal bone transducer. A hot spot was created in the phantom, and the entire setup was then manually pushed back and forth along the bore axis during heating. Temperature images were created during this motion, and the temperature of the sonication was compared to sonication temperature in a stationary setup. The results showed the temperature during motion closely matched that the stationary sonication.

Currently we are in the process of adapting the pulse sequence for in-vivo studies, acquiring images on normal volunteers to assess the need for flow compensation, optimal flyback EPI trajectories, and multicoil configuration in the presence of the ultrasound transducer.

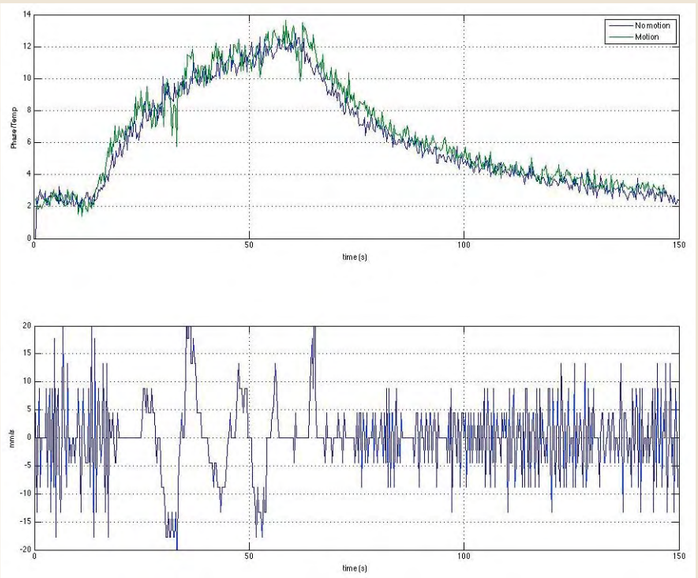

The top plot shows two sonications, one moving (at the estimated velocity of the bottom plot) and one stationary. Both are heated in the same location. The change in temperature matches well between them.

References/Funding Source

Holbrook AB, Kaye E, Rieke V, Santos JM and K Butts Pauly. MR Temperature Imaging of a Moving Phantom Using a Fast, High-Resolution Pulse Sequence and Referenceless PRF Thermometry. Seventh International MRI Symposium. Baltimore, MD. 12-13 September, 2008.
R01 CA077677
P41 RR009784
R01 CA111981
R01 CA121163

Magnetic Resonance Spectroscopy

Slice-selective Tunable-flip Adiabatic Low peak-power Excitation (STABLE) Pulse

P. Balchandani[1], J. Pauly[2], D. M. Spielman[1]
Departments of [1]Radiology and [2]Electrical Engineering

Adiabatic pulses are useful in achieving uniform excitation profiles in the presence of B1 inhomogeneity. BIR-4 pulses have been shown to achieve adiabatic excitation with user-selectable flip angles. However, these pulses are neither spatially nor spectrally selective. The BIR-4 pulse design has been extended through the use of gradient modulation techniques to create slice-selective adiabatic excitation pulses [3-5]. Unfortunately, these techniques require high RF amplitude, typically above the maximum output of the RF amplifiers available on most commercial human scanners. They also require high gradient amplitude and slew rate. In this work, we have developed an alternative gradient modulated approach that achieves adiabatic slice selection with significantly lower RF peak power requirements. Our Slice-selective Tunable-flip AdiaBatic Low peak-power Excitation (STABLE) pulse consists of an oscillating gradient in conjunction with a BIR-4-like RF envelope that is sampled by many short spatial subpulses in order to achieve spatial selectivity.

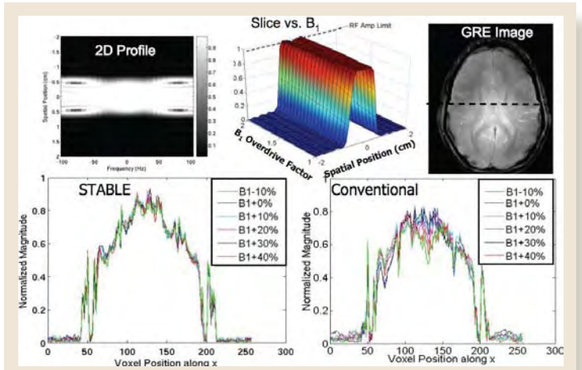

Figure 1: STABLE RF pulse. Top row: 2D profile, slice selectivity versus B1, and GRE image from normal volunteer. Bottom row: horizontal cross section across several images obtained using the STABLE pulse scaled to a range of B1 values, and horizontal cross section of several images obtained using a standard sinc 90° pulse scaled to a range of B1 values.

References/Funding Source

Priti Balchandani, John Pauly and Daniel Spielman. "Slice-selective Tunable-flip AdiaBatic Low peak-power Excitation (STABLE) pulse," Magn Reson Med. 2008;59:1072-8.
Lucas Foundation
NIH RR09784
NIH MH080913

In vivo Hyperpolarized ^{13}C Magnetic Resonance Spectroscopy of Ethanol-Modulated Pyruvate Metabolism

D. M. Spielman[1], D. Mayer[1,2], Y. Yen[3], J. Tropp[4], R. E. Hurd[3], A. Pfefferbaum[2,5]
Departments of [1]Radiology and [4]Psychiatry and Behavioral Sciences, Stanford University, [2]SRI International, Menlo Park, CA and [3]GE Healthcare

Ethanol is primarily metabolized in the liver via the breakdown of ethanol to acetaldehyde and acetaldehyde to acetate. These two reactions are catalyzed by the enzymes alcohol dehydrogenase (ADH) and acetaldehyde dehydrogenase (ALDH), with both requiring reducing the coenzyme nicotinamide adenine dinucleotide (NAD+) to NADH. Hence, ethanol consumption leads to an accumulation of excess NADH in the liver and when extreme is associated with adverse medical conditions including fatty liver disease, hepatitis, cirrhosis, and hepatocellular carcinoma. To date, direct measurements of liver ethanol metabolism have been largely limited to in vitro and ex vivo studies. Here we present a noninvasive method for monitoring this process in vivo. In particular, recent developments in magnetic resonance spectroscopy (MRS) of hyperpolarized ^{13}C-labeled substrates offer dramatically increased sensitivity. Unfortunately, the transient nature of the signal enhancement can severely hinder the observation of many metabolic pathways. We circumvent this temporal limitation by focusing on NADH, a coenzyme common to both ethanol and pyruvate metabolism. Ethanol is used to create an altered rat liver metabolic state characterized by elevated NADH. This skewed metabolic state, which can be generated over an unrestricted time interval, is then interrogated using a bolus injection of hyperpolarized [1-^{13}C]pyruvate, a non-toxic easily polarized and rapidly metabolized substrate. Using this approach, we report an approximately two-fold increased rate of rat liver pyruvate-to-lactate production in the presence of ethanol. Viewed in a more general context, this in vivo MRS assay of changes in NADH concentrations may likely have much broader applications beyond studies of liver metabolism. Mitochondrial ALDH (ALDH2) activity has an important role in neuro- and cardioprotection from oxidative stress, and we further envision the development MRS-detectable molecular imaging reporters[9] using genes which regulate NADH production.

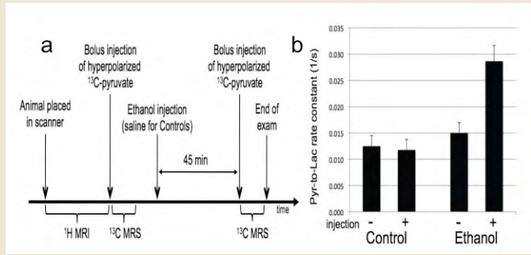

Figure 1. Summary of overall study design and primary findings. (a) Timing diagram for both MRI/MRS acquisitions and ethanol injections. (b) An approximately two-fold increase in pyruvate-to-lactate conversion is seen in the rat liver when pyruvate is given in combination with ethanol. Error bars represent ± s.e.m. (N = 4 controls, N = 6 ethanol).

References/Funding Source

The Lucas Foundation
NIH P41 RR09784
NIH P50 CA114747
NIH R01 AA005965
GE Healthcare

Fast Dynamic In Vivo Metabolic Imaging Using Hyperpolarized $^{13}C_1$-Pyruvate

D. Mayer[1,2], Y. Yen[3], J. Tropp[3], A. Pfefferbaum[2,4], R. E. Hurd[3], D. M. Spielman[1]
Departments of [1]Radiology and [4]Psychiatry, Stanford University, [2]SRI International, Menlo Park, CA and [3]GE Healthcare

Dynamic nuclear polarization can be used to create hyperpolarized compounds with magnetic resonance (MR) signal-to-noise ratio enhancements on the order of 10,000-fold. Both exogenous and normally occurring endogenous compounds can be polarized, and their initial concentration and downstream metabolic products can be assessed using MR spectroscopy. Given the transient nature of the hyperpolarized signal enhancement, fast imaging techniques are a critical requirement for real-time metabolic imaging. We report on the development of an ultrafast, multislice, spiral chemical shift imaging sequence, with subsecond acquisition time, achieved on a clinical MR scanner. The technique was used for dynamic metabolic imaging in rats, with measurement of time-resolved spatial distributions of hyperpolarized $^{13}C_1$-pyruvate and metabolic products $^{13}C_1$-lactate and $^{13}C_1$-alanine, with a temporal resolution of as fast as 1 second. Metabolic imaging revealed different signal time courses in liver compared to kidney. These results demonstrate the feasibility of real-time, hyperpolarized metabolic imaging and highlight its potential in assessing organ-specific kinetic parameters.

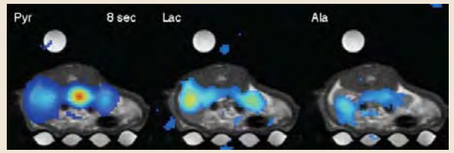

Figure 1. Real-time metabolic imaging. Images show one of 20 temporal frames from a dynamic MRSI movie depicting the inflow of pyruvate into the rat kidney and it's subsequent conversion to lactate and alanine. Parameters: spiral MRSI, 5 mm in-plane resolution, 6 mm slice, 1 temporal frame/s.

References/Funding Source

D. Mayer, Y.-F. Yen, Y.S. Levin, J. Tropp, A. Pfefferbaum, R.E. Hurd, D.M. Spielman "Ultra-Fast In Vivo Metabolic Imaging in the Rat after Injection of Hyperpolarized 13C1-Pyruvate at 3 Tesla", Proc ISMRM, 16th Annual Meeting, Toronto, 2008, 1755.
The Lucas Foundation
NIH RR09784
NIH AA05965
NIH AA13521-INIA
NIH CA114747

Tissue-specific T_2 of Hyperpolarized ^{13}C Metabolites

Y. Yen[1], P. Le Roux[2], D. Mayer[3,4], D. Spielman[3], J. Tropp[1], A. Pfefferbaum[3], R. Hurd[1]
[1]GE Healthcare, USA and [2]GE Healthcare, France, [3]Department of Radiology, Stanford University
[4]SRI International, Menlo Park, CA.

T_2 relaxation time of ^{13}C-metabolites is difficult to measure *in vivo* because of the small ^{13}C natural abundance. Large signal enhancement by hyperpolarized ^{13}C techniques makes it feasible to measure T_2 of ^{13}C-metabolites *in vivo*. A recent study [1] measuring T_2 from slice-selective data on animals suggested that there are multiple T_2 components for each metabolite and the T_2 signal sustains relatively long in tumor. The origin of these multiple components remains unknown. In order to investigate this further, we developed a new technique to excite a small voxel on the organ of interest and measure T_2 from the voxel in a single-shot acquisition.

The voxel excitation is achieved with a combination of a selective 90° SLR pulse [2] and two pairs of 180° quadratic-phase SLR pulses. The quadratic pulses provide a large bandwidth with a modest increase in B1. A CPMG echo train is employed to measure T_2 of the excited voxel signal. Spectra of 604 points and 19.2kHz bandwidth are collected every 42ms for a total of 8s. The figure shows ^{13}C-pyruvate T_2 curves acquired from an axial slice (blue) through rat kidney, a 2.6cc voxel on the kidney (green), and a 2.6cc voxel on vessels (red) in the same rat, normalized to the slice data. These curves have different T_2 characteristics. Curve fitting will be performed to quantify the T_2 and weighting factor of each component.

This new sequence will allow us to compare T_2 of normal and malignant tissues in order to optimize the imaging contrast-to-noise between them.

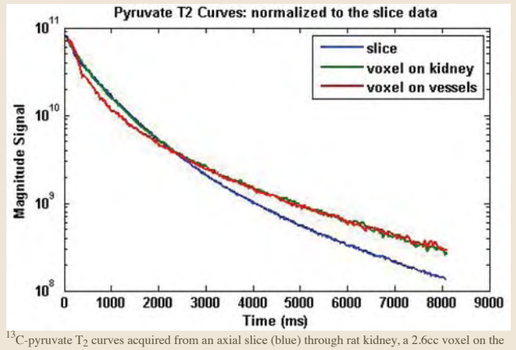

^{13}C-pyruvate T_2 curves acquired from an axial slice (blue) through rat kidney, a 2.6cc voxel on the kidney (green), and a 2.6cc voxel in between the two kidneys where large vessels are located (red) in the same rat. The curves were normalized to the slice data.

References/Funding Source

[1] Y-F. Yen, et al. Proceedings of ISMRM, 2008;1747.
[2] J. Pauly, et al. IEEE Trans Med Imaging, 1991;10:53-65.
2008 World Molecular Imaging Congress, September 10-13, 2008, Nice, France. Abstract number: 1402.
NIH RR09784
NIH P50 CA114747
NIH R01 AA005965

Parallel MRSI Reconstruction with Arbitrary Trajectories using K-space Sparse Matrices

M. Gu[1], C. Liu[1], D. Spielman[1]
Department of [1]Radiology, RSL

Parallel imaging reconstruction has been successfully applied to magnetic resonance spectroscopic imaging (MRSI) to reduce scan times. For undersampled k-space data on a Cartesian grid, the reconstruction was achieved in image domain using sensitivity encoding (SENSE) algorithm for each spectral data point. Alternative methods for reconstruction with undersampled Cartesian k-space data were the SMASH and GRAPPA algorithms that did the reconstruction in k-space domain. To reconstruct undersampled MRSI data with arbitrary k-space trajectories, image-domain based iterative SENSE algorithm has been applied at the cost of long computing times. In this work, a new k-space domain based parallel spectroscopic imaging reconstruction with arbitrary k-space trajectories using k-space sparse matrices (KSPA) was applied to MRSI with spiral k-space trajectories

Exploiting the sparsity of the reconstruction matrix, the KSPA MRSI performed parallel reconstruction with significantly reduced memory requirement. In addition, by applying a single reconstruction matrix, it achieved much faster reconstruction than the iterative SENSE method. With 8-channel phased-array acquisition, 32x32cm FOV, 64x64 matrix size, the reconstruction time using the KSPA method was 3 minutes for a reduction factor of 2 on a 2GHz Pentium PC while the reconstruction time using the iterative SENSE method was over 20 minutes. The proposed reconstruction method was performed for both phantom and in-vivo studies. Figure 1 showed spectra from representative voxels from an in-vivo study with reduction factors of 1, 2, 3 and 4. Spectroscopic images very similar to that reconstructed with fully sampled spiral k-space data were also obtained at these reduction factors.

The algorithm demonstrated its flexibility of reconstruction using undersampled data on arbitrary k-space trajectories and its efficiency with significantly reduced computing times and thus provided a suitable solution for MRSI applications where the minimum scan time was the limitation.

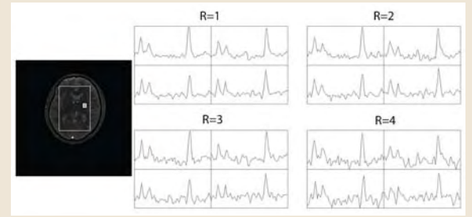

Figure 1. Spectra from representative brain voxels as indicated by the small boxes for reduction factors of 1, 2, 3 and 4. The PRESS volume is indicated with the larger box inside the brain.

References/Funding Source

Gu, et al. ISMRM 2008 annual conference.
NIH RR 09784
NIH CA098523
the Lucas foundation

Visualizing Mouse Tumor Xenografts with MRI using Magnetotactic Bacteria

M. R. Benoit[1], D. Mayer[2], Y. Barak[1], I. Y. Chen[2,3,4], W. Hu[5], Z. Cheng[2,4], S. X. Wang[5], D. M. Spielman[2,4], S. S. Gambhir[2,3,4], A. Matin[1]
Departments of [1] Microbiology & Immunology, [2]Radiology, [3]Bioengineering, [4]Molecular Imaging Program, Stanford (MIPS) and [5]Materials Science & Engineering

The sensitivity of magnetic resonance imaging (MRI) is often enhanced by the use of contrast agents. Contrast agents capable of targeting specific tissues are desired to improve MRI specificity. One class of contrast agents, known as superparamagnetic iron oxide (SPIO) particles, resembles magnetic particles produced by magnetotactic bacteria. Because many bacterial species are known to colonize tumors in mice following intravenous delivery, we examined whether the magnetotactic bacterium *Magnetospirillum magneticum* AMB-1 could colonize mouse tumors and be visualized with MRI. Curiously, when cultured under low iron conditions, AMB-1 produced increased positive contrast using T1-weighted MRI. We hypothesized that this was the result of ultra small magnetic particles, and confirmed this hypothesis using transmission electron microscopy. Because positive contrast often provides advantages for molecular imaging, we sought to exploit the positive contrast of AMB-1 for imaging cancerous tumors. To investigate positive contrast *in vivo*, athymic mice bearing 293T tumor xenografts (n=4) were injected intratumorally with AMB-1 resulting in a 2.0-fold increase compared to control tumors injected with bacterial growth medium (p<0.02). Upon tail-vein delivery of 1x10^9 AMB-1 in 4 mice, a 1.4-fold higher positive contrast was observed in tumors compared to controls receiving medium only (p<0.01). The accumulation of magnetotactic bacteria in tumors was further confirmed by radio-labeling AMB-1 with ^{64}Cu and performing microPET; and by Prussian Blue staining of tumor sections (for iron). These findings demonstrate that magnetotactic bacteria can colonize mouse tumors and enhance MRI positive contrast. Because bacterial magnetite is genetically encoded, the potential also exists to transfer the genes responsible for magnetite production to a non-bacterial delivery system.

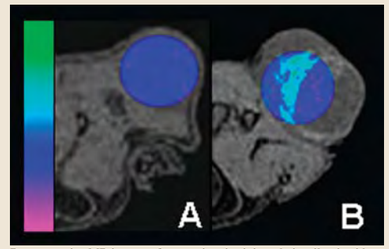

Representative MR images of tumors in mice injected via tail-vein either with the bacterial growth medium, MSGM (Control, A), or with 1×109 AMB-1 suspended in MSGM (B). The color bar shows normalized signal intensity within the gradient color maps.

References/Funding Source

ICMIC Program
NIH/NCI P50 (CA114747(SSG))
NIH RR09784
NIH/NIGMS F32GM077827 to MRB

Self-refocused Spatial-Spectral Pulse Pair for Imaging of Cells Labeled with SPIO Nanoparticles

P. Balchandani[1], J. Pauly[2], P. Yang[3], M. Yamada[4], D. M. Spielman[1]
Departments of [1]Radiology, [2]Electrical Engineering, [3]Cardiovascular Medicine, [4]School of Medicine

We have developed a self-refocused spatial-spectral (SPSP) pulse pair to achieve slice-selective, short-echo-time, spin-echo imaging of off-resonant spins. Using separate, phase-matched, SPSP 90° and 180° pulses to create a spin echo would lengthen the minimum echo time considerably and result in increased signal dephasing. A self-refocused SPSP pulse pair is essentially a phase-matched 90° SPSP pulse and 180° SPSP pulse combined into one pulse through a series of approximations, resulting in a considerably shorter echo time than possible with two separate pulses. Thus, the self-refocused SPSP pulse pair is suitable for any application requiring spatial and spectral selectivity at short echo times. Slice-selective positive-contrast imaging of superparamagnetic iron-oxide (SPIO) nanoparticle-labeled cells is one such application. When used with standard imaging sequences, the SPIO nanoparticles lead to signal dephasing and act as a negative contrast agent. However, negative contrast agents cannot be distinguished from voids in the image and can suffer from partial volume effects. To avoid these errors, several techniques have been proposed for positive contrast imaging of SPIO-labeled cells. One of these techniques uses spectrally selective pulses to image off-resonan water near the labeled cells. Although these spectrally selective pulses enable flexible selection of the excited frequency range, they are not slice-selective, resulting in interfering background signal. The SPSP self-refocused pulse pair we have developed enables slice-selective imaging of off-resonant frequencies, hence eliminating background signal from sources of off-resonance outside the slice of interest.

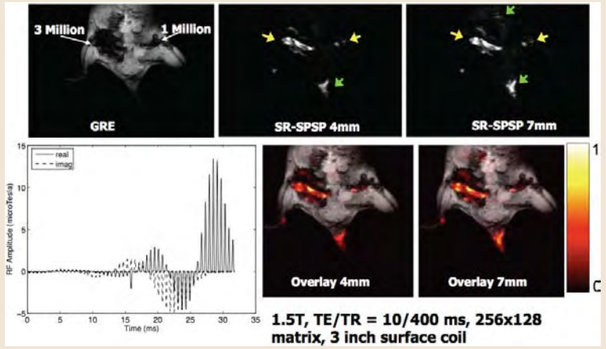

Figure 1: (A) GRE image of phantom with SPIO-labeled cells, (B) Positive contrast image of phantom using self-refocused pulse pair and (C) labeled cell concentrations. (D) GRE image of mouse with SPIO-labeled cells injected into hind legs and (E) Positive contrast image using self-refocused pulse.

References/Funding Source

P. Balchandani, J. Pauly, P. Yang, M.i Yamada, D. Spielman. "Self-refocused spatial-spectral pulse pair for positive contrast imaging of cells labeled with superparamagnetic iron-oxide (SPIO) nanoparticles" oral presentation at ISMRM Annual Meeting, Toronto, May 2008.
Lucas Foundation
NIH RR09784

Reproducibility Study of Whole-Brain ^{1}H Spectroscopic Imaging with Automated Quantification

M. Gu[1], D-H. Kim[2], D. Mayer[1,3], E. Sullivan[4], A. Pfefferbaum[4], D. Spielman[1]
Departments of [1]Radiology, [4]Psychiatry and Behavioral Sciences, Stanford University, Department of [2]Electrical Engineering, Yonsei University, Seoul, Korea; [3]SRI, Menlo Park, CA

A reproducibility study of proton magnetic resonance spectroscopic imaging (1H-MRSI) of the human brain was conducted to evaluate the reliability of an automated 3D in vivo spectroscopic imaging acquisition and associated quantification algorithm. A PRESS-based pulse sequence was implemented using dualband spectral-spatial RF pulses designed to fully excite the singlet resonances of choline (Cho), creatine (Cre) and N-acetyl aspartate (NAA) while simultaneously suppressing water and lipids. 1% of the water signal was left to be used as a reference signal for robust data processing, and additional lipid suppression was obtained using adiabatic inversion recovery. Spiral k-space trajectories were used for fast spectral and spatial encoding yielding high-quality spectra from 1 cc voxels throughout the brain with a 13 minute acquisition time. Data were acquired with an 8-channel phased-array coil and optimal SNR for the combined signals was achieved using a weighting based on the residual water signal. Automated quantification of the spectrum of each voxel was performed using LCModel. Figure 1 showed reconstructed metabolite maps and metabolite concentration ratio maps with associated high resolution structural images from one representative scan.

The reliability of the data acquisition and processing method was evaluated from a reproducibility study. The complete study consisted of 8 healthy adult subjects to assess inter-subject variations and 2 subjects scanned 6 times each to assess intra-subject variations. The reproducibility was conducted for 5 brain regions: frontal lobe, parietal lobe, occipital lobe, temporal lobe and basal ganglia and thalamus. The largest inter-subject regional coefficient of variance (CV) was 12.1% and the largest intra-subject regional CVs for each subject were 12.7% and 6.6% respectively. The coefficients of variation as measured by the proposed volumetric 1H-MRSI sequence and associated processing algorithm were comparable to or slightly better than literature reports for standard PRESS and STEAM sequence

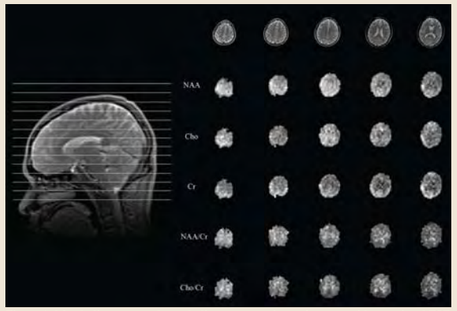

Figure 1. Metabolite maps and metabolite concentration ratio maps with associated FSE images from one representative scan.

References/Funding Source

Gu, et al. MRM, In Press 2008.
NIH RR 09784
NIH CA098523
the Lucas foundation

Glutamatergic Pathways in Children with and at Risk for Developing Mania

M. K. Singh[1], D. M. Spielman[2], K. Chang[1]
The Departments of [1]Psychiatry and Behavioral Sciences and [2]Radiology

Objective: We aimed to compare concentrations of glutamatergic metabolites in bipolar offspring and healthy controls to examine whether decreases in prefrontal glutamate concentrations occur in bipolar offspringand prior to the onset of mania.

Methods: 9–18 year old children and adolescents with a familial risk for bipolar I or II disorder (22 offspring with established history of mania,"BD," and 15 with subsyndromal symptoms without mania, "SS"), and 17 healthy controls ("HC") were examined using proton magnetic resonance spectroscopy (1H-MRS) at 3T to study glutamatergic concentrations in an 8 cc (2 x 2 x 2 cm) anterior cingulate cortex (ACC) voxel. Data was processed using LCModel (Provencher, 2001).

Results Table 1. ACC 1H-MRS Glutamatergic Quantification in Bipolar Offspring vs Healthy Controls

Subject Group	BD Mean (SD)	SS Mean (SD)	HC Mean (SD)	F Statistic	P	Effect Size, *f*
N	22	15	17			
Glutamate/Creatine	1.53 (0.33)	1.55 (0.31)	1.61 (0.30)	0.24	0.79	0.09
Glutamine/Creatine	1.14 (0.36)	1.19 (0.33)	1.02 (0.23)	1.21	0.31	0.21
Glx/Creatine	2.68 (0.47)	2.74 (0.56)	2.63 (0.34)	0.22	0.8	0.09
Glutamate*	9.24 (1.91)	9.26 (1.50)	10.11 (1.54)	1.50	0.23	0.24
Glutamine*	6.83 (2.19)	7.08 (1.43)	6.50 (1.51)	0.42	0.66	0.12
Glx*	16.07 (2.43)	16.34 (2.11)	16.6 (1.75)	0.30	0.74	0.10

*Absolute concentrations to tissue water using LCModel; Glx=Glutamate/Glutamine; BD=Offspring with Bipolar Disorder; SS=Offspring with subsyndromal symptoms; HC=Healthy Controls; SD=Standard Deviation.

Results: Trends for decreased glutamate concentrations in the ACC were seen in BD and SS groups compared to HC that did not reach statistical significance.

Conclusions: These results may be limited by a cross-sectional design, co-occurring diagnoses, or medication exposure. Nevertheless, glutamatergic function may be important in the characterization of offspring of bipolar parents. Longitudinal studies are necessary to determine if early neurochemical changes can predict the development of mania. Improved methods for identifying children with certain neurochemical vulnerabilities may inform preventive and early intervention strategies prior to the onset of mania.

References/Funding Source

M. K. Singh, D. Spielman, K. Chang. Glutamatergic Pathways in Children with and at Risk for Developing Mania. 55th Annual Meeting of the American Academy of Child and Adolescent Psychiatry, Chicago, Oct. 2008, accepted.
The Lucas Foundation
NIH P41-RR09784; NIMH K23 MH064460; NARSAD
The Hahn Family
The Klingenstein Third Generation Foundation

Neurochemical Correlates of Response to Quetiapine in Youth with Bipolar Depression

K. Chang[1], M. DelBello[1], M. Howe[1], N. Mills[1], H. Bryan[1], C. Adler[1], M. Rana[1], J. Welge[1], D. Spielman[2], S. Strakowski[2]
The Departments of [1]Psychiatry and Behavioral Sciences and [2]Radiology
Stanford University School of Medicine

Objective: Mood stabilizers have been reported to affect brain concentrations of myo-inositol (mI) and N-acetylaspartate (NAA). We wished to study the effects on these neurochemicals, and possible predictors of response, of quetiapine in adolescents with bipolar depression.

Methods: Twenty-five adolescents with bipolar depression participated in an 8-week placebo-controlled trial of quetiapine monotherapy. Subjects were scanned at baseline and after 8 weeks with ^{1}H-MRS at 3T, with 8cm^3 voxels placed in right and left dorsolateral prefrontal cortex (DLPFC) and medial prefrontal cortex (ACC). LC Model was used to calculate absolute concentrations of NAA and mI.

Results: 26 subjects had pre- and post-treatment scans (mean age = 15.6 years, 9 males). Of these subjects, 5/16 subjects receiving quetiapine (QUET) and 5/10 receiving placebo (PBO) were responders (50% decrease in CDRS score). There was no significant difference in baseline ACC mI concentrations between the responders and non-responders (4.1 +/- 1.3 vs. 4.2 +/- .48, p = 0.78). There was no significant difference in the change in ACC and DLPFC NAA levels in the QUET group vs PBO group (ACC: -0.55 +/- 1.3 vs. +0.25 +/- 1.5, p = .23; R DLPFC: -0.55 +/- 1.3 vs. 0.18 +/- 0.86, p = .24; L DLPFC: -.04 +/- 0.91 vs. +0.29 +/- 0.61, p = 0.40).

Conclusions: We found baseline ACC mI levels did not predict response to quetiapine in adolescents with bipolar depression. Furthermore, there were no differences in the change in NAA concentrations between the QUET and PBO groups. Larger studies including different brain regions would help to clarify the effects of quetiapine on neurochemistry.

References/Funding Source

K. Chang; M. DelBello; M. Howe; Neil Mills; H. Bryan; C. Adler; M. Rana; J. Welge; D. Spielman, S. Strakowski, Neurochemical correlates of response to quetiapine in youth with bipolar depression, 55th Annual Meeting of the American Academy of Child and Adolescent Psychiatry, Chicago, Oct. 2008, accepted.
Lucas Foundation
NIH P41-RR09784

Molecular Imaging

Manganese-Enhanced Magnetic Resonance Imaging (MEMRI) Highlights Injured Peripheral Nerves in Neuropathic Pain

D. Behera[1], S. Kamaya[2], S.W. Lee[3], E. Graves[4], D. Yeomans[5], H. Dhatt[6], G. E.Gold[1], S. Biswal[1]
The Departments of [1]Radiology-MIPS, [4]Radiation Oncology, [5]Anesthesia, [6]School of Medicine, Stanford University
[2]University of Colorado, Boulder; [3]School of Medicine, Asian Medical Center, Seoul, South Korea

Objective: Manganese (Mn)-enhanced MRI (MEMRI) is a surrogate method to interrogate calcium fluxes in nervous system since Mn2+ is T1 shortening agent and physiologically follows calcium. Our purpose is to validate MEMRI for detection of changes in lumbar nerves related to nociception.

Methods: Animal experiments were approved by Stanford IACUC. A neuropathic pain model was created by Spared Nerve Injury (SNI) of the left sciatic nerve of Sprague-Dawley rats. Animals with SNI, uninjured animals (control) and opioid (buprenorphine)-treated SNI animals (n=3 in each group) were injected with MnCl2 (30mM IP). The lumbar cord and plexus were scanned with a volume coil in a 3T magnet 24 hours after MnCl2 administration and one week after surgery. T1-weighted GRE (TR/TE/Flip angle 800/15ms/15º, 234µm2) were obtained. Using CMIR_Image analysis software, ROIs on bilateral lumbar nerves were used to quantify manganese enhancement, which were normalized to background signal in the muscle. Allodynia was measured through the number of paw withdrawal responses (PWR) to mechanical stimulation. The data was analyzed with statistical tools on an Excel spreadsheet ($p<0.05$).

Results: Behavioral measurements confirmed the presence of allodynia (higher PWR) in the neuropathic pain model while the uninjured and opioid-treated injured groups had significantly lower PWR. There was increased enhancement in the lumbar nerve roots and nerves in the SNI group (3.7+/-0.7) compared to the control group (2.2+/-1.1) and opioid-treated group (2.1+/-0.4) ($p<0.03$) (Figure).

Conclusion: Animals with neuropathic pain in the left hindpaw show increased manganese uptake in the lumbar plexus on MEMRI in vivo, which correlates with the PWR (r2=0.6). MEMRI is a form of functional MR neurography and a promising modality for highlighting the pain-activated sensorineural pathway in the spinal cord.

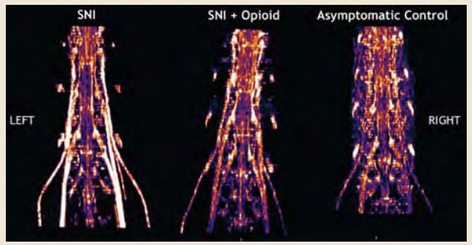

Representative MEMRI (3D MIP, posterior projection) of lumbar cord/plexus in left hindpaw of the Spared Nerve Injury (SNI) model, SNI + Opioid and Asymptomatic Control. Increased T1-weighted signal enhancement in the SNI animal compared to SNI + opioid and asymptomatic control animals.

Site-Specifically Biotinylated VEGF Protein for Imaging VEGFR-2

H. Wang[1], K. Chen[1], Z. Liu[2], G. Niu[1], X. Chen[1]
Department of [1]Radiology, MIPS, Stanford University, [2]Medical Isotopes Research Center, Peking University, China

Objectives: $VEGF_{121}$ loses its receptor affinity after chemically modified with bulky molecules such as fluorescent dyes. To remedy this, we produced $VEGF_{121}$-Avi fusion protein, which can be site-specifically biotinylated at K residue within the Avi-tag by BirA enzyme. The resulting site-specifically biotinylated $VEGF_{121}$-Avi (VEGF-Avi-b) was characterized in vitro and its optical imaging properties were evaluated by using VEGF-Avi-b-streptavidin-IRDye800 (SA800) complex (abbreviated as VEGF-SA800) in tumor-bearing mice.

Methods: Recombinant $VEGF_{121}$-Avi was expressed and purified. The binding affinity of $VEGF_{121}$-Avi was evaluated by receptor binding assay. The site-specific biotinylaion was performed using BirA enzyme, and confirmed by western blot and mass mapping. The formation of VEGF-SA800 was confirmed by cell staining, SDS-PAGE and western blot. VEGF-SA800 was injected into 67NR-tumor bearing mice and its tumor targeting efficacy evaluated by CRI Maestro imaging system.

Results: The $VEGF_{121}$-Avi was successfully expressed and purified. The binding affinity of $VEGF_{121}$-Avi to PAE/KDR cells was 3.12±0.54 nM, which was comparable to that of wild-type $VEGF_{121}$. $VEGF_{121}$-Avi was site-specifically biotinylated by BirA as assessed by western blot and mass mapping. VEGF-Avi-b was able to form stable complex with SA800. As shown in Figure 1, VEGF-SA800 and SA800 has comparable tumor uptake at early time points but the difference becomes very obvious at 48 h p.i.

Conclusions: Site-specifically biotinylated $VEGF_{121}$-Avi is a novel molecule well-suited for streptavidin binding and VEGFR targeted imaging.

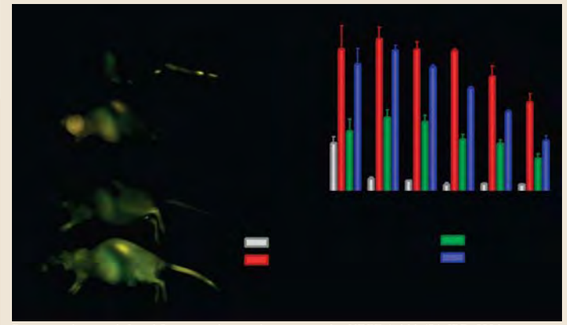

Representative near-infrared fluorescent images demonstrates that VEGF-Avi-bio/SA-IRDy800 has VEGFR-2 specific tumor uptake and high contrast.

References/Funding Source

ICMIC P50 CA114747
CCNE U54 CA119367

Tracking Mesenchymal Stem Cells in vivo

H. Wang[1], F. Cao[1], A. De[1], Y. Cao[1], C. Contag[1], S. S. Gambhir[1], J. Wu[1], X. Chen[1]
Department of [1]Radiology, MIPS

Objectives: To track the distribution and differentiation of mesenchymal stem cells (MSC) in tumor-bearing mice.

Methods: The murine breast cancer 4T1 cells and MSCs were labeled with rLuc-mRFP and fLuc-eGFP reporter gene, respectively. Two tumor models were established by injecting the 4T1- rLuc-mRFP cells intravenously or subcutaneously. Animals were divided into 3 groups and were injected with MSC-Fluc-eGFP cells (1) 4 days after 4T1-rLuc-mRFP intravenous (i.v.) injection; (2) 1 week after subcutaneous (s.c.) injection of 4T1-rLuc-mRFP cells, in the third group, healthy mice were injected with MSC-Fluc-eGFP cells and served as control. The tumor growth was monitored by rLuc BLI. The fate of MSC-Fluc-eGFP cells was monitored by fLuc BLI. The co-localization of MSC-Fluc-eGFP and 4T1-rLuc-mRFP cells was examined by ex vivo fluorescence microscope. The osteogenic and adipogenic differentiation of MSC-Fluc-eGFP was investigated by Alizarin Red S and oil red staining respectively. The mechanism underlying the different differentiation propensity of MSCs in different tissue was investigated.

Results: The 4T1 and MSCs were successfully labeled with rLuc-mRFP and Fluc-eGFP reporter gene respectively. When injected intravenously, MSCs were trapped in lung during the first 2 days in all groups. Then, the MSCs survived, proliferated, and differentiated only in tumor sites as shown in Fig1. The colocalization of RFP+ tumor cells and GFP+ MSCs were further confirmed by ex vivo fluorescence examination. Interestingly, the MSCs homing to lung 4T1 tumor differentiated into osteoblast cells whereas the MSCs homing to s.c. 4T1 tumor differentiated into adipocytes.

Conclusions: The MSCs can home to both lung metastasis tumor and subcutaneous tumor. The fate of MSCs homing to lung tumor or s.c. tumor are distinctly different.

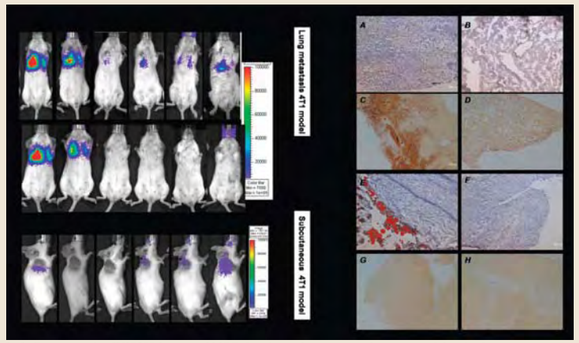

Left: Representative IVIS200 images of MSCs homing to lung metastasis tumor model and subcutaneous tumor model. Right: Representative images showed different differentiation propensity of the MSCs at lung tumor site or s.c. tumor site.

References/Funding Source

DOD Breast Cancer Research Program (BCRP) Idea Award
W81XWH-07-1-0374
ICMIC P50 CA114747; CCNE U54 CA119367
SAIRP R24 CA93862

Radio-Labeled BBN-RGD Heterodimer for Prostate Cancer Imaging

Z. Li[1], Z. Wu[1], K. Chen[1], E. Ryu[1], X. Chen[1]
Department of [1]Radiology, MIPS, Stanford University

Cyclic RGD peptides and bombesin (BBN) analogs have been radiolabeled for imaging integrin $\alpha_v\beta_3$ and gastrin-releasing peptide (GRP) receptor (GRPR) expression respectively in various cancer types. However, tracers derived from monomeric RGD and BBN suffer from relatively low tumor accumulation and retention as well as unfavorable in vivo kinetics. In this study, we developed both ^{18}F-labeled and ^{64}Cu-labeled BBN-RGD heterodimers for positron emission tomography (PET) imaging of PC-3 tumor xenografted mice.

Methods: BBN hetero-dimer (BBN-RGD) was synthesized from bombesin(7-14) and c(RGDyK) through a glutamate linker. BBN-RGD peptide was then labeled with ^{18}F and ^{64}Cu via ^{18}F-SFB prosthetic group and DOTA chelating group respectively. The integrin and GRPR receptor binding characteristics of these heterodimeric peptide tracers were evaluated in vitro by cell binding assay and in vivo by quantitative microPET imaging studies.

Results: BBN-RGD based tracers had comparable $\alpha_v\beta_3$ integrin binding affinity with c(RGDyK) and comparable GRPR binding affinity with BBN(7-14). ^{18}F-FB-BBN-RGD had significantly higher tumor uptake (3.8 ± 0.3%ID/g) compared with monomeric RGD (1.9 ± 0.2%ID/g) and monomeric bombesin (1.1 ± 0.2%ID/g) peptide tracer analogs [time point?]. The receptor specificity of BBN-RGD based heterodimeric tracers were confirmed by effective blocking of the uptake in PC-3 tumor. Compared with their monomeric analogs, radio-labeled BBN-RGD had much higher quality images.

Conclusion: Dual integrin $\alpha_v\beta_3$ and GRPR recognition showed significantly improved tumor targeting efficacy and pharmacokinetics compared with monomeric RGD and BBN analogs. The same heterodimeric ligand design may also be applicable to other receptor systems.

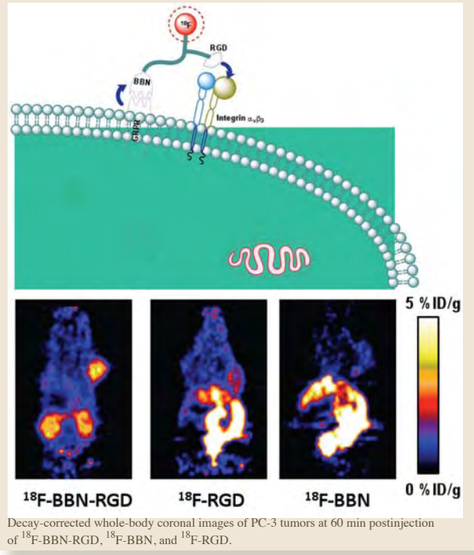

Decay-corrected whole-body coronal images of PC-3 tumors at 60 min postinjection of ^{18}F-BBN-RGD, ^{18}F-BBN, and ^{18}F-RGD.

References/Funding Source

Li Z-B et al. J Nucl Med 2008;49:453-61.
NCI R01 CA119053
NCI R21 CA121842
NCI R21 CA102123
NCI P50 CA114747
NCI U54 CA119367
NCI R24 CA93862
DOD W81XWH-07-1-0374
DOD W81XWH-04-1-0697
DOD W81XWH-06-1-0665
DOD W81XWH-06-1-0042
DOD DAMD17-03-1-0143

Quantum Dot Based Dual Functional Probe for Optical/PET Imaging of Tumor VEGFR

K. Chen[1], Z. Li[1], H. Wang[1], W. Cai[1], X. Chen[1]
Department of [1]Radiology, MIPS, Stanford University School of Medicine

Objectives: To date, in vivo imaging of quantum dots (QDs) has been mostly qualitative or semiquantitative. It is necessary to develop a dual-function PET/near-infrared fluorescence (NIRF) probe for accurate assessment of tumor-targeting efficacy of QDs.

Methods: QD705 surface was conjugated with DOTA chelator for ^{64}Cu-labeling and PET imaging, and with $VEGF_{121}$ protein for VEGFR-2 targeting in a subcutaneous U87MG tumor model. The efficiency of this optical/PET dual functional probe was evaluated in vitro, in vivo, and ex vivo.

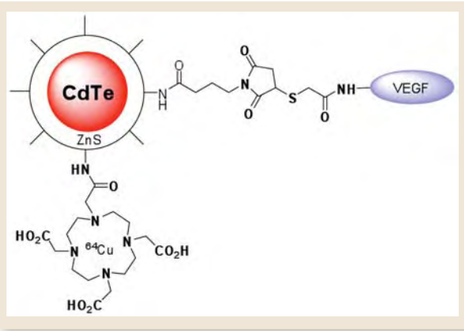

Results: DOTA-QD-$VEGF_{121}$ binds VEGFR-2 with high affinity and specificity based on competitive cell binding assay and fluorescence cell staining. Both NIRF and PET imaging of ^{64}Cu-DOTA-QD705-$VEGF_{121}$ demonstrated quick tumor contrast and increased tumor signal with time, however, optical imaging is qualitative while PET imaging is quantitative. Prominent RES uptake (liver, spleen and lymph nodes) was also observed. ^{64}Cu-DOTA-QD705 on the other hand did not show any visible tumor uptake throughout the experiment. Ex vivo PET and NIRF imaging were also carried out to further confirm the in vivo imaging results in major organs. Immunofluorescence staining of VEGFR2 on frozen U87MG tumor section confirmed that ^{64}Cu-DOTA-QD705-$VEGF_{121}$ specifically targets the tumor vasculature through VEGF/VEGFR-2 binding and only a very small fraction of QD may extravasate.

Conclusions: This is the first study to use QD-based NIRF imaging and PET imaging to specifically target tumor vascular VEGFR-2 and quantitatively evaluate the targeting efficacy.

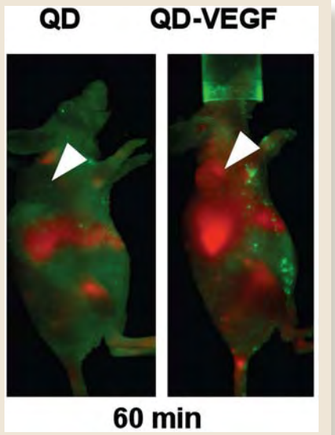

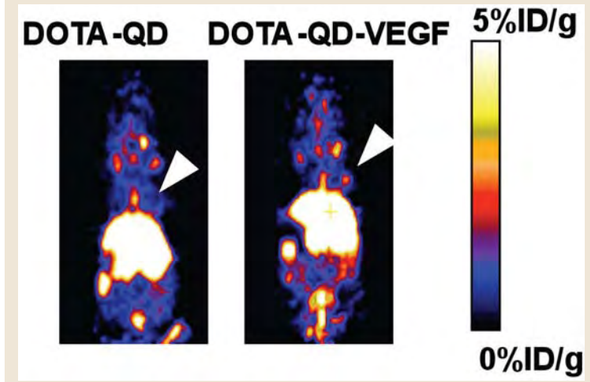

Positron emission tomography (PET) and near-infrared fluorescence (NIRF) imaging of U87MG tumor-bearing mice with 64Cu-DOTA-QD-VEGF.Arrows indicate the tumor.

References/Funding Source

Chen,K et al. Eur J Nucl Med Mol Imaging. 2008 Jun 20. [Epub ahead of print]
NCI R01 CA119053
NCI R21 CA121842
NCI R21 CA102123
NCI P50 CA114747
NCI U54 CA119367
NCI R24 CA93862
DOD W81XWH-07-1-0374
DOD W81XWH-04-1-0697
DOD W81XWH-06-1-0665
DOD W81XWH-06-1-0042
DOD DAMD17-03-1-0143

Quantitative PET Imaging of VEGF Receptor Expression

K. Chen[1], W. Cai[1], Z. Li[1], H. Wang[1], X. Chen[1]
Department of [1]Radiology, MIPS, Stanford University School of Medicine

Objectives: VEGF/VEGFR signaling pathway plays pivotal roles in regulating tumor angiogenesis. Since VEGFR expression is highly dynamic during tumor progression, quantitative imaging of VEGFR will facilitate the planning of whether, and when, to start anti-angiogenic treatment and enable more robust and effective monitoring of such treatment.

Methods: $VEGF_{121}$ was conjugated with DOTA and labeled with ^{64}Cu for PET imaging of mice bearing different sized human glioblastoma U87MG tumors (n = 15). Western blotting of tumor tissue lysate was performed to correlate the VEGFR expression level with ^{64}Cu-DOTA-$VEGF_{121}$ uptake in the tumors. Immunofluorescence staining was also carried out to validate the imaging results.

Results: The specific activity of ^{64}Cu-DOTA-VEGF121 was 3.2 ± 0.1 GBq/mg with radiochemical purity of >98%. The uptake of ^{64}Cu-DOTA-$VEGF_{121}$ in the tumor peaked when the tumor size was about 100-200 mm3 during the exponential growth phase. Both small and large tumors had lower tracer uptake indicating that the window with high VEGFR expression was quite narrow. Immunofluorescence staining revealed that the tumor had minimal VEGFR-1 expression while the VEGFR-2 expression level is quite different. Most importantly, the tumor uptake value obtained from PET imaging had good linear correlation with the relative tumor tissue VEGFR-2 expression (r2 = 0.68 based on 4h time point PET quantification).

Conclusions: The tumor uptake of ^{64}Cu-DOTA-VEGF121 measured by microPET imaging reflects tumor VEGFR-2 expression level in vivo. This is, to our knowledge, the first report of quantitative PET imaging of VEGFR-2 in living subjects. Such correlation is critical for future treatment planning and treatment monitoring applications in both cancer and other angiogenesis-related diseases

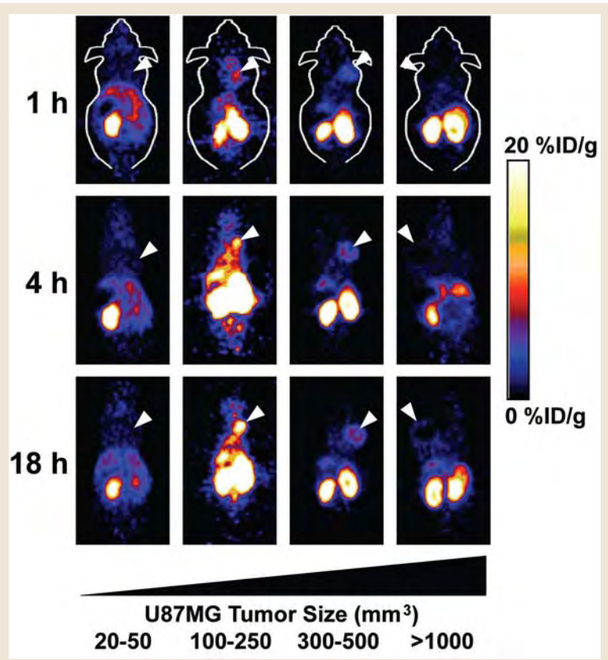

microPET images of U87MG human glioblastoma tumor-bearing mice after intravenous injection of 64Cu-DOTA-VEGF121. Arrows indicate the tumors.

References/Funding Source

Chen,K et al. Molecular imaging and Biology. In press
NCI R01 CA119053
NCI R21 CA121842
NCI R21 CA102123
NCI P50 CA114747
NCI U54 CA119367
NCI R24 CA93862
DOD W81XWH-07-1-0374
DOD W81XWH-04-1-0697
DOD W81XWH-06-1-0665
DOD W81XWH-06-1-0042

Ultrasmall c(RGDyK)-coated Fe3O4 Nanoparticles and Their Specific Targeting to Integrin Alpha(v)Beta3-rich Tumor Cells

J. Xie[1,2], K. Chen[1], H. Y. Lee[1], C. Xu[2], A. R. Hsu[1], S. Peng[2], S. Sun[2], X. Chen[1]
Departments of [1]Radiology, MIPS, Stanford University, [2] Chemistry, Brown University, Providence, RI

Fe_3O_4 nanoparticles synthesized from high temperature decomposition have the advantages over those made from the conventional co-precipitation method in that there is better control over the particles' magnetic moment, size, and size distribution, therefore, making them potentially better contrast agents for MR imaging. Those as-synthesized hydrophobic particles were then subjected to a ligand exchange treatment, preceded by simply mixing the particles with a home-made dopamine-PEG ligand. Due to the higher affinity between the dopamine moiety and the surface Fe atoms, the original organic coating was replaced with the new ligand, i.e. making the particles PEGylated. Such PEGylation rendered the particles water soluble, with the overall size tunable from 30 nm to 90 nm via changing the PEG lengths, as evidenced by dynamic light scattering (DLS) studies. Marginal size change in mimic physiology environment (PBS plus 10% PBS, 37 ˚C) for 24 hour incubation verified those PEGylated nanoparticles' superior stability; and their anti-RES-uptake feature was confirmed by an *in vitro* macrophage uptake test. Both features are important for specific targeting applications. Those particles were then conjugated with various biovectors, such as signal peptide and antibodies, which would guide the particles' cellular distribution. For example, nuclear localization signal (NLS) peptide conjugated NPs could transpass HeLa cell nuclear membrane, which are otherwise impermeable to the particles. And EGFR-antibody conjugated nanoparticles were found to concentrate on A431 cell membranes, through the antibody-antigen interaction. Furthermore, RGD peptide conjugated Fe_3O_4 nanoparticles were administrated intravenously into U87MG bearing mice, and their successful *in vivo* targeting was confirmed by the T_2 signal reduction at the tumor site on the MRI map. Recently, we developed a novel procedure to synthesize ultra-small Fe_3O_4 nanoparticles. In such a system, 4-methylcatechol was used as the surfactant in high temperature decomposition, and was coated onto the as-synthesized particles. Afterwards, amine terminated species, in this case RGD peptide, could be conjugated onto the particle surface through a one-step Mannich reaction. Such synthesis and conjugation avoid the elsewhere needed ligand exchange step. More importantly, RGD peptide, an agent for $\alpha_v\beta_3$-integrin targeting, also served as a stabilizing agent in the particle preparation, therefore maximally reducing the overall particle size. Their r_2 relativity was measured to be 165 $mM^{-1}S^{-1}$, much higher than the commercial Feridex NPs (104 $mM^{-1}s^{-1}$), attributed to the ultra-thin coating. After intravenous administration into U87MG bearing mice, a 42% signal reduction was observed at the tumor site on the T_2 weighted map. The ultra-small size might have great influence on the particles' biodistribution, such as reducing the RES uptake and enhancing extravasation. The detailed study is underway.

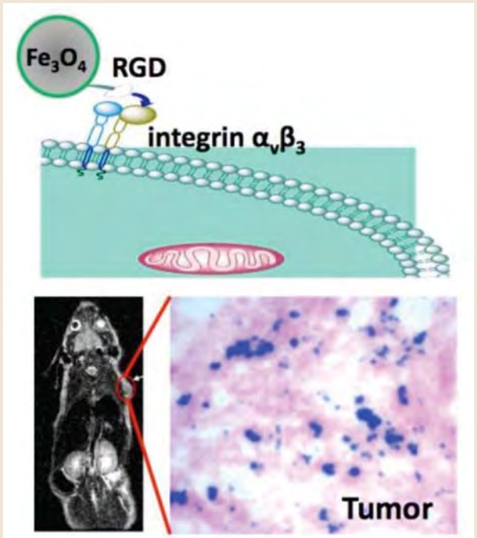

The illustration (top) shows how a RGD peptide-coated iron oxide nanoparticle binds with an integrin-rich tumor cell. At bottom left is a MRI of a mouse with the implanted U87MG tumor (red circle). At bottom right is an optical image that reveals iron oxide nanoparticles (blue) amassed in the tumor area (pink).

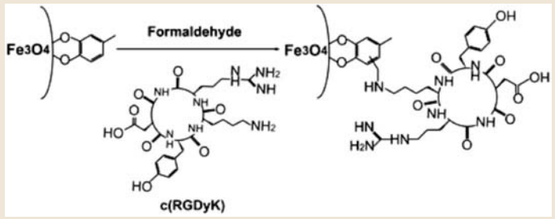

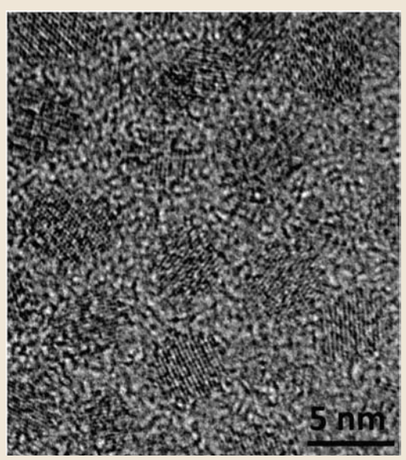

References/Funding Source

Jin X et al. J Am Chem Soc 2008;130:7542-3

Positron Emission Tomography Imaging of Vascular Endothelial Growth Factor Receptor Expression after Experimental Stroke

W. Cai[1], R. Guzman[2], A. R. Hsu[1], G. Sun[2], H. Zhao[2], M. Moseley[1], G. K. Steinberg[2], X. Chen[1]
The Departments of [1]Radiology, MIPS and RSL and [2]Neurosurgery Stanford University School of Medicine

Background and Purpose: Molecular imaging becomes increasingly important as new potential therapies for stroke emerge. In this study, we evaluated the kinetics of VEGFR expression during post-stroke angiogenesis in a rat model.

Methods: In female Sprague-Dawley rats, stroke was created by permanent distal middle cerebral artery occlusion (dMCAo). The rats were subjected to weekly MRI, ^{18}F-FDG PET, and ^{64}Cu-DOTA-VEGF$_{121}$ PET scans after surgery. Several control experiments were performed to confirm the VEGFR specificity of ^{64}Cu-DOTA-VEGF$_{121}$ uptake in the stroke area. Ex vivo histology and autoradiography using ^{125}I-VEGF$_{165}$ was carried out to validate the imaging results.

Results: The stroke in the rat brain was confirmed by T2-weighed MRI and ^{18}F-FDG PET. The stroke size based on MRI was relatively stable over time while the size of the "cold spot" in ^{18}F-FDG PET varied to a certain extent, likely due to inflammation. ^{64}Cu-DOTA-VEGF$_{121}$ uptake in the stroke area peaked at about 10 days after surgery, indicating angiogenesis as confirmed by ex vivo histology. VEGFR specificity of ^{64}Cu-DOTA-VEGF$_{121}$ uptake was confirmed by significantly lower uptake of ^{64}Cu-DOTA-VEGF$_{mutant}$ than ^{64}Cu-DOTA-VEGF$_{121}$ in the stroke area, low ^{64}Cu-DOTA-VEGF$_{121}$ uptake in the brain of sham-operated rats and ^{125}I-VEGF$_{165}$ autoradiography.

Conclusions: For the first time, we successfully evaluated the VEGFR expression kinetics non-invasively in a stroke rat model. Monitoring VEGFR expression in vivo after stroke may be translated into the clinic to determine the right timing for stroke therapy and to monitor the therapeutic efficacy by imaging post-stroke angiogenesis.

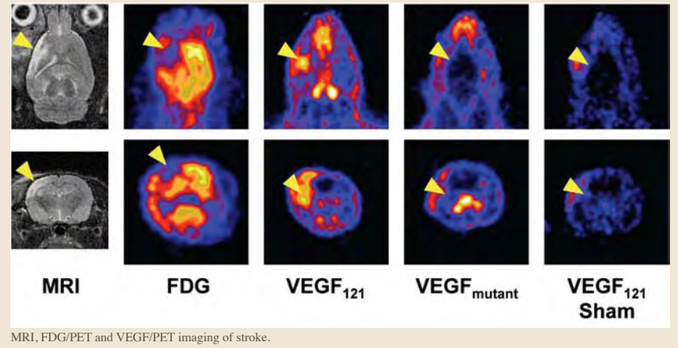

MRI, FDG/PET and VEGF/PET imaging of stroke.

References/Funding Source

Cai W et al. Stroke, in press, 2008

Transcriptional and Functional Profiling of Human Embryonic Stem Cell-Derived Cardiomyocytes

K. D. Wilson[1,3], F. Cao[1], R. A. Wagner[2], X. Xie[1], M. Drukker[5], R. C. Robbins[4], S. S. Gambhir[1,3], I. L. Weissman[5], J. C. Wu[1,2]
The Departments of [1]Radiology, [2]Cardiology, [3]Bioengineering, Cardiothoracic Surgery, [5]Developmental Biology

Human embryonic stem cells (hESCs) have the potential to serve as a limitless source of replacement cells for the regeneration of infarcted myocardium. However, the cellular and molecular phenotypes of hESC-derived cardiomyocytes (hESC-CMs) remain poorly characterized. To better understand the molecular networks underlying hESC-CM differentiation, we used microarrays to analyze both the mRNA and microRNA (miRNA) profiles of differentiating hESCs (n=24 total microarrays). Our results demonstrate that the hESC-CM transcriptome is similar to fetal heart tissue, in which early embryonic and mesodermal genes such as OCT4 and TWIST1 are downregulated, and cardiovascular and structural genes such as β-actin and vascular collagens are upregulated. Furthermore, we identified a signature group of miRNAs that are upregulated in hESCs. We also identified specific patterns of miRNA expression during hESC-CM differentiation, suggesting a regulatory role for miRNAs in cellular development. To understand functional aspects, we injected 1x10^6 hESC-CMs or PBS into SCID mice after LAD ligation (n=21 and n=12, respectively). Echocardiography showed moderate improvement by 8 weeks after transplantation (12.5±4.2% improvement over controls, P=0.03). To demonstrate long-term engraftment, molecular imaging technology was used to track the fate of transplanted hESC-CMs stably expressing GFP and firefly luciferase. Signal activity fell by 90% within the first 3 weeks of transplantation, indicating significant cell death, but remained stable thereafter through 8 weeks. Finally, postmortem histology for GFP confirmed engraftment of transplanted hESC-CMs. In conclusion, we have used molecular and functional profiles to shed significant insights into the regenerative ability of hESC-CMs.

References/Funding Source

California Institute of Regenerative Medicine

Molecular Imaging of Tumor Matrix Metalloproteinase 2 Expression Using ^{18}F-Chlorotoxin

G. Ren[1], Z. Liu[1], Z. Miao[1], Z. Cheng[1]
The Department of [1]Radiology, MIPS, Stanford University School of Medicine

Matrix metalloproteinase 2 (MMP-2) plays an important role in cancer metastasis and has become an attractive target for both cancer imaging and therapy. PET imaging technology provides opportunities to examine molecular targets in sensitive and quantitative ways. We have aimed to screen and optimize ^{18}F labelled Chlorotoxin ([^{18}F]FB-Cltx) peptides for PET imaging of MMP2 by evaluations of their in vitro and in vivo biological properties. The synthesis of the [^{18}F]FB-Cltx conjugate was successfully achieved through coupling of [^{18}F]SFB with the ε-amino group of the lysine residue in the Cltx (Figure A). The radiochemical purity of the labeled Cltx was over 95% as verified by analytic HPLC analysis. MicroPET imaging studies clearly demonstrated that this probe preferentially accumulated in the MMP2 positive tumors such as C6, U87MG, MDA-MB-435, and B16F10. High uptake was also observed in the kidney and urinary bladder, while liver uptake was significantly lower than tumor uptake ($P < 0.05$) (Figure B and C). The in vivo biodistribution of [^{18}F]FB-Cltx at 3.5 h was examined with nude mice bearing B16F10 mouse melanoma and MDA-MB-435 human breast cancer. In both tumor models, the radiolabeled complex displayed rapid blood clearance, 0.05 ± 0.02, and 0.17 ± 0.03 %ID/g blood uptake was observed at 3.5 h post-injection for B16F10 and MDA-MB-435 tumor bearing mice, respectively. Furthermore, [^{18}F]FB-Cltx showed low accumulation in most of the normal organs, while much higher tumor uptakes, in both tumor models. This results in good tumor-to-normal tissue ratios, the tumor-to-muscle ratio was 13.59 ± 0.41 to 8.90 ± 1.20 for B16F10 and MDA-MB-435, respectively. Overall, this preliminary study suggests the ^{18}F labeled Cltx is a highly promising agent for tumor MMP-2 imaging.

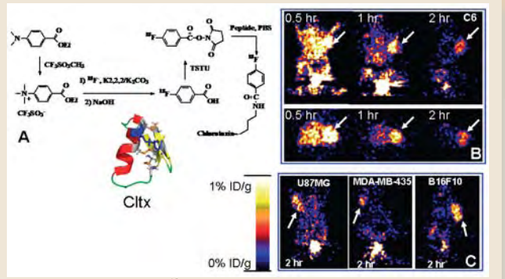

Figure. (A) Radiosynthesis of [^{18}F]FB-Cltx. (B) Coronal and transaxial microPET images of a C6 tumor bearing mouse at 0.5, 1 and 2 hr after tail vein injection of [^{18}F]FB-Cltx. (C) Coronal microPET images of mice bearing different tumors at 2 hr after tail vein injection of [^{18}F]FB-CLtx. The location of tumors is indicated by arrows.

References/Funding Source

NCI SAIRP
NCI P50 CA114747
Start-up funds from Radiology

Small Animal PET Imaging of HER2 Expression Using Site-Specific ^{18}F Labeled Affibody Molecules

Z. Cheng[1], O. Padilla De Jesus[2], M. Namavari[1], A. De,[1] J. Levi[1], J. M. Webster[2], R. Zhang[2], B. Lee[2], F. A. Syud[2], S. S. Gambhir[1]
Department of [1]Radiology, MIPS, [2]Global Research, General Electric Company

Human epidermal growth factor receptor type 2 (HER2) is a well established tumor biomarker over-expressed in a wide variety of cancers that serves as a molecular target for therapeutic intervention. HER2 also serves as a prognostic indicator of patient survival or a predictive marker of response to antineoplastic therapy. Development of ^{18}F labeled biomolecules for positron emission tomography (PET) imaging of HER2 is very important because it may provide a powerful tool for early detection of HER2 positive tumor recurrence and monitoring HER2 based tumor treatment. In this study, anti-HER2 monomeric $Z_{HER2:477}$ and dimeric $(Z_{HER2:477})_2$ Affibody proteins, were radiofluorinated in reasonable radiochemical yield (13-18%) using site-specific oxime chemistry. The resulting radiofluorinated Affibody molecules were then evaluated as a potential molecular probe for microPET HER2 imaging in SKOV3 tumor mouse models. The radiolabeled bioconjugates, ^{18}F-FBO-$Z_{HER2:477}$ and ^{18}F-FBO-$(Z_{HER2:477})_2$, both displayed specific HER2 binding ability in vitro. Biodistribution and microPET imaging studies further showed that ^{18}F-FBO-$Z_{HER2:477}$ had rapid and high SKOV3 tumor accumulation with quick clearance from normal tissues, while ^{18}F-FBO-$(Z_{HER2:477})_2$ displayed poor in vivo performance (low tumor uptake and tumor-to-normal tissues ratios). The specificity of ^{18}F-FBO-$Z_{HER2:477}$ for SKOV3 tumors was confirmed by its lower uptake upon pre-treatment of tumor mice with HER2 targeting agents Z_{HER2} and Herceptin. Moreover, microPET imaging study revealed that ^{18}F-FBO-$Z_{HER2:477}$ had better tumor imaging quality than that of ^{18}F-FBO-$(Z_{HER2:477})_2$. ^{18}F-FBO-$Z_{HER2:477}$ could clearly identify HER2 positive tumor with good contrast. Overall, these data demonstrate that ^{18}F-FBO-$Z_{HER2:477}$ is a promising PET probe for imaging HER2 receptor expression in living mice. It holds high potential for translation into clinical application. The radiofluorination method developed can also be used as a general strategy for the site-specific labeling of ^{18}F onto other proteins. Affibody is an attractive protein scaffold for further development of PET probes for other molecular targets.

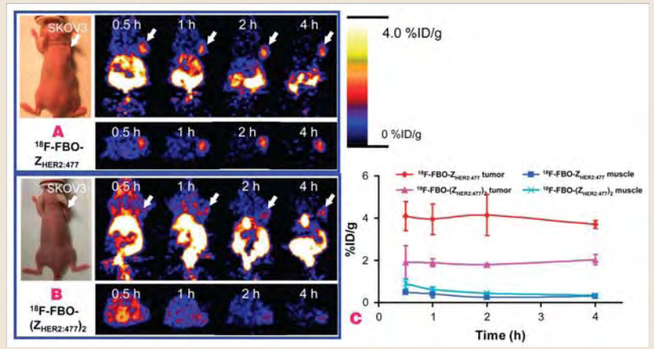

In vivo HER2 tumor targeting specificity of ^{18}F-FBO-$Z_{HER2:477}$. One hour biodistribution results (A) and tumor-to-normal tissues ratios (B) for ^{18}F-FBO-$Z_{HER2:477}$ with or without pretreatment of either 300 μg of $Z_{HER2:477}$ or 500 μg of Herceptin. The ^{18}F-FBO-$Z_{HER2:477}$ SKOV3 tumor uptake is significantly inhibited by $Z_{HER2:477}$ or Herceptin ($P < 0.05$) (N = 3).

References/Funding Source

J Nucl Med. 2008;49(5):804-13.
Medical Diagnostics
GE Healthcare
NCI SAIRP
NCI P50 CA114747

^{18}F Radiolabeled α-Melanocyte-Stimulating Hormone for Melanoma Imaging

Z. Liu[1], G. Ren[1], Z. Miao[1], Z. Cheng[1]
Department of [1]Radiology, MIPS,
Stanford University School of Medicine

Cutaneous malignant melanoma is one of the most lethal cancers. The most important approach for improvement of survival of patients with melanoma still remains early diagnosis, along with accurate staging of disease extent. Therefore, there is a need to develop imaging agents with high sensitivity and specificity for melanoma small lesions and metastases. The α-MSH receptor (melanocortin type 1 receptor, or MC1R) plays an important role in the proliferation and differentiation of melanocytes, and has been found to be over-expressed in most murine and human melanoma metastases, making it a promising molecular target for melanoma imaging and therapy. In our previous research, we designed and synthesized a rhenium cyclized peptide, Ac-d,Lys-ReCCMSH(Arg^{11}) (Figure). This novel metallopeptide showed great in vivo behavior for melanoma MC1R targeting. We thus hypothesized it could be an ideal peptide labeled with ^{18}F for PET imaging of melanoma. The Ac-d, Lys-ReCCMSH(Arg^{11}) was then synthesized using solid phase peptide synthesis (SPPS) followed by rhenium cyclization. The ^{18}F radiolabeling was achieved by conjugation the Ac-d,Lys-ReCCMSH(Arg^{11}) with a radiosynthon, ^{18}F-SFB, which was obtained from a GE FX-FN synthetic module. The in vivo biodistribution and microPET imaging studies of the radiofluorinated compound are under investigation.

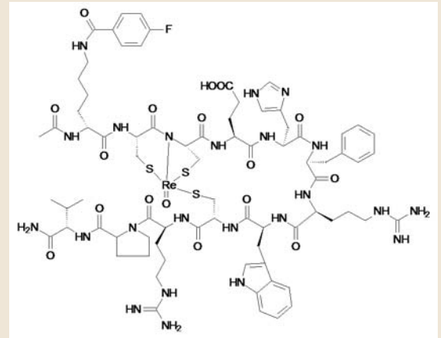

Schematic structures of Ac-d,Lys(FBA)-ReCCMSH(Arg^{11}).

References/Funding Source

Start-up funds from Radiology

PET-CT Fly-through Virtual Bronchoscopy Lesion Quantification & Parameters Affecting 3D Visualization

D. Yerushalmi,[1,2,5], R. Mullick[6], A. Quon[2,4], R. Fahrig[2], N. J. Pelc[1,2], J. I. Fann[3,7], S. S. Gambhir[1,2,4,5]
Departments of [1]Bioengineering, [2]Radiology, MIPS or RSL, [3]Cardiothoracic Surgery, [4]Nuclear Medicine, [5]Bio-X Program, [6]GE Global Research; [7]Cardiothoracic Surgery, Palo Alto Veterans Administration, Menlo Park, CA

Virtual bronchoscopy using FDG PET-CT is a promising tool relevant to diagnostics, treatment planning, and interventional guidance. To realize the clinical utility of this modality, a more thorough understanding of quantitative limitations is required. Previous work has demonstrated the feasibility of localizing lesions using 3D fusion images. Here we present a strategy for investigating the effect of parameters including PET threshold, colormap, and opacity selection for 3D visualization of endoluminal lesions of the airways and for assessing the physical properties of lesions of different sizes morphologies and activities. An anatomically accurate plastinated porcine heart-lung phantom was used to simulate the airways and peripheral structures. Flat and polypoid capsules measuring between 4-10mm were filled with 0.5-1 μCi of Fluorine-18 activity, introduced into the trachea using a flexible bronchoscope, and placed at locations along the bronchial tree. PET and CT images were acquired sequentially on a PET-CT scanner and reconstructed at 2.5mm and 5mm using the filtered-backprojection and OSEM algorithms respectively. Images were visualized in virtual bronchoscopy and volume-rendered fly-around image formats using a commercial software tool. Visualization parameters were optimized for fusion images. Lesion dimensions and activity concentration were measured based on axial images. Fly-around perspective and fly-through views clearly show focal tracer activity with respect to known anatomical landmarks. Lesion dimensions were found to have an overall relative error of 0.10±0.08mm (σ^2=0.72mm, N=2). Capsule size was found to be dependent on PET threshold parameter settings and careful opacity and color map parameter assignment were necessary to avoid artifacts. Future work will further characterize the limitations of this new modality both in phantom and in patient data.

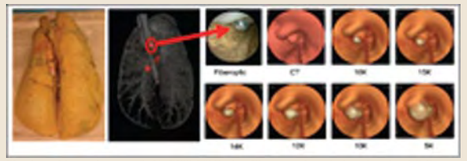

Plastinated lung phantom (left), PET-CT Fusion Fly-around rendering showing FDG PET lesions in red (middle). Red arrow indicates location of one lesion as viewed using fiberoptic bronchoscopy, CT-only fly-through virtual bronchoscopy and PET-CT virtual fly-through virtual bronchoscopy as a function of PET threshold cutoff value (right).

References/Funding Source

D. Yerushalmi, A. Quon, R. Fahrig, N.J. Pelc, J.I. Fann, S.S. Gambhir, "PET-CT Fly-through Virtual Bronchoscopy – Lesion Quantification & Parameters Affecting 3D Visualization" to Academy of Molecular Imaging, September 2007. (Abstract)
NCI ICMIC P50 (CA114747)
Canary Foundation

Intravital Imaging of Targeted Nanotube Delivery to Individual Tumor Cells and Neovasculature in Living Subjects

Bryan Smith[1], Zhuang Liu[2], Cristina Zavaleta[1], Ricky Tong[3], Abhijit De[1], Hongjie Dai[2], Sanjiv Sam Gambhir[1]
Departments of [1]Radiology MIPS, [2]Chemistry, [3]School of Medicine, Stanford University School of Medicine

Nanoparticles comprising a variety of materials, shapes, and sizes have become ubiquitous in molecular imaging, particularly for cancer diagnosis and treatment. Because these nanoparticles are predominantly intended for parenteral administration, deep understanding of nanoparticle behavior in tumor vasculature on the cellular-to-subcellular level is essential to the field. In particular, the transition of diagnostic and therapeutic nanoparticles from the lab-to-clinic and optimization of their design/physical properties will likely result with the support of such studies.

Single-walled-carbon-nanotubes (SWNTs) were conjugated to RGD peptides (targeting $\alpha_v\beta_3$-integrins expressed on tumor neovasculature and some tumor cells) and Cy5.5 fluorophores in order to probe their binding properties in two mouse tumor models using intravital microscopy. Dorsal skinfold chambers were surgically implanted into mice and EGFP-SKOV3 or EGFP-U87MG tumor cells (the latter express $\alpha_v\beta_3$-integrins) were inoculated. Imaging consisted of injecting AngioSense750 to visualize the tumor vasculature prior to injection of ~5pmol SWNTs. Three lasers excited the fluorophores and three output channels were employed to reconstruct individual/overlaid images and videos of SWNTs in the vasculature.

Twelve mice (SKOV-3, U87MG, and no tumor) were imaged with RGD-SWNTs and controls. Mice were imaged during injection and ~4 and ~10 hours, ~1, ~3, ~7, and ~21 days post-injection. Unlike controls, RGD-SWNTs were observed to bind to some tumor vessels at 4 hours post-injection. Within a day, RGD-SWNTs extravasated in U87MG tumor beds. In <3 days, RGD-SWNTs were observed binding to some individual tumor cells in U87MG tumors, but not SKOV-3 tumors. Control SWNTs extravasated in U87MG tumor, but were not associated with cells as much as RGD-SWNTs. Raman imaging verified the presence and amount of SWNTs within the chambers. These findings support for the first time the imaging of SWNTs delivered from blood vessels to tumor cells (including binding), allowing much greater understanding of these novel nanoparticles' potential in living subjects.

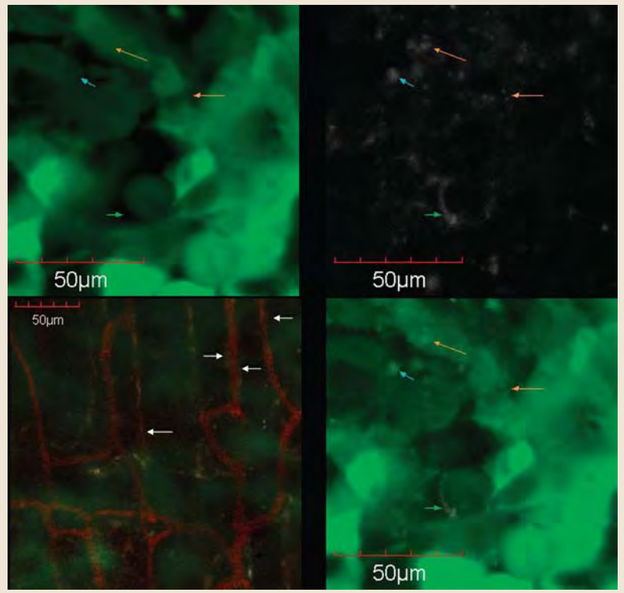

The image shows EGFP-labelled tumor cells in the dorsal window chamber of a mouse which had systemically received an injection of Cy5.5-SWNT-RGD about 1 day earlier. In the upper left panel, EGFP cancer cells are visible. In the upper right panel, SWNTs are visible by reference to their Cy5.5 signal. In the bottom right panel, it is apparent that cy5.5-SWNT-RGD (grayscale) decorates the cell surface and the inside of many cells within the tumor (some examples given by arrows). The image in the bottom left panel displays blood vessels (red) in the tumor (green) of the same mouse a few hours earlier. Extravasation of Cy5.5-SWNT-RGD is apparent by reference to the Cy5.5 color (gray) near and on many of the blood vessels (arrows indicate a few examples).

References/Funding Source

National Cancer Institute Center of Cancer Nanotechnology Excellence Grant U54 CA119367
NIH R25T postdoctoral training grant

Multiplexed Imaging in Living Mice Using Non-invasive Raman Spectroscopy in Conjunction with Raman Nanoparticles

C. L. Zavaleta[1], I. Walton[2], B. Doering[2], G. Davis[2], B. Shojaei[2], S. S. Gambhir[1]
Department of [1]Radiology, MIPS, [2]Oxonica Inc., Mt View, CA

Raman spectroscopy is a newly developed non-invasive preclinical imaging technique that offers picomolar sensitivity and multiplexing capabilities to the field of molecular imaging. In this study we demonstrate, for the first time, the ability to separate 10 spectrally-unique batches of surface enhanced Raman scattering (SERS) nanoparticles in living mice using Raman spectroscopy. Initial in-vivo evaluation consisted of 4 separate subcutaneous injections, each containing 6.6 fmol of a different SERS nanoparticle, and a fifth injection containing a mixture of various concentrations of the 4 SERS nanoparticles. Our post-processing software, which uses a direct classical least squares algorithm to linearly unmix spectra, was able to spectrally separate all four SERS nanoparticles while correctly determining the mixture's associated SERS concentrations with a 2.42% relative fitting error. Next, we subcutaneously injected 10 spectrally-unique SERS nanoparticles in a mouse—each at a separate location—then mapped the area of interest using our optimized Raman microscope to evaluate cross-talk amongst their spectra. Our post-processed results showed little to no cross-talk amongst individual nanoparticles; however, there were differences in their absolute Raman intensities, which would make them harder to multiplex in deeper tissues, due to increased noise. Based on these spectral results, we simultaneously injected the five most intense and spectrally-unique SERS nanoparticles intravenously to non-invasively evaluate their natural accumulation in the liver. Two hours post injection, Raman imaging commenced and revealed that in all mice (n=3) four of the five SERS nanoparticles were successfully identified and spectrally separated, whereas the fifth was minimally detectable in the liver due to its lower Raman intensity. These results show great potential for multiplexed imaging, where several targeted SERS probes injected simultaneously could detect multiple disease processes.

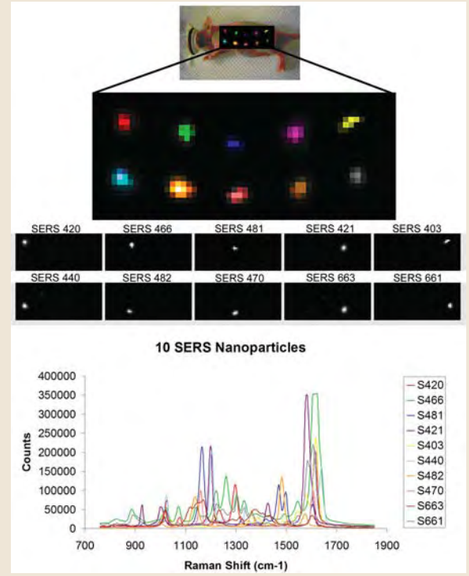

Legend: Raman map showing 10 unique SERS nanoparticles injected subcutaneously in a live mouse. Each color represents a different SERS particle as depicted in the middle panel where each particle was separated out into its own spectral channel. Notice the clear depiction of each subcutaneous injection showing little to no cross-talk between each of the SERS nanoparticles within the 10 post processed channels (lower panel). The graph at the bottom depicts the unique Raman spectra associated with each of the SERS nanoparticles and is color coded to match each injection site on the Raman map acquired above.

A Comparison between Spectral and Time Domain Imaging Systems for Imaging Quantum Dots in Small Living Animals

A. de la Zerda[1], M. L. Schipper[1], S. Keren[1], B. R. Smith[1], J. S.T. Ng[1], S.S. Gambhir[1]
The Department of [1]Radiology Molecular Imaging Program At Stanford (MIPS)
Stanford University School of Medicine

Recently, there has been an increasing interest in imaging Quantum Dots (QDots) in small living subjects. There are two main types of optical imaging systems: time-domain imaging (TDI) and spectral-imaging (SI). TDI acquires the time-response of the target to a short laser pulse whereas SI acquires an image at a range of wavelengths (spectrum). Quantifying the performance and tradeoffs between TDI and SI for QDot imaging is of great interest to the molecular imaging community.

We compared 3 commercially available instruments for Qdots fluorescence imaging: eXplore-Optix(TDI) by ART, Maestro(SI-A) by CRI, and IVIS-Spectrum(SI-B) by Xenogen. We compared the instruments for: a) Sensitivity: the smallest detectable QDot concentration, b)Multiplexing capabilities: the ability to resolve the signal of one QDot type in the presence of another, c)Depth dependence: The decay of contrast and resolution as a function of depth. For a) and b), we imaged a dilution series of 705nm and 800nm QDots. For c), we imaged a liquid phantom with QDot inclusions at the bottom and varied the depth of the inclusions.

The sensitivity of TDI was found to be an order of magnitude higher than the SI systems, capable of detecting QDot concentrations of 50pM versus 1nM with the SI systems. However, SI-A was the best instrument for multiplexing QDots, resolving the signal of 705nm QDots in the presence of 1000 times more 800nm QDots. The SI-B and TDI were only capable of imaging ratios of 1:100 and 1:10, respectively. The degradation of contrast and resolution as a function of depth was smallest with the TDI system. The SI-B showed slightly superior results compared to the SI-A system in that regard.

This comparison study shows that TDI is superior to SI for experiments employing a single Qdot type. However, for multiplexing of several Qdot types, SI is clearly superior.

References/Funding Source

NCI ICMIC P50 (CA114747)
Canary Foundation

A New Simulation Tool for Photoacoustic Molecular Imaging Validated with an Experimental Imaging System

A. de la Zerda[1], S. Keren[1], S. Vaithilingam[1], O. Oralkan[1], P. Khuri-Yakub[1], S.S. Gambhir[1]
The Department of [1]Radiology, MIPS, Stanford University School of Medicine

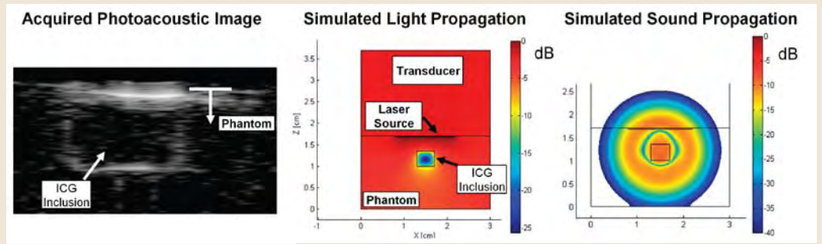

(a) Experimental photoacoustic image, vertical slice through a 100μM ICG inclusion. The boundaries of the inclusion are clearly seen.
(b) Simulated light propagation through a tissue mimicking phantom containing a 100μM ICG inclusion.
(c) Simulated sound propagation.

Photoacoustic molecular imaging is a promising imaging modality that overcomes the resolution and depth limitations of optical imaging but maintains a high contrast by using contrast agents which are highly absorbing and targeted towards diseased tissues. An essential tool for photoacoustic molecular imaging is a simulation platform that can predict, given a photoacoustic system geometry, the smallest detectable probe concentration, resolution, depth of detection, and the tradeoffs between them.

A finite element simulation platform was developed in Matlab and verified experimentally against our photoacoustic imaging system. The simulator models the propagation of light in tissue by solving the Helmholtz equation with Neumann boundary conditions to account for light reflections. It then simulates the energy conversion from light to sound (photoacoustic effect) using the Gruneisen coefficient. Lastly, propagation of acoustic waves through the tissue to the transducer is modeled by the wave equation taking into account acoustic attenuation. The simulator supports multiplexing different photoacoustic contrast agents with overlapping absorption spectra. We compared the simulator results for a semi-infinite tissue phantom to an analytical solution and found the solutions to perfectly match.

To verify the simulations, we created a tissue mimicking phantom in which cylindrical inclusions of the photoacoustic contrast agent, Indocyanine Green (ICG), were inserted. ICG concentrations varied from 20μM to 200μM. The acoustic signals acquired by the transducer (Fig. 1a), correlated within 10% to the simulated data (Fig. 1b, 1c).

Our finite-element simulator proved capable of simulating realistic photoacoustic imaging systems. Such simulator is also an essential component for iterative reconstruction algorithms. Our simulation platform holds significant promise to guide and optimize the design of future photoacoustic molecular imaging systems.

A Large 2D CMUT Array for 3D Photoacoustic Imaging

S. Vaithilingam[1], T. Ma[1], C. Yildiz[1], K. Park[1], X. Zhuang[1], I. O. Wygant[1], Y. Furukawa[1], A. Kamaya[2], O. Oralkan[1], M. Kupnik[1], R. B. Jeffrey Jr.[2], B. T. Khuri-Yakub[1]
[1]Edward L. Ginzton Laboratory and the Department of [2]Radiology

Motivation: Many photoacoustic imaging systems rely on mechanically-scanned single-focus transducers or a 1D array of transducers: neither alternative can provide true 3D images in real-time. Our proposed system is based on large two dimensional capacitive micromachined ultrasonic transducer (CMUT) arrays with integrated electronics and fiber optics for true 3D photoacoustic imaging. Our research aims to provide technology for a handheld probe to allow freehand real-time 3D photoacoustic imaging.

Statement of Contribution: We fabricate a 64x64-element CMUT array by using direct wafer bonding and local oxidation of silicon (LOCOS) in combination with trench-isolated through-wafer interconnects to connect to each element independently. This allows flip-chip bonding of the CMUT array to a custom-designed integrated circuit. Thus, each transducer element has its own dedicated low-noise preamplifier. The laser excitation is delivered through optical fibers. For the image reconstruction we utilize synthetic aperture imaging along with coherence weighting.

Results: As proof of concept that a larger 2D array will improve the image quality, we mechanically scanned a 16x16 element CMUT array at center frequency 2.5 MHz, integrated with transmit-receive front-end electronics, in x and y directions to simulate the aperture of a 64x64 element CMUT array. A 6 ns pulsewidth, 690 nm laser pulse illuminated the phantom with an intensity of 14 mJ/cm^2. The phantom consisted of three transparent fishing wires with a diameter of 150 μm and two black colored fishing wires with a diameter of 180 μm. In the 3D volume rendered images of the phantom (Figure) we overlaid the photoacoustic image (red) on the pulse-echo image (white). Both the photoacoustic and pulse-echo images were reconstructed using synthetic aperture focusing combined with coherence weighting.

Discussion and Conclusions: This experiment demonstrates that by changing from a 16x16 to a 64x64 element array we are able to realize a photoacoustic imaging system with significantly improved image quality. Our latest CMUT fabrication technology in combination with integrated electronics and fiber optics allows us to realize such a 3D photoacoustic imaging system.

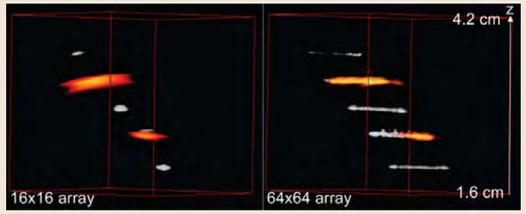

The Universal Donor Mouse: A Mouse Expressing a TRI-FUSION Reporter Gene in all Tissue

R. T. Tong[1], P. Ray[2], S. S. Gambhir[2]
[1]School of Medicine, Stanford; [2]Department of Radiology, MIPS

Imaging live animals using reporter genes is a rapidly advancing field. We have created a universal donor mouse, in which harvested cells or tissues from that mouse can be monitored using multiple imaging modalities. This transgenic mouse has ubiquitous expression of a tri-fusion reporter gene, which harbors a bioluminescence [a mutated thermo-stable firefly luciferase (*Luc*)], a fluorescence [a monomeric red fluorescence protein (*mRFP*)] and a positron emission tomography (PET) reporter gene [truncated herpes simplex virus type 1 sr39 thymidine kinase (*TK*)]. The tri-fusion reporter gene is driven by a chicken β-actin promoter. We first demonstrated high expression levels of the tri-fusion reporter proteins when the gene was transfected in various human and murine cell lines. We then created the transgenic mouse by inserting the gene construct into its genome. While the transgenic mouse has strong bioluminescence and PET (^{18}F-FHBG) signals (Figure 1), the RFP signal is much weaker. Isolated solid organs and bone marrow show strong bioluminescent signals when compared to wild type mice (N = 3 per group) (Figure 2). Presently, the signals persist for 5 generations, and no toxicity has been observed. To demonstrate the contribution of host cells from the transgenic mouse to tumor development, B16 melanoma cells were implanted subcutaneously in the transgenic mice (N = 4). After about two weeks, bioluminescence and PET signals could be detected inside the tumors, representing host cells from the transgenic mouse migrating into the tumor mass. This transgenic mouse model will serve as an important tool in multiple fields such as cancer, stem cell and transplant biology.

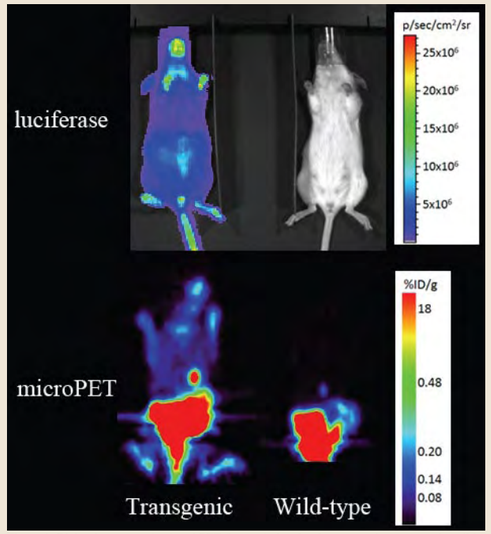

Figure 1: Bioluminescence (top) and PET (bottom) signals of a transgenic mouse and a wild type mouse.

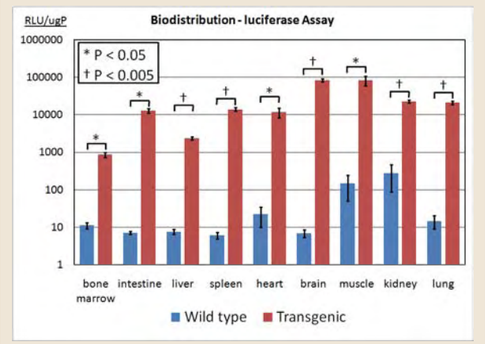

Figure 2: Luciferase activities in individual solid organs and bone marrow in transgenic mice. Solid organs and bone marrow from wild type mice were also used as control.

References/Funding Source

CAMS 2007 New York City, New York Oct 20, 2007
RSNA
Society of Nuclear Medicine
Stanford Med Scholar

Temperature Sensitive Liposomes for Local Drug delivery Using Focused Ultrasound

M. Larabi[1], M. Mackanos[2], R. Shinde[2], C. Contag[2], S. Guccione[1]
Department of [1]Radiology, RSL and the [2]Molecular Imaging Program At Stanford (MIPS)
Stanford University School of Medicine

After using hyperthermia and liposome drug delivery these past decades, these technologies have recently been used together in clinical trial. The encouraging results obtained in the first phase of the clinical study of doxorubicin temperature-sensitive liposomes (TSL) has opened a new way for early cancer detection and therapy. Local delivery of therapeutic drugs will increase drug concentration at the site of treatment for maximum efficacy, and reduce systemic drug exposure. Additionally, through specific molecular targeting, we can bind these liposomes to other sites of disease for local drug delivery. As an initial evaluation, luciferin was encapsulated in the liposome to provided release characteristics after heating. In the first step, we have, using an easy process, developed temperature-sensitive, stable liposomes. These new and innovative formulations have given very encouraging results on the stability and release profile upon heating in vitro in serum and in presence of cells. These heat-sensitive liposomes accumulate in the RES organs and can be used to deliver chemotherapy locally by using focused ultrasound. In our *in vitro* toxicity evaluation, the temperature-sensitive liposome, with or without Luciferin, did not show any membrane toxicity of cell aggregation at 1 mg/ml of lipids and/or 5 mg/ml of Luciferin. Recently, similar results were obtained with Doxorubicin and Paclitaxel encapsulated thermosensitive liposomes. The long-term goal of this project is to use focused ultrasound to heat and release chemotherapy to tumor lesions using targeted, heat-sensitive liposomes.

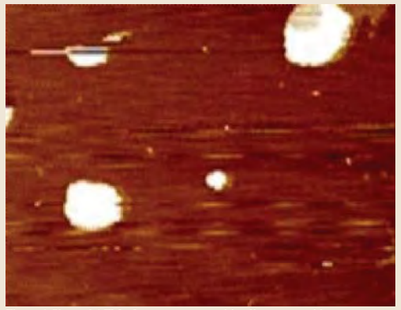

Figure 1 Showed AFM of temperature sensitive liposomes with encapsulated Luciferin.

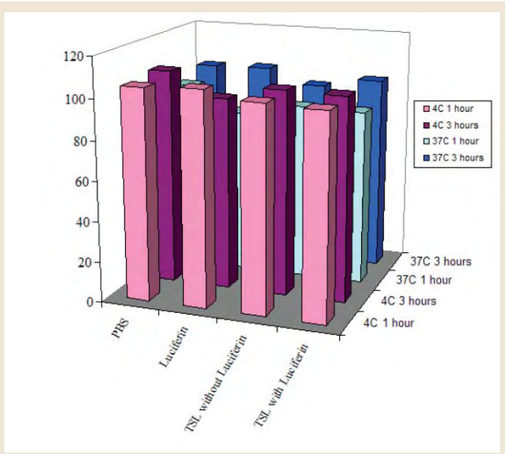

Figure 2 Influence of the TSL on the RBC *in vitro* on the cell aggregation and the membrane toxicity.

References/Funding Source

Lucas foundation
Goldhirsh Foundation
DOD grant
Bio-X

Laser-mediated Local Delivery of Liposome Contents after Systemic Administration

M. A. Mackanos[1], M. Larabi[2], R. Shinde[1], D. M. Simanovskii[3], S. Guccione[2], C. H. Contag[1,2,3,4]
Departments of [1]Pediatrics, [2]Radiology RSL,[4]Microbiology and Immunology, [3]Hansen Experimental Physics Laboratory

Liposomal formulations of drugs have been shown to enhance drug efficacy by prolonging circulation time, increasing local concentration and reducing off-target effects. Use of lasers as a thermal source could improve control of drug release from the liposomes with minimal collateral tissue damage. Methods of assessing local release after systemic delivery are needed for effective development of these tools. Here we use in vivo bioluminescence imaging to investigate the spatiotemporal distribution of luciferin, used as a model small molecule, and demonstrate laser-induced release from liposomes in animal models. The thermosensitive liposome used exhibits a phase change above 42 °C by forming open pores with MPPC, thus releasing its drug contents, whereas the DSPE-PEG2000 prolongs the in-vivo circulation time of the liposomes. These liposomes were tested for luciferin release between 37 and 45°C in PBS and serum using bioluminescence measurements, and a 3.5 fold increase in bioluminescence was observed when the liposomes were heated. In-vivo studies were performed on transgenic reporter mice that express luciferase constitutively throughout the body thus providing a noninvasive readout for investigating methods of controlled delivery. An Nd:YLF laser was used (527 nm) to heat tissues and induce rupture of the intravenously delivered liposomes. A 3-fold increase in drug release was observed in the laser-heated foot, as quantified by IVIS50. These data demonstrate laser-mediated control of small molecule delivery that offers control of local delivery.

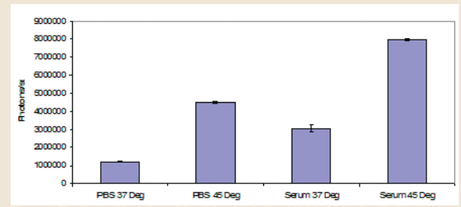

Figure 1: The thermal imaging of the right paw during Nd:YLF laser irradiation at 650 mW, 240 Hz, with a 1 cm elliptical laser spot is show from the FLIR mid-infrared thermal imaging system.

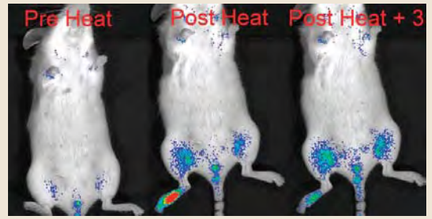

Figure 2: This image is from the bioluminescent imaging of one of the laser irradiated mice. The imaging was done one minute prior to laser heating, immediately after laser heating, and 3 minutes after laser heating. The image shows a clear difference between the bioluminescence signal seen in the laser heated right paw and the unheated left paw.

References/Funding Source

Lucas Foundation
Phil Allen Trust
Goldhirsh Foundation
U.S. Department of Defense-Medical Free Electron Laser Program administered by the Air Force Office of Sponsored Research; grant number FA9550-04-1-0045.

Performance Characterization of a High Resolution, 3-D Positioning PET Scintillation Detector

A. Vandenbroucke[1,2], A. M. K. Foudray [2], F. W. Y Lau[1,2,3], C. S. Levin[1,2], P. D. Olcott[3,4], P. D. Reynolds[1,2]
Departments of [1]Radiology, [3]Electrical Engineering, [4] Bioengineering, and [2]Molecular Imaging Program
At Stanford (MIPS), Stanford University School of Medicine

We are building a novel high resolution, high sensitivity PET scanner with a new concept for a three dimensional positioning photon detector. The concept is based on detector modules built out of an 8x8 array of 1x1x1 mm3 LSO crystals coupled to a Position Sensitive Avalanche Photo-diode (PSAPD). In our configuration, the 511 keV photons interact with the detector modules edge-on, the crystal segmentation and PSAPD thus enables a 1 mm resolution depth of interaction measurement (see Figure).

The data presented here shows the performance of a block of the above described detector modules. A dedicated holding frame was constructed in order to perform the measurements. Additionally, an intermediate PCB was designed and built so that various readout schemes could easily be implemented and studied. The charge from the PSAPD was further amplified and shaped by a commercially available ASIC.

The spatial resolution of our detector concept was obtained by analyzing the Point Spread Function (PSF) as measured by moving a 500 micron wide Na-22 source across the detector's edge. A Gaussian fit to the PSF yielded an average spatial resolution of 0.85 +/- 0.07 mm.

At the same time both energy and coincident time resolution were analyzed. The 511 keV photopeak energy resolution was measured to be 14.1 +/- 0.2 % and the coincident time resolution was 3.11 +/- 0.06 ns. No significant variation of either energy and time resolution across the LSO array and PSAPD surface were observed.

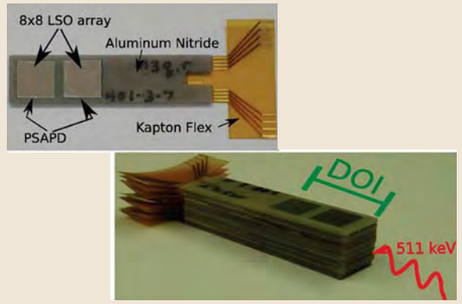

The lower picture shows a top view of one of the dual LSO-PSAPD based detector modules used in the setup. The various parts are indicated in the figure. Right shows a stack of these modules. 511 photons enter the detectors edge-on.

References/Funding Source

R01 CA119056
R33 EB003283
Belgian American Educational Foundation Fellowship

Study of Scintillation Crystal Array Parameters for an Advanced PET Scanner

A. Vandenbroucke[1], C.S. Levin[1]
Department of [1]Radiology, MIPS
Stanford University School of Medicine

We are constructing a high resolution, high sensitivity PET detector with depth of interaction capability. The detector is built out of crystal arrays coupled to Position Sensitive Avalanche Photodiodes

(PSAPDs). In order to optimize the system, various crystal configurations were considered. To determine the best performance configuration, coincident data were obtained by placing a Na-22 source in between a small LSO crystal coupled to a PMT and the crystal array under study coupled to a PSAPD.

The first comparison was between scintillator materials. Both LSO and LYSO crystals were considered. As shown in the Figure, LYSO yielded a 10 % better energy resolution at 511 keV (14.8 +/- 0.6 vs 13.6 +/- 0.6) as well as an about 10% improved coincident time resolution (4.9 +/- 0.3 vs 4.0 +/- 0.3). Additionally, the coincidence timing measurements showed a different signal arrival time dependent on the geometrical position of the crystal on the PSAPD. Up to 20 ns time difference between the corner crystals and those on the center were seen. This behavior is due to the position dependent RC constant of the PSAPD.

Different array reflector and surface configurations were also investigated. All configurations were made of LSO crystals which either had a specular (VM2000) or a diffuse (Lumirror) reflector on their top surface and different surface finishes and inter-crystal reflector conditions.

Data showed no significant differences versus the surface finishes in any of the observables. While the arrays with inter-crystal reflector showed an overall better crystal identification capability, these

crystals showed an about 10% worse energy and time resolution. The model without (with) intercrystal reflector showed an energy resolution of 13.0 +/- 0.5 (14.2 +/- 0.8) and a time resolution of 2.6 +/- 0.1 ns (3.1 +/- 0.2 ns). In summary, we have shown that an array configuration made out of 1x1x1 mm3 LYSO crystals is favorable for our detector configuration.

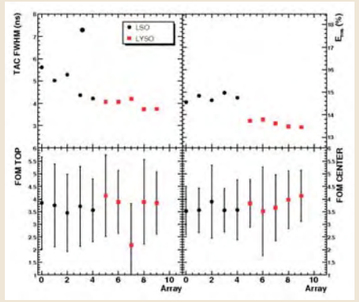

Comparison of the time (upper left) and energy resolution (upper right) between 6 LSO and 5 LYSO crystal arrays. The lower panels show a similar crystal identification capability expressed by a Figure of Merit (FOM) describing the ratio of the distance between the various position peaks and their width..

References/Funding Source

R01 CA119056
R33 EB003283
Belgian American Educational Foundation Fellowship

1mm^3 Resolution LSO-PSAPD-based Breast-dedicated PET System

F. W. Y. Lau[1,2,5], A. Vandenbroucke[2,5], P. D. Reynolds[1,2,5], C. Fang[3], P. D. Olcott,[4,5], M. A. Horowitz[1], C. S. Levin[2,5]
Departments of [1]Electrical Engineering, [2]Radiology, [3]Mechanical Engineering, [4]Bioengineering, [5]Radiology, MIPS

We are developing a breast-dedicated PET (Positron Emission Tomography) system in an effort to increase the role of PET in the detection, diagnosis, staging, biopsy, and monitoring of breast cancer. The system consists of two 16 cm x 9 cm x 2 cm panels constructed using 8x8 arrays of 1 mm^3 LSO scintillation crystals and Position Sensitive Avalanche Photodiodes (PSAPDs) as the detector elements.

Our detectors and electronics can position individual photon interactions in the LSO with energies from 200 to 590 keV. By accepting low energy events due to Compton interactions, we will have a 114% increase in coincidence detection efficiency compared to existing systems that only accept events in the 511 keV photo-peak.

The system contains 2240 detectors, so multiplexing the detector signals simplifies the electronics. We present a circuit that multiplexes two PSAPDs together without significantly degrading performance. Without (with) multiplexing, the measured energy resolution is 14.6% ± 0.8% (14.4% ± 0.8%) FWHM at 511 keV and paired coincidence time resolution is 7.3 ns ± 0.2 ns (7.3 ns ± 0.2 ns) FWHM.

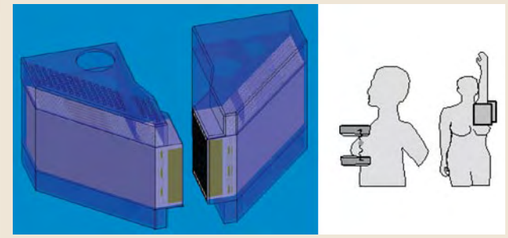

Imaging panels and two possible orientations of the imaging panels.

The figure of merit we use to quantify crystal identification was only ~10% worse for the multiplexing case for all energies from 200 to 590 keV, and it was possible to segment all 64 crystals in an 8x8 array of 1x1x1 mm^3 LSO. This multiplexed architecture results in a 40% reduction in wire routing density and a 33% reduction in channel count.

We devised a charge division method that splits the common signal of the PSAPD into a high gain common and a low gain common. This scales the signals to fit the input dynamic range of the electronics and improves time resolution.

The detector performance is temperature dependent, so we are designing mechanical structures and cooling systems to regulate the temperature. A finite volume simulation indicates that the temperature variation across the detector panel is only four degrees Celsius.

References/Funding Source

F.W.Y. Lau, A. Vandenbroucke, P.D. Reynolds, P.D. Olcott, M.A. Horowitz, C.S. Levin, "Front-end Electronics for a 1mm^3 Resolution LSO-PSAPD-based PET System with Multiplexing," to be presented at IEEE Medical Imaging Conference and Nuclear Science Symposium 2008.
R01 CA119056
R33 EB003283
Stanford Bio-X Fellowship

Convex Optimization of Coincidence Time Resolution for High Resolution PET systems

P. D. Reynolds[1,2], P. D. Olcott[2,3], G. Pratx[1,2], F. Lau[1,2], C. S. Levin[2]
Departments of [1]Electrical Engineering, [3]Bioengineering, and [2]Radiology, MIPS
Stanford University School of Medicine

We implemented a novel method to calibrate and improve coincidence time resolution using list-mode data for a high resolution PET system. We compensate for correlated noise factors by formulating the coincidence time resolution as a convex optimization problem. Once the problem was formulated, it could be solved through a number of methods. We use a direct method to the solution as well as an iterative method.

The convex optimization problem is setup as a least squares problem with the solution being a correction for each trigger event time stamp based on a function of a constant time delay and of the correlated noise factors. The least squares problem can be solved directly via a pseudo-inversion, though the inversion grows as order n^2 with the number n correction factors. We also use an iterative method of single-coordinate descent to solve the problem.

The algorithm is demonstrated using 36 channel pulser data on a NOVA RENA-3 readout ASIC, correcting for channel time delay as well as for correlated noise leakage from the fast timestamp signals. The combined timing corrections improved pulser resolution from greater than 15 ns to less than 4 ns for all channels.

The algorithm is also demonstrated with two detectors in electronic coincidence. The detectors comprise 8x8 arrays of 1x1x1 mm^3 LSO crystals coupled to position sensitive avalanche photodiodes (PSAPD). The commons of each PSAPD were coupled to the RENA-3 readout ASIC. A Na-22 point source was used to generate coincident 511 keV photons. The coincidence time difference is gated to be in the 511 keV peak and corrected for per crystal time delay, signal amplitude and leakage from the time signals. The

two array system had a raw paired time resolution of 16.38±0.05 ns FWHM. The calibrated system had a paired time resolution of 7.30±0.02 ns FWHM.

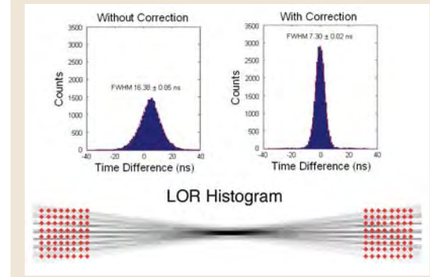

Timing histograms before and after correction for two detectors in coincidence. The line of response histogram is shown to demonstrate coincident pairings. Crystal locations are shown as red dots.

References/Funding Source

To appear in Nuclear Science symposium and Medical Imaging Conference Record, 2008.
Work funded by NIH R01CA119056
NIH R33 EB003283
NIH R01CA120474

Can Large-area Avalanche Photodiodes be used for a Clinical PET/MRI Block Detector?

H. Peng[1], P. D. Olcott[1], V. Spanoudaki[1], C. S. Levin[1]
Department of [1]Radiology, MIPS
Stanford University School of Medicine

We are studying a high resolution, Anger-logic based PET block detector design that uses large-area (~1 cm^2) avalanche photodiodes (APD). The crystal resolving ability in a crystal flood histogram is of our primary concern in this work. The figure of merit (FOM) is defined as the average peak-to-valley ratio (PVR) for the corner crystals and its neighboring crystals along the diagonal line. Using a Monte-Carlo simulation tool, we systemically optimized the detector design for crystal resolution, taking into account following factors: the width of the LYSO crystal, the optical diffuser thickness, the surface finish of crystals, the separation between APD arrays, and the signal-to-noise (SNR) of the system. An 8x8 array of 2.75x2.75x20 mm^3 LYSO crystals with specular reflectors on four sides is the optimum crystal design, which produced a FOM of about 43.2 with the SNR modeled to be around 90. Two light guide configurations were studied to address the light compression at the edge and corner of the crystal array: 1) a special 9 mm thick dual layer optical diffuser. The diffuser's edges have low reflective coefficient (~1%) from 0 to 2 mm while the remaining portion of the edge (2-9 mm) has high reflective coefficient (~96%) using specular reflectors. 2) the customized slotted 9 mm optical diffuser that minimizes the light sharing among four PSAPDs for the edge and corner crystals.

Our simulation results indicate that a SNR of at least 50 is required to resolve all 64 crystals which produced a FOM of 1.94, which is limited by both the light collection efficiency and the APD's shot noise. Based on the simulation results, a prototype block detector (8x8 LYSO, crystal size: 2.75x3.00x20 mm^3) and electronics were built. The preliminary flood map we obtained shows that an 8x8 crystal array is well resolved and the global energy spectrum exhibits an energy resolution of 12.9+/-0.3% for the 511 keV photopeak.

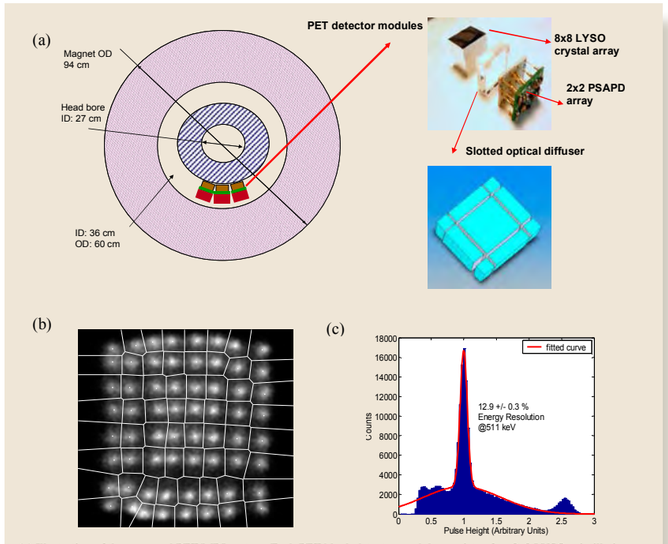

(a) Illustration of the proposed PET/MRI system. Each PET block detector module consists of an 8x8 LYSO scintillation crystal, light diffuser, 2x2 APD array (1 cm^2 area APDs), and custom readout electronics. (b) The flood map of the detector after Anger logic. (c) The global energy spectrum of the built block detector.

References/Funding Source

To appear in *Nuclear Science symposium and Medical Imaging Conference Record, 2008*.
GE Healthcare

Photon Multiple Interactions in a High Resolution PET System that Uses 3D Positioning Detectors

Y. Gu[1,2], C. S. Levin[2]
Departments of [1]Electrical Engineering, [2]Radiology, MIPS

We are developing 1 mm^3 resolution PET systems capable of positioning the 3-D coordinates of individual photon interactions in the detectors. One such PET system comprises two parallel and opposing detector panels, each assembled from 2200 pixellated LSO crystal arrays coupled to position sensitive avalanche photodiodes (PSAPD). The LSO-PSAPD pairs are arranged in 1100 dual-PSAPD flex cable modules.

We are studying analog multiplexing of the signals from each PSAPD within each module to reduce wire density. However, positioning ambiguity arises under this scheme if both PSAPDs are involved in a given photon event due to multiple interactions. In addition, since lower energy interactions in the detector generate less charge in the PSAPDs, they likely have worse spatial resolution. The primary objective of this study is to assess the effects of photon multiple interactions on the proposed multiplexing scheme. The second goal is to quantify the expected effect of accepting lower energy multiple detector interactions on system photon sensitivity. The system's characteristic Compton scatter patterns were also studied, which suggested row search across the panel face as the preferred initial direction of coincidence trigger search in the firmware logic.

Monte Carlo simulations revealed that less than 0.3% of all events interacting with a dual-LSO-PSAPD module would suffer from positioning ambiguity if the two PSAPDs within a module were multiplexed. To quantify effects of multiple interactions photon on overall photon sensitivity, the relationship between the minimum acceptable energy of interactions and the corresponding population of events falling within the 511 keV±12% window was studied. Compared to a system that acquires only photoelectric interactions ≥400 keV, the proposed data acquisition system designed to acquire all interactions ≥200 keV is expected to realize an improvement of effective sensitivity by factors of 1.5 and 3.8, respectively, for singles and coincidence photons.

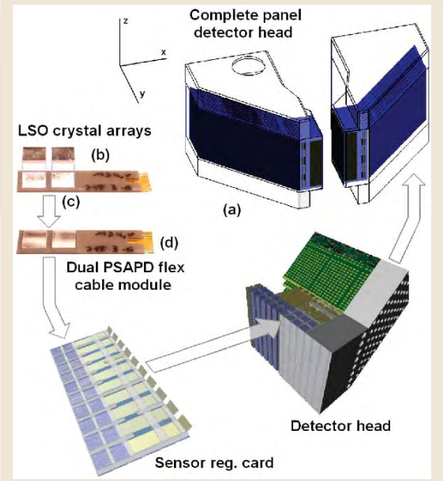

High resolution breast PET system overview.

References/Funding Source

To appear in *Nuclear Science symposium and Medical Imaging Conference Record, 2008*.
National Institute of Health grants R01 CA119056
R33 EB003283

Pulse Width Modulation: A Novel Readout Scheme For High Energy Photon Detection

P. D. Olcott[1,2], C. S. Levin[1]
Departments of [1]Radiology, MIPS, [2]Bioengineering
Stanford University School of Medicine

In standard PET scintillation detection, the energy, timing, and location of the incoming photon are recovered using analog signal processing techniques. The energy and location information are processsed using an analog-to-digital (ADC) converter that samples an analog value that is proportional to the integral of the charge created by the scintillation event. We propose to change the paradigm and modulate the width (rather than amplitude) of a digital pulse to be proportional to the integral of the charge created. The analog value of the outgoing digital pulses is recovered by using a time-to-digital converter in the back-end electronics, without the need for an ADC. Note that in this new scenario the same time-to-digital converter used to record the time of the event is used to recover the amplitude.

The main performance parameter that must be optimized is the dynamic range versus the dead-time of the front-end detector. The goal is an 8-bit dynamic range for this pulse-width modulation (PWM) scheme, which is adequate for high resolution PET detectors based on semiconductors such as avalanche photodiode (APD) or cadmium zinc telluride (CZT).

A novel circuit has been designed and simulated for the proposed PWM readout scheme. This circuit is different than previously developed time over threshold pulse width modulation circuits used in high energy physics. Using a standard JFET charge sensitive preamplifier connected to the pulse width modulation circuit, SPICE simulations predict there will be a 13.5% integral non-linearity over the input dynamic range for PET signals. For a fully 511 keV signal, the maximal pulse width required is 15 us. The maximal pulse width can be reduced for higher count rate applications, but at the price of a compromising dynamic range.

PWM techniques simplify the routing to the back end electronics without degrading the performance of the system. A readout architecture based on PWM processes digital rather than analog pulses, which can be easily multiplexed, enabling one to achieve very high channel density required for ultra-high resolution PET systems.

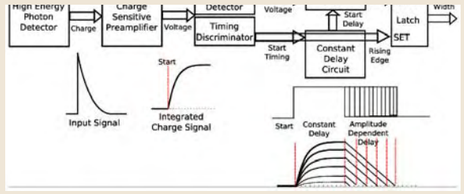

Pulse width modulation circuit converts the amplified and filtered electronic charge signal from the detector into a digital signal. The timing is encoded as the first rising edge, and each edge transition encodes a unique analog value. In this current implementation, one energy and one time is encoded into a single digital signal.

References/Funding Source

R01 CA119056
R33 EB003283
R01 CA120474
Society of Nuclear Medicine Molecular Imaging Predoctoral Fellowship

Novel Electro-optical Coupled PET Detectors for Whole Body Clinical PET/MR

P. D. Olcott[1,2], C. S. Levin[1]
Departments of [1]Radiology, MIPS, [2]Bioengineering
Stanford University School of Medicine

A new MR compatible PET detector design is being developed that uses electro-optical coupling to bring the amplitude and arrival time information of high speed scintillation pulses out of an MR system. Electro-optical coupling consists of a magnetically insensitive photodetector connected to a high gain, high speed, low noise preamplifier. The preamplifier directly drives a high speed VCSEL (HFE4192-581) laser diode that is connected to a multi-mode fiber 10 meters in length. The single mode fiber is read by a high performance photodiode (HFD3180-203), amplified and connected to standard PET electronics. This scheme essentially acts as an "optical wire" and, compared to signal transmission over standard co-axial cables, will have almost no influence on a MR system since the optical fibers are not conductive. Since the high speed analog signals are coupled by fibers, the only electrical connections to the PET detector consist of DC power cables which can be made anti-resonant to reduce loading on the RF coils within the MR system.

Using an 8 x 8 mm^2 large area, high gain avalanche photodiode coupled to a 8 x 8 x 2 mm^3 LSO sheet crystal in coincidence with an LSO-PMT detector, we measured and compared the energy and coincidence time performance for a standard coaxial cable connection and for the novel electro-optical signal transmission scheme proposed. Energy resolution at 511 keV was not significantly different between the two signal transmission methods (13.2 +/- 1.1% and 13.3 +/- 1.1%, respectively) but coincidence time performance was slightly degraded from 3.2 +/- 0.2 ns to 4.3 +/- 0.5 ns. However, the benefits of avoiding large bundles of co-axial cables, and their effect on MR performance outweigh the effects of this slight time resolution degradation.

High speed analog modulation using the VCSEL laser was successful and paves the way for a MR compatible PET block detector that has a very significantly reduced electronic footprint than a standard MR compatible PET detector. This enables the creation of a large axial FOV whole body clinical PET system that will have very little influence on whole body clinical MR system data.

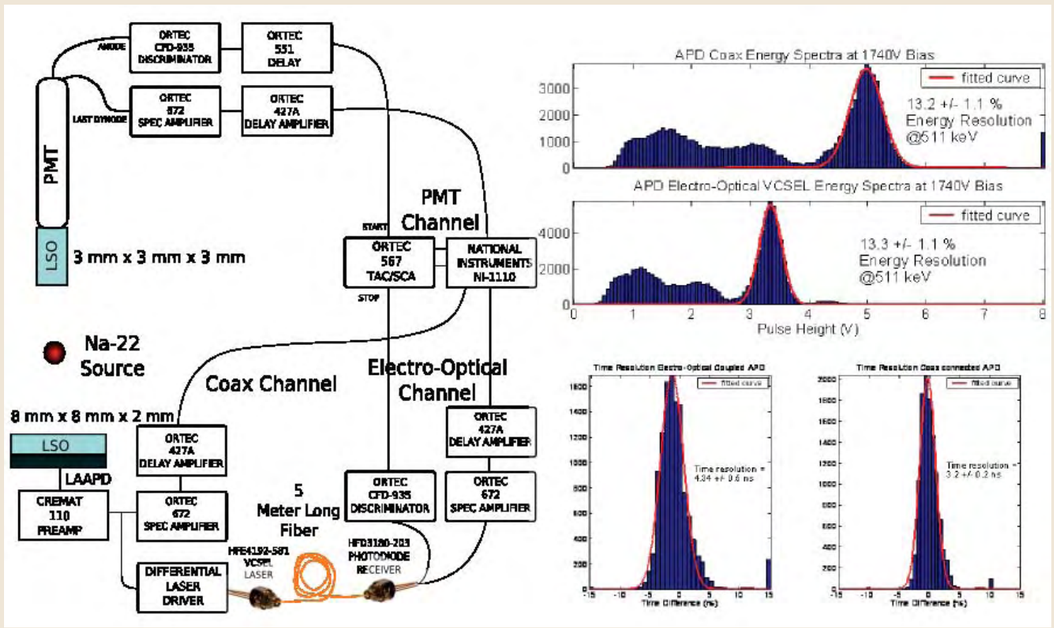

The data acquisition setup (left) produced electronic signals from large area high gain APD photodetectors irradiated from a Na-22 source. The signals were coupled over fiber and the energy and timing resolution were measured. There was no degradation in energy resolution, and a small, 30% degradation in timing resolution.

References/Funding Source

P. D. Olcott, C. S. Levin, "Novel Electro-optical coupled PET detectors for whole body clinical PET/MR", 2008 IEEE Medical Imaging Conference, Dresden Germany
GE PET/MR Industrial Research Project
Society of Nuclear Medicine Molecular Imaging Predoctoral Fellowship

A Multi-Collimation PET Image Reconstruction Algorithm

G. Chinn[1], C. Levin[1]
Department of [1]Radiology, MIPS
Stanford University School of Medicine

We evaluated a new image reconstruction algorithm using a Bayesian projector for multi-collimation PET systems. We are developing a PET system using high spatial and energy resolution 3-D detectors made from cadmium zinc telluride with cross-strip anodes and cathodes. This PET system can collimate photon pairs by coincidence timing and can collimate single photons by the kinematics of Compton scatter within the detector (Compton collimation). Compton collimation of single photons can dramatically increase overall photon sensitivity by making use of events that are discarded by conventional PET systems. However, Compton collimation offers lower spatial resolution than coincidence measurements. Previously, we showed that conventional maximum likelihood reconstruction by the list-mode ordered subset expectation-maximization (OS-EM) algorithm for these "multi-collimation" data sets yields no measurable improvement over images reconstructed using high-resolution coincidence collimation alone. We also studied a Bayesian projector function with non-uniform emission probability along the line of response weighted by an image prior generated from the low-resolution (Compton collimation) channel, to reconstruct the high-resolution (coincidence) channel. In this work, we investigated a novel approach using priors generated by reconstructing images from the high-spatial resolution coincidence data followed by post-reconstruction smoothing with a new spatially varying 3-D filter function and the Perona-Malik gradient anisotropic diffusion filter. For Monte Carlo simulations of spherical sources in a cylinder, the SNR for ROIs drawn in the spheres and the background both improved by over 20%.

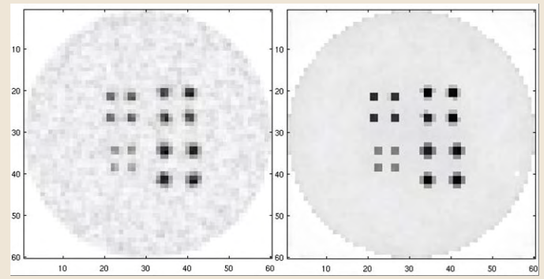

Shown are the reconstructed images for phantom 1 (idealistic energy blur model). (Left) The OS-EM algorithm using only coincidence events was used to reconstruct the image with 2 iterations, 10 subsets per iteration. (Right) The list-mode OS-EM algorithm was used to combine coincidence and single photons with a single iteration and 5 subsets. The Bayesian projector was used for Compton collimation and the standard projector was used for coincidence events.

References/Funding Source

IEEE Nuclear Science and Medical Imaging Conference, Honolulu, Hawaii 2008
NIH NIBIB R33 EB003283
NCI R01 CA119056
NIH R01 CA120474
UCBCRP 121B-0092

Study of a High Resolution, 3-D Positioning Cross-Strip Cadmium Zinc Telluride Detector for PET

Y. Gu[1,2], J. Matteson[3], R. T. Skelton[3], A. A. Deal[3], E. A. Stephan[3], F. Duttweiler[3], T. M. Gasaway[3], C. S. Levin[2]
Departments of [1]Electrical Engineering and [2]Radiology, MIPS, [3]Center for Astrophysics and Space Sciences, University of California at San Diego

We are studying ultra-high resolution PET systems built using Cadmium Zinc Telluride (CZT) detectors. The performance of a novel 1 mm resolution PET detector capable of positioning the 3-D coordinates of individual 511 keV photon interactions is investigated. The detectors used are 40×40×5mm^3 monolithic CZT crystals, and employ crossstrip readout to obtain high spatial resolution. Promising characteristics of CZT compared to scintillation detectors for PET include i) >95% inter-module packing fraction that promote >86% intrinsic detection efficiency for 511 keV photons in an "edge-on" detector arrangement; ii) an intrinsic spatial resolution defined by the anode and cathode strip pitch and the signal pulse heights; iii) capability of measuring the 3-D interaction coordinates of incoming photons, and iv) <3% FWHM energy resolution at 511 keV.

In the prototype setup, two pairs of opposing 40x40x5 mm^3 detector slabs are positioned 8cm apart and oriented to face incoming annihilation photons edge-on. Each CZT detector has 7 cathode strips covering the top 40×40mm^2 face and 38 anode strips interspersed with steering electrodes spanning the bottom face; the anode strips are oriented orthogonal to the cathodes.

The setup for measuring the energy resolution used a 250 μm diameter ^{22}Na annihilation photon point source; data was acquired as the source was moved along the center line between the opposing detector faces. The anode spectra showed an energy resolution of 3.1±0.2% at 511 keV, which corresponds well with prior studies on an earlier prototype designed for gamma-ray astronomy. For evaluating the detectors' spatial resolution a ~0.6mm diameter collimated beam of 122 keV single photons was used. The average spatial resolution value across the detector was measured to be 0.9±0.008 mm transverse to the collimated beam. The findings validate that the CZT-based detector concept has excellent performance and shows great promise for a high resolution PET system.

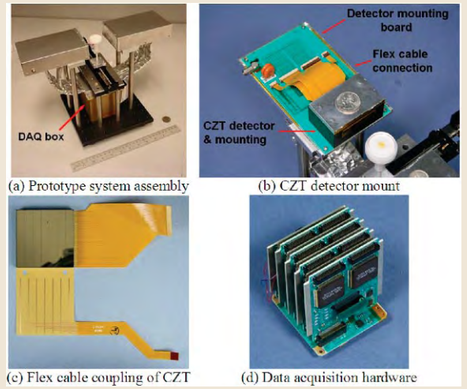

(a) Prototype system assembly (b) CZT detector mount
(c) Flex cable coupling of CZT (d) Data acquisition hardware

Prototype assembly and experimental setup comprising two "edge-on" CZT detector pairs, associated interconnections, readout electronics, and mechanical fixtures.

References/Funding Source

To appear in Nuclear Science symposium and Medical Imaging Conference Record, 2008.
National Institute of Health grant R01 CA120474

Maximum a Posteriori Event Positioning in High-Resolution PET CZT Detectors

G. Pratx[1], C. S. Levin[1]
Department of [1]Radiology, MIPS
Stanford University School of Medicine

Objectives: Cadmium-Zinc-Telluride (CZT) is a semi-conductor that can be used for PET detectors. It has high energy and spatial resolution, but low photo-fraction which means that 511 keV photons often create multiple interactions in the detectors. However, the 3-D location of each individual interaction can be read out. A challenge is to correctly estimate the first interaction, which best defines the correct line of response along which the two annihilation photons traveled. Previously, we had proposed a maximum-likelihood (ML) approach. In this work, we investigate a robust maximum a posteriori (MAP) positioning method.

Methods: The set of all possible sequences of interactions is generated. The ML criteria evaluate the consistency of the energy and position measurements. Robustness is added by considering multiple paths within the detector voxels. An accurate physical model of the a priori distribution is incorporated to compute the a posteriori probabilities. This model is based on the exponential attenuation law and the Klein Nishina formula. For fast computation, we have used graphics processing units to parallelize the algorithm. Results: To evaluate the algorithm, we generated simulated data using Monte-Carlo for CZT-based PET systems. Using MAP reduced the number of mispositioned events, which resulted in a reduction of the tails of the point-spread function and a higher contrast recovery for small lesions (see figure). The reconstructed size of "sphere" lesions was also smaller for MAP compared to all other positioning methods.

Conclusion: The MAP positioning method we have developed relies on a robust statistical framework that takes into account the stochastic properties of the imaging system. As a result, it performs better than all the other positioning methods we have tried, yielding improved quality images in which lesions are more easily identified.

References/Funding Source

R01 CA119056
R33 EB003283
R01 CA120474

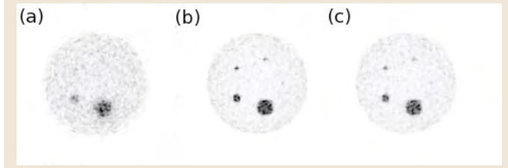

Reconstructed phantom using (a) interaction weighted mean, (b) ideal positioning, (c) MAP

Fast Maximum Likelihood Image Reconstruction via PCG without a Line Search

G. Pratx[1], Andrew Reader[2], C. S. Levin[1]
Department of [1]Radiology, Stanford, [2]Montreal Neurological Institute, QC, Canada

Objectives: Maximum Likelihood (ML) image reconstruction using the preconditioned conjugate gradient algorithm (ML-PCG) has been shown to converge to the ML estimate faster than expectation maximization (ML-EM). ML-PCG is however slower in the early iterations than ordered-subset (OS) EM, but ML-PCG is still preferred for converged regularized image reconstruction because of limit cycles. ML-PCG requires the computation of an optimal step size α for each iteration, which is conventionally computed by doing an iterative 1D line search, and often tens of iterations are needed (i.e. ~17% of the reconstruction time). We have derived a new analytical approximation for α that is accurate and 100X faster to compute.

Methods: The new formulation for α was derived directly from the log-likelihood for an inhomogeneous Poisson process, and requires just two scalar products (using the ML gradient direction and the projection of the current search direction, which are readily available in normal ML-PCG). The new method was evaluated on simulated 2D PET data.

Results: The accuracy of the new analytical α, compared to a line search, was assessed for two noise levels for different iterations. At the 1X noise level, the error in evaluating α was 0.8% RMSE (maximum error 2.0%). At the 4X noise level, the error was 1.7% RMSE (4.7% max error) (see Figure). Appealingly, the RMSE decreases to 0 at higher iterations. The method was then used in place of the line search in ML-PCG. In terms of mean-square error and log-likelihood, the resulting algorithm converges as fast as regular PCG to the exact same ML solution, but in 17% less time.

Conclusions: We have derived a new analytical expression for the optimal step size α, eliminating the need for an iterative line search. This formulation is accurate and fast, yielding a convergent ML-PCG algorithm.

References/Funding Source

R01 CA119056
R33 EB003283
R01 CA120474

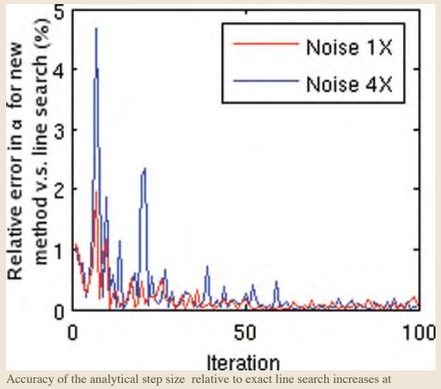

Accuracy of the analytical step size relative to exact line search increases at higher iterations.

Image siRNA Silencing in vivo with a Ribozyme-Mediated Reporter

M. K. So[1], G. Gowrishankar[1], S. Hasegawa[1], J. Rao[1]
Department of [1]Radiology, MIPS
Stanford University School of Medicine

Purpose: In recent years there is a great deal of interest in taking RNAi-based therapeutic to the pre-clinics. The ability of monitoring the efficacy of RNAi based drugs in vivo would help accelerate clinical translation. We present a new approach to image the specific siRNA mediated suppression on target RNA expression in vivo based on group I introns *Tetraymena thermophila* ribozyme, a class of catalytic RNA molecules, capable of catalyzing cis- and trans-splicing reactions.

Methods: We designed plasmid constructs containing the trans-splicing ribozyme, an engineered reporter mRNA, and an antisense sequence against an mRNA target. These constructs were able to bind the mRNA target and produce a fusion mRNA that could be translated into functional reporter enzymes. Firefly luciferase reporter has been exploited to image the mRNA of a dominantly negative p53 (p53DN) gene. Hydrodynamic injections were performed to deliver the ribozyme reporter and the p53DN expressing constructs along with p53 specific or negative control siRNAs to the livers of nude mice (n=6-8 each sample).

Results: *In vitro*, the p53-splicing dependant luciferase signal dropped significantly (89%) in the presence of the p53-specific siRNA but not with the negative control siRNA. The decrease in the luciferase activity correlated well with the drop in the p53 RNA levels (R^2=0.97). An 87% drop in splicing-dependant luciferase output was observed only in the mice injected with the p53-specific siRNA.

Conclusion: We present an RNA reporter construct based on trans-splicing ribozyme and have demonstrated its utility in direct imaging of the siRNA mediated specific suppression in gene expression in vitro and in vivo. This method may be applied to other targets to determine their siRNA efficacy in living subjects.

References/Funding Source

MK So, G Gowrishankar, S Hasegawa, JK Chung, J Rao. Imaging target RNA and siRNA mediated gene silencing in vivo with ribozyme based reporters. *ChemBioChem* 2008, in press.
DOD Breast Cancer Research Program IDEA award (W81X-WH-06-1-0251)
NCI ICMIC@Stanford (1P50CA114747)
Career Award at the Scientific Interface from the Burroughs Wellcome Fund
NCI's Small Animal Imaging Resource Program (SAIRP R24CA92862)
Stanford Cancer Biology Training Grant postdoctoral fellowship (PHS NRSA 5T32 CA09302-29) to GG

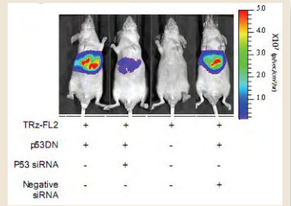

Bioluminescent imaging of siRNA mediated silencing of p53 expression in living mice. Ribozyme based RNA reporter (TRz-FL2), p53 dominantly negative gene (p53DN) and siRNA (p53 specific or negative) are introduced via hydrodynamic delivery to the mouse livers.

Quantum Dot Based Nanosensors for MMP Sensing

Z, Xia[1], Y. Xing[1], M. K. So[1], J. Rao[1]
Department of [1]Radiology, MIPS
Stanford University School of Medicine

Matrix metalloproteases (MMPs) are a family of secreted endopeptidases that play a crucial role in defining the cellular environment through regulated degradation and processing of extracellular matrices. MMPs are upregulated in almost every type of human cancer. MMP over-expression correlates with advanced tumor stage, increased invasion and metastasis, and shortened survival. To detect and image MMPs, we explored a novel and general strategy based on semiconductor nanocrystals (quantum dots, or QDs) and bioluminescence resonance energy transfer (BRET) -- an energy transfer process between a bioluminescent protein and a fluorescent acceptor. When a mutant of the bioluminescent protein *Renilla* luciferase (Luc8) was coupled to the QDs, the energy generated by Luc8 in the oxidation of the substrate coelenterazine can be transferred to QDs non-radiatively and produce the QD light emission.

Based on this QD-BRET technology, we designed a nanosensing system where Luc8 is linked to the QD through an MMP-cleavable peptide substrate (Scheme 1). In the absence of MMP, the QD conjugate can produce QD emission due to the BRET from Luc8. When the MMP is present, the peptide linker will be cleaved, leading to the releasing of the Luc8 from the QD and thus the disruption of the BRET. An intein-mediated protein splicing chemistry was applied to site-specifically ligate the fusion of the peptide substrate and the Luc8 to QDs so the MMP hydrolysis can cleave the Luc8 from the QDs. Several QD-BRET sensors were prepared for MMP-2, MMP-7, and urokinase detection in buffer, tumor lysates, and in mouse serum with a sensitivity of a few ng/mL. Multiplexed detection of several proteases using QD-BRET probes has also been achieved. We envision that the system would find wide applications such as in real-time monitoring of MMP activity in clinic samples and in facilitating the screening of inhibitors for MMPs as novel cancer therapeutics.

References/Funding Source

Z Xia, Y Xing, MK So, A Koh, R Sinclair, J Rao. Multiplex detection of protease activity with quantum dot nanosensors prepared by intein-mediated specific bioconjugation. *Submitted*.
DOD Breast Cancer Research Program Concept Award
NCI Centers of Cancer Nanotechnology Excellence (1U54CA119367-01).

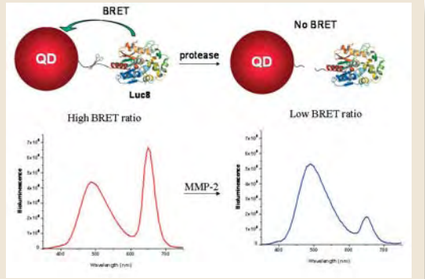

QD-BRET based nanosensors for MMP sensing. A) Schematic of the nanosensor made of a QD and luciferase proteins (Luc8) that are linked to the QD through an MMP peptide substrate. B) MMP-2 cleavage leads to the decrease in the QD emission and an increase in the Luc8 emission, resulting in the decrease of the BRET ratio.

Multi-echo Parallel Imaging Accelerated fMRI with Susceptibility-induced Off-resonance Compensation

H. Schmiedeskamp[1], R. D. Newbould[1], K. P. Pruessmann[2], R. Bammer[1]
Department of [1]Radiology, Stanford, [2]Institute for Biomedical Engineering, University and ETH, Zurich, Switzerland

Fast imaging sequences such as EPI suffer from image distortions and dropouts, precluding fMRI in areas of strong field inhomogeneities. In-plane distortion can be reduced by parallel imaging, however through-plane intra-voxel dephasing remains. The most prominent technique to overcome signal dropouts is z-shimming [1], which introduces multiple refocusing gradients in z-direction to rephase spins at certain off-resonance frequencies. The additional scan time necessary to acquire at least 2 images with different z-shim gradients is an issue. In this study, we propose using a multi-echo EPI approach together with parallel imaging to acquire multiple echo trains following a single signal excitation. Different z-shim gradients are applied to compensate for susceptibility-induced signal loss.

Using PERMEATE [2] (R=2, matrix size=96x96), three echoes fit into the acquisition time required for a single echo measurement with a near-optimal TE of 50 ms at 1.5T. The refocusing gradient in the slice-select direction was reduced to induce a z-shim gradient prior to the first echo train, resulting in high signal coverage mainly from dropout regions. A second refocusing gradient in z-direction was applied following the first echo train to fully rephase the spins in regions without strong off-resonance effects. A breath-holding experiment was performed to stimulate functional activation all over the brain. The different echo images were then combined for fMRI analysis.

The results (Fig. 1) show restored fMRI activation in typical dropout regions. In uniform regions, the signal was not compromised. Our susceptibility-compensated multi-echo fMRI acquisition technique can be used to acquire fMRI data with whole-brain coverage without significant reduction in sensitivity. The averaging of two echo images (echoes 2 and 3) restores most of the sensitivity loss caused by parallel imaging. Furthermore, this technique does not prolong scan time compared to standard acquisition sequences, making it a valuable alternative for whole-brain fMRI measurements.

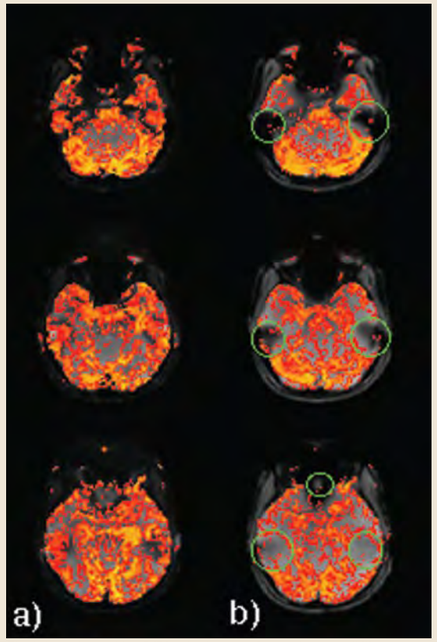

Fig. 1 shows the resulting fMRI activation maps from a) the susceptibility-compensated method and b) a separate 3-echo fMRI experiment using a regular rephasing gradient (no z-shimming). The fMRI signal could be successfully restored in the aforementioned dropout regions (encircled in green in the non-compensated experiment).

References/Funding Source

[1] Frahm et al, MRM 6:474-480, 1988
[6] Newbould et al, MRM 58:70-81, 2007
NIH 2R01EB002711
NIH 1R21EB006860
NIH P41RR09784
Lucas Foundation
Oak Foundation

Calibration Free Distortion Correction for Propeller EPI

S. Skare[1], J. Andersson[2], R. Bammer[1]
Department of [1]Radiology, RSL, Stanford University, [2]Oxford Centre for Functional MRI of the Brain (FMRIB), Oxford University, United Kingdom

The Short Axis readout Propeller EPI (SAP-EPI) pulse sequence [1] can reduce geometric distortions in high-resolution DTI. When combined with GRAPPA (R=3), distortion reductions of up to one order of magnitude have been achieved [2]. In this work, we present a distortion correction method that corrects the remaining distortion in the blades images using a generalization of the reversed gradient polarity method [3-4], in which one common distortion field is estimated for an arbitrary number of differently distorted blade images.

Prior to correction, each blade was zerofilled in k-space along the k_x direction, Fourier transformed, and counter-rotated by its nominal blade angle, making N temporary blade images, $I_{1..N}$, of the same size and patient orientation, but distorted along a unique direction, $\mathbf{v}_j$. A corrected blade, f_j, is obtained by resampling I_j based on the distortion field $d(\mathbf{c})$ along the direction $\mathbf{v}_j$, and intensity modulated according to

$$f_j = I_j\left(d(\mathrm{C})\mathrm{v}_j\right)\left(1 + D_{\mathrm{v}_j}\left(d(\mathrm{C})\right)\right) \quad [1]$$

where $D_{v_j}(d(\mathbf{c}))$ denotes the directional derivative of $d(\mathbf{c})$ along $\mathbf{v}_j$. To find a suitable $d(\mathbf{c})$, the following cost function is minimized iteratively:

$$O(\mathrm{C}) = \sum_{\mathrm{x}\in V}\left(\frac{1}{N-1}\sum_{j=1}^{N}\left(\frac{1}{N}\sum_{=1}^{N} f_k - f_j\right)^2\right) \quad [2]$$

In Fig. 1, distorted blade images for a phantom scan are shown on top of the propeller blades. The corresponding zerofilled and counter-rotated blades are shown above with white arrows indicating their individual distortion direction. Below, the variance maps before (top) and after (bottom) correction is given in conjunction with the corresponding $d(\mathbf{c})$.

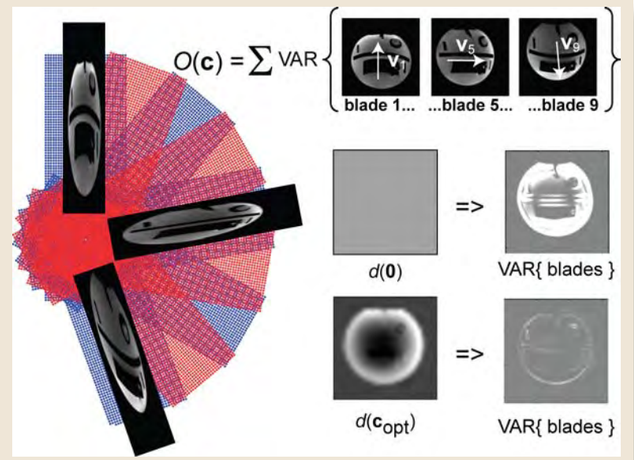

Distortion correction procedure. A distortion field, d(c), is found by minimizing the cost function, O(c). Variance maps over blades before and after correction shown to the bottom-right.

References/Funding Source

[1] Skare S et al. Magn Reson Med 2006;55(6):1298-1307.
[2] Skare S. 2006; Seattle. ISMRM. p 857. [3] Andersson J, Miller K. Personal Communication 2007.
[4] Chang H, Fitzpatrick J. IEEE Trans Med 1992;11:319–329.
R01EB002711
R21EB006860
P41RR09784
Swedish Research Council (K2007-53P-20322-01-4)
the Lucas foundation
the Oak foundation

GRAPPA-accelerated Readout-Segmented EPI for High Resolution Diffusion-Weighted Imaging

S.J. Holdsworth[1], S. Skare[1], R.D. Newbould[1], A. Nordell[2], R. Bammer[1]
Departments of [1]Radiology RSL and [2]Clinical Neuro Science, Karolinska Institute, Sweden

Introduction: Readout mosaic segmentation (RS-EPI) has been suggested as an alternative approach to EPI for high resolution diffusion-weighted imaging (DWI) (1). In RS-EPI scheme, segments of *k*-space (or 'blinds') are acquired along the readout direction. This reduces geometric distortions due to the decrease in echo spacing. In this work, peripherally cardiac gated and non-gated RS-EPI-DW images are acquired with the use of parallel imaging. We develop methods to both navigator-correct and correct for rigid-body motion between partial-Fourier RS-EPI blinds. It is assessed whether the RS-EPI scan time can be reduced through the use of non-gated acquisitions with minimally overlapping blinds using a typical set of scan parameters we are using for high resolution DW acquisitions at 3T.

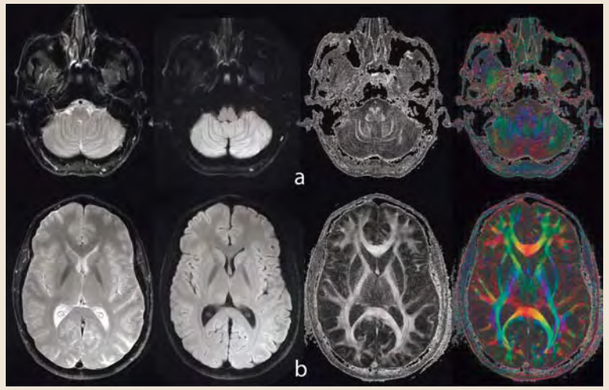

High-resolution DTI at 3T at the level of (a) the cerebellum, and (b) the corpus callosum. From left to right depicts the b =, b = 1000 isoDWI, FA, and FA with 1 st eigenvector color encoding. The scan parameters were as follows: B = 15, W = 64, 480 x 480 target resolution, R = 3, NEX = 3, 4mm slice thickness, FOV = 24cm, 2 b = 0 and 1 b = 1000 s/mm 2 scan along 15 non-collinear directions, TR/TE=3sec/60ms, 35min total scan time. Retrospective motion correction was applied on each diffusion-weighted image before final tensor processing.

Results: It is shown that patient handling can be simplified with the use of non-gated DW-RS-EPI acquisitions. Our experiments indicate that blind overlap is not necessarily required, even for uncooperative patients. With rigid-body and navigator correction, DW-RS-EPI remained robust even in the presence of relatively large rigid body motion.

We demonstrate that a combination of the RS-EPI *k*-space trajectory and parallel imaging results in high resolution T2-weighted and DW images with minimal geometric distortions. Clinical DW-RS-EPI images showed great improvement in geometric distortion properties compared with GRAPPA-accelerated EPI. This is particularly noticeable in regions around the auditory canals, nasal cavity, brain stem, and areas adjacent to the hemorrhagic lesions.

A target in-plane resolution of 480 x 480 chosen for the figure is beyond what is even used currently for most of the conventional scans. With a slice thickness of 4mm the voxels were anisotropic, but served to demonstrate the potential of such a high in-plane resolution for future developments in DTI and beyond. With this resolution and color FA maps at hand, for example, the different layers of the tapetum, the thalamic projections of the optic radiation, and the superior longitudinal fasciculus can be easily separated.

Summary: It is demonstrated that the combination of parallel imaging and the RS-EPI *k*-space trajectory results in images with reduced geometric distortions and exquisite spatial resolution at 3T in a scan time that is both clinically relevant, and considerably shorter than other high resolution DWI schemes.

References/Funding Source

(1) Porter D et al. ISMRM 2004;442.
S. J. Holdsworth, S. Skare, R. D. Newbould, R. Guzmann, N. H. Blevins, R. Bammer. *Readout-segmented EPI for rapid high resolution diffusion imaging at 3T.* European Journal of Radiology, 65 (2008) 36–46
S.J. Holdsworth, S. Skare, R. Newbould A. Nordell, R. Bammer, *"Practical Considerations for GRAPPA-Accelerated Readout-Segmented EPI in Diffusion-Weighted Imaging"*, #4 ISMRM 2008
S.J. Holdsworth, S. Skare, R. Newbould A. Nordell, R. Bammer, *"GRAPPA-Accelerated Readout-Segmented EPI for High Resolution Diffusion Imaging"*, #757 ISMRM 2008
NIH 2R01EB002711
NIH 1R21EB006860
Center of Advanced MR Technology at Stanford (P41RR09784)
Lucas Foundation
Oak Foundation
Swedish Research Council (K2007-53P-20322-01-4)

Single Step Non-Linear Diffusion Tensor Estimation In the Presence of Microscopic and Macroscopic Motion

M Aksoy[1], C Liu[1], M Moseley[1], R Bammer[1]
Department of [1]Radiology, RSL
Stanford University School of Medicine

The correction of motion artifacts is an essential prerequisite for reliable DTI. Due to the marked sensitive of diffusion sequences to small motion (e.g. brain pulsation), correction methods have thus far been focused mostly on correcting phase terms resulting from such microscopic motion. Effects on the processed diffusion tensor due to gross subject motion have been considered only in a few studies and only in the case of single shot sequences. For a multi-shot sequence, however, the rotational motion might cause each shot to be encoded with a different net diffusion encoding direction. Obviously, individual diffusion weighted images and ultimately the diffusion tensor information will suffer from substantial errors if this effect is not adequately addressed. In this study, we demonstrate the extent of the confounding effects from microscopic and macroscopic patient motion on DTI data and propose a non-linear approach to solve the diffusion tensor-signal equation for image reconstruction and tensor processing using Non-Linear Conjugate Gradient (NL-CG) optimization.

In the presence of microscopic and macroscopic motion, the obtained k-space data for a multi-shot & multi-coil scan is given by:

$$d_{\gamma,\delta,\xi}(\kappa)=\frac{1}{n_\rho}\sum_\rho m(\mathbf{r}_\rho)e^{-\sum_{i,j}[\mathbf{b}_{\delta,\xi}]_{i,j}[\mathbf{D}(\mathbf{r}_\rho)]_{i,j}}s_{\gamma,\delta,\xi}(\mathbf{r}_\rho)e^{-j\mathbf{k}_{\delta,\xi,\kappa}\cdot\mathbf{r}_\rho}$$

Due to the rotational motion, each interleaf will undergo a different diffusion encoding, as given by the ξ-dependence of the $\exp(-\mathbf{b}_{\delta,\xi}\mathbf{D})$ term. Therefore, it becomes evident that it is impossible to reconstruct an individual image with uniform diffusion-encoding. Thus, it becomes necessary to estimate the diffusion tensors **D** directly from the unity of all complex k-space data *d* that were acquired for all diffusion encoding directions. For this, we define a cost function, given by:

$$f(\mathbf{D},m)=\sum_{\gamma,\delta,\xi,\kappa}\left|d_{\gamma,\delta,\xi}(\kappa)-\frac{1}{n_\rho}\sum_\rho m(\mathbf{r}_\rho)e^{-\sum_{i,j}[\mathbf{b}_{\delta,\xi}]_{i,j}[\mathbf{D}(\mathbf{r}_\rho)]_{i,j}}s_{\gamma,\delta,\xi}(\mathbf{r}_\rho)e^{-j\mathbf{k}_{\delta,\xi,\kappa}\cdot\mathbf{r}_\rho}\right|^2$$

which will lead to minimum norm estimates of **D** and *m* by minimizing the discrepancy between the acquired k-space data, d, and the synthesized k-space data under consideration of motion in the diffusion tensor signal equation (right term).

For this study, a diffusion-weighted spin echo spiral in & out sequence was used. The spiral-in part was used to acquire a low resolution navigator image for each interleaf while the spiral-out part was used to acquire individual interleaves for the reconstruction of a final high resolution image.

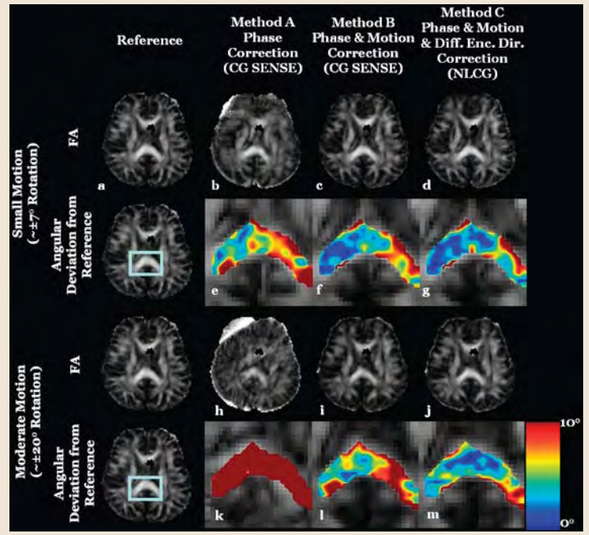

The FA maps and angular deviation maps obtained from an in-vivo experiment, reconstructed using the three different reconstruction methods. For both degrees of motion, the FA maps reconstructed with no motion correction show serious motion artifacts (b,h). With the application of motion correction using method B, these artifacts are significantly reduced (c,i). Application of method C gives FA maps of similar quality. However, method C gives more accurate tensor orientations compared to method B, as shown by the lowered angular deviation of the major eigenvectors from the reference orientations (f,g,l,m).

References/Funding Source

M Aksoy, C Liu, M Moseley, R Bammer, "Single Step Non-Linear Diffusion Tensor Estimation In the Presence of Microscopic and Macroscopic Motion", Magnetic Resonance in Medicine, Volume 59, Issue 5 , Pages 1138 - 1150
NIH 2R01EB002711
NIH 1R21EB006860
Center of Advanced MR Technology at Stanford (P41RR09784)
Lucas Foundation
Oak Foundation

Fully Automated System for Automated Analysis of Diffusion and Perfusion Images

M. Straka[1], G. Albers[2], R. Bammer[1]
Departments of [1]Radiology, RSL, [2]Neurology

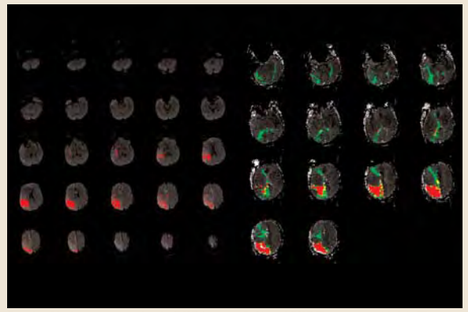

Result of lesion segmentation in DWI images (left) and PWI Tmax maps (right). The colors in Tmax maps indicate lesions for Tmax > 4s (green), Tmax > 6s (yellow) and Tmax > 8s (red). The DWI lesion size was 40ccm, whereas Tmax lesion size was 114 ccm (>4s), 52 ccm (>6s) and 44s (>8s).

Background: Perfusion and diffusion imaging can identify patient subgroups that are likely to benefit form reperfusion therapies. However, the use of MRI findings for patient selection in clinical trials is hindered by the lack of a automated method to rapidly process and analyze PWI and DWI images. We aimed to develop and test a fully automated MRI analysis software tool that 1) calculates PWI maps and 2) identifies DWI and PWI lesion volumes, both in real-time.

Methods: RAPID (Rapid Analysis of Perfusion Imaging Data) is a native C/C++ application with parallel computing to ensure fast data processing. The software processes raw DWI and PWI images and generates ADC, DWI and PWI Tmax maps. RAPID automatically segments DWI and PWI lesions and outputs the maps and lesion volume measurements to the scanner and the hospital PACS system.

Results: RAPID seamlessly integrates with MRI scanner software and the hospital PACS system. DWI and PWI maps with lesion segmentation and lesion volume assessment are available for online viewing on the hospital PACS system within 8 minutes after raw data was acquired. RAPID was tested using 30 data sets; the sensitivity for identifying a PWI-DWI mismatch pattern using the "DEFUSE" mismatch classification as the gold standard was 93% with a sensitivity of 53%. Lower sensitivity was due to inclusion of artifacts in the segmented PWI lesions leading to overestimation of the PWI lesion volume in eight cases. Three types of artifact were observed: artifact in the ventricles, artifact in the contra-lateral hemisphere or posterior fossa and movement artifact.

Conclusion: RAPID is a fully automated and fast software application that has great promise for use in multi-center clinical trials that require PWI-DWI mismatch assessment for patient selection. Reduction of existing artifacts is being addressed with modifications in both the RAPID program and PWI acquisition protocol.

References/Funding Source

private philanthropist donor

A Real Time Optical Motion Correction System Using a Single Camera and 2D Marker

M. Aksoy[1], R. Newbould[1], M. Straka[1], S. Holdsworth[1], S. Skare[1], J. Santos[2], R. Bammer[1]
Departments of [1]Radiology, RSL and [2]Electrical Engineering

Due to the prolonged acquisition time, motion correction in MRI becomes a must for achieving clinically acceptable image quality. This becomes especially important in the case of children and patients suffering from a medical condition that keeps them from staying still. Motion correction schemes can be classified as retrospective, where the motion correction is done after the data acquisition is completed, and prospective, where the motion correction is achieved in real-time during data acquisition. In general, retrospective schemes suffer from limited resolution and inability to correct for all types of motion. Previous prospective motion correction schemes utilized optical systems where the camera system had to be placed outside the scanner bore, but this requires sub-millimeter stereo position accuracy over a field of view of several meters. In this study, we use a shielded in-bore camera system that only requires a single camera and 2D marker, rather than at least two cameras and a 3D marker.

The presented real time optical motion correction system is capable of correcting in quasi real-time for both in-plane and through-plane rigid body motion. Our preliminary results show that the proposed system is effective in correcting for rigid body motion related artifacts. Both the intrinsic camera calibration and extrinsic scanner-camera calibration are semi-automatic and can be carried out each time with a relatively small overhead to the scanner usage time. This scheme can be used with more than one camera, which may add stability to the measurement, but at the cost in increased system complexity.

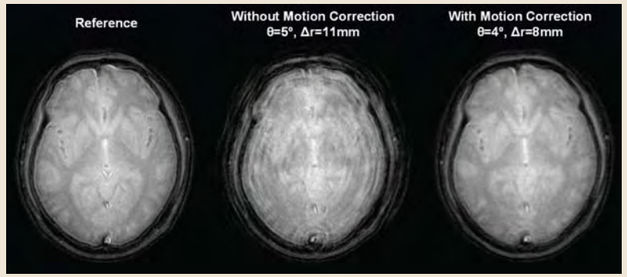

In-vivo images reconstructed with and without real time motion correction. Reference image obtained with no motion is shown on the left. The artifacts were apparent when motion was present (middle). Application of real time prospective motion correction significantly removed these artifacts (right).

References/Funding Source

M Aksoy, R Newbould, M Straka, S Holdsworth, S Skare, J Santos, R Bammer, "A Real Time Optical Motion Correction System Using a Single Camera and 2D Marker" ,Anuual Meeting of ISMRM in Toronto, Canada 3-9 May 2008
NIH 2R01EB002711
NIH 1R21EB006860
Center of Advanced MR Technology at Stanford (P41RR0978 4),
Lucas Foundation
Oak Foundation

Using DCE-MRI To Visualize Blood Flow in Head and Neck Tumors

R. Freiberg[1], Q. Le[1]
Department of [1]Radiation Oncology, Stanford University School of Medicine

Over the past year we have been utilizing the Lucas Center's unique capability to perform DCE MRI's for Dr. Quynh-Thu Le's investigator initiated trial, "A Multi-Institutional Phase II study of Radiation and GW572016 (Lapatinib) for Patients with Stage III-IV Head and Neck Cancer Who Cannot Tolerate Concurrent Chemoradiotherapy. LAP #109855" As part of our correlative studies we are assessing the blood flow to the tumors before and after a Lapatinib run in phase. With the help of Sandra Rodriguez and Anne Sawyer at the Lucas Center, eligible subjects undergo a protocol developed by the radiology teams at Duke University and Stanford University, designed to highlight the blood vessels in head and neck cancers. Four patients have been accrued to the study and three underwent sequential DCE MRI without any problem. Data were transmitted over a secure network connection to our collaborators who are responsible for the analysis of the information. In addition, images acquired during the scan are transmitted to our own facility (PACS) and are dictated to the patient record. Information gathered from these studies will contribute to our knowledge of how Lapatinib works, specifically its activity on tumor angiogenesis. The valuable service that the Lucas Center provides to investigators at Stanford University not only enables us to thoroughly investigate the effects of our study drug, but also allows us to carry out important correlative studies and cultivate collaborations with other institutions, keeping us at the leading edge of medical research.

Targeted Contrast Enhancement Using Linear System Theory

D. Kopeinigg[1,2], D. Fleischmann[1], M. Straka[1], R. Stollberger[2], R. Bammer[1]
Department of [1]Radiology, Stanford, Department of [2]Radiology, Medical University, Graz, Austria

"Targeted Contrast Enhancement Using Linear System Theory" is an attempt to improve contrast-enhanced angiography. The primary aim is to identify realistic patient specific injection protocols that result in a desired enhancement profile in the intravascular system. A vascular system characterization is performed by de-convolving a test bolus profile with an opacification profile resulting from a test bolus injection into the vascular system. Introducing a "forward approach" that takes physiological and technical constraints (maximum injection flow speed, recirculation) into account, allows the computation of an optimal injection profile.

A graphical user interface was developed and paired with modern optimization methods. This was used to generate injection sequences that lead to target enhancement profiles in the intravascular systems that closely resemble the desired enhancement profiles in a minimum-norm sense.

The in-vitro and in-vivo studies performed showed promising results. Fewer image artifacts and minimization of artery-vein overlays are likely outcomes of this project. The need to use less contrast agent is of particular importance in patients with an increased risk for Nephrogenic Systemic Fibrosis or Nephrogenic Fibrosing Dermopathy (NSF/NFD), other adverse reactions or children.

References/Funding Source

NIH 1R01EB002771+S1
NIH 1R21EB006860
NIH P41RR09784
Lucas Foundation
TU Graz
The authors are grateful to Bracco Diagnostics for providing the contrast agent to support these experiments

Role of Aberrant Behavior and Fragile X Mental Retardation Protein in Neuroanatomy

D. Gothelf[1,2], J. A. Furfaro[3], F. Hoeft[3], M. A. Eckert[4], S. S. Hall[3], R. O'Hara[5], H. W. Erba[3], J. Ringel[3], K. M. Hayashi[6], S. Patnaik[3], B. Golianu[7], H, C. Kraemer[5], P. M. Thompson[6], J. Piven[8], A. L. Reiss[1]
[1]Behavioral Neurogenetics Center, Child Psychiatry Dept, Schneider Children's Medical Center of Israel, Israel; [2]Tel Aviv University, Israel; [3]Center for Interdisciplinary Brain Sciences Research (CIBSR), Stanford; [4]Dept of Otolaryngology, Medical University of South Carolina, Charleston, SC; [5]Dept of Psychiatry and Behavioral Sciences, Stanford; [6]Laboratory of Neuroimaging, Dept of Neurology, UCLA School of Medicine; [7]Anesthesia, Stanford; [8]Dept of Psychiatry, University of North Carolina, Chapel Hill, NC

Introduction: Fragile X syndrome provides a model for elucidating critical linkages among gene, brain, and cognition in children with serious neurodevelopmental disorders.

Specific Aims: To determine how neuroanatomic variation in children and adolescents with fragile X syndrome is linked to reduced levels of the fragile X mental retardation-1 protein and to aberrant cognition and behavior.

Methods: In 84 children and adolescents with the fragile X and 72 controls matched for age and sex, brain morphology was assessed with volumetric, voxel-based, and surface-based modeling approaches.

Results: Fragile X showed significantly increased caudate nucleus and decreased posterior cerebellar vermis, amygdala, and superior temporal gyrus. A receiver operating characteristic analysis identified the combination of a large caudate with small posterior cerebellar vermis, amygdala, and superior temporal gyrus as distinguishing children with fragile X from control subjects. Large caudate and small posterior cerebellar vermis were associated with lower FMRP levels and more pronounced cognitive deficits and aberrant behaviors. Abnormal development of specific brain regions characterizes a neuroanatomic phenotype associated with fragile X syndrome and may mediate the effects of FMR1 gene mutations on the cognitive and behavioral features of the disorder.

References/Funding Source

Gothelf, D., Furfaro, J.A., Hoeft, F., Eckert, M.A., Hall, S.S., O'hara, R., Erba, H.W., Ringel, J., Hayashi, K.M., Patnaik, S., Golianu, B., Kraemer, H.C., Thompson, P.M., Piven, J., and Reiss, A.L. Neuroanatomy of fragile X syndrome is associated with aberrant behavior and the fragile X mental retardation protein (FMRP). Ann Neurol 2008;62(1):40-51.
NIMH (MH50047, MH01142)
NICHD (HD31715)
"Lynda and Scott Canel Fund forFragile X Research" (A.L.R.)
NIBIB (EB01651)
NCRR (RR019771) (P.M.T.)
NARSAD Young Investigator Award (D.G.)

3D SAP-EPI for Self-Navigated T1w Spoiled Gradient Echo Imaging

S.J. Holdsworth[1], S. Skare[1], A. Nordell[2], R.D. Newbould[1], R. Bammer[1]
Department of [1]Radiology, RSL, Stanford, Department of [2]Clinical Neuro Science, Karolinska Institute, Sweden

Introduction: 3D T1-w Spoiled Gradient Echo (SPGR) imaging is routinely used due to its high gray-white matter contrast and isotropic resolution. While the short TR makes the total scan time reasonable (~3-10 mins), certain patients have difficulties in remaining still during the scan, which leads to image ghosting and the need for reacquiring the data.

Short-axis readout propeller EPI (SAP-EPI) (1) has been suggested as an alternative approach to EPI to achieve higher resolution without the penalty of increasing distortions. In the SAP-EPI scheme individual EPI 'blades' are rotated through a central strip in *k*-space, which similar to PROPELLER allows for 2D motion correction between the blades. To achieve the above goal for 3D imaging, a 3D GRE version of the SAP-EPI sequence is implemented here, by acquiring 3D 'bricks'. The acquisition of one brick can be performed with full brain coverage in a couple of seconds, making the risk of intra-brick motion (ghosting) small and leaving only the inter-brick 3D motion to be corrected. We demonstrate motion and distortion-corrected human data from controlled motion experiments showing images with good T1-w gray/white matter contrast acquired in a sub-minute scan time.

Methods & Results: The 3D SAP-EPI sequence was performed on a 1.5T whole-body MRI unit (GE Excite) and an eight-channel head coil. Two human 3D SAP-EPI datasets were acquired, the second with both through- and in-plane rotation. Blade data were mixed such that every second blade was chosen from the rotated dataset. All bricks together are simultaneously motion and distortion corrected (2,3). Human data showing uncorrected and corrected data is shown in the accompanying figure.

Summary: We have presented an efficient propeller-based readout method that does not require the acquisition of FSE readouts, and enables the fast acquisition of T1w-SPGR images. Its inherent ability to allow motion- and geometric- distortion correction without the acquisition of any extra data makes 3D SAP-EPI a promising alternative sampling strategy to standard 3D T1w SPGR – a technique that often suffers from ghosting artifacts due to motion.

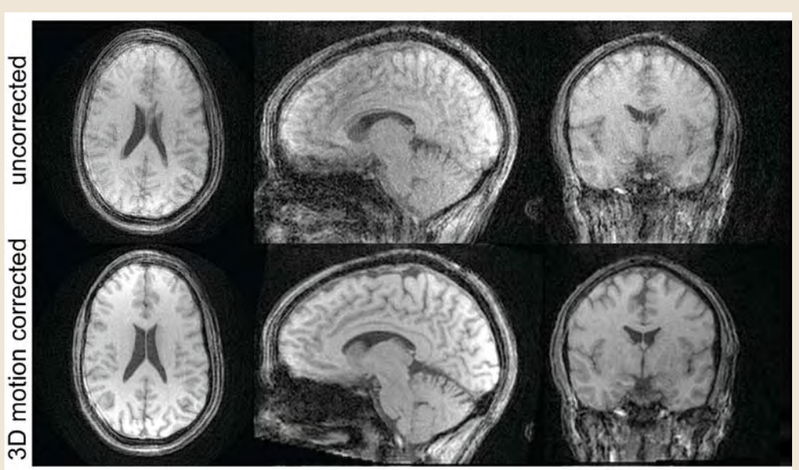

Human brain scans acquired with 3D SAP-EPI in the presence of 3D rigid-body motion. For 3D SAP-EPI, blades from two datasets with different brain orientations are mixed followed by 3D motion and distortion correction. Scan parameters were: Excitation with 5-lobe Sinc RF pulse (no fat sat); voxel size = 1.3x1.3x1.6 mm3; FOV = 25 cm^3; final volume resolution = 192x192x128; 8 blades of size 64x192x128; 180º sweep in x-y plane; a GRAPPA-acceleration factor = 3; NEX = 3; Full Fourier; TR/TE/FA = 40 ms/17 ms/60º; brick frame rate = 5s; total scan time = 2:35 mins.

References/Funding Source

(1) Skare S. et al. MRM 2006;55:1298-1307. (2) Andersson JL. Neuroimage 2003;20(2):870-888. (3) Skare S. MRM 2005;54(1):169-181
S.J. Holdsworth, S. Skare, A. Nordell, R. Newbould, R. Bammer, "3D SAP-EPI for Self-Navigated T1w Spoiled Gradient Echo Imaging", #1352 ISMRM 2008
NIH 2R01EB002711
NIH 1R21EB006860
Center of Advanced MR Technology at Stanford (P41RR09784)
Lucas Foundation
Oak Foundation
Swedish Research Council (K2007-53P-20322-01-4)

3D SAP-EPI for the fast acquisition of Susceptibility-Weighted Images

K. Marty[1], S.J. Holdsworth[1], S. Skare[1], R. Bammer[1]
Department of [1]Radiology, RSL
Stanford University School of Medicine

Introduction: Susceptibility-weighted imaging (SWI) has been utilized as a relatively new type of contrast in MRI (1). SWI consists of using both magnitude and phase images to provide improved conspicuity of venous blood vessels and other sources of susceptibility effects. Typically the SWI acquisition uses a high-resolution, three-dimensional gradient echo (GRE) sequence. However, the GRE acquisition used for SWI suffers from a long scan time (~7 mins) which decreases patient through-put and increases the chances of motion artifacts. A GRE-EPI-based trajectory has been proposed as a faster alternative, however the images may suffer from considerable blurring and geometric distortion artifacts. A short-axis readout propeller EPI (SAP-EPI) trajectory (2,3) has been suggested as an alternative approach to GRE-EPI to achieve higher resolution without the penalty of increasing distortions. The 3D SAP-EPI trajectory allows the acquisition of k-space in an efficient fashion (~2 mins), using a sampling scheme that can detect and correct for 3D rigid body motion and distortion. Here we show initial human SWI images acquired with our 3D SAP-EPI sequence.

Methods & Results:3D GRE and 3D SAP-EPI SWI acquisitions were performed on a 1.5T whole-body MRI unit (GE Excite) and an eight-channel head coil. The accompanying figure shows a comparison between SWI images acquired with 3D GRE (32 partitions, scan time of 7 mins) and 3D SAP-EPI (64 partitions, scan time = 2 mins). Although the resolution and conspicuity of the vessels in the GRE is better, our initial 3D SAP-EPI show images with high SNR; a reasonably low extent of geometric distortion; and a better extent of brain coverage in a faster scan time.

Summary: Here we have presented SWI images acquired with an efficient propeller-based readout method which has an inherent ability to allow motion- and geometric-distortion correction. Future work would therefore be to perform motion experiments and compare the images with 3D GRE – a technique that is prone ghosting artifacts due to motion. With its significantly shorter scan time, our initial data suggests that 3D SAP-EPI may be a useful alternative to GRE, particularly in uncooperative patients.

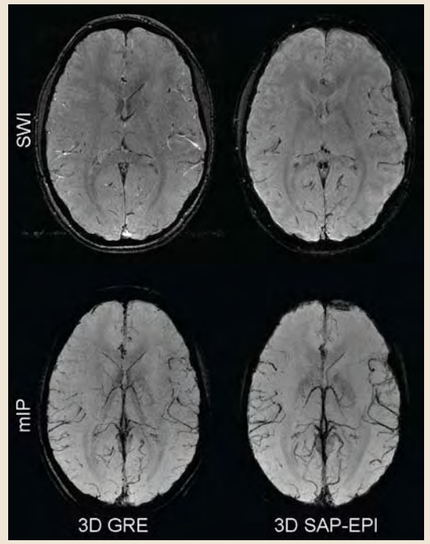

Human brain scans acquired with 3D GRE and 3D SAP-EPI (Top) SWI images (Bottom) SWI minimum intensity projection. The 3D GRE sequence was acquired with the following parameters: a target in-plane resolution = 512 x 256; slice thickness = 4mm; velocity compensation in all three directions; phase FOV = 0.75; TR = 52ms; 32 partitions; scan time 7min. The 3D SAP-EPI sequence used: 2-lobe sinc pulse with fat saturation; a target in-plane resolution of 360 x 360; GRAPPA-acceleration factor = 3; NEX = 3; 64 partitions; 8 blades of width 64; Full Fourier; TR = 60ms; scan time 2 min. Both sequences used a partition thickness of 2 mm, a FOV = 25 cm; TE = 40ms and a FA = 20º. For the SWI post-processing, a high-pass Hanning window filter is applied to the phase image followed by the creation of a normalized phase mask. This phase mask is multiplied by the magnitude image to increase the conspicuity of the vascular system.

References/Funding Source

(1) Haacke E. et al. MRM 52:612–618 (2004)
(2) Skare S. et al. MRM 2006; 55:1298-1307.
(3) Holdsworth S.J et al. #1352 ISMRM 2008
S.J. Holdsworth, S. Skare, A. Nordell, R. Newbould, R. Bammer, "3D SAP-EPI for Self-Navigated T1w Spoiled Gradient Echo Imaging", #1352 ISMRM 2008
NIH 2R01EB002711
NIH 1R21EB006860)
Center of Advanced MR Technology at Stanford (P41RR09784)
Lucas Foundation
Oak Foundation
Swedish Research Council (K2007-53P-20322-01-4)

Non-Cartesian Parallel Reconstruction Using Null Operations (NC-PRUNO)

J. Zhang[1,2], C. Liu[1], M. Moseley[1]
Departments of [1]Radiology, RSL, [2]Electrical Engineering

Non-Cartesian parallel imaging has been widely used since the innovation of conjugate gradient SENSE (CG-SENSE) reconstruction algorithm (1). Recently, several k-space reconstruction methods have also been developed for non-Cartesian trajectories (2-4). In most of these methods, each Cartesian k-space sample is synthesized one by one by linearly combining some acquired samples. Here we present a novel iterative reconstruction approach, in which we compute all missing interleaved non-Cartesian samples while assuring the consistency of all acquired samples at the same time. This method is based on our recently developed method for Parallel Reconstruction Using Null Operations (PRUNO) that has been applied for Cartesian trajectory. Here we demonstrate an algorithm for non-Cartesian Parallel Reconstruction Using Null Operations (NC-PRUNO).

In parallel imaging, due to the smoothness of coil sensitivity profiles, nearby k-space samples from multi-channels are highly correlated. Approximately, a certain subset of local neighbors may exhibit a linear dependence that is also shift invariant. Thus, there exists a non-zero linear operator, which nulls the corresponding subset of local samples. As in other auto-calibration based methods, we assume that a fully sampled k-space region is available. Then by choosing different neighbor templates, we can obtain multiple null operators from data calibration. Combining these null operations and griddings into encoding matrices, we can establish a linear system equation between missing interleaves of non Cartesian samples and acquired ones, for example, multi-shot spirals. And this equation can be efficiently solved by using an iterative conjugate-gradient approach, similar to non-Cartesian SENSE reconstruction. The algorithm has been successfully implemented and applied to variable density spirals (Fig 1).

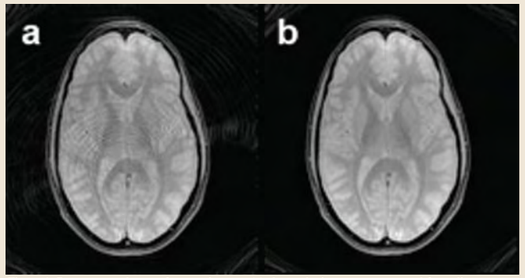

Figure 1: Reconstructed sum-of-square images. (a) shows the image reconstructed from direct regridding; (b) shows the image reconstructed from NC-PRUNO.

Here we have demonstrated a k-space iterative non-Cartesian parallel imaging method. The reconstruction is efficient since we don't need to do multiple data calibrations for every Cartesian sample or for every block of samples. Another advantage of NC-PRUNO is that it truly maintains the consistency of all acquired samples.

References/Funding Source

1. Pruessmann K, et al, Magn Recon Med, 46, 638-651, 2001;
2. Yeh E, et al, Magn Reson Med, 53, 1383-1392, 2005;
3. Liu C, et al. Proc 15th ISMRM, #332, 2007;
4. Lustig M, et al, Proc 15th ISMRM #333, 2007;
5. Griswold M, et al, Magn Reson Med, 47, 1202-1210, 2002;
6. Griswold M., et al, Magn Reson Med, 54, 1553-1556, 2005.
NCRR P41 RR09784
Lucas Foundation
NIH-1K99NS057943

Parallel Reconstruction Using Null Operations (PRUNO)

J. Zhang[1,2], C. Liu[1], M. Moseley[1]
Departments of [1]Radiology, RSL, [2]Electrical Engineering

As an auto-calibrated k-space parallel imaging method, GRAPPA (1) has shown its advantages in some applications when accurate coil sensitivity maps are difficult to obtain. However, there are two main drawbacks for GRAPPA, especially under large imaging acceleration. Here we propose an iterative k-space-based Parallel Reconstruction Using Null Operations (PRUNO) to overcome these shortcomings.

In parallel imaging, the coil sensitivity profiles are usually very smooth and k-space spectra are very compact. As a result, nearby k-space samples from multi-coils are highly correlated and some subsets of them may be approximately linearly dependent. In other words, there exists a non-zero, linear and shift-invariant operators, which nulls a selected local set of samples. By choosing different neighbor templates, we can obtain multiple null operators. The coefficients of each operator can be calibrated on ACS similar to GRAPPA. These operators essentially reveal the correlations among all samples and we can use them to formulate a linear equation between all k-space samples. In other words, by solving this equation, each of the unknown k-space samples from a certain channel can be linearly synthesized by from acquired samples among all coils. And a final reconstruction can be accomplished following this coil-by-coil k-space filling. Since each of the null operation is simply composed of 2D convolution and matrix summation, we can further develop an efficient iterative conjugate gradient method to solve the linear equation, which is similar to the iterative approach of non-Cartesian SENSE (4). Our preliminary simulation and *in vivo* results suggest that PRUNO can significantly improve the accuracy of image reconstruction compared to GRAPPA, as shown in Fig 1. Another advantage of PRUNO is that it doesn't require a large number of ACS lines and the number of necessary ACS lines doesn't depend on the reduction factor. According to our results, 2 to 4 ACS lines are sufficient for most reconstructions even with large reduction factors.

References/Funding Source

1. Griswold M, et al, Magn Reson Med, 47, 1202-1210, 2002.
2. Griswold M, et al, Magn Reson Med, 54, 1553-1556, 2005.
3. Liu C, et al. Proc 15th ISMRM, #332, 2007.
4. Pruessmann K, et al, Magn Recon Med, 46, 638-651, 2001
NCRR P41 RR09784
Lucas Foundation
NIH-1K99NS057943

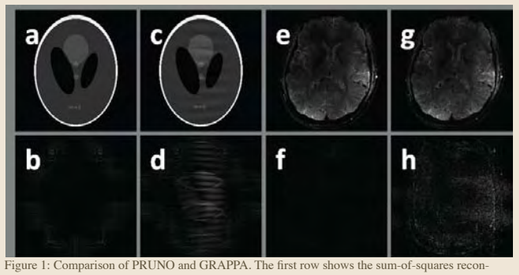

Figure 1: Comparison of PRUNO and GRAPPA. The first row shows the sum-of-squares reconstruction results using PRUNO and GRAPPA at 4-fold acceleration. Each image is compared with its corresponding Fourier reconstruction from full samples. The resulted magnified error images are displayed in the second row (shown at 5X). Among these images, the first and third columns are reconstructed using PRUNO. And the other two columns are results from GRAPPA.

Auto-Calibrated Parallel Imaging Reconstruction Using k-Space Sparse Matrices (kSPA)

C. Liu[1], J. Zhang[1,2], M. E. Moseley[1]
Departments of [1]RSL, [2]Electrical Engineering

A non-iterative parallel imaging reconstruction algorithm that utilizes **k**-space sparse matrix (kSPA) was recently introduced for arbitrary sampling patterns. The kSPA algorithm computes a sparse reconstruction matrix in **k**-space. This algorithm was shown to be particularly useful for a wide range of applications including 3D imaging, functional MRI (fMRI), perfusion-weighted imaging, diffusion tensor imaging (DTI) and massive parallel imaging, where a large number of images have to be reconstructed. The original algorithm requires the acquisition of low-resolution coil sensitivity maps. Methods for auto calibration become important in cases where sensitivity maps are difficult to obtain. Here we present an auto-calibrated kSPA algorithm for arbitrary trajectories that does not require the explicit estimation of coil sensitivities. We show that the sparse reconstruction matrix can be estimated directly from calibration data. In addition, we show that the calibration data can be located in any region of **k**-space.

One key result of the proposed auto-calibrated kSPA algorithm is that the reconstruction kernel can be computed using calibration data acquired at any location. To accomplish that we only need to translate the surrounding sampling points to center at a set of grid points in the middle of the calibration region. We then repeat the reconstruction for each coil to form the final image similar to the GRAPPA algorithm.

The auto-calibrated kSPA algorithm for parallel imaging reconstruction that can be applied to arbitrary **k**-space sampling trajectories. The sparse reconstruction matrix is solely determined by using the calibration data acquired on a region of 16x16 pixels. We also show that this calibration data in principle can be acquired at any region of **k**-space. For noisy data, better performance is achieved when the calibration data is acquired in the center of **k**-space where signal-to-noise ratio (SNR) is generally higher. Compared to the original kSPA technique, the proposed technique reconstructs each coil image separately and it does not require the explicit information of coil sensitivities. In cases where accurate sensitivity is difficult to obtain, auto-calibrated kSPA is more convenient.

References/Funding Source

Liu C, Zhang J, Moseley ME. Auto-Calibrated Parallel Imaging Reconstruction Using K-Space Sparse Matrices (KSPA). Proceedings of the ISMRM, 2008, Toronto, Ontario.
NIH-1K99NS057943
Lucas Foundation
NCRR P41RR09784

Correcting PWI-Based CBF Measurements for Arterial Input Function Partial Volume and Nonlinear Contrast Relaxivity: Comparison with a Xenon CT Gold Standard

G. Zaharchuk[1], R. Bammer[1], M. Straka[1], R. D. Newbould[1], J-M. Olivot[2], M. Mlynash[2], M. G. Lansberg[2], G. W. Albers[2], M. E. Moseley[1]
Departments of [1] Radiology, RSL and [2]Neurology

Bolus perfusion-weighted imaging (PWI) images provide reasonable relative CBF estimates and correlate well with gold standard methods such as H2O PET. One large problem is that the global CBF scaling factor varies between patients, such that absolute PWI-based CBF measurements are not reliable. Variable partial voluming (PV) of the arterial input function (AIF) is likely a major determinant of these variations. Since the superior sagittal sinus is larger than the typically chosen AIF arteries, the ratio of area under the curve of the AIF and the venous output function (VOF) may mitigate PV errors and improve the precision of PWI CBF. There is also evidence that the relationship between Gd concentration and $\Delta R2^*$ relaxivity is nonlinear at the concentrations found within large blood vessels.

Using a gold standard xeCT CBF measurement, we examined whether PWI CBF estimates can be made more precise (i.e., less intersubject variability) by correcting for PV and bulk blood (BB) nonlinear contrast relaxivity.

In our hands, PWI CBF maps created from single-shot EPI images underestimate xeCBF, have about 25% patient-to-patient variability, and have poor global CBF correlation with bias that is dependent on the baseline xeCBF levels. These factors limit diagnostic confidence of quantitative mrCBF measurements in individual patients. Limitations of the current study include the use of global CBF values for each technique; it is possible that there is better correlation for different tissue types (i.e., white vs gray matter) or based on CBF level (such as PWI overestimation of xeCBF in regions with large cortical vessels); examining this relationship will be a focus of future work. Further refinement in algorithms to remove PV artifact and to account for BB nonlinear relaxivity, coupled with improved AIF morphology achievable with multiecho sequences may lead to improvements in quantitative PWI CBF.

References/Funding Source

Zaharchuk G, Bammer R, Straka M, Newbould R, Olivot JM, Mlynash M, Lansberg M, Albers GW, Moseley M. Correcting PWI-Based CBF Measurements for Arterial Input Function Partial Volume and Nonlinear Contrast Relaxivity: Comparison with a Xenon CT Gold Standard. Proceedings of the ISMRM, 2008, p. 628, Toronto, Ontario
NIH 2R01EB002711
NIH 1R21EB006860
NIH P41RR09784
PERFUSE
Lucas foundation
Oak foundation

In Vivo Higher-Order Contrast Measured with Generalized Diffusion Tensor Imaging Using Higher-Order Tensors

C. Liu[1], S. C. Mang[2], M. E. Moseley[1]
Department of [1]Radiology, Stanford, Department of [2]Neuroradiology, University of Tuebingen, Germany

The higher order tensor (HOT) model by Liu et al proposes to quantitatively characterize general diffusion processes using a series of diffusion tensors with increasing orders. Each order of these tensors offers a well defined physical interpretation, with the second order tensor meaning the second order cumulant (covariance matrix), the third order tensor meaning the third order cumulant (skewness tensor), and the fourth order tensor meaning the fourth order cumulant (kurtosis tensor) and so on so forth. We present a very first in vivo implementation of generalized diffusion tensor imaging (GDTI) with HOT. Higher order diffusion tensors up to order four are measured. We further propose a set of techniques to generate higher order diffusion contrast. These higher order contrasts provide a vast amount of extra quantitative information, new visualization tools and potential biomarkers.

We have shown a successful measurement of higher order tensors up to order four. Those higher order tensors provide extra quantitative information of underlying tissue architecture that is not present in the second order model. Although we only have illustrated two examples of higher order contrast, many more contrasts measures can be defined accordingly. Although the exact physical and biological nature of these indexes is yet to be understood, it is clear that both LC and FA4 provide information that is independent of second order measures. This higher

order information also improves fiber tractography in regions where multi-modal diffusion exists and the second order model may fail. These higher order contrasts provide additional quantification of tissue integrity. In a deceased state, such as stroke and trauma, cellular damages in tissue could alter the diffusion property and possibly change the higher order contrast as a consequence of reduced non-Gaussian diffusion.

References/Funding Source

Liu C, Mang S, Moseley ME. In Vivo Higher-Order Contrast Measured with Generalized Diffusion Tensor Imaging Using Higher-Order Tensors. Proceedings of the ISMRM, 2008, p. 38, Toronto, Ontario.
NIH-1K99NS057943
Lucas Foundation
NCRR P41RR09784
German Academic Exchange Service
("DAAD-Doktorandenstipendium")

Matrix Formulation and Tikhonov-Regularized HYPR Reconstruction

M. Haeberlin[1,2], S. Skare[1], R. D. Newbould[1], K. P. Pruessmann[2], R. Bammer[1]
Department of [1]Radiology, Stanford, [2]Institute for Biomedical Engineering, University and ETH, Switzerland

A comparison between HYPR, common filtered backprojection (Iradon), CG-HYPR and the proposed method (Regularized CG HYPR). The main advantage of the proposed method is in the convergence behavior of the CG, which is stable. It also inherits HYPR's ability to suppress streak artifacts common in inverse Radon reconstructions. Without regularization, CG diverges and yields unacceptable results.

HYPR (HighlY constrained backPRojection) has previously been proposed by Mistretta *et al*. [1] as a non-iterative image reconstruction method for time-resolved MRA and has evolved ever since to tackle a multitude of reconstruction problems including less sparse data, such as those obtained with perfusion or diffusion imaging [7, 6]. The HYPR algorithm, however, exhibits an inherent inconsistency between the acquired projection data and the HYPR-synthesized projection data. To minimize this inconsistency Griswold *et al*. [2] recently proposed a Conjugate Gradients (CG) approach. Although self-regularizing, the CG method exhibits inherent instability in ill-posed problems which requires further regularization methods. A simple approach to stabilize the solution is Tikhonov regularization [8]. Tikhonov regularization has previously been proposed not only for MRI but also for backprojection-data, such as obtained with PET and CT [3, 4]. In extension to the work of Griswold [2] and Older [5], we put the backprojection reconstruction into a matrix formalism framework. The matrix formalism helps better understand HYPR and its variant, CG-HYPR. Moreover, it allows one to incorporate regularization techniques as demonstrated in this work by including Tikhonov regularization.

References/Funding Source

Maximilian Häberlin et al., "Matrix Formulation and Tikhonov-Regularized HYPR Reconstruction", Procs. ISMRM 2008
NIH 2R01EB002711
NIH 1R21EB006860
NIH P41RR09784
Lucas foundation
Oak foundation
Swiss-American Society

Modulation of Resting-State Brain Networks by COMT in Children

M. E. Thomason[1], D. J. Yoo[1], I. H. Gotlib[1], G. H. Glover[1,2]
Departments of [1]Psychology and [3]Radiology, RSL

Recent research has investigated the association between the COMT gene and schizophrenia, in part because of the involvement of COMT in the catabolic clearance of dopamine. In particular, the COMT Val allele has been associated with cognitive difficulties, such as problems in working memory and in the processing of information. In this context, the present study was designed to examine the effects of the COMT Val/Met polymorphism on neural functional connectivity in a sample of 9-15-year-old healthy children. More specifically, we examined both functional connectivity in resting-state brain networks and anatomical connectivity across discrete systems. For each child, we identified an executive network and a paralimbic network. We selected *a priori* regions of interest on the basis of dopamine neuron concentration, as well as control areas. We found that Val carriers demonstrated reduced functional connectivity in regions that subserve executive processing (e.g., prefrontal cortex). Importantly, Met homozygosity was associated with greater functional connectivity in regions with high concentrations of dopamine neurons (e.g., caudate, putamen, anterior cingulate, orbitofrontal cortex, prefrontal cortex). These data suggest that the COMT Val allele disrupts the functional connectivity of the executive and paralimbic networks in healthy children, and highlight the importance of examining the association of this polymorphism with cognitive functioning in samples of healthy individuals.

References/Funding Source

MH074849 to IHG
MH071996 to MET

Fiber Tracts Connecting Mid-Fusiform and Lateral Occipital Face-Selective Regions

J. Yoon[1], G. Golarai[1], M. B. Shachar[1], R. F. Dougherty[1], S. Hong[1], A. Liberman[1], K. Grill-Spector[1]
Department of [1]Psychology

Introduction: Functional neuroimaging studies of face processing reveal a network of regions involved in face processing, including a region in the fusiform gyrus (FFA), a region in lateral occipital cortex (OFA) and a region in the posterior STS. Models of face processing suggest a projection from OFA to the FFA (e.g., Haxby et al, 2000). Lesions to the FFA or the OFA are sufficient to induce prosopagnosia even when the rest of the network is structurally intact. This suggests that the FFA and OFA are necessary for successful face identification (Barton et al, 2002; Rossion et al, 2003; Steeves et al, 2006). However, little is known about the anatomical connections between the FFA and OFA.

Method: We acquired functional magnetic resonance imaging (fMRI) and diffusion tensor imaging (DTI) data in healthy adults and adolescents on a 3T GE scanner. In fMRI, subjects viewed images of faces, objects, scenes and textures in short blocks. FFA was defined as a face-selective region (faces > scenes & objects; $p<10^{-3}$) in the mid fusiform gyrus and OFA was defined with the same contrast, within the lateral occipital cortex. ROIs were defined in gray matter, then dilated to protrude into white matter. For fiber-tracking, we seeded the entire right hemisphere, tracked all fibers using Streamlines Tracking Technique (STT: Mori et al, 1999). Fibers were classified by their endpoints: Type 1 - endpoints in the FFA; Type 2 - endpoints in the OFA; Type 3 - endpoints in both FFA and OFA.

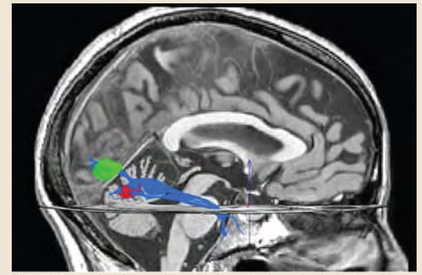

Fibers (blue) tracked from regions with face-selective activation in the mide-fusiform gyrus (red) and lateral occipital cortex (green).

Preliminary results: In four adults, fibers with endpoints in either the FFA or OFA (Types 1 and 2) projected to the temporal pole and frontal lobe. These pathways are likely to comprise portions of the inferior longitudinal fasciculus and inferior fronto-occipital fasciculus, respectively. We also found fibers of Type 3 which directly connect the FFA and OFA in the right hemisphere in 3 out of 4 adults. We will further examine the development of this pathway in a larger sample of adults and adolescents.

Conclusion: These findings suggest that the FFA and OFA are directly connected by white matter fiber tracts in adults, supporting the hypothesis that these two regions are part of a cortical network for processing faces. These initial findings enable us to measure individual differences in the diffusion properties of OFA-FFA fiber pathways and how they relate to performance in face recognition tasks.

References/Funding Source

NSF: BCS-0617688
NIH: 1R21EY017741
Klingenstein Fellowship in Neuroscience to KGS
NIH grant EY015000

Cognitive and Neural Basis of Memory in Older Aviators Genetically at risk for Alzheimer's Disease

M. M. Adamson[1, 2], B. Hutchinson[3], A. Wagner[3], J. L. Taylor[1,2]
[1]Department of Veterans Affairs and Sierra-Pacific MIRECC, Palo Alto, CA, Departments of [2]Psychiatry and Behavioral Sciences, [3]Psychology; Stanford University

The APOE ε4 allele is a major genetic risk factor Alzheimer's Disease (AD). Furthermore, over 25% of the general population are ε4 carriers. To enhance early identification of AD, studies are assessing the impact of ε4 on memory in older nondemented carriers. The literature is inconsistent and few studies have examined the impact of APOE ε4 in older professionals performing complex "real-world" tasks, such as flying an airplane. Results from our cross-sectional study in pilots from the Stanford/VA Aviation Study (n = 50) show that ε4 heterozygous carriers have lower Visual Paired Associate (VPA) recall scores than non-carriers despite no difference in hippocampal or frontal lobe volumes (Adamson *et al*., 2008). Aviators continuously employ visuo-spatial navigation in familiar and unfamiliar environments while flying, and this ability to fly an airplane has previously provided an ideal platform to study aging workers (Taylor *et al*., 2007). Therefore, the current fMRI study aims to investigate the impact of APOE ε4 on the neural mechanisms associated with memory during encoding of word lists in Rey Auditory Verbal Learning Test and route (Fig 1.A.) and survey (Fig 1.B.) perspectives in a perspective dependent task (Shelton & Gabrieli, 2002; 2005). Preliminary analysis of the BOLD response during the two perspectives in the perspective dependent task shows that route perspective activates hippocampus and parahippocampal region bilaterally (Fig 1.Ci: route vs. dot control). When compared to survey, route recruits additional activity in the left region ((Fig 1.Ciii: route vs. survey). The control task, not used previously, provides a better platform for extracting MTL activity than fixation. Forty actively flying, FAA medically certified aviators with a range of aviation expertise are being recruited for the study. We predict that ε4 carriers will show overall lower activation than non-carriers during memory encoding in MTL regions (specifically the hippocampus), prefrontal, parietal and anterior cingulate regions.

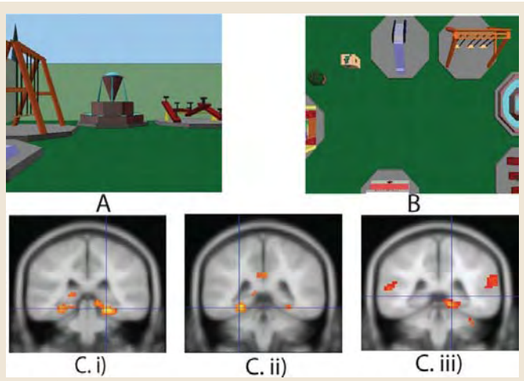

Figure 1 (File name: Taylor_Adamson_apoepilots.tif): Perspective dependent task: A. route perspective; B. survey perspective; & C. BOLD signal in MTL regions (hippocampus and parahippocampus areas): i) route vs. dot control; ii) survey vs. dot control, & iii) route vs. survey.

References/Funding Source

Adamson, M., Hutchinson, B., Rapakko, S., Samarina, V., Kennedy, Q., Rosen, A., Wagner, A., & Taylor, J. Neural Correlates of Perspective-Dependent Spatial Memory in Middle-aged and Older Pilots. [Poster for International Neuropsychological Society, Hawaii, Feb, 2008.]
Adamson, M., Landy, K.M., Duong, S., Fox-Bosetti, S., McCoy, D., Ashford, W.J., Murphy, G.M., Weiner, M., & Taylor, J.L. APOLIPOPROTEIN E ε4 influences on episodic recall and brain structures in aging pilots. (In Press).
Shelton, A. L., & Gabrieli, J. D. (2002). Neural correlates of encoding space from route and survey perspectives. J Neurosci, 22(7), 2711-2717.
Shelton, A. L., & Gabrieli, J. D. (2004). Neural correlates of individual differences in spatial learning strategies. Neuropsychology, 18(3), 442-449.
Taylor, J. L., et al. (2007). Pilot age and expertise predict flight simulator performance: A 3-year longitudinal study. Neurology, 68, 648-654.
P30AG017824 (Taylor: Pilot Grant 4.1)
R01 AG021632-04S1 (Adamson: Diversity Supplement).

Neural Correlates of Inhibitory Deficits in Depression

J. P. Hamilton[1], I. H. Gotlib[1]
Department of [1]Psychology

Although memory biases for negatively valenced stimuli have been reliably associated with depression and have been postulated to play a critical role in the maintenance of this disorder, the neural bases of these biases have received little attention. In this study, we tested a model of heightened memory sensitivity for negative information in depression in which neural mechanisms that normally facilitate memory for affective material are over-recruited during encoding of negative material in depression. We used functional magnetic resonance imaging to examine amygdala activity and functional connectivity with the hippocampus and caudate-putamen during successful encoding—as assessed by a recognition memory probe one week following scanning—of negative, neutral, and positive pictures by 14 depressed and 12 nondepressed individuals. Depressed individuals demonstrated greater memory sensitivity than did nondepressed participants to negative, but not to neutral or positive, stimuli. The right amygdala was more active and showed greater functional connectivity with the hippocampus and caudate-putamen during encoding of subsequently remembered negative, but not neutral or positive, stimuli in depressed than in control participants. The degree of memory-related right amygdala responsivity in the depressed participants was significantly correlated with depressive severity. These findings support the formulation that, in remembering negative information better than nondepressed persons, depressed individuals over-recruit a neural network involved more generally in enhancing memory for affective stimuli, and that the degree to which they over-recruit this system is related to the severity of clinical symptomatology.

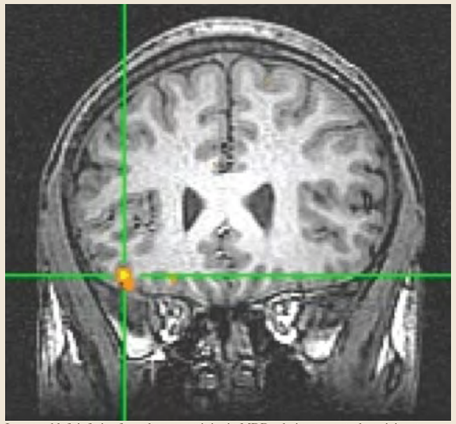

Increased left inferior frontal gyrus activity in MDD relative to control participants during expelling of negative versus neutral verbal material.

References/Funding Source

MH592599 to IHG

Modulation of Resting-State Networks by Anxiety in Adolescents

M. E. Thomason[1], D. J. Yoo[1], I. H. Gotlib[1], G. H. Glover[1,2]
Departments of [1]Psychology and [3]Radiology, RSL

Investigators have recently hypothesized that resting state-brain networks represent underlying functional activity, as well as anatomical connectivity, across discrete systems. The present study was designed to examine ways in which intrinsic activity may differ in two discrete resting-state systems, the default mode network (DMN) and the paralimbic network (PLN), in children as a function of levels of self-reported anxiety. Because anxiety in adolescence is a risk factor for generalized anxiety disorder and major depressive disorder, we hypothesized that children with higher levels of anxiety will show greater functional connectivity in regions of the DMN and PLN that have been implicated in anxiety, depression, and in the processing of negative affect. We examined 32 healthy children ages 9-16 in a 6-minute resting-state fMRI scan, and identified the DMN and PLN for each child. We used simple regression to identify significant clusters in these networks that varied as a function of levels of anxiety. We found greater connectivity strength in children with higher anxiety in middle frontal (BA9), left amygdala, anterior cingulate (BA25), and thalamic regions of the DMN, and precuneus (BA7), superior temporal (BA38/22), putamen, frontal, and thalamic regions of the PLN. In contrast, we observed greater connectivity strength in children with lower levels of anxiety in the left insula, and in middle temporal (BA21) and postcentral gyrus regions of the DMN, and anterior cingulate (BA24/31) and superior frontal (BA8/10) regions of the PLN. Significant clusters in these regressions comparing different levels of anxiety identify patterns of functional connectivity that underlie adolescent anxiety and that effects observed in MDD and in mood induction paradigms. It appears that anxiety in adolescents is associated with changes in resting functional brain connectivity. Continued delineation of the maturation of these systems will afford the opportunity for earlier detection and prevention of child psychopathology.

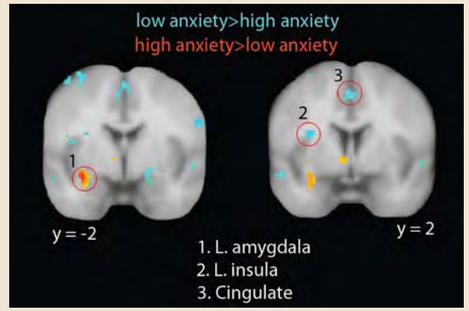

Increased connectivity strength in limbic regions in high anxiety children compared to their low anxiety counterparts. $p < 0.05$.

References/Funding Source

MH074849 to IHG
MH071996 to MET

Neural Correlates of Inhibitory Deficits in Depression

I. H. Gotlib[1], J. P. Hamilton[1], J. Joormann[2]
Department of [1]Psychology, Stanford,
Department [2]Psychology, University of Miami, FL

Depression is a widely diagnosed and highly debilitating disorder. Recurrent and often unintentional and uncontrollable negative thoughts are a hallmark feature of depressive episodes. Not only are these ruminative thoughts a debilitating symptom of depression, but they have also been associated with vulnerability to the onset of depression, the recurrence of depressive episodes, and the maintenance of negative affect. It is still unclear, however, why some people are especially prone to ruminate. Difficulties in executive functions in working memory, specifically inhibitory deficits, in depression have been proposed as an important underlying mechanism of rumination. In the present study, we used a modified Sternberg task to investigate neural correlates of the ability to remove irrelevant negative material from working memory in depressed and nondepressed participants. Thirteen participants meeting criteria for Major Depressive Disorder (MDD) and 15 age and sex-matched healthy control participants have been run in this study so far. fMRI was used to measure neural activation during the presentation of a cue that indicated that negative, positive, or neutral material should be expelled from working memory. Comparisons of trials in which the participants were instructed to expel negative material with trials in which participants were instructed to expel positive or neutral material show increased left inferior frontal gyrus (IFG) activity in depression during expel instructions. These findings support the formulation that depression is associated with unnecessary elaboration of negative material and point to the left IFG, a structure involved in maintenance of verbal information, in subserving this finding.

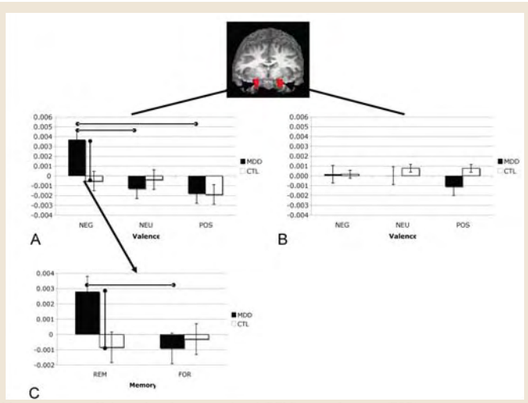

Mean contrast coefficient values from remembered (REM) versus forgotten (FOR) contrast across valence and group variables in peak left amygdala (A; −19, −4, −12) and right amygdala (B; 17, −5, −12) voxels, and REM versus fixation and FOR versus fixation for negative stimuli in each group (C).

References/Funding Source

MH592599 to IHG

Genetic Variation in the COMT Gene Alters Brain Blood Flow in Children

M. E. Thomason[1], G. H. Glover[2], I. H. Gotlib[1]
Departments of [1]Psychology and [2]Radiology, RSL

Maintenance of the brain's structural and functional integrity is ensured by the efficient delivery of blood in response to energy demands imposed by neural activity. A specific gene that has been found to be associated with differences is cognitive functioning and patterns of neural activation is the catechol-O-methyltransferase (COMT) gene, which codes for an enzyme that catabolizes dopamine. A relatively frequent val158met polymorphism in the general population, characterized by a methionine (met) to valine (val) substitution at codon 158, results in lower levels of COMT enzymatic activity and, consequently, in higher levels of extracellular dopamine, for met-allele carriers relative to val-allele carriers. The present study was designed to examine brain blood perfusion as a function of this COMT polymorphism, which should lead to a better understanding of the role of COMT in brain function. We studied resting cerebral and cerebellar perfusion in 42 9-15-year-old children using flow-sensitive alternating inversion recovery (FAIR) imaging. Met-carriers (N = 29) showed greater blood flow in prefrontal (BA 10, 11, 47), temporal (BA 21, 22, 37, 38), parahippocampal (BA 34), and lateral cerebellar (posterior lobe) regions. In contrast, Val/Val homozygotes (N = 13) had increased resting blood flow in temporal (BA 38, 39) and occipital regions (BA 18, 19) and, most notably, in the vermis of the cerebellum (0, -70, -22). Importantly, the regions that are characterized by greater blood flow in each group are implicated in behaviors that have been found to be differentially advantaged in the two groups. That is, whereas Met-carriers have been found to outperform Vals on high-order cognitive tasks (PFC, temporal lobe, parahippocampus), Val homozygotes appear to have an advantage in affective and emotional processing and regulation (cerebellar vermis).

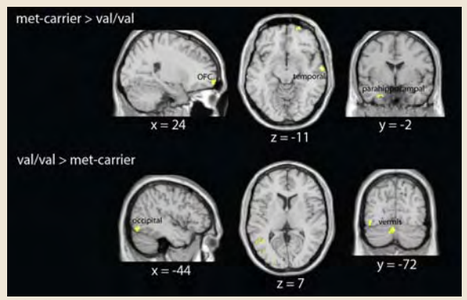

Main effects of genotype on resting brain perfusion: met-carriers compared to val/val homozygotes, p < 0.01, uncorrected.

References/Funding Source

MH074849 to IHG
MH071996 to MET

Abnormal Cortical Activation During Response Inhibition in 22q11.2 Deletion Syndrome

D Gothelf[1,2], F Hoeft[3], C Hinard[4], J F. Hallmayer[3], J Van Dover Stoecker[3], SE Antonarakis[5], MA Morris[4], AL Reiss[3]
[1]Behavioral Neurogenetics Center, Child Psychiatry Dept, Schneider Children's Medical Center of Israel, Petah Tiqwa, Israel; [2]Sackler Faculty of Medicine, Tel Aviv University, Tel Aviv, Israel; [3]Center for Interdisciplinary Brain Sciences Research (CIBSR), Stanford; [4]Service of Medical Genetics, Geneva University Hospitals, Geneva, Switzerland; [5]Dept of Genetic Medicine and Development, University of Geneva Medical School, Geneva, Switzerland

Introduction: 22q11.2 deletion syndrome (22q11.2DS) is a well-known genetic risk factor for schizophrenia. The catechol-O-methyltransferase (COMT) gene falls within the 22q11.2 minimal critical region of the deletion.

Specific Aims: To investigate brain activation during executive function in 22q11.2DS and those will different COMT polymorphisms.

Methods: Brain activity, as measured by functional magnetic resonance imaging (fMRI) during a Go/NoGo, response inhibition task was assessed in adolescents with 22q11.2DS (n = 13), typically developing (TD) controls (n = 14), and controls with developmental disability (DD, n = 9). Subjects with 22q11.2DS were also genotyped for the COMT Met/Val polymorphism.

Results:Groups did not differ on task performance. However, compared to both control groups, the 22q11.2DS group showed greater brain activation within left parietal regions. Comparison of brain activation between 22q11.2DS Met and Val subgroups revealed significantly increased activation (Met>Val) in the cingulate but not the dorsolateral prefrontal cortex. These preliminary findings suggest that adolescents with 22q11.2DS compensate for executive dysfunction via recruitment of parietal regions. Further, the COMT Met subgroup of 22q11.2DS may recruit additional cingulate activation for tasks requiring attention and inhibition. 22q11.2DS is a unique model for learning about the deleterious effects of decreased dosage of the COMT gene on brain function.

References/Funding Source

Gothelf, D., Hoeft, F., Hinard, C., Hallmayer, J.F., Van Dover Stoecker, J., Antonarakis, S.E., Morris, M.A., and Reiss, A.L. Abnormal cortical activation during response inhibition in 22q11.2 deletion syndrome. Human Brain Mapp 2007;28(6):533-542.
NIMH (MH50047, MH01142)
NICHD (HD31715)
"Lynda and Scott Canel Fund for Fragile X Research" (A.L.R.)
NIBIB (EB01651)
NCRR (RR019771) (P.M.T.)
NARSAD Young Investigator Award (D.G.)

Differential Associations with SES and Brain Activation in Dyslexic vs Typical Adolescent Readers

J. Black[1], C. Ho[1], J. Heitzmann[1], N. Zakerani[1], A. Reiss[1], F. Hoeft[1]
[1]Center for Interdisciplinary Brain Sciences Research (CIBSR)
Stanford University School of Medicine

Introduction: Extant work suggests that socioeconomic status (SES) is a robust predictor of reading ability, with higher SES related to greater reading proficiency. One study that examined the relationship between SES and reading-related brain activation suggests that SES modulates the relationship between phonological skills and brain activation in young children with various reading ability (Noble et al. Dev Sci 2006).

Specific Aims: To extend this finding and examine the association between SES and brain activation during phonological processing independently in adolescents with and without dyslexia.

Methods: Participants were 33 healthy, right-handed, English-speaking adolescents (12 males; 19 dyslexic). A composite SES score was calculated for each group independently through exploratory factor analysis of three scores (parental education, occupation, and family income). During fMRI, participants performed a real-word rhyme judgment task. Simple correlations between brain activation and SES were conducted using statistical parametric mapping (SPM2) (p-value=.005, extent threshold=10).

Results:Among typical readers, there was a significant positive correlation between SES and brain activation in the left hemisphere frontal and parieto-temporal regions as well as right frontal regions. Among dyslexic readers, significant positive correlations were found between SES and brain activation in right frontal regions similar to typical readers. Dyslexic readers showed no significant correlation in left hemisphere language regions though there were significant negative correlations in the right hemisphere regions homologous to that found on the left hemisphere in typical readers. The correlation between fMRI task performance and SES was not significant for typical readers (r=-.20, $p < .49$), though for dyslexic readers the correlation was tending toward significance (r=.41, $p < .08$).

References/Funding Source

Black, J.M., Ho, C., Heitzmann, J., Zakerani, N., Reiss, A.L., and Hoeft, F. Differential Associations with Socioeconomic Status and Brain Activation in Dyslexic versus Typical Adolescent Readers. Organization for Human Brain Mapping. June 2008; Melbourne Australia
Child Health Research Program (CHRP) from Stanford University School of Medicine (F.H.).

A medial prefrontal view of emotion regulation in humans: basic mechanisms and relevance to anxiety and mood disorders

A. Etkin[1], K. E. Keller[1], J. M. Anguiano[1], V. Menon[1], A. F. Schatzberg[1]
Department of [1]Psychiatry and Behavioral Sciences

Individuals with anxiety or mood disorders experience exaggerated or inappropriate emotional reactions, often despite deliberate and effortful attempts at emotion regulation. In this talk I will describe a limbic-medial prefrontal circuit involved in evaluating and regulating emotion outside of awareness, using a task employing salient emotionally conflicting stimuli. In healthy subjects, emotional conflict was associated with emotion-generation activity in the amygdala and insula, and emotion monitoring activity in the dorsomedial prefrontal cortex (PFC). Emotional conflict resolution was associated with activation of the ventromedial PFC and ventral anterior cingulate, and top-down regulation of limbic regions. Patients with generalized anxiety disorder (GAD) were unable to resolve emotional conflict, while those with major depressive disorder (MDD) resolved conflict similarly as controls. In GAD, failure to activate the ventromedial PFC to resolve emotional conflict was associated with limbic hyperactivation. Moreover, relative to matched controls, dorsomedial PFC responses to emotional conflict were of opposite directions in GAD (hypoactivated) and MDD (hyperactivated). Thus, an emotion regulation approach focusing on the dissociable roles of different medial prefrontal regions can provide valuable insight into the neural mechanisms underlying clinical disorders of anxiety or mood. These data also highlight the importance of understanding implicit forms of emotion regulation.

References/Funding Source

Etkin A, Anguiano JM, Keller KE, Menon V, Schatzberg AF (2008) Alterations in frontolimbic systems for emotion regulation in major depression and generalized anxiety Society of Biological Psychiatry, Washington, D.C.
Lucas Center pilot grant entitled: "Exploring the relationship between brain activity, interregional connectivity, and autonomic responsivity in healthy subjects and patients with generalized anxiety disorder" and internal funds

Gender Differences in the Mesocorticolimbic System During Computer Game-Play

F. Hoeft[1], C. L. Watson[1], S. R. Kesler[1], K. E. Bettinger[1], A. L. Reiss[1]
[1]Center for Interdisciplinary Brain Sciences Research (CIBSR)

Introduction: Little is known about the underlying neural processes of playing computer / video games, despite the high prevalence of its gaming behavior, especially in males.

Specific Aims:To investigate the neural correlates of gender difference in video-game play.

Methods: A functional magnetic resonance imaging study contrasting a space-infringement game with a control task.

Results:Males showed greater activation and functional connectivity compared to females in the mesocorticolimbic system. These findings may be attributable to higher motivational states in males, as well as gender differences in reward prediction, learning reward values and cognitive state during computer video games. These gender differences may help explain why males are more attracted to, and more likely to become "hooked" on video games than females.

References/Funding Source

Hoeft, F., Watson, C.L., Kesler, S.R., Bettinger, K.E. and Reiss, A.L. Gender differences in the mesocorticolimbic system during computer game-play. J Psychiatr Res 2008;42:253-258.

Passionate Love Attenuates Acute Pain Via Involvement of Dopaminergic Reward System Pathways

J. W. Younger[1], A. Aron[2], S. C. Parke[3], S. C. Mackey[1]
Departments of [1]Anesthesia and [3]Human Biology, Stanford, [2]Psychology, Stony Brook University, Stony Brook, NY

Recent neuroimaging studies suggest that passionate love recruits dopaminergic reward system circuitry, which has also been shown to produce analgesia. We hypothesized that feelings of passionate love would suppress acute thermal pain.

Six healthy individuals who were in the first 6 months of a romantic relationship, and who were passionately in love with their partner, completed a functional magnetic resonance imaging (fMRI) protocol in which they were exposed to three thermal stimulus intensities (none, low, and high) during completion of three tasks (viewing pictures of their beloved, viewing pictures of an equally attractive acquaintance, and performing a cognitively-demanding distraction task). Following each presentation, participants rated their pain on a visual analog scale via a button box. Functional MRI images were collected using a 3 Tesla GE scanner, adult head coil, and standard spiral in/out BOLD sequences with whole brain and brainstem coverage.

Self-reported pain was predicted by an interaction of task and stimulus intensity ($\chi^2 = 44.13$, $p < .0001$). Both the distraction task and beloved-pictures task significantly reduced self-reported pain in the model. The beloved task was associated with a 46% reduction of low intensity pain and a 13% reduction of high intensity pain. A significant, positive correlation was found between participants' self-reported degree of love with their partner, and their analgesic response in the beloved task ($r = .56$, $p = .028$). Above and beyond the acquaintance and distraction tasks, viewing pictures of the beloved was associated with decreased pain-related activity in the posterior anterior cingulate cortex and putamen, and increased activity in the ventral tegmental area, caudate and dorsolateral prefrontal cortex.

Our findings confirm the results of previous studies which show that evoked feelings of passionate love activate reward system pathways. We further demonstrate that activation of those systems via passionate love is associated with analgesia to acute, painful stimuli, via an apparently distinct neural mechanism from distraction.

References/Funding Source

International Association for the Study of Pain conference 2008
John and Dodie Rosekranz Pain Research Endowment

Voxel Based Orphometry Analysis of Patients with Chronic Neuropathic Pain

M. J. Barad[1], T. Ueno[2], R. Moulton[1], J. Younger[1], G. Glover[3], S. Mackey[1]
Departments of [1]Anesthesia, Stanford and [3]Radiology, Stanford,[2]Kyushu University, Fukuoka, Japan

Complex regional pain syndrome (CRPS) is a debilitating chronic neuropathic pain condition. Central mechanisms have been proposed to play a role in the generation and maintenance of many chronic pain conditions. In this study, our aim was to investigate regional gray matter volume differences between CRPS patients and controls through the imaging technique of voxel based morphometry.

Eighteen right-handed patients with upper extremity CRPS (mean age 41.7±11.3) meeting standard criteria for CRPS were matched with 25 right-handed controls (age 35.0±14.0). An additional strict match was performed with a subset of the original group containing 12 female patients (mean age 44.0 ±9.7) with right upper extremity CRPS and 12 age matched female controls (mean age 45.8±10.7). Voxel-based morphometry analyses were performed on high-resolution T1 magnetic resonance images using VBM 5.1 provided by Dr. Christian Gaser. Non-linearly warped modulated gray matter images were then submitted to an analysis of variance (ANOVA) ($p= 0.01$ corrected).

In the rough match, there was overall statistically smaller gray matter volume [$t(41)=3.714$, $p=0.001$], white matter volume [$t(41)=3.800$, $p<0.001$] and total brain volumes [$t(41)=3.736$, $p=0.001$]. We found that CRPS patients, compared to controls, had significantly reduced gray matter in the middle cingulate cortex. Additionally, when regressing age, the roughly matched group demonstrated significant bilateral gray matter reduction in the posterior insula extending into the secondary somatosensory cortex and the right primary motor cortex. In the strictly matched group, we found similar significant reduction of gray matter in the posterior cingulate gyrus, the bilateral posterior insula and secondary somatosensory cortex with extension into the bilateral primary sensory and motor cortex.

We observe significant gray matter reductions in CRPS patients, indicating abnormalities in both sensory and emotional processing of somatic information in these patients. These findings agree with previous studies that show gray matter reductions associated with chronic pain.

References/Funding Source

International Association for the Study of Pain conference, 2008
NIH NINDS R01 NS053961
Mentored Research Training Grant from the Foundation for Anesthesia Education and Research
John and Dodie Rosekranz Pain Research Endowment

Morphometry Differentiates Fragile X Syndrome and Control Boys of Ages One to Three

F. Hoeft[1], A. A. Lightbody[1], H. Hazlett[2], S. Patnaik[1], J. Piven[2], A. L. Reiss[1]
[1]Center for Interdisciplinary Brain Sciences Research (CIBSR), Stanford University, [2]Neurodevelopmental Disorders Research Center, University of North Carolina, Chapel Hill NC

Introduction: Studies of genetic disorders such as fragile X syndrome (FXS) which is a disorder caused by a single gene mutation resulting in abnormal dendritic and synaptic pruning, together with healthy individuals may provide valuable information to study gene, brain-behavior relationship.

Specific Aims: To examine morphometric spatial patterns that differentiate between FXS from controls in early childhood.

Methods: Voxel-based morphometry was examined in a total of 101 children of ages 1 to 3; 51 boys with FXS, 32 typically developing (TD) boys and 18 boys with idiopathic developmental delay (DD).

Results:In addition to aberrant brain structures reported previously in older individuals with FXS, we found reduced gray matter volumes in regions such as the hypothalamus, insula and medial and lateral prefrontal cortices. Further, multivariate pattern classification analyses discriminated FXS from TD and DD controls with over 90 % prediction accuracy. The spatial patterns that classified FXS from controls included those that may have been difficult to identify previously using other methods (e.g. amygdala, posterior vermis, hippocampus). These findings are critical in understanding interplay among gene, environment, brain and behavior, and signify the importance of examining detailed spatial patterns of healthy and perturbed brain development.

References/Funding Source

Hoeft, F., Lightbody, A.A., Patnaik, S., Hazlett, H.C., Piven, J., Reiss, A.L. Morphometric Brain Patterns Differentiate Boys with Fragile X Syndrome, Typical Development and Developmental Delay in Early Childhood. Arch Gen Psychiatr (in press)
MH64708-05 (A.L.R., J.P.)
MH61696 (J.P.)
HD03110-36 (J.P.)
Child Health Research Program (CHRP) from Stanford University School of Medicine (F.H.).

Overdrive of Humor-Related Brain Responses in Cataplexy

A. L. Reiss[1], F. Hoeft[1], A. S. Tenforde[1], W. Chen[2], D. Mobbs[1,3], E. J. Mignot[2]
[1]Center for Interdisciplinary Brain Sciences Research (CIBSR) and the [2]Center for Narcolepsy, Howard Hughes Medical Institute, Stanford, [3]MRC-Cognition and Brain Sciences Unit, Cambridge University, UK

Introduction: Cataplexy is a core symptom of narcolepsy, a sleep disorder affecting 1 in 2,000 persons. Cataplexy is most often triggered by strong emotions such as those associated with laughter.

Specific Aims: To examine neural systems underlying humor processing in individuals with narcolepsy.

Methods: We performed a functional magnetic resonance imaging (fMRI) study in 24 individuals with and without narcolepsy while they watched funny still cartoons. We also examined separately, a subject who experienced a cataplectic attack during the scan and compared both with healthy and with narcolepsy individuals. We measured their subjective ratings of funniness of the cartoons (in all subjects) and cataplectic symptoms (in the patients).

Results:Relative to controls, subjects with narcolepsy showed increased activation in several regions related to humor processing. Increased activation was also observed in ventrostriatal and thalamic regions typically associated with rapid-eye movement (REM) sleep, and in the ventrolateral prefrontal cortex, a region related to inhibitory control. In contrast, the subject experiencing the cataplectic attack showed dramatic reductions across these same regions as well as the dorsolateral prefrontal and primary motor cortices. These findings contribute to the elucidation of neural mechanisms underlying a propensity for cataplectic symptoms in individuals with narcolepsy.

References/Funding Source

Reiss, A.L., Hoeft, F., Tenforde, A.S., Chen, W., Mobbs, D., and Mignot, E.J. Anomalous hypothalamic responses to humor in cataplexy. PLoS ONE 2008;3(5):e2225.
Funded by NIH 23724
Howard Hughes Medical Institute

Aberrant Neural Function during Emotion Attribution in Females with Fragile X Syndrome

C. C. Hagan[1], F. Hoeft[2], A. Mackey[2], D. Mobbs[3], A. L. Reiss[2]
[1]University of York, United Kingdom; [2]Center for Interdisciplinary Brain Sciences Research (CIBSR), Stanford
[3]MRC-Cognition and Brain Sciences Unit, Cambridge University, UK

Introduction: Fragile X (FraX) syndrome is caused by mutations of the FraX mental retardation-1 gene - a gene responsible for producing FraX mental retardation protein (FMRP). The neurocognitive phenotype associated with FraX in females includes increased risk for social anxiety, depression, and attention deficit.

Specific Aims: To investigate the neurobiological systems underlying emotion attribution in females with FraX syndrome.

Methods: While undergoing fMRI, ten high-functioning females with FraX syndrome and ten typically developing (TD) female subjects were presented with photographs of happy, sad, and neutral faces and instructed to determine the facial emotion.

Results:No significant group differences were found for the recognition of sad and happy faces although the FraX group showed poorer recognition of neutral faces. Controlling for IQ and performance accuracy, TDs had greater activation than the FraX group in the caudate for sad compared to scrambled faces, and in the anterior cingulate cortex (ACC) for neutral compared to scrambled faces. In the FraX group, FMRP levels positively correlated with activation in the dorsal ACC for neutral, happy, and sad faces when independently compared to scrambled faces. Significantly greater negative correlation between IQ and insula activation for neutral relative to scrambled faces was observed in FraX compared to TD. Significantly greater positive correlation between IQ and ACC activation for neutral relative to scrambled faces was observed in TD compared to FraX. Though emotion recognition is generally spared in FraX syndrome, the social anxiety circuit (i.e., ACC, caudate, and insula) that modulates emotional responses to facial stimuli may be disrupted.

References/Funding Source

Hagan, C.C., Hoeft, F., Mackey, A., Mobbs, D., and Reiss, A.L. Aberrant Neural Function during Emotion Attribution in Females with Fragile X Syndrome. J Am Acad Child Adolesc Psychiatr (in press).
MH50047
Canel Family research fund

DTI in Williams Syndrome

F. Hoeft[1], N. Barnea-Goraly[1], B. W. Haas[1], G. Golarai[1], D. Ng[1], D. Mills[2], J. Korenberg[3], U. Bellugi[4], A. Galaburda[5], A. L. Reiss[1]
[1]Center of Interdisciplinary Brain Sciences Research (CIBSR), Stanford; [2]Psychology, Emory University, Atlanta, GA; [3]Pediatrics, Cedars Sinai Medical Center, Human Genetics, UCLA; [4]Laboratory for Cognitive Neuroscience, Salk Institute for Biological Studies, La Jolla, CA; [5]Neurology, Beth Israel-Deaconess Medical Center, Boston, MA

Introduction: Cognitive hallmarks of Williams syndrome (WS) include severe visuospatial deficits, and relative strengths in face and object processing (Meyer-Lindenberg et al., 2006). Functional neuroimaging data has indicated anomalous functional connectivity of the dorsal stream in WS.

Specific Aims: To investigate whether WS has aberrant connectivity of dorsal stream white matter tracts which may link between genetic and visuospatial abnormalities in WS.

Methods: We used diffusion tensor imaging to examine white matter integrity in the dorsal and ventral streams among individuals with Williams syndrome (WS) compared to two control groups (typically developing and developmentally delayed) and using three separate analysis methods (whole brain, region of interest, and fiber tractography).

Results:All analysis methods consistently showed that fractional anisotropy (FA, a measure of microstructural integrity) was higher in the right superior longitudinal fasciculus (SLF) in WS compared to both control groups. There was a significant association with deficits in visuospatial construction and higher FA in WS individuals. Comparable increases in FA across analytic methods were not observed in the left SLF or the bilateral inferior longitudinal fasciculus (ILF) in WS subjects. Taken together, these findings suggest a specific role of right SLF abnormality in visuospatial construction deficits in WS.

References/Funding Source

Hoeft, F., Barnea-Goraly, N., Haas, B., Golarai, G., Ng, D., Mills, D., Korenberg, J., Bellugi, U., Galaburda, A., and Reiss, A.L. More is not always better: Increased fractional anisotropy of superior longitudinal fasciculus associated with poor visuospatial abilities in Williams syndrome. J Neurosci 2007;27:11960-11965.
P01 HD033113-12 (NICHD).

Functional and Morphometric Brain Dissociation Between Dyslexia and Reading Ability

F. Hoeft[1,2], A. Meyler[3], A. Hernandez[1], C. Juel[4], H. Taylor-Hill[1], J. L. Martindale[1], G. McMillon[1], G. Kolchugina[1], J. M. Black[1], A. Faizi[1], G. K. Deutsch[1], W. T. Siok[1,5], A. L. Reiss[2], S. Whitfield-Gabrieli[1,6], J. D. E. Gabrieli[1,6]
[1]Psychology, [2]CIBSR, [4]Education, Stanford Univ; [3]Psychology, Carnegie Mellon Univ, Pittsburgh, PA; [5]Humanities and State Key Laboratory of Brain and Cognitive Sciences, Univ of Hong Kong, Hong Kong, China. [6]Brain and Cognitive Sciences, MIT Cambridge, MA

Introduction: In functional neuroimaging studies, individuals with dyslexia often exhibit both hypoactivation, often in left parieto-temporal cortex, and hyperactivation, often in left inferior frontal cortex.

Specific Aims:To perform fMRI and VBM analyses to interpret the differential relations of hypoactivation and hyperactivation to dyslexia.

Methods: We measured brain activation and grey matter morphology in dyslexic adolescents.

Results:Relative to the age-matched group (n=19, mean 14.4 years), the dyslexic group (n=19, 14.4 years) exhibited hypoactivation in left parietal and bilateral fusiform cortices, and hyperactivation in left inferior and middle frontal gyri, caudate, and thalamus. Relative to the reading-matched group (n=12, 9.8 years), the dyslexic group (n=12, 14.5 years) also exhibited hypoactivation in left parietal and fusiform regions, but equal activation in all four areas that had exhibited hyperactivation relative to age-matched controls. In regions that exhibited atypical activation in the dyslexic group, only the left parietal region exhibited reduced grey matter volume relative to both control groups. Thus, areas of hyperactivation in dyslexia reflected processes related to the level of current reading ability independent of dyslexia. In contrast, areas of hypoactivation in dyslexia reflected functional atypicalities related to dyslexia itself independent of current reading ability, and related to atypical brain morphology in dyslexia.

References/Funding Source

Hoeft, F., Meyler, A., Hernandez, A., Juel, C., Taylor-Hill, H., Martindale, J.L., McMillon, G., Kolchugena, G., Black, J.M., Faizi, A., Deutsch, G.K., Siok, W.T., Reiss, A.L., Whitfield-Gabrieli, S., and Gabrieli, J.D.E. Functional and morphometric brain dissociation between dyslexia and reading ability. Proc Natl Acad Sci USA 2007;104(10):4234-4239.
William and Flora Hewlett Foundation
Richard King Mellon Foundation
BrightStar Inc.

Neuroanatomical Correlates of Reading Development in Adolescents with Dyslexia

C. Ho[1], A. Gantman[1], J. Black[1], J. Heitzmann[1], N. Zakerani[1], A. Reiss[1], F. Hoeft[1]
[1]Center for Interdisciplinary Brain Sciences Research (CIBSR), Stanford
Stanford University School of Medicine

Introduction:Dyslexia is a developmental condition that affects much as 17% of children (Shaywitz, 1994). In examining the neurobiology of dyslexia, voxel-based morphometry (VBM) studies have shown reduced gray matter density and volume in the left parieto-temporal and left occipito-temporal regions of dyslexic readers when compared to normal readers (Brown et al., 2001; M. A. Eckert et al., 2005; Silani et al., 2005).

Specific Aims:Using VBM, this longitudinal study will extend upon previous studies by examining the structural correlates of reading development in adolescent dyslexic readers.

Methods:Twenty two adolescents with dyslexia were followed up for 2.5 years. Participants' IQ and word identification (WID) abilities were tested at baseline and follow-up. High resolution anatomical scans were collected at baseline for optimized and modulated VBM analysis. Whole brain regression analyses between local gray and white matter volumes and delta standard scores (ss) were performed, while regressing out baseline age, IQ and WID scores as nuisance variables.

Results:Significant correlations were found between delta WID-ss and regional gray matter volumes. Delta WID-ss was found to be positively correlated with gray matter volumes in the Right Postcentral Gyrus, Inferior Parietal Lobule, Precentral Gyrus, Medial Frontal Gyrus, and Superior Frontal Gyrus. Delta ID-ss was found to be negatively correlated with gray matter volumes in the Right Fusiform Gyrus, Superior Temporal Gyrus, Parahippocampal Gyrus, and Claustrum. No significant correlations were found between delta ID-ss and white matter volumes. These results may suggest an association between reading capacity and the development of compensatory strategies in dyslexic readers.

References/Funding Source

Ho, C., Gantman, A., Black, J.M., Heitzmann, J., Zakerani, N., Reiss, A.L., and Hoeft, F. Neuroanatomical Correlates of Reading Development in Adolescents with Dyslexia: A Longitudinal Study. Organization for Human Brain Mapping. June 2008; Melbourne Australia
Brown, W. E., Eliez, S., Menon, V., Rumsey, J. M., White, C. D., & Reiss, A. L. (2001). Preliminary evidence of widespread morphological variations of the brain in dyslexia. Neurology, 56, 781-783.
Eckert, M. A., Leonard, C. M., Wilke, M., Eckert, M., Richards, T., Richards, A., et al. (2005). Anatomical signatures of dyslexia in children: unique information from manual and voxel based morphometry brain measures. Cortex, 41, 304-315.
Shaywitz, S. E., Fletcher, J. M., & Shaywitz, B. A. (1994). Issues in the definition and classification of attention deficit disorder. Topics in Language Disorders, 14, 1-25.
Silani, G., Frith, U., Demonet, J. F., Fazio, F., Perani, D., Price, C., et al. (2005). Brain abnormalities underlying altered activation in dyslexia: a voxel based morphometry study. Brain, 128, 2453-2461.
Child Health Research Program (CHRP) from Stanford University School of Medicine (F.H.).

Inferior Frontal Activation Predicts Development of Compensatory Reading Skills in Dyslexia

F. Hoeft[1], C. Ho[1], J. Heitzmann[1], C. Hulme[2], H. Lyytinen[3], B. McCandliss[4], J. D. E. Gabrieli[5], A. L. Reiss[1]
[1]Center for Interdisciplinary Brain Sciences Research (CIBSR), Stanford; [2]University of York, York, UK; [3]University of Jyväskylä, Finland; [4]Sackler Institute, New York, NY; [5]Massachusetts Institute of Technology, Cambridge, MA

Introduction: About one-fifth of individuals with developmental dyslexia develop compensatory skills for reading by the time they reach adulthood but the mechanisms remain unknown.

Specific Aims: Investigation of brain activation patterns that predict future reading gains in dyslexic children.

Methods: We studied 45 children with and without dyslexia with a baseline fMRI and behavioral testing, and followed them up for an average of 2.5 years.

Results:Eleven of the 25 adolescents with dyslexia no longer fulfilled the criteria of dyslexia at the time of follow-up. Greater right inferior frontal activation during a phonological processing task at baseline predicted gains of reading skills in the dyslexic group, suggesting that this region is critical for the development of compensatory skills. None of the behavioral measures of reading and cognitive abilities used in the study predicted gains in reading. Greater reading improvement in the control group on the other hand, was predicted by lesser baseline reading skills and lesser left frontal activation including inferior frontal and precentral regions. Our study suggests one potential mechanism in which individuals with dyslexia may develop compensatory skills for reading. The inclusion of neuroimaging measures may enhance our ability to predict reading outcomes and children's responsiveness to educational interventions.

References/Funding Source

Hoeft, F., Ho, C., Heitzmann, J., Hulme, C., Lyytinen, H., McCandliss, B., Gabrieli, J.D.E., and Reiss, A.L. Inferior Frontal Activation Predicts Development of Compensatory Reading Skills in Dyslexic Adolescents. American Educational Research Association (AERA). March 2008; NYC NY USA
Child Health Research Program (CHRP) from Stanford University School of Medicine (F.H.).

Predicting Gains In Reading Abilities Using Diffusion Tensor Imaging (DTI) In Dyslexia

N. Zakerani[1], B. McCandliss[2], C. Ho[1], J. Heitzmann[1], J. M. Black[1], X. R. Ojo[1], J. D.E. Gabrieli[3], A. L. Reiss[1], F. Hoeft[1]
[1]Center for Interdisciplinary Brain Sciences Research (CIBSR), Stanford, [2]Sackler Institute, New York, NY; [3]Massachusetts Institute of Technology, Cambridge, MA

Introduction: Predicting reading outcome is important for the early identification and remediation of reading disabilities.

Specific Aims: The present study investigated the relationship between white matter integrity and individual differences in reading gains in adolescents with dyslexia.

Methods: We performed DTI and a battery of behavioral tests in 20 children (age 14.1 + 1.9) with dyslexia and followed them for 2.5 years.

Results:Individual differences in baseline fractional anisotropy (FA) measured by Reproducible Objective Quantification Scheme (ROQS) and reading scores (in 67 typical and poor readers) replicated findings from Niogi & McCandliss (Neuropsychologia 2006); single word reading scores correlated positively with left Centrum Semiovale FA values. As a group, children with dyslexia showed significant gains in standard scores of reading over 2.5 years (5 + 7.3, p = 0.007). Greater gains in decoding regressing out baseline age, IQ and decoding scores, were predicted by greater FA values of the bilateral Superior Coronal Radiata (SCR; right (r = 0.64) left (r = 0.59), not significantly different between hemispheres), but not FA of other fibers. These findings provide evidence of white matter pathways that may be associated with the development of compensatory mechanisms in dyslexia.

References/Funding Source

Zakerani, N., McCandliss, B., Ho, C., Heitzman, J., Black, J.M., Ojo, X.R., Gabrieli, J.D.E., Reiss, A.L., and Hoeft, F. Predicting Gains In Reading Abilities Using Diffusion Tensor Imaging (DTI) In Adolescents With Dyslexia. Cognitive Neuroscience Society Annual Meeting. April 2008; San Francisco, CA, USA
Child Health Research Program (CHRP) from Stanford University School of Medicine (F.H.).

Neural Basis of Resilient Readers in Dyslexia

J. Heitzmann[1], C. Ho[1], A. Reiss[1], F. Hoeft[1]
[1]Center for Interdisciplinary Brain Sciences Research (CIBSR)

Introduction: Only recently has it been explored that some dyslexic readers may classify as 'resilient readers' because of their average or above average text comprehension skills.

Specific Aims: To investigate the neural basis of resilient readers,

Methods: A total of 62 healthy native English speakers between 6-16 years of age (mean 13.4, standard deviation (SD) 2.6) participated in our study. Among them, 31 children were skilled readers and 31 were dyslexic readers with and without poor reading comprehension skills (15 and 16 children, respectively). We performed voxel-based morphometry (VBM) and examined differences in regional gray and white matter volume (GMV, WMV) in dyslexic adolescents with and without poor reading comprehension. We also performed phonological and semantic processing tasks utilizing functional magnetic resonance imaging (fMRI) to identify whether there were corresponding differences in brain activation.

Results: Whole brain analysis of GMV regressing out total GMV showed significantly greater GMV in the left parieto-temporal region in the Dys[NormComp] compared to the Dys[PoorComp] Group ($p<0.01$ corrected). This cluster included two distinct peaks in the left posterior superior temporal gyrus (pSTG) and inferior parietal lobule (IPL). There were no significant differences in WMV. Post-hoc region-of-interest analysis showed significantly greater GMV in controls compared to Dys[NormComp] and Dys[PoorComp] combined ($t(59)=2.09$, $p=0.04$), but not compared to Dys[NormComp] only ($t(59)=0.72$, $p=0.48$).

Corresponding to the cognitive characteristics, left parieto-temporal activation during rhyme judgment showed no significant difference between Dys[NormComp] and Dys[PoorComp], but Dys[NormComp] compared to Dys[PoorComp] showed significantly greater activation during semantic categorization in this region.

Results: The findings suggest that the left parieto-temporal region is spared in resilient readers, despite their poor phonological processing. Further research is necessary to corroborate these results.

References/Funding Source

Heitzmann, J., Ho, C., Reiss, A.L., Gabrieli, J.D.E., and Hoeft, F. Resilient Readers in Dyslexia Show Spared Left Parieto-Temporal Region. Organization for Human Brain Mapping. June 2008; Melbourne Australia
The William & Flora Hewlett Foundation
Richard King Mellon Foundation
BrightStar, Inc.
Stanford Child Health Research Program (CHRP)

Decreased Amygdalar Volume in Familial Subsyndromal Bipolar Disorder

A. Karchemskiy[1], A. Garrett[1], M. Howe[1], N. Adleman[1], D. Simeonova[1], A. Reiss[1], K. Chang[1]
Department of [1]Psychiatry and Behavioral Sciences
Stanford University School of Medicine

Objective: Children of parents with bipolar disorder (BD) ("bipolar offspring"), especially those with symptoms of depression, mania, and/or attention-deficit/hyperactivity disorder (ADHD), have been shown to be at high-risk for developing BD. This study examines amygdala volumes in bipolar offspring, who have early mood symptoms but no full blown bipolar diagnosis.

Methods: A sample of 22 subsyndromal bipolar offspring subjects (12.3 +/- 2.5 years old) and 22 healthy controls group-matched for age, gender, handedness, and IQ (13.1 +/- 2.7 years old) participated in the study. All subsyndromal subjects met criteria for ADHD and had moderate mood symptoms, with a score of >10 on the Young Mania Rating Scale or a score of >30 on the Children's Depressive Rating Scale – Revised. MRI was performed on a 3T GE scanner, using coronal 3D volumetric spoiled gradient echo series, and data analyzed using BrainImage software v. 5.3.7. Amygdalae were traced on positionally normalized brain stacks and volumes were compared using ANCOVA, with total brain volume and age as covariates.

Results: Bipolar offspring with subsyndromal BD had significantly smaller amygdalar volumes (10.6% decrease; p = 0.015), driven by a decrease in right amygdala (p = 0.031). The figure shows a scatterplot of amygdala volumes in subsyndromal and control subjects.

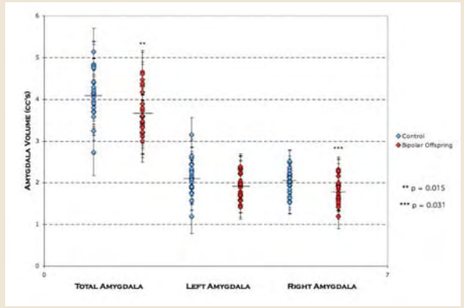

Preliminary Spectral Results from Key Regions of Interest

Conclusions: Decreased amygdalar volume, which might be associated with abnormal emotional regulation, may present as a trait finding before the onset of full mania. Whether the degree of the amygdalar volume decrease can be a predictor of which subsyndromal individuals will develop BD can be explored by longitudinal studies of subsyndromal bipolar offspring.

References/Funding Source

Klingenstein Third Generation Foundation (Chang)
NIH MH64460-01 (Chang)

Identification of Genetic and Neurobiologic Risk Factors for the Development of Early-Onsest Bipolar Disorder

K. Chang[1], M. Howe[1], A. Garrett[1], R. Kelley[1], E. Weitz[1], M. Pease[1], A. Reiss[1]
Department of [1]Psychiatry and Behavioral Sciences

Bipolar disorder (BD) is a chronic disorder carrying high morbidity and mortality. Up to 2-4% of the U.S. population may be affected by bipolar spectrum disorders. Numerous twin and family studies have supported the high heritability of BD. It is becoming increasingly clear that the genetic basis of BD is likely due to multiple inherited genes of small to moderate effect, which can combine in various ways to provide varying risk for BD.

This study aims to identify structural and functional characteristics of the amygdala and prefrontal cortex, as well as allelic variants, that predict BD in children at risk. We will compare our findings to unaffected siblings, bipolar offspring who are largely symptom free and thus are at reduced risk of BD development. This discordant sibling design will control for large environmental factors and will allow both risk factors and protective factors to be ascertained.

In particular, we will determine the association between BD risk and the serotonin transporter. The serotonin transporter protein is involved with regulating the concentration of available synaptic serotonin and thus may have widespread effect on mood and mood regulation. The presence of the s-allele of the serotonin transporter protein may confer increased risk for depression when combined with stressful life events. This finding has been replicated in children with histories of maltreatment. Therefore, the s-allele of 5-HTT may confer risk for development of mood disorders, including BD, particularly in the context of psychosocial stress.

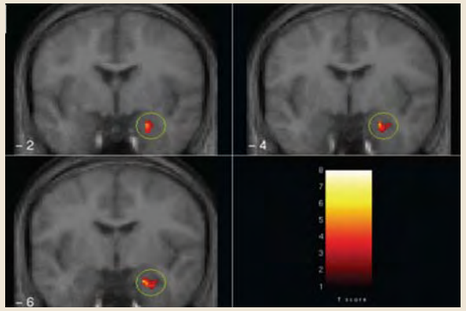

Preliminary Spectral Results from Key Regions of Interest.

We will also study the characteristics of the amygdala and prefrontal cortex that confer risk for BD. The amygdala is particularly relevant to the pathophysiology of BD, and demonstrates activation abnormalities during functional imaging studies of adults with BD. Our lab has demonstrated activation of the amygdala during the presentation of fearful facial expressions (see Figure), and will use a similar paradigm to study amygdala activation in children at risk for BD. Volumetric findings in adults with BD have been mixed, but 6 of 7 pediatric studies show decreased amygdala volumes in BD. Our lab has also found decreased amygdala volume in pediatric BD. This study will examine amygdala volume in children at risk for BD and their unaffected siblings.

References/Funding Source

NIMH R01 MH077047-01 (Chang)

Genetically Regulated Sociability: Hyper amygdala Reactivity and Event-Related Responses to Positive Social Stimuli in Williams Syndrome

B. W. Haas[1], D. Mills[2], A. Yam, F. Hoeft[1], U. Bellugi[3], A. Reiss[1]
[1]Center of Interdisciplinary Brain Sciences Research (CIBSR), Stanford University; [2]Psychology, Emory University, Atlanta, GA; [3]Laboratory for Cognitive Neuroscience, Salk Institute for Biological Studies, La Jolla, CA

The drive towards social engagement is a fundamental characteristic of the human species. Scientific pursuits have not yet fully determined the neural and genetic basis of social drive in humans. Williams syndrome (WS) is a genetic disorder caused by a hemizygous microdeletion on chromosome 7q11.23. WS is associated with a compelling symptom profile characterized by relative deficits in visiospatial function and preserved and in some cases enhanced social function. We examined the neural basis of social drive in WS by assessing brain function in WS participants during two types of social stimuli, negative (fearful) and positive (happy) emotional facial expressions. Here, we report a double dissociation such that WS participants exhibited absent amygdala reactivity to negative (fearful) social stimuli, and heightened amygdala reactivity to positive (happy) social stimuli compared to controls. Furthermore, by using ERP we report that WS participants exhibited reduced N200 response to negative (fearful) social stimuli and heightened P300-500 response to positive (happy) social stimuli compared to controls. This study provides evidence that specific genetic deletions (such as in WS) may not only influence the reduction (or absence) of brain function, but in some cases enhance brain function during psychological processing.

References/Funding Source

Haas, B.W., Mills, D., Yam, A., Hoeft, F., Bellugi, U., Reiss, A.L. (2008). Genetically Regulated Sociability: Hyper Amygdala Reactivity and Event-Related Responses to Positive Social Stimuli in Williams Syndrome. Platform Presentation given at the 12th International Professional Conference on Williams Syndrome. Anaheim, CA.
P01 HD033113-12 (NICHD)
T32 MH19908

Aberrant Brain Activation During Gaze Processing in Males with Fragile X Syndrome

C. Watson[1], F. Hoeft[1], A. Garrett[1], S. Hall[1], A. Reiss[1]
[1]Center for Interdisciplinary Brain Sciences Research (CIBSR)

Introduction: Eye contact is a fundamental component of human social behavior. Individuals with fragile X syndrome, particularly males, avoid eye contact and display other social deficits. To date, this behavior in fragile X syndrome has only been studied in females who show lesser degrees of gaze aversion.

Specific Aims: To determine the neural correlates of the perception of direct eye gaze in adolescent males with fragile X syndrome using functional magnetic resonance imaging.

Methods: Participants: 13 adolescent males with fragile X syndrome, 10 developmentally-delayed and 13 typically-developing controls

Main Outcome Measures: Behavioral performance and brain activation during functional magnetic resonance imaging were evaluated during the presentation of faces with eye-gaze directed to or averted away from subjects. Whole-brain and gaze-related regions-of-interest analyses and regression analyses with task performance were performed.

Results: Significantly greater activation was observed bilaterally in prefrontal cortices in controls compared to fragile X syndrome participants who, in contrast, demonstrated elevated left insula activation to direct eye gaze stimuli. Furthermore, compared to controls, males with fragile X syndrome showed sensitization in the left amygdala with repeated exposure to direct gaze.

References/Funding Source

Accepted for publication in Archives of General Psychiatry.
MH50047
Canel Family research fund.

Insular Volume Reduction in William's Syndrome using Real-Space Morphometry

J. Cohen[1], U. Bellugi[2], A. Karchemsky[1], B. Haas[1], A. L. Reiss[1]
[1]Neuroimaging Lab, Department of Psychiatry and Behavioral Sciences, Stanford, [2]Laboratory for Cognitive Neuroscience, Salk Institute for Biological Studies, La Jolla, CA.

Functional imaging in humans and anatomical data in monkeys have implicated the insula as a multimodal sensory integrative brain region. There is a topographic organization of insular connections that mirror its cytoarchitechtonic regions. Previous attempts to measure the insula have utilized either indirect or automated methods. This study was designed to develop a reliable method for obtaining volumetric magnetic resonance imaging (MRI) measurements of the human insular cortex, and to validate that method by examining the anatomy of insular cortex in adults with William's syndrome (WS) and healthy age-matched controls. Statistical reliability was obtained among three raters for this method, supporting its reproducibility not only across raters, but within different software packages. The procedure described here utilizes native-space morphometry as well as a method for dividing the insula into functional sub-regions estimated from cytoarchitechtonics. Reliability was calculated in both ANALYZE (n=3) and BrainImageJava (N=5) where brain scans were measured once in each hemisphere by each rater. This highly reliable method revealed total, anterior, and posterior insular volume reduction bilaterally (all p's < .001) in WS, after accounting for reduced total brain volumes in these participants. Although speculative, the reduced insula volums in WS may represent a neural risk for the development of hyperaffiliative social behavior with increased specific phobias, and implicate the insula as a critical limbic integrative region. Native-space quantification of the insula may be valuable in the study of neurodevelopmental or neuropsychiatric disorders related to anxiety and social behavior.

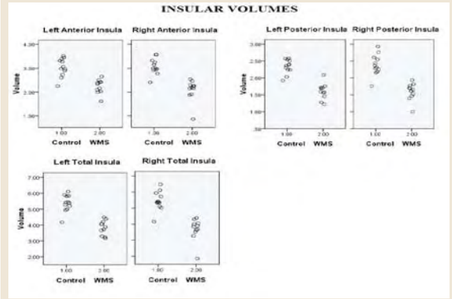

Scatter plots of insular volumes for each participant by ROI, hemisphere and group. Volumes are in cm^3.

References/Funding Source

Cohen, J., Bellugi, U., Karchemsky, A., Haas, B., Reiss, A.L., 2007. Insular volume reduction in William's syndrome using real-space morphometry. Presented at the Organization of Human Brain Mapping, Melbourne, Australia.
NICHD (P01 HD033113-12)

Structural Brain Differences between Autistic and Typically-Developing Siblings

K. Steinman[1], L. Lotspeich., S. Patnaik[3], F. Hoeft[3], A. Reiss[3]
[1]Child Neurology, Department of Neurology, UCSF, San Francisco, CA; [2]Psychiatry & Behavioral Sciences, Stanford;
[3]Center of Interdisciplinary Brain Sciences Research (CIBSR)

Introduction: Morphologic brain differences have been identified between children with autism and typically-developing children, though findings have been inconsistent across studies. One potential cause is the variability in brain morphology resulting from the influence of multiple genetic and environmental factors on brain development. A strategy to control for such factors is to compare brain structure between siblings discordant for autism.

Specific Aim: To assess the relationship between brain morphology and autism using voxel-based morphometry to examine siblings discordant for autism.

Methods: Participants included 27 same-gender sibships consisting of one child with autistic disorder (AU; confirmed with ADI-R and ADOS-G) and one typically-developing sibling (TD). Subjects were between 6-13 years old, and all pairs were less than 4 years apart. High-resolution structural magnetic resonance images were pre-processed (including modulation) and analyzed (paired t-test covarying for age, gender, and total gray/white matter volume) using SPM5 and VBM5.1 (p=0.01 corrected).

Results: With VBM, we demonstrated that AU had greater grey matter volume than TD in the right insula and posterior perisylvian region and the left insula and inferior temporal lobe. AU had greater white matter volume in the right temporal stem and inferior temporal lobe. AU had less grey matter volume than TD in right anterior parietal lobe, and less white matter volume in posterior corpus callosum. Further work will examine the relationship between brain region volume differences and abnormal language and behavioral measures.

Progress: Presented at the International Meeting for Autism Research 2008 Annual Meeting. Manuscript in progress to be submitted for peer-reviewed publication.

References/Funding Source

Steinman K, Lotspeich L, Patnaik S, Hoeft F, Reiss A. Structural brain differences between autistic children and their typically-developing siblings: a voxel-based morphometry analysis, International Meeting for Autism Research, 7th Annual Meeting, 2008.
Grant K01 MH001832 from the National Institute for Mental Health
KJS is supported by the NINDS Neurological Sciences Academic Development Award (NS01692).

Neurochemical Characterization of Child Offspring of Parents with Bipolar Disorders

M. Singh[1], D. Spielman[2], R. Kelley[1], V. Azor, A. Reiss[1], K. Chang[1]
Departments of [1]Psychiatry and Behavioral Sciences, and Radiology, RSL, Stanford University School of Medicine

Bipolar disorder (BD) is a common and serious psychiatric disorder associated with a high risk of suicidality, co-occurring psychiatric disorders, psychosocial and academic problems, and substance use. Investigating biomarkers for illness development through use of proton magnetic resonance spectroscopy (^{1}H-MRS) in high-risk BD would aid in predicting the development of mania and help elucidate the neuropathological etiology of BD. Preliminary data suggest that individuals with and at high risk for BD exhibit abnormalities in neurometabolites including N-acetyl aspartate (NAA), phosphocreatine/creatine, myoinositol (mI), and glutamate in prefrontal and subcortical brain regions. However, prior ^{1}H-MRS studies have shown conflicting results, examining only single structures at a time, and limiting examination to symptomatic offspring, which cannot determine whether findings are affective-state dependent or trait-related endophenotypes inherent to the pathophysiology of BD. An initial step in characterizing abnormalities in early-onset BD is to compare the concentrations of specific metabolites across several selected regions among prodromally symptomatic versus healthy asymptomatic siblings ('symptom-discordant siblings') of bipolar parents, and versus healthy controls using magnetic resonance spectroscopic imaging (MRSI). MRSI is a non-invasive technique that provides a spatial distribution of specific neurochemical metabolites, enabling simultaneous evaluation of metabolites across several brain regions (Figure 1). Studying discordant sibling pairs controls for shared environment and helps discern which inherited risk factors are *not* related to BD development, and allows for the assessment of any neuroprotective biochemical markers that might be preventing symptom manifestation. In this proposal, we will determine the MRSI-detectable neurochemical characteristics of familially at-risk offspring of bipolar adults. Based on previous findings, we hypothesize that compared to healthy controls, bipolar offspring sibling pairs will demonstrate decreases in NAA in the amygdala and the cerebellar vermis and increases in mI in the anterior cingulate cortex.

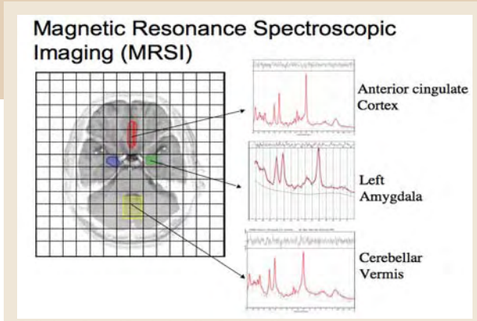

Preliminary Spectral Results from Key Regions of Interest.

References/Funding Source

1. Cecil KM, DelBello MP, Sellars MC, Strakowski SM (2003), Proton magnetic resonance spectroscopy of the frontal lobe and cerebellar vermis in children with a mood disorder and a familial risk for bipolar disorders. J Child Adolesc Psychopharmacol 13(4):545-55.
2.Gallelli KA, Wagner CM, Karchemskiy A, Howe M, Spielman D, Reiss A,Chang KD. N-acetylaspartate levels in bipolar offspring with and at high-risk for bipolar disorder. Bipolar Disord 2005: 7: 589–597.
NARSAD Young Investigator Award (Singh)
Pediatric Research Fund-Child Health Research Program Pilot Award for Early Career Investigators (Singh)
NIMH R01 MH077047-01 (Chang)

Neural Correlates of Response Inhibition in Pediatric Mania

M. Singh[1], K. Chang[1], P. Mazaika[1], A. Garrett[1], N. Adleman[1], R. Kelley[1], M. Howe[1], A. Reiss[1]
[1]Center of Interdisciplinary Brain Sciences Research (CIBSR)
Stanford University School of Medicine

Objective: To evaluate brain activation during a Go/NoGo response inhibition task in children with bipolar disorder, hypothesizing that compared to healthy controls, children with bipolar disorder will exhibit anomalous prefrontal activation during NoGo compared to Go epochs.

Methods: Children (ages 9-18 years) with bipolar I or II disorder ("BD," N=26) and age, gender, and IQ comparable healthy children ("HC," N=22) without any psychiatric diagnosis were given a Go/NoGo task during whole brain functional magnetic resonance imaging (fMRI). A group analysis was performed to compare NoGo to Go epochs.

Results: BD children had no statistically significant group differences from HC in response inhibition as determined by percentage correct on NoGo trials (p=0.11), reaction times needed for correctly responding in Go trials (Z=0.86, p=0.39), or reaction times for false alarms (Z=0.82, p=0.41). In the NoGo minus Go contrast, the BD group showed increased activation in the right dorsolateral prefrontal cortex (DLPFC) compared to HC (T(46) = 4.21, p<0.001).

Conclusions: Children with BD show accurate NoGo trial performance but increased activation in the DLPFC relative to controls, suggesting increased recruitment of executive control regions to maintain accurate response inhibition. Further studies relating these results to mood regulation in children with BD are warranted.

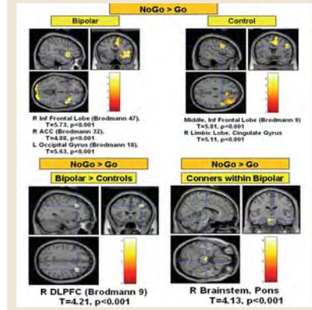

Areas of greater activation during the Go/NoGo task in the NoGo minus Go (NoGo > Go) contrast in subjects with bipolar disorder compared with controls.

References/Funding Source

Presented at the 53rd Annual Meeting of the American College of Neuropsychopharmacology, Boca Raton, FL, December 9-12, 2007.
Helena Anna Henzl-Gabor Young Women in Science Fund
National Institute of Mental Health (K23 MH064460 – Dr. Chang)
National Alliance for Research on Schizophrenia and Depression (NARSAD)
Hahn Family
Klingenstein Third Generation Foundation
GlaxoSmithKline
Abbott Laboratories

Limbic and Corpus Callosum Aberrations in Adolescents with Bipolar Disorder: A Tract-Based Spatial Statistics Snalysis

N. Barnea-Goraly[1], K. D. Chang[1], A. Karchemmskiy[1], M. E. Howe[1], A. L. Reiss[1]
Center for Interdisciplinry Brain Sciences Research (CIBSR)
Stanford University School of Medicine

Background: Investigation of brain structure and function in children and adolescents with bipolar disorder (BD) offers the opportunity to observe changes that are more clearly linked to the disorder itself, as children and adolescents are less likely to have prolonged medication exposure, drug abuse and concurrent medical problems. Converging evidence from genetic and neuroimaging studies indicate that white matter abnormalities may be involved in BD, yet there are no published whole brain analyses of white matter integrity in adolescents with this disorder.

Methods: We used Diffusion Tensor Imaging (DTI) and Tract-Based Spatial Statistics (TBSS), a whole-brain voxel-by voxel analysis, to investigate white matter structure in 21 adolescents with BD, who also are offspring of at least one parent with BD, and 18 age- and IQ- matched control subjects. Fractional anisotropy (FA) and trace values were used as variables in this analysis. In addition, we correlated between FA values, behavioral measures and medication exposure.

Results: Adolescents with BD had lower FA values than control subjects in the fornix, the left mid-posterior cingulate gyrus, throughout the corpus callosum, in fibers extending from the fornix to the thalamus, as well as in parietal and occipital corona radiata bilaterally. There were no significant between-group differences in trace values.

Conclusion: Significant white matter tract alterations in adolescents with BD were observed in regions involved in emotional, behavioral and cognitive regulation. These results suggest that alterations in white matter are present early in the course of disease.

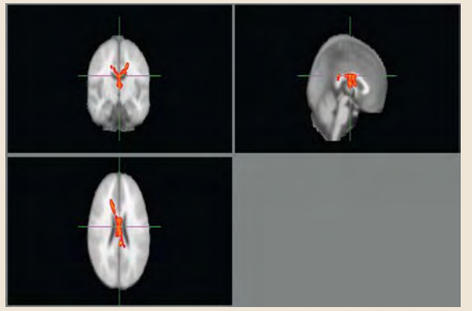
Figure 1: Coronal (A), sagittal (B) and axial (C) views of regions of significant FA differences between adolescents with BD and controls Group differences are mapped onto an average FA image (group difference were "thickened" for visualization purposes).

References/Funding Source

Klingenstein Third Generation Foundation (Chang)

Investigation of Cortical Complexity in Children with Autism, Their Autism-Discordant Siblings, and Controls

N. Barnea-Goraly[1], E. Walter[1], A. L. Reiss[1]
[1]Center for Interdisciplinry Brain Sciences Research (CIBSR)
Stanford University School of Medicine

Autism is a severe neurobiological condition with a strong genetic component and onset in early childhood. Several structural brain abnormalities have been associated with autism, but none have been consistently replicated and no single abnormality is seen in all persons with autism. A potential factor contributing to these inconsistencies is the inherent difficulty in controlling for genetic and environmental variables that influence brain morphology. In this study, we propose to investigate brain-surface complexity in siblings discordant for autism, thus allowing us allow to gain greater experimental control of genetic and environmental factors that influence brain development.

In this proposal we describe plans to use an innovative whole-brain analysis of brain-surface complexity to assess the relation between brain-surface morphology and autism in 27 same-gender sibling-pairs discordant for autism, as well as in 27 control subjects age- and gender- matched to the siblings of subjects with autism. In addition, we propose to assess the relation between brain-surface complexity and behavioral features of autistic subjects.

We hypothesize that brain regions important for social cognition, communication, and face recognition will be altered in children with autism when compared to their unaffected siblings and controls. In addition, we hypothesize that abnormal shape in these regions will be correlated with severity of social and communication impairments in subjects with autism. This information will help to specify which neuroanatomical regions are most highly associated with autism. A better understanding of the neurobiological underpinning of autism will eventually allow for the identification of meaningful sub-groups of individuals with this condition and the development of more targeted treatments for cognitive and behavioral symptoms.

References/Funding Source

Autism Speaks – Physician/Investigator Beginning Autism Research Award
NIH grant # 5R03MH082291-02

Motion Correction and Artifact Repair for High Motion Clinical Subjects

P. Mazaika[1], S. Whitfield-Gabrieli[2], A. Reiss[1], G. Glover[3]
[1]Center for Interdisciplinary Brain Sciences Research (CIBSR), Stanford; [2]Department of Brain and Cognitive Sciences, MIT, Cambridge, MA; [3]Department of Radiology, RSL

A key issue to improve mental health is to better understand the abnormal cognitive processing in mentally impaired populations. Thousands of fMRI data sets from clinical subjects have been collected at the Lucas MRI Center over the last decade. However, the data is difficult to analyze because the clinical subjects often moved during a scan session. Based on fMRI phantom experiments at Lucas Center, we developed new data analysis algorithms to automatically correct for large motions and repair artifacts in the data.

The new algorithms are embedded into staged software releases for different user communities. The earliest version, data visualization and artifact repair, has been implemented as a plug-in toolbox for standard neuroimaging software (SPM2 and SPM5). This software was fully documented and has been downloaded more than 500 times from the CIBSR (Center for Interdisciplinary Brain Sciences Research) website. (http://cibsr.stanford.edu).

The second stage includes corrections for large motions. This software was implemented in 2007 within CIBSR as a semi-automatic approach to analyze clinical subject data. Software with the motion correction algorithms has been applied to over 200 data sets from pediatric clinical subjects with conditions such as bipolar disorder, FraX syndrome, Turner syndrome, and ADHD.

The results after motion correction showed there were remaining artifacts from spontaneous deep breaths of some subjects. New updates to the software in 2008 include automatic detection of deep breath artifacts and detection of outlier subjects who are very different from the rest of the group.

The overall goal of this research and tool development is to exploit existing fMRI data to help better understand the neural correlates of neurodevelopmental and neurogenetic disorders.

References/Funding Source

Motion Correction and Artifact Repair for High Motion Clinical Subjects, by Paul Mazaika, S. Whitfield-Gabrieli, A. Reiss and G. Glover. Presentation at Human Brain Mapping meeting, June 10, 2007.
NIMH grant K25MH077309-01
Software available http//cibsr.stanford.edu/tools/ArtRepair/ArtRepair.htm

Turner Syndrome: Linking Genes, Brain, and Behavior

S. Kesler[1], B. Dunkin[1], T. Nichols[1], H. Baumgartner[1], E. K. Neely[2], J. Hallmayer[3], A. Reiss[1]
[1]Center for Interdisciplinary Brain Sciences Research (CIBSR), [2]Pediatric Endocrinology, [3]Psychiatry and Behavorial Sciences, Stanford University School of Medicine

Introduction: Turner syndrome (TS) provides a model for elucidating critical linkages among X chromosome gene function, brain development, and cognition.

Specific Aims: To determine the neurobiologic and genetic correlates of visual-spatial skills, emotion processing and executive function impairments in girls with TS compared to controls.

Methods: Cognitive-behavioral and neuroimaging assessments (including volumetric MRI, functional MRI, DTI and 1H MRS) are administered to 100 subjects with TS and 50 age matched female controls. Subjects are re-assessed at 12-18 months. Local subjects additionally participate in cognitive intervention programs designed to improve visual-spatial planning or math skills. Subjects enrolled in the intervention programs are assessed before and after the intervention.

Results: Preliminary analysis of 9 girls with TS and 9 controls indicated that girls with TS are significantly less accurate than controls in judging facial emotion. Compared to controls, girls with TS fail to deactivate certain regions when viewing negative faces vs. neutral or scrambled faces. They show more activation than controls when viewing neutral faces vs. negative faces. Seven girls with TS have completed the planning intervention. They demonstrated significantly improved planning and processing speed performance as well as significantly increased brain activation in frontal-parietal regions. Two girls with TS have completed the math training program. They demonstrated significantly improved geometry, measurement and mental calculation performance and significantly increased brain activation in frontal-striatal-parietal regions.

Progress: Planning intervention results presented at the International Neuropsychology Society meeting February 7, 2008.

References/Funding Source

NICHD: R01 HD049653-01A1

Neurochemical Effects of Quetiapine in Youth with Bipolar Disorder

K. Chang[1], M. DelBello, M. Howe[1], N. Mills[2], R. Kelley[1], H. Bryan[2], C. Adler[2], M. Rana[1], J. Welge[2], D. Spielman[1], S. M. Strakowski[2]
Department of [1]Psychiatry and Behavioral Sciences, Stanford University, Department of [2]Psychiatry, University of Cincinnati, Cincinnati, OH

Mood stabilizers have been reported to affect brain concentrations of myo-inositol (mI) and N-acetylaspartate (NAA). We wished to study the effects on these neurochemicals, and possible predictors of response, of quetiapine in adolescents with bipolar depression.

Methods: Twenty-five adolescents with bipolar depression participated in an 8-week placebo-controlled trial of quetiapine monotherapy. Subjects were scanned at baseline and after 8 weeks with ^{1}H-MRS at 3T, with 8cm^{3} voxels placed in right and left dorsolateral prefrontal cortex (DLPFC) and medial prefrontal cortex (ACC). LC Model was used to calculate absolute concentrations of NAA and mI.

Results: 26 subjects had pre- and post-treatment scans (mean age = 15.6 years, 9 males). Of these subjects, 5/16 subjects receiving quetiapine (QUET) and 5/10 receiving placebo (PBO) were responders (50% decrease in CDRS score). There was no significant difference in baseline ACC mI concentrations between the responders and non-responders (4.1 +/- 1.3 vs. 4.2 +/- .48, p = 0.78). There was no significant difference in the change in ACC and DLPFC NAA levels in the QUET group vs PBO group (ACC: -0.55 +/- 1.3 vs. +0.25 +/- 1.5, p = .23; R DLPFC: -0.55 +/- 1.3 vs. 0.18 +/- 0.86, p = .24; L DLPFC: -.04 +/- 0.91 vs. +0.29 +/- 0.61, p = 0.40).

Conclusions: We found baseline ACC mI levels did not predict response to quetiapine in adolescents with bipolar depression. Furthermore, there were no differences in the change in NAA concentrations between the QUET and PBO groups. Larger studies including different brain regions would help to clarify the effects of quetiapine on neurochemistry.

References/Funding Source

AstraZeneca

Retinal Position and Object Category Effects in Human Lateral Occipital Cortex

R. Sayres[1,2], K. Grill-Spector[1,2]
The Department of [1]Psychology and [2]Neurosciences

Object-selective regions of human cortex, including the lateral occipital complex (LOC), are known to be sensitive to the retinotopic position of object stimuli, as well as the category of object. However, there has been little quantitative measure of the extent, organization or relative magnitude of these effects. Further, the relationship between different functionally-defined cortical regions is unclear: while the LOC is defined by preferential responses to objects over non-object images, the retinotopic maps LO-1 and LO-2 are known to be located in the vicinity. We sought to relate measures of object selectivity and retinotopy with a series of fMRI experiments. We imaged six subjects in a 3T MRI scanner using a standard retinotopic stimuli, as well as block-design experiments in which different object categories were presented at six distinct retinotopic positions. We then examined responses in region LO, a subset of the LOC positioned posterior to hMT+ along the lateral cortical surface.

We found substantial retinotopic modulation by checkerboard wedge and ring stimuli in LO. LO exhibited a modest overlap with LO-1 and LO-2, and retinotopic modulation in LO extended well beyond the boundaries of LO-1 and LO-2. Further, LO showed a pronounced lower visual field bias: more LO voxels represented the lower contralateral visual field during the retinotopic mapping experiment, and the mean LO response was higher to objects presented below fixation than above fixation. Finally, we examined how object category and retinal position affect the distributed response across LO. We found a stronger effect of position than category on the distributed LO response: response patterns to two stimuli were more correlated if the category was the same, than the position. These results indicate that retinal position affects BOLD response at least as strongly as category, and these effects may be explained by retinotopic organization in LO.

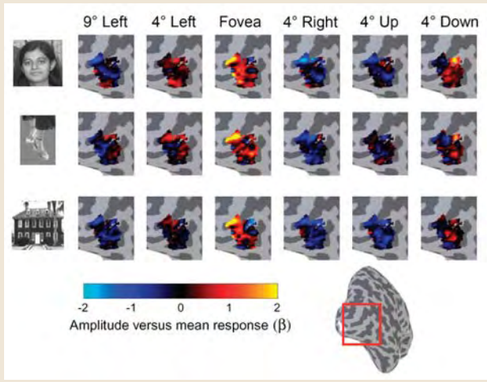

Example LO distributed response patterns to different object categories and stimulus positions shown on the lateral aspect of the right hemisphere cortical surface for subject S2, Each panel shows the amplitude (beta weight from a general linear model) after subtracting the mean beta in each voxel across all conditions. Inset: Inflated right cortical hemisphere, with red square indicating the zoomed region.

References/Funding Source

Sayres R, Grill-Spector K (2008). Relating retinotopic and object-selective responses in human lateral occipital cortex. J Neurophysiol. 100(1):249-67. Epub 2008 May 7.
NEI 5 R21 EY016199-02
NEI 5 F31 EY015937
Whitehall Foundation grant 2005-05-111-RES

Reward- and Interference-Based Modulations of Memory

B. A. Kuhl[1], A. T. Shah[1], S. DuBrow[1], A. D. Wagner[1,2]
The Department of [1]Psychology and [2]Neurosciences

Declarative memory formation is known to be influenced by interference from competing memories as well as motivational factors such as the anticipation of reward. While interference has a deleterious effect on encoding and frequently elicits activation in left ventrolateral prefrontal cortex (VLPFC), reward anticipation has been shown to facilitate encoding through engagement of mesolimbic structures. Although reward anticipation and interference have distinct effects, the extent of interactions between the neural systems engaged by each remains unclear. In the present study, we used functional MRI to characterize neural responses related to reward and interference in the context of a paired associate memory task. During scanning, each paired associate encoding trial was preceded by a cue indicating the potential reward if the pair could be later remembered (either 'high' or 'low' reward trials). While some pairs were novel, others contained elements previously associated with other stimuli (no interference vs. interference trials, respectively). Behaviorally, subsequent recall was superior for pairs preceded by a high reward cue at encoding relative to pairs preceded by a low reward cue. In addition, pairs that suffered interference were more poorly remembered than those without interference. During associative encoding (a) anticipation of reward was accompanied by engagement of mesolimbic structures, including midbrain and ventral striatum, whereas (b) mnemonic interference elicited activation in VLPFC. Critically, successful memory formation was related to the magnitude of activation in both mesolimbic and VLPFC regions, indicating that these regions jointly influence encoding. Moreover, mesolimbic structures modulated by reward were also sensitive to the presence of interference, while prefrontal areas modulated by interference were also sensitive to reward, suggesting potential interactive effects between reward and interference effects. These data indicate that mesolimbic and prefrontal structures collectively support declarative memory formation by promoting gains associated with reward and mitigating losses associated with interference.

Reference/Funding Source

NIMH (5R01–MH080309 and 5R01–MH076932)
Alfred P. Sloan Foundation

Prefrontal and Medial Temporal Correlates of Response Learning Contributions to Repetition Priming

A. Race[1], S. Shanker[2], N. J. Clement[2], A. D. Wagner[1,2]
[1]Neurosciences and The Department of [2]Psychology

Repeated perceptual and conceptual processing of a stimulus results in behavioral facilitation (priming) and functional activation reductions in prefrontal and posterior neocortical regions. Emerging evidence suggests that priming effects may also stem from the formation, and subsequent retrieval, of medial-temporally dependent stimulus-response associations. The present fMRI study aimed to characterize neural responses associated with (a) perceptual repetition, (b) conceptual repetition, and (c) response repetition. During initial exposure, participants performed one of two semantic classification tasks on words. Subsequently, these initially encountered (old) words were represented along with a set of new words. Half of the old words were classified in the same manner as during the initial encounter (within-task repetition), and half were classified according to the other task (across-task repetition). Of the across-task trials, half required the same response as was previously appropriate (response repetition) and half a different response (response switch). Behavioral evidence for response learning was observed: reaction times were faster for across-task response-repeat items compared to both across-task response-switch and novel items. Moreover, a response-switch cost was observed for across-task response-switch items compared to novel items, providing further evidence of stimulus-response learning. Initial fMRI analyses revealed: (a) decreased activation in frontal and occipito-temporal regions for within-task items, and (b) medial temporal and frontal sensitivity to response-repetition for across-task items. These data implicate multiple prefrontal, posterior neocortical, and medial temporal contributions to repetition-related behavioral facilitation.

References/Funding Source

Race, E., S. Shanker, N. J. Clement, A. D. Wagner, 2007. Prefrontal and medial temporal correlates of response learning contributions to repetition priming. Abstracts of the Society for Neuroscience, San Diego, USA.
NIMH (1R01-MH080309-01)
NSF (BCS 0401641)

Repetition Suppression and Category Selectivity in Human Ventral Cortex: Evidence for the Scaling Model

K. S. Weiner[1], J. Vinberg[1], R. Sayres[1,2], Kalanit Grill-Spector[1,2]
The Department of [1]Psychology and [2]Neurosciences

The reduction in neural activity to repeated stimuli in ventral cortex is known as repetition-suppression (RS). It is unknown whether RS measured with fMRI reflects reduced firing of neural populations responding to repeated stimuli (referred to as "scaling"), or whether RS reflects a reorganization of the neural representation from the narrowing of the neurons' tuning width (referred to as "sharpening"). Here we examined: (1) Does RS scale or sharpen the mean fMRI responses in category-selective ventral cortical regions? (2) Does the profile of RS vary across regions or time scales? and (3) Does repetition change the distributed pattern of response to object categories across ventral cortex? The same nine subjects were scanned with high-resolution fMRI in a short-lagged (SL, immediate repetitions) and a long-lagged (LL, mean of 20 stimuli between repeats) experiment in which they viewed repeated and nonrepeated images of cars, houses, faces, flowers, guitars and limbs. We measured the effects of RS and category selectivity using region of interest (ROI) analyses of the mean response within five ROIs defined from separate localizer scans with selectivity to either limbs, faces, houses or objects. We conducted regression analyses between repeated and nonrepeated conditions for each experiment. In the attached figure, we plotted the ratio of the beta values from each category for each subject for nonrepeated and repeated trials for the SL and LL experiments, respectively. Here, each point represents a different subject and each color represents a different category. Each of these regressions was highly significant for both experiments (SL: all $R^2 \geq .439$, $p \leq$ 10e-8 in category-selective regions; LL: all $R^2 \geq .727$, $p \leq$ 10e-9 in category-selective regions). Taken together, our data support the scaling model of RS and suggests that the same neural mechanisms underlie repetition effects in the SL and LL experiments.

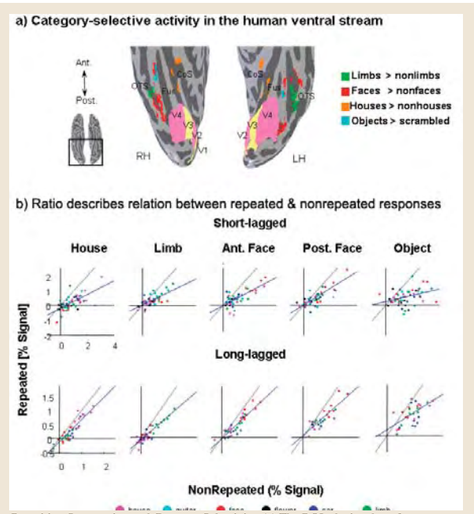

Repetition Suppression and Category Selectivity. (a) The ROIs depicted are face-selective (red), house-selective (orange), limb-selective (green), and object-responsive (cyan). Early visual areas V1-V4 are illustrated in pink (V2, V4) and beige (V1, V3). Inset: Inflated reconstruction of both cortical hemispheres with black square indicating the zoomed region. (b) Regression analysis to test predictions of scaling and sharpening models. The top row represents the Short-Lagged experiment, while the bottom row represents the Long-Lagged experiment. Each column is a different ROI. Each point represents the beta values from each subject with repeated conditions on the y-axis and nonrepeated conditions on the x-axis. Each color represents a different condition. The dotted black line represents when x=y and no RS occurs, while the solid blue line illustrates the results of each regression.

The Impact of Social Belief on the Neurophysiology of Learning and Memory

J. Chen[1], D. Shohamy[4], V. Ross[1], B. Reeves[2], A. Wagner[1,3]
The Departments of [1]Psychology, [2]Communication, [3]Neurosciences, Stanford, The Department of [4]Psychology, Columbia University, New York, NY

How does belief in the social status of an instructor providing performance-based feedback impact learning and subsequent memory representation? In two experiments, we measured physiological and neural correlates of episodic and incremental learning to elucidate the impact of social vs. non-social feedback. In Experiment 1, skin conductance (SC) was acquired while subjects engaged in a two-phase learning and generalization task. In the first phase, subjects learned face-scene associations using trial-and-error feedback. In the second phase, subjects were probed to generalize what they learned to novel stimulus combinations. Belief in the presence of a social other was manipulated by embedding the learning phase in an interaction with a virtual instructor, who provided performance-based feedback in the form of animated affirmations or rebukes. One group was informed that the instructor was computer-controlled (Agent), while the other was informed that the instructor was experimenter-controlled (Avatar). Importantly, all other aspects of the task were held constant except for this belief manipulation. Analyses of SC and behavioral performance revealed (a) higher SC in the Avatar vs. Agent group during learning, and (b) a correlation between learning-phase changes in SC and subsequent generalization (Agent, r^2=.30; Avatar, r^2=.32). Multiple regression revealed superior generalization in the Avatar vs. Agent group (p=.003) when controlling for SC, revealing that social belief facilitates episodic encoding that supports later generalization. In Experiment 2, an independent group of subjects underwent functional MRI scanning while performing the same learning and generalization task. Initial fMRI analyses revealed learning-phase changes in striatal activation, as well as greater activity in ventral striatum and hippocampus during correct relative to incorrect trials. Moreover, midbrain and prefrontal regions displayed a greater learning-phase change in activation in the Avatar relative to Agent group, suggesting that social belief may impact memory by modulating reward processes during feedback-based learning.

References/Funding Source

J. Chen, D. Shohamy, V. Ross, B. Reeves, & A. Wagner (2008). The impact of social belief on the neurophysiology of learning and memory. To be presented for: Society for Neuroscience, Washington, D.C.
NIMH (5R01–MH080309)
NSF
Stanford Media-X Program

Study-Test Perceptual Similarity and Recognition Memory: Neural Correlates of Item Memory Strength

R. K. Olsen[1], N. Davidenko[1], J. Drucker[1], A. D. Wagner[1,2]
The Department of [1]Psychology and [2]Neurosciences

Recognition memory decisions can be based on the perceived memory strength elicited by a test probe. One factor that is posited to influence memory strength is the degree of perceptual similarity between studied stimuli and test probes. Systematic manipulation of study-test perceptual similarity may provide leverage on the behavioral and neural bases of recognition decisions. In this experiment, we parametrically varied the degree of perceptual similarity between studied items and test probes to examine the impact of similarity on perceived memory strength and on the neural correlates of memory strength at retrieval. At study, shapes were encoded during performance of a size judgment task. At test, functional MRI (fMRI) measured neural responses as subjects made memory decisions about three types of test probes that varied in similarity to studied items: studied shapes, unstudied shapes that were morphs between a studied and an unstudied shape, and unstudied shapes. Subjects indicated whether they recognized the shape as old or new. Behavioral results revealed that memory strength increased as a function of study-test perceptual similarity. Initial fMRI analyses focused on the effect of perceived memory strength on retrieval-phase activation when encountering each of the three probe types. For all probe types, activation was reduced in perirhinal cortex for items perceived as previously studied compared to items perceived as novel. That is, when holding the study status of the test probe constant greater perceived memory strength was associated with reduced perirhinal activation. An analysis that incorporated similarity and perceived memory strength further revealed that as perceptual similarity and memory strength increased, activation in medial temporal and prefrontal cortical areas decreased. These results indicate that perceived memory trace strength varies with study-test perceptual similarity and is associated with decreases in MTL cortical activation, furthering understanding of how item memory strength is signaled in the brain.

References/Funding Source

Society for Neuroscience Annual Conference, November 2008
NIMH (5R01–MH076932
NSF
NARSAD

Harnessing the Ventral Attentional Network to Promote Rather than Detract from Episodic Encoding

M. R. Uncapher[1], J. B. Hutchinson[1], A. D. Wagner[1,2]
The Department of [1]Psychology and [2]Neurosciences

Neuroimaging studies of episodic memory have demonstrated that engagement of dorsal parietal cortex during an experience is predictive of subsequent memory for the experience. Dual-attention theories of lateral parietal function posit that dorsal and ventral parietal subregions support 'top-down', goal-directed attentional allocation and 'bottom-up' capture of attention by unexpected or salient stimuli, respectively. When viewed through the lens of attention, the dorsal parietal correlates of encoding can be interpreted to signify that dorsal attention mechanisms facilitate episodic encoding. By contrast, ventral parietal activation has been shown to correlate negatively with subsequent memory. The present functional MRI study sought to determine whether ventral parietal mechanisms can facilitate rather than detract from encoding, specifically when event information is captured in a bottom-up manner. Participants were scanned while incidentally encoding stimuli in a variant of the Posner cueing paradigm. On each trial, participants were cued (leftward or rightward pointing arrow) to expect a stimulus in one of two spatial locations (left or right of central fixation). Participants judged whether the stimulus was a real or a nonsense object. Approximately 10 min post-scanning, recognition memory for the real objects was assessed. Subsequent memory for both validly- and invalidly-cued objects was well above chance. The fMRI data revealed enhanced activity in dorsal parietal regions during the cue period (suggestive of top-down attentional allocation), and in ventral parietal regions for invalidly- vs. validly-cued objects (suggesting bottom-up attentional capture). Activation in ventral parietal cortex correlated with the later mnemonic fate of the object, being greater during trials for which the object would be later recognized vs. forgotten. Critically, the magnitude of this subsequent memory effect was larger for objects that appeared in the unexpected vs. expected location. These findings indicate that, when recruited, bottom-up attention mechanisms subserved by ventral parietal cortex can enhance the capture of event information in episodic memory.

References/Funding Source

NIMH (5R01–MH080309 and 5R01–MH076932)
Alfred P. Sloan Foundation

Episodic Retrieval and Parietal Cortex: Relating Memory to Visuo-Spatial Attention

J. B. Hutchinson[1], M. R. Uncapher[1], D. W. Bressler[3], M. A. Silver[4], A. D. Wagner[2]
The Department of [1]Psychology, [2]Psychology & Neurosciences Program, [3]Vision Science Graduate Program, Stanford University; [4]Helen Wills Neuroscience Institute and School of Optometry, UC Berkeley, CA

Episodic retrieval is a multi-process act that has long been known to depend on the medial temporal lobe and prefrontal cortex. More recently, a large body of neuroimaging evidence indicates that lateral posterior parietal cortex (PPC)--including the intraparietal sulcus and inferior parietal lobule--is engaged during event remembering. Given the rich literature demonstrating PPC involvement in visuo-spatial attention, a debate has emerged over the degree to which PPC activations during episodic retrieval can be understood as reflecting the engagement of parietal attentional processes during remembering. Resolution of this debate may partially come from within-subject analysis of the overlap between parietal correlates of episodic retrieval and (a) topographically organized maps of spatial attention within the intraparietal sulcus (IPS1-IPS4) and (b) ventral parietal structures implicated in bottom-up (reflexive) attentional orienting. To this end, the present functional MRI study examined the relationship between recognition memory and visuo-spatial attention effects in parietal cortex at the single-subject level. During the memory task, subjects encoded visually presented words, and were scanned during a subsequent recognition memory test that probed item recognition and source recollection. In a separate session, subjects performed (a) a covert visuo-spatial attention task that mapped topographically organized regions along the IPS that subserve goal-directed visuo-spatial attention, and (b) a reflexive (Posner cuing) attentional orienting task that engaged ventral parietal cortex. While the fMRI episodic retrieval data revealed mnemonic effects in IPS and IPL, initial analyses suggest that the localization of these IPS effects were predominantly non-overlapping with the IPS regions demonstrating topographically organized spatial attention maps. Additionally, ventral parietal regions recruited during the memory task were largely distinct from regions elicited by target detection during the Posner cuing task. Taken together, these findings suggest a possible anatomical and functional distinction between mechanisms associated with episodic retrieval and processes of top-down and bottom-up spatial attention.

References/Funding Source

Society for Neuroscience, Annual Meeting, 2008
NIMH (5R01–MH080309 and 5R01–MH076932)
Alfred P. Sloan Foundation
Fight for Sight Foundation

Cortical Maps and White Matter Tracts Measured Following 40 Years of Visual Deprivation

N. Levin[1], S. O. Dumoulin[1], R. F. Dougherty[1], B. A. Wandell[1]
Department of [1]Psychology

Early visual deprivation changes neural development. But what happens when vision is restored? Cases of sight salvage in adult life, after long deprivation periods, are extremely rare. The impact of deprivation followed by salvage on visual pathways and visual field maps has not been reported previously. MM, a 53 year-old male, lost his left eye and became blind in the right due to corneal damage at the age of 3. At age 46, MM received a right eye corneal stem-cell transplant. High resolution visual field maps and population receptive field sizes were estimated using fMRI; white matter was measured using diffusion tensor imaging (DTI) and fiber tractography. The loss of an eye and subsequent degeneration of the optic nerve results in increased radial diffusivity in MM's optic tracts. The size, diffusivity and position of the optic radiation were similar to controls. The apparent synaptic connectivity in foveal V1 differs significantly from controls: MM's occipital pole did not map the central visual field and population receptive field sizes were almost twice the size of those measured in controls. There was an organized peripheral visual field map in anterior calcarine, similar to that of controls. The cross-sectional area of MM's occipital callosal fiber group was smaller than the area in controls, suggesting a reduction in intra-cortical white matter volume due to visual deprivation. Correcting MM's retinal image has not restored normal cortical organization, seven years post-surgery. The continuing deficits in his cortical organization may explain why visual performance remains substantially limited compared to controls.

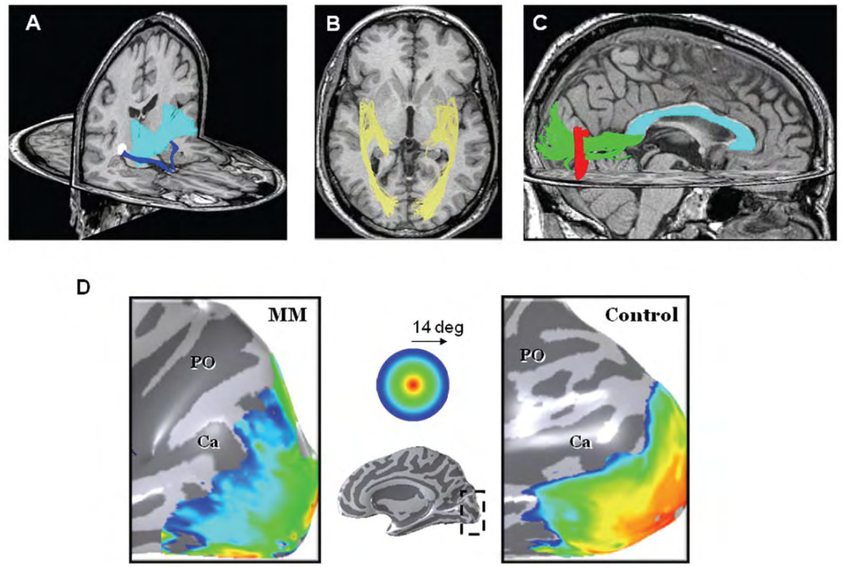

A) Three dimensional rendering of the fibers in the optic tracts (blue) and the posterior limbs of the internal capsule (cyan) are shown superimposed on axial and coronal slices. (B) Rendering of the optic radiation (yellow) superimposed on an axial slice viewed from below. (C) The inter-hemispheric occipital-callosal fibers are presented as green fiber bundle that connects the occipital-lobe (red) and the corpus callosum (cyan). (D) Eccentricity maps on the medial aspect of the right hemisphere in MM (left) and a control (right). The stimuli extended from fixation to 14 degrees. There is an organized peripheral map (green to blue) in MM's anterior calcarine. The large confluent fovea representation (red-orange) that is prominent in the control is nearly absent in MM. The data are shown on smoothed images of occipital cortex; dark shading is within a sulcus and light shading a gyrus. Ca = calcarine sulcus, PO = parieto-occipital sulcus.

Improving Perfusion-Weighted MR Imaging of CBF by Correcting for Partial Volume and Nonlinear Contrast Relaxivity

G. Zaharchuk[1], R. Bammer[1], M. Straka[1], R. D. Newbould[2], J. Rosenberg[1], J-M. Olivot[3], M. Mlynash[3], M. G. Lansberg[3], N. E. Schwartz[3], M. M. Marks[1], G. W. Albers[3], M. E. Moseley[1]
[1]Radiology, [3]Neurology and Neurological Sciences, Stanford; [2]Clinical Imaging Centre, GSK, London, UK

Background and Purpose: Using xenon computed tomography (xeCT) CBF as a gold standard, we examined whether dynamic susceptibility contrast (DSC) MRI-based absolute CBF measurements can be improved by accounting for partial volume (PV) of the arterial input function (AIF) and the nonlinear contrast relaxivity of bulk blood (BB).

Methods: 13 patients with cerebrovascular disease underwent xeCT and single-shot gradient echo DSC within 24 hrs. PV was measured as the ratio of the area under the AIF and the venous output function (VOF) concentration versus time curves. A correction was applied to account for the nonlinear relaxivity of bulk blood (BB) in the AIF and VOF.

Results: Global xeCT CBF was 44.8±15.9 ml/100g/min (mean±SD). BB correction decreased CBF by a factor of 4.7±0.5, but did not affect precision. The least-biased CBF measurement was with BB correction but without PV correction (47.9±19.6 ml/100 g/min, coefficient of variation (COV)=37%). Precision improved with PV correction, although absolute CBF was mildly underestimated (33.9±11.5 ml/100 g/min, COV=28%).

Conclusions: AIF partial volume and nonlinear contrast relaxivity corrections improve DSC CBF maps, though they still underestimate xeCT values by about 20% with 28% patient-to-patient variability, and only moderately correlate with gold-standard xeCT CBF. These factors limit diagnostic confidence of quantitative DSC CBF measurements in individual patients.

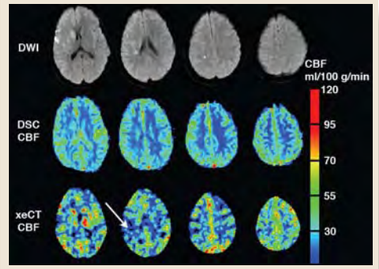

Example of a typical co-registered data set, including DWI, DSC CBF map, and xeCT CBF map. The high signal on DWI represents acute cerebral ischemia. High CBF signal on the DSC MRI map presumably represents artifact from large vessels, and partially obscures an area of low CBF on the xeCT study (arrow).

References/Funding Source

Zaharchuk G, Bammer R, Straka M, Newbould RD, Olivot JM, Mlynash M, Lansberg MG, Albers GW, Moseley ME, Correcting PWI-based CBF measurements for arterial input function partial volume and nonlinear contrast relaxivity: comparison with a xenon CT gold standard, Proc ISMRM, Toronto, Canada 2008: 628.
NIH (2R01EB002711, 1R21EB006860, P41RR09784, K23 NS051372)
the Lucas foundation
the Oak foundation

Arterial Spin Label Findings in Patients with Normal Bolus Perfusion-Weighted Imaging – Identification of the "Watershed Sign"

G. Zaharchuk[1], A. Shankaranarayan[2], D.C. Alsop[3], M. Straka[1], R. Bammer[1], N.J. Fischbein[1], M. E. Moseley[1], S.W. Atlas[1]
[1]Radiology, Stanford, Stanford, CA; [2]ASL-West, General Electric Medical Systems, Menlo Park, CA, [3]Department of Radiology, Beth Israel Deaconess Hospital, Boston, MA

Purpose: Bolus contrast perfusion-weighted imaging (PWI) is a widely used technique for assessing cerebrovascular disease. Arterial spin labeling (ASL) is a noncontrast perfusion method that may yield additional information. This study reports ASL imaging findings in patients with normal PWI studies.

Materials and Methods: Patients with suspected or known cerebrovascular disease underwent brain imaging at 1.5T supplemented with ASL and bolus PWI. Pseudocontinuous ASL images were acquired with a background-suppressed 3D fast-spin-echo readout. Bolus contrast PWI was performed using gradient-echo echo planar imaging, and maps of relative cerebral blood volume (rCBV), relative cerebral blood flow (rCBF), mean transit time, and AIF normalized time-to-peak of the residue function (Tmax) were created.

Results: 41/139 patients (29%) had normal bolus PWI studies (mean age 63±15 yrs, range: 21-89 years). Of these, 23 patients (56%) also had normal ASL studies. The others had varying degrees of ASL signal dropout with surrounding cortical hyperintensities in the bilateral MCA-ACA and MCA-PCA borderzones, which we term a "watershed sign." Patients with a watershed sign were older than normals (71±11 vs. 57±16 yrs, $p<0.005$). 5 patients had additional focal findings: 2 with high ASL signal near diffusion lesions; 2 with high ASL signal corresponding to slow or stagnant flow in a vascular structure; and 1 with low ASL signal in surgical resection cavities.

Conclusion: About half of patients with normal bolus contrast PWI have low ASL signal in the MCA-ACA and MCA-PCA watershed regions that may reflect decreased CBF and/or prolonged arterial arrival time. In a smaller subgroup, focal abnormalities were identified that were not visible on bolus contrast PWI.

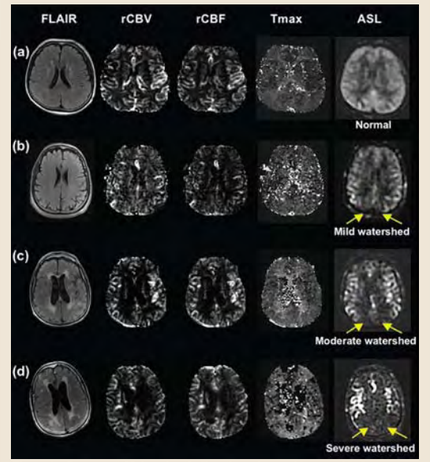

Figure 1: Common ASL imaging findings in patients with normal bolus perfusion-weighted imaging (PWI). Many ASL studies had signal dropout in the bilateral MCA-ACA and MCA-PCA borderzones with serpiginous high signal in the surrounding cortex, which we have termed a "watershed sign." This ranged from mild to severe as shown above. In the severe case, only the proximal segments of the MCA and ACA are visualized with complete lack of parenchymal ASL signal. Fluid-attenuated inversion recovery (FLAIR) images as well as maps from bolus PWI (rCBV, rCBF, and Tmax) are shown for comparative purposes.

Neuroimaging: Functional MRI (fMRI)

Learning to Like: Social Observation Influences Prefrontal Activation for Viewing Others

J. C. Cooper[1], T. Kreps[1], A. Aron[2], B. Knutson[1]
Department of [1]Psychology, Stanford University, Stanford, CA, Department of [2]Psychology, Stony Brook University, Stony Brook, NY

How do we learn who to like? Observing others provides an important source of information. Often, people make enduring positive and negative judgments of others based on limited observation. Little is known, though, about how the brain builds positive or negative social impressions on the basis of observation. We scanned participants with event-related FMRI in a novel social prediction task. Participants observed the outcomes round-by-round of a six-person repeated public goods game and made predictions about how much was donated on each round. Participants were not told in advance that the donation profiles of each player in the game were designed to be more or less generous. Participants were accurate at estimating each player's average donation, and formed strong impressions of each player. After observation, generous players were liked more, while selfish players were liked less. To investigate how participants' impressions changed over time, we fitted a single-parameter associative learning model to each participant's predictions, and used that model to create individualized regressors of each player's estimated generosity (average donation) over time. When participants viewed the faces of each player, activation in ventromedial prefrontal cortex correlated positively with model estimates of generosity. When receiving feedback about actual donation amounts, activation in anterior striatum and parahippocampal cortex correlated positively with unexpectedly high donations. Finally, when making predictions about donation outcomes in each round, activation in the ventromedial prefrontal cortex correlated with predicting higher rather than lower donations. This study is among the first to examine how observation changes both emotional impressions of others and neural responses to them. The effects suggest that brain networks involved in learning about rewards for ourselves are also engaged in learning about reward for other people. The effects are also consistent with the hypothesis that others we like are processed in the brain similar to other kinds of rewards.

References/Funding Source

Cooper, J.C., Kreps, T., Aron, A., & Knutson, B., "Learning to like: social observation influences prefrontal activation for viewing others," abstract, Society For Neuroeconomics 2008 Annual Meeting (Park City, UT, United States)
FINRA Investor Education Foundation (2006-07-004)
NIMH training grant 5T32MH020006-10.

Interleaved Spiral-In/Out with Application to fMRI

C. Law[1,2], G. Glover[1]
Departments of [1]Radiology, RSL and [2]Electrical Engineering

The conventional spiral-in/out trajectory (1) samples k-space sufficiently in the spiral-in path and sufficiently in the spiral-out path, thereby enabling creation of separate images. We propose an *interleaved spiral-in/out* trajectory comprising a spiral-in path that gathers half of the k-space data, and a complimentary spiral-out path that gathers the other half. Readout duration is thereby reduced by approximately half, offering two distinct advantages: reduction of signal dropout due to susceptibility-induced field gradients (at the expense of signal-to-noise ratio), and higher spatial resolution when readout duration is identical to the conventional method. Two reconstruction methods can be used; both involve temporal filtering (UNFOLD) (2) to remove aliasing artifacts. Empirically, interleavedspiral-in/out images are free from false activation resulting from *signal piling-up* around air/tissue interface which is common in conventional spiral-out method. Comparisons with conventional methods under hypocapnia reveal greater frontal-orbital activation volumes, and slight loss of volumes in whole-brain averages. (Figure)

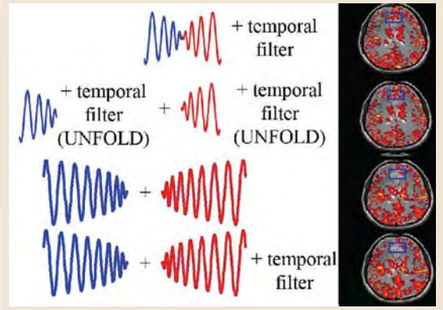

Activation maps (t-score, p<0.001). Top two images are gathered with interleaved spiral-in/out trajectory but reconstructed differently. Bottom two images are gathered with conventional spiral-in/out trajectory. The purpose of using temporal filtering in the last image is to reduce noise for fair comparison. Rectangular ROIs drawn on images indicate susceptibility induced signal loss regions.

With the compact readout duration of interleaved spiral-in/out trajectory, repetition time can be reduced such that more time frames are gathered in a fixed scan time; so as to increase SNR efficiency and temporal resolution. On the other hand, interleaved spiral-in/out gives higher spatial resolution than conventional spiral-in/out if readout duration is fixed.

What motivated our choice of spiral sampling, instead of Cartesian, is motion insensitivity, low distortion, and the potential for high speed of acquisition when used in conjunction with acceleration techniques like parallel imaging. The proposed method is easy to incorporate into parallel imaging technique such as spiral SENSE (3,4), for example. Combining parallel imaging with interleaved spiral-in/out can further reduce readout duration (and signal dropout); certainly a direction for continuing research.

References/Funding Source

Submitted to Magnetic Resonance in Medicine (under revision).
1. Glover GH, Law CS. Spiral-in/out BOLD fMRI for increased SNR and reduced susceptibility artifacts. Magn Reson Med 2001;46(3):515-522.
2. Madore B, Glover GH, Pelc NJ. Unaliasing by Fourier-encoding the overlaps using the temporal dimension (UNFOLD), applied to cardiac imaging and fMRI. Magnetic Resonance in Medicine 1999;42(5):813-828.
3. Qian Y, Zhang Z, Stenger VA, Wang Y. Self-calibrated spiral SENSE. Magnetic Resonance in Medicine 2004;52(3):688-692.
4. Weiger M, Pruessmann KP, Österbauer R, Börnert P, Boesiger P, Jezzard P. Sensitivity-encoded single-shot spiral imaging for reduced susceptibility artifacts in BOLD fMRI. Magnetic Resonance in Medicine 2002;48(5):860-866.
NIH RR 09784
the Lucas Foundation
GE Health Care

Sliding Window SENSE Calibration for Reducing Noise in fMRI

C. Law[1,2], C. Liu[1], G. Glover[1]
Departments of [1]Radiology, RSL, [2]Electrical Engineering, Stanford.

We propose a self-calibrated parallel imaging fMRI method in which sensitivity profiles are calculated dynamically using a sliding window approach: averaging a small number of consecutive fully-sampled multishot images. This technique provides an SNR gain over conventional SENSE reconstruction. For conjugate gradient CG-SENSE reconstruction (1,2) used here, profiles are updated at every time frame. No spatial smoothing is performed so as to retain thermal noise in sensitivity profiles. Sliding window width determines similarity between thermal noise in sensitivity profiles and thermal noise in the windowed raw data. Narrower window width yields more similarity and provides better noise cancellation in the reconstructed image time-series. This *sliding window* technique is especially applicable to acquisition of high spatial-resolution images (where thermal noise dominates over physiological noise). Activation from visual stimulation is revealed where conventional sensitivity calculations falter.

We compare this proposed *sliding window* parallel imaging technique with a conventional *reference frame* method and an *all-frame* method, as well as with the conventional fully-sampled two-shot reconstruction. In the *reference frame* method, four image time frames from the beginning of a time series are averaged and smoothed with spline interpolation. In the *all-frame* method, data acquired over the whole time-series is averaged to calculate coil sensitivity. In all comparisons, our proposed technique demonstrates enhanced BOLD activation and less noise. The improvement is most significant for high resolution, thin slice, and low SNR cases.

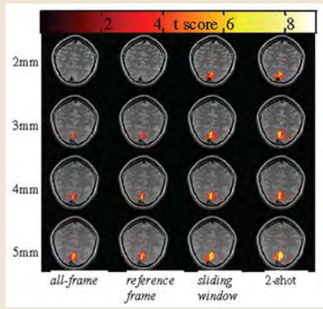

Activation maps for one volunteer (p<0.005). Same data was processed using different sensitivity profile calculation methods. Sliding window yields greater activation than all-frame and reference frame; especially at thin slices. Results from sliding window is statistically the same as those using 2¬shot reconstruction.

References/Funding Source

Proc. Intl. Soc. Mag. Reson. Med. 16 (2008) 2451, 1504. Magnetic Resonance of Medicine (accepted).
1. Pruessmann KP et al., Magn Reson Med. 2001; 46(4):638-651.
2. Liu et al., Magn Reson Med. 2005; 54(6) :1412-1422.
NIH RR09784
NIH-1K99NS057943-01
Lucas Foundation
GEMS

Parametric fMRI Study of Working Memory in Obstructive Sleep Apnea patients

O. Prilipko[1], N. Huynh[1], A. R. Peralta[1], V. Tantrakul[1], J. Kim[1], M. Lee[1], M. Henry[2], C. Guilleminault[1], C. Kushida[1]
[1]Stanford Sleep Clinic and Center for Human Sleep Research, Department of[2]Psychology

Introduction: Functional magnetic resonance imaging (fMRI) studies enable the investigation of neural correlates underlying behavioral performance. In the present study we investigate the working memory (WM) function of patients with untreated obstructive sleep apnea (OSA) and compare the results to previous fMRI studies of healthy subjects as well as the only previous fMRI study of WM in OSA patients.

Methods: A parametric fMRI experiment with four levels of a spatial N-back task was used to investigate the pattern of cortical activations across the various degrees of load in 21 patients with moderate or severe OSA.

Results: We found activations in a similar cortical network in patients as the one previously described in healthy subjects, involving the supplementary motor area, dorsolateral prefrontal cortex (DLPFC), precentral and parietal regions. The activity in these regions increased linearly with increasing load. Similarly, a deactivation pattern was found in posterior and anterior cingulate, bilateral parahippocampal gyri and medial frontal regions previously described as a" default network". Activation in these regions linearly decreased with increasing load. Furthermore, an inverted-U shape trend of activation was observed in posterior cingulum, thalami and occipital regions, as well as right insula and left parietal and left DLPFC. The latter observation may represent a reflection of the observed decrease of behavioral performance at maximal load.

Conclusion: Our results indicate that the same cortical regions are involved in WM function in OSA patients as in healthy subjects and that, similarly, some components of this network demonstrate a capacity-constrained response. This is in contrast with the results of the prior WM fMRI study (Thomas et al.), which revealed an absence of activation in the DLPFC of OSA patients.

References/Funding Source

Oral presentation at APSS 2008, abstract published in Sleep 2008 (abstract suppl):31, pA152
Respironics, Resmed, Covidien, Swiss National Foundation for Scientific Research

Chronic Pain Remodels the Brain's Salience Network: A Resting-State fMRI Study

M. D. Greicius[1], M. Barad[2], T. Oeno[2], S. Mackey[2]
Departments of [1]Neurology and Neurological Sciences and [2]Anesthesiology
Stanford University School of Medicine

Background: The persistent nature of chronic pain makes it difficult to study using traditional functional imaging protocols. Here we applied resting-state functional MRI (fMRI) to a homogenous sample, patients with complex regional pain syndrome (CRPS), to investigate changes in brain network connectivity induced by chronic pain.

Methods: Thirteen female patients with CRPS and sixteen age-matched female controls underwent an eight-minute resting-state fMRI scan on a 3 Tesla scanner. Independent component analysis (ICA) was used in an automated, investigator-independent approach to detect three resting-state networks of interest related to vision, episodic memory processing (the default-mode network), and salience detection [1-3]. Two-sample t-tests were performed to compare connectivity within each network between patients and controls. Within the pain group, correlation analyses were performed to assess the effects of pain severity on connectivity in the salience network.

Results: Connectivity in the default mode and visual networks did not differ between groups. The pain group demonstrated increased connectivity in the salience network. Further this network was expanded in the pain group to include regions such as the left sensory-motor cortex not detected in the control group. Within the pain group, connectivity in the salience network was correlated with pain severity.

Discussion: The salience network is believed to be critical for assessing the relevance of stimuli (whether internally or externally generated) and adjusting the autonomic nervous system and internal milieu accordingly[2]. Our results show that in patients with chronic pain the salience network has expanded to incorporate a number of regions implicated in the perception of acute pain. We interpret these findings as showing that persistent pain has merged two distinct networks—one for pain and one for salience that normally interact only in the setting of acute pain—into a single network. Our findings demonstrate that chronic pain remodels a canonical resting-state brain network and can be considered a disorder of abnormally enhanced neural connectivity.

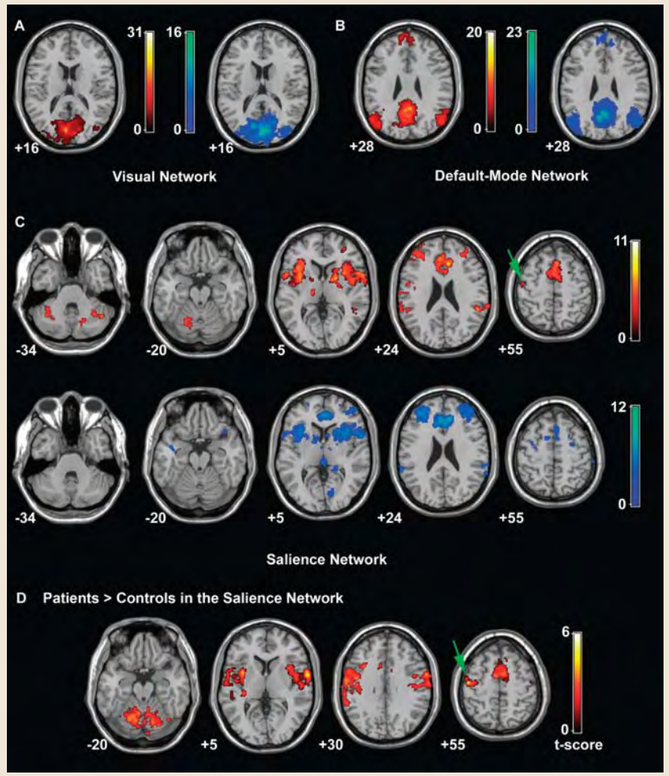

Connectivity in the visual (A) and default mode (B) networks did not differ between pain patients (red) and controls (blue). In the salience network pain patients showed increased connectivity (C). Regions of the salience network with significantly increased connectivity in patients are shown in (D). The green arrow indicates the left sensory-motor region.

References/Funding Source

1 Greicius et al., *Proc Natl Acad Sci* 2004 2 Seeley et al., *J Neurosci* 2007 3 Beckmann et al., *Philos Trans R Soc Lond*, 2005
Gary Glover for his expertise and his spiral in/out protocol
John and Dodie Rosekranz Pain Research Endowment
the Foundation for Anesthesia Education and Research
NIH NS048302
NIH NS053961

Functional Magnetic Resonance Imaging of Spinal Cord Nociception in Humans

J. E. Brown[1], J. Kornelsen[2], D. Watcha[3], G. Glover[4], S. Mackey[5]
[1]Neurosciences, Stanford; Department of [2]Psychology, University of Winnipeg, Canada; Departments of [3]Biology, [4]Radiology, [5]Anesthesia; Stanford University, Stanford, CA, United States

The experiments described here examine the feasibility of fMRI to characterize neuronal activity along the left-right, dorso-ventral, and rostro-caudal axes of the human spinal cord.

Functional MRI was conducted on 23 healthy volunteers using an 8-channel phased array spine coil. Eight 2mm sagittal slices were prescribed parallel to the rostro-caudal axis of the spinal cord (single-shot partial-ky fast spin-echo pulse sequence, 20x20cm field of view, 128x128 matrix, 10 second TR, 39 msecond TE). Thermal stimuli were applied to the right volar forearm using a rapid-heating, contact heat, evoked potential stimulator. Three experiments were conducted: 1) repetitive fist-clenching: 60 seconds of opening and closing the fist at a rate of ~1/2 Hz alternated with 60 seconds of passive rest (N=12), 2) tonic noxious stimulation: 60 seconds of 45°C alternated with 60 seconds of 40°C rest (N=8), 3) phasic noxious stimulation: 60 seconds of linearly ramped oscillation between 45°C and 40°C at a rate of 1/3Hz, alternated with 60 seconds of 40°C rest (N=9). Phasic and tonic noxious stimulation resulted in a 4.69% ± 0.57% (mean ± 1SE) and 4.22% ± 0.23% signal increase, respectively. Noxious stimulation resulted in significantly more spinal cord activity in the dorsal half of the spinal cord than in the ventral half (paired t-test, t(15)=-1.770, p=0.05) and in significantly more spinal cord activity in the ipsilateral side of the spinal cord than in the contralateral side (paired t-test t(15)=-1.759, p=0.05). During noxious stimulation of the forearm, spinal cord activity was centered on spinal cord segment C5. Fist clenching did not produce a significant lateralization of activity across the left-right or dorso-ventral axes of the spinal cord; however, along the rostro-caudal axis activity was greatest at spinal cord segments C8/T1.Future studies will investigate how spinal cord nociception is correlated with pain perception.

References/Funding Source

International Association for the Study of Pain conference 2008

Accelerated Three-Dimensional Through-Slice Shimming for Functional MRI

J-J. Hsu[1], G. H. Glover[1]
Department of [1]Radiology, RSL
Stanford University School of Medicine

Because of the shape and the magnetic susceptibility of the brain, the homogeneity of the imaging magnetic field required for MRI can not be achieved, resulting in signal loss and image distortion. Correcting this problem is essential because the affected areas, e.g., the frontal lobe, are of great interest in understanding higher level brain functions. One type of approaches is the so-called *z*-shimming, which corrects the through-slice inhomogeneity and is commonly implemented with two-dimensional imaging methods. We have shown [1] that three-dimensional imaging is more efficient because it offers more choices of shims, which is not an available feature of 2D imaging, and thus generates images of higher quality. In this work, we further increase the temporal efficiency of 3D *z*-shimming by including an accelerated data acquisition technique known as the UNFOLD method [2]. Along the fMRI time course, either the even or odd k_z-lines are collected in each time frame. Thus the number of time frames per unit time is doubled. The parity of the k_z-line collection alternates along the time frames. Low-pass Fourier-transform filtering and the maximum intensity projection are used to reconstruct the fMRI images (see Refs. [1] and [2] for details).

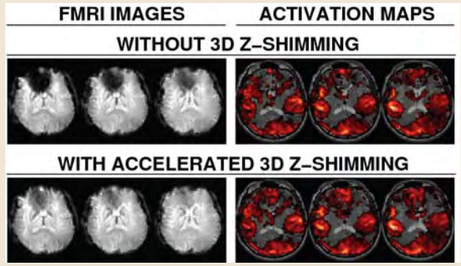

Sample fMRI images and activation maps (color coded) obtained with and without accelerated 3D *z*-shimming.

References/Funding Source

[1] G.H. Glover, 3D z-shim method for reduction of susceptibility effects in BOLD fMRI, Magn Reson Med 42, 290 (1999).
[2] B Madore, G.H. Glover, N.J. Pelc, Unaliasing by Fourier-encoding the overlaps using the temporal dimension (UNFOLD), applied to cardiac imaging and fMRI, Magn Reson Med 42, 813 (1999).
NIH RR09784
Richard M. Lucas Foundation

In FIG. 1, the results of fMRI of a normal volunteer are shown (nine-cycle block-designed breath-hold task, B_0 = 3.0 T, 64×64 matrix by spiral readout, T_E = 30 ms, T_R = 70 ms to acquired one k_z-line, 25 k_z-lines per time frame, total 180 time frames). As seen in the figure, the magnetic field inhomogeneity results in serious signal loss in the frontal areas. Our accelerated 3D *z*-shimming can restore the signal in these areas considerably and, consequently, more activation (red pixels) is detected. The success of this novel development suggests that accelerated (partial *k*-space) acquisition can significantly improve temporal resolution of 3D *z*-shimming without the activation detectability being compromised.

Using fMRI to Differentiate Neural Activity in Depressed Adolescents in Response to Emotional Phrases

N. E. Adleman[1,2], K. D. Chang[3], A. Garrett[1], N. Barnea-Goraly[1], M. Howe[3], A. L. Reiss[1]
[1]Center for Interdisciplinary Brain Sciences Research (CIBSR), [2]Interdisciplinary Program in Neurosciences, [3]Pediatric Bipolar Disorders Program; Stanford University School of Medicine

Our study employed a novel functional imaging task to elucidate differences in brain function of this circuitry between healthy and depressed adolescents and, further, to identify potential differences between pediatric MDD and BD. The data from this study supports the role of abnormal, decreased amygdala processing in mood disorders with mood severity inversely correlated with amygdala activation to negative self-relevant emotional phrases (see figure 1). Although this finding is opposite to many amygdala findings in adults, we hypothesize that this is due to developmental changes in the amygdala, supported by the fact that our data is consistent with a study that found blunted amygdala in 5 female children with MDD (Thomas, 2001).

This study is the first to demonstrate neurofunctional differences between depressed adolescents with MDD and BD. The clear activation differences between such small groups of currently depressed MDD and BD subjects illustrates it may, indeed, be possible to differentiate these phenomonologically similar diseases using neuroimaging technology, as we hypothesized. The results indicate that patients with MDD and BD may have different healthy neural resources available to them,reflecting unique neurofunctional characteristics that might be delineated further in order to uncover separate underlying pathophysiologies.

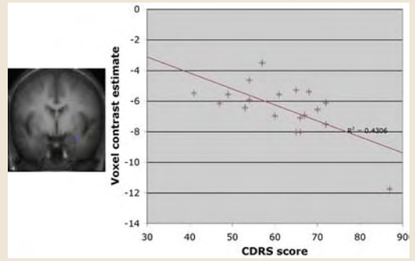

Inverse correlation between depressive symptom severity on day of scan (measured by CDRS) and response of right amygdala cluster to negative versus neutral phrases in adolescent depressed subjects.

Strengths of this study include the unique subject populations and the fact that the subjects were almost entirely unmedicated. In addition, this analysis controlled for depressive symptom severity, IQ, pubertal status, and home environment measures between the BD and MDD groups, allowing for differences specifically associated with the underlying subject disease to be isolated. Finally, limiting this study to females prevents gender differences in emotion processing, brain structure, and development, from confounding the study results. The main weakness of this study is the small sample sizes. Future research with more subjects is warranted.

References/Funding Source

Adleman, N.E., Chang, K.D., Garrett, A., Barnea-Goraly, N., Howe, M., Reiss, A.L., 2008. Using fMRI to differentiate neural activity in depressed adolescents in response to personally-relevant emotional phrases. 14th Annual Meeting of the Organization for Human Brain Mapping, Melbourne, Australia, June 15-19, 2008: Poster presentation and abstract.
Rocky Family Endowed Fund in Child and Adolescent Psychiatry
Howard Hughes Predoctoral Fellowship in Biological Sciences to NEA

Decoding Neural Signatures of Recognition Memory States Based on Distributed Patterns of fMRI Activity

J. Rissman[1], A. D. Wagner[1]
Department of [1]Psychology and the Neuroscience Program
Stanford University School of Medicine

While the brain responds differently when it experiences a novel sensory stimulus as compared to a previously encountered stimulus, conventional functional magnetic resonance imaging (fMRI) data analysis approaches, utilizing univariate statistics to compare voxel activity levels across task conditions, cannot reliably capture these mnemonic effects on single trials. We sought to exploit the wealth of information represented in distributed fMRI activity patterns, using a multi-voxel pattern analysis approach to decode the mnemonic status of individual stimuli. Prior to scanning, participants studied 200 color photographs of human faces. Subsequently, participants were scanned while they made recognition memory decisions about the 200 studied faces intermixed with 200 novel faces. For each test face, participants indicated whether they 1) recollected having studied the face, 2) were highly confident they studied it, 3) thought they studied it, 4) thought they did not study it, or 5) were highly confident they did not study it. After fMRI data preprocessing, we trained a back-propagation neural network classifier model to detect brain activity patterns that maximally differentiate encounters with studied stimuli from those with novel stimuli. The classifier was iteratively trained on 90% of the dataset with the remaining 10% of trials used to assess the classifier's ability to generalize its "knowledge" to new data. Using this approach, the trained classifier achieved above-chance classification of the objective mnemonic status of the test stimuli (i.e., studied vs. unstudied). This effect held even when the training set equated the number of studied and unstudied stimuli given each subjective response, effectively de-correlating objective mnemonic status from subjectively experienced memory strength. Separately derived classifier models exhibited a significant ability to classify the subjective status of stimuli (i.e., perceived memory strength) and to differentiate recollection-based responses from familiarity based responses. The neural signatures of these various mnemonic states were explored by extracting the 'importance value' of each voxel to a particular classification outcome. Despite the highly distributed nature of the underlying representations, classification outcomes were largely tied to activity levels in a core set of prefrontal, parietal, medial temporal, and visual association regions. The implications of these results for understanding the neural signals mediating human recognition memory will be discussed.

References/Funding Source

Rissman, J. and Wagner, A.D. Decoding neural signatures of recognition memory states based on distributed patterns of fMRI activity, To be presented at the Society for Neuroscience Annual Meeting, Washington, DC, November 2008.
NIMH (5R01–MH076932 and NRSA #)
NARSAD
Alfred P. Sloan Foundation

Building the Lucas Center

The View in 2008


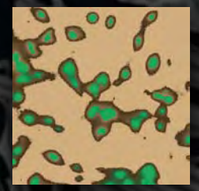
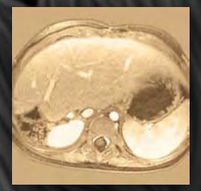
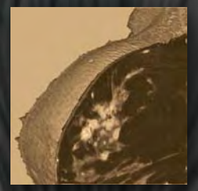
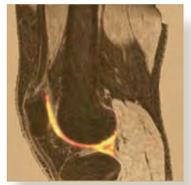
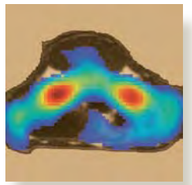
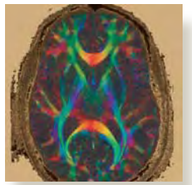


Publications and Presentations

Peer-Reviewed Presentations at Scientific Meetings

ISMRM 2008

Alley MT, Hargreaves BA, Daniel BL, Beatty PJ, Brau AC.	High-resolution 3D bilateral breast imaging using slice direction autocalibrated parallel imaging.
Balchandani P, Pauly J, Yang P, Yamada M, Spielman DM.	Self-refocused spatial-spectral pulse pair for positive contrast imaging of cells labeled with superparamagnetic iron-oxide (SPIO) nanoparticles. Oral presentation.
Balchandani P, Spielman DM, Pauly J.	Slice-selective Tunable-flip AdiaBatic Low peak-power Excitation (STABLE) pulse. Oral presentation; chosen as Young Investigators Award finalist.
Beatty P, Beaulieu CF, Brau A, Busse R, Gold G, Han E, Stevens K.	Isotropic MRI of the ankle at 3.0T using 3D-FSE-Cube with Extended Echo Train Acquisition (XETA).
Chen C, Kijowski R, Hargreaves B, Reeder S, Busse R, Brau A, Beatty P, Gold G.	3D-FSE-Cube for Rapid Assessment of Cartilage Morphology in the Knee.
Chen J, Watkins R, Butts Pauly K.	Optimization of Encoding Gradients for Magnetic Resonance Acoustic Radiation Force Imaging.
Gold G, Busse R, Stevens K, Han E, Brau A, Beatty P, Beaulieu C.	Isotropic MRI of the Ankle using 3D-FSE-Cube with extended echo train acquisition (XETA).
Granlund K, Hargreaves B.	Multi-frequency water-fat separation and off-resonance correction for 3D spiral breast imaging.
Gu M, Kim DH, Mayer D, Sullivan E, Pfefferbaum D, Spielman DM.	Reproducibility Study of Whole-Brain Spectroscopic Imaging with Automated Quantification.
Gu M, Liu C, Spielman DM.	Parallel Spectroscopic Imaging Reconstruction with Arbitrary Trajectories using k-space Sparse Matrices.
Gu M, Mayer D, Sullivan EV, Pfefferbaum A, Spielman D.	Reproducibility Study of Whole-Brain 1H Spectroscopic Imaging with Automated Quantification.
Han M, Hargreaves BA.	Accelerated bilateral DCE 3D spiral breast imaging: comparison between TSENSE and TGRAPPA.
Han M, Hargreaves BA.	Slab-phase modulation combined with parallel imaging in bilateral breast imaging.
Hargreaves BA, Daniel BL.	Dynamic contrast-enhanced breast MRI using dual-resolution 3D spiral imaging.
Hargreaves BA.	Partially dephased SSFP for elimination of dark bands.
Holbrook A, Barrera J, Santos J, Butts Pauly K, Popelka G.	Real Time Sleep MRI and Physiologic Monitoring of Patients with Obstructive Sleep Apnea.
Holbrook A, Josan S, Bouley D, Daniel B, Butts Pauly K.	Acute and Chronic Magnetization Transfer Ratio Observations in Canine Cryoablation.
Hope M, Hope T, Ordovas K, Meadows A, Saloner D, Reddy G, Alley M, Higgins C.	Clinical evaluation of aortic coarctation with 4D flow MR imaging.
Hope T, Hope M, Bammer R, Alley M.	Combination of parallel imaging and a cut-corner acquisition for neurovascular 4D-flow.
Hsu JJ, Zaharchuk G, Glover GH.	Fast simultaneous measurement of the RF flip angle and the longitudinal relaxation time for quantitative MRI
Josan S, Kaye E, Pauly J, Daniel B, Butts Pauly K.	Improved Half RF Slice Selectivity in Presence of Eddy Currents with Quadratic Phase Saturation.
Josan S, van den Bosch M, Rosenberg J, Daniel B, Butts Pauly K.	MRI-guided Cryoablation - Acute Cryolesion Assessment with T1, T2 Imaging.
Josan S, Watkins R, Daniel B, Butts Pauly K	Reduction of RF Heating of Interventional Cryoprobes using Chokes.
Kaye E, Lynch S, Caires C, Butts Pauly K	Proton Resonant Frequency Shift and R2* in Frozen Ex Vivo Renal Tissue at 7T.
Koo S, Hargreaves B, Andriacchi T, Gold G	Automatic Segemnetation of Articular Cartilage from MRI: A Multi-Contrast and Multi-Dimensional Approach
Koo S, Hargreaves B, Gold G, Dragoo J.	Accuracy of Building a Three-Dimensional Model of a Complex Articular Cartilage Defect from 1.5T MRI
Lu W, Butts K, Gold G, Pauly J, Hargreaves B	Towards Artifact-free MRI Near Metallic Implants.
Lu W, Yu H, Shimakawa A, Alley M, Reeder S, Hargreaves BA.	Noise considerations in water-fat separation with bipolar multi-echo sequences.
Mayer D, Yen YF, Levin YS, Tropp J, Pfefferbaum A, Hurd RE, Spielman DM.	Time-Resolved Metabolic Imaging in the Rat after Injection of Hyperpolarized 13C1-Pyruvate at 3 Tesla.
Mayer D, Yen YF, Levin YS, Tropp J, Pfefferbaum, Hurd RE, Spielman DM.	Ultra-Fast In Vivo Metabolic Imaging in the Rat after Injection of Hyperpolarized 13C1-Pyruvate at 3 Tesla.
Newbould R, Alley M, Ropele S, Bammer R	T1 mapping of MT effects in bSSFP.
Nnewihe A, Staroswiecki E, Bangerter N, Hargreaves BA.	Dual tuned helmholtz coil for breast cancer imaging.

ISMRM 2008

Park Y, Elayaperumal S, Daniel B, Kaye E, Butts Pauly K, Black R, Cutkosky M.	MRI-compatible Haptics: Feasibility of using optical fiber Bragg grating strain-sensors to detect deflection of needles in an MRI environment.
Rieke V., Butts Pauly K.	Contribution of temperature dependent T1-change, slice thickness and positioning to an artifact in temperature images of FUS heating.
Rieke V., Newbould R., Bammer R., Butts Pauly K.	Referenceless multi-coil Reconstruction.
Santos J, Butts Pauly K, Popelka G, Pauly J.	Real-Time MRI of Swallowing in Upright Position.
Schmitz A, van den Bosch M, Rieke V, Dirbas F, Butts Pauly K, Mali W, Daniel B	3.0-T MRI-guided focused ultrasound ablation versus MRI-guided needle-wire placement for the preoperative localization of non-palpable breast tumors: an experimental study.
Staroswiecki E, Bangerter N, Gurney P, Gold G, Holdsworth S, Grafendorfer T, Hargreaves B	In Vivo Measurement of 23Na T2* in Human Articular Cartilage at 3T and 7T.
Wong SH, Watkins RD, Kupnik M, Butts Pauly K, Khuri-Yakub BT.	MRI Temperature Mapping of a CMUT design for HIFU.
Zaharchuk G, Bammer R, Straka M, Newbould RD, Olivot JM, Mlynash M, Lansberg MG, Albers GW, Moseley ME.	Correcting PWI-based CBF measurements for arterial input function partial volume and nonlinear contrast relaxivity: comparison with a xenon CT gold standard.

RSNA 2007

Atlas SW.	Key Health Care Trends in Asian Emerging Markets. GE Healthcare Asian Pacific American Forum.
Barth RA.	Refresher Course: MR Imaging of the Fetal Neck and Chest: Review of the Clinical Indications. Normal Anatomy, and Correlation with Postnatal Outcome.
Blankenberg FG.	Oncologic Imaging in the Era of Molecular Medicine/Molecular Imaging Advances in Oncology/Apoptosis: Oncologic Imaging.
Chuyeshov G, Kukuk M, Napel S	Localizing a guidewire in three dimensions during endovascular interventions using single-view fluoroscopy and a stereo roadmap: method and feasibility study.
Do BH, Maley JE, Biswal S.	Feedback natural language processing of fractures in unstructured reports of emergency department plain films. Oral presentation.
Fischbein N.	Imaging Anatomy Relevant to Contouring of Nasopharyngeal carcinoma.
Gold G, Busse R, Stevens K, Han E, Brau A, Beatty P, Chen C, Beaulieu C.	Isotropic MRI of of the Musculoskeletal System with 3D-FSE-XETA.
Hernandez A, MacKenzie JD, Gonzalez L, Pena A, Ruppert K, Khrichenko D, Jawad AF, Wells L, Smith-Whitley K, Jaramillo D.	Quantitative Diffusion-Weighted MR Imaging of the Hips in Pediatric Patients with Sickle Cell Disease at Risk for but without Evidence of Avascular Necrosis.
Iagaru A, Mittra E, Le Q, Quon A, Gambhir SS.	18F FDG PET/CT in Nasopharyngeal Carcinoma: What Do We Need to Scan?
Iagaru A, Mittra E, Quon A, Daniel B, Ikeda D, Herfkens R, McDougall IR, Gambhir SS.	18F FDG PET/CT Evaluation of Patients with Breast Cancer.
Iagaru A, Rodriguez CA, El-Maghraby T, Quon A, Gambhir SS, McDougall IR.	18F FDG PET/CT Evaluation of Patients with Cervical Cancer.
Kim B, Mittra E, Dhatt H, Do BH, Graves E, Biswal S.	Increased 18F-FDG Uptake is Observed within the Spinal Canal in Low Back Pain Patients. Oral presentation.
Kukuk M, Rosenberg J, Napel S.	Co-Visualization of Stereoscopic and Monoscopic Images for Instrument Navigation in the Interventional Room.
Lee SW, Graves E, Jeon TJ, Lee SH, Gold GE, Biswal S.	Validation of Manganese-Enhanced Magnetic Resonance Imaging (MEMRI) as a Method to Detect Changes in the Spinal Cord Following Painful Stimuli. Oral presentation.
Leung A.	Case Based Review: Diffuse Lung Disease. Mentoring of Radiology Faculty. Pneumonia for Radiologists: A Practical Approach.
Leung A.	Thoracic Manifestations of Connective Tissue Disease. Pulmonary Grand Rounds; Stanford University Medical Center; April 4, 2008; Stanford, CA.

RSNA 2007

MacKenzie JD, Hernandez A, Gonzalez L, Pena A, Ruppert K, Khrichenko D, Jawad AF, Wells L, Smith-Whitley K, Jaramillo D.	Diffusion-Weighted Imaging in Early Avascular Necrosis - Quantification of the Apparent Diffusion Coefficient in the Hips of Sickle Cell Patients with Early Avascular Necrosis.
Mittra E, Iagaru A, Le Q, Fischbein N, McDougall IR, Gambhir SS, Quon A.	18F FDG PET/CT in the Management of Patients with Nasopharyngeal Carcinoma.
Olsen DA, Paik DS, Roos JE, Napel S, Rubin GD.	External Validity of Cross-Validation on Computer-aided Detection (CAD) of Lung Nodules Enabled by the LIDC Dataset.
Olsen DA, Roos JE, Paik DS, Napel S, Rubin GD.	Influence of Lung Nodule Characteristics on Computer-aided Detection (CAD) based on the Lung Imaging Database Consortium (LIDC) CT Dataset.
Paik DS, Olsen DA, Roos JE, Rubin GD.	A Novel Parametric Free-response ROC (FROC) Methodology; Radiological Society of North America 93rd Scientific Assembly and Annual Meeting Program; November 25-30, 2007; Chicago, Illinois.
Pelc NJ.	Dual-Energy CT: Technical Aspects.
Roos JE, Olsen DA, Paik DS, Napel S, Liu EG, Rubin GD.	Potential Equalization of Radiologists' Diagnostic Performance with the use of Computer Aided Detection (CAD) as a Second Reader in Lung Nodule Detection on Chest CT.
Sundaram P, Beaulieu CF, Shi R, Yee J, Olcott E, Napel S, Shin L, Edwards B.	A Pilot Study Evaluating the Efficiency Of "Patch View": A New Paradigm for Reviewing the Output of a Computer-Aided Polyp Detection Method.
Sundaram P, Beaulieu CF, Shi R, Yee J, Olcott EW, Napel S.	A Pilot Study Evaluating the Efficiency Of "Patch View": A New Paradigm for Reviewing the Output of a Computer-Aided Polyp Detection Method.
Willmann JK, Chen K, Rollins M, Wang DS, Chen X, Gambhir SS.	Molecular Imaging of Therapeutic Angiogenesis in Murine Hindlimb Ischemia using PET and ^{64}Cu-labeled Vascular Endothelial Growth Factor121.
Willmann JK, Paulmurugan R, Chen K, Gheysens O, Chen X, Gambhir SS.	Ultrasonic Imaging of Tumor Angiogenesis with Contrast Microbubbles Targeted to Vascular Endothelial Growth Factor Receptor Type 2 in Mice.
Yi C, Olsen DA, Roos JE, Paik DS, Napel S, Rubin GD.	Characteristics of True Positive (TP) Lung Nodules Detected by Computer-aided Detection (CAD) but Subsequently Rejected by Radiologists on Chest MDCT Scans.

SNM 2008

Blankenberg FG.	Imaging chronic pain with annexin V-128 in a rodent model of spared nerve injury.
Blankenberg FG.	Radiotherapy of 4T1 tumors with Lu-177-DOTA-PEG-scVEGF.
Blankenberg FG.	Time domain optical imaging of sterile soft tissue abscesses with Cy5.5-scVEGF.
Cai W, Guzman R, Hsu AR, Sun G, Zhao H, Moseley M, Steinberg GK, Chen X.	Positron Emission Tomography Imaging of Vascular Endothelial Growth Factor Receptor Expression after Experimental Stroke.
Chen K, Cai W, Li Z, Wang H, Chen X.	Quantitative PET imaging of VEGF receptor expression.
Chen K, Li Z, Wang H, Cai W, Chen X.	Quantum dot based dual functional probe for optical/PET imaging of tumor VEGFR.
Iagaru A, Mittra ES, Gambhir SS, Goris ML.	Can 111In-Ibritumomab Imaging Predict the Outcome of 90Y-Ibritumomab (Zevalin®) Therapy in Refractory Non-Hodgkin's Lymphoma.
Li ZB, Chen K, Chen X.	^{68}Ga-labeled Multimeric RGD Peptides for microPET Imaging of Integrin $\alpha v\beta 3$ Expression.
Li ZB, Chen K, Wu Z, Wang H, Niu G, Chen X.	^{64}Cu-Labeled Polyethylenimine (PEI) for Cell Trafficking and Tumor Imaging by microPET.
Li ZB, Lee HY, Chen K, Hsu AR, Xu C, Xie J, Sun S, Chen X.	PET/MRI Dual Modality Tumor Imaging Using RGD Conjugated Radiolabeled Iron Oxide Nanoparticles.
Li ZB, Wu Z, Chen K, Ryu E-K, Chen X	Radio-Labeled BBN-RGD Heterodimer for Prostate Cancer.
Mittra ES, Quon A, McDougall IR, Gambhir SS, Iagaru A.	18F-FDG PET/CT in the Evaluation of Pediatric Sarcomas.
Pratx G, Levin CS.	Maximum a Posteriori Event Positioning in High-Resolution PET CZT Detectors.
Pratx G, Reader AJ, Levin CS.	Fast Maximum Likelihood Image Reconstruction via PCG without a Line Search.
Wang H, Cao F, De A, Gambhir S, Wu J, Chen X.	Trafficking the fate of mesenchymal stem cells in vivo.
Wang H, Chen K, Niu G, Chen X.	Site-specifically biotinylated VEGF121 for tumor angiogenesis imaging.

SMI 2008

Biswal S, Cheng D, Levashova Z, Tait J, Vanderheyden JL, Blankenberg F.	Subjects Suffering from Inflammatory Arthritis Demonstrate Increased Cy5.5-labeled Annexin V Uptake in the Central Nervous System. Poster presentation.
Cai W, Chen K, Li ZB, Gambhir SS, Chen X.	Dual Functional Quantum Dot-Based Probe for Near-Infrared Fluorescence and Positron Emission Tomography Imaging of Cancer.
Cai W, Ebrahimnejad A, Chen K, Cao Q, Li Z-B, Tice DA, Chen X.	Quantitative PET Imaging of EphA2 Expression in Tumor-Bearing Mice.
Cai W, Guzman R, Chen K, Hsu AR, Bliss T, Sun G, Wang H, He L, Li ZB, Maag AL, Hori N, Zhao H, Steinberg GK, Chen X.	PET Imaging of VEGFR Expression in Stroke.
Cao F, Li Z-B, Chen K, Wang H, Cai W, Chen X, Wu JC.	PET Imaging of Angiogenesis Formation in Teratoma from Human Embryonic Stem Cells.
Cheng Z, Blum G, Gheysens O, Bogyo M, Gambhir SS.	Activity based probes for microPET imaging of cathepsin B. Poster presentation.
Cheng Z, De Jesus OP, De A, Webster J, Gheysens O, Levi J, Namavari M, Wang S, Zhang R, Faisal S, Gambhir SS.	MicroPET imaging of HER2 expression using ^{64}Cu labeled synthetic affibody molecules. Poster presentation.
Cheng Z, Zhang L, Graves E, Xiong Z, Dandekar M, Chen X, Gambhir SS.	Evaluation of ^{18}F-labeled-alpha-melanocyte stimulating hormone analog for melanocortin 1 receptor imaging. Poster presentation.
Chinn G, Levin CS.	High Resolution PET Image Reconstruction Algorithm that Incorporates Single as well as Coincidence Photons.
Jeon TJ, Lee SW, Biswal S.	The Presence of Relatively Small Number of Mesenchymal Stem Cells Promotes Accelerated Growth in Osteosarcoma Tumor Xenografts.
Keren S, Zavaleta C, Cheng Z, Gheysens O, Gambhir SS.	Noninvasive molecular imaging of small living subjects using Raman spectroscopy and Raman nanoparticles. Oral presentation.
Kimura RH, Cheng Z, Gambhir SS, Cochran JR	Molecular imaging of tumor angiogenesis with a new class of affinity matured integrin-binding cystine-knot miniproteins. Oral presentation.
Lau F, Olcott P, Horowitz M, Levin CS.	Noise Performance of PSAPD-based PET Multiplexing Circuits. Joint meeting, Academy of Molecular Imaging and Society for Molecular Imaging; Sep 7-11, 2007; Providence, RI.
Lee SW. Graves E, Jeon TJ, Lee SH, Gold GE, Biswal S.	Validation of Manganese-Enhanced Magnetic Resonance Imaging (MEMRI) as a Method to Detect Changes in the Spinal Cord Following Painful Stimuli. Poster presentation.
Lee HY, Lee SH, Lee JH, Koh AL, Wu B, Wang X, Wang S, Nishimura DG, Biswal S, Cho SH, Chen X.	In Vitro and In Vivo Test of PVP-coated Iron Oxide Nanoparticles as Liver-Specific MRI Contrast Agent.
Lee HY, Li Z-B, Chen K, Lee S-H, Lee J-H, Nishimura DG, Cho SH, Biswal S, Chen X.	Radiolabeled Iron Oxide Nanoparticle Conjugate for PET/MRI Dual Modality Imaging of Tumor Vasculature.
Lee SH, Lee SW, Biswal S.	Inhibition of Hepatic Phagocytosis of Superparamagnetic Iron Oxides (SPIOs) using Polyinositic Acid (PIA). Poster presentation.
Li ZB, Niu G, Wang H, Ploug M, Chen X.	microPET Imaging of Urokinase-type Plasminogen Activator Receptor Expression Using a ^{64}Cu-Labeled Linear Peptide Antagonist.
Li ZB, Wu Z, Cao Q, Dick DW, Tseng JR, Gambhir SS, Chen X.	Orthotopic Brain Tumor Imaging with ^{18}F-2-Fluorodeoxysorbitol (^{18}F-FDS).
Li ZB, Wu Z, Chen K, Chin FT, Chen X.	Click Chemistry for ^{18}F-Labeling of RGD Peptides and microPET Imaging of Tumor $\alpha_v\beta_3$ Integrin Expression.
Li ZB, Wu Z, Chen K, Ryu EK, Chen X.	^{18}F-Labeled BBN-RGD Heterodimer for Prostate Cancer.
Namavari M, Cheng Z, Zhang R, De A, Levi J, Hoerner J, Wang S, Syud FA, Gambhir SS.	A novel method for direct site-specific radiolabeling of peptides using [^{18}F]FDG. Poster presentation.
Namavari M, De Jesus OP, Cheng Z, De A, Kovacs E, Levi J, Wang S, Zhang R, Hoerner J, Grade H, Syud FA, Gambhir SS.	Direct site-specific radiolabeling of a protein via [^{18}F]benzaldehyde. Oral presentation.
Niu G, Cai W, Chen K, Chen X.	Noninvasive monitoring of early response to anti-Hsp90 therapy with microPET by use of ^{64}Cu-DOTA-cetuximab.
Peng H, Olcott P, Foudray AMK, Levin CS.	Evaluation of a Fully Digital Data Acquisition for PET Systems.
Peng H, Olcott P, Pratx G, Foudray AMK, Chinn G, Levin CS.	Performance Study of a High-Resolution CZT-Based PET Camera for Breast Imaging.
Pratx G, Chinn G, Levin CS.	Fast Fully-3D List-Mode OSEM for High-Resolution PET using PC Graphics Hardware.

SMI 2008

Ray P, Lutz A, Cheng Z, Cochran FV, Junutula AR, Gambhir SS.	Noninvasive imaging of an epithelial cell adhesion molecule (EpCAM) antibody in mouse models of ovarian cancer. Poster presentation.
Rodriguez-Porcel M, Brinton TJ, Chen IY, Gheysens O, Lyons J, Ikeno F, Willmann JK, Wu L, Wu JC, Yeung AC, Yock PG, Gambhir SS.	Reporter Gene Imaging Following Percutaneous Delivery in Swine: Moving Towards Clinical Applications.
Rodriguez-Porcel M, Cai W, Gheysens O, Chen IY, Chen K, He L, Willmann JK, Wu JC, Li Z, Mohamedali K, Kim S, Rosenblum MG, Chen X, Gambhir SS.	Imaging of VEGF Receptor in a Rat Myocardial Infarction Model using Positron Emission Tomography.
Ryu EK, Wu Z, Balboni G, Lazarus LH, Chen X.	Synthesis and evaluation of potent ^{18}F-labeled δ-opioid receptor agonist.
Schipper ML, Cheng Z, Koh AL, Lee SW, Bentolila LA, Iyer G, Keren S, Ebenstein Y, Li J, Rao J, Chen X, Wu AM, Weiss S, Gambhir SS.	MicroPET-based biodistribution of quantum dots in living mice. Poster presentation.
Schipper ML, Iyer G, Koh AL, Cheng Z, Ebenstein Y, Keren S, Bentolila LA, Zerda A, Li J, Smith BR, Rao J, Chen X, Wu AM, Sinclair R, Weiss SS, Gambhir SS.	Particle size, surface coating, and pegylation influence the biodistribution of quantum dots in living mice. Poster presentation.
Smith BR, Cheng Z, De A, Gambhir SS.	Direct visualization of RGD-quantum dot binding in tumor neovasculature using intravital microscopy and living mice. Poster presentation.
Wang H, Cai W, Chen K, Li ZB, Chen X.	Efficient In Vivo Tumor Targeting of a RGD-TNF Fusion Protein.
Wang H, Cai W, Chen K, Li ZB, He L, Chen X	A VEGFR2 Specific PET Tracer.
Willmann JK, Chen K, Wang H, Paulmurugan R, Rollins M, Cai W, Wang D, Chen IY, Lutz AM, Gheysens O, Rodriguez-Porcel M, Chen X, Gambhir SS.	Assessment of therapeutic angiogenesis in murine hindlimb ischemia using a 64Cu-labeled vascular endothelial growth factor-121 PET.
Willmann JK, Paulmurugan R, Chen K, Gheysens O, Rodriguez-Porcel M, Lutz AM, Chen IY, Chen X, Gambhir SS.	Ultrasonic imaging of tumor angiogenesis with contrast microbubbles targeted to vascular endothelial growth factor receptor type 2 in mice.
Zavaleta C, Keren S, Cheng Z, Schipper M, Chen X, Liu Z, Dai H, Gambhir SS.	Use of non-invasive Raman spectroscopy imaging in living mice for evaluation of tumor targeting with carbon nanotubes. Poster presentation.
Zhang X, Peng H, Pratx G, Chinn G, Levin CS.	A Minimum-Angular-Difference Algorithm for Sequencing Multiple Interactions of 511KeV Photons in High-Resolution CZT PET Detectors.

Other Scientific Meeting Presentations

Other Presentations 2008

Atlas SW.	Advances in Brain MRI: Evolution of Technology and Emerging Applications. First Annual Symposium on Advanced MRI; Fudan University School of Medicine; June 21, 2008; Shanghai, China.
Atlas SW.	Advances in Imaging Technology: What Are The Drivers? India Society of Neuroradiology 10th Annual Conference; November 13-15, 2007; Mumbai, India.
Atlas SW.	Advances in MR Technology: Rationale and Significance. 6th Annual Clinical Applications in High Field MR Imaging. Stanford University School of Medicine; October 14, 2007; Las Vegas, Nevada.
Atlas SW.	Advances in MRI. Lucid Advanced Medical Diagnostics; November 16, 2007; Hyderabad, India.
Atlas SW.	Advances in MRI: Rationale and Future Directions. General Electric Healthcare; Advanced MRI Users Group; February 26, 2008; Sao Paulo, Brazil.
Atlas SW.	Current Imaging of Stroke: What is True and What Might Be. 6th Symposium on Neurosciences FLENI; May 14, 2008; Buenos Aires, Argentina.
Atlas SW.	Current MRI of Brain Tumors: Fundamentals and Advanced Applications. 6th Symposium on Neurosciences FLENI; May 14, 2008; Buenos Aires, Argentina.
Atlas SW.	Emerging Advances in MR of the Brain. Department of Radiology, Stanford University School of Medicine; May 1-2, 2008; Las Vegas, Nevada.
Atlas SW.	Imaging Brain Tumors: Fundamentals and Advances. India Society of Neuroradiology 10th Annual Conference; November 13-15, 2007; Mumbai, India.
Atlas SW.	Imaging Diseases of the Eye and Orbit. India Society of Neuroradiology 10th Annual Conference; November 13-15, 2007; Mumbai, India.
Atlas SW.	Key Trends in Health Care in Asia: Implications for China. Special Seminar, Peking University School of Business; April 21, 2008; Peking, China.
Atlas SW.	MRI in Brain Tumors: Update. Department of Radiology, Stanford University School of Medicine; May 1-2, 2008; Las Vegas, Nevada.
Atlas SW.	Stroke Imaging: Current Status. India Society of Neuroradiology 10th Annual Conference; November 13-15, 2007; Mumbai, India.
Atlas SW.	Stroke Imaging: What Is, and What Might Be. Italian Society of Neuroradiology Annual Course and Meeting; University of Bologna School of Medicine; November 2, 2007; Bologna, Italy.
Atlas SW.	The Future of Health Care in America. Hoover Institution; November 30, 2007; Stanford, CA.
Atlas SW.	The Future of MRI: Rationale and Emerging Applications. 6th Symposium on Neurosciences FLENI; May 14, 2008; Buenos Aires, Argentina.
Bangerter N, Starosweiecki E, Gurney P, Hargreaves B, Gold G.	High Resolution In Vivo Sodium MRI of Articular Cartilage at 3T and 7T. International Workshop on Imaging in Osteoarthritis; November 2007; Salzburg, Austria.
Barnes P, Galaznik J, Krasnokutsky M, Plunkett J, Ophoven J, Squier W.	CT in Infant Dysphagic Choking ALTE. 55th Annual Meeting of the Society for Pediatric Radiology; May 8-10, 2008; Scottsdale, AZ.
Barnes P, Galaznik J, Krasnokutsky M.	CT in Infant Dysphagic Choking Acute Life Threatening Event (ALTE – a mimic of child abuse). Scientific Paper Sessions, Society for Pediatric Radiology, Scottsdale AZ, May 6-10, 2008; American Society of Pediatric Neuroradiology / American Society of Neuroradiology; May 31-Jun 5, 2008; New Orleans, LA.
Barnes P, Keller KA.	Imaging Findings in Congenital Rickets. 55th Annual Meeting of the Society for Pediatric Radiology; May 8-10, 2008; Scottsdale, AZ.
Barth RA.	Fetus-in-fetu with 9 Fetoform Parts. American Institute of Ultrasound in Medicine; March 12-15, 2008, San Diego, CA.
Beaulieu CF.	Four lectures, UCSF CME course on Musculoskeletal MRI. November 16, 2007; San Francisco, California.
Beaulieu CF.	Technical Aspects of Musculoskeletal MRI. Stanford Postgraduate Course; October 29, 2007; Monterey, California.
Beaulieu CF.	Two lectures, Society of Computed Body Tomography and MRI; March 31, 2008; Charleston, South Carolina
Beaulieu CF.	Visiting Professor, Duke University Medical Center Department of Radiology. Grand Rounds and Resident Case Conference; March 27, 2008; Durham, North Carolina.
Besier TF, Beaupré GS, Gold G, Fredericson M, Delp SL.	Muscle forces at the knee during walking and running in patients with patellofemoral pain. American Society of Biomechanics; August 2007; Stanford California.
Besier TF, Delp SL, Gold G, Beaupré GS.	Influence of quadriceps muscle force distributions on cartilage stresses at the patellofemoral joint during running. American Society of Biomechanics; August 2007; Stanford California.
Biswal S, Lee S, Kamaya S, Behera D, Graves E, Gold G.	Imaging Pain and Nociception with Manganese-Enhanced MRI (MEMRI). Moncoda Award Winner, Best Contrast Media Paper. Society of Body Computed Tomography and MR; Mar 30-Apr 4, 2008; Charleston, SC.
Blankenberg FG.	Children's Oncology Group, Special Emphasis Panel/Scientific Review group 2008/01 NCI-HR Meeting; October 22-23, 2007; Washington, DC.
Blankenberg FG.	Multi-modality imaging of atherosclerosis. Nuclear Medicine Grand Rounds; January 22, 2008; Stanford, CA.
Blankenberg FG.	The use of sc-VEGF as a radiotherapeutic agent. MIPS Small Animal Imaging Workshop; Nov 8, 2007; Stanford, CA.

Blankenberg FG.	Working Group Reviewer. NIH Panel Meeting for NSLS-II (National Synchrotron Light Source); April 27-28, 2008; Bethesda, MD.
Chan FP, Newman B, Perry SB, Feinstein JA.	Evaluation of Contrast Injection Strategies in CT Angiography of Cavopulmonary Connections. 55th Annual Meeting of the Society for Pediatric Radiology; May 8-10, 2008; Scottsdale, AZ.
Chan FP, Nguyen ET, Feinstein JA, Perry SB, Reddy VM, Hanley FL.	Replacement of Catheter Angiography with CT Angiography for the Evaluation of Pulmonary Artery Anatomy in Neonatal Pulmonary Atresia with Ventricular Septal Defect. 55th Annual Meeting of the Society for Pediatric Radiology; May 8-10, 2008; Scottsdale, AZ.
Chan FP, Wong H, Vasanawala SS, Feinstein JA, Dubin AM, Newman B.	Inter-observer Variability and Accuracy in the Diagnosis of Aberrant Coronary Artery in Children Using Coronary CT Angiography. 55th Annual Meeting of the Society for Pediatric Radiology; May 8-10, 2008; Scottsdale, AZ.
Chang P, Ramamoorthy C, Williams J, Chan FP.	Characteristics of Anesthesia Complications in Pediatric Patients who Underwent Cardiovascular CT and MRI Examinations. 55th Annual Meeting of the Society for Pediatric Radiology; May 8-10, 2008; Scottsdale, AZ.
Chari R, Gambhir SS, Geevarghese S, Geller DA, Iagaru A, Meschder A, Nemunaitis J, Reid TR, Sze DY, Tanabe K.	Efficacy of an Oncolytic Herpes Simplex Virus (NV1020) in Patients with Colorectal Cancer Metastatic to Liver. American Society of Clinical Oncology Annual Meeting; May 30-Jun 3, 2008; Chicago, IL.
Chen IY, Gheysens O, Ray S, Padmanabhan P, Ramasamy P, Loening AM, Rodriguez-Porcel M, Willmann JK, Sheikh AY, Hoyt G, Robbins RC, Biswal S, Wu JC, Gambhir SS.	Indirect imaging of transgene expression using a versatile, bidirectional cardiac gene therapy vector with combined transcriptional targeting and amplification strategies. Joint meeting, Academy of Molecular Imaging and Society for Molecular Imaging; Sep 7-11, 2007; Providence, RI.
Chinn G, Levin CS.	PET Image Reconstruction with a Bayesian Projector for Multi-Electronic Collimation Schemes. IEEE (Institute of Electrical & Electronics Engineers) Nuclear Science Symposium and Medical Imaging Conference; October 27-November 3, 2007; Honolulu, HI.
Choi G, Shin LK, Taylor C, Cheng C.	Quantification of the deformation of the human iliac arteries with hip and knee flexion: implications for stent-graft design. Summer Bioengineering Conference (SBC); June 25-29, 2008; Marco Island, FL.
Deshmukh S, Rubesova E, Barth RA.	Literature Review: Normative Fetal Lung Volume by Gestational Age on MRI. 55th Annual Meeting of the Society for Pediatric Radiology; May 8-10, 2008; Scottsdale, AZ.
Deshmukh S, Rubesova E, Rosenberg J, Hintz SR, Barth RA.	Subjective versus objective MRI measurement of fetal lung volumes. 55th Annual Meeting of the Society for Pediatric Radiology; May 8-10, 2008; Scottsdale, AZ.
Dhanani RS, Kothary N, Hunt S, Kuo WT, Hofmann LV, Sze DY.	Comparison of Outcomes Between TIPS Performed with 8 mm and 10 mm Diameter Stent-Graft Devices. Society of Interventional Radiology 33rd Annual Scientific Meeting; March 15-20, 2008; Washington, D.C.
Do, Huy.	16th Annual Summer Diagnostic Imaging Update (four presentations). Stanford University School of Medicine, Department of Radiology; July 8-11, 2008; Jackson Hole, Wyoming.
Do, Huy.	Advances in Neuroradiology and Sports Medicine Imaging. Radiology Continuing Medical Education, Stanford University School of Medicine, Department of Radiology; May 2-5, 2008; Las Vegas, NV.
Do, Huy.	Pathway to Excellence: Advancing Interventional Radiology 3rd Annual Fellows Conference. Stanford University School of Medicine, Department of Radiology; June 4-6, 2008; Chicago, Il.
Draper C, Besier T, Santos J, Gold G, Beaupré G, Delp S.	Measurements of in vivo patellofemoral joint kinematics with real-time MRI. American Society of Biomechanics; August 2007; Stanford, CA.
Fischbein N.	CN VII: Anatomy and Pathology. 41st Annual Meeting of the American Society of Head and Neck Radiology; Sep 30, 2007; Seattle, WA.
Fischbein N.	Nasopharynx: Anatomy and Patterns of Cancer Spread. 46th Annual Meeting of the American Society of Neuroradiology; Jun 2, 2008; New Orleans, LA.
Ganguly A, Schneider A, Keck B, Bennett NR, Fahrig R.	In Vivo Imaging of Superficial Femoral Artery (SFA) Stents for Deformation Analysis. Proceedings of the Society of Photographic Instrumentation Engineers (SPIE); Feb 18-20, 2008; San Diego, CA.
Girard-Hughes E, Fahrig R, Mehdizadeh A, Boese J, Lauritsch G, Wang PJ, Zei PC, Hsia HH, Moore T, Rosenberg J, Al-Ahmad A.	Comparison of gated vs. non-gated cardiac c-arm CT (Dyna CT) of the left atrium and pulmonary veins in humans. 13th Annual Meeting of the Boston Atrial Fibrillation Symposium; January 17-19, 2008; Boston, MA.
Girard-Hughes E, Al-Ahmad A, Mehdizadeh A, Boese J, Lauritsch G, Wang PJ, Zei PC, Hsia HH, Moore T, Rosenberg J, Fahrig R.	The impact of atrial fibrillation on the accuracy of three-dimensional imaging of the left atrium: A study using ECG gated multisweep c-arm CT (DynaCT Cardiac). Annual Meeting of the Heart Rhythm Society; May 14-17, 2008; San Francisco, CA.

Gold G, Staroswiecki E, Nnewihe A, Bangerter N, Hargreaves B.	In Vivo Full Joint Sodium MRI of the Knee for Proteoglycan Assessment. Osteoarthritis Research Society International; September, 2007;
Goris ML, Iagaru A, Zhu H, Mari C	Comparison of Efficacy and Toxicity of Bexxar and Zevalin in the Management of Refractory Non-Hodgkin's Lymphoma. European Association of Nuclear Medicine Annual Congress; October 13-17, 2007; Copenhagen, Denmark.
Guccione S, Jang T, Yang Y-S, Cao H, Haddix T, Glantz M, Le Q, Recht L, Harsh G.	Osteopontin (OPN) expression correlates with glioma aggressiveness. Society for Neuro Oncology Annual Meeting, November 15-18, 2007; Dallas, TX.
Guccione S, Yang Y-S, Choi S.	Molecular imaging and therapy platform: Pre-selecting responding tumors to antiangiogenic therapy. Society for Neuro Oncology Annual Meeting, November 15-18, 2007; Dallas, TX.
Hargreaves B, Bangerter N, Staroswiecki E, Gurney P, Grafendorfer T, Nnewihe A, Daniel B, Gold G.	Co-Registered Sodium and Proton MRI of Osteoarthritis and Breast Cancer. Lauterbur Award Winner, Best MRI Paper. Society of Body Computed Tomography and MR; March-April 2008; Charleston, South Carolina.
Heilmaier C, Sutter R, Lutz AM, Weishaupt D, Marincek B, Willmann JK.	Dynamic MRI of the liver with parallel acquisition technique for mapping of the hepatic vascular anatomy: comparison with 64-detector row computed tomography. Annual meeting, Swiss Society of Radiology; May 29-31; St. Gallen, Switzerland.
Heit JJ, Georganos SA, Dodd RL, Jayaraman MV, Do HM.	Extravertebral osteoplasty using cement for treatment of non-healing fractures of the pubic ramus and clavicle. Society of Interventional Radiology 33rd Annual Scientific Meeting; March 15-20, 2008; Washington, D.C.
Higgins LJ, van den Bosch M, Hwang G, Paulmurugan R, Kothary N, Kuo WT, Sze DY, Katzenberg R, Gambhir LV, Hofmann LV.	J Vasc Interv Radiol. 2008;19:S135.
Hofmann LV.	Advances in Clinical Care: Coagulation and Hemostasis. Society of Interventional Radiology 33rd Annual Scientific Meeting; March 15-20, 2008; Washington, D.C.
Hofmann LV.	Aortoiliac Interventions. Society of Interventional Radiology 33rd Annual Scientific Meeting; March 15-20, 2008; Washington, D.C.
Hofmann LV.	Arterial Intervention: Visceral Vascular Intervention. International Symposium on Endovascular Therapy (ISET); Jan 22, 2008; Hollywood, FL.
Hofmann LV.	Arterial Lysis. Pathway to Excellence. Advancing interventional radiology. Fellows Conference, June 5, 2008.
Hofmann LV.	Bam! DVT Disasters. 9th Annual Interventional Radiology Summit at Squaw; February 22, 2008; Lake Tahoe, California.
Hofmann LV.	Concurrent Session 6: Interactive Session: My Worst Complication. International Symposium on Endovascular Therapy. International Symposium on Endovascular Therapy (ISET); Jan 23, 2008; Hollywood, FL.
Hofmann LV.	Culprit Lesions and DVT. 9th Annual Interventional Radiology Summit at Squaw; February 22, 2008; Lake Tahoe, California.
Hofmann LV.	Deep Vein Thrombosis. Pathway to Excellence. Advancing interventional radiology. Fellows Conference, June 5, 2008
Hofmann LV.	Film Panel Revisited. Society of Interventional Radiology 33rd Annual Scientific Meeting; March 15-20, 2008; Washington, D.C.
Hofmann LV.	Full Metal Jacket: The Best Way to Treat Chronic DVT. International Symposium on Endovascular Therapy (ISET); Jan 23, 2008; Hollywood, FL.
Hofmann LV.	IVC Filters. Department of Medicine, Stanford University; Oct 16, 2007; Stanford, CA.
Hofmann LV.	Molecular Image-Guided Interventions: Your Future. 9th Annual Interventional Radiology Summit at Squaw; February 22, 2008; Lake Tahoe, California.
Hofmann LV.	Pulmonary Embolism. Pathway to Excellence. Advancing interventional radiology. Fellows Conference, June 5, 2008.
Hofmann LV.	SFA Intervention, Stroke, DVT Management. International Symposium on Endovascular Therapy (ISET); Jan 23, 2008; Hollywood, FL.
Hofmann LV.	Thrombolytic Therapy for Arterial Disease. Society of Interventional Radiology 33rd Annual Scientific Meeting; March 15-20, 2008; Washington, D.C.
Hofmann LV.	Venous Thrombolysis. Society of Interventional Radiology 33rd Annual Scientific Meeting; March 15-20, 2008; Washington, D.C.
Iagaru A, McDougall IR.	18F FDG PET/CT in the Management of Papillary Thyroid Cancer, with an Emphasis on Thyroglobulin, TSH and Lesion SUVmax Values. European Association of Nuclear Medicine Annual Congress; Oct 13-17, 2007; Copenhagen, Denmark.

Iagaru A, Mittra E, Quon A, Gambhir SS.	18F FDG PET/CT in Head and Neck Cancers: What is the Definition of Whole-Body Scanning? American College of Neuropsychopharmacology Annual Meeting; Feb 14-17, 2008; Newport Beach, CA.
Iagaru A, Quon A, Jacobs C, Marina N, McDougall IR, Gambhir SS.	Osseous and soft tissue sarcomas: when can 18F FDG PET/CT evaluation provide useful information? European Association of Nuclear Medicine Annual Congress; Oct 13-17, 2007; Copenhagen, Denmark.
Iagaru A, Zhu H, Mari C, Knox SJ, Ganjoo K, Goris ML.	131I-Tositumomab (Bexxar®) vs. 90Y-Ibritumomab (Zevalin®) in Refractory/Relapsed Non-Hodgkin?s Lymphoma. American College of Neuropsychopharmacology Annual Meeting; Feb 14-17, 2008; Newport Beach, CA.
Iagaru A	Sarcomas: Classification, Diagnosis, and Therapeutic Approaches with an Emphasis on the Role of 18F FDG PET/CT. Northern California Chapter SNM Annual Meeting; Feb 28, 2008; Pleasanton, CA.
Josan S, Chen J, Holbrook A, van den Bosch M, Bouley D, Daniel B, Butts Pauly K.	World Conference on Interventional Oncology; June 22-25, 2008; Los Angeles, CA.
Kamaya A, Hunt S, Edwards B, Jeffrey B, Garcia G.	Screening for Hepatocellular Carcinoma Using Ultrasound Harmonics. Oral presentation American Roentgen Ray Society; April 14, 2008; Washington, D.C.
Kamaya A, van de Ven SM, van den Bosch MA, Kwong A, Rosenberg J, Lo G, Ikeda DM.	Reproducibility of scoring systems used for breast density and breast parenchymal pattern assessment on X-ray mammography. American Society of Clinical Oncology; May 2008; Chicago, Illinois.
Kang B, Sze DY, Razavi MK.	Treatment failure after uterine artery embolization for symptomatic uterine fibroids: significance of ovarian arterial collateral vessels in predicting the outcome. Cardiovascular and Interventional Radiological Society of Europe; Sep 8-12, 2007;Athens, Greece.
Karrasch M, Geevarghese SK, de Haan H, Sze D, Chari R.	Radiological and clinical benefit to second line NV1020 oncolytic virus and CPT-11/bevacizumab treatment in a patient with progressive metastatic colorectal cancer. World Congress on GI Cancer/Perspectives in Colorectal Cancer; Sep 7-8, 2007;Miami, FL.
Kaye E, Butts Pauly K,	MR Parameters of Frozen Tissue: Proton Resonant Frequency and R2. 45th Annual Meeting, Society for Crybiology; July 20-23, 2008; Charlotte, NC.
Keller KA, Barnes PD.	Imaging Findings in Congenital Rickets (a mimic of child abuse). Scientific Paper Session, Society for Pediatric Radiology; May 6-10, 2008; Scottsdale AZ.
Keren S, Zavaleta C, Cheng Z, Gheysens O, Gambhir SS.	Noninvasive molecular imaging of small living subjects using Raman spectroscopy and Raman nanoparticles. Poster presentation, NCI Nanotechnology Alliance Investigators Meeting; Oct 16-18, 2007; Chapel Hill, NC.
Koo S, Hargreaves B, Bangerter N, Andriacchi T, Gold G.	Automatic Segementation of Knee Articular Cartilage From MRI: A Multi-Contrast and Multi-Dimensional Approach. International Workshop on Imaging in Osteoarthritis. Salzburg, Austria; November, 2007.
Kothary N, Kuo WT, Louie J, Hofmann LV, Sze DY.	Safety and Efficacy of Ethanolamine for Embolization of Gastric Varices in Patients with Portal Hypertension. Society of Interventional Radiology 33rd Annual Scientific Meeting; March 15-20, 2008; Washington, D.C.
Kraitchman D, Hofmann LV.	Serial MRI Evaluation of Stem Cell Efficacy Using Allogeneic, MR-labeled Stem Cells in a Rabbit Peripheral Arterial Disease Model: Comparison to X-ray Angiography and Histology. American Heart Association (AHA) Scientific sessions; Nov 7, 2007; Orlando, FL.
Kuo WT, van den Bosch MA, Hofmann LV, Louie JD, Kothary N, Sze DY.	Catheter-Directed Embolectomy, Fragmentation, and Thrombolysis for the Treatment of Massive Pulmonary Embolism After Failure of Systemic Thrombolysis. American College of Chest Physicians Annual Scientific Meeting; October 20-25, 2007; Chicago, Illinois.
Kuo WT, van den Bosch MA, Sze DY, Gould MK, Kothary N, Hofmann LV.	Catheter-Directed Therapy for Massive Pulmonary Embolism: Systematic Review and Meta-Analysis of the Modern Technique. Society of Interventional Radiology 33rd Annual Scientific Meeting; March 15-20, 2008; Washington, D.C.
Larabi M, Mackanos M, Shinde R, Contag C, Guccione S.	Temperature sensitive liposomes for local drug delivery using focused ultrasound. AACR-NCI-EORTC International Conference on Molecular Targets and Cancer Therapeutics, October 22-26, 2007; San Francisco, CA.
Larabi M, Mackanos M, Shinde R, Contag C, Guccione S.	Temperature sensitive liposomes for local drug delivery using focused ultrasound. Nano Science and Technology Institute Conference; June 1-5, 2008; Boston, MA.
Lau F, Olcott P, Horowitz M, Levin CS.	Noise Analysis of PSAPD PET Detector Front-End Multiplexing Circuits. IEEE (Institute of Electrical & Electronics Engineers) Nuclear Science Symposium and Medical Imaging Conference; October 27-November 3, 2007; Honolulu, HI.
Levi J, De A, Cheng Z, Gambhir SS.	Novel substrates for bioluminescence imaging with improved properties. Poster presentation, joint meeting Academy of Molecular Imaging and Society for Molecular Imaging; Sep 7-11, 2007; Providence, RI.
Levin CS.	Integrating Positron Emission Tomography and Magnetic Resonance Imaging. Presented to GE Executives of the Global Climate and Energy Project (GCEP); June 4, 2008; Lucas Learning Center; Stanford, CA.
Levin CS.	Introduction to the Small Animal Imaging Workshop at Stanford. Small Animal Imaging Workshop 2007; November 7-10; Stanford, CA.

Levin CS.	New Imaging System Technologies to Enhance the Molecular Sensitivity of Positron Emission Tomography. Philips Molecular Imaging Lecture Series 2007; December 3; Clark Center, Stanford CA.
Levin CS.	New imaging system technologies to enhance the molecular sensitivity of positron emission tomography; Department of Engineering Physics, Tsinghua University; June 17, 2008; Beijing, China.
Levin CS.	Optical Imaging Physics and Instrumentation: Brief Overview. Small Animal Imaging Workshop 2007; November 7-10; Stanford, CA.
Levin CS.	Organ-Specific Positron Emission Tomography Camera for More Sensitive Cancer Imaging. University of Connecticut Department of Electrical and Computer Engineering; April 11, 2008; Storrs, Connecticut.
Levin CS.	Organ-Specific Radionuclide Cameras for More Sensitive Cancer Imaging. Department of Engineering Physics, Tsinghua University; June 17, 2008; Beijing, China.
Levin CS.	PET Instrumentation that can be Operated Within an MRI System. Ninth Annual Academy of Molecular Imaging and SNM PET/CT Symposium; VA Palo Alto Health Care System; June 7, 2008; Palo Alto, CA.
Levin CS.	PET Instrumentation that can Operate Within a Magnetic Resonance Imaging (MRI) System; Department of Engineering Physics, Tsinghua University; June 17, 2008; Beijing, China.
Levin CS.	Radionuclide Imaging Physics and Instrumentation: Brief Overview. Small Animal Imaging Workshop 2007; November 7-10; Stanford, CA.
Levin CS.	Spatial Resolution Limits of Radionuclide Tomography. Nuclear Medicine Grand Rounds 2008; February 19; Stanford CA
Lillaney P, Bracken J, Ganguly A, Fahrig R, Rowlands JA.	Development of an MR compatible rotating anode x-ray tube. Proceedings of the Society of Photographic Instrumentation Engineers (SPIE); Feb 18-20, 2008; San Diego, CA.
Liu Z, Cai W, Chen X, Dai H.	Biomedical Application of Single-walled Carbon Nanotubes, from In Vitro to In Vivo. 2007 Materials Research Society (MRS) Fall meeting; Nov 26-30, 2007; Boston, MA.
MacKenzie JD, Hernandez A, Gonzalez L, Pena A, Ruppert K, Khrichenko D, Jawad AF, Wells L, Smith-Whitley K, Jaramillo D.	Magnetic Resonance Imaging in Early Avascular Necrosis - Quantification of the Apparent Diffusion Coefficient in the Hips of Sickle Cell Patients. Sickle Cell Disease Association of America and National Institues of Health 35th Annual Convention; September 17-22, 2007; Washington, D.C.
MacKenzie JD.	MR Arthrography Made Simple: Indications and Techniques. 55th Annual Meeting of the Society for Pediatric Radiology; May 8-10, 2008; Scottsdale, AZ.
Melvin JS, Mackenzie JD, Wells L, Sennett BJ.	Magnetic Resonance Imaging and the HAGL Lesion: Four arthroscopically confirmed cases of false positive MRI diagnosis. American Academy of Orthopedic Surgeons; March 5-9, 2008; San Francisco, California.
Mescheder A, Chari R. Geevarghese S, Geller D, Karrasch M, Nemunaitis J, Senzer N, Reid T, Sze D, Tanabe K	Preliminary clinical profile of an oncolytic herpes simplex virus (NV1020) prior to second-line chemotherapy, in patients with colorectal cancer metastatic to liver. Amer Soc Clin Oncol GI Symposium; May 30-Jun 3, 2008;Orlando, FL.
Mittra E, Iagaru A, Fisher G, Kuntz P, Quon A, Gambhir SS.	Value of 18F FDG PET/CT for the Restaging of Colorectal Cancer after Treatment with Erbitux. American College of Neuropsychopharmacology Annual Meeting; Feb 14-17, 2008; Newport Beach, CA.
Moseley M.	MR Physics for the Next Generation. American Society of Neuroimaging; Jan 17-20, 2008; Tucson, AZ.
Moseley M.	The Present Situation and the Future Prospect of Molecular Imaging. Plenary Lecture. Japanese Society of Radiological Technology (JSRT). Apr 4-6, 2008; Yokohama, Japan.
Moseley M.	MR Physics for the Next Generation. Japanese Society of Radiological Technology (JSRT). Apr 4-6, 2008; Yokohama, Japan.
Moseley M.	Molecular Imaging in Stroke. Invited Lecture. The Princeton Conference; Apr, 2008; Houston, TX.
Moseley M.	Small Animal MRI. Invited Lecture. Small Animal Imaging Workshop; Clark Center, Stanford; Nov 2007; Stanford, CA.
Moskowitz P.S.	Three 3-hour Workshops: Managing Your Vital Resources; Values-Based Use of Your Time and Money; Surviving and Thriving in Your Medical Marriage. Medical Career Transitions: Shift Happens. Physicians' Wellness Retreat; Palo Alto Medical Foundation; April 26-27, 2008; Chaminade Resort, Soquel, California.
Moskowitz PS.	A Wellness Curriculum for California Physicians: Concepts and Proposed Structure. Invited Presentation, Education Committee, Medical Board of California; April 24, 2008; Sacramento, California.
Moskowitz PS.	Interesting Cases from LPCH at Stanford, 2007-2008. Annual Meeting Pacific Coast Pediatric Radiologists Association; July 31 - August 3, 2008; Silverado Resort, Napa Valley, California.
Moskowitz PS.	Interesting Pediatric Radiology Cases from LPCH at Stanford. Children's Hospital of Auckland; January 4, 2008; Auckland, New Zealand.
Moskowitz PS.	Interesting Pediatric Radiology Cases from LPCH at Stanford. Westmeade Children's Hospital; January 23, 2008; January 30, 2008; February 4, 2008; Sydney, Australia.

Moskowitz PS.	Living Well is the Best Revenge: Career and Life Planning for the Busy Physician. A three hour workshop for physicians and spouses. Physician Well Being Retreat. Santa Clara County Medical Association; September 29, 2007; Sunnyvale, California.
Moskowitz PS.	Surviving and Thriving in the Medical Marriage. Annual Meeting, California Medical Association Alliance; September 15, 2007; Stockton, California.
Moskowitz PS.	The Need for Physician Renewal. Invited Presentation, Medical Board of California; November 2, 2007; San Diego, California.
Moskowitz PS.	The Six Domains of Balance: Definitions and Strategies. Faculty Symposium on Work-Life Balance; Stanford University School of Medicine; March 5, 2008; Stanford, California.
Moskowitz PS.	Well-Being and the Quest for Balance: Career and Life Planning for the Busy Radiologist; lecture and three-hour workshop. Annual meeting, Western Angiographic and Interventional Society; September 21-25, 2008; Ritz Carleton Hotel, Kappaula, Maui.
Mueller MA, Mayer D, Seifert B, Marincek B, Willmann JK.	Effect of direct contrast-enhanced 3D MR venography findings on diagnosis and therapeutic decisions in patients with recurrent lower limb varicose veins. Annual meeting, Swiss Society of Radiology; May 29-31; St. Gallen, Switzerland.
Newman B.	Unilateral systemic venous obstruction and lymphatic congestion. 55th Annual Meeting of the Society for Pediatric Radiology; May 8-10, 2008; Scottsdale, AZ.
Newman B, Feinstein JA, Cohen RA, Feingold B, Kreutzer J, Chan FP.	Portosystemic shunts associated with L-Isomerism. 55th Annual Meeting of the Society for Pediatric Radiology; May 8-10, 2008; Scottsdale, AZ.
Newman B.	The ABC's of Vascular Rings. 16th Annual Summer Diagnostic Imaging Update 2008; Stanford University Department of Radiology; July 8-11, 2008; Jackson Hole, WY.
Newman B.	Congenital Lung Anomalies: Current Concepts and Controversies. 16th Annual Summer Diagnostic Imaging Update 2008; Stanford University Department of Radiology; July 8-11, 2008; Jackson Hole, WY.
Newman B.	Imaging Pulmonary Infection in Children. 16th Annual Summer Diagnostic Imaging Update 2008; Stanford University Department of Radiology; July 8-11, 2008; Jackson Hole, WY.
Newman B.	Low Dose CT Imaging in CF Patients. 10th Annual International Symposium on Multidetector-Row CT; Stanford University Department of Radiology; May 13-16, 2008; Las Vegas, NV.
Newman B.	Common Vascular Rings – The ABC's of Imaging Interpretation. 10th Annual International Symposium on Multidetector-Row CT; Stanford University Department of Radiology; May 13-16, 2008; Las Vegas, NV.
Olcott PD, Lau F, Cajipe VB, Clajus M, Tumer TO, Volkovskii A, Levin CS.	Data Acquisition System Design for a 1 mm^3 Resolution PSAPD-Based PET System. IEEE (Institute of Electrical & Electronics Engineers) Nuclear Science Symposium and Medical Imaging Conference; October 27-November 3, 2007; Honolulu, HI.
Olivot JM, Mlynash M, Zaharchuk G, Straka M, Bammer R, Lansberg MG, Moseley ME, Albers GW.	Perfusion-magnetic resonance imaging Tmax and mean transit time compared to stable xenon computed tomography cerebral blood flow. European Stroke Conference; May 13-16, 2008; Nice, France.
Pelc NJ.	Principles, Advantages and Limitations of Dual Energy CT. 16th Annual Diagnostic Imaging Update. Stanford University Department of Radiology; March 17-21, 2008; Kauai, HI.
Pelc NJ.	Recent Advances and Future Directions in MR Imaging. 16th Annual Diagnostic Imaging Update. Stanford University Department of Radiology; March 17-21, 2008; Kauai, HI.
Peng H, Levin CS.	Study of Potential PET Spatial Resolution Improvement in PET/MRI Dual Modality. Joint meeting, Academy of Molecular Imaging and Society for Molecular Imaging; Sep 7-11, 2007; Providence, RI.
Peng H, Olcott P, Foudray AMK, Levin CS.	Evaluation of Free-Running ADCs for High Resolution PET Data Acquisition. IEEE (Institute of Electrical & Electronics Engineers) Nuclear Science Symposium and Medical Imaging Conference; October 27-November 3, 2007; Honolulu, HI.
Peng H, Olcott PD, Pratx G, Foudray AMK, Chinn G, Levin CS.	Design Study of a High Resolution Breast-Dedicated PET System Built from Cadmium Zinc Telluride Detectors. IEEE (Institute of Electrical & Electronics Engineers) Nuclear Science Symposium and Medical Imaging Conference; October 27-November 3, 2007; Honolulu, HI.
Pratx G, Chinn G, Levin CS.	Fully 3D List-Mode OSEM on PC Graphics Hardware: Quantitative Studies. IEEE (Institute of Electrical & Electronics Engineers) Nuclear Science Symposium and Medical Imaging Conference; October 27-November 3, 2007; Honolulu, HI.
Pratx G, Levin CS.	Accurately Positioning Events in a High-Resolution PET System that uses 3D CZT Detectors. IEEE (Institute of Electrical & Electronics Engineers) Nuclear Science Symposium and Medical Imaging Conference; October 27-November 3, 2007; Honolulu, HI.
Pruemmer M, Rohkohl C, Fahrig RA, Lauritsch G, Hornegger JM.	Cardiac C-arm CT: image-based gating. Proceedings of the Society of Photographic Instrumentation Engineers (SPIE); Feb 18-20, 2008; San Diego, CA.

Ray P, Lutz A, Cheng Z, Cochran FV, Junutula AR, Gambhir SS.	Noninvasive imaging of an epithelial cell adhesion molecule (EpCAM) antibody in mouse models of ovarian cancer. Poster presentation.
Ren PG, Lee SW, Biswal S, Goodman SB.	Systemic trafficking of macrophages induced by bone cement particles in nude mice. Annual meeting, Orthopedic Research Society; March 2-5, 2008; San Francisco, CA.
Rieke V, Chen J, Holbrook A, Bouley D, Diederich C, Sommer G, Butts Pauly K	High Intensity Ultrasound Ablation of the Canine Prostate: Monitoring and Post -Procedural Assessment with Magnetic Resonance Imaging. World Conference on Interventional Oncology; June 22-25, 2008; Los Angeles, CA.
Roos JE.	Airway Disease: From Large to Small. 16th Annual Winter Diagnostic Imaging Update; Stanford University Department of Radiology; January 7-11, 2008; Beaver Creek, Colorado.
Roos JE.	Computer Assisted Detection (CAD) of Lung Nodules in Chest CT: Are We Ready for Prime Time? 16th Annual Winter Diagnostic Imaging Update; Stanford University Department of Radiology; January 7-11 2008; Beaver Creek. Colorado.
Roos JE.	Idiopathic Interstitial Pneumonias (IIP): What Every Radiologist Should Know. 16th Annual Winter Diagnostic Imaging Update; Stanford University Department of Radiology; January 7-11, 2008; Beaver Creek, Colorado.
Roos JE, Olsen DA, Paik DS, Napel S, Rubin GD	Computer-aided detection (CAD) of pulmonary nodules in chest CT: Do radiologists benefit equally from CAD? European Congress of Radiology; March 7-11 2008; Vienna, Austria.
Roos JE.	Cardiac CT: Technique and Post-Processing; Resident Education: A Module or Cardiac Imaging, Armed Forces Institute of Pathology, Walter Reed Army Medical Center; April 28, 2008; Washington, D.C.
Roos JE.	CT of Coronary Artery Disease; Resident Education: A Module or Cardiac Imaging, Armed Forces Institute of Pathology, Walter Reed Army Medical Center; April 28, 2008; Washington, D.C.
Roos JE.	Who Benefits From Lung CAD? 10th Annual International Symposium on Multidetector–Row CT; Stanford University Department of Radiology; May 13-16, 2008; Las Vegas, Nevada.
Roos JE.	Strategies for Efficient Chest CT Interpretation. 10th Annual International Symposium on Multidetector-Row CT; Stanford University Department of Radiology; May 13-16, 2008; Las Vegas, Nevada.
Roos JE.	Chest CT Technical Advances. 2008 Summer Symposium on State of the Art Imaging; July 21-26, 2008; Stanford, California.
Rubesova E, Newman B, Dutta S, Hartman G, Rosenberg J, Barth RA.	Management of Bronchopulmonary Malformations: Results of the SPR and ESPR Survey. 55th Annual Meeting of the Society for Pediatric Radiology; May 8-10, 2008; Scottsdale, AZ.
Rubesova E, Newman B, Dutta S, Hartman G, Rosenberg J, Barth RA.	Management of Bronchopulmonary Malformations: Results of the SPR and ESPR Survey (Paper & Poster). Annual Meeting of the European Society for Pediatric Radiology; June 4-7, 2008; Edinburgh, Scotland.
Schipper ML, Iyer G, Koh AL, Cheng Z, Ebenstein Y, Aharouni A, Keren S, Bentolila LA, Zerda A, Li J, Smith BR, Rao J, Chen X, Wu AM, Banin U, Sinclair R, Weiss SS, Gambhir SS.	Particle size, surface coating, and pegylation influence the biodistribution of quantum dots in living mice. Poster presentation, NCI Nanotechnology Alliance Investigators Meeting; Oct 16-18, 2007; Chapel Hill, NC.
Schmitz AC, van den Bosch MA, Rieke V, Dirbas FM, Butts-Pauly K, Mali WP, Daniel BL.	3.0T MRI-guided focused ultrasound ablation versus MRI-guided needle wire placement for the pre-operative localization of non-palpable breast tumors: an experimental study. European Congress of Radiology; March 7-11 2008; Vienna, Austria.
Sherbondy AJ, Dougherty R, Ben-Shachar M, Cheung S, Napel S, Wandell BA.	Identifying the most likely white matter pathways between two brain regions. Society for Neuroscience Annual Meeting; November 2007; San Diego, California.
Shin LK, Chan J, Jeffrey RB.	Ultrasonography of abnormal neck lymph nodes. American Society of Head and Neck Radiology. Sep 26-30, 2007; Seattle, WA.
Shin LK.	CT colonography: key recent studies. 10th Annual International Symposium on Multidetector-Row CT. Stanford University Department of Radiology; May 13-16, 2008; Las Vegas, NV.
Shin LK.	MDCT of active arterial bleeding – what does it mean? 10th Annual International Symposium on Multidetector-Row CT. Stanford University Department of Radiology; May 13-16, 2008; Las Vegas, NV.
Smith BR, Cheng Z, De A, Gambhir SS.	Direct visualization of RGD-quantum dot binding in tumor neovasculature using intravital microscopy and living mice. Poster presentation, NCI Nanotechnology Alliance Investigators Meeting; Oct 16-18, 2007; Chapel Hill, NC.
Sommer G.	Multimodality Single Kidney Function: How and Why? Workshop, Society of Uroradiology Abdominal Radiology Course; Feb 17-22, 2008; Rancho Mirage, CA.
Sommer G.	Female Pelvic MRI. 16th Annual Diagnostic Imaging Update, Stanford University Department of Radiology; Jan 8, 2008; Vail, Colorado.
Sommer G.	Prostate MRI: A Critical Look. 16th Annual Diagnostic Imaging Update, Stanford University Department of Radiology; Jan 8, 2008; Vail, Colorado.

Other Presentations 2008

Sommer G.	CT Urography Update. 16th Annual Diagnostic Imaging Update, Stanford University Department of Radiology; Jan 8, 2008; Vail, Colorado.
Sommer G.	Current Concepts of Magnetic Resonance Imaging. Stanford University Department of Radiology. Oct 2007; Monterey, CA.
Starman J, Tognina C, Virshup G, Star-Lack J, Mollov I, Fahrig R.	Parameter investigation and first results from a digital x-ray flat panel detector with forward bias capability. Proceedings of the Society of Photographic Instrumentation Engineers (SPIE); Feb 18-20, 2008; San Diego, CA.
Stevens K.	Temporal progression of cystic angiomatosis. International Skeletal Society; September 2007; Budapest, Hungary.
Sutter R, Nanz D, Weishaupt D, Pfammatter T, Marincek B, Willmann JK.	Assessment of aortoiliac and renal arteries: MR angiography with parallel acquisition technique versus conventional MR angiography and digital subtraction angiography. Annual meeting, Swiss Society of Radiology; May 29-31; St. Gallen, Switzerland.
Sze DY, Chari R, Geller D, Nemunaitis J, Reid T, Tanabe K.	Phase I/II study of the oncolytic herpes virus NV1020 to treat liver-dominant metastatic colorectal cancer. J Vasc Interv Radiol. 2008;19:S25.
Sze DY, Gambhir SS, Chari R, Geller DA, Iagaru A, Mescheder A, Nemunaitis J, Reid TR, Tanabe K.	Imaging Characteristics and Response after Intraarterial Administration of the Oncolytic Herpes Virus NV1020 to Treat Hepatic Colorectal Metastases. American Society of Clinical Oncology Annual Meeting; May 30-Jun 3, 2008; Chicago, IL.
Tward DJ, Siewerdsen JH, Fahrig R, Pineda AR.	Cascaded systems analysis of the 3D NEQ for cone-beam CT and tomosynthesis. Proceedings of the Society of Photographic Instrumentation Engineers (SPIE); Feb 18-20, 2008; San Diego, CA.
Tye GA, Rosenberg J, Kuo WT, Kothary N, Sze DY, Hofmann LV.	Oral Contraceptive-Induced Deep Venous Thrombosis: A Correlation With May-Thurner Syndrome. Society of Interventional Radiology 33rd Annual Scientific Meeting; March 15-20, 2008; Washington, D.C.
Vance CJ, Newbould RD, Rubesova E, Barth RA, Bammer R.	Normal Values of Relaxation Times of Human Placenta at 1.5 Tesla. Fetal MRI Congress and Course; May 15-18, 2008; Vienna, Austria.
Wong H, Vasanawala SS, Newman B, Dubin AM, Chan FP.	Referral Patterns Favor the Use of Coronary MR Angiography for the Evaluation of Aberrant Coronary Artery in Older Children. 55th Annual Meeting of the Society for Pediatric Radiology; May 8-10, 2008; Scottsdale, AZ.
Yang Y-S, Vaithilingam S, Oralkan O, Khuri-Yakub P, Guccione S,	Photoacoustic contrast agents for in vivo imaging; Nano Science and Technology Institute Conference; June 1-5, 2008; Boston, MA.
Zaharchuk G, Augustin M, Fischbein NJ, Skare S, Rosenberg J, Newbould RD, Lansberg MG, Kemp S, Wijmann C, Moseley ME, Albers GW, Bammer R.	Clinical assessment of standard and GRAPPA parallel diffusion imaging: effects of acceleration factor and spatial resolution. American Society of Neuroradiology; May 31-Jun 5, 2008; New Orleans, LA.
Zaharchuk G, Shankaranarayan A, Alsop DC, Newbould RD, Straka M, Bammer R, Moseley ME.	Pseudocontinuous arterial spin labeling imaging findings in clinical patients with normal bolus perfusion-weighted imaging. American Society of Neuroradiology; May 31-Jun 5, 2008; New Orleans, LA.
Zaharchuk G.	Overview and comparison of quantitative CBF imaging techniques. 2nd International Symposium on Flow Measurement in Cerebrovascular Surgery; Sep 14, 2007; San Diego, CA.
Zavaleta C, Keren S, Cheng Z, Schipper M, Chen X, Liu Z, Dai H, Gambhir SS.	Use of non-invasive Raman spectroscopy imaging in living mice for evaluation of tumor targeting with carbon nanotubes. Poster presentation, NCI Nanotechnology Alliance Investigators Meeting; Oct 16-18, 2007; Chapel Hill, NC.
Zhu L, Star-Lack J, Green M, Fahrig R.	Metal artifact correction using hybrid kV and MV imaging. Oral presentation, 10th International Electronic Portal Imaging and Positioning Devices Workshop (EPI2K8); May 20-22, 2008; San Francisco, CA

Published Papers

Advani R, Maeda L, Lavori P, Quon A, Hoppe R, Breslin S, Rosenberg SA, Horning SJ.
Impact of positive positron emission tomography on prediction of freedom from progression after Stanford V chemotherapy in Hodgkin's disease. J Clin Oncol. 2007 Sep 1;25(25):3902-7.

Ai L, Rouhanizadeh M, Wu JC, Takabe W, Yu H, Alavi M, Li R, Chu Y, Miller JD, Heistad DD, Hsiai T
Shear stress influences spatial variations in vascular Mn-SOD expression: implications for LDL nitration. Am J Physiol Cell Physiol. 2008;294(6):C1576-85.

Aksoy M, Liu C, Moseley ME, Bammer R.
Single-step nonlinear diffusion tensor estimation in the presence of microscopic and macroscopic motion. Magn Reson Med. 2008 May;59(5):1138-50.

Al-Ahmad A, Wigstrom L, Sandner-Porkristi D, Wang PC, Zei PC, Boese J, Lauritsch G, Moore T, Chan F, Fahrig R.
Time-resolved three-dimensional imaging of the left atrium and pulmonary veins in the interventional suite--a comparison between multisweep gated rotational three-dimensional reconstructed fluoroscopy and multislice computed tomography. Hearth Rhythm 2008;5(4):513-519.

Alam MR, Dixiti V, Kang H, Li ZB, Chen X, Juliano R
Intracellular Delivery of an Anionic Antisense Oligonucleotide via Receptor Mediated Endocytosis. Nucl Acid Res. 2008;36(8):2764-76.

Arakawa H, Marks MP, Do HM, Bouley DM, Strobel N, Moore TT, Fahrig R.
Experimental study of intracranial hematoma detection with flat panel detector C-arm CT. American Journal of Neuroradiology 2008;29(4):766-772.

Assimes TL, Knowles, JW, Basu A, Iribarren C, Southwick A, Tang, H, Absher D, Li J, Fair JM, Rubin GD, Sidney S, Fortmann SP, Go AS, Hlatky MA, Myers RM, Risch N, Quertermous T.
Susceptibility locus for clinical and subclinical coronary artery disease at chromosome 9p21 in the multi-ethnic ADVANCE Study. Hum Mol Genet. 2008 Apr 28. [Epub ahead of print]

Atlas SW.
Managing the Health Care Myth. Hoover Digest 2007;Winter (4).

Au T, Thorne S, Korn M, Sze D, Kirn D, Reid T.
Minimal hepatic toxicity of Onyx-015: spatial restriction of coxsackie-adenoviral receptor in normal liver. Cancer Gene Ther 2007;14:139-150.

Au T, Thorne S, Korn M, Sze D, Kirn D, Reid T.
Minimal hepatic toxicity of Onyx-015: spatial restriction of coxsackie-adenoviral receptor in normal liver. Cancer Gene Ther. 2007;Feb;14(2):139-50. Epub 2006 Dec 1.

Augustine EM, Spielman DM, Barnes PD, Sutcliffe TL, Dermon JD, Mirmiran M, Clayton DB, Ariagno RL.
Can magnetic resonance spectroscopy predict neurodevelopmental outcome in very low birth weight preterm infants? J Perinatol. 2008 Jul 10. [Epub ahead of print].

Balchandani P, Pauly J, Spielman DM.
Interleaved narrow-band PRESS sequence with adiabatic spatial-spectral refocusing pulses for 1H MRSI at 7T. Magn Reson Med. 2008 May;59(5):973-9.

Balchandani P, Spielman DM.
Fat suppression for 1H MRSI at 7T using spectrally selective adiabatic inversion recovery. Magn Reson Med. 2008 May;59(5):980-8.

Balchandani P, Pauly J, Spielman DM.
Slice-selective tunable-flip adiabatic low peak-power excitation pulse. Magn Reson Med. 2008 May;59(5):1072-8.

Barnes PD, Krasnokutsky M.
Imaging of the central nervous system in suspected or alleged nonaccidental injury, including the mimics. Top Magn Reson Imaging. 2007;18(1):53-74.

Biswal S, Resnick DL, Hoffman JM, Gambhir SS.
Molecular imaging: integration of molecular imaging into the musculoskeletal imaging practice. Radiology 2007;Sep;244(3):651-71.

Breen M, Butts K, Chen L, Saidel G, Wilson D.
MRI guided thermal ablation therapy: model and parameter estimates to predict cell death from MR thermometry images. Annals of Biomedical Engineering 2007; 35(8):1391-1403.

Burt JR, Iribarren C, Fair JM, Norton LC, Mahbouba M, Rubin GD, Hlatky MA, Go AS, Fortmann SP.
Atherosclerotic Disease, Vascular Function and Genetic Epidemiology (ADVANCE) Study. Incidental findings on cardiac multidetector row computed tomography among healthy older adults: prevalence and clinical correlates. Arch Intern Med. 2008 Apr 14;168(7):756-61.

Cai W, Chen X.
Multimodality Molecular Imaging of Tumor Angiogenesis. J Nucl Med. 2008;49(Suppl 2):113S-128S.

Cai W, Chen K, Li Z, Gambhr SS, Chen X.
Dual-function probe for PET and near-infrared fluorescence imaging of tumor vasculature. J Nucl Med. 2007 Nov;48(11):1862–70.

Cai W, Chen X.
Preparation of peptide conjugated quantum dots for targeted cancer imaging. Nat Protocol. 2008;3:89-96.

Cai W, Chen X.
Nanoplatforms for Targeted Molecular Imaging in Living Subjects. Small 2007; Nov;3(11):1840-54.

Cai W, Ebrahimnejad A, Chen K, Cao Q, Li Z-B, Tice DA, Chen X.
Quantitative RadioimmunoPET Imaging of EphA2 in Living Mice. Eur J Nucl Med Mol Imaging 2007;34(12):2024-2036.

Cai W, Niu G, Chen X.
Molecular Imaging of the HER-Kinase Axis in cancer. Eur J Nucl Med Mol Imaging 2008;35(1):186-208.

Caires C, Guccione S.
Synthesis, structure, and reactivity of borate ester coordinated organobismuth compounds. Organometallics 2008;27(4):747-752.

Cao F, Sadrzadeh AH, Abilez OJ, Blundo J, Wang H, Pruitt B, Zarins C, Wu JC.
In vivo imaging and evaluation of biomatrices for improvement of stem cell engraftment in vivo. Tissue Engineering & Regenerative Medicine 2007;1(6):465-8.

Cao F, van der Bogt KE, Sadrzadeh A, Xie X, Sheikh AY, Wang H, Connolly AJ, Robbins RC, Wu JC. Spatial and temporal kinetics of teratoma formation from murine embryonic stem cell transplantation. Stem Cells & Development 2007;Dec;16:883-891.

Cao Q, Cai W, Li ZB, Chen K, He L, Li H-C, Hui M, Chen X. PET of Acute and Chronic Inflammation in Living Mice. Eur J Nucl Med Mol Imaging 2007;34(11):1832-42.

Cao Q, Li Z-B, Chen K, Wu Z, He L, Neamati N, Chen X Evaluation of Biodistribution and Anti-tumor Effect of a Dimeric RGD Peptide-paclitaxel Conjugate in Mice with Breast Cancer. Eur J Nucl Med Mol Imaging 2008 Mar 29; [Epub ahead of print].

Chan C, Paulmurugan R, Gheysens O, Kim J, Chiosis G, Gambhir SS. Molecular imaging of the efficacy of heat shock protein 90 inhibitors in living subjects. Cancer Res 2008;68:1:216-26.

Chen J, Daniel BL, Diederich CJ, Bouley DM, van den Bosch MA, Kinsey AM, Sommer G, Butts Pauly KB. Monitoring prostate thermal therapy with diffusion-weighted MRI. Magn Reson Med 2008;Jun;59(6):1365-72.

Chen JL, Gittleman A, Barnes PD, Change KW. Utility of temporal bone computed tomographic measurements in the evaluation of inner ear malformations. Arch Otolaryngol Head Neck Surg. 2008;134:50-56.

Chen K, Li Z-B, Wang H, Cai W, Chen X. Modification of Quantum Dot for Dual Modality Imaging of Tumor Vascular VEGFR. Eur J Nucl Med Mol Imaging. 2008 Jun 20. [Epub ahead of print]

Cheng Z, Xiong Z, Subbarayan M, Chen X, Gambhir SS. ^{64}Cu-labeled alpha-melanocyte-stimulating hormone analog for microPET imaging of melanocortin 1 receptor expression. Bioconjugate Chemistry 2007;18:765-772.

Cheng Z, Padilla De Jesus O, Namavari M, De A, Levi J, Webster JM, Zhang R, Lee B, Syud FA, Gambhir SS. Small-Animal PET Imaging of Human Epidermal Growth Factor Receptor Type 2 Expression with Site-Specific ^{18}F-Labeled Protein Scaffold. Journal of Nuclear Medicine 2008;May;49(50:804-13.

Chew K, Stevens K, Wang TG, Fredericson M, Lew H. Introduction to musculoskeletal diagnostic ultrasound Part 2. American Journal of Physical Medicine and Rehabilitation 2008;87(3)238-248.

Chin FT, Namavari M, Levi J, Subbarayan M, Ray P, Chen X, Gambhir SS. Semi-automated Radiosynthesis and Biological Evaluation of [^{18}F]FEAU: A Novel PET Imaging Agent for HSV1-tk/sr39tk Reporter Gene Expression. Mol Imaging Biol. 2008;10:82-91.

Chinn G, Levin CS. PET Image Reconstruction with a Bayesian Projector for Multi-Electronic Collimation Schemes. Conference Record of the 2007 IEEE Nuclear Science Symposium and Medical Imaging Conference; 2799-2802.

Chun HJ, Wilson K, Huang M, Wu JC. Integration of genomics, proteomics, and imaging for cardiac stem cell therapy (Review article). European Journal Nuclear Medicine & Molecular Imaging 2007;34:S20-S26.

Chung HH, Razavi MK, Sze DY, Frisoli JK, Kee ST, Dake MD, Hellinger JC, Kang BC. Portosystemic pressure gradient during transjugular intrahepatic portosystemic shunt with Viatorr stent graft: what is the critical low threshold to avoid medically uncontrolled low pressure gradient related complications? J Gastroenterol Hepatol. 2008;Jan;23(1):95-101.

Creusot R, Yaghoubi S, Kodama K, Dang D, Dang V, Breckpot K, Thielemans K, Gambhir SS, Fathman C. Tissue-targeted therapy of autoimmune diabetes using dendritic cells transduced to express IL-4 in NOD mice. Clin Immunol 2008,May;127(2):176-87.

De la Zerda A, Gambhir SS. Drug delivery: keeping tabs on nanocarriers. Nature Nanotechnology 2007;2:745-46.

Desser TS. Simulation based training: the next revolution in Radiology education? J Am Coll Radiol. 2007 Nov;4(11):816-24.

Do HM. Comments on Brain AVM Embolization with Onyx. American Journal of Neuroradiology 2007;28:178 (Editorial).

Duan Y, Catana A, Meng Y, Yamamoto N, He S, Gupta S, Gambhir SS, Zern M. Differentiation and enrichment of hepatocyte-like cells from human embryonic stem cells in vitro and in vivo. Stem Cells. 2007 Dec;25(12):3058-68.

Elkins CJ, Alley MT. Magnetic resonance velocimetry: applications of magnetic resonance imaging in the measurement of fluid motion. Exp. Fluids. 2008;43:823-858.

Fahrig R, Ganguly A, Lillaney P, Bracken J, Rowlands JR, Wen Z, Yu H, Rieke V, Santos JM, Pauly KB, Sze DY, Frisoli JK, Daniel BL, Pelc NJ. Design, performance, and applications of a hybrid x-ray/MR system for interventional guidance. Proc IEEE 2008;96:468-480.

Fair JM, Kiazand A, Varady A, Mahbouba M, Norton L, Rubin GD, Iribarren C, Go AS, Hlatky MA, Fortmann SP. Ethnic differences in coronary artery calcium in a healthy cohort aged 60 to 69 years. Am J Cardiol. 2007 Sep 15;100(6):981-5.

Fazel SS, Mallidi HR, Lee RS, Sheehan MP, Liang D, Fleischman D, Herfkens R, Mitchell RS, Miller DC. The aortopathy of bicuspid aortic valve disease has distinctive patterns and usually involves the transverse aortic arch. J Thorac Cardiovasc Surg. 2008;Apr;135(4):901-7

Foudray AMK, Levin CS. Bayesian Estimator for Angle Recovery: Event Classification and Reconstruction in Positron Emission Tomography. Journal of Bayesian Inference and Maximum Entropy Methods in Science and Engineering, American Institutes of Physics, 2007;954:362-371

Freeman-Walsh CB, Fahrig R, Ganguly A, Rieke V, Daniel BL. A hybrid radiography/MRI system for combining hysterosalpingography and MRI in infertility patients: initial experience. AJR 2008;Feb;190(2):W157-60.

Friedland S, Benaron D, Coogan S, Sze DY, Soetikno R. Diagnosis of chronic mesenteric ischemia by visible light spectroscopy during endoscopy. Gastrointest Endosc. 2007 Feb;65(2):294-300.

Gambhir SS. Molecular imaging of cancer: from molecules to humans. Introduction. J Nucl Med 2008 Jun;49; Suppl 2:1S-4S.

Ganguly A, Gold G, Butts K, Mayer D, Mosley M, Pelc N, Fahrig R. Quantitative Evaluation of the Relaxivity Effects of Iodine on Gd-DTPA Signal for MR arthrography. J Magn Reson Imaging. 2007;Jun;25(6):1219-25.

Gao F, Kar S, Zhang J, Qiu B, Walczak P, Larabi M, Xue R, Frost E, Qian Z, Bulte JW, Yang X. MRI of intravenously injected bone marrow cells homing to the site of injured arteries. NMR Biomed. 2007 Nov;20(7):673-81.

Goerke A, Loening A, Gambhir SS, Swartz J. Cell-free metabolic engineering promotes high-level production of bioactive Gaussia princeps luciferase. Metab Eng. 2008;May-Jul;10:3-4:187-200.

Gold G, Busse R, Beehler C, Han E, Baru A, Beatty P, Beaulieu C. Isotropic MRI of the Knee with 3D-FSE-xeta (eXtended Echo Train Acquisition) – Initial Experience in Healthy Volunteers. Amer J Roentgen 2007;May;188(5):1287-93.

Gold G, Pappas G, Blemker S, Whalen S, Campbell G, McAdams T, Beaulieu C. Abduction and External Rotation in Shoulder Impingement: An Open MRI Study on Healthy Volunteers. Radiology 2007;Sep; 244(3):815-22.

Goris ML, Zhu HJ, M.D. Robinson TE. A critical discussion of Computer Analysis in Medical Imaging. Proceedings of the Thoracic Society 2007;4:347-349.

Graves E, Zhou H, Chatterjee R, Keall P, Gambhir SS, Contag C. Design and evaluation of a variable aperture collimator for conformal radiotherapy of small animals using a microCT scanner. Medical Physics 2007 Nov;34(11):4359–67.

Gutgemann I, Stevens K, Loftus D, Schmidt-Wolf IGH, George TI. VEGF and osteosclerosis in POEMS syndrome. Annals of Hematology 2008;87:87.

Ha BY, Ahmed A, Sze DY, Razavi MK, Simpson N, Keeffe EB, Nguyen MH. Long-term survival of Patients with unresectable hepatocellular carcinoma treated with transcatheter arterial chemoinfusion. Aliment Pharmacol Ther. 2007;Sep15;26(6):839-846.

Hara W, Loo BW Jr, Goffinet DR, Chang SD, Adler JR, Pinto HA, Fee WE, Kaplan MJ, Fischbein NJ, Le QT. Excellent local control with stereotactic radiotherapy boost after external beam radiotherapy in patients with nasopharyngeal carcinoma. Int J Radiat Oncol Biol Phys. 2008;71:393-400.

Hartung D, Petrov A, Haider N, Fujimoto S, Blankenberg FG, Fujimoto A, Virmani R, Kolodgie FD, Strauss HW, Narula J. Radiolabeled Monocyte Chemotactic Protein 1 for the detection of inflammation in experimental atherosclerosis. J Nucl Med. 2007 Nov;48(11):1816-1821.

Heilmaier C, Sutter R, Lutz AM, Seifert B, Weishaupt D, Marincek B, Willmann JK. Mapping of the hepatic vascular anatomy by dynamic contrast-enhanced parallel magnetic resonance imaging: comparison with 64-detector row computed tomography. Radiology 2007;Dec;245:872-880.

Heilmaier C, Sutter R, Lutz AM, Seifert B, Willmann JK. Dynamic MRI of the liver with parallel MR acquisition technique: characterization of focal liver lesions and mapping of the hepatic vasculature in a single MRI session. Rofo 2008;180:440-448.

Hoffman J, Gambhir SS, Kelloff G. Regulatory and reimbursement challenges for molecular imaging. Radiology 2007 Dec;245(3):645-60.

Holzbaur K, Delp S, Gold G, Murray W. Moment-generating capacity of upper limb muscles in healthy adults. J Biomech. 2007;40(11):2442-9.

Hope MD, Meadows AK, Hope TA, Ordovas KG, Reddy GP, Alley MT, Higgins CB. Evaluation of bicuspid aortic valve and aortic coarctation with 4D flow magnetic resonance imaging. Circulation. 2008;117:2818-2819.

Hope TA, Markl M, Wigstrom L, Alley MT, Miller DC, Herfkens RJ. Comparison of flow patterns in ascending aortic aneurysms and volunteers using four-dimensional magnetic resonance velocity mapping. J. Magn. Reson. Imaging. 2007;Dec;26(6):1471-1479.

Hoxworth JM, Glastonbury CM, Fischbein NJ, Dillon WP. Focal opacification of the olfactory recess on sinus CT: just an incidental finding? American Journal of Neuroradiology 2008;29:895-7.

Hsu AR, Chen X. Advances in anatomical, functional and molecular imaging of angiogenesis. J Nucl Med. 2008;49(4):511-514.

Hu W, Wilson RJ, Koh A, Fu A, Faranesh AZ, Earhart CM, Osterfeld SJ, Han S-J, Xu L, Guccione S, Sinclair R, Wang SX. High-moment antiferromagnetic nanoparticles with tunable magnetic properties. Advanced Materials 2008;20(8);1479-1483.

Hundt W, Yuh EL, Steinbach S, Bednarski MD, Guccione S. Comparison of continuous vs. pulsed focused ultrasound in treated muscle tissue as evaluated by magnetic resonance imaging, histological analysis, and microarray analysis. Eur Radiol. 2008;18:993-1004.

Hundt W, Yuh EL, Bednarski MD, Guccione S. Gene expression profiles, histologic analysis, and imaging of squamous cell carcinoma model treated with focused ultrasound beams. Am J Roentgenol. 2007 Sep;189(3);726-36.

Hundt W, Steinbach S, O'Connell-Rodwell CE, Mayer D, Bednarski MD, Guccione S. Tumor tissue characterization evaluating the Luciferase Activity under the control of a hsp70 promoter and MR imaging in Three Tumor Cell Lines. Eur J Radiol. 2008 Mar 6. [Epub ahead of print]

Hwang GL, Patel TH, Hofmann LV. Role of image-guided vascular intervention in therapeutic angiogenesis translational research. Expert Rev Cardiovasc Ther. 2007 Sep;5(5):903-15.

Iagaru A, Chen X, Gambhir SS. Molecular Imaging Can Accelerate Anti-Angiogenic Drug Development. Nat Clin Pract Oncol. 2007;Oct;4(10):556-7.

Iagaru A, Kalinyak J, McDougall IR. 18F FDG PET/CT in the Management of Thyroid Cancer. Clin Nucl Med. 2007;Sep;32(9):690-5

Iagaru A, Mari C, Gambhir SS. Follicular dendritic sarcoma within a focus of Castleman's disease. Serial FDG PET/CT in the follow up of recurrence with histopatholigic confirmation. Revista Espanola Medicina Nuclear Journal 2007;26(1):40-45.

Iagaru A, Masamed R, Chawla S, Menendez L, Fedenko A, Conti PS. 18F FDG PET and PET/CT Evaluation of Response to Neoadjuvant Chemotherapy in Musculoskeletal and Soft-Tissue Sarcomas. Clin Clin Nucl Med. 2008;Jan;33(1):8-13.

Iagaru A, Peterson D, Quon A, Dutta S, Twist C, Daghighian F, Gambhir SS, Albanese C. Case study: 123I MIBG Mapping with Intraoperative Gamma Probe for Recurrent Neuroblastoma. Mol Imaging Biol. 2008 Jan-Feb;10(1):19-23.

Illes J, Atlas SW. Risks and benefits of the new medical imaging enterprise. Virtual Mentor AMA. 2007;9:99-103.

Jayaraman MV, Marcellus ML, Hamilton S, Do HM, Campbell D, Chang SD, Steinberg GK, Marks MP. Neurologic complications of arteriovenous malformation embolization using liquid embolic agents. American Journal of Neuroradiology 2008;29:242-246.

Kakuda W, Lansberg MG, Thijs VN, Kemp SM, Bammer R, Wechsler LR, Moseley ME, Marks MP, Albers GW DEFUSE Investigators. Optimal definition for PWI/DWI mismatch in acute ischemic stroke patients. J Cereb Blood Flow Metab. 2008 May;28(5):887-91.

Kamaya A. Book Review: Clinical Magnetic Resonance Imaging Third Edition. Abdominal Imaging 2007;Oct;33(1):126.

Kaneoya K, Ueda T, Suito H, Nanazawa Y, Tamaru J, Isobe K, Naya Y, Tobe T, Motoori K, Yamamoto S, Rubin GD, Minami M, Ito H Functional computed tomography imaging of tumor-induced angiogenesis: preliminary results of new tracer kinetic modeling using a computer discretization approach. Radiat Med. 2008 May;26(4):213-21.

Kashefi A, Zhao H, Chen X. Molecular Imaging as the Main Part of Our Decision-Making and Treatment Strategies in Stroke. Front Biosci. 2008;13:1535-1556.

Kelly ME, Guzman R, Sinclair J, Bell-Stephens TE, Bower R, Hamilton S, Marks MP, Do HM, Chang SD, Adler JR, Levy RP, Steinberg GK. Multimodality treatment of posterior fossa arteriovenous malformations. J Neurosurg. 2008;Jun;108(6):1152-61.

Keren S, Gheysens O, Levin C, Gambhir SS. A comparison between a time domain and continuous wave small animal optical imaging system. IEEE Trans Med Imaging 2008;27:1:58-63.

Keren S, Zaveleta C, Cheng Z, de La Zerda A., Gheysens O, Gambhir SS. Noninvasive molecular imaging of small living subjects using Raman spectroscopy. Proceedings of the National Academy of Science (USA) 2008;Apr;105(15):5844-9.

Khan S, Kurland G, Newman B. Controlled - Ventilation Volumetric CT Scan in the Evaluation of Acquired Pulmonary Lobar Emphysema. Pediatric Pulmonology 2007 Dec;42:1222-1228

Kim DH, Henry R, Spielman DM. Fast multivoxel two-dimensional spectroscopic imaging at 3 T. Magn Reson Imaging. 2007;25(8):1155-61.

Kim YS, Yang C-, Wang J, Wang L, Li Z-B, Chen X, Liu S. Effects of Targeting Moiety, Linker, Bifunctional Chelator and Molecular Charge on Biological Properties of ^{64}Cu-Labeled Triphenylphosphonium Cations. J Med Chem. 2008;May 22;51(10):2971-84.

Kinsey A, Diederich C, Rieke V, Nau W, Butts Pauly K, Bouley D, Sommer G. Transurethral ultrasound applicators with dynamic multi-sector control for prostate thermal therapy: In vivo evaluation under MR guidance. Med Phys 2008;May;35(5).

Konukoglu E, Acar B, Paik D, Beaulieu C, Rosenberg J, Napel S. Polyp enhancing level-set evolution of colon wall: method and pilot study. IEEE Trans Med Imaging 2007;26(12):1649-56.

Korosoglou G, Gilson WD, Schär M, Ustun A, Hofmann LV, Kraitchman DL, Stuber, M. Hind limb ischemia in rabbit model: T2-prepared versus time-of-flight MR angiography at 3 T. Radiology 2007 Dec;245(3):761-9. Epub 2007 Oct 19.

Kuo WT, Kee ST. Wire loop methods for retrieval of trapped inferior vena cava filters: 10-f versus 16-f sheath technique. J Vasc Interv Radiol. 2008;19;6:956-7.

Kuo WT, Loh CT, Sze DY. Emergency retrieval of a G2 filter after complete migration into the right ventricle. J Vasc Interv Radiol. 2007;Sep;18(9):1177-1182.

Kuo WT, Sze DY, Hofmann LV, Goldhaber SZ. Catheter-directed intervention for acute pulmonary: a shining saber. Chest 2008;Jan;133(1):317-318.

Kuo WT, van den Bosch MA, Sze DY, Gould MK, Kothary N, Hofmann LV. Catheter-directed therapy for massive pulmonary embolism: Systematic review and meta-analysis of the modern technique. J Vasc Interv Radiol. 2008;19:S6. ABSTRACT

Lau F, Olcott P, Horowitz M, Levin CS. Noise Analysis of PSAPD PET Detector Front-End Multiplexing Circuits. Conference Record of the 2007 IEEE Nuclear Science Symposium and Medical Imaging Conference; 3212-3219.

Lansberg MG, Thijs VN, Bammer R, Olivot JM, Marks MP, Wechsler LR, Kemp S, Albers GW. The MRA-DWI Mismatch Identifies Patients With Stroke Who Are Likely to Benefit From Reperfusion. Stroke. 2008 Jul 17. [Epub ahead of print]

Le QT, Koong A, Lieskovsky YY, Narasimhan B, Graves E, Pinto H, Brown JM, Spielman D. In vivo1h magnetic resonance spectroscopy of lactate in patients with stage IV head and neck squamous cell carcinoma. Int J Radiat Oncol Biol Phys. 2008;71(4):1151-7.

Lee HY, Lee S-H, Xu C, Xie J, Lee J-H, Wu B, Koh AL, Wang X, Sinclair R, Wang SX, Nishimura DG, Biswal S, Sun S, Cho SH, Chen X. Synthesis and characterization of PVP-coated large core iron oxide nanoparticles as MRI contrast agent. Nanotechnology 2008;19:Epub ahead of print.

Lee HY, Li ZB, Chen K, Hsu AR, Xu C, Xie J, Sun S, Chen X. PET/MRI Dual Modality Tumor Imaging Using Conjugated Radiolabeled Iron Oxide Nanoparticles. J Nucl Med. 2008;49:1371-1379.

Lee P, Weerasuriya DK, Lavori PW, Quon A, Hara W, Maxim PG, Le QT, Wakelee HA. Donington JS, Graves EE, Loo BW Jr. Metabolic tumor burden predicts for disease progression and death in lung cancer. Int J Radiat Oncol Biol Phys. 2007 Oct 1;69(2):328-33.

Lee SW, Greve JM, Leaffer D, Lollini L, Bailey P, Gold GE Biswal S. Early findings of small animal MRI and small animal computed tomography correlate with histological changes of a rat model of rheumatoid arthritis. NMR in Biomed 2007;21(5):527-36.

Levashova Z, Backer M, Backer JM, Blankenberg FG. Direct site-specific labeling of the Cys-tag moiety in sc VEGF with technetium 99m. Bioconjug Chem. 2008;19(5):1049-1054.

Levi J, De A, Cheng Z, Gambhir SS. Bisdeoxycoelenterazine derivatives for improvement of bioluminescence resonance energy transfer assays. Journal of American Chemical Society 2007;129:11900-1.

Levin CS. New Imaging Technologies to Enhance the Molecular Sensitivity of Positron Emission Tomography. Proceedings of the IEEE 2008;96;Mar(3):439-67.

Levin YS, Mayer D, Yen YF, Hurd RE, Spielman DM. Optimization of fast spiral chemical shift imaging using least squares reconstruction: application for hyperpolarized (13)C metabolic imaging. Magn Reson Med. 2007;58:245-52.

Lew C, Pineda AR, Clayton D, Spielman D, Chan FP, Bammer R. SENSE phase-constrained magnitude reconstruction with iterative phase refinement. Magn Reson Med. 2007 Nov;58(5):910-21.

Li Z, Wu J, Sheikh A, Kraft D, Cao F, Xie X, Patel M, Gambhir SS, Robbins R, Cooke J. Differentiation, survival, and function of embryonic stem cell derived endothelial cells for ischemic heart disease. 2007 Sep 11;116(11 Suppl):I46-54.

Li Z, Wu JC, Sheikh AY, Kraft D, Cao F, Xie X, Patel M, Gambhir SS, Robbins RC, Cooke JP, Wu JC. Differentiation, survival, and function of embryonic stem cell-derived endothelial cells. Circulation 2007;116:I46-I54.

Li Z, Yoriyasu S, Huang M, Cao F, Xie X, Connolly AJ, Yang P, Wu JC. Comparison of reporter gene and iron particle labeling for tracking fate of human embryonic stem cells and differentiated endothelial cells in living subjects. Stem Cells 2008;26(4):864-73.

Li ZB, Chen K, Chen X. ^{68}Ga-labeled Multimeric RGD Peptides for microPET Imaging of αvβ3 Integrin Expression. Eur J Nucl Med Mol Imaging. 2008;35:1100-1108.

Li ZB, Niu G, Wang H, He L, Ploug M, Chen X. MicroPET Imaging of Urokinase-type Plasminogen Activator Receptor Expression Using a ^{64}Cu-Labeled Linear Peptide Antagonist. Clin Cancer Res. 2008;14:4758-4766.

Li ZB, Wu Z, Cao Q, Tseng J, Gambhir SS, Chen X. The Synthesis of 2-Deoxy-2-[^{18}F]fluoro-sorbitol (^{18}F-FDS) and Its Potential Application in Molecular Imaging. Mol Imaging Biol. 2008;10:92-98.

Li ZB, Wu Z, Chen K, Ryu E-K, Chen X. ^{18}F-Labeled BBN-RGD Heterodimer for Prostate Cancer Imaging. J Nucl Med. 2008;49(3):453-461.

Lin BW, Schraga ED, Stevens KJ. Pediatrics, Limp. eMedicine 2008;June (electronic publication).

Lin S, Xie X, Patel MR, Yang YH, Li Z, Cao F, Gheysens O, Zhang Y, Gambhir SS, Rao JH, Wu JC. Quantum dot imaging for embryonic stem cells. BMC Biotechnology 2007;Sep;7:1-10.

Liu C, Bammer R, Moseley ME. Parallel imaging reconstruction for arbitrary trajectories using k-space sparse matrices (kSPA). Magn Reson Med. 2007 Dec; 58(6):1171-81

Liu YI, Shin LK, Kamaya A, Jeffrey RB. An unusual imaging and clinical presentation of papillary thyroid carcinoma. J Ultrasound Med. 2008 Aug;27(8):1241-4.

Liu Z, Davis C, Cai W, He L, Chen X, Dai H. Circulation and Long-Term Fate of Functionalized, Biocompatible Single-Walled Carbon Nanotubes in Mice Probed by Raman Spectroscopy. Proc Natl Acad Sci U S A. 2008 Feb 5;105(5):1410-5.

Lu W, Hargreaves BA. Multi-resolution field map estimation using golden section search for water-fat separation. Magn Reson Med. 2008;60;Jun;(1):236-244.

Lu W, Yu H, Alley MT, Shimakawa A, Reeder SB, Hargreaves BA. Water-fat separation with bipolar multi-echo sequences. Magn Reson Med 2008;60;Jun(1):198-209.

Luo J, Ho P, Buckwalter M, Hsu T, Lee L, Zhang H, Kim D, Kim S, Gambhir SS, Steinman L, Wyss-Coray T. Glia-dependent TGF-beta signaling, acting independently on the TH17 p-pathway, is critical for initiation of murine autoimmune encephalomyelitis. Journal of Clinical Investigation 2007 Nov;117(11):3306–15.

Lutz A, Ray P, Willmann J, Drescher C, Gambhir SS. 2-Deoxy-2-[F-18] Fluoro-D: glucose accumulation in ovarian carcinoma cell lines. Mol Imaging Biol 2007 Oct;9(5):260–66.

Lutz AM, Ray P, Willmann JK, Gambhir SS. 2-Deoxy-2-[F-18]fluoro-D-glucose-accumulation in ovarian carcinoma cell lines. Mol Imaging Biol 2007;Sep-Oct;9:260-266.

MacKenzie JD, Gonzales L, Hernandez A, Ruppert K, Jaramillo D.	Diffusion weighted and diffusion tensor imaging for pediatric musculoskeletal disorders. Pediatric Radiology 2007;Aug;37(8):781-8.
MacKenzie JD, Hernandez A, Gonzalez L, Pena A, Ruppert K, Khrichenko D, Jawad AF, Wells L, Smith-Whitley K, Jaramillo D.	Diffusion-Weighted Imaging in Early Avascular Necrosis - Quantification of the Apparent Diffusion Coefficient in the Hips of Sickle Cell Patients with Early Avascular Necrosis. Radiological Society of North America; Nov 25-30, 2007; Chicago, IL.
MacKenzie JD, Hernandez A, Gonzalez L, Pena A, Ruppert K, Khrichenko D, Jawad AF, Wells L, Smith-Whitley K, Jaramillo D.	Magnetic Resonance Imaging in Early Avascular Necrosis - Quantification of the Apparent Diffusion Coefficient in the Hips of Sickle Cell Patients. Sickle Cell Disease Association of America and National Institutes of Health 35th Annual Convention; Sep 17-22, 2007; Washington DC.
MacKenzie JD, Nazario-Larrieu J, Cai T, Ledbetter MS, Duran-Mendicuti MA, Judy PF, Rybicki FJ.	Reduced-dose CT: effect on reader evaluation in detection of pulomonary embolism. AJR Am J Roentgenol. 2007 Dec;189(6):1371-1379.
MacKenzie JD, Nazario-Larrieu J, Cai T, Ledbetter SM, Duran-Mendicuti MA, Vargas TM, Judy PF, Rybicki FJ.	Lower Dose Computed Tomography for the Detection of Acute Pulmonary Embolism. American Journal of Roentgenology 2007;Dec;189(6):1371-9.
Margolis D, Hoffman J, Herfkens R, Jeffrey R, Quon A, Gambhir SS.	Molecular imaging techniques in body imaging. Radiology 2007 Nov;245(2):333–56.
Massoud T, Singh A, Gambhir SS.	Noninvasive Molecular Neuroimaging using Reporter Genes Part I, Principles Revisited. Am Journal of Neuroradiol 2008;29(2):229-34.
Massoud T, Singh A, Gambhir SS.	Noninvasive molecular neuroimaging using reporter genes: Part II, experimental, current, and future applications. Am J Neuroradiol. 2008;Mar;29(3):409-18.
Mayer D, Kim DH, Spielman DM, Bammer R.	Fast parallel spiral chemical shift imaging at 3T using iterative SENSE reconstruction. Magn Reson Med. 2008 Apr;59(4):891-7.
McAdams TR, Biswal S, Stevens KJ, Beaulieu CF, Mandelbaum BR.	Tibial aperture bone disruption after retrograde versus antegrade tibial tunnel drilling: a cadaveric study. Knee Surg Sports Traumatol Arthrosc 2008; published electronically 6/3/2008.
McMullan DM, Reddy VM, Gottliebson WM, Silverman NH, Perry SB, Chan FP, Hanley FL, Riemer RK.	Morphological studies of pulmonary arteriovenous shunting in a lamb model of superior cavopulmonary anastomosis. Pediatr Cardiol. 2008 Jul;29(4):706-12.
Miller JC, Thrall JH, Golding S, Frija G, Glazer GM, Ringertz HG, Krestin GP.	Reinventing radiology in a digital and molecular age: summary of proceedings of the Sixth Biannual Symposium of the International Society for Strategic Studies in Radiology (IS3R) August 25-27, 2005. Radiology. 2007 Sep;244(3):633-8.
Minn AY, Fisher PG, Barnes PD, Dahl GV.	A syndrome of irreversible leukoencephalopathy following pediatric allogeneic bone marrow transplantation. Pediatr Blood Cancer. 2007;48(2):213-217.
Müller MA, Mayer D, Seifert B, Marincek B, Willmann JK.	Effect of direct contrast-enhanced 3D MR venography findings on diagnosis and therapeutic decisions in patients with recurrent lower limb varicose veins. Radiology 2008; 247:887-895.
Namavari M, De Jesus O, Cheng Z, De A, Kovacs E, Levi J, Zhang R, Joshua K, Hoerner J, Grade H, Syud F, Gambhir SS.	Direct site-specific radiolabeling of an affibody protein with 4-[18F] fluorobenzaldehyde via oxime chemistry. Mol Imaging Biol. 2008;Jul-Aug;10(4):177-81.
Namavari M, Padilla De Jesus O, Cheng Z, De A, Kovacs E, Levi J, Wang S, Zhang R, Hoerner J, Grade H, Syud FA, Gambhir SS.	Direct site-specific Radiolabeling of an Affibody Protein with [^{18}F]Fluorobenzaldehyde via Oxime Chemistry. Molecular Imaging & Biology 2008;10:177-81.
Nguyen JT, Peterson JS, Biswal S, Beaulieu CF, Fredericson M.	Stress-related injuries around the lesser trochanter in long-distance runners. Am J Roentgenol 2008;190:1616-1620.
Niederkohr RD, Hwang BJ, Quon A.	FDG PET/CT detection of a gossypiboma in the neck. Clin Nucl Med. 2007 Nov;32(11):893-5.
Niederkohr RD, Rosenberg J, Shabo G, Quon A.	Clinical value of including the head and lower extremities in 18F-FDG PET/CT imaging for patients with malignant melanoma. Nucl Med Commun. 2007 Sep;28(9):688-95.
Niu G, Cai W, Chen K, Chen X.	Non-invasive PET imaging of EGFR degradation induced by heat shock protein 90 inhibitor. Mol Imaging Biol. 2008;10:99-106.
Niu G, Cai W, Chen X.	Quantification of HER2 Expression by Molecular Imaging. Front Biosci. 2008;13:790-805
Norton JA, Ham CM, Van Dam J, Jeffrey RB Jr, Longacre TA, Huntsman DG, Chun N, Kurian AW, Ford JM	CDHI truncating mutations in the E-cadherin gene: an indication for total gastrectomy to treat hereditary diffuse gastric cancer. Ann Surg 2007;245(6):873-9.
Oakes D, Frisoli JK, Mitchell RS, Sze DY, Harris J, van der Starre PJA.	Intraoperative monitoring of elephant trunk kinking with transesophageal echocardiography. J Cardiothorac Vasc Anesth. 2007 Aug;21(4):584-6.
Olcott P, Lau F, Cajipe V, Clajus M, Tumer T, Volkovskii A, Levin CS.	Data Acquisition System Design for a 1 mm^3 Resolution PSAPD-Based PET System. Conference Record of the 2007 IEEE Nuclear Science Symposium and Medical Imaging Conference; 3206-3211.
Olcott PD, Habte F, Levin CS, Foudray AMK.	Performance Characterization of a Miniature, High Sensitivity Gamma-Ray Camera. IEEE (Institute of Electrical & Electronics Engineers) Transactions on Nuclear Science 2007; 54(5):1492-1497.

Olivot JM, Mlynash M, Thijs VN, Kemp S, Lansberg MG, Wechsler L, Schlaug G, Bammer R, Marks MP, Albers GW.	Relationships Between Infarct Growth, Clinical Outcome, and Early Recanalization in Diffusion and Perfusion Imaging for Understanding Stroke Evolution (DEFUSE). Stroke. 2008 Jun 19. [Epub ahead of print]
Park BH, Hwang T, Liu TC, Sze DY, Kim JS, Kwon HC, Oh SY, Han SY, Yoon JH, Hong SH, Moon A, Speth K, Park C, Ahn YJ, Daneshmand M, Rhee BG, Pinedo HM, Bell JC, Kirn DH.	Use of a targeted oncolytic poxvirus, JX-594, in patients with refractory primary or metastatic liver cancer: a phase I trial. Lancet Oncol 2008;Epub May 19.
Paulmurugan R, Tamrazi, A, Katzenellengogen J, Katzenellenbogen B, Gambhir SS.	A human estrogen receptor (ER){alpha} mutation with differential desponsiveness to nonsteroidal ligands: novel approaches for studying mechanism of ER action. Mol Endocrinol 2008. Jul;22(7):1552-64.
Peng H, Olcott P, Foudray AMK, Levin CS.	Evaluation of Free-Running ADCs for High Resolution PET Data Acquisition. Conference Record of the 2007 IEEE Nuclear Science Symposium and Medical Imaging Conference; 3328-3331.
Peng H, Olcott P, Pratx G, Foudray AMK, Chinn G, Levin CS.	Design Study of a High Resolution Breast-Dedicated PET System Built from Cadmium Zinc Telluride Detectors. Conference Record of the 2007 IEEE Nuclear Science Symposium and Medical Imaging Conference; 3700-3704.
Peng PD, Spain DA, Tataria M, Hellinger JC, Rubin GD, Brundage SI.	CT angiography effectively evaluates extremity vascular trauma. Am Surg. 2008 Feb;74(2):103-7.
Pitman MB, Abele J, Ali SZ, Duick D, Elsheikh TM, Jeffrey RB, Powers CN, Randolph G, Rensgaw A, Scoutt L.	Techniques for thyroid FNA: a synopsis of the National Cancer Institute Thyroid Fine-Needle Aspiration State of the Science Conference. Diagn Cytopathol. 2008 Jun;36(6):407-24.
Poon M, Rubin GD, Achenbach S, Attebery TW, Berman DS, Brady TJ, Jacobs JE, Hecht HS, Lima JA, Weigold WG.	Consensus update on the appropriate usage of cardiac computed tomographic angiography. J Invasive Cardiol. 2007 Nov;19(11):484-90.
Pratx G, Levin CS.	Accurately Positioning Events in a High-Resolution PET System that uses 3D CZT Detectors. Conference Record of the 2007 IEEE Nuclear Science Symposium and Medical Imaging Conference; 2660-2664.
Pratx G, Levin CS.	Maximum a Posteriori Event Positioning in High-Resolution PET CZT Detectors. J. Nucl. Med. Meeting Abstracts 2008;May;49:61.
Pratx G, Reader AJ, Levin CS.	Fast Maximum Likelihood Image Reconstruction via PCG without a Line Search. J. Nucl. Med. Meeting Abstracts 2008;May;49:61.
Pu J, Roos J, Yi CA, Napel S, Rubin GD, Paik DS.	Adaptive border marching algorithm: Automatic lung segmentation on chest CT images. Computerized Medical Imaging and Graphics 2008; 32:452-62.
Quon A, Chang ST, Chin F, Kamaya A, Dick DW, Loo BW Jr, Gambir SS, Koong AC.	Initial Evaluation of (18)F-florothymidine (FLT) PET/CT scanning for primary pancreatic cancer. European Journal of Nuclear Medicine and Molecular Imaging. 2008 Mar;35(3):527-31.
Rackow-Penner R, Gold G, Daniel B, Stevens K, Rosenberg J, Mazin S, Pauly J, Glover G.	Reduction of Truncation Artifacts in Rapid 3D Articular Cartilage Imaging. J Magn Reson Imaging 2008;27: 860-865.
Rackow-Penner R, Gold G, Daniel B, Stevens K, Rosenberg J, Mazin S, Pauly J, Glover G.	Reduction of Truncation Artifacts in Rapid 3D Articular Cartilage Imaging. J Magn Reson Imaging 2008;Apr;27(4):860-5.
Rakshe T, Fleischmann D, Rosenberg J, Roos JE, Straka M, Napel S.	An improved algorithm for femoropopliteal artery centerline restoration using prior knowledge of shapes and image space data. Medical Physics 2008;Jul;35(7):3372-82.
Raman R, Raman B, Napel S, Rubin GD.	Improved Speed of Bone Removal in CT Angiography (CTA) Using Automated Targeted Morphological Separation: Method and Evaluation in CTA of Lower Extremity Occlusive Disease. J Comput Assist Tomogr. 2008;32(3):485-91.
Raman R, Raman B, Napel S, Rubin GD.	Semi-automated Quantification of the Mass and Distribution of Vascular Calcification using Multidetector CT: Method and Evaluation. Radiology 2008;247(1):241-50.
Reid TR, De Haan H, Karrasch M, Sze D.	Tumor response after repeated intrahepatic infusion of oncolytic herpes simplex virus NV1020 prior to second-line chemotherapy. Proc Amer Soc Clin Oncol. 2007;25:A459.
Reid TR, De Haan H, Karrasch M, Sze D.	Tumor response after repeated intrahepatic infusion of oncolytic herpes simplex virus NV1020 prior to second-line chemotherapy. Proc Amer Soc Clin Oncol. 2007;25:A459.
Rieke V, Butts Pauly K.	Echo Combination to Reduce PRF Thermometry Errors From Fat. J Magn Reson Imaging. 2008;Mar;27(3):376-90.
Rieke V, Butts Pauly K.	MR Thermometry; Invited Review paper for the special issue, “Interventional MRI Update.” JMRI 2008;Feb;27(2):376-90.
Rieke V, Diederich CJ, Nau WH, Ross AB, Kinsey A, Sommer G, Butts Pauly K.	Referenceless MR Thermometry for Monitoring Thermal Ablation in the Prostate, IEEE Transactions on Medical Imaging 2007;26(6):813-821.

Robinson TE, Trapnell BC, Goris ML. Quantitative chest CT imaging during treatment of idiopathic pulmonary proteinosis utilizing aerosolized GM-CSF therapy. American Journal of Respiratory and Critical Care Medicine 2007;175:A141.

Rodriguez-Porcel M, Brinton TJ, Chen I, Gheysens O, Lyons J, Ikeno F, Willmann JK, Wu L, Wu JC, Young AC, Yock P, Gambhir SS. Percutaneous delivery and non-invasive imaging of gene therapy in a porcine model. J Am Coll Cardiol 2008;51:595-597.

Rodriguez-Porcel M, Brinton TJ, Chen IY, Gheysens O, Lyons J, Ikeno F, Willmann JK, Wu L, Wu JC, Yeung AC, Yock P, Gambhir SS. Reporter gene imaging following percutaneous delivery in swine: moving toward clinical applications. Journal of American College of Cardiology 2008;51(5):595-7.

Rodriguez-Porcel M, Cai W, Gheysens O, Willmann JK, Chen K, He L, Chen IY, Wu JC, Zibo L, Mohamedali KA, Rosenblum MG, Chen S, Gambhir SS. Imaging of VEGF receptor in a rat myocardial infarction model using positron emission tomography. J Nucl Med. 2008;Apr;49(4):667-673.

Rodriguez-Porcel M, Cai W, Gheysens O, Willmann JK, Chen K, He L, Chen IY, Wu JC, Wang H, Mohamedali KA, Rosenblum MG, Li ZB, Kim S, Chen X, Gambhir SS Imaging of VEGF receptor in a rat myocardial infarction model using PET. J Nucl Med 2008;49(4);667-73.

Rogers WM, Dobo E, Norton JA, Van Dam J, Jeffrey RB, Huntsman DG, Kingham K, Chun N, Ford JM, Longacre TA. Risk-reducing total gastrectomy for germline mutations in E-cadherin (CDH1): pathologic findings with clinical implications. Am J Surg Pathol. 2008 Jun;32(6):799-809.

Rose J, Mirmiran M, Butler EE, Lin Cy, Barnes PD, Kermoian R, Stevenson DK. Neonatal microstructural development of the internal capsule on diffusion tensor imaging correlates with severity of gait and motor deficits. Dev Med Child Neurol. 2007;49:745-750.

Rubin DL, Desser TS. A Data Warehouse for Integrating Radiologic and Pathologic Data. JACR 2008 March;5(3):210-217.

Ryu E-K, Chen X. Molecular imaging for Alzheimer's disease. Front Biosci. 2008;13:777-789.

Ryu EK, Wu Z, Chen K, Lazarus LH, Markzak E, Sasaki Y, Ambo A, Salvadori S, Ren C, Zhao H, Balboni G, Chen X. Synthesis and Evaluation of a Potent and Selective ^{18}F-Labeled δ-Opioid Receptor Antagonist. J Med Chem. 2008 Mar;27;51(6):1817-23.

Salles A, Nino-Murcia M, Jeffrey RB. CT of pancreas: minimum intensity projections. Abdom Imaging 2008;33(2):207-13.

Sato M, Figueiredo M, Burton J, Johnson M, Chen M, Powell R, Gambhir SS, Carey M, Wu L. Configurations of a two-tiered amplified gene expression system in adenoviral vectors designed to improve the specificity of *in vivo* prostate cancer imaging. Gene Therapy 2008;19:1-11.

Schellenberg D, Goodman KA, Lee F, Chang S, Kuo T, Ford JM, Fisher GA, Quon A, Desser TS, Norton J, Greco R, Yang GP, Koong AC. Gemcitabine Chemotherapy and Single-Fraction Stereotactic Body Radiotherapy for Locally Advanced Pancreatic Cancer. Int J Radiat Oncol Biol Phys. 2008;Apr 3. [Epub ahead of print]

Schernthaner R, Fleischmann D, Lomoschitz F, Stadler A, Lammer J, Loewe C. Effect of MDCT angiographic findings on the management of intermittent claudication. Am J Roentgenol. 2007;Nov;189(5):1215-22.

Schipper M, Nakayama-Ratchford N, Davis C, Kam N, Chu P, Liu Z, Sun X, Dai J, Gambhir SS. Preliminary toxicology studies of single walled carbon nanotubes in mice. Nature Nanotechnology 2008 Mar;3:216-21.

Schipper ML, Cheng Z, Lee SW, Bentolila LA, Iyer G, Rao J, Chen X., Wu AM, Weiss SS, Gambhir SS. microPET-based biodistribution of quantum dots in living mice. Journal of Nuclear Medicine 2007;48:1511-1518.

Schipper ML,Goris ML, Gambhir SS. Evaluation of Herpes Simplex Virus 1 Thymidine Kinase-Mediated Trapping of (131)I FIAU and Prodrug Activation of Ganciclovir as a Synergistic Cancer Radio/Chemotherapy. Molecular Imaging and Biology 2007;9:110-116.

Shi J, Jia B, Liu Z, Yang Z, Yu Z, Chen K, Chen X, Liu S, Wang F. ^{99}mTc-Labeled Bombesin(7-14)NH2 with Favorable Properties for SPECT Imaging of Colon Cancer. Bioconj Chem. 2008;19(6):1170-8.

Shi R, Napel S, Rosenberg JK, Shin LK, Freeman CB, Mogensen MA, Joshi AJ, Pankhudi P, Beaulieu CF. Transparent rendering of intraluminal contrast for 3D polyp visualization at CT colonography. J Comput Assist Tomogr 2007;31:773-9.

Singh A, Massoud T, Deroose C, Gambhir SS. Molecular imaging of reporter gene expression in prostate cancer: an overview. Seminars in Nuclear Medicine 2008;39(1):9–19.

Smith BR, Cheng Z, De A, Koh AL, Gambhir SS. Real-time intravital imaging of RGD-quantum dot binding to luminal endothelium in mouse tumor neovasculature. Nano Letters 2008 Apr 4; [Epub ahead of print].

Stebbins GT, Nyenhuis DL, Wang C, Cox JL, Freels S, Bangen K, deToledo-Morrell L, Sripathirathan K, Moseley M, Turner DA, Gabrieli JD, Gorelick PB. Gray matter atrophy in patients with ischemic stroke with cognitive impairment. Stroke. 2008 Mar;39(3):785-93.

Stebbins GT, Smith CA, Bartt RE, Kessler HA, Adeyemi OM, Martin E, Cox JL, Bammer R, Moseley ME. HIV-associated alterations in normal-appearing white matter: a voxel-wise diffusion tensor imaging study. J Acquir Immune Defic Syndr. 2007 Dec 15;46(5):564-73.

Stevens KJ, Dragoo JL. Anterior cruciate ligament tears and associated injuries. Topics in Magnetic Resonance Imaging 2007;17(5):247–362.

Stillman AE, Rubin GD, Teague SD, White RD, Woodard PK, Larson PA. Structured reporting: coronary CT angiography: a white paper from the American College of Radiology and the North American Society for Cardiovascular Imaging. J Am Coll Radiol. 2008 Jul;5(7):796-800.

Stuber M, Gilson WD, Schär M, Kedziorek DA, Hofmann LV, Shah S, Vonken EJ, Bulte JW, Kraitchman DL. Positive contrast visualization of iron oxide-labeled stem cells using inversion-recovery with ON-resonant water suppression (IRON). Magn Reson Med. 2007 Nov; 58(5):1072-7.

Sun S, Zhuge F, Rosenberg J, Rubin GD, Napel S. Learning-Enhanced Simulated Annealing: Method, Evaluation, and Application to Lung Nodule Registration. International Journal of Applied Intelligence 2008;28(1):83-99.

Sundara P, Zamorodian A, Beaulieu C, Napel S. Colon polyp detection using smoothed shape operators: preliminary results. Med Image Anal 2007;12;99-119.

Sundaram P, Zamorodian AJ, Beaulieu CF, Napel S. Colon Polyp Detection using Smoothed Shape Operators: Preliminary Results. Medical Image Analysis 2008;12(2):99-199.

Sutter R, Nanz D, Lutz AM, Pfammatter T, Seifert B, Struwe A, Heilmaier C, Weishaupt D, Marincek B, Willmann JK. 3D MR angiography with parallel acquisition for assessment of the aortoiliac and renal arteries: comparison with conventional 3D MR angiography and digital subtraction angiography. Radiology 2007;Oct;245:276-284.

Sze DY, Kao JS, Frisoli JK, McCallum SW, Kennedy WA, Razavi MK. Persistent and recurrent postsurgical varicoceles: venographic anatomy and treatment with N-butyl cyanoacrylate embolization. J Vasc Interv Radiol. 2008 Apr;19(4):539-545.

Tang XN, Wang Q, Koike MA, Cheng D, Goris ML, Blankenberg FG, Yenari MA. Monitoring the protective effects of minocycline treatment with radiolabeled annexin V in an experimental model of focal cerebral ischemia. J Nucl Med. 2007 Nov;48(11):1822-1828.

Tang XN, Wang Q, Koike MA, Cheng D, Goris ML, Blankenberg FG, Yenari MA. Monitoring the Protective Effects of Minocycline Treatment with Radiolabeled Annexin V in an Experimental Model of Focal Cerebral Ischemia. Journal of Nuclear Medicine 2007;48:1822-1828.

Thomas AJ, Stevens K, Goodman SB. Utility of Judet oblique views in the preoperative assessment of acetabular osteolysis. American Journal of Orthopedics 2007; 36(7):107-108.

Tran DN, Fleischmann D, Rakshe T, Roos JE, Rosenberg J, Straka M, Napel S. Femoropopliteal Artery Centerline Interpolation using Contralateral Shape. Medical Physics 2007;34(9):3428-35.

Van de Venne JE, Van Hoenaker FM, Parizel PM, Butts Pauly K, Lang RK. Reduction of metal artifacts in musculoskeletal MR imaging. JBR-BTR 2007;Sept-Oct;90(5):345-9.

Van den Bosch M, Daniel BL, Rieke V, Butts RK, Kermit E, Jeffrey SS. MRI-guided radiofrequency ablation of breast cancer: preliminary clinical experience. J Magn Reson Imaging. 2008;Jan;27(1):204-8.

Van den Bosch MA, Higgins L, Hwang G, Katzenberg R, Willmann JK, Paulmurugan R, Kuo WT, Kothary N, Sze DY, Gambhir SS, Hofmann LV. A novel rat hepatocellular carcinoma model designed for in vivo evaluation of image-guided therapies. J Vasc Interv Radiol. 2008;19:S136. ABSTRACT

Van den Bosch MA, Hofmann LV, Miller DC, Mitchell RS, Dake MD, Sze DY. Factors portending endoleak formation after thoracic aortic stent-graft repair of aortic dissection. J Vasc Interv Radiol. 2008;19:S18. ABSTRACT

Van den Bosch MA, Sze DY, Hofmann LV. Quiz Page: Fibromuscular dysplasia of the Renal artery. Am J Kidney Dis. 2007 May;49(5):43-44

Veervagu A, Hou LC, Hsu AR, Cai W, Greve JM, Hoang S, Chen X, and Tse V. Characterization of Angiogenesis in GL26 Murine-Derived Glioblastoma Multiforme. Neurol Res. 2008 Jul 25. [Epub ahead of print]

Venisnik K, Olafsen T, Gambhir SS, Wu A. Fusion of gaussia luciferase to an engineered anti-carcinoembryonic antigen (CEA) antibody for in vivo optical imaging. Mol Imaging Biol 2007 Oct;9(5):266–77.

Vertinsky AT, Barnes PD. Macrocephaly, increased intracranial pressure, and hydrocephalus in the infant and young child. Top Magn Reson Imaging. 2007;18(1):31-51.

Vidarsson l, Cunningham L, Gold G, Pauly J. T2-selective Magnetization Preparation Pulses. IEEE Transactions in Medical Imaging 2007;Jul;26(7):981-9.

Walker T, Chen T, Bergeron CM, Fischbein NJ, Kaplan MJ, Monfared A. Radiology quiz case 1. Ameloblastoma. Arch Otolaryngol Head Neck Surg. 2008;Mar;134(3):328, 330.

Walls Z, Puttaraju M, Temple G, Gambhir SS. A generalizable strategy for using pre-mRNA levels in living subjects using spliceosome-mediated RNA trans-splicing. J Nucl Med. 2008;Jul;49(7):1146-54.

Wang H, Cai W, Chen K, Li Z-B, He L, Chen X. A new PET tracer specific for vascular endothelial growth factor receptor 2. Eur J Nucl Med Mol Imaging 2007;34(12):2001-2010.

Wang H, Chen K, Cai W, Li Z, He L, Kashefi A, Chen X Integrin Targeted Imaging and Therapy with RGD4C-TNF Fusion Protein. Mol Cancer Ther. 2008;7(5):1044-53.

Wang H, Chen X. Site-specifically modified fusion protein for molecular imaging. Front Biosci. 2008;13:1716-1732.

Willmann JK, Chen K, Wang H, Paulmurugan R, Rollins M, Cai W, Wang D, Chen I, Chen S, Gambhir SS. Monitoring of the Biologic response to murine hind limb ischemia using ^{64}Cu-labeled vascular endothelial growth factor-121 Positron Emission Tomography. Circulation 2008;Feb;117(7):915-22.

Published Papers

Willmann JK, Paulmurugan R, Chen K, Gheysens O, Rodriguez-Porcel M, Lutz AM, Chen I, Chen S, Gambhir SS.	Ultrasonic imaging of tumor angiogenesis with contrast microbubbles targeted to vascular endothelial growth factor receptor 2 in mice. Radiology 2008 Feb;246(2):508-18
Willmann JK, van Bruggen N, Dinkelborg LM, Gambhir SS.	Molecular Imaging in Drug Development. Nature Reviews Drug Discovery 2008;Jul;7:591-607.
Wong H, Desser TS, Jeffrey RB.	Transient Hepatic Attenuation Differences in Computed Tomography from Extrahepatic Portal Vein Compression. Radiology Case Reports 2008;3(1):1-7.
Wong S, Watkins R, Kupnik M, Butts Pauly K, Khuri-Yakub BT.	Feasibility of MR-temperature mapping of ultrasonic heating from a CMUT. IEEE Trans Ultrason Ferroelectr Freq Control 2008;Apr;55(4):811-8.
Wootton-Gorges SL, Buonocore MH, Kuppermann N, Marcin JP, Barnes PD, Neely EK, DiCarlo J, McCarthy T, Glaser NS.	Cerebral proton magnetic resonance spectroscopy in children with diabetic ketoacidosis. Am J Neuroradiol. 2007;28(5):895-899.
Wu JC, Narula J.	Molecular imaging in cardiology. (Editorial) Current Opinions in Biotechnology 2007;18(1):1-3.
Wu JC.	Can radionuclide imaging predict future response to stem cell therapy? (Editorial) J Nuclear Cardiology 2008;15(3):308-10.
Wu Z, Li Z-B, Cai W, Chin FT, Li F, Chen X.	^{18}F-labeled mini-PEG spacered RGD dimer (^{18}F-FPRGD2): synthesis and microPET imaging of $\alpha_v\beta_3$ integrin expression. Eur J Nucl Med Mol Imaging 2007;34(11):1823-1831.
Wu Z, Li Z-B, Cai W, He L, Chin FT, Li F, Chen X.	MicroPET Imaging of Tumor αvβ3 Integrin Expression Using 18F-labeled PEGylated Tetrameric RGD Peptide (18F-FPRGD4). Nucl Med. 2007 Sep;48(9):1536-44.
Xie J, Chen K, Lee HY, Xu C, Hsu AR, Peng S, Chen X, Sun S.	Ultra-Small c(RGDyK)-Fe3O4 Nanoparticles and Their Specific Targeting to Integrin αvβ3-rich Tumor Cells. J Am Chem Soc. 2008;130:7542-3.
Yaghoubi S, Creusot R, Ray P, Fathman CG, Gambhir SS.	Multimodality imaging of T-cell hybridoma trafficking in collagen-induced arthritic mice: image-based estimation of the number of cells accumulating in mouse paws. J Biomed Opt 2007;Nov-Dec;12(6):064025-1–11.
Yang C-T, Wang J, Kim Y-S, Sreerama SG, Cao Q, Li Z-B, He Z, Chen X, Liu S.	64Cu-Labeled Triphenylphosphonium and Triphenylarsonium Cations as Highly Tumor-Selective PET Imaging Agents. J Med Chem. 2007 Oct 18;50(21):5057-69.
Zaharchuk G, Martin AJ, Dillon WP.	Noninvasive imaging of quantitative cerebral blood flow changes during 100% oxygen inhalation using arterial spin-labeling MR imaging. Am J Neurorad 2008;29:663-667.
Zaharchuk G.	Theoretical basis of magnetic resonance imaging techniques to measure cerebral blood volume, cerebral blood flow, and permeability. Am J Neurorad 2007;28:1850-1858.
Zhang SJ, Wu JC.	Comparison of imaging techniques for tracking cardiac stem cell therapy. Journal of Nuclear Medicine 2007;48(12):1916-1919.
Zhao Y, Kuge Y, Zhao S, Morita K, Inubushi M, Strauss HW, Blankenberg FG, Tamaki N.	Comparison of 99mTc-annexin A5 with 18F-FDG for the detection of atherosclerosis in ApoE-/- mice. Eur J Nucl Med Mol Imaging. 2007 Nov;34(11):1747-1755.
Zhu L, Yoon S, Fahrig R.	A short-scan reconstruction for cone-beam CT using shift-invariant FBP and equal weighting. Medical Physics 2007;34(11):4422-38.
Zhuge Z, Sun S, Rubin GD, Napel S.	A Directional Distance Aided Method for Medical Image Segmentation. Medical Physics 2007;34(12):4562-76.
Zilber S, Epstein N, Lee S-W, Larsen M, Ma T, Smith RL, Biswal S, Goodman SB.	Mouse femoral intramedullary injection model: technique and microCT scan validation. Journal of Biomed Mater Res B Appl Biomater 2008;84(1):286-90.

Books and Book Chapters

Books

Atlas SW (ed).	Magnetic Resonance Imaging of the Brain and Spine; 4th edition; Lippincott Williams & Wilkins Publishers, Philadelphia-New York, 2009. (in press).
MacKenzie JD, Karasick D.	Imaging Rheumatoid Arthritis. In: Weissman B, ed. Imaging Arthritis. (in press).
Dalinka M, Mackenzie JD.	Avascular Necrosis (AVN) – with emphasis on imaging and differential diagnosis. In: Weissman B, ed. Imaging Arthritis. (in press).

Book Chapters

Atlas SW, Do H.	Intracranial Vascular Malformations and Aneurysms. In: Magnetic Resonance Imaging of the Brain and Spine; 4th edition; Scott W. Atlas (ed). Philadelphia-New York: Lippincott Williams & Wilkins; 2009.
Atlas SW, Thulborn K.	Intracranial Hemorrhage. In: Magnetic Resonance Imaging of the Brain and Spine; 4th edition; Scott W. Atlas (ed). Philadelphia-New York: Lippincott Williams & Wilkins; 2009.
Barnes P.	Neuroimaging in the Evaluation of Pattern and Timing of Fetal and Neonatal Brain Abnormalities. In: Stevenson D, Benitz W, Sunshine P (eds). Fetal and Neonatal Brain Injury; 4rd edition; Cambridge University Press; 2008. In press.
Beer A, Niu G, Chen X, Schwaiger M.	Tumor Vascular Imaging. In: Molecular Imaging: Principles and Practice; Ralph Weissleder, Sanjiv S Gambhir, Brian D Ross, Alnawaz Rehemtulla, eds. Hamilton, Ontario, Canada. BC Decker, Inc.
Biswal S.	Molecular Imaging of Rheumatoid Arthritis and Osteoarthritis. In: Bruno M (ed) Arthritis in Color. Elsevier, Philadelphia PA. (in-press).
Cai W, Chen X.	Multimodality Agents. In: Molecular Imaging: Principles and Practice; Ralph Weissleder, Sanjiv S Gambhir, Brian D Ross, Alnawaz Rehemtulla, eds. Hamilton, Ontario, Canada. BC Decker, Inc.
Cai W, Gambhir SS, Chen X.	Molecular Imaging of Tumor Vasculature. In: Methods in Enzymology: Angiogenesis; David Cheresh, ed. Philadelphia, PA. Elsevier.
Chan C, Gambhir SS.	In: V. Ntziachristos, ed. (in press).
Dalinka M, MacKenzie JD.	Avascular Necrosis (AVN) - with emphasis on imaging and differential diagnosis. In: Imaging Arthritis, Weissman B, ed (accepted for 2008 publication).
Gambhir SS.	Primer on Multimodality Molecular Imaging. New York, New York. Springer-Verlag (in press).
Gold G.	Introduction to MRI of Arthritis. In: Arthritis in Color (in press).
Gold G.	MRI of Arthritis: Advanced Sequences. In: Arthritis in Color (in press).
Iyer M, Gambhir SS.	Non-invasive imaging strategies to visualize gene expression in living subjects. In: Chung L, Isaacs W, Simons J, eds. Prostate Cancer - Biology, Genetics, and the New Therapeutics. 2nd edition. New York, New York: Humana Press (Springer); 2007.
Iyer M, Gambhir SS.	Non-invasive imaging strategies to visualize tissue-specific gene expression using transcriptional amplification approaches. In: Schuster DP, Blackwell T, eds. Molecular Imaging of the Lungs. New York, New York. Marcel Dekker, Inc. (in press).
Jeffrey B	Topics in Radiology Audio Series (Audio Chapter) – Johns Hopkins University School of Medicine/Oakstone Publishing, October 15, 2007.
Joseph P, Atlas SW.	Artifacts. In: Magnetic Resonance Imaging of the Brain and Spine; 4th edition; Scott W. Atlas (ed). Philadelphia-New York: Lippincott Williams & Wilkins; 2009.
Kuo WT.	Transjugular Intrahepatic Portosystemic Shunt. In: Anesthesiologist's Manual of Survical Procedures. Jaffe RA, Samuels SI (eds). Lippincott Williams & Wilkins (in press).
Larabi M.	Nanoparticle therapy in parasites diseases: Possibility and reality! In: Nanotherapeutics: Drug Delivery Concepts in Nanoscience. Alf Lamprecht, ed. Hackensack, NJ; World Scientific Publishing Company, Inc.; 2008.
Levin CS.	Imaging system physics, technology, and methods for visualization and quantification of reporter gene expression in living subjects. In: Reporter Gene Imaging. Gambhir, Yaghoubi (eds). Cambridge University Press 2008.
Levin CS.	Instrumentation and methods to combine small animal PET with other imaging modalities. In: Molecular Imaging: Principles and Practice. Gambhir, Weissleder, Ross, Rehemtulla (ed). BC Decker Inc. 2008. In press.
Li Z-B, Chen X.	MicroPET, microSPECT, and NIR fluorescence imaging of biomolecules in vivo Microfluids, Nanotechnologies, and Physical Chemistry (Science). In: Separation, Detection, and Analysis of Biomolecules; James W. Lee, ed. New York, New York: Humana Press (Springer); 2007.
Li ZB, Chen X.	Click Chemistry for Molecular Imaging. In: Recent Advances of Bioconjugate Chemistry in Molecular Imaging. Xiaoyuan Chen, ed. Trivandrum, Kerala, India. Research Signpost.
MacKenzie JD, Karasick D.	Imaging Rheumatoid Arthritis. In: Imaging Arthritis, ed Weissman B (accepted for 2008 publication).
Massoud T, Gambhir SS.	Bioluminescence reporter gene imaging in small animal models of cancer. In: Padani A, Choyke P, eds. New Techniques in Oncological Imaging. New York, New York. Taylor and Francis Books (in press).
Massoud T, Paulmurugan R, Gambhir SS	Molecular imaging of intracellular signal transduction in reporter gene imaging. Yaghoubi S, Gambhir SS, eds. Cambridge University Press (in press).

Book Chapters

Newman B, Effmann E.	Lung Masses. In: Slovis T, ed. Caffey's Pediatric Diagnostic Imaging. 11th edition. Philadelphia, Pennsylvania: Elsevier Inc.; 2008.
Newman B.	Imaging the chest. In: Rudolph's Textbook of Pediatrics. 22nd edition. New York, New York; McGraw-Hill (in press).
Niu G, Chen X.	Radiopharmaceuticals and Medical Imaging. In: Development of Therapeutic Agents; Shayne C. Gad, ed. John Wiley & Sons, Hoboken, NJ.
Nusbaum AO, Rapalino O, Fung KM, Atlas SW.	White Matter Disease and Inherited Metabolic Disorders. In: Magnetic Resonance Imaging of the Brain and Spine; 4th edition; Scott W. Atlas (ed). Philadelphia-New York: Lippincott Williams & Wilkins; 2009.
Pelc NJ, Alley MT, Listerud J, Atlas SW.	Fundamentals of flow and hemodynamics. In: Atlas SW, ed. Magnetic resonance imaging of the brain and spine. 4th edition. Philadelphia, Pennsylvania: Lippincott Williams & Wilkis; 2008.
Ray S, Biswal S, Gambhir SS.	Monitoring gene and cell therapies in living subjects with molecular imaging technologies. In: Templeton NS, Lasic DD (eds.) Gene Therapy: Therapeutic Mechanisms and Strategies. 3rd edition. Marcel Dekker, New York (in press).
Stevens KJ	MRI of the extremities. In: Clinical Emergency Radiology; Cambridge University Press, Cambridge, U.K. (in press).
Towbin A, Newman B.	Syndromes and chromosomal disorders and the heart. . In: Slovis T, ed. Caffey's Pediatric Diagnostic Imaging. 11th edition. Philadelphia, Pennsylvania: Elsevier Inc.; 2008.
Towbin A, Newman B.	Systemic diseases affecting the heart. In: Slovis T, ed. Caffey's Pediatric Diagnostic Imaging. 11th edition. Philadelphia, Pennsylvania: Elsevier Inc.; 2008.
Van Tassell P, Mafee M, Atlas SW, Galetta S.	The Orbit and Visual System. In: Magnetic Resonance Imaging of the Brain and Spine; 4th edition; Scott W. Atlas (ed). Philadelphia-New York: Lippincott Williams & Wilkins; 2009.
Vertinsky T, Jayaraman MV, Do HM.	Radiographic Evaluation of Lesions within the Vertebrae. In: Tumors of the Spine. Kim DH, Chang UK, Kim SH, Bilsky MH (eds) 121-183. Philadelphia, PA: Saunders Elsevier; 2008.
Wintermark M, Wirt MD, Mukherjee P, Zaharchuk G, Barbier E, Dillon WP.	Brain: Modern Techniques and Anatomy. In: Magnetic Resonance Tomography. Berlin Heidelberg: Springer-Verlag; 2007.
Xie J, Chen X.	Surface modification and bioconjugation of nanoparticles. In: Nanoplatform-Based Molecular Imaging. Xiaoyuan Chen, ed. John Wiley & Sons, Hoboken, NJ.

Papers Submitted or In Press

Aggarwal A, Olsen D, Napel S, Rubin GD, Paik DS.	Lung Nodule CAD False Positive Reduction Using a Novel Non-parametric Shape Analysis Approach in Chest CT. Medical Physics; June 2008 (submitted).
Backer MV, Levashova Z, Levenson R, Blankenberg FG, Backer JM.	Cysteine-Containing Fusion Tag for Site-Specific Conjugation of Therapeutic and Imaging Agents to Targeting Proteins. In: Otvos L, ed. Methods in Molecular Biology, Peptide-Based Drug Design. New York, New York: Humana Press, 2008. (in press).
Barral JK, Pelc NJ, Pauly JM, and Nishimura DG	Accurate Reconstruction Method for Truncated Projection Reconstruction-MRI data. IEEE Trans Med Imag (submitted).
Besier T, Fredericson M, Gold G, Delp S, Beaupré G.	The influence of femoral and tibial internal and external rotation on cartilage stresses within the patellofemoral joint. Journal of Orthopaedic Research (in press).
Besier T, Fredericson M, Gold, Beaupré G, Delp S.	Muscle forces at the knee during walking and running in patellofemoral pain patients and pain-free controls. Journal of Biomechanics. Submitted.
Besier T, Gold G, Delp S, Fredericson M, Beaupre G.	The Influence of Femoral Internal Rotation on Cartilage Stresses within the Patellofemoral Joint. J Ortho Research 2008 (in press).
Blankenberg F.	In Vivo Detection of Apoptosis. J Nucl Med. (in press).
Blankenberg F.	Monitoring of treatment-induced apoptosis in oncology with PET and SPECT. Curr Pharm Des. (in press).
Bracken J, Lillaney P, Fahrig R, Rowlands J.	Closed bore XMR (CBXMR) systems for aortic valve replacement: Investigation of rotating-anode x-ray tube heat loadability. Med. Phys. 2008 (submitted).
Butts Pauly K, Diederich CJ, Rieke V, Bouley D, Chen J, Nau WH, Ross AB, Kinsey AM, Sommer G.	MR-guided high intensity ultrasound ablation of the prostate. Topics Magn Reson Imaging 2007. (in press)
Cai W, Chen X.	Imaging of Integrins as Biomarkers for Tumor Angiogenesis. Curr Pharm Des. (in press).
Cai W, Guzman R, Hsu AR, Sun G, Wang H, Bliss T, He L, Chen K, Li ZB, Maag AL, Hori N, Zhao H, Moseley M, Steinberg GK, Chen X.	Positron Emission Tomography Imaging of Vascular Endothelial Growth Factor Receptor Expression after Experimental Stroke. Stroke. (in press).
Caires C, Guccione S.	Synthesis, structure, and reactivity of borate ester coordinated organobismuth compounds. Organometallics (accepted).
Cao Q, Cai W, Niu G, He L, Chen X.	Multimodality Imaging of IL-18bp-Fc Therapy of Experimental Lung Metastasis. Clin Cancer Res. (in press).
Chen C, Lu W, Johns C, Hargreaves B, Reeder S, Delp S, Siston R, Gold G.	Multi-Echo IDEAL-GRE Water-Fat Separation for Rapid Assessment of Cartilage Morphology – Initial Experience. Radiology. Submitted.
Chen K, Cai W, Li Z-B, Wang H, Chen X.	Quantitative PET imaging of VEGF receptor expression. Mol Imaging Biol. (in press).
De la Zerda A, Zavaleta C, Keren S, Vaithilingam S, Bodapati S, Liu Z, Levi J, Ma TJ, Oralkan O, Cheng Z, Chen X, Dai H, Khuri-Yakub BP, Gambhir SS.	Photoacoustic Molecular Imaging in Living Mice Utilizing Targeted Carbon Nanotubes. Nat Nanotechnol. in press.
Desser T, Kamaya A.	Ultrasound of Thyroid Nodules. Neuroimaging clinics of North America. Accepted for publication.
Do BH, Tseng JR, Rosenberg J, Lee S-W, Mari CA, Quon A, Biswal S.	Pattern of 18F-FDG uptake in the spinal canal in patients with non-central nervous system malignancy. Radiology 2008 (accepted).
Draper C, Santos J, Kourtis L, Besier T, Beaupré G, Gold G, Delp S.	Accuracy of measuring joint motion using real-time MRI: A phantom study. Journal of Magnetic Resonance Imaging (in press).
Draper C, Santos J, Kourtis L, Besier T, Beaupre T, Gold G, Delp T.	Accuracy of Measuring Joint Motion Using Real-time MRI: A Phantom Study. J Magn Reson Imaging 2008 (in press).
Gerber R, Kamaya A, Miller S, Cronin D, Dwyer B, Chueh J, Conner K, Barth R	Fetus-in-fetu: Eleven fetoid forms in a single fetus, review of the literature, and imaging. Journal of Ultrasound in Medicine. Accepted for publication.
Ghosh MG, Renier C, Goris M, Mari C, Schipper ML, Gavrielov A, Nowels K, Gambhir SS, Wapnir IL.	In vitro and in vivo differences in NIS activity with retinoic acid, lactogenic hormones and dexamethasone. BMC Cancer. Submitted.
Gu M, Kim DH, Mayer D, Sullivan EV, Pfefferbaum A, Spielman D.	Reproducibility Study of Whole-Brain 1H Spectroscopic Imaging with Automated Quantification. Magn Reson Med. (in press).
Han M, Daniel BL, Hargreaves BA.	Accelerated bilateral dynamic contrast-enhanced 3D spiral breast MRI using TSENSE. J Magn Reson Imaging (accepted).
Heit JJ, Georganos SA, Dodd RL, Jayaraman MV, Do HM.	Extravertebral osteoplasty using cement for treatment of non-healing fractures of the pubic ramus and clavicle. Journal of Vascular and Interventional Radiology (submitted).
Holman H-Y, Bjornstad KA, Martin MC, Mckinney WR, Blakeley EA, Blankenberg FG	Mid-infrared reflectivity of experimental atheromas. J Biomed Opt. (in press).

Holman HYN, Blankenberg FG.	Mid-Infrared Reflectivity of Mouse Atheromas: A Case Study. DASIM Book. In: Moss D, ed. Biomedical Applications of Synchrotron Infrared Microspectroscopy 2008. (in press).
Hu W, Wilson RJ, Koh A, Fu A, Faranesh AZ, Earhart CM, Osterfeld SJ, Han S-J, Xu L, Guccione S, Sinclair R, Wang SX.	Nanoimprinted high-moment antiferromagnetic nanoparticles with multiplex functionality. Advanced Materials (accepted).
Huang M, Chan D, Jia F, Xie X, Li Z, Hoyt G, Robbins RC, Chen X, Giaccia A, Wu JC.	Molecular Imaging of RNA Interference Therapy Targeting Prolyl Hydroxylase-2 for Treatment of Myocardial Ischemia. Circulation. (in press).
Hundt W, O'Connell-Rodwell CE, Mayer D, Bednarski MD, Guccione S.	Tumor tissue characterization evaluating the Luciferase Activity under the control of a hsp70 promoter and MR imaging in Three Tumor Cell Lines. European Journal of Radiology 2008 (accepted).
Iagaru A, Gambhir SS, Goris ML.	90Y-Ibritumomab (Zevalin®) Therapy in Refractory Non-Hodgkin?s Lymphoma: Observations from 111In-Ibritumomab Pre-Treatment Imaging. J Nucl Med. 2008 (in press).
Iagaru A, Goris ML, Gambhir SS.	Perspectives of Molecular Imaging and Radioimmunotherapy in Lymphoma. Radiol Clin North Am. 2008;Jul;46(4) (in press).
Iagaru A, Goris ML, Gambhir SS.	Perspectives of Molecular Imaging and Radioimmunotherapy in Lymphoma. Radiologic Clinics of North America (in press).
Iagaru A, Goris ML.	Rhabdomyosarcoma diffusely metastatic to the bone marrow: suspicious findings on 99mTc-MDP bone scintigraphy confirmed by 18F-18 FDG PET/CT and bone marrow biopsy. Eur J Nucl Med Mol Imaging. 2008 (in press).
Iagaru A, Mittra ES, McDougall IR, Quon A, Gambhir SS.	18F FDG PET/CT Evaluation of Patients with Ovarian Carcinoma. Nucl Med Commun. 2008 (in press).
Iagaru A, Wang, Y, Mari C, Quon A, Goris ML, Horning S, Gambhir SS.	18F FDG PET/CT Evaluation of Response to Therapy in Lymphoma: When is the Optimal Time for the First Re-evaluation Scan? Clin Nucl Med. 2008 (in press).
Kamaya A, Shin L, Desser T, Chen B.	Emergency Gynecologic Imaging. Seminars in Ultrasound, CT, and MRI. Accepted.
Keenan K, Kourtis L, Besier T, Lindsey D, Gold G, Delp S, Beaupre G.	New resource for the computation of cartilage biphasic material properties with the interpolant response surface method. Biomechan. Model. Mechanobiol (in review).
Kelly ME, Guzman R, Sinclair J, Bell-Stephens TE, Bower R, Hamilton S, Marks MP, Do HM, Chang SD, Adler JR, Levy RP, Steinberg GK.	Multimodality treatment of posterior fossa arteriovenous malformations. Journal of Neurosurgery (accepted).
Kim D, Gu M, Cunningham C, Chen A, Baumer F, Glenn O, Vigneron D, Spielman D, Barkovich A.	Fast 3D 1H-MRSI of the Pediatric Brain with Motor Dysfunction. JMRI (in press).
Koo S, Giori N, Gold G, Dyrby C, Andriacchi T	Accuracy of cartilage thickness measurement in MRI changes with Cartilage Thickness: Laser Scanner Based Validation of In Vivo Osteoarthritis Cartilage. Journal of Biomedical Engineering 2008 (in press).
Kuo WT, van den Bosch MA, Hofmann LV, Louie JD, Kothary N, Sze DY.	Catheter-directed embolectomy, fragmentation, and thrombolysis for the treatment of massive pulmonary embolism after failure of systemic thrombolysis. Chest 2008; (in press).
Larabi M, Mackanos M, Shinde, R, Contag C, Guccione S	Temperature sensitive liposomes for local drug delivery using focused ultrasound (submitted).
Lee DS, Kamaya A, Jeffrey RB.	Islet Cell Tumors of the Pancreas: Spectrum of MDCT Findings. A Pictorial Essay. Applied Radiology. Accepted for publication.
Lee S-W, Padmanabhan P, Ray P, Gambhir SS, Doyle TD, Contag C, Goodman SB, Biswal S.	Stem cell-mediated accelerated bone healing observed with in vivo molecular and small animal imaging. J Orthop Res; 2008 (accepted).
Lim M, Bower R, Steinberg S, Guccione S.	The predictive value of serum myeloperoxidase for vasospasm in patients with aneurysmal subarachnoid hemorrhage. J Neurosurgery 2008 (submitted).
Lim M, Yang Y-S, Choi S, Bower R, Sims L, Wang Y, Samra R, Cheshier S, Haddix T, Vogel H, Tse V, Harsh G, Guccione S.	Vascular targeted nanoparticle therapeuty for GBM. Cancer Research (submitted).
Liu Y, Shin L, Kamaya A, Jeffrey RB.	An Unusual Imaging and Clinical Presentation of Papillary Thyroid Carcinoma. Journal of Ultrasound in Medicine. Accepted.
Liu Z, Chen K, Davis C, Sherlock S, Cao Q, Chen X, Dai H	Drug delivery with carbon nanotubes for in vivo cancer treatment. Cancer Res. (in press).
Lu A, Pauly J, Butts Pauly K.	Improved Slice Selection for R2* Mapping during Cryoablation with Eddy Current Compensation. JMRI (in press).
Mackanos M, Larabi M, Shinde R, Simanovskii D, Guccione S, Contag C.	Laser-mediated local delivery of liposome contents after systemic administration (submitted).
MacKenzie JD, Vasanawala S.	Advances in Pediatric Body MRI. Radiology Clinics of North America (in press).
Mazin SR and Pelc NJ	A Fourier Rebinning Algorithm for Cone Beam CT. Med Phys (submitted).
McKenzie CA, Reeder SB, Brau ACS; Pineda AR, Yu H, Shimakawa A, Pelc, NJ and Brittain JH	Abdominal IDEAL Imaging with Self Calibrating Parallel MRI. Magn Reson Med (submitted).

Melvin JS, Mackenzie JD, Nacke E, Sennett BJ, Wells L.	Magnetic Resonance Imaging and the HAGL Lesion: Four arthroscopically confirmed cases of false positive MRI diagnosis. American Journal of Roentgenology (in press).
Mittra ES, Iagaru A, Quon A, Fischbein N.	Skull base neoplasms. PET Clinics. 2008; Jul;2(3): (in press).
Newman B, Grosse-Wortmann L, Charron M, Yoo SJ.	A Pitfall of Radioisotope Quantification of Qp/Qs in a Patient with Severe Postoperative Pulmonary Venous Obstruction. Clinical Nuclear Medicine (in press).
Pineda AR and Pelc NJ	To Bin or Not to Bin? The Effect of Detector Cell Size on Noise and Detectability in CT. Med Phys (submitted).
Pu J, Roos J, Yi CA, Napel S, Rubin GD, Paik DS.	Adaptive Border Marching Algorithm: Automatic Lung Segmentation on Chest CT Images. Computerized Medical Imaging and Graphics 2008 May; (in press).
Renier C, Yao C, Goris ML, Ghosh M, Katznelson L, Nowles K, Gambhir SS, Wapnir I	Endogenous NIS expression and activity in triple negative breast cancers. Breast Cancer Research (in press).
Rubin D, Rodriguez C, Shah P, Beaulieu CF.	iPad: semantic annotation and markup of radiological images. AMIA Annual Symposium, peer reviewed manuscript. Accepted for publication pending revisions, June 2008.
Shachaf C, Gentles A, Elchuri S, Sahoo D, Soen Y, Sharpe O, Perez O, Chang M, Mitchel D, Robinson W, Nolan G, Dill D, Plevritis SK, Felsher D.	Genomic and proteomic analysis reveals a threshold level of MYC required for tumour maintenance. Cancer Research (in press).
Shahbaba N, Prenosil E, Jain A, Plevritis SK.	A modified Dirichlet process mixture model for clustering phophopeptides based on their response to anti-cancer drug perturbation. Proceedings of the 2008 International Conference on Bioinformatics and Computational Biology (accepted).
Sherbondy AJ, Dougherty RF, Ben-Shachar M, Cheung SH, Napel S, Wandell BA.	ConTrack: Finding the Most Likely Pathways Between Brain Regions. Journal of Vision 2008;April (in press).
Siston R, Giori N, Cromie M, Goodman S, Gold G, Maloney W.	Averaging different alignment axes improves femoral rotational alignment in navigated total knee arthroplasty. Journal of Bone and Joint Surgery (in press).
Sommer FG, Bouley D, Frisoli J, Pierce L, Sandner-Porkristl D, Fahrig R.	Determination of 3-dimensional zonal renal volumes using contrast enhanced CT. J Comput Assist Tomogr. (in press)
Staroswiecki E, Bangerter N, Gurney P, Grafendorfer T, Daniel B, Gold, G, Hargreaves	In Vivo Sodium Imaging with a 3D Cones Trajectory at 3T and 7T. Magn Resnon Med. Submitted.
Stevens K, Busse R, Brau A, Han E, Beatty P, Beaulieu C, Gold G.	Isotropic MRI of the Ankle with 3D-FSE-Cube: Initial Experience in Healthy Volunteers. Radiology (in press).
Stevens K, Busse RF, Han E, Brau AJ, Beatty P, Beaulieu CF, Gold GE.	Isotropic MRI of the Ankle with 3D-FSE-Cube: Initial experience in healthy volunteers. Accepted by Radiology 2008;April.
Stevens K, Griffiths, KL, Zatz LM, Mahadevan S, Leung ANC.	Discordance rates between preliminary and final radiology reports on cross-sectional imaging studies at a level one trauma center. Accepted by Academic Radiology 2008;March.
Strauss HW, Blankenberg FG, Vanderheyden J-L, Tait J.	Imaging of Apoptosis. In: Schwaiger M, ed. Molecular Imaging – Handbook of Experimental Pharmacology. 2008. (in press).
Vandevenne J, Vanhoenacker F, Beaulieu CF, MD, Bergman AG, Butts Pauly K, Dillingham MF, Lang PK.	All-in-one MR arthrography of the shoulder in a vertically open MR unit. Acta Radiologica (in press).
Vandevenne JE, Vanhoenacker F, Beaulieu CF, et al.	All-in-one MR arthrography of the shoulder in a vertically open MR unit. Acta Radiologica 2008; (in press).
Vertinsky AT, Schwartz NE, Fischbein NJ, Rosenberg J, Albers GW, Zaharchuk G.	Comparison of multidetector CT angiography and magnetic resonance imaging of cervical artery dissection. Am J Neurorad. 2008 (in press).
Wang ZJ, Joe BN, Coakley FV, Zaharchuk G, Busse RF, Yeh BM.	Urinary oxygen tension measurement in humans using MR imaging. Acad Radiol. 2008 (in press).
Wen Z, Fahrig R, Williams ST and Pelc NJ	Shimming with Permanent Magnets for the X-ray Detector in a Hybrid X-ray/MR System. Med Phys (submitted).
Wen Z, Reeder SB, Pineda AR, and Pelc NJ	Noise Considerations of Three-Point Water-Fat Separation Imaging Methods. Med Phys (submitted).
Wong H, Desser TS, Jeffrey RB.	Transient Hepatic Attenuation Differences in Computed Tomography from Extrahepatic Portal Vein Compression. Radiology Case Reports 2007 (in press).
Wong SH, Kupnik M, Watkins RD, Butts Pauly K, Khuri-Yakub BT.	Evaluation of wafer bonded CMUTs with rectangular membranes featuring high fill factor, Ultrasonics, Ferroelectrics and Frequency Control. IEEE Transactions (in press).
Yaghoubi SS, Jensen MC, Satyamurthy N, Budhiraja S, Paik DS, Czernin J, Gambhir SS	Non-Invasive Detection of Therapeutic Cytolytic T Cells with [18F]FHBG Positron Emission Tomography in Glioma Patients. Nature Clinical Practice Oncology 2008 (submitted).
Yang Y-S, Sims L, Guccione S.	Changes in glucose uptake after nanoparticle-based anti-angiogenic therapy: PET and MRI correlations. Cancer Research (submitted).
Zavaleta C, Keren S, Cheng Z, Schipper M, Liu Z, Chen X, Dai H, Gambhir SS	Non-invasive Raman Spectroscopy in Living Mice for Evaluation of Tumor Targeting with Carbon Nanotubes. Nano Lett. (in press).

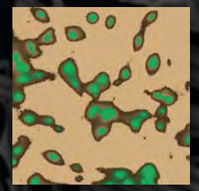

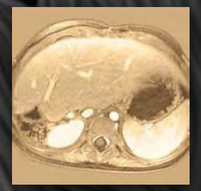

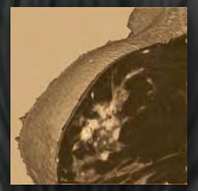

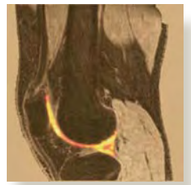

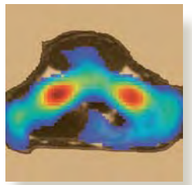

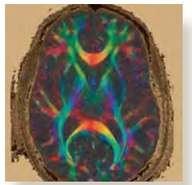

Funded Research Projects

NIH Supported Research

PI	Type	Title
Roland Bammer, PhD	R01	**Improving SENSE MRI for Spiral and Echo-Planar Imaging
	R21	*Real-Time MRI Motion Correction System
Christopher Beaulieu, MD, PhD	R01	Three-Dimensional CT Colonography
Francis Blankenberg, MD	R01	Imaging Apoptosis in vivo with Technetium 99m Annexin
Kim Butts Pauly, PhD	R01	iMRI Methods for Cancer Diagnosis and Treatment
	R01	MR-Image Guided Focused Ultrasound for Treatment of Liver and Renal Cancer
Catie Chang	F32	*Temporal Characteristics of Intrinsic Brain Networks
Xiaoyuan Chen, PhD	R01	*Radiolabeled RGD Peptides for Breast Cancer Imaging and Therapy
	R01(MPI)	*Carbon Nanotubes as Multifunctional Spectroscopic Markers & Delivery Agents for Cancer Therapy
	R21	Quantum Dots for NIR Fluorescence Imaging of Tumor Angiogenesis
Bruce Daniel, MD	R01	Magnetic Resonance Imaging of Breast Cancer
	R01	Techniques for MRI-Guided Cryosurgery of Prostate Cancer
Rebecca Fahrig, PhD	R01	*MR Compatible X-Ray Tube
	R21	*Efficient Scatter Correction
Sam Gambhir, MD, PhD	P50	In Vivo Cellular and Molecular Imaging Center at Stanford
	R01	Reporter Imaging of Protein-Protein Interactions
	R01	Multimodality Imaging of Cell Mediated Gene Transfer
	R01	***Imaging Cytolytic T Cells in Ca Pts using Reporter Gener/Reporter Probes
	R25	Stanford Molecular Imaging Scholars (SMIS)
	U54	Center of Cancer Nanotechnology Excellence Focused on Therapy Response (CCNE-TR)
Gary M. Glazer, MD	T32	**Advanced Techniques for Cancer Imaging
Gary Glover, PhD	P41	Center for Advanced Magnetic Resonance Technology at Stanford (CAMRT)
Garry Gold, MD	R01	Rapid MRI for Evaluation of Osteoarthritis
	R01	Real-Time MRI and 3D Modeling: Development and Application to Patellofemoral Pain
Craig Levin, PhD	R01	Advanced PET System Dedicated to Breast Cancer Imaging
	R01	*Enhancing Molecular Cancer Imaging with Cadmium Zinc Telluride PET
	R13	Workshop on the Nuclear Radiology of Breast Cancer
	R33	New Scintillation Light Detection Concepts for PET
Chunlei Liu, PhD	K99	High Resolution Diffusion-Weighted magnetic Resonance Imaging at 300-Micron Level
Michael Moseley, PhD	R01	Improved PWI Methodology in Acute Clinical Stroke
Sandy Napel, PhD	R01	Efficient Implementation of 3D Vascular Image Data
Norbert Pelc, ScD	R01	Inverse Geometry CT for Dose-efficient Volumetric Imaging
Laura Pisani, PhD	F32	Fetal Functional Magnetic Resonance Imaging

* New for 2008
** Longstanding projects renewed for new funding cycle beginning 2008
*** New for 2009

For additional awards, see Awards and Honors pages 24-25, and Trainee Awards pages 30-31.

PI	Type	Title
Sylvia Plevritis, PhD	R01	Cost-Effectiveness Analysis of Lung Cancer Screening
	U01	Breast Cancer Trend Analysis Using Stochastic Simulation
	U56	Computational Modeling of Cancer Biology
Jianghong Rao, PhD	R01	***Nanosensors Based on quantum Dots and BRET
	R01 (MPI)	* Actively Controlled and Targeted Single-Molecule Probes for Cellular Imaging
Geoffrey Rubin, MD	R01	Improving Radiologist Detection of Lung Nodules with CAD
Graham Sommer, MD	R01	**Precise MRI-Directed Sonic Ablation of Prostate Cancer
Dan Spielman, PhD	R01	*IH MRSI of the Human Brain at 7T
Joseph Wu, MD, PhD	K08	Molecular Imaging of Cardiac Cell Transplantation
	R21	*Biological Insights into Dynamics of Stem Cell Differentiation & Misbehavior
	R21/R33	*Nanostructuring and Molecular Imaging of Engineered Cardiovascular Tissues
Annelise Barron	Sub (CCNE)	*Targeted, biocompatible, multivalent contrast agents based on core-shell star polymer nano-particles for MR and NIR imaging
Sandip Biswal	Sub (ICMIC)	*Imaging Cancer Pain with Manganese-Enhanced MRI
Francis Blankenberg, MD	Sub (U of Wash)	Membrane Binding and Imaging Applications of Annexins
Xiaoyuan Chen, PhD	Sub (Purdue)	99mPTc-Labeled Cyclic RGD Peptide Tetramers for Breast Cancer Imaging
Zhen Cheng	Sub (ICMIC)	*A Novel Rhenium Cyclized Peptide for Pre-clinical Imaging of Melanoma Metastases
Rebecca Fahrig, PhD	Sub (Sunnybrook)	Low Cost Digital X-ray Detectors Using Liquid Crystals
	Sub (Univ Hlth Network)	Image Science for the New X-Ray: Taking NEQ to Task
Gary Glover, PhD	Sub (UCI)	Functional Imating Research in Schizophrenia Testbed
Garry Gold, MD	Sub (UCSF)	Data Coordinating Center for Osetoarthritis Initiative
Beverly Mitchell	Sub (ICMIC)	*Synthesis and Use of 18F-fluoro-9-B-D-arabinofuranosylguanine as an Imaging Agent for the Detection of Diseases of T cell origin
Sandy Napel, PhD	Sub (BioE)	SIMBIOS - Physics-Base Simulation of Biological Structures
David Paik	Sub (NCBO)	***Cancer Nanotechnology Knowledgebase for Nanoparticle Analysis and Design
Dan Spielman, PhD	Sub (U of Miami)	*Partnership for MR Spectroscopic Imaging Data
Juergen Willmann	Sub (ICMIC)	*Molecular Ultrasound for Monitoring Anti-Angiogenic Cancer Treatment: Comparison with PET-CT

* New for 2008
** Longstanding projects renewed for new funding cycle beginning 2008
*** New for 2009

For additional awards, see Awards and Honors pages 24-25, and Trainee Awards pages 30-31.

Other Government Supported Research

PI	Type	Title
Xiaoyuan Chen, PhD	DOA	Alpha-v Integrin Targeted PET Imaging of Breast Cancer Angiogenesis and Low-Dose Metronomic Anti-Angiogenic Chemotherapy Efficacy
	DOD	Mesenchymal Stem Cell as Targeted-delivery Vehicle in Breast Cancer
	DOD	Molecular Imaging of Ovarian Carcinoma Angiogenesis
Zhen Cheng, PhD	CBCRP	*Novel Small Proteins for PET Imaging of Breast Cancer
Adam de la Zerda, BS	DOD	***Early Assessment of Breast Cancer Therapy Responses Using Photoacoustic
Brian Hargreaves, PhD	CBCRP	Multinuclear MRI of Breast Tumors
	VA	Cartilage Compression Study for VA
Gang Niu, PhD	DOD	*Imaging Heat Shock Protein 90 (Hsp90) Activity in Hormone-Refractory Prostate Cancer
Rakow-Penner	DOD	Improving Breast Cancer MRI
	CBCRP	***Functional Breast MRI with BOLD Contrast
Jianghong Rao, PhD	DOA	Ribozyme-Mediated Imaging of p53 Expression in Breast Tumor Cells
Joseph Wu, MD, PhD	CIRM	*In Vivo Imaging of Human Embryonic Stem Cell Derivatives and Tumorigenicity

* New for 2008
** Longstanding projects renewed for new funding cycle beginning 2008
*** New for 2009

Stanford Supported Research

PI	Type	Title
Terry Desser, MD	Wallenberg	Learning Radiology in Simulated Environments
Huy Do, MD	OTL	A Novel Non-Invasive Device for Occluding Cerebral Aneurysms
Garry Gold, MD	Wallenberg	Learning Radiology in Simulated Environments
Sandy Napel, PhD	BioX IIP	A Novel Transducer Array and Intelligent Software for Automated Detection of Asymptomatic Carotid Artery Stenosis

* New for 2008
** Longstanding projects renewed for new funding cycle beginning 2008
*** New for 2009

For additional awards, see Awards and Honors pages 24-25, and Trainee Awards pages 30-31.

Foundation Supported Research

PI	Type	Title
Sandip Biswal, MD	Weston Havens	Nerves on Fire: 'Imaging Pain with Manganese-Enhanced Magnetic Resonance Imaging'
Qizhen Cao, PhD	TRDRP	*Alpha7-nAChR Targeted Imaging and Tx of Lung C
Zhen Cheng, PhD	SNM	*Engineered Small Proteins for HER2 Imaging
Qizhen Feng, PhD	AHA	Cellular Therapy for the Ischemic Myocardium: In Vivo Characterization of Biology and Physiology
Carmel Chan, PhD	Susan G. Komen Foundation	Imaging the Efficacy of Heat Shock Protein 90 Inhibitors in Human Breast Cancers
Hyung Chun, PhD	SNM	Integration of Imaging and Genomics for Characterization of Cardiac Stem Cell Therapy
Sam Gambhir, MD, PhD	Canary Fd	Center of Excellence in Early Detection of Cancer
	Doris Duke	Molecular Imaging of Cancer with a Voltage Sensor
Samira Guccione, PhD	Brain tumor Society	*Anti-angiogenic Targeted-Nanoparticle Therapy in Tumors
Mei Huang, PhD	AHA	Molecular Imaging of Non-Viral Cardiac Gene therapy
Zonjin Li, MD, PhD	SNM Pilot Rsch	*Molecular Imaging of Stem Cell Differentiation and Function
MacKenzie/Vasanawala	Soc for Pediatric Radiology	*Evaluation of Pediatric Diseases with Hyperpolarized Carbon-13 MRI
Peter Olcott, MS	SNM	*Optically Coupled Pulse Width Modulation PET Detectors for Combined Whole Body Clinical PET/MR Systems
Jianghong Rao, PhD	BWF	Career Award at the Scientific Interface
	HFSP	Imaging mRNA in Synaptic Plasticity
	Texas A&M/Gates Fd	*Development of Fluorogenic Probes for In Vivo Imaging of TB
David Wang, MD	RSNA	*Ultrasound-mediated Suicide Gene Therapy with MolecularlyTargeted Microbubbles in a Murine Model of Tumor Angiogenesis
Juergen Willmann, MD	RSNA Seed	*Development and Validation of a Multi-Target Contrast Agent for Contrast Enhanced US Imaging of Tumor Angiogenesis in Early Stage Pancreatic Cancer
Joseph Wu, MD, PhD	ACCF	Multi-Modality Imaging of Cardiac Stem Cell
	AHA	In Vivo Tracking of Stem Cells in the Ischemic Myocardium
	BWF	*Molecular and Cellular Mechanisms of Cardiac Regeneration
Greg Zaharchuk, MD, PhD	GE	Perfusion Territory Imaging Using Arterial Spin Labeling in Moyamoya Patients
Michael Zeineh, MD, PhD	RSNA	*Ultra-High Resolution Clinical Imaging of the Human Medial Temporal Lobe with 7T MRI

* New for 2008
** Longstanding projects renewed for new funding cycle beginning 2008
*** New for 2009

For additional awards, see Awards and Honors pages 24-25, and Trainee Awards pages 30-31.

Industry Supported Research

PI	Type	Title
Terry Desser, MD	Berlex Labs	Simulation-based Medical Training Exercise in Management of Contrast Media Adverse Reactions for Residents
Rebecca Fahrig, PhD	Siemens	*Perfusion Imaging using C-arm CG: Brain and Liver
	Siemens	*Cardiac Imaging Using C-arm CT: EP Registration and Perfusion
	Siemens	Gated 3D DynaCT for Cardiac Applications
	Varian	*Correction Approaches for Amorphous Silicon Detector Non-Idealities
Sam Gambhir, MD, PhD	GE Healthcare	Multimodality Molecular Pre-Clinical Imaging
	GE Healthcare	Cell Tracking
	Schering AG	Collaborative Research Agreement: Project 1: Tumor Lymphangiogenesis Imaging Project 2: PET Imaging of Breast Cancer Using Fructose Analogues
Gary M. Glazer, MD	GE Healthcare	GE PACS System
	GE Healthcare	Destination Digital
Garry Gold, MD	GlaxoSmithKline	Sodium MRI at 3.0T for Drug Discovery
	GE Healthcare	Advanced Orthopedic MR Imaging
Robert Herfkens, MD	GE Healthcare	Body and Vascular Imaging
Debra Ikeda, MD	ART, Inc.	SSC-311 Adjunctive Efficacy Study of the SoftScan Optical Breast Imaging System
Nishita Kothary, MD	Siemens	Clinical Feasibility and Evaluation of RoRo (Rotational Mapping); Optimal Imaging Protocol of HCC Undergoing TACE Utilizing DynaCT; & Needle Guided Procedures Utilizing DynaCT, Laser Guidance, and 2D3D Registration
Craig Levin, PhD	GE Healthcare	Combined PET MR System
Michael Marks, MD	Micrus Endovascular	Safety and Efficacy of Cerecyte Polymer Filled Coil in Patients with Intracranial Aneurysms
Norbert Pelc, ScD	GE Healthcare	CT X Ray
	GE Healthcare	Interventional MR Guidance
Geoffrey Rubin, MD	Cook Medical	Zenith TX2 Thoracic TAA Endovascular Graft
Dan Spielman, PhD	SRI International	In Vivo Diffusion and Spectroscopic Brain Imaging in Alcoholism
Daniel Sze, MD, PhD	Angiotech	*A Prospective Randomized Multi-centered Safety and Efficacy Evaluation of the Bio-seal Biopsy Track Plug for Reducing Pneumothorax Rates Post Lung Biopsy Procedures
	Cook Medical	Zenith TX2 Thoracic TAA Ebdovascular Graft
	Cook, Inc.	The Zilver PTX Drug Eluding Vascular Stent in the Above the Knee Femoral-popliteal Artery
	Gore Medical	A Clinical Study Comparing Use of the Bifurcated EXCLUDER Endovascular Prosthesis to Open Surgical Repair in the Primary Treatment of Infrarenal Abdominal Arotic Aneurysms
	Gore Medical	A Clinical Study comparing the Use of the Modified Bifurcated EXCLUDER Endoprosthesis to Open Surgical Repair in the Primary Treatment of Infrarenal Abdominal Aortic-Aneurysms
	Gore Medical	A Clinical Study Evaluating the Use of the Thoracic EXCLUDER Endoprostheis in the Treatment of Descending Thoracic Aortic Diseases
	Gore Medical	Evaluation of the GORE TAG Thoracic Endoprothesis for Treatment of Descending Thoracic Aneurysms
	Gore Medical	Treatment IDE for Use of the GORE TAG Thoracic Endoprosthesis in Subjects with Descending Thoracic Aortic Aneurysms Requiring Surgical Repair
	Gore Medical	Evaluation of the GORE TAG Thoracic Endoprothesis for Treatment of Complex Pathology of the Descending Thoracic Aorta

* New for 2008
** Longstanding projects renewed for new funding cycle beginning 2008
*** New for 2009

For additional awards, see Awards and Honors pages 24-25, and Trainee Awards pages 30-31.

Industry Supported Research

PI	Type	Title
Daniel Sze, MD, PhD	Gore Medical	*Evaluation of the GORE TAG Thoracic Endoprosthesis-45 mm for the Primary Treatment of Aneurysm of the Descending Thoracic Aorta
Shreyas Vasanawala, MD	GE Healthcare	Advanced Pediatric MR Imaging
Joseph Wu, MD, PhD	Geron	Imaging of Human Embryonic Stem Cells in the Heart and Skeletal Muscles

* New for 2008
** Longstanding projects renewed for new funding cycle beginning 2008
*** New for 2009

Projects made possible in part by industry seed funding grants

PI	Type	Title
Daniel Spielman , PhD	GE Healthcare	Parallel Imaging Methods Optimized for Magnetic Resonance Spectroscopic Imaging of Hyperpolarized 13 C-labeled Substrates
Brian Hargreaves , PhD	GE Healthcare	32-channel Bilateral Form-Fitted Breast MRi Coil Array
Graham Sommer, MD	GE Healthcare	Dynamic Contrast Enhancement of Prostate Cancer and BPH
Greg Zaharchuk , MD, PhD	GE Healthcare	Perfusion Territory Imaging Using Arterial Spin Labeling in Moyamoya Patients
Sandip Biswal , MD	GE Healthcare	Nerves on Fire: Imaging Pain with Teslascan
Michael Zieneh, MD, PhD	GE Healthcare	High Field MRI (7T) Imaging of Temporal Lobe

* New for 2008
** Longstanding projects renewed for new funding cycle beginning 2008
*** New for 2009

For additional awards, see Awards and Honors pages 24-25, and Trainee Awards pages 30-31.

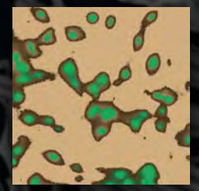

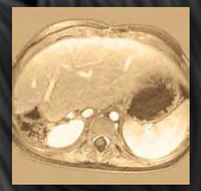

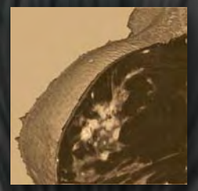

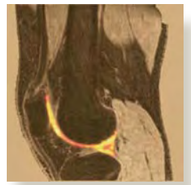

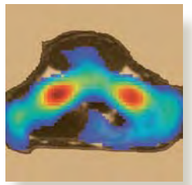

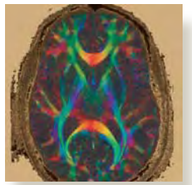

Collaborators

Building the Lucas Center

The View in 2008

Collaborating Stanford Departments

We work with almost three hundred faculty, postdoctoral fellows, students, and research staff from across the University. We wish to thank you all for the friendly, productive collaborations that we enjoy all year long. Stanford departments with whom we have long-standing research projects include the following:

Aeronautics and Astronautics
Anesthesia
Applied Physics
Bioengineering
Cancer Biology
Cancer Center
Chemistry
Computer Sciences
Comparative Medicine
Developmental Biology
Electrical Engineering
ENT
Functional Restoration
Health Research and Policy
Infectious Diseases
Materials Science and Engineering
Mechanical Engineering
Medical Informatics
Medicine
Microbiology and Immunology
Neurobiology
Neurology and Neurological Sciences
Neurosurgery
OB/GYN
Opthalmology
Orthopedics/Orthopedic Surgery
Pediatrics/Neonatology
Psychiatry and Behavioral Sciences
Psychology
Radiation Oncology
Stanford Center for Biomedical Ethics
Stroke Center
Surgery
Urology

Collaborators Outside of Stanford

We also enjoy many collaborations with foundations, agencies, institutions, and industry for whose support we are indeed thankful. We look forward to continued success in these collaborative endeavors as well.

Advanced Research Technologies, Inc.
Alza Corporation
Angiotech
Berlex
Canary Foundation
Cedars Sinai, Los Angeles
Chiron Corporation
Colorado State University—Boulder
Concentric Medical, Inc.
Cook Incorporated
Cook Medical Institute, Inc.
Diversified Diagnostic Products, Inc.
FeRx, Inc.
Fred Hutchinson Cancer Research Center
GE Healthcare
Genentech
Geron
Glaxo Smith Kline
Intronn Inc.
Medimmune Inc.
Micrus Corporation
Nova R&D Inc.
Palo Alto Veterans Administration
Pfizer
Prostate Cancer Foundation
Richard M. Lucas Cancer Foundation
Riken, Saitama, Japan
Schering AG
Sidney E. Frank Foundation
Siemens Corporate Research
Siemen's Medical Solutions
SRI International
U-Systems
University of California, Berkeley
University of California, Davis
University of California, Irvine
University of California, Los Angeles
University of California, San Francisco
University of California, San Diego
University of Texas, A & M
University of Texas, Austin
Varian Associates
Wallenberg
W.L. Gore and Associates